Strathclyde Institute of Pharmacy and Biomedical Sciences

University of Strathclyde

Glasgow G4 0RE

Submitted September 2025

Using a fluorescent dual-reporter in *Streptomyces* to study *bldA*-dependant gene expression

Jack William Stone

Principal Investigator: Professor Paul A Hoskisson

Secondary Supervisor: Professor Iain S Hunter

Doctoral Thesis submitted in fulfilment of the requirement for the degree of Doctor of Philosophy.

Declaration of Authenticity and Author's Rights:

This thesis is the result of the author's original research. It has been composed by the author and has not been previously submitted for examination which has led to the award of a degree.

The figures used in this thesis are the result of work carried out by myself, with the exceptions of **Fig. 4.1**, **Fig 4.2**, **Fig. 4.4**, and **Fig. 4.5** which were generated with the assistance of Professor Paul A Hoskisson.

Signed:

Date:

Acknowledgements

Firstly, I would like to express my deepest gratitude to my fantastic supervisor: Professor Paul Hoskisson. Over the last 4 years, Paul has always been available to everyone in his group, including myself. His assistance and guidance throughout the last 4 years, as well as his encouragement and inspirational ideas have been invaluable in building up my confidence in both my research and my ideas. He has also been a much-needed mentor for networking across the community and has introduced me to many scientists in the field, something I will always be thankful for. I would also like to thank my secondary supervisor Prof Iain S Hunter for his own suggestions and assistance in developing my own ideas for my project throughout the course of my studies.

I must also thank the academics that make up 'The Microgroup ', especially Paul Herron, Kate Duncan, Leighton Pritchard, Morgan Feeney, Gail McConnell and Arnaud Javelle, all of which have contributed their own knowledge and have influenced my work throughout my time in Glasgow. My thanks go out to the University of Strathclyde for funding my studentship through the Research Excellence Award and for being my home for the last 3 years. I would especially like to thank Allison and everyone from the autoclave suite for their technical work over my time at Strathclyde. I would also like to thank the larger Microgroup for being great people to work alongside for the last three years, in particular everyone from the past and previous Hoskisson Group (John Munnoch, John Bruce, James, Dan, Kaisha, Molly, Robyn and Katherine) for being there for me and making every day of working in the Hamnett Wing a blast. It might have taken me a while (a long while) for me to open out of my shell a bit, but you all truly made my time at Strathclyde an unforgettable experience. So, with that said, James, Dan, Molly, Robyn, the Johns (Munnoch and Bruce), the Toms (Hender and Harris), Kaisha, Katherine, Liam, Charlie, Elmira, Adrianna, Eilidh, Emily, Angelika, Darren, Kirstyn, Khedidja, Lizzy, Becca, Stuart, Anil and Derya, thank you for the great times, it was a blast.

Ally, Holly, Dave, Logan, Hannah, Lily, John. I wanted to thank each of you for all the great nights out, the evenings of drinks, and being a thoroughly great group of people who have helped me get through the hard patches during my time in Glasgow. I genuinely would not have been able to get through this without you guys. Lily and John, we go back to even before Strathclyde, all the way to Birmingham, so who could have seen me ‘following ‘you all the way to Glasgow to continue working in research! You helped me break ground in socialising with everyone here and have helped me form lifelong friends as a result, and that’s something I will always be grateful for. Holly and Logan, where to start…Every time I walk in and see you both there, I know I’m in for a good day solely because you guys are there. Turns out microbiology and immunology do mix! Dave, your infectious laugh and banter never fail to brighten my mood. Ally, I love our chats and that evening watching King of Staten Island in your flat stands out to this day. Hannah, your constant positive attitude, and our occasional optimistic bus chats always set the tone for the day. I love you all.

Thank you to my friends who were always willing to pick up a game for an hour or two to unwind after long nights. That goes to Jack, Liam, Chris, Paddy, the Sams, and John Munnoch. Thanks for all the nights of games and laughs that I sorely needed after long days in the lab. Jack, my best friend of 25 years, Liam and John, my FPS squad, Chris and the Sams, the League Lads, and Paddy, who was happy to play whatever. I couldn’t choose a better group of lads to unwind with. Finally, and most importantly, a huge thank you to my Mum, Dad, Harry and Nan. Thank you for putting up with me for the last 30 years. Thank you for always having time for a chat and continuously showing an interest in my work, even if the closest we got to a scientific conversation was ‘Is this a bacteria? ‘. Thank you for talking some sense into me when things weren’t going well. Simply put, thank you for everything.

This Thesis Is Dedicated To:

William ‘Bill’ Gilbert

&

Carl Gilbert

I hope I made you proud.

Abstract

With rising antimicrobial resistance, new strategies are needed to discover and improve antibiotics. Improved genetic tools may accelerate antibiotic discovery and production. Many existing antimicrobial compounds are natural products of *Streptomyces* bacteria. In *Streptomyces*, the Leucine-tRNA^{UAA} (encoded by *bldA*) decodes the rare TTA codon, and loss of *bldA* results in deficiencies in aerial hyphae, sporulation and antibiotic production. Expression of *bldA* is reported to be repressed by the global regulator BldD in *Streptomyces coelicolor.* Reporter assays, including fluorescent proteins and RNA aptamers, are widely used to monitor gene regulation, and their combination offers a promising genetic tool.

This thesis describes the design, construction, and validation of the 'Broccomyces 'dual-reporter system, which combines the Broccoli aptamer (transcriptional output) and a modified version of mCherry (TTA-mCherry, translational output). Broccomyces was tested in *S. coelicolor* using the *bldA* translational control system. TTA-mCherry levels varied with *bldA* availability, confirming translational reporter viability, however the Broccoli transcriptional reporter was non-functional in liquid media. Unexpectedly, TTA-mCherry was also expressed in *bldA*-deficient backgrounds, suggesting alternative mechanisms for decoding rare codons. The Broccomyces system was further tested under the *ccaR* promoter in *S. clavuligerus* and demonstrated utility for quantifying the translational effects of 5`UTR mutations relevant to antibiotic production.

TTA-mCherry detection in a *bldA*-deficient background prompted whole genome sequencing of a historical *bldA*$^{-}$ strain, highlighting hundreds of previously undocumented mutations, with potential regulatory effects. An isogenic *bldA* deletion strain in *S. coelicolor* M145 was subsequently created and characterised through complementation, metabolite profiling, utilisation assays and transcriptomics. Analysis indicates the *bldA* tRNA impacts far more than morphological development and antibiotic production. This work establishes Broccomyces as a versatile translational reporter and demonstrates the wider regulatory role of *bldA*, with implications for engineering antibiotic production in *Streptomyces*.

Previously published material:

The results of *Chapter 5* (Genomic Characterisation of the *Streptomyces coelicolor bldA* mutant J1700) have been published in the following research article:

Stone JW., Munnoch JT., Hoskisson PA (2025). Whole-genome sequencing of the *Streptomyces coelicolor bldA39* mutant (J1700) reveals hundreds of previously unknown mutations. *Access Microbiol*. 7(2): 000958.v3.

Contribution: Investigation, Formal Analysis, and Original Draft preparation

Contents

Chapter 1: Introduction

1.1 The importance of antimicrobials and antimicrobial resistance

An antimicrobial is an agent that kills micro-organisms or inhibits their growth (Purssell, 2019). One of the first clinically relevant antimicrobials discovered was penicillin, a β-lactam produced by the fungus *Penicillium spp* (Fleming, 1929). The discovery of penicillin launched a golden age of antibiotic discovery, leading to the detection of a multitude of antibiotic classes, such as aminoglycosides, macrolides, carbapenems and many more (Hutchings, Truman and Wilkinson, 2019). Using antimicrobials to treat infections caused by pathogens is one of the greatest advancements in medicine, however, the over-use of antimicrobials, the dissemination of antimicrobial resistance-conferring genes and the spread of novel antibiotic resistances are contributing factors that have led to the current antimicrobial resistance crisis (Llor and Bjerrum, 2014., Salam *et al*, 2023).

Antimicrobial resistance (AMR) occurs when microorganisms evolve mechanisms that results in drugs being used against them becoming less effective. There are multiple mechanisms that microbes can develop to counteract antimicrobials, including modification of the antimicrobial, modification of the target of the antimicrobial, increased efflux of the antimicrobial and blocking antimicrobial uptake (Reygaert, 2018., Souque, Ojeda and Baym, 2024). Mechanisms of antimicrobial resistance typically fall into four categories: limiting drug update, target modification, drug inactivation or drug efflux (Reygaert, 2018). The diversity of mechanisms that lead to resistance means that microorganisms can evolve resistance whenever they are exposed to sub-minimum inhibitory concentrations of antimicrobials, utilising one or more of the mechanisms described above. Given the rise of such resistance in the clinical, there is a need to respond.

The Review on Antimicrobial Resistance, which was commissioned by the UK government, suggested that the increased occurrence of antimicrobial resistance could be responsible for 10 million annual deaths by 2050 (O'Neill, 2014). While there are some who dispute these

predictions (de Kraker *et al*, 2016., National Office of Animal Health, 2016), the World Health Organisation (WHO) and various other research groups concur that AMR is an urgent issue that required worldwide action to address, with the WHO stating that 'AMR is one of the top 10 global public health threats facing humanity ' (Prestinaci, Pezzotti and Pantosti, 2015., WHO, 2021., US CDC, 2019).

As a result of the increase in worldwide AMR, there is an urgent need to develop and introduce new antimicrobial products to the clinic to combat the AMR crisis. Novel strategies are required to discover new drug molecules and to enhance the effectiveness or the production of currently used antimicrobial compounds. Many of the clinically used antimicrobial drugs utilised today are natural products of complex biological factories found in *Streptomyces* bacteria, belonging to the phylum Actinomycetota (Barka *et al*, 2015., De Simeis and Serra, 2021).

1.2 An Overview of Actinomycetota

Actinomycetota (formerly Actinobacteria) is a diverse phylum of filamentous, non-motile Gram-positive bacteria, well known for their high guanine + cytosine (GC) content in their DNA, with some *Streptomyces* bacteria possessing over 70% GC content (Ventura *et al*, 2007, Oren, 2024). In recent years, the nomenclature of Actinomycetota changed as the International Committee on Systematics of Prokaryotes (ICSP) voted to include phylum in the rules of the International Code of Nomenclature of Prokaryotes (ICNP), resulting in the change of classification from Actinobacteria to Actinomycetota (Oren and Garrity, 2021, Oren, 2024). Members belonging to Actinomycetota are found ubiquitously, both in terrestrial and aquatic environments, where they have been documented to be of great ecological importance due to their contributions in soil systems (Servin *et al*, 2008., Bhatti *et al*, 2017). Actinomycetota are also of significant use in agriculture, biotechnology and medicine, with the phylum famously producing two-thirds of all naturally derived antibiotics and various anticancer and antifungal compounds (Barka et al., 2015).

Actinomycetota is one of the largest taxonomic units within the Bacteria domain. Members of the Actinomycetota phylum are incredibly diverse, including a range of human pathogens (*Mycobacterium, Corynebacterium, Nocardia, Propionibacterium, Tropheryma*), soil bacteria (*Streptomyces, Micromonospora*), and human gastrointestinal commensals (*Bifidobacterium*), exhibiting a vast assortment of morphologies from coccoid to highly differentiated branched mycelial forms (Barka et al., 2015, Ventura et al., 2007). Whilst *Streptomyces* and *Mycobacterium* represent two of the most highly studied and characterized genera, the phylum Actinomycetota contains over 300 other genera, many of which are greatly under researched in comparison to more well-documented species (Gao and Gupta, 2012., Parte, 2014., Zhi, Li and Stackebrandt, 2009;). This lack of research be partially attributed to the sheer diversity of Actinomycetota members. This becomes especially apparent when investigating species that are capable of colonizing and surviving in extreme conditions such as freezing or high temperatures, radioactively or chemically contaminated sites, arid deserts soils, or deep marine environments (Gao and Gupta, 2012).

Mycelial forming Actinomycetota are often referred to as Actinomycetes, a designation utilized as early as 1877, meaning 'ray fungus' (Waksman, 1950). This name can likely be attributed to the typical mycelial growth and reproduction through sporulation exhibited by *Actinomycetes*, suggesting an association with fungi, and names such as '*Streptomyces*' ('twisted fungus') reflects the possession of both fungal and bacterial properties and demonstrates the previously uncertainty of organism classification (Hopwood, 2015). In the late 1970s, Carl Woese realised that 16S rRNA sequencing, a technique where 16S ribosomal RNA (rRNA) containing both variable and highly conserved regions, which can be amplified and compared in order to establish phylogenic relationships, had value as a taxonomic tool (Woese and Fox, 1977., Woese, 1987). 16S rRNA gene sequencing confirmed that Actinobacteria are truly bacteria, with only superficial similarities to fungi as a result of convergent evolution (Hopwood, 2015). However, classification of Actinomycetota remains a complex and ever-adjusting terrain as further sequencing and discovery of novel species and

genera leads to regular updates in taxonomic structure and composition of the Actinomycetota phylogenetic tree (Barka *et al*, 2015., Oren and Garrity 2021., Seshadri *et al*, 2022).

1.3 The Genus *Streptomyces*

Streptomyces bacteria are Gram-positive, spore-forming, mycelial Actinomycetota that were first characterised in 1943 by Waksman and Henrici (Waksman and Henrici, 1943). They are ubiquitous in soil, producing the secondary metabolite geosmin, which gives soil its earthly smell; giving an indication as to how widespread growth of *Streptomyces* is in the natural world, as well as being saprophytes, helping to promote organic matter decomposition (Seipke Kaltenpoth and Hutchings, 2012). They are responsible for the production of a plethora of bioactive molecules including antibiotics, antifungal, antiviral, anti-cancer and immunosuppressive molecules (Wright and Bibb, 1992). The *Streptomyces* genus is part of the family *Streptomycetaceae*, which is found in the order of *Streptomycetales* and the Actinomycetota *(*formerly Actinobacteriota) phylum (Anderson and Wellington, 2001., Stackebrandt, Rainey and Ward-Rainey, 1997). The *Streptomycetaceae* family also includes other bacterial genera, such as *Kitasatospora*, *Streptacidiphilus* and *Yinghuangia*, all of which are phenotypically and genotypically similar to *Streptomyces* (Kim *et al*, 2003., Nouioui *et al*, 2018., Omura *et al*, 1982). Due to the similarities between the two genera, *Kitasatospora* was originally defined as a *Streptomyces* species, however complete 16S ribosomal RNA analysis by Zhang and colleagues revealed significantly higher levels of meso-diaminopimelic acid in *Kitasatospora* cell wall hydrolysates when compared to *Streptomyces,* allowing for distinguishment between the two species (Zhang *et al*, 1997).

As previously noted, the genus *Streptomyces* possess genomes with a high GC content (Subramaniam *et al*, 2020). The study by Subramaniam *et al*, (2020) which reported on genome sequences from 16 *Streptomyces* strains, showed that the GC content in *Streptomyces* species averages above 70%, concurring with previously established literature

(Hopwood, 2007). Unlike many other bacterial species, *Streptomyces* possess a large genome. The model Gram-negative bacterium *Escherichia coli* has a genome size of 4.6 Mbp, by comparison, the complete genome sequence of *Streptomyces coelicolor* A3(2) is 8.6 Mbp long (which at the time of the study, was the largest number of genes ever recorded in a bacterium), with a GC content of 72.1%, which further confirms the presence of high GC content in the genomes of *Streptomyces* species (Bentley *et al*, 2002). This species of *Streptomyces* additionally contains two plasmids: the linear plasmid SCP1 and the circular plasmid SCP2, with lengths recorded at 356kb and 31kb for each plasmid respectively (Bentley *et al*, 2004., Haug *et al*, 2003). Four of the antibiotics produced by *S. coelicolor* are well-characterized, including actinorhodin, undecylprodigiosin, coelimycin and calcium-dependant antibiotic (CDA) (Bednarz *et al,* 2021., Ryding *et al*, 2002., Schlimpert and Elliot, 2023). *Streptomyces clavuligerus*, another member of the genus and an important industrial strain due to the production of clavulanic acid (CA), possesses a 6.8 Mbp genome, along with four linear plasmids: pSCL1-pSCL4, whose size varies from 10kbp to 1.8Mbp (Song *et al*, 2010). Both the *S. clavuligerus* genome and its four plasmids contain high GC content levels, with the genome possessing a G+C content percentage of 72.69% and the plasmids ranging from 70.07% to 71.96%.

Streptomyces clavuligerus ATCC 27064 was originally described by Higgens and Kastner as a new producing two new β -lactam antibiotics and earned its name due to the clubbed shape of its spore-bearing hyphal branches (Higgens and Kastner, 1971). *S. clavuligerus* produces a number of clinically significant antibiotics, including cephamycin C, deacetoxycephalosporin C, pencillin N and clavulanic acid, which itself functions as β-lactamase inhibitor (Brown *et al,* 1976., Paradkar, 2013). While clavulanic acid is not an effective antibiotic by itself, when it is combined with a penicillin-class antibiotic, it assists in overcoming antibiotic resistance in bacteria that secrete β-lactamases, which cleaves the β -lactam ring, inactivating the antibiotic. The β-lactamase inhibiting activity of clavulanic acid makes it a clinically significant antimicrobial agent and one of the WHO essential medicines (WHO, 2021). *S. clavuligerus* is

also responsible for the production of non- β lactam antibiotics like holomycin and the antibiotic complex MM 19290 (Baggaley *et al*, 1997).

1.4 Morphology and Lifecycle of *Streptomyces* species

Streptomyces species are predominantly found in the soil, which can be a challenging environment to inhabit due to the variety of other microbes, animal and plant life found abundantly in soil (Kaltenpoth, 2009., Khan *et al*, 2023., Seipke *et al,* 2012). Additionally, the levels of nutrients such as nitrogen, carbon and phosphorus can vary due to factors including competition between soil-dwelling organisms. *Streptomyces* species survive in this environment by secreting a range of compounds to help it compete with other soil-dwelling bacteria. Specialised metabolites and bioactive compounds assist *Streptomyces* in scavenging nutrients from its environment (Berdy, 2005., Chater *et al*, 2010). *Streptomyces* also possess a complex life cycle that aids them with the fluctuating levels of nutrients available in their environment.

Development of a *Streptomyces* cell begins with a single dormant spore, from which one or more germ tubes emerge in the presence of suitable nutrient conditions (Chen *et al*, 2022). The germ tubes extend by apical growth at the hyphal tips, with additional branches growing from the lateral walls of the spore (Jones and Elliot, 2018). This growth results in the formation of a network of dense, branching vegetative hyphae, which is known as the vegetative mycelium. In response to nutrient limitation, *Streptomyces* activate a developmental growth phase; where non-branching aerial hyphae are produced, growing upwards from the surface of the colony (Jones *et al*, 2017). It is during this phase when regulators known as the bald (*bld*) genes coordinate the genes required for *Streptomyces* to produce the aerial hyphae. Mutation in these *bld* genes result in colonies unable to make aerial hyphae, giving them a bald appearance (Elliot *et al*, 1998). The *bld* genes are tightly connected to other physiological changes in *Streptomyces*, including the onset of secondary metabolite production, with many

of these genes pleiotropically acting on the sporulation and secondary metabolite pathways (McCormick and Flärdh, 2012). A second class of developmental mutants, the white (*whi*) mutants, are also known. These genes control the maturation of aerial hyphae, but mutants in these genes fail to complete their development into mature unigenomic spores, resulting in spores that fail to produce the characteristic grey pigment and remain white in colour (Flärdh and Buttner, 2009). An overview of the lifecycle of *Streptomyces* can be seen in **Fig. 1.1**.

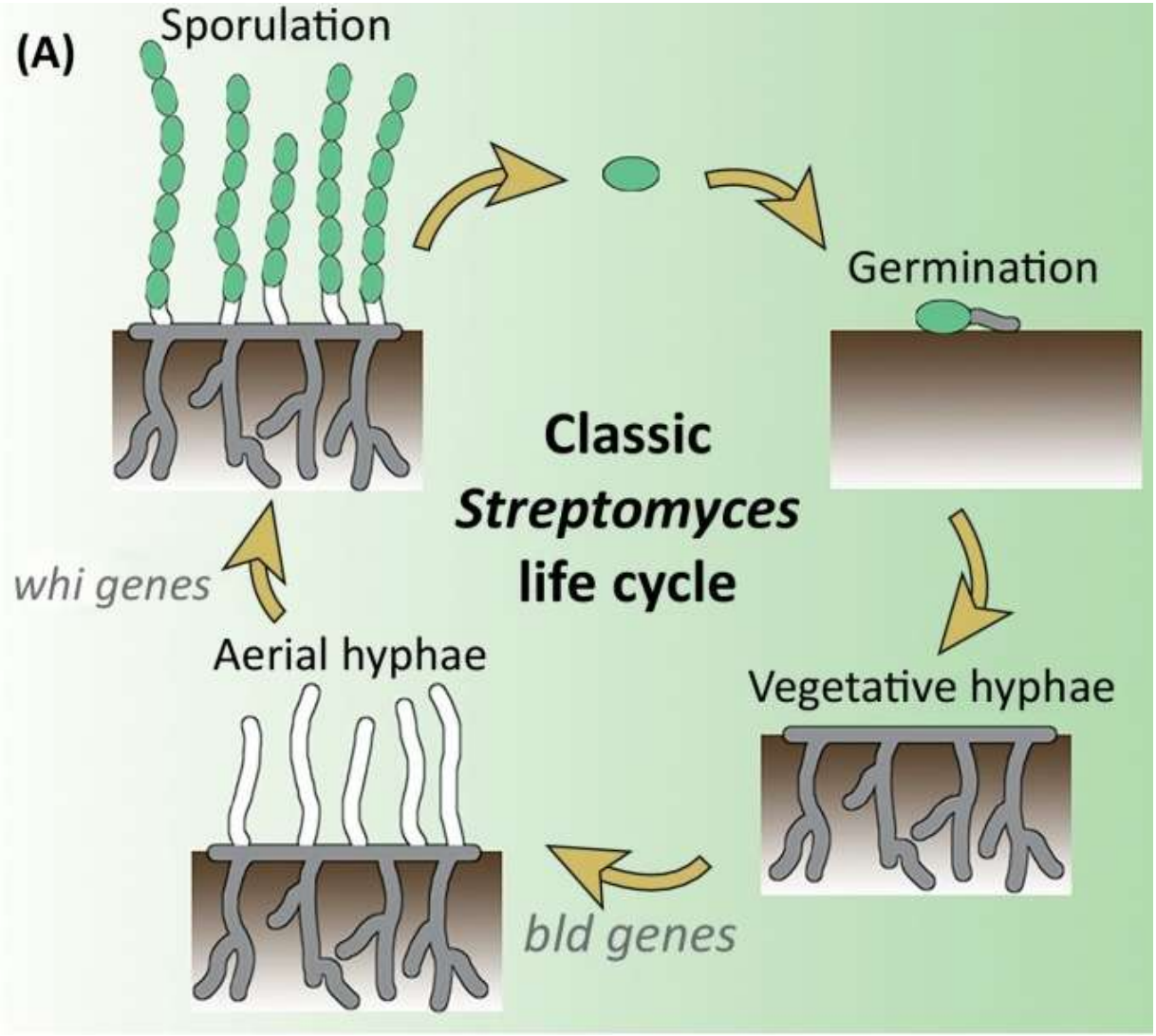

Fig. 1.1 Life cycle of *Streptomyces* bacteria. Germinated spores grow and produce vegetative hyphae while in the presence of nutrients. Once nutrient levels deplete, production of vegetative hyphae ceases and aerial hyphae production begins, eventually leading to mature spore chain sporulation and dispersal of matured spores. Adapted from Jones and Elliot, 2017.

1.4.1 *Streptomyces* spores and spore germination

The *Streptomyces* life cycle starts with a single spore, that is highly resistance to dessication, possibly contributing to streptomycete abundance in soils (Kalakoutskii and Agre, 1976). *Streptomyces* spores also possess active ribosomes and a pre-existing pool of mRNAs which are crucial for the earliest step in spore germination (Quirós *et al*, 1986). *Streptomyces* spores contain a spore wall comprised of two sections, an outer and an inner wall, measuring 12μm and 30 μm respectively (Glauert and Hopwood, 1961). This spore wall has been reported as integral to maintaining the spore's dormant nature and is constantly maintained. The protein NepA was the first bacterial cell wall protein recorded for its importance in maintaining the spore wall, as deletion of *nepA* allowed for germination in poor nutrient conditions, such as in fresh water (De Jong *et al*, 2009).

Upon encountering suitable levels of nutrients, the spore begins to germinate. Three phases are involved with germination: darkening, swelling of the spore, and germ tube emergence (Hardisson *et al*, 1978). The first phase, darkening, involves water intake, swelling and reduced heat resistance, attributed to the loss of spore hydrophobicity. To induce the darkening phase of germination, the presence of bivalent cations (Ca^{2+}, Mg^{2+}, Mn^{2+}, Zn^{2+}, and Fe^{2+}) is required (Eaton and Ensign, 1980., Salas *et al*, 1983). Early in the germination process, the spores uncoat, leading to accumulated calcium in the spore envelope being released over time; a process controlled by calcium-binding protein CabC. Reduced CabC function leads to spores germinating prematurely, while overexpression of CabC production leads to delayed germination. During the uncoating process, hydrolases are reactivated to enable lysis and reconstruction of peptidoglycan in the cell wall to allow for the take up of nutrients. This has been characterized by Haiser *et al*, by showing that *rpfA* and *swlA* mutants, which are genes that encode for hydrolases, exhibit reduced germination (Haiser *et al*, 2009).

The swelling of the spore phase is caused by the influx of water from the previous phase. During this phase, a significant decline in trehalose concentration is seen in *Streptomyces*, along with an increase in glucose concentration, indicating restored functionality of the trehalase enzyme (McBride and Ensign, 1987). Hydration of the spore additionally re-activates proteins and ribosomes preserved while the spore was in dormancy. After the reactivation of the ribosomes, new proteins are able to be translated from the mRNA pool present in each spore (Strakova *et al*, 2013), with which, the spores become metabolically active and are able to utilize energy sources to obtain further nutrients such as carbon and nitrogen. Carbon and nitrogen are required for the emergence of germ tubes, as carbon levels fluctuate through the pentose phosphate and glycolytic pathways (Salas *et al*, 1984). The obtained energy and carbon nutrients are used for protein translation and DNA replication. Eventually, the swelled spores are able to detect external nutrients and adjust their metabolic pathways accordingly. In 2012, Strakova and colleagues determined that this is caused by the activity of pleiotropic regulators acting on transcriptional and translational levels, including BldD, cyclic AMP-receptor protein Crp, anti-sigma factors and ribonuclease RNase II (Strakova *et al*, 2012)

The final phase of germination, germ tube emergence, occurs after spore swelling. Either one or two germ tubes grow out of the spore and elongate via apical tip extension, with the tubes rising from the inner wall of the spore (Glauert and Hopwood, 1961). The site of germ tube emergence is thought to the governed by the protein SsgA, which is located at the sites of germ tip appearance (Noens *et al*, 2007). During dormancy, DNA synthesis is not carried out, however the onset of DNA synthesis coincides with germination. During germination, DNA synthesis is carried out by a single replisome, however, once appropriate hyphae length is reached, two or three DNA replisomes have been observed in previous literature (Wolánski *et al*, 2011). The number of replisomes double/triple in germinating spores compared to dormant spores and further double inside the germ tubes (Ruban-Ośmiałowska *et al*, 2006). After germination and the emergence of multiple germ tubes, the germ tubes form a network of hyphae that *Streptomyces* utilises to scavenge for nutrients in its local environment.

1.4.2 Early Lifecycle: Vegetative Mycelium

Germination of the *Streptomyces* spores and outgrowth results in the formation of a network of hyphae for nutrient scavenging. Hyphae grow through tip extension and branch laterally, which results in two new hyphae that concurrently grow via apical tip extension (Flärdh and Buttner, 2009., McCormick and Flärdh, 2012). After branching, new cell poles are required for the production of new hyphal branches.

The protein DivIVA, a homologue of DivIVA found in *Bacillus subtilis*, plays a crucial role in the formation of new cell poles (Cha and Stewart, 1997, Edwards and Errington, 1997). In *S. coelicolor,* Flärdh and colleagues highlighted that DivIVA is an essential protein in the life cycle of *Streptomyces* spores, as partial deletion of the protein resulted in hyphal growth defects, while overexpression of the protein lead to dramatically altered cell shapes, affecting tip extension and causing hyperbranching (Flärdh, 2003). When properly functioning, DivIVA is a self-assembling coiled-coil protein that specifically localises at sites where lateral hyphae will emerge, and at newly growing hyphal tips, where it interacts with another protein, Scy (*Streptomyces cytoskeletal* element), to form a multiprotein complex through a process involving the Ser/Thr kinase AfsK (Hempel *et al*, 2008., Hempel *et al*, 2012). Previous literature has shown that a third protein, FilP (Filament-forming protein) is involved in the DivIVA-Scy multiprotein complex (Fröjd and Flärdh, 2019). Research into DivIVA phosphatases in *Streptomyces* showed that Ser/Thr/Tyr protein phosphatase SppA is able to dephosphorylate DivIVA, affecting hyphal branching and tip extension, with *sppA* mutants demonstrating growth arrests (Passot *et al*, 2021). To obtain the necessary nutrients, hydrolytic enzymes such as cellulases, lignocellulases and chitinases are secreted into the surrounding environment (Chater *et al*, 2010., Schrempf, 2001). Cellulose and chitin are the most abundant polysaccharides on Earth and, when broken down, they represent an important source of carbon for streptomycetes. Streptomycetes possess a vast arsenal of hydrolytic enzymes and are able to extract carbon from a wide range of sources, such as agarase, which allows colonies to grow on substrates containing agar as the sole carbon source (Stanier, 1942).

1.4.3 Vegetative to Aerial: The *bld* gene regulatory network

Upon the depletion of nutrients or stress *Streptomyces* switch from vegetative mycelium production to reproductive aerial mycelium formation (McCormick and Flärdh, 2013, Xu *et al*, 2022). The transition from vegetative to aerial mycelium coincides with the production of secondary or specialised metabolites such as antibiotics (Hopwood, 2007., Bibb, 2005). Originally, it was thought that the role of the antibiotics produced by *Streptomyces* in a soil environment was for inhibitory or bactericidal purposes, to reduce competition for nutrients, however later research highlighted that only sub-inhibitory concentrations of antibiotics are produced by *Streptomyces* in a soil environment (Waksman, 1961., Davies, 2006., Aminov, 2009). Rather than causing an inhibitory effect on neighbouring bacteria, the sub-lethal concentrations of antibiotics produced in the soil have been shown to alter gene expression in non-producing species, such as *Salmonella* Typhimurium (Goh *et al*, 2002). Sub-inhibitory concentrations of protein biosynthesis inhibiting antibiotics, such as streptomycin and rifampicin, have been noted to shift nutrient use in co-cultures, which alters nutritional boundaries within an environment occupied by several bacterial strains (Jauri *et al*, 2013).

To initiate the growth of aerial hyphae, important regulators are required. These regulators are encoded for by the *bld* genes (Claessen *et al*, 2006., Bush *et al*, 2013., Avramova *et al*, 2023). When mutations occur in the *bld* genes, the formation of aerial hyphae is blocked, producing a bald (*bld*) phenotype, which can be clearly distinguished from Wild-Type *Streptomyces*. The *bld* mutants are also pleiotropically deficient in antibiotic production (Elliot *et al*, 1998, Hackl and Bechthold, 2015). So far, 12 of the *bld* genes (*bldA* to *bldN*) and their gene products have been identified, in which mutations can result in a *bld* phenotype (Bibb *et al,* 2000, Claessen *et al*, 2006, Guyet *et al*, 2014). However, other studies have shown that mutations in genes outside of the *bld* genes can also confer a *bld* phenotype, as mutations to *devA* (a GntR-like transcriptional regulator), *ramR* (a transcriptional activator for the *ramCSAB* operon) and the chaplin genes have all been previously shown to result in an ability to erect aerial hyphae (Hunt *et al,* 2005, Hoskisson *et al*, 2006, Bibb *et al*, 2012).

In-depth research has been carried out to determine the order of activation for the *bld* regulatory pathways. The gene *bldD* is a well-documented global regulator and transcription factor in *Streptomyces*, that autoregulates itself by binding a dimer of the protein BldD to its promotor, leading to reduced transcription (Elliot *et al*, 2001, Yan *et al*, 2020). BldD binds with 3`, 5`-cyclic diguanylic acid (cyclic-di-GMP), to form an active repressor which facilitates the dimerization of BldD, allowing it to activate or repress its associated target genes (den Hengst *et al,* 2010, Tschowri *et al*, 2014). The BldD regulon contains approximately 167 genes, including those important for both development, such as *bldA*, *adpA* (also known as *bldH*), *ftsZ* and *ssgA,* and secondary metabolite production, such as *nsdA*, *bldA, bldC*, and *leuA* (den Hengst *et al*, 2010). As BldD also functions as an autorepressor, the reduction in *bldD* expression, through reduced cyclic-di-GMP levels and autorepression triggers further development through a regulatory network of the previously mentioned genes, allowing previously repressed developmental genes to be expressed. There are two more well-documented Bld regulators in the development network of *Streptomyces*, to sustain vegetative growth. This includes *bldC,* which produces a small DNA-binding protein related to the DNA-binding MerR family (Hunt *et al*, 2005). While the protein is only 68 amino acids long, it has been shown to be integral to antibiotic biosynthesis. *Streptomyces bldC* mutants have been documented to be deficient in antibiotic production, as well as aerial mycelium formation (Schumacher *et al*, 2018). The other Bld regulator is BldO, a direct, second repressor of *whiB* (alongside BldD), showing that BldO solely targets expression of *whiB,* and that Δ*bldO* strains possess a hypersporulation phenotype (Bush *et al*, 2017). This also indicates that BldO may act as a safeguard against premature development. A third gene in the *bld* regulatory complementation grouping of Nodwell et al., (1996) is *bldG,* encoding an anti-anti-sigma factor which is involved in the regulation of the UshX and ApgA anti-sigma factors (Sevcikova *et al*, 2010).

Perhaps the most well-documented of the *bld* mutants in *Streptomyces* is *bldA* (White and Bibb, 1997, Hackl and Bechthold, 2015, Koshla *et al*, 2019). The gene *bldA* encodes a unique

tRNA in *Streptomyces* species which translates a UUA codon into the amino acid leucine (Leu-tRNA^{UAA}) (Lawlor *et al*, 1987). Genes that contain the TTA codon are reliant on the presence of *bldA* for gene expression. The TTA codon contains regulators for morphological development, such as AdpA (Takano *et al*, 2003, McCormick and Flärdh, 2012); as well as regulators for antibiotic biosynthesis, such as *actII-ORF4* in the actinorhodin gene cluster (Fernández-Moreno *et al*, 1991., Liu *et al*, 2013). The *bldA* is believed to regulate antibiotic production through enabling translation of cluster-situated regulatory genes in *Streptomyces* (Nodwell, 1996). As such, *Streptomyces* that are deficient in *bldA* are pleiotropically defective in aerial mycelium production, sporulation and/or antibiotic production, however *bldA* mutants are still viable and able to produce vegetative mycelium (Piret and Chater, 1985., Chater and Chandra, 2008).

1.4.4 Aerial Mycelium and Sporulation

The *bld* regulatory network also controls the formation of a hydrophobic protein sheath. This hydrophobic sheath is comprised of rodlin proteins, chaplin proteins and SapB, a lantibiotic-like lanthionine containing peptide that acts as a biosurfactant to facilitate the upward growth of newly produced aerial hyphae (Elliot *et al*, 2003., Capstick *et al*, 2007). This hydrophobic sheath is commonly known as the 'rodlet layer '. The interactions of rodlin and chaplin proteins causes the formation of fibrils, which provides the characteristic hydrophobic layer found on spores. The rodlet layer itself is comprised of hydrophobic chaplin proteins, which are organised into rods by the rodlin proteins RdlA and RdlB. Deletion of the chaplin genes (*chpA-chpH*) results in a phenotype that is severely deficient in the production of aerial hyphae. The *bld* mutants are unable to produce any aerial hyphae and therefore, are unable to sporulate, however, previous research has proven that supplementation with the SapB peptide restores aerial hyphae formation in *bld* mutants (Willey *et al*, 1991). Along with a myriad of other genes, *bldD* regulates the gene expression of the *adpA* gene, as the expression of AdpA requires the

presence of *bldA*, which itself is directly regulated by *bldD*. The absence of *bldA* results in the inability to produce AdpA due to the presence of a TTA codon in *adpA* (Takano *et al*, 2003). AdpA is a transcriptional pleiotrophic regulator that controls the expression of hundreds of genes associated with morphological differences, secondary metabolite production and chromosome regulation (Rabyk *et al*, 2018). Along with these factors, AdpA plays a critical role in the development of aerial hyphae; as it regulates the transcription of the ECF sigma factor and *amfR*, a gene encoding a protein required for aerial mycelium formation (Yamazaki *et al*, 2003). Mutants containing a deletion of *adpA* are unable to produce aerial hyphae and affects the expression of a large number of genes across multiple pathways in *Streptomyces*, including *ramR*, *cutRS* and *bldN* (Guyet *et al*, 2014).

Old vegetative mycelium is cannibalised through the secretion of proteases to supply nutrients for aerial hyphae growth, as well as the production and secretion of protease inhibitors to protect new mycelium (Wolański *et al*, 2011). Expression of genes encoding proteases and protease inhibitors are also regulated by AdpA. Once the aerial hyphae are fully grown, the multigenomic filaments undergo synchronous septation. This causes a generation of genomic pre-spore compartments which, when matured, form dormant pigmented spores. Transition from aerial hyphae to sporulation requires the activation of regulators known as *whi* genes, their name given due to mutations in these genes resulting in the absence of the grey polyketide spore pigment, leaving *Streptomyces* aerial hyphae appearing white.

While it is responsible for the promotion of several genes, the protein BldD is also responsible for the repression of genes associated with sporulation, including *bldN* and *whiG*. Upon reduced transcription of *bldD*, *whiG* is no longer repressed and is able to be translated (Chater, 2001). The *whiG* gene encodes the RNA polymerase sigma factor σ whiG, which in turn, activates the expression of other *whi* genes required for the onset of sporulation, namely *whiA, whiB, whiG, whiH* and *whiI* (Chater *et al*, 1989, Chater, 2001). All five of the *whi* genes are required for correct sporulation septation. The aerial hyphae themselves contain the proteins WhiA and WhiB, which, when aerial hyphae growth reduces, modify into A* and B* forms,

which lead to growth cessation. The *whiH* gene product is a GntR-like regulatory protein, which has been shown to negatively regulate its own transcription (Ryding *et al*, 1998).

The *whi* genes are also required for the transcription of the *sigF* and *ftsZ* genes, both of which are important for later sporulation. Large amounts of FtsZ protein assemble to form a ring-like structure, called the Z-ring, inside a cell that is about to divide. This is a requirement for cell division and, thus, for sporulation septation to occur. The gene *sigF* encodes the late-sporulation sigma factor σ^F, in which mutations can cause defects in pre-spore compartment maturation, leading to irregular spores with thin spore-walls and reduced pigmentation (Kelemen *et al*, 1996). σ^F, along with WhiD (a paralogue of the early-spore protein WhiB) are responsible for final spore maturation and the pigmentation with the grey polyketide spore pigment, leaving fully grown *Streptomyces* colonies appearing with a grey surface. An overview of the sporulation regulation network in *Streptomyces* can be seen in **Fig. 1.2**.

Unlike the endospores of the Firmicutes, spores of *Streptomyces* are primarily dispersal rather than survival vehicles (Chater, 2006, Elliot and Flärdh, 2020). They are dispersed by water, wind and the movement of animals living in the soil or through aerially attaching to the surface of soil particles to be translocated to areas containing higher concentrations of nutrients (Becher *et al*, 2020). Once a spore has entered an area with a sufficient level of nutrients required for growth, the life cycle repeats again.

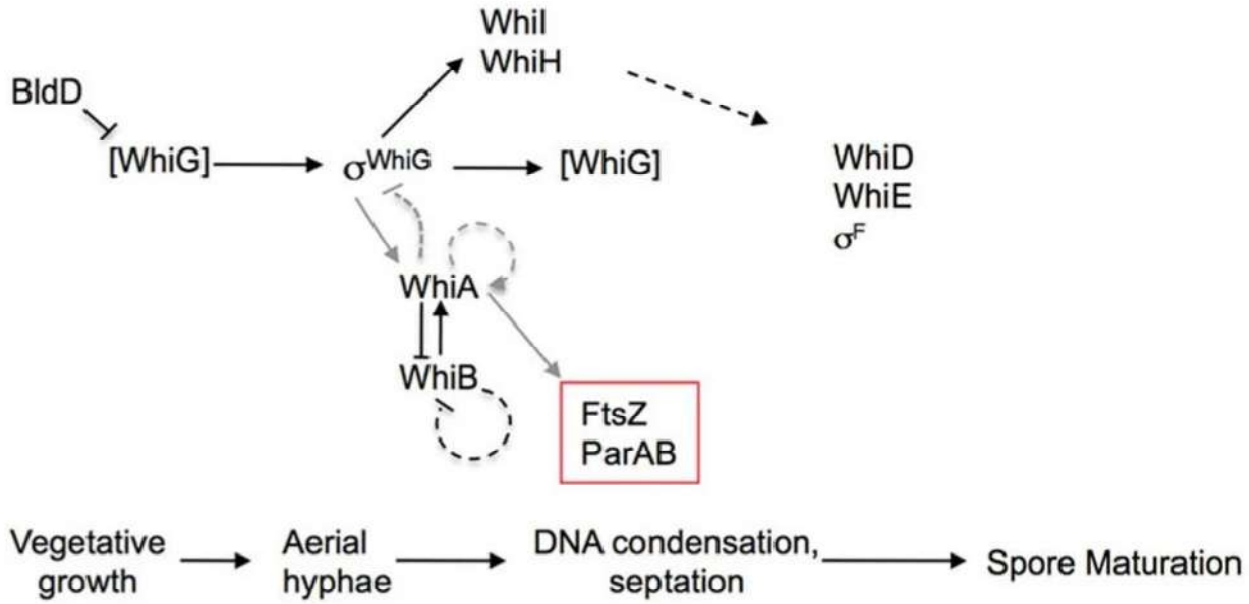

Fig. 1.2: Sporulation regulation network in *Streptomyces*. The core genes associated with the transition from aerial hyphae production to sporulation and septation. Adapted from Kaiser and Stoddard, 2011.

1.5 *Streptomyces coelicolor*

Perhaps the most prominently known *Streptomyces* is the species *Streptomyces coelicolor*, which is often used as a model organism. *S. coelicolor* is a free-living saprophytic bacterium with key roles in many metabolic processes and biotransformations in soil. *S. coelicolor* A3(2) is the model organism for the *Streptomyces* genus and it is the M145 strain, a plasmid-free derivative of the A3(2) strain, lacking the native linear 363Kb SCP1 plasmid and the circular 31.4Kb SCP2 plasmid, which is employed as the primary wild-type organism in this study (Yamasaki, Redenbach and Kinashi, 2001; Haug et al., 2003; Hoskisson and van Wezel, 2019).

Originally discovered by R. Müller in 1908, *S. coelicolor* was named for production of a striking blue pigment; coelicolor being translated as ‘sky color’ from Latin. When Professor Sir David Hopwood began his study of *Streptomyces* genetics, he chose what he believed to be a strain of *S. coelicolor* as his model organism, later to become A3(2), as the characteristic red and blue pigments made for ideal markers. However, advances in genetic analysis techniques would later determine that this strain is more closely related to a strain documented by Waksman and Curtis, known as *Streptomyces violaceoruber* ISP5049, rather than *S. coelicolor* Müller. However, to reduce confusion the A3(2) strain remains referred to as *S. coelicolor* (Kutzner and Waksman, 1959, Hoskisson and van Wezel, 2019)

S. coelicolor A3(2) has a singular chromosome of approximately 8.66 Mbp with a centrally located origin of replication and a GC content of 72.12% (Bentley et al., 2002). The chromosome is generally considered to possess a core, which contains essential genes, and two chromosome arms, containing genes of non-essential function for the survival of the organism (Bishop *et al*, 2004). The core extends from approximately 1.5 Mb to 6.4 Mb, with the left arm being 1.5 Mb in length and the right arm being 2.3Mb in length (Bentley et al., 2003). The genome possesses 7825 coding sequences, with the chromosomal ends carrying terminal inverted repeats with covalently linked proteins to protect the free 5` ends. This

chrosomal structure allows for a loss of more than 1 Mbp of genome sequence at either chromosome end to be tolerable to *S. coelicolor* (Hoskisson and van Wezel, 2019).

1.6 Secondary metabolites in *Streptomyces coelicolor* and *Streptomyces clavuligerus*

S. coelicolor possesses more than 20 biosynthetic gene clusters (BGCs) that encode for natural products, which play crucial ecological roles, by providing *S. coelicolor* with a competitive advantage by inhibiting the growth of rival microorganisms. Among its most well-characterized natural products are undecylprodigiosin (RED), actinorhodin (ACT), coelimycin and calcium-dependant antibiotic (CDA).

1.6.1 Undecylprodigiodin

Undecylprodigiosin is a red-coloured antibiotic produced by *Streptomyces coelicolor*, belonging to the prodigiosin family, a group of secondary metabolites characterized by a unique tripyrrole ring system found in their structure (White and Bibb, 1997, Lee *et al*, 2024). Undecylprodigiosin is produced through the RedH-mediated condensation of 4-methoxy-2,2'-bipyrrole-5-carboxaldehyde (MBC) and 2-undecylpyrrole, which are assembled by two distinct sets of enzymes encoded by the *red* gene cluster (Feitelson, Malpartida and Hopwood, 1985, Cerdeño, Bibb and Challis, 2001). Undecylprodigiosin biosynthesis is controlled by the *red* biosynthetic gene cluster, which includes regulatory genes and enzymes responsible for its production. Key genes in the *red* BGC include RedG, which facilitates the formation of a tripyrrole structure of undecylprodigiosin, and RedD, which acts as a transcriptional activator of the pathway (Sydor *et al,* 2011, White and Bibb, 1997, Narva and Feitelson 1990). Undecylprodigiosin (RED) has also been investigated for its anticancer, antimalarial and immunosuppressant capabilities, in addition to its antimicrobial capacity (Williamson *et al*,

2006, Stankovic *et al*, 2014). Previous research has shown that the *bldA* leucine^{UAA} tRNA is essential for normal RED production, as *bldA* mutants fail to produce RED, emphasising the tight regulatory connection between differentiation and secondary metabolism in *S. coelicolor* (White and Bibb, 1997). Biosynthetic gene cluster annotation reveals that the *red* biosynthetic gene cluster consists of 22 open reading frames, including five core biosynthetic genes, nine additional biosynthetic genes, two regulatory genes and six other genes (**Fig 1.3**)

1.6.2 Actinorhodin

Actinorhodin is a polyketide antibiotic produced by *S. coelicolor*. Actinorhodin's BGC (the *act* BGC) contains biosynthetic enzymes and genes responsible for the export of the antibiotic, leading to extracellular visualisation of the antibiotic in the form of a blue-pigmented product (Bystrykh *et al*, 1996, Fernádez-Moreno *et al,* 1991). Actinorhodin has been shown to exhibit bacteriostatic activity, primarily against Gram-positive bacteria, making it an important model for studying polyketide biosynthesis and function (Mak and Nodwell, 2017).

An important characteristic of actinorhodin, as noticed by Bystrykh *et al* (1996) is its use as a natural pH indicator, as actinorhodin is red at an acidic pH and blue at an alkaline pH. The biosynthesis of actinorhodin is controlled by the *act* biosynthetic gene cluster, which contains enzymes for polyketide chain assembly and tailoring modifications. Transcriptional regulators, such as ActII-ORF4, activate the pathway in response to environmental and developmental signals (Fuiji *et al*, 1996, Liu *et al*, 2021). Like RED, actinorhodin (ACT) production is developmentally regulated and is influenced by *bld* genes, with *bldA* mutants often show delayed, reduced or abolished actinorhodin production, highlighting the potential role of *bldA* translational regulation in secondary metabolism (Guthrie and Chater, 1990).

The *act* biosynthetic gene cluster in *Streptomyces coelicolor* is located in a core region of the genome at 5.52 Mb. The 22Kb *act* cluster of *S. coelicolor* consists of 22 open reading frames, including two core polyketide synthase biosynthetic genes, nine additional biosynthetic genes,

two regulatory genes, two transport-related genes, a resistance gene and six other genes (Taguchi *et al*, 2007; **Fig 1.3**)

1.6.3 Coelimycin and CDA

Coelimycin is a cryptic polyketide antibiotic encoded by the *cpk* gene cluster, often silent under standard laboratory conditions but inducible through specific environmental or genetic modifications (Pawlik, Kotowska and Kolensiński, 2010). Production of coelimycin is regulated by both the *scbA*-*scbR* quorum-sensing system and global regulators, such as BldD and the leucine-tRNA^{BldA} (Kotowska *et al*, 2024). By being regulated by the BldD and BldA, this links coelimycin expression to *S. coelicolor* development. First synthesized as a colourless antibiotic by Gottelt *et al*, 2010, coloured coelimycins (P1 and P2) are formed when coelimycin it forms adducts with *N*-acetylcysteine or glutamate respectively, which do not possess antibacterial activity.

The calcium dependant antibiotic (CDA) is a non-ribosomal lipopeptide antibiotic, which requires calcium ions for its antibiotic activity (Hopwood and Wright, 1983). CDA functions by disrupting bacterial membranes through the production of trans-membrane channels, which leads to ion leakage and cell death. Controlled by the *cda* gene cluster, CDA production is influenced by developmental and environmental factors, including calcium availability and global regulators like Bld and Whi proteins (Bum Kim *et al*, 2004, Liu *et al*, 2013). This trend of secondary metabolism linked to Bld proteins, including *bldA*, makes *bldA* an ideal target for investigation into specialized metabolite production in *Streptomyces*.

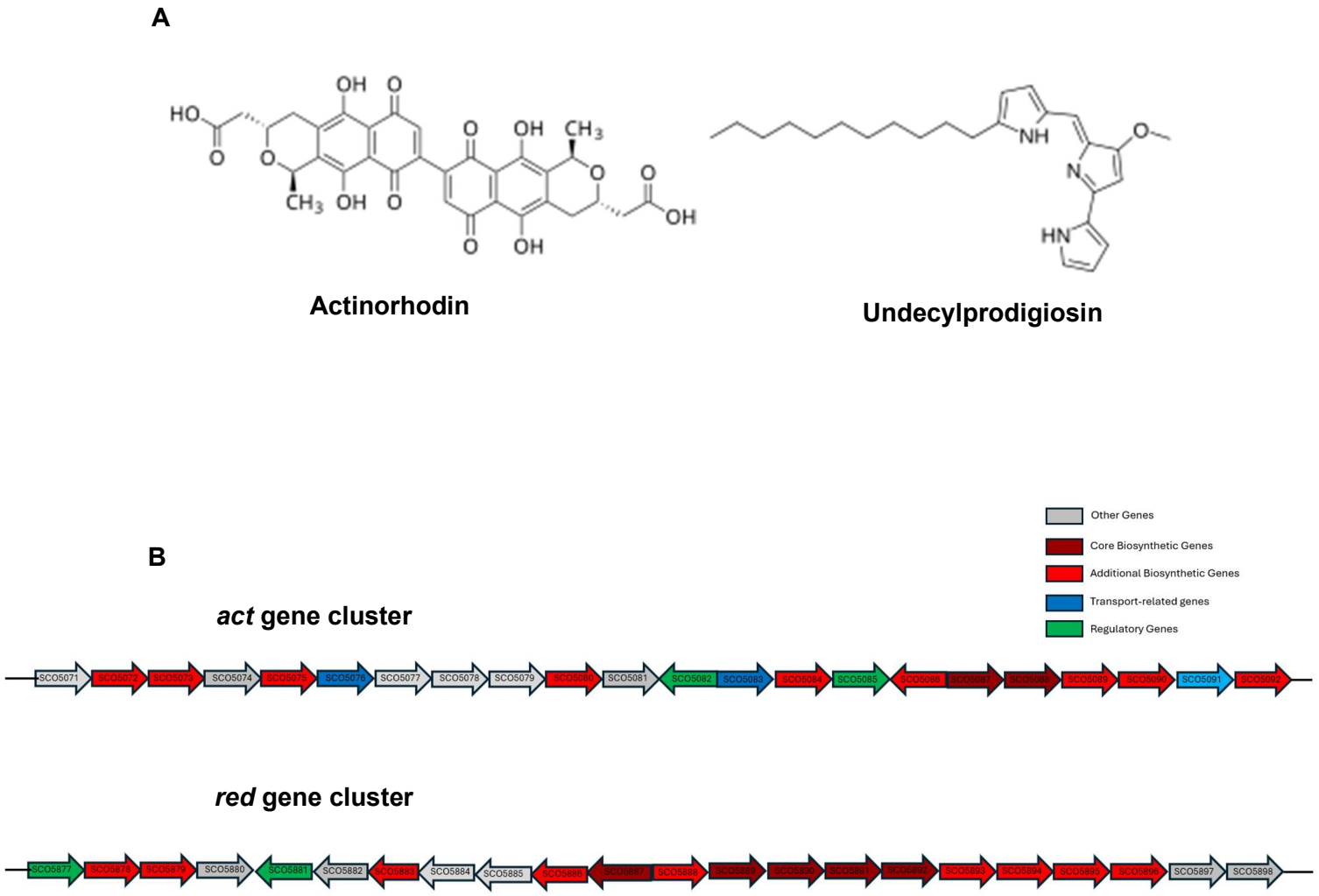

Fig. 1.3: Two of the core specialised metabolites documented in *S. coelicolor*: Actinorhodin and Undecylprodigiosin. A: The chemical structure of Actinorhodin and Undecylprodigiosin. Actinorhodin's structure makes it redox-active, resulting in its usability as a pH indicator. Undecylprodigiosin's hydrophobic tail influences its solubility and membrane interactions. **B: The *act* and *red* gene clusters**. The *act* gene cluster is comprised of 22 genes from SCO5071-SCO5092. The *red* gene cluster is comprised of 22 genes, from SCO5877-SCO5898. The *act* and *red* gene clusters were detected using antiSMASH (Blin *et al*, 2023)

1.6.4 Clavulanic acid

One of the more important characteristics of *S. clavuligerus* is that it produces the ß-lactamase inhibitor clavulanic acid. It is the production of clavulanic acid that brings high pharmaceutical value to *S. clavuligerus*. ß-lactams target the peptidoglycan layer of bacterial cell walls, which consist of N-acetyl glucosamine (GlcNAc) and N-acetyl-muramic acid (MurNAc). β-lactam antibiotics function by disrupting cell wall synthesis, through binding to penicillin-binding proteins (PBPs), which are essential enzymes for forming cross-links in the GlcNAc-MurNAc peptidoglycan mesh, resulting in weak cell walls and eventual cell lysis (Bush and Bradford, 2016). However, certain bacteria produce ß-lactamases, which hydrolyze the ß-lactam ring structure, resulting in deactivation of the ß-lactam (Aggarwal, Chaudhary and Bala (2008). The inhibitory properties of clavulanic acid make it an unusual, non-classical ß-lactam compound, as it has previously been shown to inhibit a variety of ß-lactamases, such as narrow-spectrum ß-lactamases, ESBLs and even cephalosporinases (Shahid et al., 2009).

Clavulanic acid is a suicide inhibitor, that works by permanently inactivating the enzyme through chemical reactions at the active site (Drawz and Bonomo, 2010). Clavulanic acid contains a β -lactam ring that binds to the β-lactamase active site and inactivates the enzyme, restoring the antibacterial effect of β-lactam antibiotics, such as amoxicillin; a common β-lactam-β-lactamase inhibitor combination. This inhibition restores the antimicrobial activity of β-lactam antibiotics against lactamase-secreting resistant bacteria. Despite this, some bacterial strains that are resistant even to such combinations have emerged, such as the clinically relevant S130G mutation found in the SHV-1 and TEM- 1β-lactamases, commonly found in *E. coli* and *K. pneumoniae,* resulting in a 330-fold resistance increase to clavulanic acid (Pagan-Rodriguez *et al*, 2004, Sulton *et al*, 2005). Such an extreme increase in resistance may indicate a potential mode of action for clavulanic acid, by binding to the serine residue, which would result in the restructuring of the clavulanic acid molecule, creating a much more reactive species that attacks another amino acid in the active site.

1.7 Translation control in *Streptomyces*

Gene expression in *Streptomyces* is regulated at both transcriptional and translational levels, with translational control being an important layer of regulation in *Streptomyces*, as it is used to adjust gene expression during stress responses, such as heat-shock, nutrient availability, and during development (Jeong et al, 2016, Bucca et al, 2018). By controlling mRNA translational efficiency without altering mRNA levels, *Streptomyces* bacteria are able to coordinate both complex developmental processes and specialised metabolism of antimicrobial agents. One of the most understood examples of translational control in bacteria is attenuation in amino acid biosynthetic operons, which results in premature transcription termination (Gollnick and Babitzke, 2002, Melior *et al*, 2019). Attenuation relies on both transcription and translation, where a leader sequence (found between the promoter and the start codon of an operon) contain several codons of the relevant amino acid (such as Trp codons in the *trp* operon in *E. coli*) (Klug *et al*, 2019). In attenuation, the ribosome stalls at the attenuator region of the leader sequence, typically to repress genes in the presence of their own product (Naville and Gautheret, 2009). In amino acid biosynthetic operons, there are typically four sequence motifs, which form alternate hairpins dependant on the abundance of the associated amino acid (Yanofsky, 2000). When the relevant amino acid is already abundant in the intracellular environment, ribosomes translate the leader peptide sequence motifs, allowing two of the motifs to form a hairpin structure, which terminates further transcription (Baggett *et al*, 2017). In contrast, when amino acid levels are low, ribosomes stall at the previously mentioned relevant amino acid codons found in the first sequence motif, causing the formation of an alternative hairpin structure and prevents the formation of the transcription terminator hairpin, allowing RNA polymerase to continue transcription of biosynthetic genes to continue (Ashniev *et al*, 2022).

In *Streptomyces*, translational control extends further than classical attenuation to include rare codon regulation. As previously discussed in **Section 1.4.3,** the *bldA* gene encodes the only tRNA able to decode the rare leucine-UUA codon, meaning that genes containing UUA codons

are conditionally expressed, adding a unique layer of regulation. A number of antibiotic biosynthetic clusters in *Streptomyces* contain UUA codons within their coding sequence, making their expression dependent on the presence of the leucine-tRNA^{BldA}, effectively linking translation control to secondary metabolism (Liu *et al*, 2013). When *bldA* is silent, these genes cannot be properly translated, and production of the gene product is repressed. This means that the leucine-tRNA^{BldA} serves as a translational checkpoint for *Streptomyces*, coordinating morphological development and sporulation with secondary metabolism. This allows *Streptomyces* to synchronize secondary metabolite production with developmental stage and environmental signals (Chater *et al*, 2010, Makitrynskyy *et al*, 2013). A representation of both the cloverleaf and three-dimensional tRNA structure can be seen in **Fig. 1.4**.

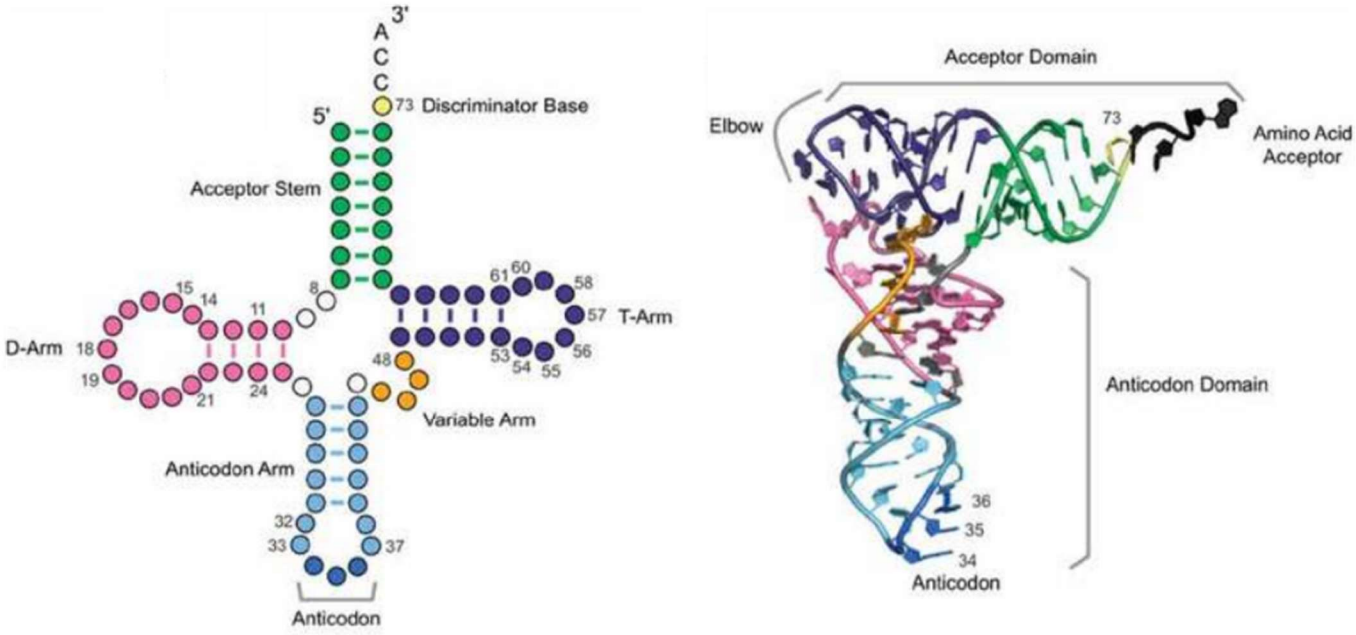

Fig. 1.4. Schematic of cloverleaf and three-dimensional tRNA structure. The anticodon loop contains a triplet sequence that base-pairs with a complementary codon on the mRNA. The acceptor stem carries the corresponding amino acid next to the discriminator base, charged by an aminoacyl-tRNA synthetase Abbreviations: tRNA- transfer ribonucleic acid. Taken from Berg and Brandt, 2020.

1.8 The Leucine tRNA landscape in *Streptomyces coelicolor*

Transfer RNAs (tRNAs) are small, non-coding RNAs essential to translation as they link nuceleotide sequences and amino acids through codon-anticodon pairing (Raina and Ibba, 2014). As documented by Fujishima and Kanai, to function as a substrate for protein synthesis, the tRNA is charged with the corresponding amino acid by its cognate aminoacyl-tRNA synthetase (AARS), and then the aminoacyl-tRNA is delivered into the ribosome to biosynthesize proteins (Fujishima and Kanai, 2014). Each codon in mRNA is complemented by a three-nucleotide anticodon in tRNA. Each tRNA has a distinct anticodon triplet sequence relating to a specific amino acid, however some anticodons are able to pair with more than one codon due to a phenomenon known as Wobble-Base-Pairing (WBP), where the pairing of two nucleotides in RNA molecules do not follow Watson-Crick base pairing rules, which was first hypothesized by Crick in 1966 (Crick, 1966, Varani and McClain, 2000).

One of the 20 essential amino acids is leucine, a branched-chain amino acid encoded by the codons UUA, UUG, CUU, CUC, CUA, and CUG. In bacteria, the leucine amino acid is commonly used in protein biosynthesis and as a precursor for polyketides. Leucine can also be used by bacteria as a source of energy in times when other sources of carbon are limited via a process called l-leucine catabolism, where leucine is broken down into acetoacetate and acetyl-CoA through multiple reactions (Díaz-Perez *et al*, 2015). Among these leucine tRNAs, tRNA-Leu$^{(UAA)}$, tRNA-Leu$^{(GAG)}$, tRNA-Leu$^{(CAG)}$, and tRNA-Leu$^{(UAG)}$ possess long variable loops, classifying them as type II tRNA-Leu isoacceptors. In contrast, tRNA-Leu$^{(CAA)}$ has a short variable loop, making it a type I tRNA-Leu. The structural difference between type I and type II tRNAs can affect their recognition by aminoacyl-tRNA synthetases., their ribosome binding efficiency, as well as codon-anticodon interactions and decoding efficiency. However, despite the structural differences between type I and type II tRNAs, *Streptomyces coelicolor* has a single leucyl-tRNA synthetase (LeuRS) capable of aminoacylating both types (Fan *et al*, 2019).

1.9 The Role of *bldA*, *bldD* and *bld* mutants in *Streptomyces coelicolor*

As previously discussed in **Section 1.4**, the *bld* genes in *Streptomyces* species form a complex regulatory network that controls the transition from vegetative growth to aerial hyphae formation and sporulation. Mutations in *bld* genes prevent the formation of aerial mycelium, resulting in a 'bald' colony phenotype. Two of the primary components of the *bld* regulatory network are *bldD*, a master repressor that is responsible for the control the expression of many developmental genes (Elliot *et al*, 1998, den Hengst *et al*, 2010) and *bldA*, which encodes a rare leucyl-tRNA^{UAA}, which is necessary for the translation of rare UUA codons, which are found in key regulatory genes related to morphological development and specialised metabolite production (Leskiw *et al*, 1993, Hackl and Bechthold, 2015). The *bld* gene network, with *bldD* results in the repression of other developmental genes until appropriate signals are received. Once repression by BldD is lifted (due to changes in c-di-GMP levels), downstream regulatory proteins (such BldM, BldN, SmeA and WhiD) are translated; most of these regulatory proteins promote the development of aerial hyphae and sporulation (Molle and Buttner, 2000, Bibb *et al*, 2000, Molle *et al*, 2000, Ausmees *et al*, 2007).

1.9.1 *Streptomyces coelicolor: bldD*

BldD is a master transcriptional regulator that plays a crucial role in the control of morphological differentiation and secondary metabolism in *Streptomyces* species. Acting as a global repressor, BldD maintains the organism in a vegetative growth state until environmental and physiological conditions favour aerial hyphae formation and sporulation over the maintenance of vegetative mycelium (Lee *et al*, 2007). BldD contains an N-terminal helix-turn-helix (HTH) motif, a common structure for DNA-binding proteins, which allows BldD to recognize and bind to specific promoter regions of its target genes, repressing their transcription until the presence of BldD reduces (Tschowri *et al*, 2014). The C-terminal region of the BldD protein enables dimerization, which is essential for the role of BldD in DNA binding.

BldD also forms dimers, not through direct protein-protein interactions alone, but via a small molecule mediator: cyclic di-GMP (c-di-GMP). When c-di-GMP levels are high, this leads to the promotion of BldD dimerization, resulting in the repression of developmental genes and the maintenance of vegetative hyphal growth, whereas low c-di-GMP levels disrupt the BldD dimers, leading to de-repression of the target genes, which leads to aerial mycelium formation and sporulation (Schlimpert and Elliot, 2023). It has also been shown through protein purification and electrophoretic mobility shift assays from previous literature, that BldD binds to its own promotor, creating a negative autoregulatory loop and ensuring that the expression of BldD is tightly controlled (Elliot *et al*, 2003)

BldD controls a large regulon, directly repressing approximately 167 genes in *Streptomyces coelicolor*, including key developmental and secondary metabolic genes (Tschowri *et al*, 2014). This extensive regulon includes genes such as *bldN*, an ECF sigma factor responsible for the activation of genes required for aerial hyphae production, the *whi* genes (which as discussed previously, are involved in sporulation and cell differentiation), *sigF* and *sigH* (sigma factors regulating late developmental genes), *adpA*, an AraC family transcriptional regulator essential for developmental growth, and a wide scope of genes involved in antibiotic biosynthesis, including those involved in the production of the four well-documented specialised metabolites found in *S. coelicolor* (Elliot *et al*, 2001, Tschowri *et al*, 2014, Yan *et al*, 2020).

1.9.2 *Streptomyces coelicolor: bldA*

BldA is a unique regulatory element in *Streptomyces*, distinguished from other *bld* genes as it does not encode a traditional transcription factor or signalling protein. Instead, *bldA* encodes a rare tRNA-Leu^{UAA}, which is crucial for translating mRNAs containing the rare TTA codon (Lawlor, Bayliss and Chater, 1987). The TTA codon is exceptionally rare in the *Streptomyces* genome, as previous literature reports the TTA codon is found in less than 1% of coding

sequences, with between only 142 and 147 genes containing the TTA codon (Li *et al,* 2007, Hesketh *et al*, 2007, Silov *et al*, 2020). Despite its rarity, this codon appears in several key regulatory genes that control morphological development and secondary metabolism. Certain critical regulatory proteins in *Streptomyces* contain TTA codons. Without *bldA*, these mRNAs cannot be efficiently translated, halting the production of proteins essential for a variety of cellular processes including morphological development and antibiotic biosynthesis (Zacharia *et al*, 2021). While *bldA* is not a transcription factor, it's function as a rare leucine tRNA allows it to act as a global regulatory element, through translational control of master regulators (Makitrynskyy *et al*, 2013), introducing a 'bottleneck effect', and allows a single tRNA to influence a wide array of cellular processes.

Many *Streptomyces* genes involved in antibiotic production contain TTA codons, meaning that without *bldA*, these genes cannot be efficiently translated, resulting in the bald characteristic phenotype of abolished specialised metabolite production. The BGCs for actinorhodin (ACT) and undecylprodigiosin (RED) synthesis possess TTA-containing regulatory genes (White and Bibb, 1997, Trepanier *et al*, 2002). Additionally, there are other global regulators of specialised metabolism that contain TTA codons, like AdpA, which plays essential roles in morphological development across the *Streptomyces* genus (Lopez-Garcia, Santamarta and Liras, 2010, Ohnishi *et al*, 1999, Takano *et al*, 2003). The *bldA* system in *S. coelicolor* highlights how translational regulation can control complex bacterial life cycles. Since other actinomycetes (including other antibiotic-producing species) also rely on TTA codon regulation, *bldA* is a crucial factor in natural product biosynthesis.

Streptomyces coelicolor J1700 is a well-studied mutant strain that has significantly contributed to the understanding of morphological development and specialized metabolite production in *S. coelicolor*. Carrying the genotyped *bldA*39 mutation, which affects the *bldA* coding sequence, rendering it inactive (Leskiw, Bibb and Chater, 1991), *S. coelicolor* J1700 exhibits a 'bald' (Bld) appearance, characterized by a lack of aerial hyphae and sporulation (**Fig. 1.4**). This Bld phenotype is caused by the disruption of translation of TTA codon-containing genes,

essential for morphological development. *S. coelicolor* J1700 also exhibits deficiencies in specialized metabolite production, emphasizing the fundamental role of the leucine-tRNA^{BldA} in regulation of both morphological development and secondary metabolism in *S. coelicolor*.

1.9.3 *Streptomyces coelicolor: bldA* and *bldD* mutants

Previous literature has shown that both *bldA* and *bldD* can be successfully mutated, highlighting that neither is essential to *Streptomyces* viability, however deficiency in either *bldA* or *bldD* results in notable phenotypic differences and molecular changes (Lawlor, Baylis and Chater, 1987, Elliot *et al*, 1998). The deletion or inactivation of *bldA* results in bald phenotype, defined by the lack of aerial hyphae or spores, while also resulting in severely reduced or abolished specialised metabolite production (particularly ACT and RED) (White and Bibb, 1997, Hou *et al*, 2018). This phenotype is visually distinct from wild-type *Streptomyces* as *Streptomyces* colonies normally exhibit a characteristic fluffy, white aerial mycelium, which eventually turns gray due to spore maturation. Bald *Streptomyces* mutants completely lack aerial mycelium and spores, resulting in a smooth, glossy colony morphology (**Fig. 1.5**; Hackl and Bechthold, 2015., Hou *et al*, 2018). Additionally, wild-type *S. coelicolor* colonies produce distinct red and blue pigments, attributable to the specialised metabolites ACT and RED, while *bld* mutants often show reduced or absent pigmentation due to misregulated specialised metabolite biosynthesis (Hesketh *et al*, 2007).

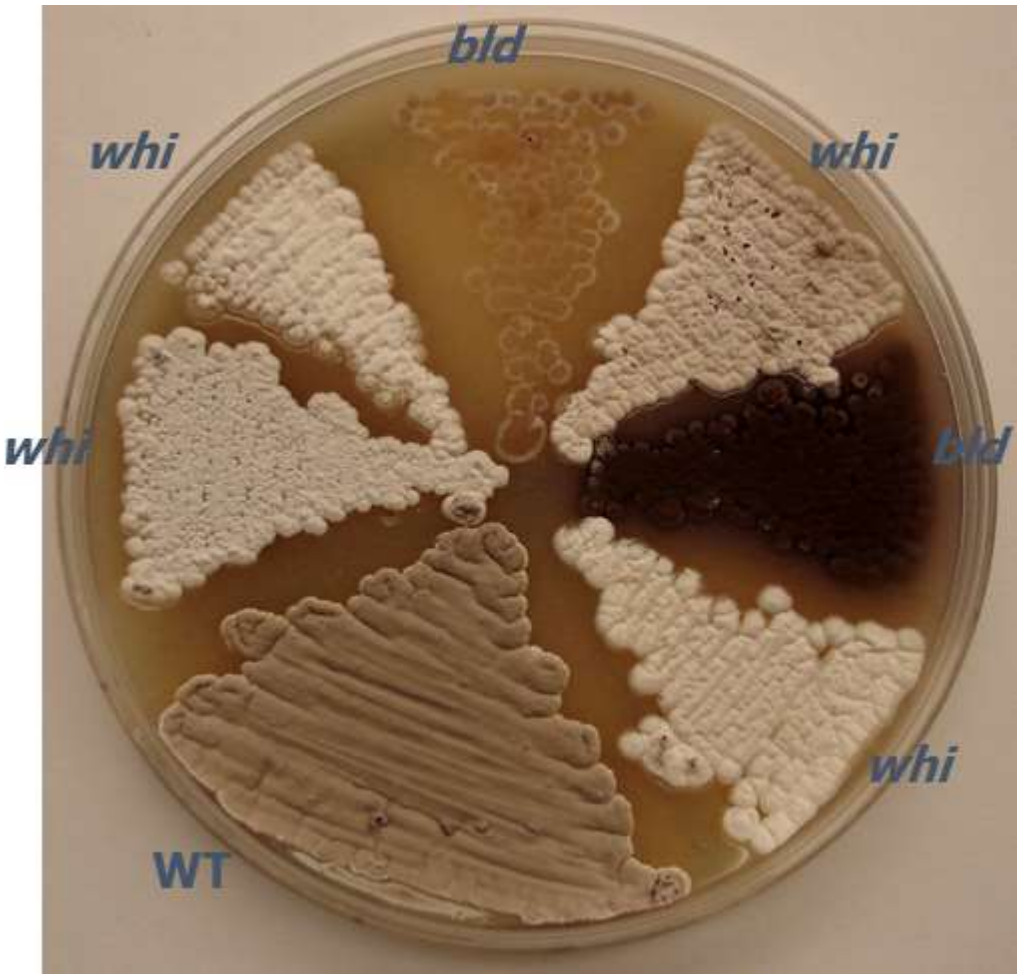

Fig. 1.5 Comparative Phenotypes of Wild-Type, *bld* and *whi* Mutants of *Streptomyces coelicolor*. The WT segment shows the wild-type strain displaying robust aerial mycelium formation and characteristic gray spore pigmentation after 5 days incubation on MS agar for 5 days. The *bld* segments depicts the characteristic bald phenotype, which exhibits an absence of aerial hyphae and sporulation. The *whi* sections exhibit white (*whi*) mutants, characterized by reduced spore pigmentation (Taken from Bennett *et al*, 2018).

1.10 Tools for studying *Streptomyces* genes and mutations

Streptomyces coelicolor serves as a model organism for studying bacterial differentiation and specialized metabolism, because of its complex lifecycle and its wide variety of specialized metabolites. Understanding the genetic and regulatory mechanisms behind *Streptomyces* development and specialized metabolite production requires a combination of genetic and molecular tools. Traditional genetic approaches, such as homologous recombination and transposon mutagenesis, are used for creating gene disruptions for the study of specific gene function (Gehring *et al*, 2000, Xu *et al*, 2017), whereas molecular techniques, such as whole-genome sequencing (WGS) and RNA sequencing (RNA-seq) are utilized in identifying genome and transcriptome alternations respectively (Fatima *et al*, 2024, Kim *et al*, 2020). In addition to genetic and molecular techniques, the use of bioinformatics can also assist in the identification of new BGCs and regulatory networks, through the use of tools such as AntiSMASH and sequencing methodologies (including Illumina, NanoPore and PacBio) to uncover previously unknown BGCs (Blin *et al*, 2023, Quainoo *et al*, 2017). The combination of these techniques is crucial in uncovering new antibiotic pathways and are important tools in AMR research.

1.7.1 Gene Deletion and Disruption

Altering *Streptomyces* genes, either through disruption of function or gene deletion, are fundamental to the study of gene function. In *Streptomyces* species, homologous recombination is commonly used, where a plasmid carrying a disrupted version of the target gene (with an inserted resistance marker) integrates into the chromosome, resulting in a gene with reduced, or no function (Netzker *et al*, 2016, Raynal *et al*, 2006). The usage of gene deletion is commonly utilised for the study of non-essential genes (as essential genes are unable to be deleted without causing unrecoverable damage to the modified bacteria), and helps to provide insight into gene function, especially in metabolic and antibiotic production

pathways (Ochi, 2016, Liu *et al*, 2021). In recent years, advancements in molecular biology techniques have opened up new paths for gene manipulation and deletion, such as the clustered regularly interspaced short palindromic repeats (CRISPR) family of DNA sequences (Cobb, Wang and Zhao, 2015, Tong *et al*, 2020). CRISPR-Cas9, a recent gene-editing technology, works by using a small guide RNA (sgRNA) to direct the Cas9 nuclease to a specific DNA sequence (based on the sgRNA). After this, Cas9 creates a double-strand break at the targeted gene, which the cell then repairs using homologous flanks of the target gene, leading to precise deletion after homologous recombination (Cobb, Wang and Zhao, 2015). It is this recombination event that results in a successful deletion as unrepaired double-stranded breaks are lethal to the cells they occur in.

Gene disruption works by nucleases inducing double-stranded breaks, leading to error-prone non-homologous end joining (NHEJ), which can result in small insertions or deletionss near the cleavage site (Aigle and Corre, 2012). These mutations can potentially result in frameshifts, which alters the reading frame downstream of the mutation, leading to significant changes in the amino acid coding sequences and often produces a non-functional protein. To this effect, gene disruption and deletion can be used to determine the role and essentiality of genes in *Streptomyces* by comparing the phenotypes of wild-type and deletion strains.

1.10.2 Plasmid-mediated Mutagenesis

Changes to the genetic code of *Streptomyces* species can be made through the use of a plasmid vector, allowing for the study of specific gene functions, as well as investigations into gene overexpression, where a gene is placed under the control of a strong promotor to increase expression compared to wild-type strains (Gehring *et al*, 2000) However, there are limitations when performing this in *Streptomyces*. As previously mentioned, a key trait of *Streptomyces* species is the presence of large genomes with high GC content, which can result in complications in gene manipulation (Kim *et al*, 2025). Additionally, *Streptomyces* restricts methylated DNA, which can cause difficulties regarding plasmid stability and replication (Alduina and Gallo, 2012). For example, *S. coelicolor* possesses a restriction

system which cleaves DNA methylated by *E. coli* modification systems, meaning that any plasmids conjugated into *S. coelicolor* must be done so through a methylation-deficient strain of *E. coli*, such as *E. coli* ET12567 (MacNeil *et al*, 1992). A helper plasmid that contains necessary conjugation machinery is also needed, and in *Streptomyces* molecular genetics, this helper plasmid is normally pUZ8002, which is documented to be derived from the RK2 plasmid, a broad-host range plasmid (Paget *et al*, 1999, Larcombe *et al*, 2024). A combination of *E.coli* ET12567 pUZ8002 and a plasmid vector containing an *oriT* are typically used to overcome this molecular obstacle and allows for successful conjugation of donor DNA into *Streptomyces* cells.

1.10.3 Reporter Gene Fusions

Reporter assays measure biological responses by introducing a reporter gene construct into live cells and then monitoring the reporter's activity, making them incredibly useful tools with regards to gene regulation. Commonly used reporters in medical research include fluorescent proteins (such as Green Fluorescent Protein (GFP)), which exhibit quantifiable fluorescence when exposed to their respective excitation spectra (Tsien, 1998); luciferases, which produce light when interacting with its substrate of interest luciferin (Brennan *et al*, 2021), and β-galactosidase, which is a reporter gene that produces a blue pigment when cells are treated with the chromogenic substrate 5-bromo-4-chloro-3-indoyl-β-D-galactoside (also known as X-gal) (Horwitz *et al*, 1964). As *Streptomyces* is documented to display *N*-acetyl-β-galactosamidase activity, β-galactosamidase reporter assays are not used in *Streptomyces* background, where instead, β-Glucuronidase assays are utilized, using the pGUS reporter plasmid (Myronovskyi *et al*, 2011) These systems allow for several detection methods, including luminescence, absorbance and fluorescence-based methods (**Fig. 1.6**), and allow for a wide variety of research applications including studying gene expression, measuring cell signalling pathways, drug target screening and the analysis of promoter strength (Boulin, Etchberger and Hobert, 2006, Debnath, Prasad and Bisen, 2009).

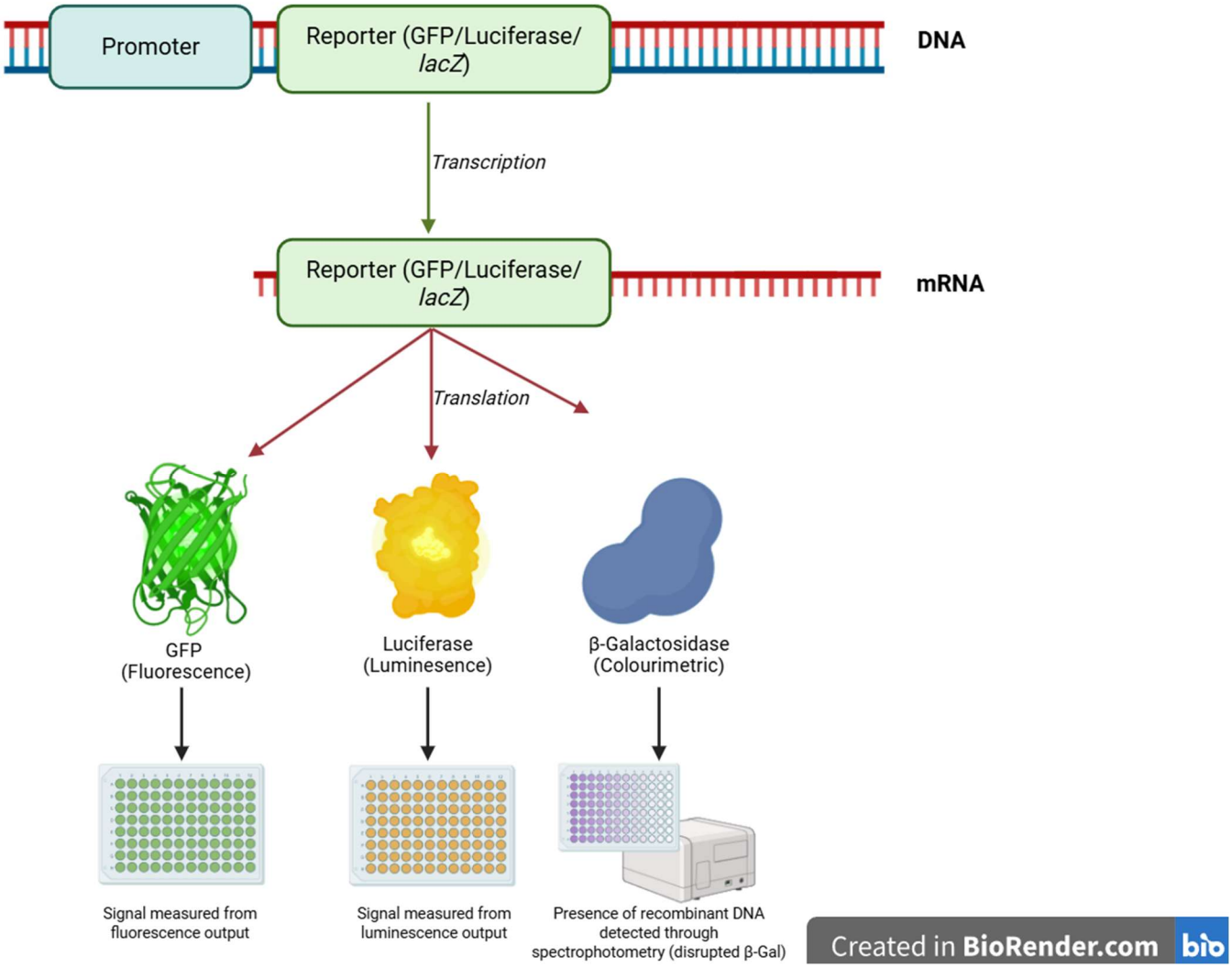

Fig. 1.6: Schematic Overview of a Reporter Gene Assay: The promoter and regulatory elements of the gene or promotor of interest are fused directly to a reporter gene (e.g., GFP, *lacZ*, or luciferase) within a vector construct. When introduced into the host cell, the endogenous regulatory signals drive the expression of the reporter, producing a measurable output, that reflects the activity of the native promoter. Abbreviations: DNA- Deoxyribonucleic acid, mRNA- Messenger ribonucleic acid, GFP- Green Fluorescent Protein, *lacZ*- gene encoding Beta-Galactosidase, β-gal- Beta-Galactosidase**.** Created with BioRender (BioRender, 2025).

Fluorescent proteins are a class of proteins that emit light when interacting with light wavelengths with their excitation spectra, making them vital tools for both molecular and cellular biology. Originally discovered in jellyfish by Shimomura and colleagues in 1962 (e.g. GFP), newer proteins have since been engineered into a variety of fluorescent colours, enabling multi-colour labelling in live-cell imaging and microscopy (Shinomura Johnson and Saiga, 1962, Heim and Tsien, 1996, Seo, Kim and Kim, 2024). These proteins can also function as genetic markers when their production is tied to a gene, making them useful tools for visualising gene expression and real time cellular dynamics. As a result, fluorescent proteins have seen widespread use in fluorescence microscopy and high-throughput reporter screening (Chudakov *et al*, 2010, Delgadillo-Guevara *et al*, 2024). While fluorescent proteins rely on encoded protein structures, RNA aptamers, a newer reporter system seeing increased use, offers an additional approach to imaging, which could be utilised in tandem with fluorescent proteins.

1.11 RNA Aptamers

RNA aptamers are RNA oligonucleotides that bind to a specific target with high affinity and specificity to their target that is comparable to antibodies. RNA aptamers are typically identified through Systematic Evolution of Ligands by EXponential enrichment (SELEX), an *in vitro* method relying on repeated exposure of oligomer molecules to populations, followed by screening and re-exposure to create a selection pressure for high affinity ligands (Kaur and Shorie, 2019). The end result of SELEX is a library of oligonucleotide sequences that demonstrate affinity to the target of interest. This library is then cloned and sequenced. SELEX was first developed by the Gold lab in 1990, however the Szostak laboratory, unaffiliated with the Gold lab also developed this technique at the same time, under the name '*in-vitro* selection ' (Tuerk and Gold, 1990., Ellington and Szostak, 1990). Since this time, SELEX has been used to generate an endless number of aptamers for both clinical and research purposes.

Aptamers can be combined with ribozymes to self-cleave in the presence of their molecule of interest. Hammerhead ribozymes (HHRs) are small RNA modules that can be integrated into a variety of mRNAs to control their stability (Ausländer *et al*, 2016). These HHRs fold into a tertiary structure where stem loop I and stem loop II form a specific interaction that is necessary for efficient self-cleaving. As the best characterized ribozyme and self-cleavage capability, the hammerhead ribozyme serves as a model system for research into RNA structure and properties. The combination of a HHR with an RNA aptamer causes self-cleavage to become dependent on the presence of the aptamer's ligand, making the combination a useful tool for gene control (Wittmann and Suess, 2012).

1.11.1 The Vegetable Aptamers: Spinach

Fluorescent RNA aptamers exhibit fluorescence when binding to their chosen ligand and have been well-documented as useful readout modules for RNA-based devices (Arora *et al*, 2015). An example of a fluorescent RNA aptamer is the RNA aptamer Spinach. An RNA mimic of green fluorescent protein (GFP) and developed by the Jaffery lab, Spinach is used for fluorescently labelling RNA and tracking RNA *in vivo* (Paige *et al*, 2011). The GFP fluorophore is comprised of three cyclized amino acids within a β-barrel structure: Serine65-Tyrosine66-Glycine67; this structure is also known as 4-hydroxybenzylidene imidazolinone, or HBI and was used as the basis for SELEX experimentation. A derivative of HBI: (Z)-4-(3,5-Difluoro-4-hydroxybenzylidene)-1,2-dimethyl-1H-imidazol-5(4H)-one, or DFHBI was designed and synthesized. The fluorescence from the 24-2/DFHBI complex was green and resembled that of the fluorescence produced by GFP, hence named the 'Spinach ' aptamer. Spinach is an 84-nucleotide long structure comprised of two helical strands and an internal bulge containing a G-quadruplex. A G-quadruplex is a secondary structure formed in guanine-rich sequences through hydrogen-bonded guanine nucleotides, detectable in both DNA and RNA (Lyons *et al*, 2017). Spinach and DFHBI are non-fluorescent when separate, however when DFHBI binds to the Spinach aptamer's G-quadruplex motif, they form a brightly fluorescent complex, resulting in an RNA analog of GFP (**Fig 1.7**) (Filonov *et al*, 2014., Huang *et al*, 2014).

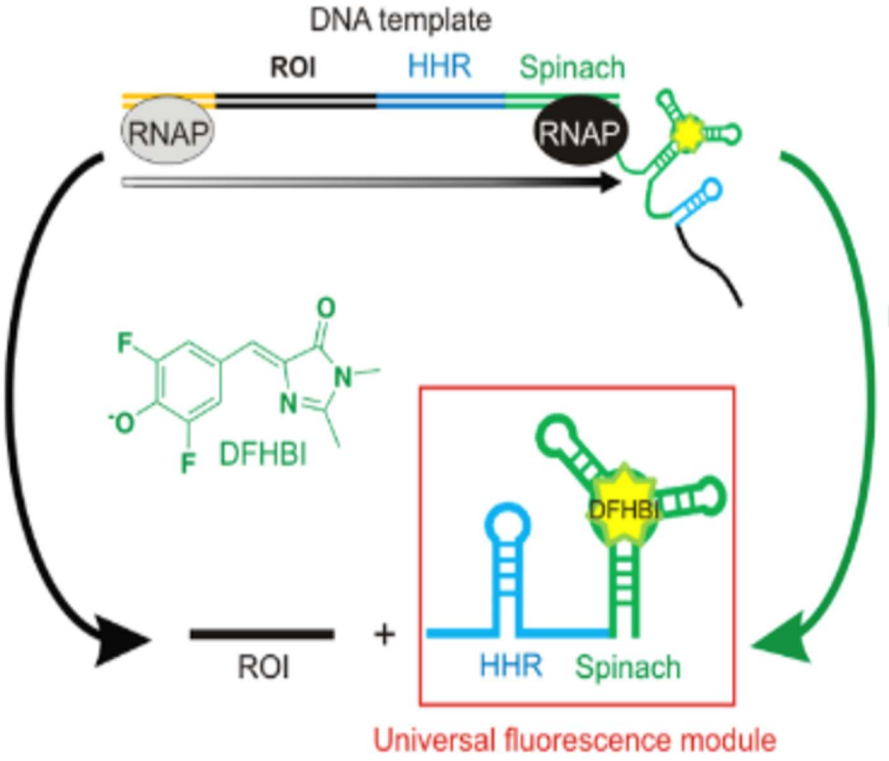

Fig. 1.7: Mechanism of Spinach-DFHBI complex fluorescence. When inserted downstream of a chosen promoter or RNA of interest, the hammerhead ribozyme-Spinach aptamer complex forms a universal fluorescence module that fluorescence in the presence of DFHBI, allowing for transcription monitoring. Abbreviations: DNA- Deoxyribonucleic acid, ROI- Region of interest, RNAP- Ribonucleic acid polymerase, HHR- Hammerhead Ribozyme, DFHBI- 3,5-Difluoro-4-hydroxybenzylidene imidazolinone. Modified from Höfer *et al*, 2013.

The fluorescence produced by the Spinach-DFHBI complex is also able to be detected while in living cells, which makes the use of fluorescent RNA aptamers as tools for imaging RNA in living cells viable. Additionally, Strack and colleagues were able to show that Spinach can be combined with other functional RNAs to serve as a completely RNA-based readout module for metabolite detection (Strack *et al*, 2014). Further advantages of using the Spinach-DFHBI complex over GFP comes with its resistance to photobleaching, a disadvantage of many fluorescent proteins, and the ability to tag Spinach to RNAs of interest, whereas GFP is a large 27kDa protein, making it unsuitable for tagging smaller biomolecules of interest such as DNA and lipids (Hink *et al*, 2000, Ouellet, 2016, Grimm and Lavis, 2022). Moreover, RNA aptamers give direct readouts of transcriptional activity, not requiring translation to give indications of promoter strength or activity, unlike traditional reporters such as β-galactosidases or fluorescent proteins.

Since the creation of Spinach, it has been adapted for uses as a small molecule sensor, as well as for monitoring transcription *in vitro* and *in vivo* in real time (Pothoulakis *et al*, 2014., Kellenburger *et al*, 2013). The use of Spinach and other fluorescent RNA aptamers as imaging tools has been invaluable to RNA research, with potential further uses including simultaneous imaging of multiple RNAs and the imaging of RNA-RNA interactions.

1.11.2 The Vegetable Aptamers: Broccoli

Since the development of the Spinach aptamer, improvements have been made to further increase fluorescence and improve aptamer stability. One of the major challenges facing aptamers is that they typically function poorly within cells, due to RNA degradation and poor intracellular folding. Further testing with the Spinach aptamer revealed while fluorescence measurements can be taken *in vivo,* it is highly unstable caused by its poor folding and thermal instability at 37ºC, leading to reduced brightness (Ouellet, 2016). Due to its *in vivo* instability, Spinach requires a tRNA scaffold when used for *in vivo* experimentation (Strack *et al*, 2013).

The poor folding of Spinach and its reduced use in an *in vivo* environment led to research into improving the intra-cellular folding capacity of Spinach for extended *in vivo* usage.

Through systematic mutagenesis of Spinach, the Jaffery Lab were able to identify mutations that conferred thermostability and improve folding, resulting in the creations of multiple Spinach analogues (Strack *et al*, 2014). These analogues include Spinach 1.1, Spinach 1.2 and Spinach2. Spinach2 is a 96-nucleotide long variant of Spinach, which exhibits improved thermal stability, intra-cellular folding and brighter fluorescence compared to the original Spinach aptamer, making it a versatile tool for RNA imaging in live cells. Due to their nomenclature, Spinach, Spinach2 and similar-named aptamers are known collectively as the 'vegetable 'aptamers (Filonov *et al*, 2015).

Advancements in the use of SELEX allowed for the production of aptamers with high compatibility with cellular expression, coupled with fluorescence-activated cell sorting (FACS) enabled the selection of aptamers based on the ability to induce fluorophore fluorescence, in addition to their ability to function intracellularly. Using this approach, the Jaffery Lab were further able to iterate on Spinach2, leading to the development of the Broccoli aptamer (Filonov *et al*, 2014). A pool of RNAs that activate the fluorescence of DFHBI were identified using SELEX. After 4-6 rounds of SELEX using a random library containing approximately 10^{14} library members, the RNA pool was cloned into bacterial expression vectors and transformed into *E. coli*. The transformed *E. coli* was further sorted through FACS in the presence of DFHBI to identify aptamers capable of producing the brightest fluorescence when forming a complex with DFHBI. This process resulted in the Broccoli RNA aptamer (Filonov *et al*, 2014).

Broccoli is a 49-nucleotide long fluorescent aptamer, shorter than both Spinach and Spinach2, along with exhibiting bright green fluorescence upon binding with either DFHBI or its improved counterpart: (5*Z*)-5-[(3,5-Difluoro-4-hydroxyphenyl)methylene]-3,5-dihydro-2-methyl-3-(2,2,2-trifluoroethyl)-4*H*-imidazol-4-one (DFHBI-1T) (**Fig. 1.8A**). Compared to Spinach2, Broccoli possesses a similar folding efficiency but has a reduced dependence on magnesium for folding and thermostability, resulting in a significant increase in brightness *in vitro*. In addition,

Broccoli does not require the use of a tRNA scaffold to support folding *in vivo*, making it a viable alternative to Spinach for *in vivo* experimentation. The Broccoli RNA forms a G-quadruplex structure that relies on potassium and sodium ions to assist in stabilising the structure of the aptamer and with DFHBI/DFHBI-1T binding (**Fig. 1.8B**; Ageely *et al*, 2016).

Furthermore, Broccoli can be dimerized (tdBroccoli), which further increases its fluorescence compared to standard Broccoli (tBroccoli) by ~1.8 fold (Filonov *et al*, 2014). Since its creation, Broccoli has further been developed into a split aptamer that can be used to visualise RNA-RNA assembly (Alam *et al*, 2017). The split Broccoli aptamer is comprised of a *Top* and *Bottom* portion, where each portion is fused onto a separate RNA molecule. Fluorescence with the split aptamer is only seen when the RNAs complex so the entire aptamer can hybridize and fold in the presence of DFHBI, allowing for the observation of RNA-RNA interactions.

Since its development, the Broccoli aptamer has found several uses (Filonov *et al*, 2014, Kartje *et al,* 2021, van der Sijs *et al*, 2024). Predominantly, it is used as a superior alternative to the Spinach and Spinach2 aptamers due to it not requiring an tRNA scaffold while showing increased levels of fluorescence. As with other fluorescent aptamers, Broccoli is commonly used for live-cell RNA imaging, with Broccoli inserted into the RNA of interest and producing a direct readout. Unlike traditional reporter systems, when using RNA aptamers there is no requirement for mRNA translation to measure activity. Broccoli has also been used to allow for imaging RNA and RNA cleavage products in gels, as well as for screening activity in RNA-altering enzymes (Filonov *et al*, 2015., Svensen and Jaffery, 2016). However, even with these uses, the Broccoli aptamer is not without its limitations. Aptamers in general are influenced by flanking sequences which can lead to folding interference, a disadvantage that also affects Broccoli (Strack *et al*, 2013., Martell *et al*, 2002).

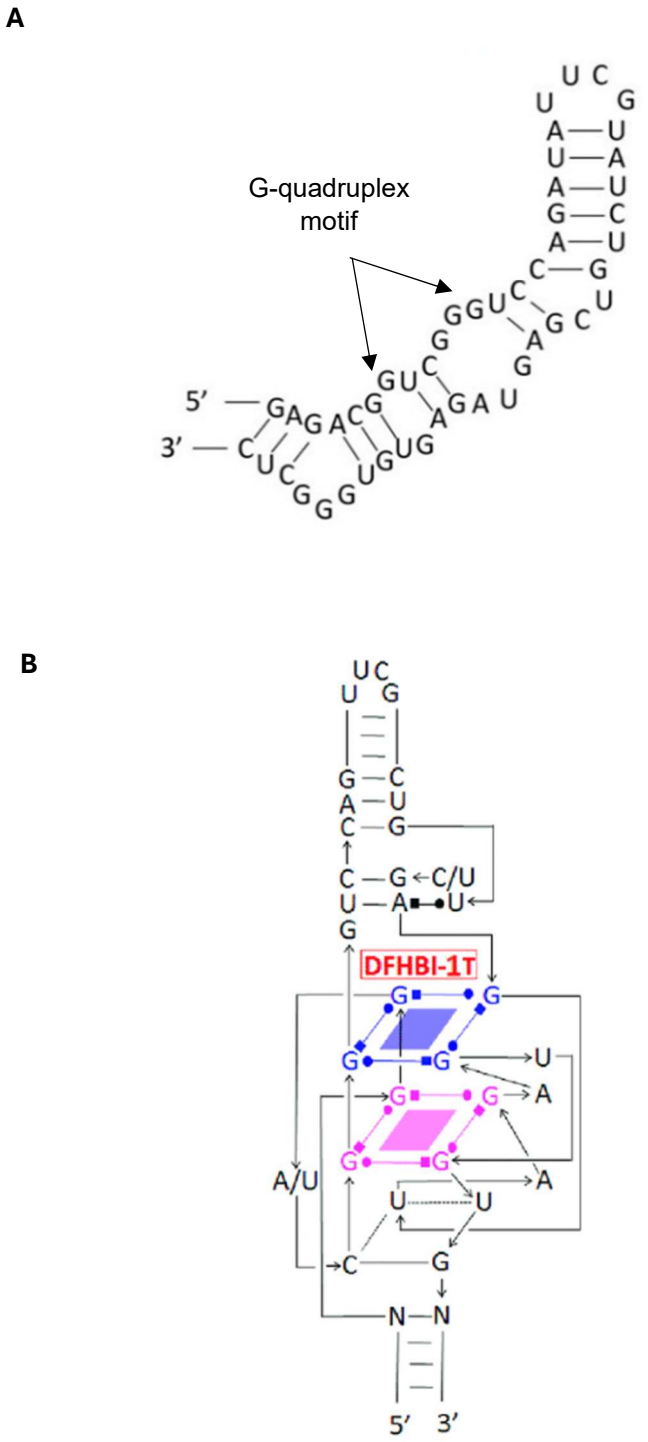

Fig. 1.8. Nucleotide Structure of the Broccoli Aptamer and Its G-Quadruplex Scaffold. A: Nucleotide composition and secondary structure of the Broccoli aptamer, showing its conserved stem-loop architecture and guanine-rich G-quadruplex motif. **B: Detailed view of the G-quadruplex scaffold**. This structure serves as the binding site for DFHBI, stabilizing the fluorophore within the RNA scaffold and enhancing fluorescence (Modified from Shanaa *et al*, 2021)

1.12 Fluorophores and DFHBI

The compound DFHBI is a fluorinated derivative of the green fluorescent protein (GFP) chromophore, which is utilised for imaging RNA in living cells, with its fluorescence activated through binding with the Spinach, Spinach2 or Broccoli aptamers. Designed by Paige *et al*, this was the compound that was used as selection pressure which led to the creation of the Spinach aptamer (Paige *et al*, 2011). Since its creation, further analogues of DFHBI have been made to increase fluorescence levels, improve binding affinity, and enhance thermodynamic parameters.

Song and colleagues iterated on the DFHBI compound by replacing the methyl substituent with a 1,1,1-trifluoroethyl group, resulting in the creation of DFHBI-1T, which displayed an increase in brightness when compared to DFHBI, along with an increased quantum yield (an efficiency measurement for photon emission and absorption) and extinction coefficient (Song *et al*, 2014). DFHBI-1T also possesses higher photostability than DFHBI, leading to improved signal efficiency and lower background fluorescence in fluorescence measurement experiments. DFHBI-1T is better suited for fluorescence detection devices that are suited for GFP imaging due to the red shift in its excitation wavelengths. Finally, the excitation and emission wavelengths for DFHBI-1T vary slightly from its parent DFHBI. While a Broccoli-DFHBI complex has an excitation and emission wavelength of 450nm and 501nm respectively, the Broccoli-DFHBI-1T complex possess an excitation and emission wavelength of 472nm and 507nm respectively. However, a trait of DFHBI-1T that is shared with DFHBI is that of its low fluorescence intensity; even though DFHBI-1T possesses higher fluorescence intensity than DFHBI, this value is still low. This is attributed to their moderate binding affinity, which limits the imaging of low abundance transcripts (Pauff *et al*, 2017., Santra *et al*, 2019). Despite this, DFHBI and DFHBI-1T remain the most widely used fluorophores in these aptamer systems. The structures for both DFHBI and DFHBI-1T can be seen in **Fig. 1.9**.

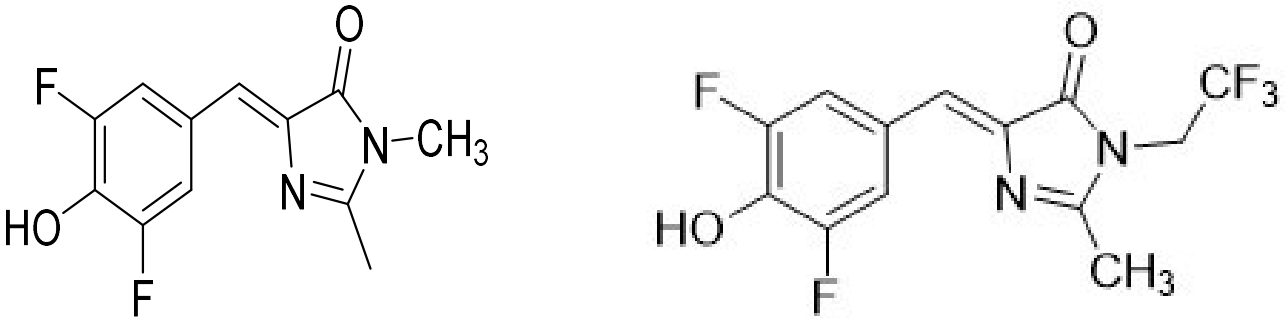

Fig. 1.9: **Chemical structures of DFHBI and DFHBI derivatives**. The parental fluorophore, DFHBI, is the most well-documented of the Spinach/Broccoli aptamer fluorophores. DFHBI-1T is documented as producing higher fluorescence than its parent, DFHBI. Abbreviations: DFHBI- 3,5-Difluoro-4-hydroxybenzylidene imidazolinone, DFHBI-1T- (5*Z*)-5-[(3,5-Difluoro-4-hydroxyphenyl)methylene]-3,5-dihydro-2-methyl-3-(2,2,2-trifluoroethyl)-4*H*-imidazol-4-one

1.13 mCherry: The Red Fluorescent Protein

mCherry is a basic red fluorescent protein, belonging to the mFruits family of monomeric red fluorescent proteins (mRFPs). Derived from the *Discosoma spp* protein DsRed, mCherry was optimized through directed evolution of mRFP, which itself is a derivative of DsRed, along with other fluorescent proteins such as mStrawberry, tdTomato and mBanana (Shaner *et al*, 2004). Out of all of the fluorescent proteins developed in the Tsien lab, mCherry possesses the highest photostability and the fastest maturation, along with pH resistance (Shaner *et al*, 2004). The mCherry chromophore is comprised of three amino acids: Gln66, Tyr67 and Gly68, which are modified post-translation into an imidazolinone. Fluorescent proteins like mCherry are used to tag cellular components, to allow them to be studied using fluorescence microscopy or spectroscopy. Spectroscopic analysis revealed mCherry has a max excitation wavelength of 587nm and a max emission wavelength between 610nm, which makes it the closest fluorescent protein to its parent mRFP1 (Shu *et al*, 2006).

The fluorescent protein mCherry is most commonly used as an instrument in fluorescence microscopy as an intracellular probe, where it assists in protein visualization and function analysis. GFP and mCherry are commonly used in tandem for co-localisation and co-expression experiments because their spectral properties allow for minimal crossover when utilised *in vivo* (Doherty *et al*, 2010). It is also possible to integrate the mCherry fluorescent protein into various genes, allowing for quantification of gene expression and protein translation based on the level of mCherry fluorescence. Although there have been many newer red fluorescent proteins since the reaction of mCherry, it is still the most widely used RFP. This is attributed to its high ratio flickering threshold to brightness compared to other red fluorescent proteins, along with respectively high quantum yield (Siegel *et al*, 2013). Compared to other red fluorescent monomers, mCherry is widely regarded as the best mRFP. This is due to its brightness efficiency, its small molecular weight for faster folding times and its superior photostability compared to other mRFPs, such as tdTomato and mStrawberry (Shaner *et al*, 2005). While tdTomato is close to mCherry in terms of photostability, its molecular weight is

twice that of mCherry which may lead to interfering with protein interaction, as well as an increased folding time compared to mCherry. As such, mCherry has become the most widely used mRFP for visualization of intracellular processes.

1.14 Scope of the Project.

Previous literature has stated that without the presence of the *bldA* leucine tRNA, TTA codons cannot be translated in *Streptomyces*, and therefore, proteins containing TTA cannot be translated. In *Streptomyces,* the *bldA* translational control of antibiotic biosynthetic genes offers an excellent example to test differences in transcription and translation of genes. To test this, a tandem Broccoli-mCherry reporter system will be designed and tested in *Streptomyces* species, and a 96-well plate-based assay developed for measuring activity. It was hypothesized that the Broccoli aptamer, if coupled with the mCherry fluorescent protein with the TTA codon early into its coding sequence could be used as a novel quantitative transcription/translation reporter system. The Broccoli aptamer has been shown to be functional in Gram-Negative bacteria such as *E. coli* (Filonov and Jaffery, 2016), but no published data exists on the use of the Broccoli aptamer in *Streptomyces* species. By inserting the construct downstream of important promotors in *Streptomyces coelicolor* and *Streptomyces clavuligerus*, it may be possible to quantify varying levels of promotor activity (transcription) and TTA-codon-dependant translation, which could simultaneously be used to detect the effects mutations have on transcription and translation for afflicted genes. While the *bldA* mutant *S. coelicolor* J1700 is well-documented in the wider literature for its deficiency in sporulation and specialised metabolite production due to its defective Leu-TTA tRNA, knowledge of the wider genome of J1700, and consequently additional mutations is currently unknown. In summary, this work in the following thesis investigates the importance of the *bldA* tRNA on *Streptomyces* gene expression, through novel assay development, whole genome sequencing, phenotypic analysis and specialised metabolite production comparisons.

1.15 Specific Aims and hypothesis

It is hypothesised that the fluorescent aptamer system can be coupled with a modified fluorescent protein to develop an orthogonal transcription/translation reporter tool for *Streptomyces.* To test this system, the well characterised *bldA* translational control system will be exploited to explore the use of the new tool.

Specific aims

- **Evaluate the functionality of the Broccoli aptamer in *Streptomyces* species**.
- **Develop a tandem Broccoli-mCherry reporter system** to test transcription and TTA-codon-dependent translation in *Streptomyces* species and design a 96-well plate-based assay for measuring activity.
- **Quantify promotor-dependent transcription and TTA-codon-dependent translation** in *Streptomyces coelicolor* and *Streptomyces clavuligerus* and assess the effects of promotor mutations on these processes.
- **Sequence the whole genome of *Streptomyces coelicolor* J1700** to identify previously undocumented mutations.

Chapter 2: Materials and Methods

2.1 Plastic Consumables and Glassware

Bacterial cells were typically grown in either Universal tubes (supplied by Elkay Laboratory Products Ltd (UK) or 250 mL Erlenmyer flasks (Supplied by either GSK or Duran, Wertheim, DE) and grown in shaking incubators, dependant on the bacteria's optimum growth temperature. Once grown to a suitable growth phase, determined via measuring the optical density at a wavelength of 600nm (OD_{600}), cells were transferred into either sterile 15ml or 50mL centrifuge tubes (supplied by Corning Incorporated, New York, USA) and centrifuged in the Heraeus Megafuge 40R (4000 x *g*). Smaller volumes of liquid culture were centrifuged using the Microfuge 16 Centrifuge by Beckman Coulter (referred to henceforth as a microfuge).

2.2 Chemical, Media, and Supplement Preparation

Media used throughout this thesis can be seen in **Table 2-1**. All media was prepared and sterilised on the same day, either through autoclaving at 121°C for 20 minutes or by filter-sterilising using passing the media through a 0.22 μm pore filter using a sterile syringe if any media components were heat-sensitive. Recipes for the media used in this study are shown in **Table 2-2**. Distilled water was dispensed by the Purite water system (UK).

Table 2-1: Media used for cultivation of *Streptomyces* and *Escherichia coli*

Media	Components	Reference
2xYT Yeast Tryptone media	16g Tryptone 10g Yeast Extract 5g Sodium Chloride (NaCl) Made up to 1000mL with distilled water (dH_2O) pH adjusted to 7.2	Kieser *et al*, 2000
L3M9	0.3g Dextrin 10g α-α-Trehalose 0.5g Di-potassium hydrogen orthophosphate (K_2HPO_4) 1g Sodium Chloride (NaCl) 1g Magnesium Sulfate ($MgSO_4$) 0.5g Calcium Chloride (CaCl) 2g Casamino acids 11g MOPS powder 1ml 10x trace salts stock solution[1] 30g ROKO Agar Made up to 1000mL with distilled water (dH_2O) pH adjusted to 6.8 ± 0.2	GSK, 2021
Lysogeny Broth (LB)	10g Tryptone 5g Yeast Extract 10g Sodium Chloride (NaCl) 1000mL distilled water (dH_2O) 20g agar-agar added for solid medium pH adjusted to 7.2	Bertani *et al*, 1951., Sambrook, Fritschi and Maniatis, 1989
Mannitol Soya Flour (MS) Agar	20g Soya Flour 20g Mannitol ($C_6H_{14}O_6$) 20g Agar-agar 1000mL tap water (H_2O)	Hobbs *et al*, 1989

Tryptic Soya Broth (TSB)	30g TSB Powder 1000mL Distilled water (dH_2O) pH adjusted to 7.2	Kieser *et al*, 2000
Yeast Extract Malt Extract (YEME) medium	3g Yeast Extract 3g Malt Extract (Oxoid) 5g Peptone 10g Glucose 340 g sucrose (34% final concentration) Up to 1L dH_2O pH adjusted to 7.5 After autoclaving: 2mL 2.5M Magnesium dichloride hexahydrate ($MgCl_2*6H_2O$) (Final concentration of 5mM)	Kieser *et al*, 2000
Super Optimal Broth with Catabolite Repression Medium (SOC)	20g tryptone, 5g yeast extract, 1mL 1M NaCl, 0.25mL1M KCl, 1mL 2M Mg2+ stock 1mL 2M glucose Up to 1L dH2O	New England BioLabs
Broccomyces Tris-Washing Buffer	4.85g Tris 0.48g Magnesium chloride ($MgCl_2$) 9.32g Potassium chloride (KCl) Up to 1L dH_2O pH adjusted to 7.2	This Study
Broccomyces HEPES Buffer	4.76g HEPES 0.48g Magnesium chloride ($MgCl_2$) (5mM) 9.32g Potassium chloride (KCl) (125mM) Up to 1L dH_2O pH adjusted to 7.2	This Study

Broccomyces M9 Buffer	6.78g disodium hydrogen phosphate (Na_2HPO_4) (47.75mM) 3g potassium dihydrogen phosphate (KH_2PO_4) (22.04mm) 0.5g Sodium chloride ($NaCl_2$) (8.56mM) 1g ammonium chloride (NH_4Cl) (18.7mM) 0.24g Magnesium sulfate ($MgSO_4$) (2mM) 0.01g Calcium chloride ($CaCl_2$) (0.1mM) 9.32g Potassium chloride (KCl) (125mM) Up to 1L dH_2O pH adjusted to 7.2	Adapted from Okuda *et al*, 2017
Supplemented PBS	10x Dulbecco's Phosphate Buffered Saline (DPBS) tablets 0.5g L-Glutamine 1000mL dH_2O pH adjusted to 7.2 After autoclaving: 20g Glucose ($C_6H_{12}O_6$) (Autoclaved separately as a 50% solution)	This study
Minimal Media	0.5g L-asparagine 0.5g K_2HPO_4 0.2g $MgSO_4$*$7H_2O$ 0.01g $FeSO_4$*$7H_2O$ 10g agar 1L dH_2O After Autoclaving: 20mL 50% glucose (filter sterilized)	Kieser *et al*, 2000

1. Contained 0.5g of FeSO4, 0.5g of $MnSO_4$ and 0.5g $ZnSO_4$ per 50mL of distilled H_20.
2. Tap water used in place of distilled water due to the micronutrients found in tap water.

Table 2-2 Antibiotic stocks and working concentrations

Antibiotic	Class	Solvent	Working concentration (μg/mL)
Apramycin	Aminoglycoside	H_2O	50
Chloramphenicol	50S ribosomal subunit targeting antibiotic	100% EtOH	25
Kanamycin	Aminoglycoside	H_2O	50
Hygromycin B	Substitute aminoglycoside	H_2O	25
Nalidixic acid	DNA gyrase inhibitor antibiotic	0.1M NaOH	25

2.3 Bacteria preparation

2.3.1 Preparation of *Streptomyces* and *E.coli* cultures

All bacterial strains used and/or generated as part of this study are listed in **Table 2-3**. *S. coelicolor* and *S. clavuligerus* strains were grown on Mannitol Soya flour (MS) and L3M9 agar respectively, for spore counting, transformation and conjugation experiments (Hobbs *et al*, 1989; GSK, 2021). Ex-conjugants of *S. coelicolor* and *S. clavuligerus* were selected on MS agar and L3M9 agar respectively, containing appropriate antibiotics for selection. Plasmids used within this study are listed in **Table 2-4**.

Typically, *Streptomyces* spores were heat-activated at 50°C for 10 minutes in a dry bath, to promote and synchronise germination. Volumes of 50-100 µL spore stocks (~1 x 10^9 CFUs/mL) were added to 900-950 µL of appropriate inoculation media for *S. coelicolor* and *S. clavuligerus* respectively (typically TSB media). These heat-activated spores were used to set up starter cultures which were left to grow at 30°C (250rpm) for 24 hours and 26°C (250rpm) for 48 hours for *S. coelicolor* and *S. clavuligerus* respectively. The starter cultures were then standardized by equalising their respective optical densities to ensure that all cultures start with the same number of cells for further experimentation. *E. coli* cells were grown on LB agar and cultured in LB broth for 16-24 hour.

2.3.2 Preparation of Glycerol Stocks

Streptomyces strain stocks were produced by streaking spore stocks for single colonies. After isolating a single colony for the specific *Streptomyces* strain, the spores from a single *Streptomyces* colony were transferred using a sterilised cotton bud to an identical agar plate and streaked to create a lawn of spores on the plate. The growth of *Streptomyces* spore plates took seven days for *S. coelicolor* on MS agar and ten days for *S. clavuligerus* on L3M9 agar. *Streptomyces* spores were harvested into a 20% glycerol solution by using a sterile cotton bud to lift the spores from the aerial hyphae. The spore-glycerol solution was then passed through

a sterilised 20mL syringe containing cotton wool to remove residual mycelium. After filtration, the spores were transferred into a cryo-tube and stored at -20°C until further use.

E. coli stocks were prepared by aliquoting 500 µL of overnight LB liquid culture into a cryotube containing 500 µL of 50% glycerol and stored at -20 °C until further use.

Table 2-3: List of *Streptomyces* and *Escherichia coli* strains utilized in this study.

Species	Description	Genotype	Reference
E. coli Subcloning Efficiency DH5α Competent Cells	*E.coli* K-12 derivative	*F- Φ80lacZΔM15 Δ(lacZYA-argF), U169, recA1, endA1, hsdR17(rk-, mk+), phoA, supE44, thi-1, gyrA96, relA1 λ-*	Grant *et al*, 1990
E. coli ET12567 pUZ8002	*E.coli* K-12 derivative	*Medam-13::Tn9 dcm-6 hsdM hsdR recF143, zij201::Tn10, galK2, galT22, ara14, lacYI, xylS, leuB6, thi-1, tonA31, rpsL136, hisG4, tsx78, mtli, glnV44, F-*	MacNeil *et al*, 1992
S. coelicolor M145	Wildtype *S. coelicolor* strain	$SCP1^-$, $SCP2^-$	Feitelson *et al*, 1983
S. coelicolor M145 + pSET152 EV	*S. coelicolor* M145 exconjugant containing pSET152.	M145, *AprR*	This study
S. coelicolor M145 + Broccomyces-*ermE*p*	*S. coelicolor* M145 exconjugant containing pSET152 expressing Broccoli/TTA_mCherry construct under control of *ermE** promoter	M145, *AprR*	This study
S. coelicolor M145 + Broccomyces-*bldDp*	*S. coelicolor* M145 exconjugant containing pSET152 expressing Broccoli/TTA_mCherry construct under control of *bldD* promoter	M145, *AprR*	This study
S. coelicolor M145 + Broccomyces-*ermE*p* ΔHHR	*S. coelicolor* M145 exconjugant containing pSET152 expressing Broccoli/TTA_mCherry construct with HHR removed, under control of *ermE** promoter	M145, *AprR*	This study
S. coelicolor M145 + Broccomyces-*bldDp* ΔHHR	*S. coelicolor* M145 exconjugant containing pSET152 expressing Broccoli/TTA_mCherry construct with HHR removed, under control of *bldD* promoter	M145, *AprR*	This study

S. coelicolor M145 + Broccomyces-*ermE*p* TGA-mCherry	*S. coelicolor* M145 exconjugant containing pSET152 expressing Broccoli/TTA_mCherry construct under control of *ermE*p*, with mutated mCherry as negative control	M145, *AprR*	This study
S. coelicolor M145 + pIJ10257	*S. coelicolor* M145 exconjugatant containing pIJ10257	M145, *HygR*	This study
S. coelicolor M145 + pIJ10257 CAA	*S. coelicolor* M145 exconjugatant containing pIJ10257 expressing the CAA tRNA	M145, *HygR*	This study
S. coelicolor M145 + pIJ10257 *bldA*	*S. coelicolor* M145 exconjugatant containing pIJ10257 expressing the *bldA* tRNA	M145, *HygR*	This study
S. coelicolor J1700	BldA mutant produced by random mutagenesis of *S.coelicolor* J1501 strain	*hisAI, uraAI, strAI, pgl*$^{-}$, SCP1^{-}, SCP2^{-}, *bldA39*	Kieser *et al*, 2000
S. coelicolor J1700 + pSET152 EV	*S. coelicolor* J1700 exconjugant containing pSET152.	J1700, *AprR*	This study
S. coelicolor J1700 + Broccomyces-*ermE*p*	*S. coelicolor* J1700 exconjugant containing pSET152 expressing Broccoli/TTA_mCherry construct under control of *ermE** promoter	J1700, *AprR*	This study
S. coelicolor J1700 + Broccomyces-*bldDp*	*S. coelicolor* J1700 exconjugant containing pSET152 expressing Broccoli/TTA_mCherry construct under control of *bldD* promoter	J1700, *AprR*	This study
S. coelicolor J1700 + Broccomyces-*ermE*p* ΔHHR	*S. coelicolor* J1700 exconjugant containing pSET152 expressing Broccoli/TTA_mCherry construct with HHR removed, under control of *ermE** promoter	J1700, *AprR*	This study
S. coelicolor J1700 + Broccomyces-*bldDp* ΔHHR	*S. coelicolor* J1700 exconjugant containing pSET152 expressing Broccoli/TTA_mCherry construct with HHR removed, under control of *bldD* promoter	J1700, *AprR*	This study
S. coelicolor J1700 + Broccomyces-*ermE*p* TGA-mCherry	*S. coelicolor* J1700 exconjugant containing pSET152 expressing Broccoli/TTA_mCherry construct under control of *ermE*p*, with mutated mCherry as negative control	J1700, *AprR*	This study

S. coelicolor J1700 + pIJ10257	*S. coelicolor* J1700 exconjugatant containing pIJ10257	J1700, *HygR*	This study
S. coelicolor J1700 + pIJ10257 CAA	*S. coelicolor* J1700 exconjugatant containing pIJ10257 expressing the CAA tRNA	J1700, *HygR*	This study
S. coelicolor J1700 + pIJ10257 *bldA*	*S. coelicolor* J1700 exconjugatant containing pIJ10257 expressing the *bldA* tRNA	J1700, *HygR*	This study
S. coelicolor J774	*S. coelicolor bldD* deficient strain	*bldD53, cysA15, pheA1, mthB2, strA1,* SCP1^{NF}. SCP2*	Merrick, 1976
S. coelicolor J774 + pSET152 EV	*S. coelicolor* J774 exconjugant containing pSET152.	J774, *AprR*	This study
S. coelicolor J774 + Broccomyces-*ermE*p*	*S. coelicolor* J774 exconjugant containing pSET152 expressing Broccoli/TTA_mCherry construct under control of *ermE** promoter	J774, *AprR*	This study
S. coelicolor J774 + Broccomyces-*bldDp*	*S. coelicolor* J774 exconjugant containing pSET152 expressing Broccoli/TTA_mCherry construct under control of *bldD* promoter	J774, *AprR*	This study
S. coelicolor J774 + Broccomyces-*ermE*p* ΔHHR	*S. coelicolor* J774 exconjugant containing pSET152 expressing Broccoli/TTA_mCherry construct with HHR removed, under control of *ermE** promoter	J774, *AprR*	This study
S. coelicolor J774 + Broccomyces-*bldDp* ΔHHR	*S. coelicolor* J774 exconjugant containing pSET152 expressing Broccoli/TTA_mCherry construct with HHR removed, under control of *bldD* promoter	J774, *AprR*	This study
S. coelicolor J774 + Broccomyces-*ermE*p* TGA-mCherry	*S. coelicolor* J774 exconjugant containing pSET152 expressing Broccoli/TTA_mCherry construct under control of *ermE*p*, with mutated mCherry as negative control	J774, *AprR*	This study
S. coelicolor JWS-Δ*bldA*	*S. coelicolor* M145 Δ*bldA* knockout	M145, Δ*bldA*	This study
S. coelicolor JWS-Δ*bldA* + pIJ10257	*S. coelicolor* JWS Δ*bldA* exconjugatant containing pIJ10257 empty vector	M145, Δ*bldA*, *HygR*	This study

S. coelicolor JWS-Δ*bldA* + pIJ10257 CAA	*S. coelicolor* JWS Δ*bldA* exconjugatant containing pIJ10257 expressing the CAA tRNA	M145, Δ*bldA*, *HygR*	This study
S. coelicolor JWS-Δ*bldA* + pIJ10257 *bldA*	*S. coelicolor* JWS Δ*bldA* exconjugatant containing pIJ10257 expressing the *bldA* tRNA	M145, Δ*bldA*, *HygR*	This study
S. clavuligerus SC6	GSK production strain	Wild-Type	GSK
S. clavuligerus SC6 + pSET152 EV	*S. clavuligerus* SC6 exconjugatant containing pSET152	*AprR*	This study
S. clavuligerus SC6 + Broccomyces-*ermE*p*	*S. clavuligerus* SC6 exconjugatant containing pSET152 expressing the Broccoli/TTA_mCherry construct under the control of the *ermE** promoter	*AprR*	This study
S. clavuligerus SC6 + Broccomyces-*ermE*p* TGA-mCherry	*S. clavuligerus* SC6 exconjugatant containing pSET152 expressing Broccoli/TTA_mCherry construct under control of *ermE*p*, with mutated mCherry as negative control	*AprR*	This study
S. clavuligerus SC6 + Broccomyces-*ccaRp*-WT	*S. clavuligerus* SC6 exconjugatant containing pSET152 expressing the Broccoli/TTA_mCherry construct under the control of the wild-type *ccaR* promoter	*AprR*	This study
S. clavuligerus SC6 + Broccomyces-*ccaRp*-M1	*S. clavuligerus* SC6 exconjugatant containing pSET152 expressing the Broccoli/TTA_mCherry construct under the control of the *ccaR* promoter with 48C>T mutation	*AprR*	This study
S. clavuligerus SC6 + Broccomyces-*ccaRp*-M2	*S. clavuligerus* SC6 exconjugatant containing pSET152 expressing the Broccoli/TTA_mCherry construct under the control of the *ccaR* promoter with 143G>A mutation	*AprR*	This study
S. clavuligerus SC6 + Broccomyces-*ccaRp*-M1M2	*S. clavuligerus* SC6 exconjugatant containing pSET152 possessing the Broccoli/TTA_mCherry construct downstream of *ccaR* promoter with 48C>T and 143G>A mutations	*AprR*	This study

Table 2-4: Plasmids used in this study

Plasmid Name	Description	Resistance	Reference
pSET152	Empty plasmid vector	Apramycin	Biermann *et al*, 1992
pSET152 Broccomyces-*ermE*p*	Broccoli/TTA-mCherry transcription/translation regulator under control of *ermE** promoter	Apramycin	This study
pSET152 Broccomyces-*bldDp*	Broccoli/TTA-mCherry transcription/translation regulator under control of *bldD* promoter	Apramycin	This study
pSET152 Broccomyces-*ermE*p* ΔHHR	Broccoli/TTA-mCherry transcription/translation regulator under control of *ermE** promoter with HammerHead Ribozyme removed	Apramycin	This study
pSET152 Broccomyces-*bldDp* ΔHHR	Broccoli/TTA-mCherry transcription/translation regulator under control of *bldD* promoter with HammerHead Ribozyme removed	Apramycin	This study
pSET152 Broccomyces-*ermE*p* TGA-mCherry	Broccoli/TTA-mCherry transcription/translation regulator under control of *ermE** promoter with TTA-mCherry functionality removed	Apramycin	This study
pSET152 Broccomyces-*ccaRp* WT	Broccoli/TTA-mCherry transcription/translation regulator under control of *ccaR* promoter	Apramycin	This study
pSET152 Broccomyces-*ccaRp* M1	Broccoli/TTA-mCherry transcription/translation regulator under control of *ccaR* promoter with mutation M1 (48C>T)	Apramycin	This study
pSET152 Broccomyces-*ccaRp* M2	Broccoli/TTA-mCherry transcription/translation regulator under control of *ccaR* promoter with mutation M2 (143G>A)	Apramycin	This study
pSET152 Broccomyces-*ccaRp* M1M2	Broccoli/TTA-mCherry transcription/translation regulator under control of *ccaR* promoter with mutation M1 (48C>T) and M2 (143G>A)	Apramycin	This study
pIJ10257	Empty plasmid vector	Hygromycin	Hong *et al*, 2005
pIJ10257_CAA	CAA tRNA overexpression vector under control of *ermE**	Hygromycin	This study
pIJ10257_bldA	UAA tRNA overexpression vector under control of *ermE**	Hygromycin	This study
pCRISPR-Cas9	Empty vector *Streptomyces* optimized gene knockout plasmid for actinomycetes	Apramycin	Tong *et al*, 2020
pCRISPR-Δ*bldA*	pCRISPR-Cas9 plasmid for deletion of Leu-tRNA^{UAA}	Apramycin	This study
pCRISPR-ΔLeu-tRNA^{CAA}	pCRISPR-Cas9 plasmid for attempted deletion of Leu-tRNA^{CAA}	Apramycin	This study
pUC19	Empty vector plasmid	Ampicillin	Norrander *et al*, 1983
pUZ8002	Empty vector plasmid	Chloramphicol/ Kanamycin	Paget *et al*, 1999

2.4 Molecular Biology

2.4.1 *Streptomyces* genomic DNA extraction

A 50mL liquid culture was incubated in a baffled flask at 30ºC for 24 hours. After incubation, 10mL of liquid culture was aliquoted into a Falcon tube and centrifuged at 4000g for 10 minutes to prepare a pellet. The pellet was then resuspended in 300 µL TE buffer containing 5mg/mL lysozyme and 0.1mg/mL RNAse A. The resuspended samples were then transferred into microfuge tubes and incubated at 37ºC for 30 minutes. After incubation, 50 µL of 10% SDS and 10µL of 20mg/mL Proteinase K were added and the solution incubated at 55ºC for a further 2.5 hours. Subsequently, 85µL of 5M NaCl was added to each sample. 400 µL of phenol/chloroform/isoamyl alcohol (25:24:1) was added to each sample, vortexed to homogenise each sample, and centrifuged at 16000g for 10 minutes.

Post centrifugation, the upper layer of each sample was removed and aliquoted into a fresh microfuge tube. To each sample 400 µL of chloroform/isoamyl alcohol (24:1) was added, after which each sample was vortexed till homogenous and centrifuged at 16,000 x*g* for 10 minutes. The aqueous upper phase of each sample was aliquoted into a new microfuge tube, where 500 µL of isopropanol was added to each microfuge tube, and mixed by inversion before being left at room temperature for 5 minutes. The samples were centrifuged at 16,000 x *g* for 10 minutes before each sample was washed with 1mL of ice cold 70% EtOH.

After washing the samples were centrifuged one final time at 16,000 x *g*, and the excess EtOH was removed before the pelleted DNA was resuspended in 100 µL nuclease free water. DNA concentrations and ratios were determined using a NanoDrop™ spectrophotometer.

2.4.2 *Streptomyces* RNA extraction

Streptomyces cultures were grown in 50mL of TSB media in an autoclaved baffled flask at 30°C for 24 hours. After incubation, 1mL of each culture was centrifuged in a benchtop centrifuge at 16,000 x *g* for 5 minutes. The supernatant was decanted, and the cell pellets were carefully resuspended in 500 μl RNAlater (SigmaAldrich). The resuspended pellets were stored at -20°C until extraction.

To extract the RNA from *Streptomyces* pellets, the tubes were thawed on ice before centrifuging at 16,000 x *g* for 5 minutes. The RNAlater supernatant was removed, and the cells were resuspended in 135 μl of TE buffer containing 15μl of 50 mg/ml lysozyme. The lysozyme stock was prepared by dissolving 50 mg of lysozyme powder in 1 ml of distilled water, which had been previously sterilised by filtration. Cell lysis was carried out at 30°C for 30 minutes. After lysis was sufficient, 525 μl of RTL buffer was added to each sample (provided by the Qiagen RNAeasy mini kit). Additionally, 10 μl β-mercaptoethanol (provided by Sigma-Aldrich) was added to each sample. The samples were inverted to ensure mixing, centrifuged and the resulting supernatant was transferred into a new microcentrifuge tube, to which 375 μl absolute ethanol was added.

RNA extraction using the RNAeasy mini kit column was carried out following the supplier's protocol, skipping the on-column DNase I digest step, which was completed by adding 20μl of 0.1mg/mL DNAse and incubating at room temperature for 1 hour

The DNAse reactions were halted by adding 2 μl of 0.25 M EDTA (final concentration of 5 mM EDTA/sample) to inhibit the enzyme activity. The resulting RNA was cleaned up using the RNAeasy mini kit column according to manufacters instructions, with the cleaned RNA eluted in 40 μl RNase-free water twice. RNA concentrations and OD_{260}/OD_{280} ratios were determined using the NanoDrop 2000c spectrophotometer.

2.4.3 Plasmid Extraction

E. coli cells were incubated overnight in 10mL of LB broth (containing the appropriate antibiotics for selection) in a shaking incubator at 37^{O}C and 250rpm. Overnight cultures were then centrifuged for 10 minutes at 2500 x *g* and the supernatant was discarded. The plasmids were extracted from the bacterial pellet using the Wizard® Plus SV Minipreps DNA Purification System from Promega. DNA concentrations and OD_{260}/OD_{280} ratios were quantified using a NanoDrop 2000 to identify the quantity of plasmid DNA extracted.

2.4.4 DNA and RNA Quantification

To quantify DNA or RNA, two commonly used instruments were utilised: the Nanodrop 2000c spectrophotometer and the Qubit fluorometer. The Nanodrop 2000c uses UV-Vis spectrophotometry to measure DNA/RNA concentration by assessing absorbance at 260 nm, requiring only 1 µL of the sample. Nanodrop quantification is best suited for checking for the presence and purity of either DNA or RNA, however it can overestimate concentration due to the presence of contaminants such guanidine residues from purification kits.

In contrast, the Qubit uses fluorescent dyes that selectively bind to DNA or RNA (with different assay kits for DNA and RNA respectively), making Qubit quantification much more accurate and sensitive than NanoDrop readings. The Qubit method involves the preparation a working solution with dye and buffer in a 1:200 ratio, the preparation of standards using 10µL of standard reagent and 190µL of working solution, and the setup of the test sample, containing 199µL of working solution and 1µL of the chosen DNA/RNA sample. The prepared samples can then be inserted into a QuBit which reads the fluorescence and correlates the concentration of DNA with the fluorescence output based on a standard curve.

2.4.5 Polymerase Chain Reactions

Primers used in this study were designed using SnapGene™ and NEBuilder™ (v2.10.5). Confirmation Polymerase Chain Reactions (PCRs) were carried out using Sigma-Aldrich RedTaq ReadyMix PCR Reaction Mix with the following specifications:

Cycle. No	Denature	Anneal	Extension	Hold
1	95ºC, 2m			
2-34	95ºC, 30s	50 ºC, 30s	72 ºC, 30s/kb	
35			72ºC, 5m	
36				4 ºC, hold

For cloning and gene deletions, Q5 High-Fidelity DNA polymerase was used provided by New England Biolabs using the following specifications:

Cycle. No	Denature	Anneal	Extension	Hold
1	98ºC, 30m			
2-34	98ºC, 30s	55-72ºC, 30s*	72 ºC, 30s/kb	
35			72ºC, 5m	
36				4 ºC, hold

*Due to the nature of Q5 High-Fidelity DNA Polymerase, NEB Tm Calculator (v1.16.7) was used to determine optimal annealing temperatures for each reaction (NEB, 2025)

All reactions were set-up following the manufacturer's instructions with approximately 10-30ng of plasmid DNA as a template. The PCR programmes used varied depending on the utilised polymerase and downstream application of the PCR products. A list of primers used throughout this study can be found in **Table 2-5.**

Table 2-5: A list of primers used in this study.

Primer Number	Primer Name	Primer Sequence (5'-3')	Tm (°C)
1	pSET152 Broccomyces check primer (Forward)	GCT GCG CCG ATG GTT TCT ACA AAG ATC G	63.2
2	pSET152 Broccomyces check primer (Reverse)	GAG CGG ATA ACA ATT TCA CAC AGG AAA CAG CTA TGA C	62.7
3	pSET152 ermE* TGA mCherry SDM test primer (forward)	AAC ATG GCC TGA ATC AAG GAG TTC ATG	59.3
4	pSET152 ermE* TGA mCherry SDM test primer (reverse)	GTC CTC CTC GCC CTT GCT	60
5	M13 Forward	GTA AAA CGA CGG CCA GT	56.0
6	M13 Reverse	CAG GAA ACA GCT ATG AC	54.8
7	pIJ10257 check primer (Forward)	CAT CAG CGA GCT GAA GAA AGA CAA TC	58
8	pIJ10257 check primer (Reverse)	GAT GCT AGT CGC GGT TGA TCG	58.1
9	CRISPR *bldA* gRNA	CGG TGG GTA GGA TCG ACG GCC GGA TGG TGG AAT GCA GAC AGT TTT AGA GCT AGA AAT	70.4
10	CRISPR *bldA* guide gRNA confirmation primer (forward)	CGG ATG GTG GAA TGC AGA CA	57.6
11	CRISPR *bldA* guide gRNA confirmation primer (reverse)	CGT AGC TGA CGC CTA CGT AAA	56.7
12	*bldA* homology template upstream primer (Forward)	TTG CGG GAT CTC GTC GAA GGC ACT AGA AGG AAG ATG ATC GGC CGG G	72.3
13	*bldA* homology template upstream primer (Reverse)	GGA CCC GCG CGG TCG ATC CCC GCA TAT AGG AGG CCA TGG GCT CCG CTT	76.7
14	*bldA* homology template downstream primer (Forward)	CGG AGC CCA TGG CCT CTA CTG TCA CGC TGC GTG	71.2
15	*bldA* homology template downstream primer (Reverse)	GGA CCC GCG CGG TCG ATC CCC CGA TAT AGG CAT CAT CGA GGA CCA CAC	73.8
16	StuI primer (forward)	GAC AAT GAC AAC AAC CAT CGC C	56.9
17	StuI primer (reverse)	GGG AAG TCG TCG CTC TCT GG	59.8
18	*bldA* tRNA knockout confirmation check primer (Forward)	CCT TGT CGA GAC GGT CAA AT	58.1
19	*bldA* tRNA knockout confirmation check primer (Reverse)	AGC ACC CTG CTG TGA ATG	55.6
20	CRISPR CAA gRNA 1	CGG TTG GTA GGA TCG ACG GCG GGA TTC GAA CCC ACG CTG TGA TTT AGA GCT AGA AAT	71
21	CRISPR CAA guide gRNA 1 confirmation primer (Forward)	GGG ATT CGA ACC CAG GCT GT	60.2
22	CRISPR CAA guide RNA 1 confirmation primer (Reverse)	CGT AGC TGA CGC CTA CGT AAA	56.7
23	CRISPR CAA gRNA 2	CGG TTG GTA GGA TCG ACG GCG TAG TCC AGC GGT AGA GAC ACT TTT AGA GCT AGA AAT	69.7

24	CRISPR CAA guide RNA 2 confirmation primer (Forward)	GTA GTC CAG CGG TAG AGA CA	55.6
25	CRISPR CAA guide RNA 2 confirmation primer (Reverse)	CAG GAC CTT CAA CTT CTT GGA	55.3
26	CRISPR CAA gRNA 3	CGG TTG GTA GGA TCG ACG GCG AGC AAC GTG TCT CTA CCG CGT TTT AGA GCT AGA AAT	71.2
27	CRISPR CAA guide RNA 3 confirmation primer (Forward)	GAG CAC CGT GTC TCT ACC GC	60.2
28	CRISPR CAA guide RNA 3 confirmation primer (Reverse)	TGT TGC CAA GGA CGT TGA ACT	59
29	CRISPR CAA gRNA 4	CGG TTG GTA GGA TCG ACG GCG CGT GGG TTC GAA TGC CAC CGT TTT AGA GCT AGA AAT	71.6
30	CRISPR CAA guide RNA 4 confirmation primer (Forward)	GCG TGG GTT CGA ATC CCA CC	61.2
31	CRISPR CAA guide RNA 4 confirmation primer (Reverse)	CCT TGT CGA GAC GGT GAA AT	59.8
32	CAA tRNA homology template upstream primer (forward)	TTG CGG GAT CTC GTC GAA GGC ACT AGA AGG CAG GGC ACC ACC ATC CTG	73.1
33	CAA tRNA homology template upstream primer (reverse)	GAA ATG AAG GAA AAG TTC CTG TAA AAC AGA GCT TGA CG	61.6
34	CAA tRNA homology template downstream primer (forward)	TCT GTT TTA CAG GAA CTT TTC CTT CAT TTC GAA GGG GC	63.6
35	CAA tRNA homology template downstream primer (reverse)	GGA CC GCG CGG TCG ATC CCC GCA TAT AGG CAT CGT CGC CAC CCA GAT G	75.2
36	CAA tRNA removal confirmation primer (forward)	TCA CCG ACG ACG GAG TAC C	58.8
37	CAA tRNA removal confirmation primer (reverse)	CTG GTT CAT GAG CGC CAG A	58.1
38	pMS82 check primer(forward)	GCA ACA GTG CCG TTG ATC GTG CTA TG	62.2
39	pMS82 check primer(reverse)	GCC ACT GGT ATT TAT GTC AAC ACC GCC	61.7

2.4.6 Agarose Gel Electrophoresis

Agarose gels of between 1-2%, dependant on the fragment sizes to be separated, were prepared by dissolving agarose in 1x TAE buffer (diluted from a 50x TAE stock solution). The 50x stock solution was made by combining 242g Tris Base, 57.1 mL of glacial acetic acid, and 200mL 0.25M EDTA stock solution and made up to a final volume of 1000mL using distilled water. The agarose/1x TAE buffer mixture was heated to allow the agarose to dissolve in the TAE buffer and allowed to cool to a suitable temperature prior to adding 1 drop of 10mg/mL Ethidium Bromide for visualisation. The agarose gel was poured into a mould and allowed to set before adding samples containing loading dye. Gels were run at 90V for 60 minutes. Finally, DNA bands in the gel were visualised using the VWE Genosmart computer.

2.4.7 Restriction Digestion

A restriction digest uses restriction enzymes to cut DNA at specific sequences, creating DNA fragments, which can be used to remove specific sections of DNA from plasmids by cleaving restriction sites near the targeted sequence. To accomplish this, 5μL of plasmid DNA was added to an microfuge tube, where 2μL of rCutSmart Buffer (supplied by New England Biolabs) was added, as well as 12μL of nuclease-free water and 1μL of the restriction enzyme. The 20μL digest was left to incubate at 37ºC for 1 hour before being removed and loaded into an agarose gel for electrophoresis, which was ran at 90V for 60 minutes. The DNA bands in the gel were visualised using the VWE Genosmart computer. The gel band containing the plasmid was then excised by placing the gel on a UV block to be able to visualise the gels, where the correct band was cut out using a scalpel, with the gel piece inserted into an microfuge tube. The excised gel was then extracted using the New England Biolabs DNA Gel Extraction Kit and following manufacturer's instructions to purify the plasmid DNA.

2.4.8 Ligation

Plasmid DNA was ligated using the T4 ligase kit with an insert to vector ratio of 3:1. *E.coli* DH5α were transformed with the ligated plasmid by heat-shocking at 42ºC for 2 minutes, incubating on ice for a further 2 minutes and recovered at 37ºC for 1 hour. The transformed DH5α was then plated on LB plates containing the appropriate antibiotics.

2.4.9 Site Directed Mutagenesis

Site Directed Mutagenesis (SDM) was performed using the Q5 ® Site Directed Mutagenesis Kit (supplied by New England Biolabs). Firstly, 1μL of the template DNA was added to an PCR tube, along with 9μL of nuclease free water, 1.25μL of the forward and reverse primer required for the site-directed mutagenesis, and 12.5μL of Q5 Hot Start High-Fidelity 2x Master Mix. The PCR was then performed under the standard conditions. Initial Denaturation: 98ºC for 30 seconds, a further 10 seconds of denaturation at 98ºC, followed by 30 seconds of annealing at 62ºC, and then extension at 72ºC for 30 seconds/kb. This cycle was repeated 25 times before a final extension of 2 minutes at 72ºC and held at 4ºC.

Next, the PCR product was subjected to a KLD reaction, comprised of 1μL of PCR product, 1μL of 10x KLD Enzyme Mix, 5μL of 2x KLD Reaction Buffer and 3μL of nuclease-free water. The reaction was incubated at room temperature for 5 minutes before 50μL of chemically competent *E. coli* DH5α was transformed with the KLD mix. After incubation on ice, 950μL of SOC media was added to the transformed DH5α, which was then incubated at 37ºC for 1 hour before plating onto LB agar containing 50μg/mL Apramycin.

2.5 Generating CRISPR-BEST gene deletions

2.5.1 Spacer Selection

SnapGene, NCBI BLAST and CRISPy-Web (Blin *et al*, 2016) were used to generate the most suitable small guide RNAs (sgRNAs) for gene deletion of the Leu^{UAA} and Leu^{CAA} tRNAs in *Streptomyces coelicolor*. The 60bp protospacers possessed 20bp belonging to a sequence inside the tRNA of interest and a pair of 20bp overhangs present on the pCRISPR plasmid to allow for accurate annealing. The entire protospacer sequence can be seen below:

CGGTTGGTAGGATCGACGGC-**N20***-GTTTTAGAGCTAGAAATAGC

*-N20 represents the custom 20bp oligonucleotide insert determined by SnapGene and CRISPy-Web.

2.5.2 Plasmid DNA Purification

10 mL overnight cultures of *E. coli* DH5α cells previously transformed with pCRISPR and pSET152 with appropriate antibiotics (Table 2.5.) were purified using the spin column-based New England Biolabs Monarch Plasmid Minipreps Kit (NEB #T1010). The purified DNA was eluted in 50 µL of nuclease free dH2O and the final concentration was measured on the NanoDrop 2000c Spectrophotometer (Thermo Fisher Scientific).

2.5.3 Introduction of sgRNA scaffold and sgRNA insertion confirmation

In accordance with the method outlined by Tong *et al,* to insert the 60bp sgRNA protospacer into the pCRISPR plasmid, a digestion of the pCRISPR plasmid was used (Tong *et al*, 2020). For single-editing purposes, FastDigest NcoI was used in a 20 µL reaction containing the following reagents:

Reagent	Volume (µL)
pCRISPR plasmid DNA	10*
FastDigest NcoI	1
10x FastDigest Buffer	2
ddH_2O	7
Total Volume	20

*800ng of pCRISPR plasmid is typically digested in a reaction, the volume used changed accordingly with the plasmid concentration

The reaction was allowed to incubate at 37°C for 1 hour to allow for adequate digestion of the plasmid contents. After 1 hour had elapsed, the reaction was treated with 1µL FastAP Thermosensitive alkaline phosphatase and incubated for a further 15 minutes. The linearized plasmid was then ran on a 1% agarose gel with 1kb ladder at 90V for 60 minutes to allow for visualisation of the bands using a GelDoc system. The resulting band was gel excised, extracted and quantified using a NanoDrop 2000c spectrophotometer.

To insert the sgRNA protospacer into the linearized pCRISPR plasmid, a 20 µL reaction was prepared with the following reagents:

Reagent	Volume (µL)
Linearized pCRISPR plasmid DNA (30ng/µl)	1*
5uM sgRNA protospacer	5
2x NEB HiFi DNA Assembly Master Mix	10
ddH_2O	4
Total Volume	20

*30ng of linearized pCRISPR plasmid is typically used in the reaction, the volume used changed accordingly with the gel extracted plasmid concentration

The reaction was incubated at 50°C for 1 hour using a BioRad Thermocycler. After sufficient ligation, 5µL of the above reaction was transformed into chemically competent *E.coli* DH5a, according to the process outlined in **Section 2.6.1**, with the resultant recovered bacteria plated onto a selective LB plate containing 50µg/mL apramycin and incubated overnight at 37°C.

Confirmation of successful sgRNA insertion was completed by screening the clones using *E.coli* colony PCR, picking up to 20 *E. coli* colonies from each completed assembly into a 96-well plate containing 200 µL LB broth supplemented with 50 µg/mL apramycin. The picked colonies were incubated at 37°C for 2 hours before 1µL from each culture well was used as template DNA for a colony PCR reaction, using the following reagents:

Reagent	**Volume (µL)**
sgRNA-TEST-F	0.5
sgRNA-TEST-R	0.5
Template DNA	1
2xRedTaq Master Mix	12.5
ddH_2O	11.5
Total Volume	20

Cycle. No	**Denature**	**Anneal**	**Extension**	**Hold**
1	95°C, 2m			
2-34	95°C, 30s	50 °C, 30s	72 °C, 30s	
35			72°C, 5m	
36				4 °C, hold

An aliquot (5µL) of the above reaction was treated with 6x DNA Gel Loading Dye and run on a 3% agarose gel, alongside 100bp ladder. The gel was made up with 1xTBE buffer with Ethidium Bromide acting as a DNA intercalating agent to visualise DNA on a GelDoc system. The gel was run at 100v for 60 minutes and visualised following electrophoresis. Given the difference in the product size is only 20bp, it is difficult to determine a successful insertion at agarose gel percentages lower than 3%. Successful clones were later grown in 10mL of supplemented LB media, miniprepped using the NEB Monarch Miniprep Kit and sent for Sanger sequencing at Eurofins Ltd to confirm the correct insertion sequence.

2.5.4 Amplification of editing templates

To create the desired editing templates upstream and downstream of the RNA of interest, firstly, *S. coelicolor* M145 genomic DNA was extracted in the methods outlined in **Section 2.4.1** via phenol-chloroform extraction. After successful extraction, the genomic DNA was stored at -20°C until further use. Then, NEBuilder, SnapGene and the database StrepDB (http://strepdb.Streptomyces.org.uk) were utilized in tandem to design primers that would amplify 1kb DNA fragments that flanked the RNA of interest, with the ends of each fragment containing 20bp of nucleotide overhang to allow the DNA fragments to successfully anneal to the pCRISPR-Cas9 plasmid (StrepDB, 2025). Using the extracted genomic DNA as a template, the following PCR conditions were used to amplify both 1kb DNA fragments:

Reagent	Volume (µL)
Forward Primer of 1kb DNA fragment (10µg/mL)	1
Reverse Primer of 1kb DNA fragment (10µg/mL)	1
Template DNA	1*
2xRedTaq Master Mix	25
DMSO	1.5 (3% vol/vol)
ddH_2O	20.5
Total Volume	50

*100ng of genomic DNA is typically used in the reaction, the volume of template DNA used changed accordingly with extracted gDNA concentration. Concentrations above 100 µg/mL were diluted to appropriate levels prior to PCR reaction.

Cycle. No	Denature	Anneal	Extension	Hold
1	95°C, 2m			
2-34	95°C, 15s	50 °C*, 30s	72 °C, 30s	
35			72°C, 5m	
36				4 °C, hold

*Annealing temperature calculated using NEBTm calculator

The resultant PCR products were analysed alongside NEB 1kb-Plus Gel Ladder on a 1% agarose gel containing ethidium bromide with 1x TBE buffer. The agarose gels were ran at 90V for 60 minutes before imaging using a GelDoc system. Successful amplification resulted in 1kb bands, which were further excised, extracted and quantified on a NanoDrop 2000c spectrophotometer.

2.5.5 Insertion of amplified homology templates into CRISPR plasmids

Following the amplification, extraction and quantification of the flanking DNA editing templates, the pCRISPR-Cas9 plasmid bearing the already inserted sgRNA was linearized via restriction enzyme digestion. The following reaction was setup for each linearization experiment using the enzyme FastDigest StuI:

Reagent	Volume (µL)
pCRISPR plasmid DNA (200ng/µL)	10*
FastDigest StuI	2
10x FastDigest Buffer	5
ddH_2O	33
Total Volume	50

*Ideally, a total of 2µg of pCRISPR-Cas9 plasmid was used for each reaction. The volume of plasmid DNA was increased or decreased dependant on the concentration of the utilized pCRISPR-Cas9 stock.

The reaction was allowed to incubate at 37°C for 1 hour before the reaction was injected with a further 1µL of FastDigest StuI and 1µL of FastAP Thermosensitive alkaline phosphatease and incubated for a further 15 minutes. The linearized product was analysed on a 1.5% agarose gel with TBE buffer containing ethidium bromide, which was ran at 90V for 60 minutes before visualisation on a GelDoc system. The linearized product was excised, extracted using a gel extraction kit, and quantified using a NanoDrop 2000c spectrophotometer. Gel

purification tended to provide much lower yields than using heat-inactivation on restriction digestion reagents, however StuI is unable to be inactivated by heat, resulting in the reliance on gel extraction to purify linearized pCRISPR-Cas9 plasmids.

Post-linearization, the two flanking 1kb DNA editing fragments were inserted into the linearized product through Gibson assembly, using the NEB HiFi DNA Assembly Master Mix kit. The required volumes of linearized plasmid and editing fragments was calculated using an online calculator, resulting in a required editing template concentration of 8.878ng/μL for each fragment. The following reagents were used as a part of each Gibson Assembly for a 10μL reaction:

Reagent	**Volume (μL)**
Linearized pCRISPR plasmid DNA (30ng/μL)	1*
Purified 1kb upstream DNA fragment (8.878ng/μL)	1
Purified 1kb downstream DNA fragment (8.878ng/μL)	1
2x NEB HiFi DNA Assembly Master Mix	5
ddH_2O	2
Total Volume	10

The combined reaction was gently mixed, centrifuged in a Mini-Centrifuge for 5 seconds and incubated at 50ºC for 60 minutes. Vortexing of the reaction was avoided to prevent DNA shearing. The entirety of the ligated product was transformed into *Escherichia coli* DH5a, using the protocol outlined in **Section 2.6.1**, and grown on LB agar supplemented with 50 μg/mL apramycin at 37ºC for 18-24 hours.

Positive colonies were screened by *E. coli* colony PCR in the same process as outlined in **Section 2.5.3**, using the primer set **StuI-F** and **StuI-R**, which were designed to flank the editing template. Successful insertion of both upstream and downstream flanking DNA fragments would result in an agarose gel band of approx. 2.1kbp. Candidates that successfully

possessed an appropriate gel band on a 1.5% agarose gel were isolated and resuspended into a 25% glycerol stock (vol/vol). Successful candidates were also grown up in 10mL of LB broth supplemented with 50 µg/mL apramycin for 18-24 hours, extracted using the NEB Monarch Minipreps kit and sent for whole plasmid sequencing.

2.5.6 Plasmid Sequencing

Microfuge tubes containing 15 µL of 50 ng/µL plasmid DNA were prepared. The microfuge tubes were then labelled and shipped off via the Plasmidsaurus whole plasmid sequencing service. Sequence results were analysed using the SnapGene® software.

2.6 Transformation of *E. coli* cells

2.6.1 Transformation of *E. coli* DH5α with plasmid DNA.

Aliquots (50 µl) of chemically competent *E. coli* DH5α were thawed on ice before adding 100 ng of plasmid DNA, with which the cells were incubated on ice for 30 minutes. The cells were then heat-shocked for 2 minutes at 42°C and incubated on ice for a further 2 minutes. Subsequently, 950µl of LB broth was added, and the cells were left to recover in a shaking incubator set to 37^{O}C, 250rpm for 60 minutes. 100µl of the incubated cells was plated onto LB plates containing the appropriate antibiotics for selection, and the remaining cells were briefly centrifuged at 16,000 x *g*. The supernatant was removed before resuspending the pellet in 100µl LB broth. Finally, the resuspended pellet was plated on LB agar plates containing the appropriate antibiotics. Plates were incubated for 16-18 hours at 37°C.

2.6.2 Transformation of *E. coli* ET12567/pUZ8002 with plasmid DNA.

Aliquots of chemically competent *E. coli* ET12567/pUZ8002 cells were thawed on ice before the addition of 100ng of plasmid DNA. The *E. coli* cells together with the plasmid were incubated on ice for 30 minutes before being heat-shocked at 42ºC for 2 minutes and subsequently incubated on ice for an additional 2 minutes. 950µl of SOC media was added to the cells, which were left to recover in a shaking incubator set to 37ºC, 250rpm for 3 hours. After recovery, 100µl of the incubated transformed cells was plated onto LB plates containing selection antibiotics, and the remaining 900µl of cells were centrifuged at 16,000 x *g* for 1 minute. The supernatant was removed before resuspending the pellet in 100µl of LB broth, which was then plated to selection LB plates. The LB plates were then incubated for 16-20 hours at 37ºC.

2.7 Conjugation

2.7.1 Conjugation from *E. coli* into *Streptomyces*

To conjugate plasmid DNA from *E. coli* strain ET12567/pUZ8002 into *S. coelicolor* or *S. clavuligerus* strains, overnight cultures of the *E. coli* ET12567/pUZ8002 strains that contain the plasmid desired for conjugation were grown in the presence of the required antibiotics in a shaking incubator, set to 37ºC and 250rpm, for 16-20 hours. From this overnight culture, 4% inoculums were made for each overnight culture and incubated at 37ºC until an OD_{600} of 0.4 was reached. L3M9 agar plates containing 10mM $MgCl_2$ were created, one for each desired conjugation. Once an OD_{600} of 0.4 was reached, the *E. coli* ET12567/pUZ8002 strains were removed from the incubator and centrifuged at 2500 *x g* for 10 minutes to pellet the bacteria. *Streptomyces* spore stocks were taken from -20ºC storage and transferred into sterile 1.5mL microfuge tubes, where they were centrifuged at 16,000 x *g* for 2 minutes. The supernatant was decanted, and this process was repeated until the entire spore stock was successfully pelleted, where it was resuspended into 500 µL of LB broth. The decanted spore stock is then

heat-shocked at 50ºC for 10 minutes and allowed to cool. For *S. coelicolor* conjugations, a total of 500µl of spore stock is utilised, however, which conjugating into *S. clavuligerus*, the entirety of a spore stock is used.

After centrifuging the *E. coli* ET12567/pUZ8002 at 2,700 x *g* for 10 minutes in the Heracus Megafuge 40R, the supernatant was removed and the samples were washed with LB media before being recentrifuged for a further 10 minutes. This process was repeated once more, after which the supernatant was removed, and the pellets were resuspended in 500 µL LB broth. The *E. coli* cells were then mixed with the relevant cooled *Streptomyces* spores and mixed well until the sample was homogenous. The mixed cells were centrifuged at 16,000 x *g* for 2 minutes, after which the supernatant was discarded, and the pellet resuspended in 100 µL of LB broth. The conjugation mix was then transferred from the microfuge tube to L3M9 + 10mM $MgCl_2$ plates and spread with plastic spreads before they were incubated for 16-20 hours at 30ºC.

The following day, the antibiotics needed for selective growth, along with 25 μgmL^{-1} naladixic acid were added to 1mL of sterile distilled water and added to their respective conjugation plates to inhibit the growth of *E. coli* and to select for *Streptomyces* spores that had successfully taken up the desired plasmid. The antibiotic mixture was dispersed evenly across the plates and allowed to seep completely into the agar before being returned to the incubator until visible ex-conjugant colonies were seen (time dependant on *Streptomyces* species, typically 7-10 days).

2.7.2 Intergeneric conjugation from *E. coli* into *Streptomyces bldA*-deficient mutants

Given *bldA* mutants are unable to sporulate, it is not possible to have a spore stock of these mutants available. An alternative method for conjugating from *E. coli* into *Streptomyces bldA*-deficient mutants is to instead use the vegetative mycelia instead of spores. To do this, a lawn

plate of *bldA*-deficient colonies was used. Aliquots (3mL) of 20% glycerol is added directly onto the plate containing *bldA* and dispersed around the plate. An inoculating loop is then used to dislodge the *bldA*-deficient mycelium from the agar plate and into the 20% glycerol solution. Once the *bldA*-deficient colonies across the lawn plate have been successfully dislodged, the colony-glycerol solution is then transferred from the plate into an microfuge tube (a sterilised 20mL syringe containing cotton wool is not used as the mycelia are needed). The microfuge tube containing the *bldA* mycelia is then centrifuged at 16,000 x *g* for 2 minutes and the supernatant is removed. The remaining mycelia is then resuspended in 500μL of LB broth, ready for conjugation with *E. coli* ET12567/pUZ8002. One lawn plate of *Streptomyces bldA* mutant colonies are needed for each conjugation and this step must be performed on the day of the conjugation as *bldA*-deficient mycelium glycerol stocks are not stable. Once the mycelia has been successfully resuspended, the process of conjugation is the same as above (2.2.7), substituting *Streptomyces* spores for the *bldA*-deficient mycelia.

2.8 *Streptomyces* gravimetric cell dry weights

The dry weight of *Streptomyces* cells contained in 1mL of a bacterial culture was determined using gravimetric analysis. Two days before culture harvest, micro glass fibre filter (purchased from Fisherbrand, 1 μm pore size) are dried at 50oC for 48 hours to remove residual moisture. On the day of culture harvest, each filter is weighed using a fine microbalance and the weight is recorded in grams accurate to four decimal places. Then, the grown cells were applied to the appropriate micro glass fibre filter and filtered through a Buchner Funnel (KIF Laboport and NALGENE 180 PVC metric tube, after which each filter is subsequently washed with three volumes of distilled water, to remove residual broth and ensure only bacterial biomass remained. Once all samples had been transferred to micro glass fibre filters, filtered using the Buchner Funnel and washed continuously, the biomass-containing filters were dried at 50°C over a period of 24 hours to remove residual moisture. The biomass for each culture was

determined by subtracting the mass of the filter from the filter containing the biomass (mg/ml). For each culture, this process is performed in technical triplicates.

2.9 Fluorescence Microscopy

A dense *Streptomyce*s spore stock (1-2x10^8 spores/mL) was diluted 1/100 and 5 µL of the diluted stock was inoculated on to MS media under a coverslip inserted at a 45^o angle. Cultures were grown at 30^{o}C for a period of either 24, 48 or 72 hours for *S. coelicolor* cultures and 72 or 168 hours for *S. clavuligerus* cultures. To visualise the bacteria displaying Broccoli-based and mCherry based fluorescence, cover slips were removed from the agar and wiped lightly with 100% methanol to remove excess media to reduce autofluorescence during visualisation. The slides were then coated in 10 µl of 40% glycerol solution as a negative control without the presence of the DFHBI-1T fluorophore to compare Broccoli fluorescence with a culture lacking Broccoli fluorescence. The DFHBI-1T fluorophore was supplied by Scientific Laboratory Supplies (Product Code: SML2697-5MG). For testing Broccoli fluorescence, sample slides were coated in 10 µL of 40% glycerol solution containing 20mM DFHBI-1T. Coated slides were then mounted to a slide and sealed with clear nail varnish.

An Olympus BX50 fluorescence wide field microscope (Olympus, Japan), coupled to a mercury fluorescence lamphouse and power supply (Olympus, Japan) was then used to acquire images of the *Streptomyces* strains. Images were acquired with a 40x UPlan Fluor Ph3 DLL objective lens (Olympus, Japan) at 490 and 617nm respectively. An Orca-100 CCD (Hamamatsu, Japan) camera was used to detect the wavelengths. ImageJ was used to analyse and scale the images. Confocal microscopy was completed using the same conditions, utilizing a Leica SP8 confocal microscope to visualize Broccoli and TTA-mCherry fluorescence using an Argon gas laser at 488nm for Broccoli fluorescence and a diode laser at 561nm for TTA-mCherry fluorescence.

2.10 Broccoli-mCherry construct fluorescence assaying

2.10.1 Quantitative fluorescence assay for visualizing transcription and translation in tandem in *Streptomyces coelicolor*

Cultures of *S. coelicolor* containing the Broccomyces dual-reporter constructs were grown in 50mL of TSB media over a period of 24 hours in a shaking incubator, at 30ºC and 250rpm,. Grown cultures were then transferred from flasks to 50mL falcon tubes and centrifuged at 4,000 x *g* for 10 minutes until pelleted. The supernatant was removed from the falcon tubes and the pelleted bacteria was washed with 20mL of Broccomyces Tris washing buffer (see Table 2-1). The washed cultures were subsequently pelleted and washed a further two times to remove residual TSB broth, before being resuspended in 5mL of Broccomyces Tris washing buffer.

In a black, 96-well plate, 2µL of 200uM 3,5-Difluoro-4-hydroxybenzylidene imidazolinone (DFHBI) fluorophore was added to wells according to a premade plate layout, with 2µL of dimethyl sulfoxide (DMSO) added to neighboring wells to function as a negative fluorophore control for each experiment. Wells containing DFHBI or dimethyl sulfoxide (DMSO) were subsequently loaded with 198µL of specific, resuspended *Streptomyces* culture according to the premade plate layout. After adding *Streptomyces* cultures, the plate was incubated at 30ºC for 15 minutes, to allow for the uptake of the DFHBI compound and sufficient interaction between the Broccoli RNA aptamer and DFHBI fluorophore. Measurements of absorbance (OD_{600}) and fluorescence were performed using a FlexStation 3 plate reader, using the excitation/emission wave lengths of 425/510nm and 590/620nm for Broccoli and TTA-mCherry respectively. For each sample, the measured Broccoli and mCherry fluorescence signals were subsequently normalized to the OD_{600} signal.

2.10.2 96-well plate fluorescence assay for visualizing transcription and translation in tandem in *Streptomyces clavuligerus* over a time course

S. clavuligerus spores containing the Broccomyces constructs were heat-shocked at 50°C for 10 minutes and pregerminated in 10mL of TSB for 48 hours in a shaking incubator at 26°C, 250rpm. After 48 hours had elapsed, the pregerminated cultures were removed from the incubator and standardised to the same optical density at OD_{600}. Then, 5mL of standardised *S. clavuligerus* cultures was transferred into 195ml of TSB and incubated for a further 24hours in a shaking incubator at 26°C, 250rpm.

After 24 hours (and every 24 hours after this point, until 168 hours have accumulated), 20ml of *S. clavuligerus* culture was transferred from their batch cultures into 50mL falcon tubes and centrifuged at 4000 x *g* for 10 minutes until pelleted. The supernatant was removed from the falcon tubes and the pelleted *S. clavuligerus* cultures were washed with 20mL of Broccomyces Tris washing buffer containing 20mg/ml of glucose and 0.5mg/ml of L-glutamine. The washed cultures were subsequently pelleted and washed a further two times to remove residual TSB (which may impact fluorescence readings), before being resuspended in 5ml of Broccomyces Tris washing buffer.

In a black, 96-well plate, 2µL of 500µM DFHBI-1T was added to wells according to a premade plate layout, with 2µL of DMSO added to neighbouring wells as a fluorophore control. Wells containing DFHBI-1T or DMSO were subsequently loaded with 198µL of resuspended *S. clavuligerus* culture to match the premade plate layout. After aliquoting each *S. clavuligerus* culture, the plate was incubated at 26°C for 15 minutes, to allow for the uptake of DFHBI-1T and suitable interaction between the Broccoli RNA aptamer and the DFHBI-1T fluorophore.

Measurements of absorbance (OD_{600}) and fluorescence were performed using a FlexStation 3 plate reader, using the excitation/emission wave lengths of 425/510nm and 590/620nm for Broccoli and TTA-mCherry respectively. For each sample, the measured Broccoli and mCherry fluorescence signals were subsequently normalized to the OD_{600} signal. This process

was repeated every 24 hours over the course of time-course experiments to determine the variation in gene transcription and translation over time.

2.11 *Streptomyces* Specialised Metabolite Yield Assays

2.11.1 Actinorhodin Antibiotic Yield Assay

Initially, 50μL (~1 x 10^7 CFUs) of *Streptomyces* spore stock to 950μL of YEME broth and heat-shocked at 50°C for 10 minutes before being added to 50mL of YEME in an autoclaved baffled conical flask and incubated at 30°C for 48 hours. When using a *bldA*-deficient *Streptomyces* strain, 200μL of suspended mycelia (the equivalent to half of one lawn plate of mycelium growth) was used instead of spores, due to *bldA* deficient *Streptomyces* being incapable of producing spores. In the case of using a *bldA* deficient *Streptomyces*, the heat-shocking step is omitted.

After 48 hours, the flasks were removed from the incubator, and the cultures were transferred into 50mL falcon tubes. The cultures were centrifuged at 4,000 x *g* for 10 minutes until pelleted, after which the supernatant was removed, and the pellet resuspended in 40mL of fresh YEME media. The optical density of each culture is then read at 600nm and recorded. After recording the OD_{600} of each culture is taken, each culture is standardised to an OD_{600} of 1.0, with a total volume of 10mL. 5mL of this standardised culture was then transferred into a new autoclaved baffled flask containing 45mL YEME (for a total volume of 50mL and an OD_{600} of 0.1), which is then incubated in a shaking incubator at 30°C, 250rpm for 120 hours. At this time, preparations are taken to perform gravimetric dry weight analysis on each tested strain (see **Section 2.8**).

Three microfuge tube for each strain was labelled. The *Streptomyces* cultures were removed from the incubator and 1mL of culture was transferred into each microfuge tube. The microfuge tubes were centrifuged at 4000 x *g* for 10 minutes, after which, 100μL of supernatant was added to three wells of a black 96-well plate. To these wells, 100μL of 1M NaOH was added before the plate was gently shaken to ensure mixing of the NaOH and the supernatant. Absorbance measurements of the supernatant/NaOH solution were taken at OD_{633}, using a FlexStation 3 plate reader to determine the amount of actinorhodin present in each well. The concentration of actinorhodin (ACT) in each sample was calculated using the Beer-Lambert Law where A is absorbance, *ε* is the molar extinction coefficient (15,135 at OD_{633} for ACT), C is the concentration of ACT and l is the used light path (2mm):

$$c = \frac{A}{\varepsilon \cdot l}$$

The cell pellet left in each microfuge tube is then used as a technical replicate for gravimetric dry weight analysis (see **Section 2.8**)

2.11.2 Undecylprodigiosin Yield Assay

Sample preparation was carried out in an identical manner to the actinorhodin yield assays (see **Section 2.11.1**), up to and including standardisation to an OD_{600} of 1.0 and inoculation into 50mL of YEME media, resulting in an OD_{600} of 0.1. At this time, preparations are taken to perform gravimetric dry weight analysis on each tested strain (see **Section 2.8**).

On the day of culture harvest, samples were removed from the incubator. For each strain, 1mL of bacterial culture was aliquoted from the flasks into microfuge tubes in triplicate for each sample. The microfuge tubes were centrifuged at 16000 x *g* for 10 minutes and washed with 0.5M HCl twice. After washing, the microfuge tubes were centrifuged once more at 16000 x *g*

for 10 minutes, and the undecylprodigiosin (RED) was extracted from the pellets by adding 0.5M HCL-Methanol. The extracted samples were incubated at 30°C for 2 hours to ensure adequate RED extraction. After incubation, the samples were centrifuged again at 16000 x *g* at 10 minutes, to pellet cell debris. 200µL of supernatant was taken from each microfuge tube and added to the well of a black 96-well plate. 200µL of 0.5M HCL-Methanol was used as a negative control for absence of RED. The complete 96-well plate was measured using a FlexStation 3 plate reader, with the absorbance for each well read at 530nm. The concentration of RED in each sample was calculated using the Beer-Lambert Law where A is absorbance, E is the molar extinction coefficient (100,500 at OD_{530} for RED), C is the concentration of RED and l is the used light path (2mm).

$$c = \frac{A}{\varepsilon \cdot l}$$

The cell pellet left in each microfuge tube is then used as a technical replicate for gravimetric dry weight analysis (see **Section 2.8**)

2.12 Carbon and Nitrogen utilisation assay in *Streptomyces*

The spores of a *Streptomyces coelicolor* colony were picked and spread onto LB agar and incubated at 30°C for two days, during the period vegetative mycelium production begins but before the growth of aerial hyphae. For *S. coelicolor* colonies exhibiting a bald phenotype, the vegetative mycelium was used in place of spores. After two days incubation, the plates were removed, and the grown cells were harvested. The harvested cells were then transferred into 20mL minimal BioLog™ inoculating fluid (IF-0a), until an optical density (OD_{600}) of 0.04 was reached (BioLog, 2025). BioLog™ Redox Dye C (200µL) was added to the inoculated BioLog™ media to visualize respiration, which is used to quantify growth.

The inoculated media was then transferred into two BioLog™ Phenotype MicroArray plates: PM1 (for carbon utilization) and PM3b (for nitrogen utilization). For PM1 plates, the inoculated IF-0a fluid, containing Redox Dye C, were added straight to each well. For PM3b plates, each well was supplemented with 20mM glucose to function as a carbon source. A total of 100µL of inoculated media was transferred into each well of each Phenotype MicroArray plate. The inoculated plates were then placed into a BioLog™ OmniLog PM system, set to incubate at 30ºC. The BioLog™ OmniLog PM system imaged each well every 15 minutes using a CCD-based camera. Colour change, resulting from NADH production and reduction of Redox Dye C, was captured over time. Both PM1 and PM3b plates were incubated in the BioLog™ OmniLog for 80 hours.

After incubation, each image is saved on the BioLog™ OmniLog system as a D5E file. These files were taken from the BioLog™ OmniLog and converted into OKA files, using the GUI software D5e_OKA Data File Converted (v1.1.1.15). The raw kinetic data from each OKA file was extracted using the OPM analysis software Kinetic (v1.3). This raw kinetic data could then be assembled into an MicroSoft Excel file, in .csv format, with one .csv for each tested strain/condition combination. The subsequent scripts used for data melting, data visualization and figure generation can be found in **Appendix 6**, along with their versions utilized for this study.

2.13 Bioinformatics

2.13.1 Whole Genome Sequencing Analysis

All whole genome sequencing carried out for the duration of this project was performed using the Illumina NovaSeq 6000 platform. *Streptomyces coelicolor* J1700 and *Streptomyces coelicolor* M145 *ΔbldA*-JWS whole genome sequencing analysis was performed using the BioConda environment, utilizing the *breseq* (v0.38.3) pipeline, by comparing the trimmed, paired end reads from the sequencing data to the closed *S. coelicolor* A3(2) genome reference obtained from NCBI under the genome assembly

ASM20383v1. The *breseq* package is a computational pipeline of software comparing whole genome sequencing data to an inputted reference genome, utilizing published software including Bowtie2 (v2.5.4) (Langmead and Salzberg, 2012), samtools (v1.20) and R (v4.4.0), using the output of one step as the input for the subsequent step. The final output of the *breseq* pipeline is a compare.html file that complies a list of evidenced mutations from inputted data. *Streptomyces coelicolor* J1700 and *Streptomyces coelicolor* M145 *ΔbldA* JWS sequencing data was analysed and compared to the reference genome *Streptomyces coelicolor* M145 with *breseq* using the following commands in command line, following the installation of the *breseq* pipeline using BioConda:

--conda breseq activate

breseq --polymorphism-prediction --num-processors 4 -r reference.gbk reads1.fastq reads2.fastq -output folder/directory

gdtools COMPARE -o compare.html -r reference.gbk input1.gd input2.gd

2.13.2 Determining Leucine codon frequency in *S. coelicolor*

The frequency of each leucine codon throughout each coding sequence in the *S. coelicolor* genome was determined using Python script (v3.11.5). The script used for this experiment can be found in **Appendix 6**.

2.13.3 RNA-sequencing analysis

Initially, RNA read counts were quantified using Salmon (v1.10.1), within the bioconda environment in Terminal (Patro *et al*, 2017). Differential expression analysis was performed using the DESeq2 package (v1.45.0) (Love *et al*, 2014). Normalization, dispersion estimation, and statistical testing were carried out following the standard DESeq2 pipeline to identify

differentially expressed genes (DEGs) between experimental groups. The DEGs were exported into a .csv, which was further used for functional analysis within R (v4.5.0).

All scripts, including R code for figure generation are provided within **Appendix 6**.

2.14 Software and Data Processing

All plotted graphs were created using GraphPad Prism (v8.0.2) (Graphpad Software, USA), unless specified otherwise. Initial analysis from data generated for the *Streptomyces coelicolor* and *Streptomyces clavuligerus* 96-well plate Broccomyces dual-reporter assay was performed in Microsoft Excel, whereas GraphPad Prism v8.0.2 was used to determine mean, standard deviation and standard error of the mean, as well as for producing graphs seen in this body of work. *Streptomyces coelicolor* dual-reporter assays, *Streptomyces clavuligerus* dual-reporter assays, as well as actinorhodin and undecylprodigiosin yield experiments were performed using the FlexStation3 platform, which utilised the SoftMax Pro 7 Microplate Data Acquisition software.

2.15 Statistics

All experiments were repeated at least three times, unless otherwise specified. When curves such as growth kinetic curves were required, the mean Cell Dry Weight (CDW) was plotted. Graphpad Prism v8.0.2 (GraphPad Software, USA) was used for all statistical data analysis and plot construction. A Kruskal-Wallis with Welch's correction was used for statistical analysis for all experiments, unless otherwise specified. Unpaired Student t-tests are used for comparison of two independent groups, where data is normally distributed with equal variances, whereas Welch's correction allows comparison of datasets with unequal variances and utilised to minimize false positive results.

For WGS and RNA-seq data analysis, Bayesian approaches integrated in the BioConda *breseq* and DESeq2 packages were used (Deatherage and Barrick, 2014). Bayesian statistics

use probabilities to infer event chances at being significant or not. This allows to account for differences in sampling sizes and provides a more robust analysis when compared to standard Student's t-tests and ANOVAs. A p <0.05 was considered significant for all tests to enable rejection of the null hypothesis.

Chapter 3: Design and Development of a dual transcription and translation reporter system in *Streptomyces coelicolor*

3.1 Introduction

In bacteria, control of gene expression occurs mainly at the levels of transcription and translation (McGary and Nudler, 2013). The mechanisms of control can be multilayered, complex and are often tightly regulated (Bervoets and Charlier, 2019). Gene expression in *Streptomyces* is no exception to this and can also be controlled at the level of transcription and translation. Many factors control gene expression with cells integrating a number of signals to control both transcription and translation to ensure appropriate temporal and spatial gene expression (Romeo *et al*, 2013). In *Streptomyces* the control of gene expression of a number of genes integral to development and specialised metabolite production are thought to be influenced by the availability of the rare Leucine $tRNA^{UAA}$ (*bldA*) (Takano *et al*, 2003). This tRNA is expressed at low levels early in the life cycle and is thought to be repressed by the global regulator *bldD* (den Hengst *et al*, 2010). The presence of *bldD* decreases at later stages of the *S. coelicolor* growth cycle, resulting in increased expression of *bldA* (Elliot *et al*, 2001, Yan *et al*, 2019). Many of the genes containing TTA codons are found in morphologically important genes or genes relating to specialised metabolite production, including clinically important antibiotics (Li *et al*, 2007). The presence of a TTA codon in an open reading frame is thought to act as an additional regulatory switch, preventing translation of specific genes when *bldA* levels are low, with expression increasing at specific stages in the lifecycle.

In the absence of the *bldA*-encoded tRNA, translation of genes containing TTA codons can be interrupted, hindering protein synthesis (Hou *et al*, 2018, Huang *et al*, 2022). This translational dependency creates a selective mechanism for controlling protein expression in a growth-phase-dependent manner (Kataoka *et al*, 1999). The tight control of *bldD* over the presence of *bldA* ensures morphological development (ie: the production of aerial hyphae and

sporulation) and metabolite production occurs at specific points in the life cycle of *Streptomyces* (Den Hengst *et al*, 2010).

Given the regulatory significance of TTA codons in *Streptomyces* gene regulation, it was hypothesised that an orthogonal reporter system could be designed to temporally and spatially visualize and quantify TTA-dependent gene expression at the level of transcription and translation.

To accomplish this, a dual-reporter system was designed. The transcriptional reporter in the proposed dual-reporter system is the Broccoli aptamer, an RNA-based fluorescent marker that binds to a specific fluorophore, where the aptamer-ligand complex produces green fluorescence (Filonov *et al*, 2014). Since its fluorescence directly correlates with RNA abundance, Broccoli serves as a transcriptional readout for promoter activity. This system does not require translation to deliver a readout, unlike many other promoter-reporter systems. The translation reporter in the system is based on mCherry, a widely used red fluorescent protein known for its high photostability and strong red fluorescence emission (Shaner *et al*, 2004). To date Broccoli has not been used in *Streptomyces* and would represent a step-forward in the development of tools for these organisms.

To establish a direct link between transcriptional activity and translational efficiency, it is essential to design a system where both reporter signals can be independently quantified. By placing the Broccoli aptamer under the control of native *Streptomyces* promoters, fluorescence output would provide a transcriptional snapshot, dependant on the activity of the promoter used. However, since transcription does not always directly equate to protein synthesis due to regulatory mechanisms such as attenuation, tRNA availability, sRNAs (Duval *et al*, 2015), incorporating mCherry as a translational reporter, would allow visualisation of protein production in the same system.

To ensure mCherry fluorescence is TTA-codon dependant and would reflect translational efficiency based on the availability of the *bldA* tRNA, the coding sequence was altered to substitute a TTA codon into mCherry, where fluorescence would rely on the availability Leu-tRNA^{UAA} is available. Combining these two reporter systems in to an orthogonal dual-reporter system would enable a better understanding of coordination of gene expression control by *bldA* through quantification of fluorescence at both the transcriptional and translational levels in *S. coelicolor*. Here, the design of an orthogonal dual-reporter system is described, which employs the fluorescent Broccoli RNA aptamer and a TTA codon-containing mCherry fluorescent protein variant. This system will be evaluated for performance in *Streptomyces* and will be used to evaluate the transcriptional and translational output of *S. coelicolor*, while under the control of constitutive and developmentally regulated promoters.

3.2 Aims of this chapter

The aims of this chapter is to design an orthogonal dual-reporter system for measuring transcription and translation of *Streptomyces* genes based on their promoters in tandem. Following the design of this dual-reporter, the impacts of the orthogonal dual-reporter system on morphology and growth rate of *S. coelicolor* will be explored and the functionality of the orthogonal dual-reporter system will be determined through fluorescent microscopy and whether the dual-reporter can be used for temporal and spatial visualisation of transcription and translation. The use of this dual-reporter system will then be optimised for use in a 96-well plate fluorescence-based assay to quantify transcriptional and translation output based on *S. coelicolor* expression from different promoters.

3.3 Results

3.3.1 The creation of Broccomyces: a dual reporter utilizing RNA aptamers and fluorescent proteins

To design an integrated synthetic transcription/translation imaging system for *Streptomyces*, it was hypothesised that the incorporation of the Broccoli aptamer into a vector containing the mCherry fluorescent reporter would create an orthogonal system for visualising transcription/translation with two colours reading out different cellular processes (**Fig 3.1**). The rational for this system is that it can be coupled to any promoter to investigate transcriptional and translational control and can be used to investigate spatial localization of these processes within specific tissues of *Streptomyces* (vegetative & aerial mycelium or spores) and temporal expression.

Considerations for the synthetic transcription/translation imaging system:

The proposed system, 'Broccomyces ', should be delivered in single copy on a widely used and well characterised vector. The control of transcription should be driven from well-characterised promoters, have a quantifiable 'read-out' and the translation of the mCherry couple potentially be made as a translational fusion protein, with any protein of interest. The use of mCherry could also have an additional control point, for example exploiting the *bldA* mediated translational control of genes through the inclusion of a TTA codon. Testing this system should use a constitutive promoter (*ermE**) and a promoter that controls expression of TTA codon containing genes or *bldA (*for example *bldD*) (Bibb *et al,* 1985, Den Hengst *et al*, 2010).

RNA is a dynamic molecule and is able to fold in to range of structures, these structures can be catalytic, bind small molecules or and act as sensors (Ouellet, 2016). These binding capabilities have been exploited as aptamers, for a range of applications. The 'vegetable fluorogenic aptamer' systems (Broccoli, Spinach etc) in combination with fluorescent proteins

to develop synthetic genetic probes that allow us to investigate and image gene expression (Ouellet, 2016). These fluorogenic aptamers are RNA equivalents of green fluorescent protein (GFP), which form a fluorescent RNA aptamer-ligand complex when bound with 3,5-difluoro-4-hydroxybenzylidene imidazolinone (DFHBI), enabling the direct imaging of RNA processes in live cells (e.g., transcription, localisation, and degradation). DFHBI and a -CH_3 derivative (DFHBI-1T) are commercially available fluorophores.

Ideally the system containing the Broccoli aptamer will be in a genetic construct that integrates into the genome (such as on a widely used integrating vector e.g. pSET152). This can be placed downstream of promoters and would represent an advantage over traditional reporter systems (ß-galactosidase, GFP etc) as there is no need for translation to occur to measure reporter activity, providing a direct readout of the RNA of interest. One issue that has arisen in the literature is the stability of the Broccoli RNA, and its susceptibility to endonucleases. This has been overcome through the use of RNA scaffolds such as the F30 scaffold from *E. coli* (Filonov *et al*, 2015) and as such should be included in any construct. Moreover, to increase the suitability of the RNA for parallel assays, incorporation of a catalytic (hammerhead) ribozyme (HHR) into the system would allow cleavage of the fluorophore binding portion of the aptamer and scaffold to yield an identical fluorescent molecule, regardless of the promoter or length of transcript. (Höfer *et al*, 2013)

Engineering a TTA codon into the mCherry gene would enable the control of mCherry translation to be governed by the availability of the *bldA*-tRNA and *bldA* expression. The expression of *bldA* is regulated by BldD in an unusual mechanism. Traditionally, the BldD dimer binds upstream of the protein sequence to prevent gene transcription, whereas for the *bldA* tRNA, the BldD dimers binds directly to the genomic sequence encoding the primary transcript of the tRNA (den Hengst *et al*, 2010). BldD is the master repressor of development in *Streptomyces,* where during vegetative growth, high levels of cyclic-di-GMP results in the formation of BldD dimers that block expression of a large regulon of genes, including a number of genes containing TTA codons (Gallagher *et al*, 2024). Amongst the best understood TTA

containing gene is the cluster situated regulator for the blue-pigmented antibiotic actinorhodin. The gene *act*II-ORF4 possesses the rare leucine-TTA codon starting at nucleotide 15 in the gene, which is believed to control translation of this regulator, ultimately controlling actinorhodin biosynthesis (Fernández-Moreno *et al*, 1991). There is an isoleucine encoded in mCherry starting at nucleotide position 34 (AUC codon), substitution of this codon with TTA for leucine would represent a conservative amino acid substitution with a similar aliphatic amino acid. This would also place the TTA codon prior to the fluorophore in mCherry eliminating any potential partial fluorophore folding. The remainder of the mCherry gene was also codon optimised for *Streptomyces* and checked for any other potential TTA codons.

Using this rational, a Broccoli/mCherry construct was designed that had a promoter driving expression of a HHR, Broccoli (including an F30 scaffold), a ribosome binding site (for efficient translation, derived from *ermE*) and a TTA codon containing mCherry gene (**Fig 3.2**). The construct was created in two forms, one with an *ermE*p* and one with *bldDp* promoter driving expression. The constructs were synthesised by Genscript cloned into the integrating vector pSET152. This vector contains a phiC31 integration site, an apramycin resistance gene and an *oriT* to facilitate conjugation into *Streptomyces* from *E. coli* with the from the ET12567 strain containing the helper plasmid pUZ8002 (Larcombe *et al*, 2024).

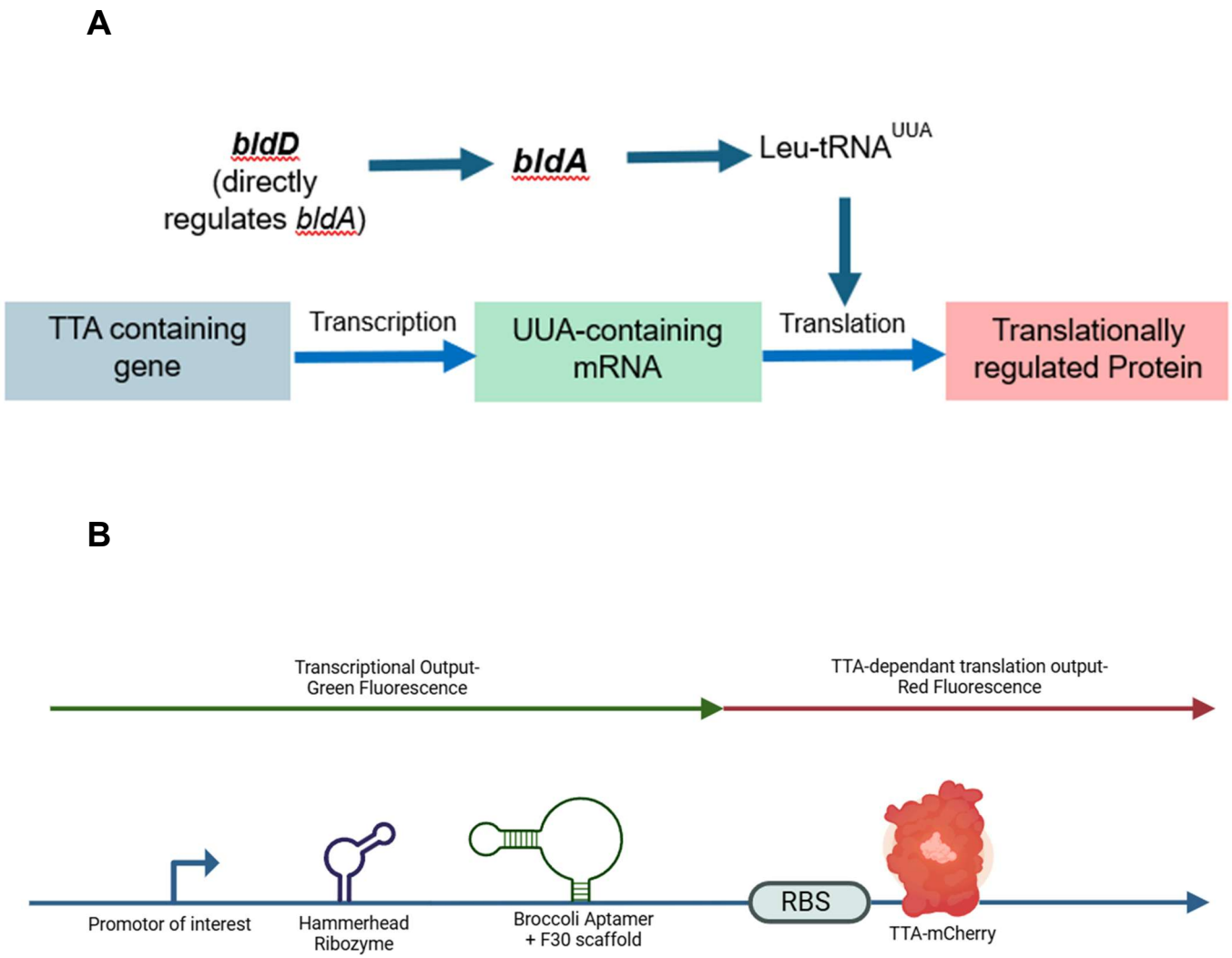

Fig. 3.1: Rationale behind the Broccomyces reporter system in *Streptomyces*. (A) Regulation of TTA-containing genes in *Streptomyces* through *bldA*-dependent translation. When *bldA* expression is low, translation of TTA-containing proteins is restricted, reducing gene expression. **B: Design of a novel fluorescence-based reporter system for TTA codon-dependent transcription and translation.** Transcriptional output is governed by Broccoli-DFHBI fluorescence output while translational output is measured through a modified mCherry, containing a TTA codon, ensuring *bldA* dependent translation of mCherry. Abbreivations: RBS- Ribozyme Binding Site. Created using Biorender (Biorender, 2025)

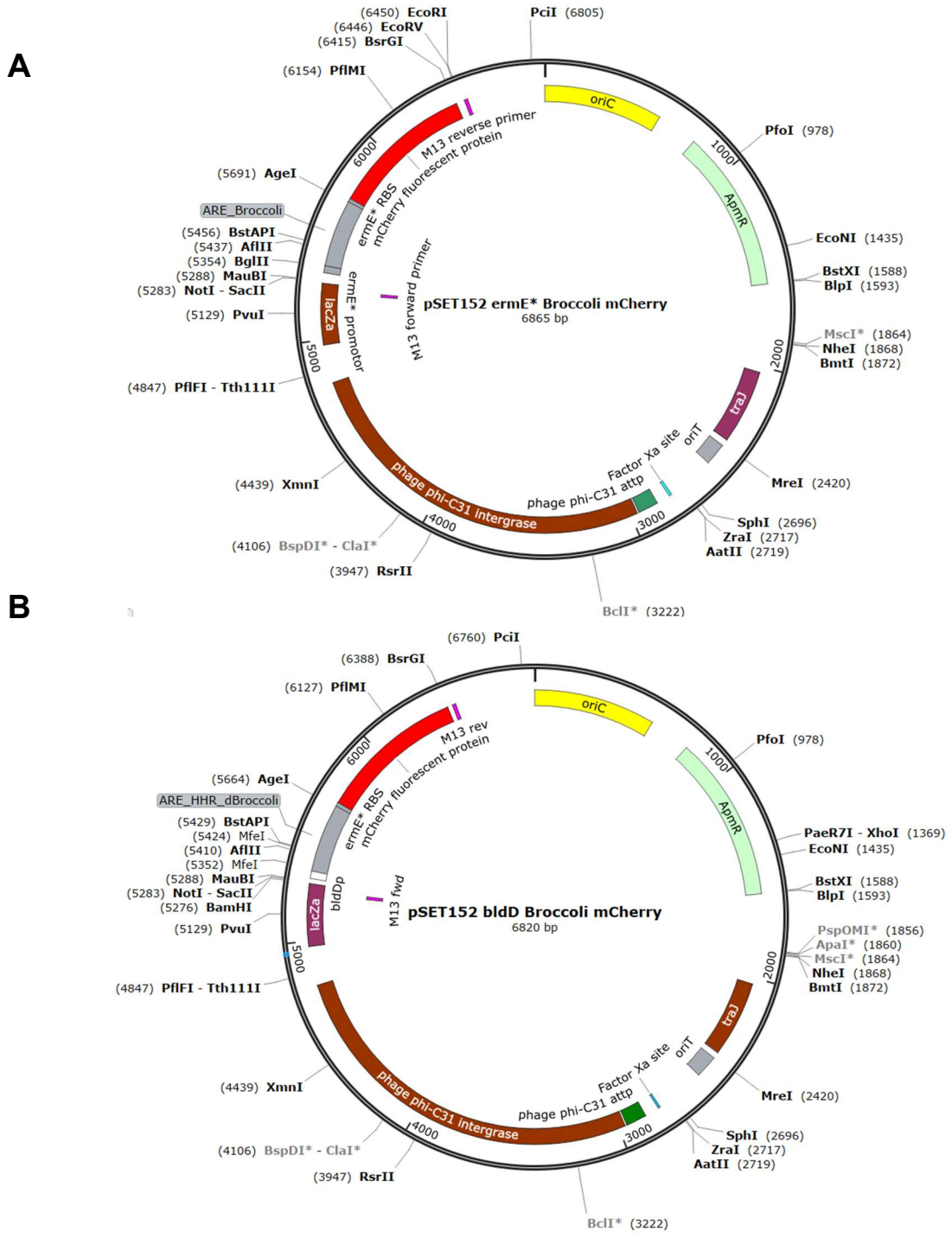

Fig. 3.2: Plasmid constructs for fluorescence-based transcriptional and translational reporter assays in *Streptomyces*. Schematic representation of the Broccomyces fluorescent reporter, designed to assess transcriptional and translational activity under different regulatory conditions. The Broccomyces reporter construct is placed under the control of either a constitutively expressed (*ermE**) (**Fig 3.2A**) or a developmentally regulated (*bldD*) (**Fig3.2B**) promoter. Plasmids synthesized by GenScript.

3.3.2 Broccomyces plasmids do not affect growth of *Streptomyces* strains

Following construction of the TTA codon-dependent transcription-translation quantification system under the control of the *ermE** and *bldD* promoters (henceforth referred to as 'Broccomyces-*ermE*p* and Broccomyces-*bldDp* respectively '), the next step was to assess if the Broccomyces plasmids affect *Streptomyces coelicolor* growth. First, the effects of the Broccomyces plasmids on *Streptomyces* colony morphology were investigated, followed by growth assays over a period of 72 hours in TSB media. This method was chosen over the widely used Optical Density measurement, most commonly used to measure bacterial growth over time, as organisms exhibiting mycelial growth (such as *Streptomyces*) produce erroneous results using this method (Hobbs et al., 1989). Primarily, this data was used to determine at which point the stationary phase of the growth cycle was reached and for specific growth rate calculations, to measure potential growth impacts following Broccomyces plasmid conjugation. An empty vector control, containing the pSET152 vector alone, was used to elucidate whether the presence of pSET152 alone impacted *S. coelicolor* growth.

Results of these experiments (**Fig. 3.3, Fig. 3.4)** show that the presence of the Broccomyces plasmids have negligible effects on *Streptomyces* colony morphology. The presence of the plasmids was confirmed in each strain by PCR using the Broccomyces check primers (primer numbers 1 and 2) (**Fig. 3.3A).** The integration of each of these vectors (**Fig. 3.3B)** has no effect on the morphological development of *S. coelicolor* colonies.

Next, the effect of the Broccomyces plasmids on overall growth of the strains was determined. *S. coelicolor* M145 reaches stationary phase of growth after ~32 hours (**Fig. 3.4)**. Analysis of the cell dry weight measurements shows that the presence of all plasmids had minimal impact on growth phase transition or specific growth rate, with all four strains reaching stationary phase at the same time and exhibiting similar growth rates. Given this, the constructs were deemed to be suitable for further investigation to determine if the fluorophores are active, via fluorescence microscopy and if the expression is localised in terms of the Broccoli and mCherry reporters within the *Streptomyces* mycelia.

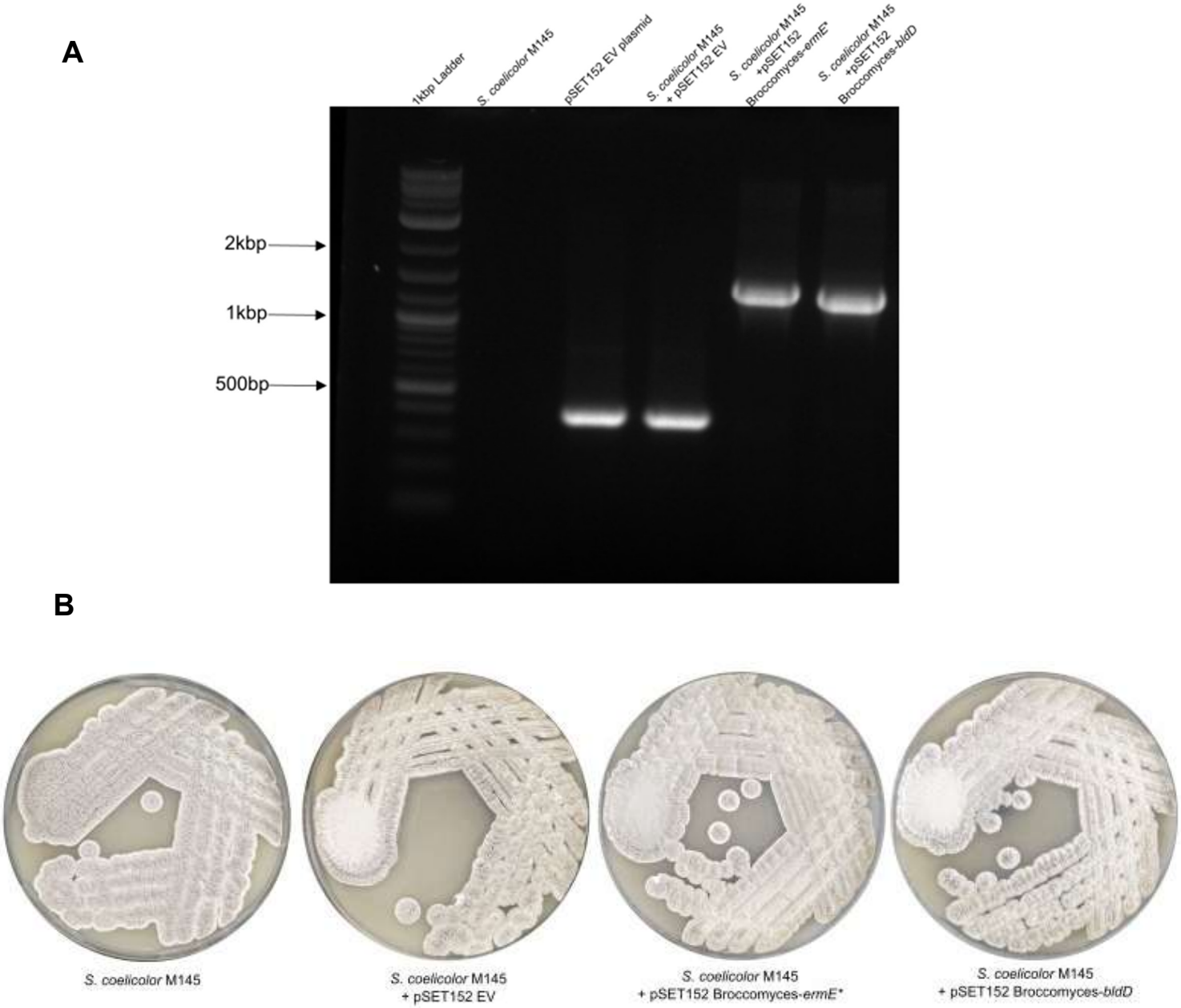

Fig. 3.3: Amplification and phenotypic comparison of Broccomyces cassettes in *S. coelicolor* M145. A) WT and transconjugant *S. coelicolor* genomic DNA was used to amplify pSET152 Broccomyces, resulting in 410bp amplicons for the empty vector plasmid and EV transconjugant and 1.5kbp amplicons for the Broccomyces-*ermE*p* and Broccomyces-*bldDp*. *S. coelicolor* M145 genomic DNA was used as a negative control for no plasmid conjugation. **B)** Phenotypic comparisons of WT-*S. coelicolor* M145 and Broccomyces transconjugants on MS plates grown at 30^{o}C for 7 days.

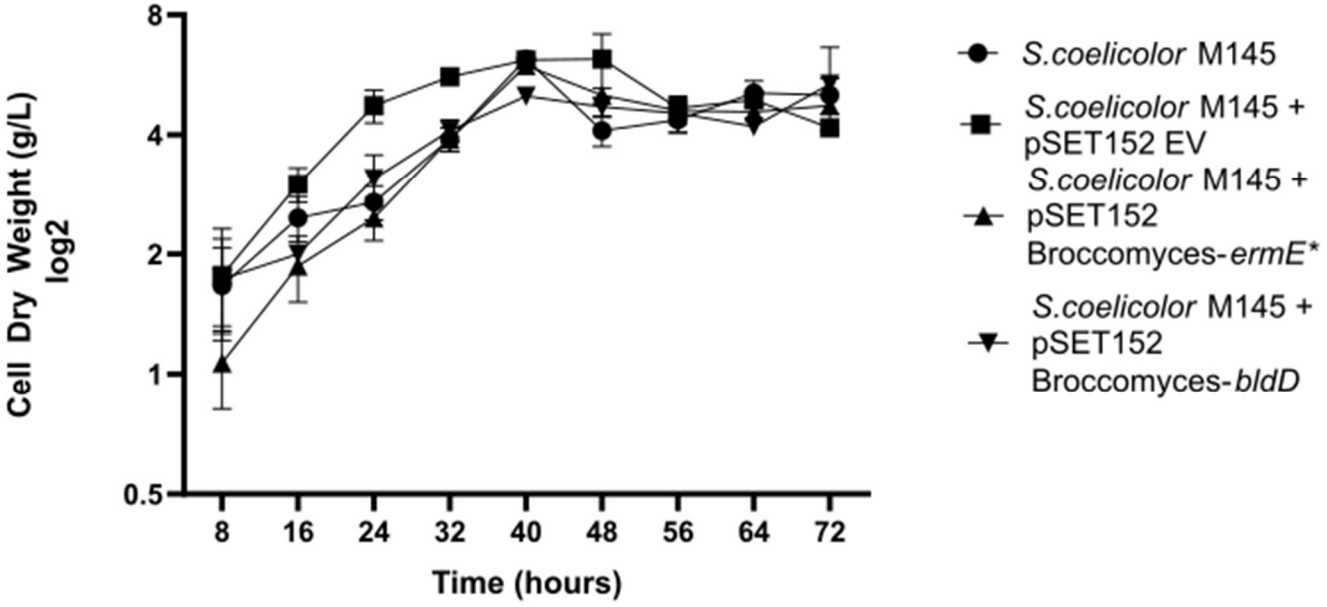

Strain	Specific Growth Rate (h^{-1})
S. coelicolor M145	0.057
S. coelicolor M145 + pSET152 EV	0.057
S. coelicolor M145 + pSET152 Broccomyces-*ermE*p*	0.053
S. coelicolor M145 + pSET152 Broccomyces-*bldDp*	0.054

Fig. 3.4: Growth of WT and Broccomyces strains in liquid culture over a period of 72 hours. Strains were measured in biological triplicates and cell dry weight (g) was used as an indicator of growth. Error bars represent the mean with standard deviation. Specific growth rates between strains shows minimal differences in growth rate, regardless of plasmid presence.

3.3.3 Fluorescent Microscopy highlights Broccoli aptamers viability in *Streptomyces*

Streptomyces coelicolor strains containing the Broccomyces construct plasmids, under the control of the *ermE** and *bldD* promoters were examined by fluorescence microscopy to determine the functionality of the Broccoli aptamer and mCherry fluorescent protein in *Streptomyces*. This approach would also allow us to determine the levels of visual fluorescence produced by either construct when driven from a constitutive promoter (*ermE*p*) and a developmentally regulated promoter (*bldDp*).

Sterilized glass cover slips were inserted into MS agar plates at a 45-degree angle, where diluted spores of *S. coelicolor* M145 Broccomyces-*ermE*p* and *S. coelicolor* M145 Broccomyces-*bldDp* were added to the point of intersection between the agar and the cover slip. *S. coelicolor* M145 lacking the fluorescent construct was utilised as a negative control for the experiments, as it should not produce fluorescence. The plates were incubated at 30ºC for 72 hours before removing the cover slips carefully from the agar to not disturb the specimens. Due to the hydrophobic nature of the aerial hyphae *Streptomyces* hyphae adhere to the cover slip.

The coverslips containing the specimens were laid across a flat surface with the growth facing downwards, where 40 µM DFHBI or 40 µM DFHBI-1T was added in 10 % (v/v) glycerol solution to the cover slip to facilitate Broccoli fluorescence. The coverslip was then mounted to a glass microscopy slide using nail varnish. Microscope slides were imaged using an Olympus Fluorescent microscope, measuring 70% gain and an exposure time of 600ms for both Broccoli and mCherry fluorescent measurement to allow normalisation of the fluorescence across images. Fluorescence measurements were obtained through removing the background fluorescence from samples where no fluorophore was added. Obtained images were analysed using the program Fiji ImageJ.

The fluorescence images indicate that the Broccoli aptamer is expressed in *Streptomyces* and is functional in the presence of the DFHBI fluorophore (**Fig. 3.5, Fig. 3.6, Fig. 3.7**). The reporter system yielded detectable fluorescence in a *Streptomyces* background when driven by both the *ermE** and *bldD* promoters when compared to the negative control, indicating potential for further fluorescence experiments (**Fig. 3.6 & Fig. 3.7**). At 24- and 48- hours of incubation on MS agar, both Broccoli and TTA-mCherry derived fluorescence seen in the Broccomyces-*bldDp* construct was higher than the fluorescence seen in the *ermE*p* construct, whereas at 72 hours, Broccomyces-*bldDp* fluorescence for both Broccoli and TTA-mCherry was lower than Broccomyces-*ermE*p*.

The *ermE** promoter is constitutively expressed in *Streptomyces* (Wang *et al*, 2013, Li *et al*, 2015) and fluorescence (Broccoli and TTA-mCherry) was observed in strains carrying this construct at all time points. Given the genetic background (*S. coelicolor* M145) is *bldA*$^{+}$*,* both strains possess the ability to translate the UUA codon in a developmentally regulated manner. Remarkably, TTA-mCherry was visible in *S. coelicolor* M145 prior to the initiation of development (24 hours). This fluorescence of TTA-mCherry demonstrates that the TTA codon in the synthetic TTA-mCherry gene is being translated even in the absence of the *bldA*-tRNA, which is expressed during the development of *Streptomyces* (Leskiw *et al*, 1993). This is contrary to what the literature suggests – TTA codons are not translated until late in growth.

While TTA-mCherry fluorescence in the *ermE** construct remains consistent at all time points, TTA-mCherry fluorescence in the Broccomyces-*bldDp* construct is barely visible at 72 hours. This reduced fluorescence is likely due to the *bldD* promoter having reduced activity later in the growth cycle (Elliot *et al*, 1998, Yan *et al*, 2019).

There is no current literature highlighting the use of the Broccoli aptamer in a *Streptomyces* background, with limited reports demonstrating functionality in high GC, Gram-positive bacteria (Bychenko *et al*, 2020, Jensen *et al*, 2023). Much of the previously established literature concerning the utilisation of the Broccoli aptamer is in Gram-negative bacteria and mammalian cells (Filonov and Jaffery, 2015, Okuda *et al,* 2017 Climent-Catala *et al*, 2023).

While the use of mCherry in *Streptomyces* species is well-documented (Thoma *et al*, 2016., Hamed *et al*, 2018, Kerr and Hoskisson, 2019), these data provide novel insights into translation of TTA codon containing genes and the potential of Broccoli aptamers *Streptomyces*. To further characterise the use of the Broccomyces vectors a high-throughput fluorescence quantification assay for *Streptomyces* was developed.

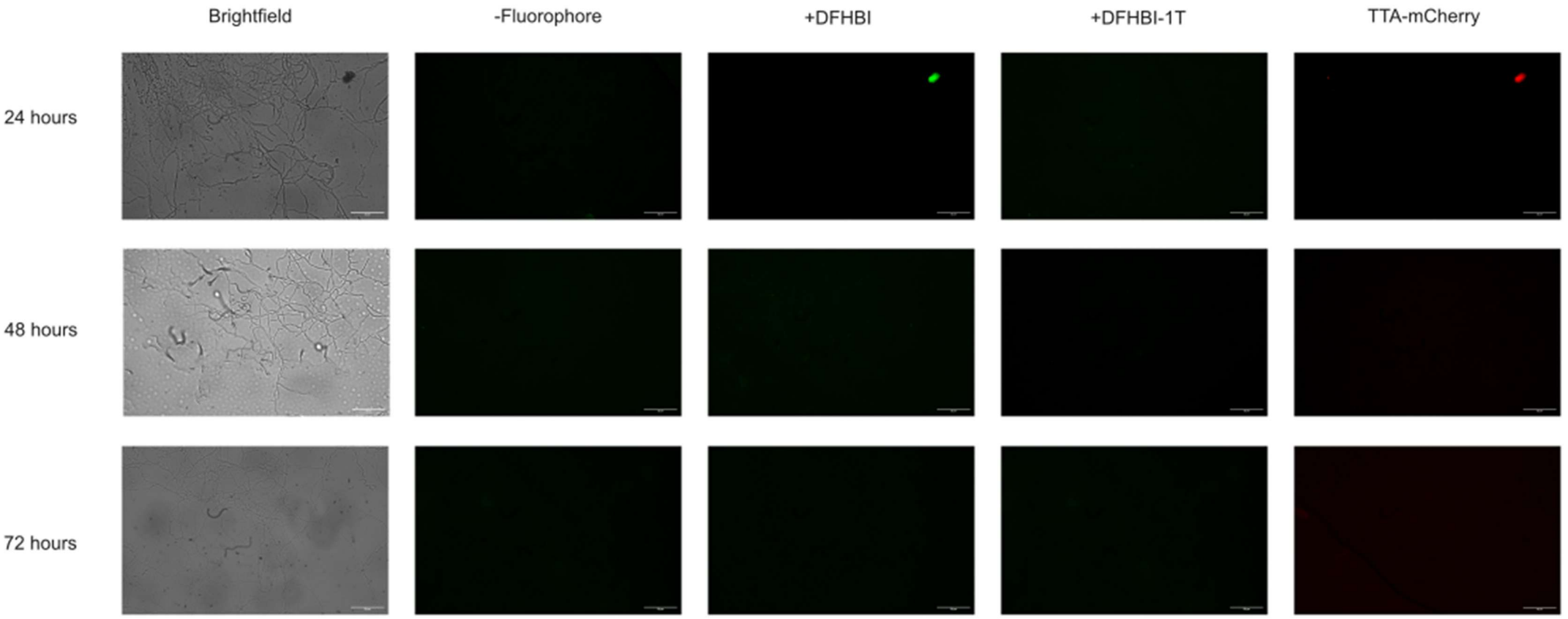

Figure 3.5: Brightfield and fluorescence microscopy of wild-type *S. coelicolor* M145 with and without DFHBI-derived fluorophores over 72 hours. Microscopy images show WT-M145 at 24, 48 and 72 hours, imaged with DFHBI, DFHBI-1T, without either fluorophore and Brightfield. The WT strain exhibits minimal Broccoli or mCherry fluorescence, serving as a negative control for determining signal specificity. Signal detected at 24 hours attributable to residual agar on cover slip. Scale bar= 25 μm

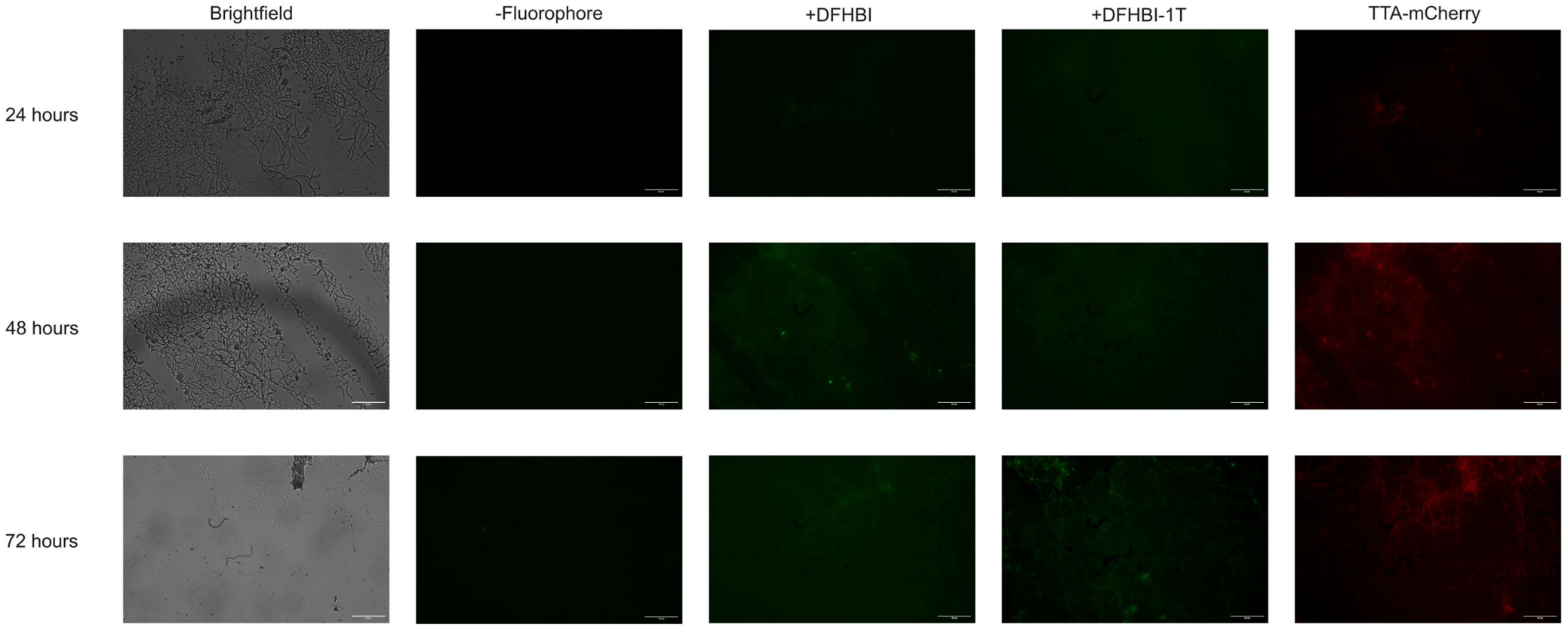

Fig. 3.6: Time course fluorescence imaging of *S. coelicolor* M145 + pSET152 Broccomyces-*ermE*p* in the presence and absence of aptamer fluorophores. Fluorescence and Brightfield microscopy of *S. coelicolor* + pSET152 Broccomyces-*ermE*p*, imaged at 24, 48 and 72 hours. Broccoli and mCherry fluorescence is detectable under both DFHBI and DFHBI-1T when compared to -fluorophore control, with signal increasing over time, consistent with constitutive promoter expression. The absence of fluorophore condition is included to show minimal background signal. Scale bar= 25 µm.

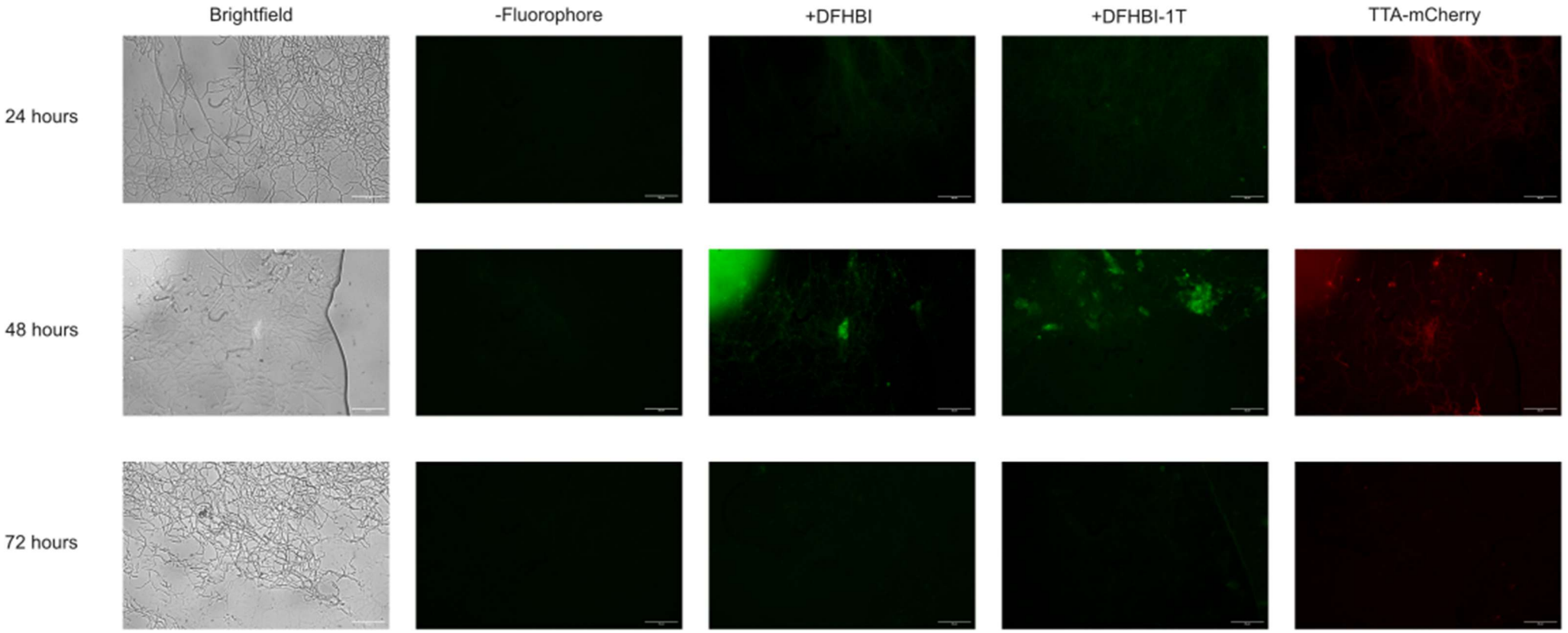

Fig. 3.7: Brightfield and Fluorescence microscopy of *S. coelicolor* M145 + pSET152 Broccomyces-*bldDp* over time under fluorophore-induced conditions. Images show Broccoli-Fluorophore (green), TTA-mCherry (red) and Brightfield light at 24, 48 and 72 hours respectively. Strong TTA-mCherry signal is detected at 24 and 48 hours, while reducing to background levels at 72 hours, consistent with developmentally regulated promoter data. Minimal fluorescence was detected in the -fluorophore control. Scale bar= 25 μm

3.3.4 Development of a 96-well plate assay to measure transcription and translation in tandem

Given that the orthogonal tandem Broccoli aptamer and TTA-mCherry transcription/translation reporter system functions in *S. coelicolor,* a more scalable method for fluorescence quantification was designed. While microscopy provided qualitative information, it is difficult to infer fluorescence quantification in multiple samples simultaneously. Therefore, it was determined that a high-throughput approach was needed to enable rapid, quantitative comparisons across multiple conditions, backgrounds and replicates. This required the design and optimisation of a 96-well plate–based fluorescence assay capable of simultaneously measuring Broccoli and TTA-mCherry fluorescent outputs from samples in liquid culture.

The design of the 96-well plate–based fluorescence assay aimed to balance sensitivity, reproducibility, and compatibility with the growth requirements of *Streptomyces coelicolor* (**Fig. 3.8**). Cultures were grown in TSB for 24 hours to balance both culture density and visualise Broccoli and TTA-mCherry in both Broccomyces strains. The cells were then washed in a supplemented PBS buffer containing 20g/L glucose as a carbon source, and 0.5g/L L-glutamine as a nitrogen source. Preliminary experiments indicated the lack of a carbon or nitrogen source in the washing buffer led to nutrient shock, impacting transcription and translation and reduced the fluorescent signal. The buffer also contained 100mM KCl and 5mM $MgCl_2$ as K^+ and Mg^{2+} ions have been previously documented to assist in stabilizing RNA structures the G-quadruplex the Broccoli aptamer is reliant on these cations for folding (Furuhata *et al*, 2019).

Following two washes in buffer to remove any residual TSB that resulted in excessive autofluorescence, the cells were transferred to a 96-well. After concentration of each cell sample through centrifugation, each well was loaded with approximately 0.5g of *Streptomyces* biomass. Two triplicate sets were prepared: one incubated with 2μM DFHBI, dissolved in

DMSO, and the other with an equivalent volume of DMSO, absent any fluorophore, as a control.

The 96-well plates were then incubated at 30°C for 15 minutes to allow Broccoli aptamer fluorophore-DFHBI binding in the dark to avoid photobleaching the DFHBI fluorophore. Following incubation, plates were read using a FlexStation3 plate reader (Molecular Devices), measuring fluorescence according to the excitation and emission spectra of the Broccoli aptamer (447nm/501nm) and mCherry (587nm/610nm). Additionally, optical density (OD_{600}) readings were used to normalize the fluorescence readings for cell density. Wild-Type (WT) *Streptomyces coelicolor* M145 was used as a negative control for the purpose of removing any culture-based autofluorescence, while *S. coelicolor* M145 possessing the pSET152 empty vector was used as an additional control strain, to demonstrate that any detected fluorescence was attributable solely to the Broccomyces constructs.

Initial trials utilising a combination of TSB media for growth, supplemented PBS for washing and final concentrations of 2μM DFHBI were used to attempt to visualize Broccoli/DFHBI fluorescence (447nm/501nm) and mCherry fluorescence (587nm/610nm) in a 96-well plate format (**Fig. 3.9**). Any fluorescence values below zero after background subtraction were reported as zero.

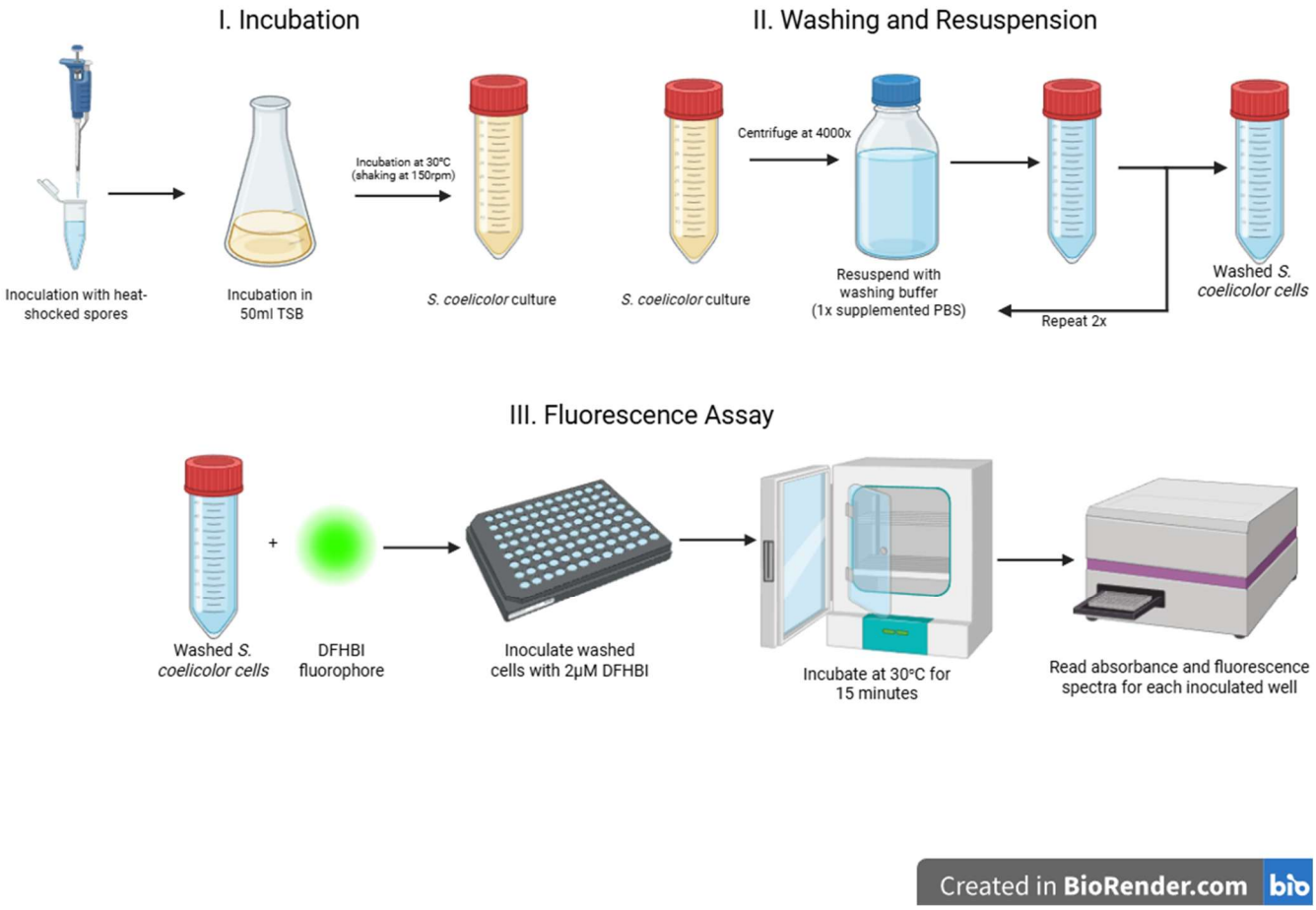

Fig. 3.8: Schematic overview of the high-throughput 96-well plate-based Broccoli/mCherry fluorescence assay. Fluorescence was recorded for both Broccoli and TTA-mCherry using a microplate reader. This assay format enables rapid and parallel screening of multiple constructs and conditions for RNA aptamer/fluorescent protein-based output. Created with BioRender (BioRender, 2025).

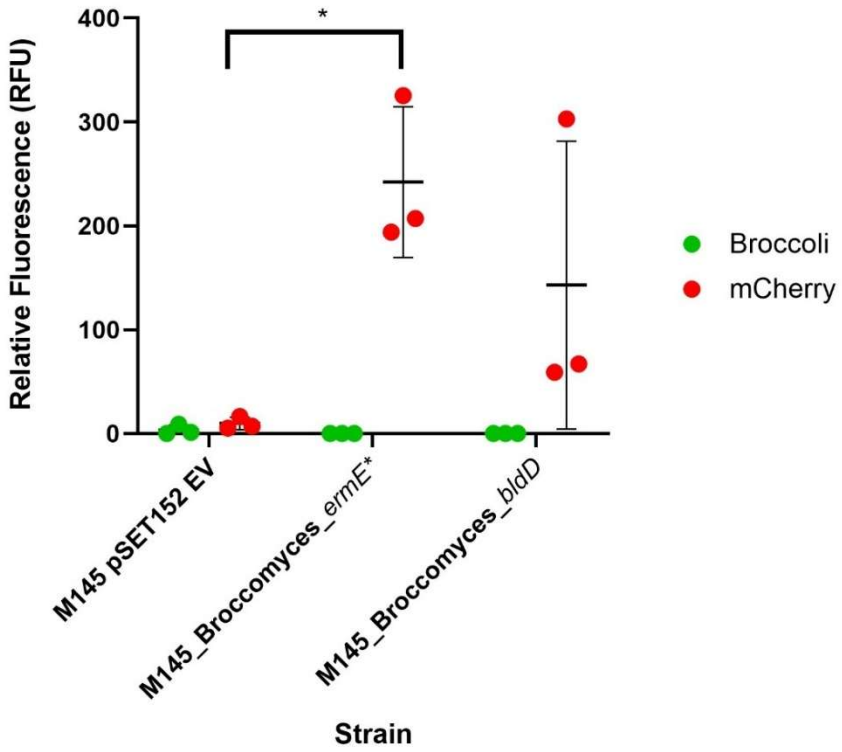

Fig. 3.9. Normalised fluorescence measurements of initial Broccomyces high-throughput assay in *S. coelicolor* M145. Fluorescence measurements were normalised to cell density (OD_{600}) to account for differences in biomass per well**.** Data was analysed by Kruskal-Wallis test (*p*= 0.0250), followed by Dunnett's multiple comparisons tests between strains (*p < 0.05, **p < 0.01)

Visualization of TTA-mCherry fluorescence was clear after 24 hours of growth in liquid culture (**Fig. 3.9)**, with signal intensity varying depending on which promoter was driving expression. The signal from *the* bldDp was much more variable than the *ermE*p* and this is likely due to the lower levels of activity of *bldDp* promoter in liquid culture.

Broccoli fluorescence was very low in these initial assays, with levels being barely above background, suggesting further optimization would be required to improve aptamer signal visibility under these conditions. *Streptomyces coelicolor* cells possessing either Broccomyces-*ermE*p* or Broccomyces-*bldDp* exhibited clear TTA-mCherry fluorescence, corresponding with growth phase after 24 hours of growth, allowing us to measure TTA codon-dependent translation through both constitutively expressed and developmentally regulated promoters. However, after the removal of background fluorescence by subtracting the values for WT *S. coelicolor* M145 from the other tested strains, Broccoli fluorescence was completely absent from the initial experiments. The inability to visualize Broccoli fluorescence in the initial 96-well plate assay suggested further optimisation was required to improve the detection of Broccoli fluorescence and overall aptamer performance and to enabling a more reliable and reproducible assay in *Streptomyces*.

3.3.5 Design of a negative fluorescence control for TTA-mCherry in *Streptomyces*

The TTA-mCherry fluorescent protein utilised as a part of the Broccomyces construct is engineered to possess the rare leucine-TTA codon starting at nucleotide position 34, replacing the native isoleucine residue. The purpose of this substitution (I11L) enables the control of mCherry translation to be governed by the availability of the *bldA* encoded TTA-tRNA. The current hypothesis is that in the absence of *bldA* expression or in strains lacking functional *bldA* expression, the TTA-tRNA is unavailable for translation, leading to stalled translation and absence of TTA-mCherry, and would serve as an indirect reporter of TTA-tRNA availability and *bldA* activity. To provide an additional control for TTA-mCherry a nonsense mutation was introduced at the same nucleotide position, by replacing the engineered TTA codon with a stop codon TGA (L11*). This mutation would cause premature translation termination of mCherry, resulting in a truncated protein and the abolishment of measureable mCherry fluorescence. Broccomyces-*ermE*p* was chosen as a suitable candidate over Broccomyces-*bldDp* because of the constitutive promoter rather than the developmentally regulated nature of *bldD*, resulting in detectable fluorescence regardless of growth phase.

The L11* substitution was created through site-directed mutagenesis (SDM) of the Broccomyces-*ermE*p* plasmid using the TGA-mCherry SDM primer set (primer numbers 3 and 4), and was verified by Sanger sequencing, using the M13_forward primer (primer number 5) and is represented in the Clustal Omega alignment (**Fig. 3.10)**. The L11* nonsense mutant served as a critical negative control demonstrating that all TTA-mCherry fluorescence detected from the Broccomyces is the result of TTA codon translation rather than any autofluorescence.

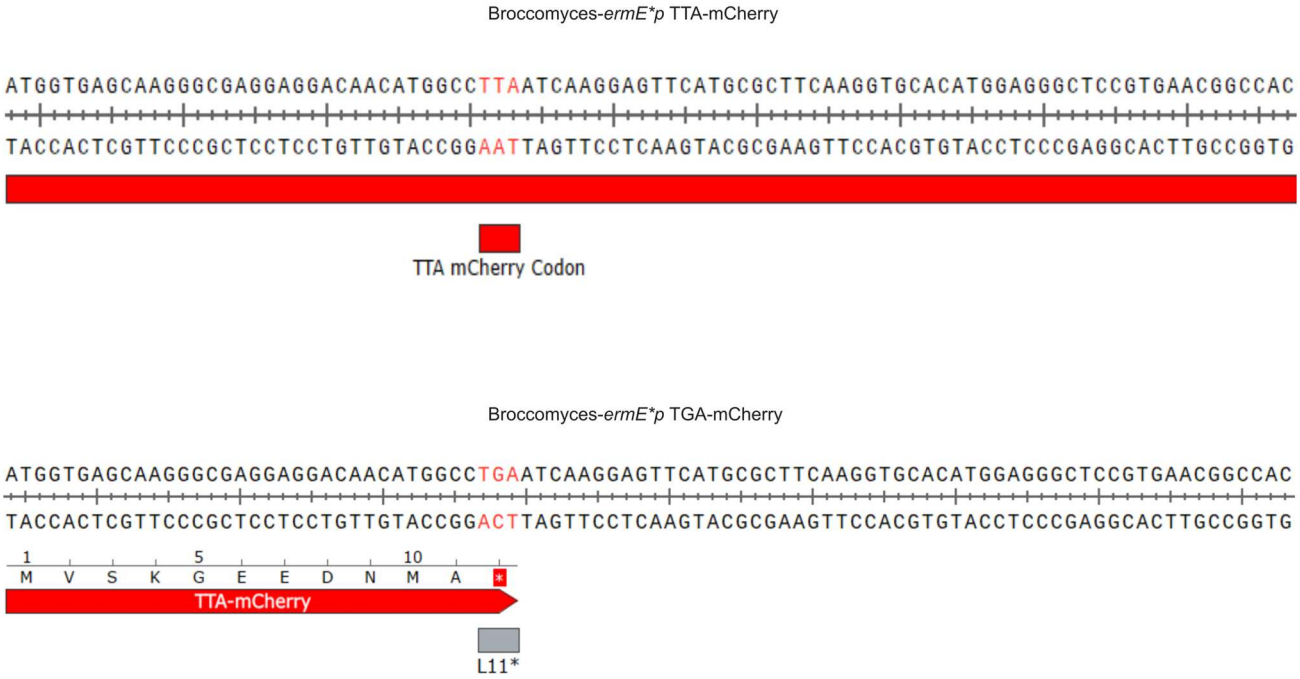

Fig. 3.10. Sanger sequencing confirms substitution of L11* mutation in mCherry. SnapGene alignment of the first 50 nucleotides of mCherry in both Broccomyces-*ermE*p* and Broccomyces-*ermE*p*-TGAmCherry. The M13_F primer was used for sequencing of the amplified region for both plasmids. The mutated codon (L11*) is highlighted.

The resulting plasmid carrying the L11* nonsense mutation in mCherry was introduced into *S. coelicolor* M145 through conjugation and examined in the 96-well plate fluorescence assay. The hypothesis being that the Broccoli amptamer activity would be unaltered and the L11* mCherry mutation would result in no detectable mCherry fluorescence from the modified construct.

Testing of the Broccomyces-*ermE*p* TGA_mCherry plasmid showed that the L11* nonsense mutation abolishes TTA-mCherry fluorescence, validating its use as a TTA-mCherry negative control (**Fig. 3.11**). The comparison between the TTA and TGA Broccomyces-*ermE*p* constructs confirms that TTA-mCherry fluorescence in Broccomyces is specifically dependent on the presence and successful translation of the engineered TTA codon. Unfortunately, visualisation of Broccoli-based fluorescence is still negliable across all conditions where the Broccoli aptamer is present.

.

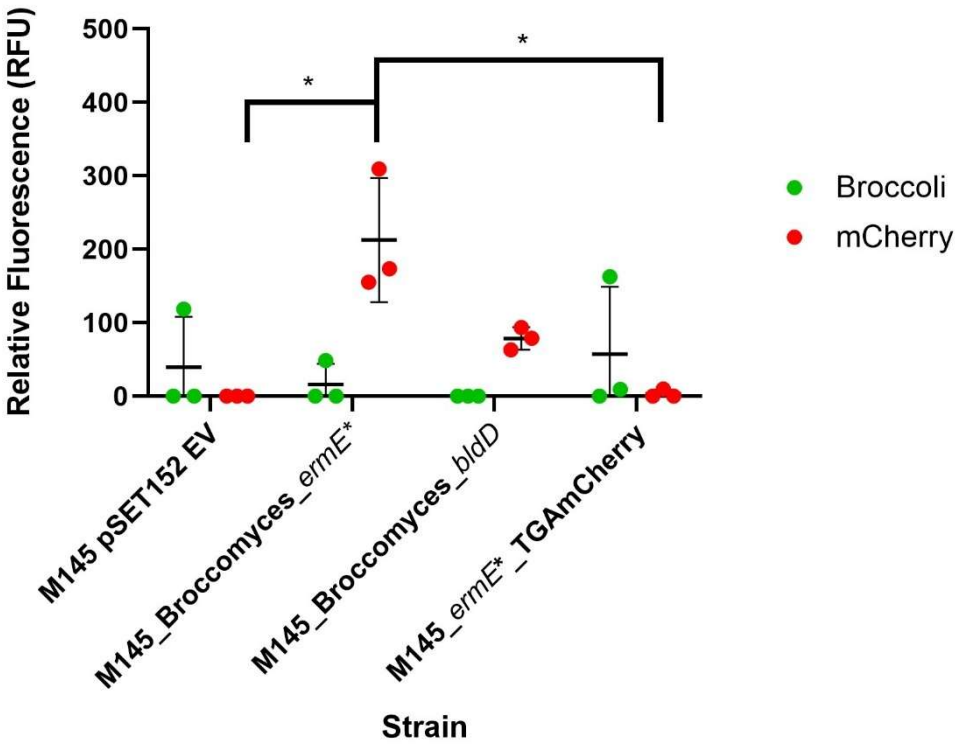

Fig. 3.11. Normalised fluorescence of Broccoli and TTA-mCherry highlights functionality of Broccomyces-*ermEp* *TGA as an mCherry negative control. Broccoli and TTA-mCherry fluorescence output was measured for the following strains: M145 pSET152 EV, M145 Broccomyces-*ermE*p,* M145 Broccomyces-*bldDp* and M145 Broccomyces-*ermE*p*-TGAmCherry. Data was analysed by Kruskal-Wallis test (p= 0.0006), followed by Dunnett's multiple comparisons tests between strains (*p < 0.05, **p < 0.01)

3.3.6 Influence of *Streptomyces* growth phase on Broccoli/DFHBI and mCherry-based fluorescence.

RNA aptamers such as Broccoli provide an alternative to traditional fluorescent protein reporter genes. *Streptomyces* bacteria possess complex life cycles, from vegetative growth to the production of aerial hyphae and secondary metabolites coinciding with late-stage growth (Jones and Elliot, 2018). It was hypothesized that the complex *Streptomyces* lifecycle may influence Broccoli-based fluorescence. To determine whether Broccoli fluorescence is influenced by *Streptomyces coelicolor* growth in liquid media, *Streptomyces coelicolor* strains possessing the Broccomyces constructs were grown in Tryptic Soy Broth (TSB) and assayed at across growth.

To prevent the formation of large mycelial aggregates, *Streptomyces* cultures were grown in Erlenmeyer flasks, containing stainless steel springs to ensure dispersed growth. At each time point, *Streptomyces* cultures were collected, washed, and transferred to clear-bottom black 96-well plates. Clear-bottom black-walled 96-well plates were chosen to minimize background fluorescence from adjacent wells. The DFHBI fluorophore was added to each well, with DMSO alone added as a Broccoli fluorescence control at each timepoint. Samples were then incubated at 30^{o}C in the absence of light for 15 minutes before being read in a FlexStation 3 fluorescence plate reader using excitation/emission settings of 447/501 nm.

Regardless of the chosen time points, Broccoli fluorescence was not detectable above background at any stage of growth (**Fig. 3.12**). This outcome suggests either poor fluorophore uptake, rapid efflux, or insufficient aptamer expression or folding in the current conditions. However, microscopy confirmed that Broccoli fluorescence was present in cells at the single-cell level, indicating that the RNA-fluorophore complex does form but that the fluorescence signal may currently be too weak or inconsistent across the *Streptomyces* population to be captured reliably in a plate-based format.

Conversely, TTA-mCherry fluorescence was successfully detected across all time points with the exception of 12 hours, likely attributable to low levels of biomass at such a small timeframe (**Fig. 3.12A**). This indicates that expression of the construct is occurring. Fluorescence intensity of TTA-mCherry was dependant on both incubation time and the tested promoter, highlighting the efficacy of the translational reporter and it is well established that proteins are more stable than RNA. Broccomyces-*ermE*p* and Broccomyces-*bldDp*, mCherry fluorescence gradually increased over time before reaching a maximum signal after 30 hours of growth (**Fig. 3.12D**), coinciding with the transition to stationary phase as seen in the previous kinetic data (see **Fig 3.4**). This suggests that *bldA*-dependent translation becomes more active during mid- to late exponential growth, which is consistent with the historical data on *bldA* being active later in growth for the translation of TTA codons.

Fluorescence of TTA-mCherry in Broccomyces-*bldDp* also peaked at 30 hours, and declined at 36 hours, mirroring the known activity of *bldD*, which functions early in the developmental program to repress sporulation genes. The increase in Broccomyces-*bldDp* TTA-mCherry activity at 24 and 32 hours can likely be attributed to rising levels of *bldA* expression, allowing TTA translation, whereas the decline observed after in later samples reflects downregulation of *bldD* as development progresses (**Fig. 3.12C to Fig. 3.12F**). It was concluded that the TTA-mCherry reporter sufficiently relies on *bldA* presence to fluoresce and reinforces the utility of protein-based reporters for monitoring gene translation in *Streptomyces.* These data also indicate that there is some translation of TTA-mCherry when availability of the *bldA*-tRNA will be limited, suggesting that other mechanisms may be at play regarding translation of *bldA*-dependent genes. Further optimisation is required to enhance the output of the Broccoli transcriptional reporter. Broccoli and TTA-mCherry fluorescence output for each Broccomyces reporter over time can be seen in **Fig. 3.13A** for Broccomyces-*ermE*p* and **Fig. 3.13B** for Broccomyces-*bldDp*, showcasing the rise and fall of *bldA*-tRNA dependant translation for both a constitutive and developmentally regulated gene promoter over time.

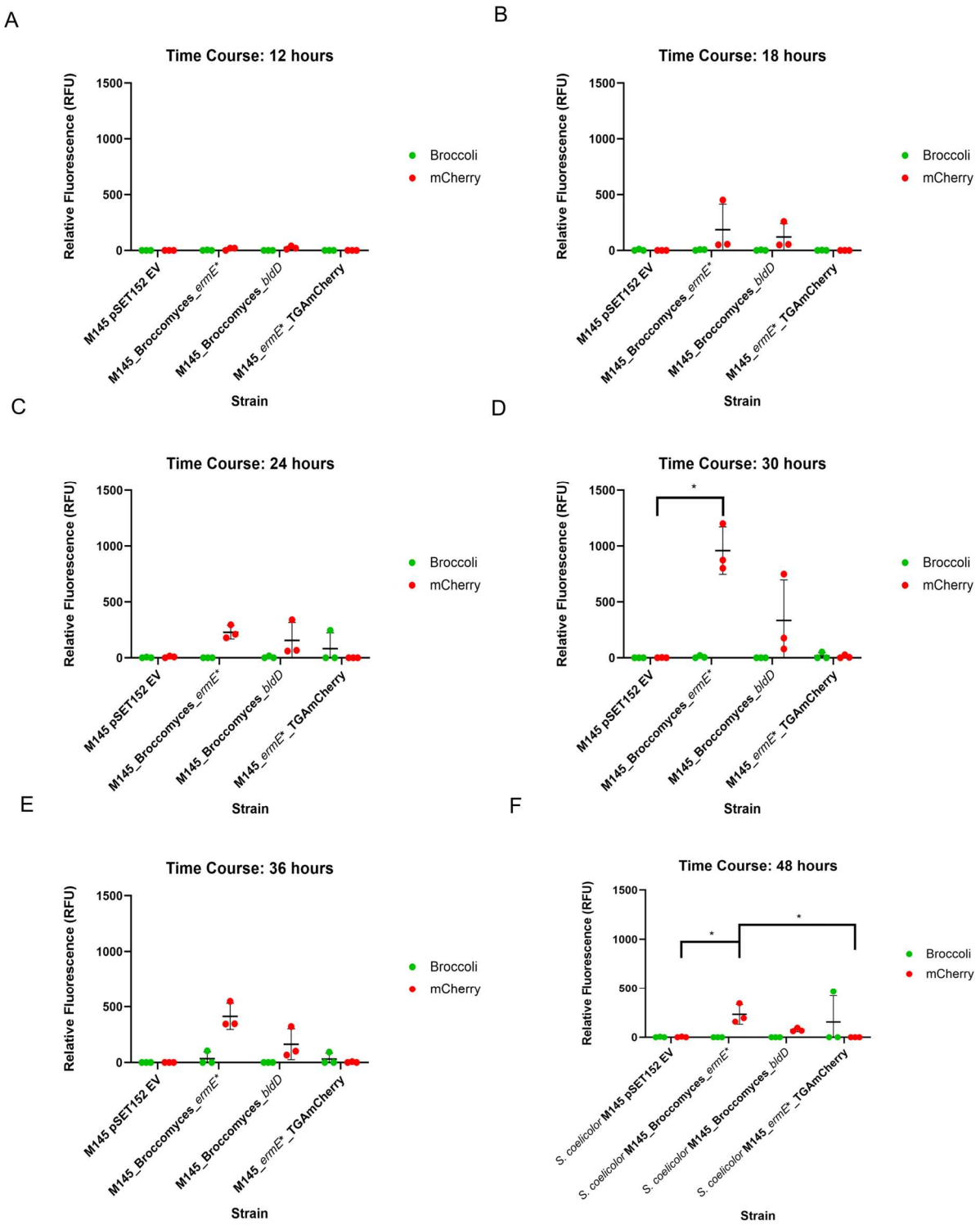

Fig. 3.12. Fluorescence time-course analysis of Broccoli/DFHBI and mCherry reporters in *Streptomyces coelicolor* across distinct growth phases. Cultures were grown in Tryptic Soy Broth (TSB) in Erlenmeyer flasks sampled at **(A)** 12, **(B)** 18, **(C)** 24, **(D)** 30, **(E)** 36, **(F)** 48 hours post-inoculation. Data was analysed with Kruskal-Wallis tests (*p*-values: **A**:0.0409, **B**:0.0045, **C**:0.0057, **D**:0:0006, **E**: 0.0009, **F**: 0.0006), followed by Dunnett's multiple comparisons tests between strain (*p < 0.05, **p < 0.01).

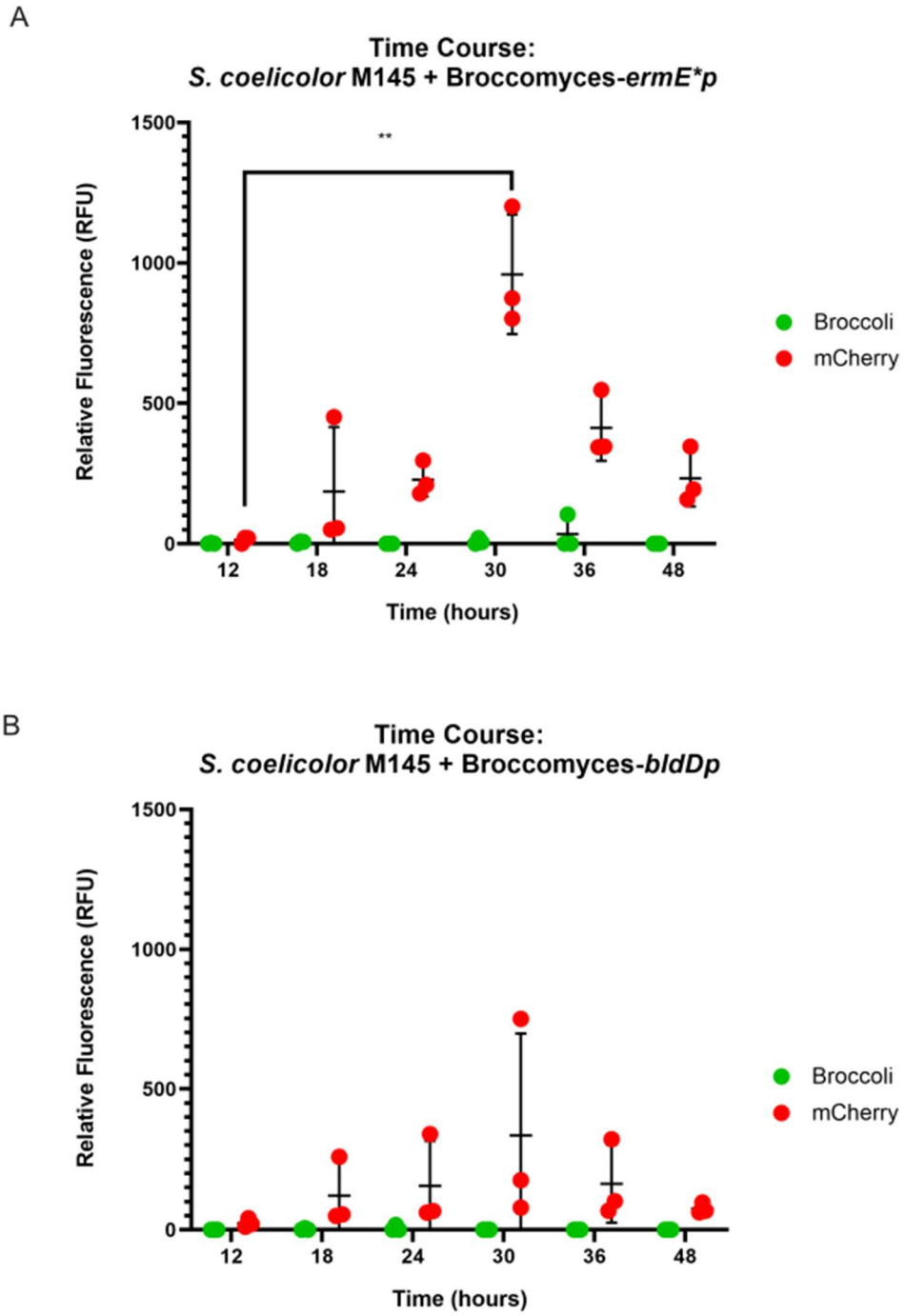

Fig. 3.13: Time course of Broccoli and TTA-mCherry fluorescence output over 48 hours, dependant on gene promoter. (A) Fluorescence output of Broccoli and TTA-mCherry dual reporter in *S. coelicolor* M145 Broccomyces-*ermE**p, driven by the constitutive *ermE*p promoter. **(B)** Fluorescence output of Broccoli and TTA-mCherry dual-reporters in *S. coelicolor* M145 Broccomyces-*bldDp*, driven by the developmentally regulated *bldD* promoter. Data was analysed with Kruskal-Wallis tests (*p*-values: **A**:0.0181, **B**:0.0757), followed by Dunnett's multiple comparisons tests between strain (*p < 0.05, **p < 0.01).

3.3.7 Buffer composition has little observable effect on Broccoli aptamer fluorescence

To further optimise the visualisation of the Broccoli aptamer efforts were focused on the post-culture handling of *S. coelicolor* M145 cells, in particular targeting the washing steps with different buffer systems to improve Broccoli fluorescence signal detection. The next approach was to test a variety of buffers to determine their impact on improving Broccoli-based fluorescence, which previous literature has shown RNA aptamers to be sensitive to buffer conditions (Stovall *et al*, 2004, Henri *et al*, 2019). The buffers chosen for testing included the previously used phosphate-buffered saline (PBS), as well as new buffers including Tris, HEPES, and M9 minimal media (see **Table 2-1**). All buffers were supplemented with the previous concentrations of glucose, L-glutamine, KCl and $MgCl_2$, for the purpose of maintaining nutrient availability and RNA aptamer stability. Every buffer was standardized to a pH of 7.5 before buffer optimisation began.

Cell cultures were grown for 24 hours prior to fluorescence analysis, as data obtained from **Fig. 3.12** suggests this growth period represents a balance between active transcriptional output and sufficient cell density for reliable fluorescence measurements, while avoiding any unwanted influence from pigmented metabolites, commonly seen in *Streptomyces* species (Alam *et al*, 2022)

Analysis of normalised fluorescence values revealed that buffer composition surprisingly had a substantial impact on the intensity or stability of TTA-mCherry fluorescence. When utilising PBS or Tris as a buffer system, TTA-mCherry fluorescence was shown to be stable across all biological replicates (**Fig. 3.14A & Fig. 3.14B**), whereas in HEPES and M9- based buffers, TTA-mCherry fluorescence for Broccomyces-*bldDp* was found to vary significantly between biological replicates (**Fig. 3.14C, Fig. 3.14D**). In contrast, Broccoli fluorescence was minimally affected by buffer composition (**Fig. 3.14)**. No buffer systems demonstrated a consistent improvement in Broccoli signal over the previously used PBS. Utilizing a Tris-based buffer

produced slight increases in normalised Broccoli fluorescence compared to PBS, observed through some biological replicates measuring slightly above background and reduced negative fluorescence values after normalisation, compared to PBS, HEPES and M9. This slight improvement in optimisation could indicate that the buffering capacity or ionic profile of Tris may better support aptamer folding or function, with Tris being used as a buffer of choice in previous Broccoli aptamer experiments (Okuda *et al,* 2017, Kartje *et al*, 2021).

It was also found that HEPES and M9-based buffers produced higher levels of deviation between biological replicates for both Broccoli and TTA-mCherry fluorescence compared to PBS and Tris-based buffers, resulting in the buffers negatively impacting the Broccomyces reporter assay. The variability in fluorescence could be attributable to the differences in composition leading to conditions affecting RNA aptamer folding, ligand binding, osmotic effects, or the in the case of M9: reduced nutrient availability due to its nature as a minimal medium (Henri *et al*, 2019). These data resulted in the omission of HEPES and M9-based buffers going forward, with the Tris-based buffer carried forward for continued optimisation, due to its contribution to consistent TTA-mCherry fluorescence across biological replicates and its improved foundation for improving Broccoli fluorescence output.

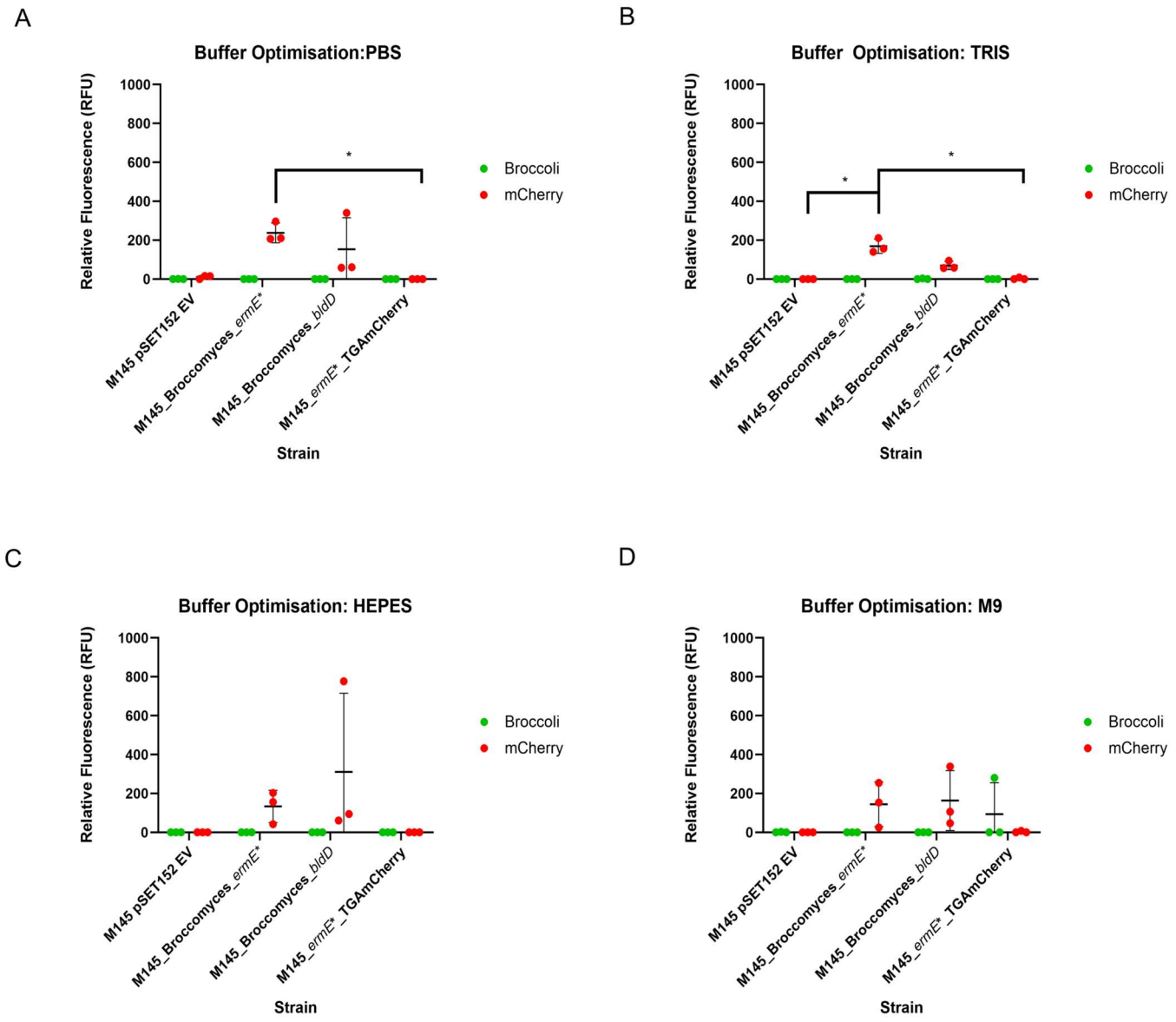

Fig. 3.14: Effect of buffer composition on Broccoli and mCherry fluorescence in *Streptomyces coelicolor* M145 harboring Broccomyces dual reporter constructs. Cells were washed post-culture in one of four buffer conditions: **(A)** PBS, **(B)** Tris, **(C)** HEPES, or **(D)** M9 minimal buffer. Each panel represents the average fluorescence intensity (± standard deviation) of three biological replicates for both reporters. Data was analysed with Kruskal-Wallis tests (*p*-values: **A**:0.0076, **B**:0.0006, **C**:0.0065, **D**:0:0105), followed by Dunnett's multiple comparisons tests between strain (*p < 0.05, **p < 0.01)

3.3.8 Utilisation of an improved fluorophore does not improve the Broccoli signal in *Streptomyces*

While DFHBI has been used previously as a fluorophore for Broccoli, it is known to produce lower levels of fluorescence when compared to its modern derivatives (Song *et al,* 2014, Filonov and Jaffrey, 2017). DFHBI-1T, a modified derivative of DFHBI, has been reported to exhibit improved fluorescence upon binding to the Broccoli aptamer, as well as improved photostability *in vivo* when compared to DFHBI (Song *et al*, 2014, Climent-Catala *et al*, 2023). To test DFHBI-1T compatibility in the Broccomyces dual reporter assay it was compared to its parent fluorophore, DFHBI.

Compared to DFHBI, DFHBI-1T possesses an additional trifluoroethyl group, resulting in an increased quantum yield, while retaining high binding affinity for the Broccoli aptamer (Song *et al*, 2014). Previous literature has shown that DFHBI-1T outperforms DFHBI, with DFHBI-1T fluorescence being between 4- and 6-fold better in both bacterial and mammalian cell backgrounds (Filonov and Jaffrey, 2016). To test the effect of DFHBI-1T compared to DFHBI in the Broccomyces constructs, the conditions of the assay were kept the same, using a final concentration of 2μM for either fluorophore. The goal was to determine whether this switch alone could produce a meaningful improvement in Broccoli signal, thereby overcoming one of the key limitations encountered with DFHBI. The Broccoli/DFHBI-1T complex possesses different excitation and emission maxima compared to Broccoli/DFHBI (Filonov and Jaffrey, 2016). As such, the corresponding excitation/emission spectra was used for each aptamer fluorophore complex (447/501 for Broccoli/DFHBI vs 472/507 for Broccoli/DFHBI-1T)

Normalised data analysis revealed a slight increase in Broccoli fluorescence when DFHBI-1T was used over DFHBI (**Fig. 3.15**). While overall Broccoli fluorescence remained near background levels, some biological replicates utilising DFHBI-1T were able to yield some measurable Broccoli fluorescence, which is an improvement over previously tested condition (**Fig. 3.13**, **Fig. 3.14**). While the Broccoli aptamer aspect of the Broccomyces constructs is still

not functioning at their full potential in *S. coelicolor* in a 96-well plate format **(Fig. 3.14)**, DFHBI-1T may offer a slight advantage over DFHBI in regard to in signal output, potentially due to its higher quantum efficiency over its progenitor (Song *et al*, 2014). Fluorescence of the mCherry-based translational reporter remained stable and unchanged in the presence of DFHBI-1T (**Fig. 3.15)**.

The use of DFHBI-1T may potentially help the development of the Broccoli aspect of the Broccomyces reporter assay in *S. coelicolor*. Using a brighter fluorophore produced a barely detectable Broccoli/fluorophore signal increase, implying successful aptamer-ligand binding is taking place, however further improvements are required before the Broccomyces constructs can be widely adopted as reporters in *Streptomyces*.

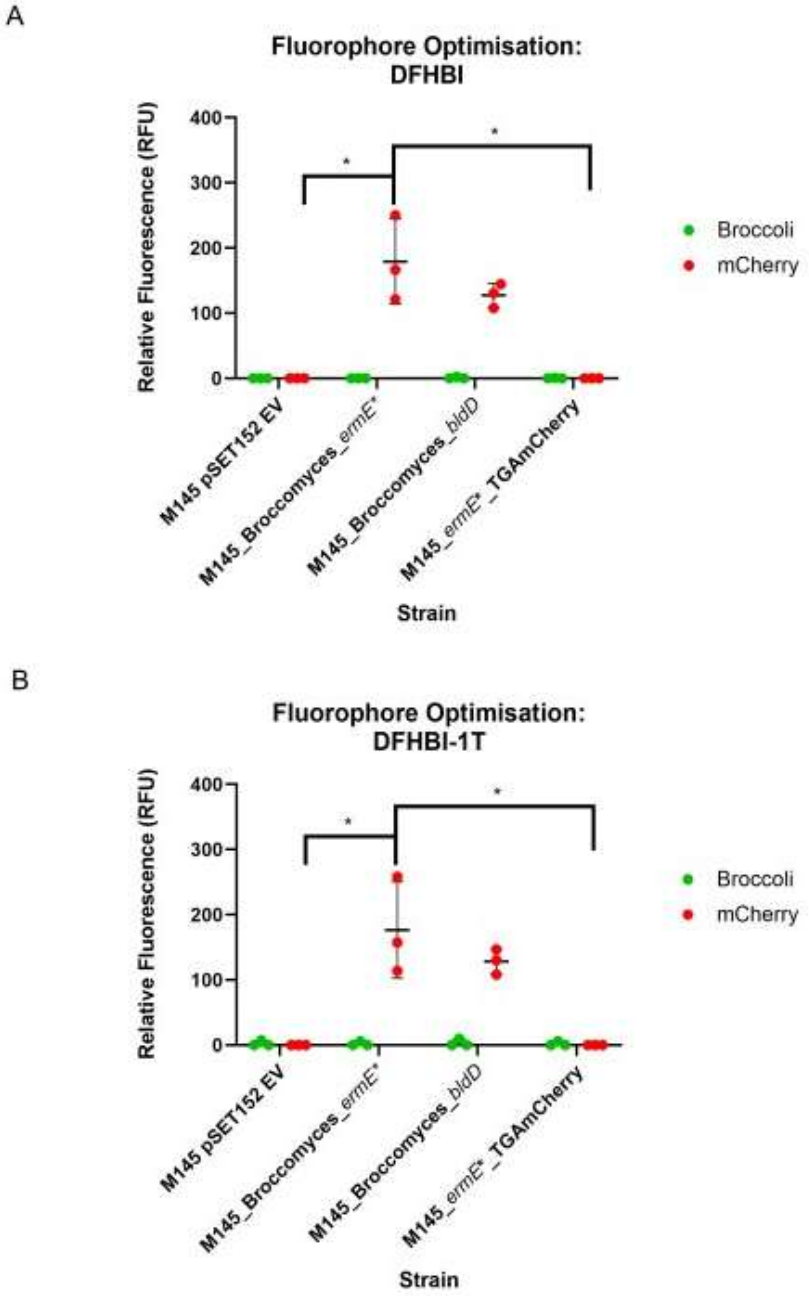

Fig. 3.15. Comparison of Broccoli and TTA-mCherry fluorescence using DFHBI and DFHBI-1T in *Streptomyces coelicolor*. Fluorescence output from Broccoli and mCherry reporters was measured under identical assay conditions, with the only variable being the fluorophore used: either **(A)** 2 µM DFHBI or **(B)** 2 µM DFHBI-1T. Data was analysed with Kruskal-Wallis tests (*p*-values: **A**:0.0026, **B**:0.0026), followed by Dunnett's multiple comparisons tests between strain (*p < 0.05, **p < 0.01)

3.3.9 Altering DFHBI or DFHBI-1T concentration has no effect on Broccoli signal

To further optimise the visualisation of the Broccoli aptamer the concentration of the DFHBI and DFHBI-1T fluorophores, which binds to the Broccoli RNA aptamer to enable its fluorescence were altered. Concentrations of DFHBI and DFHBI-1T used in previous literature appears to vary heavily dependent on the experimental methodology and the nature of each experiment (Filonov and Jaffrey, 2016, Alam *et al*, 2017, Li *et al*, 2021). As such, it was unclear whether the fluorophore concentration utilised in the initial experiment was suboptimal; either being too low, resulting in insufficient aptamer-fluorophore complex formation, or being too high, leading to elevated non-specific background fluorescence that could obscure any Broccoli-related fluorescence.

To address this, a gradient-based experiment in which the concentration of DFHBI or DFHBI-1T was increased from the lowest concentration of 1µM to the highest concentration of 40 µM. Each concentration was tested in wells containing *S. coelicolor* M145 cells harbouring the Broccomyces dual reporter constructs under previously optimized growth and wash buffer conditions. This range in fluorophore concentration was used to encompass both low- and high-end concentrations used in Broccoli aptamer assays in the literature (Okuda *et al*, 2017, Furahata *et al*, 2019, Climent-Catala *et al*, 2023). The goal from this optimisation experiment was to identify a concentration that balances higher Broccoli signal intensity with low background interference.

Despite the hypothesis that increasing the concentration of either Broccoli-specific fluorophore might improve the visualization of Broccoli/fluorophore fluorescence, the results of this experiment revealed no appreciable increase in fluorescence intensity across the tested range. Normalised fluorescence measurements remained relatively consistent from 1 µM DFHBI **(Fig. 3.16A, Fig. 3.17A)** through to 40 µM DFHBI **(Fig. 3.16F, Fig. 3.17F)**, indicating that the inability to detect Broccoli fluorescence output in S. *coelicolor* M145 strains

possessing either Broccomyces construct was not limited by the availability and quantity of either fluorophore. This find was somewhat surprising, given previous reports of functional Broccoli expression and signal detection at DFHBI concentrations of 2 μM, 20 μM, and even 40 μM in other biological systems such as *E. coli* (Filonov *et al*, 2014, Han *et al*, 2014, Filonov and Jaffrey, 2016, Yuan and Alper, 2020).

However, this data also revealed a clear drawback to using higher DFHBI concentrations as a part of our dual reporter assay. Starting from 10 μM of either fluorophore (**Fig. 3.15D, Fig. 3.16D**), an exponential increase in background fluorescence was detected in control wells containing no cells, suggesting that the DFHBI fluorophores themselves were contributing significantly to non-specific signal. When DFHBI or DFHBI-1T was utilized at 20 μM and 40 μM (**Fig. 3.15E-F, Fig. 3.16E-F**), background fluorescence levels in the blank control wells was recorded to be higher than those containing cells, regardless of whether they possessed the Broccomyces construct, resulting in normalised values reaching far below zero for all tested strains. This result compromised the accuracy and sensitivity of the dual reporter assay to the point we concluded that increasing the concentration of either fluorophore past 10 μM resulted in no benefit to improving the Broccoli aptamer signal and likely impaired the signal to background ratio of the assay.

Based on the data presented in **Fig. 3.16** and **Fig. 3.17**, it was decided that a concentration of 5μM DFHBI-1T would be utilized for all future assay conditions. The concentration of 5μM was selected as a sufficient compromise between sufficient fluorophore availability while minimizing background interference, while DFHBI-1T was chosen as the superior fluorophore, due to the potential to increase fluorescence.

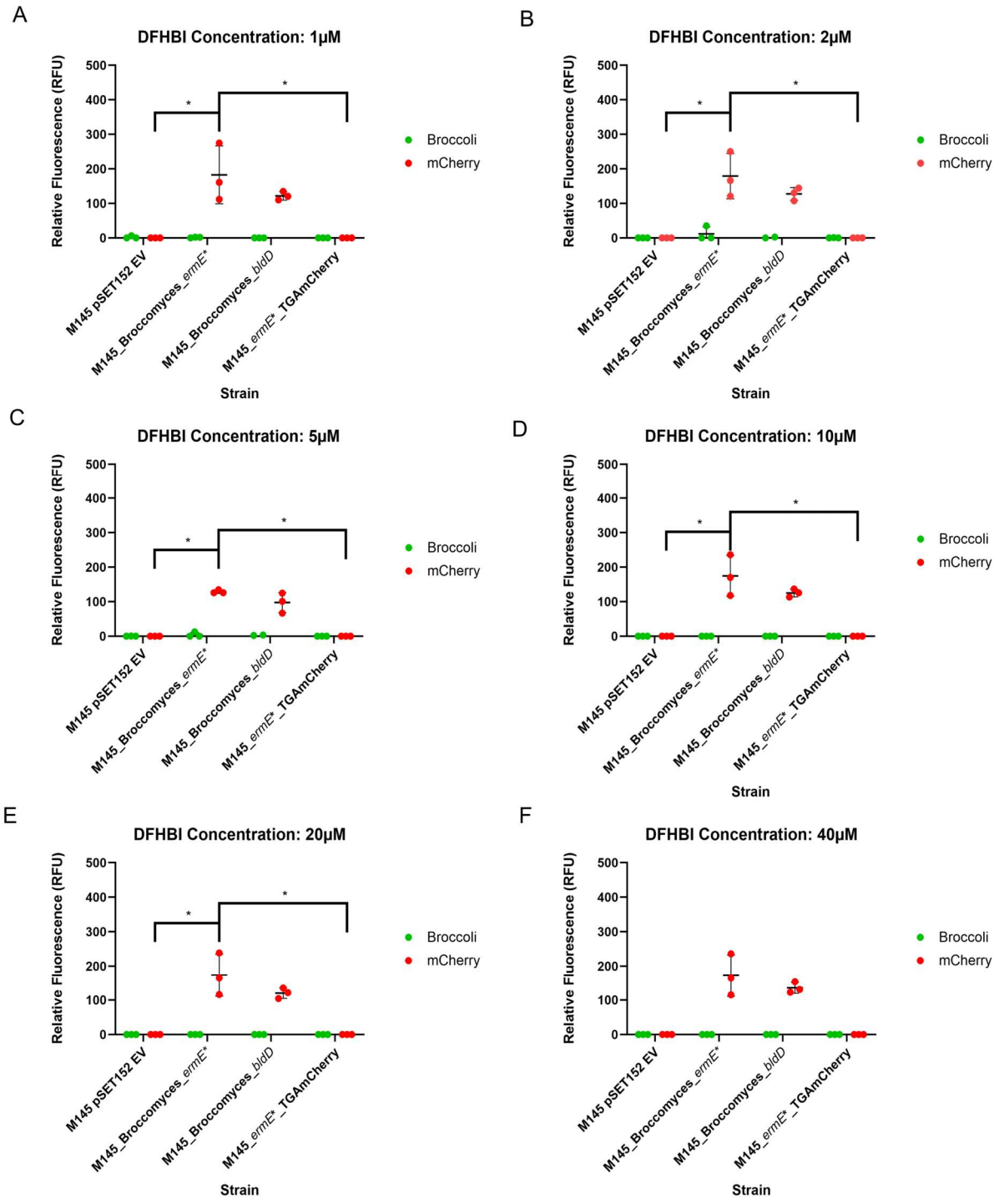

Fig. 3.16: DFHBI fluorophore concentration and its impact on Broccoli and TTA-mCherry fluorescence in *S. coelicolor* M145. Fluorescence output from the Broccoli RNA aptamer and the TTA-mCherry fluorescent protein was measured following incubation with increasing concentrations of DFHBI: **(A)** 1 µM, **(B)** 2 µM, **(C)** 5 µM, **(D)** 10 µM, **(E)** 20 µM, and **(F)** 40 µM. Each panel represents mean Broccoli fluorescence intensity across three biological replicates using Broccomyces dual reporter constructs. Data was analysed with Kruskal-Wallis tests (*p*-values: **A**:0.0026, **B**:0.0026, **C**:0.0006, **D**:0:0026, **E**: 0.0026, **F**: 0.0045), followed by Dunnett's multiple comparisons tests between strain (*p < 0.05, **p < 0.01)

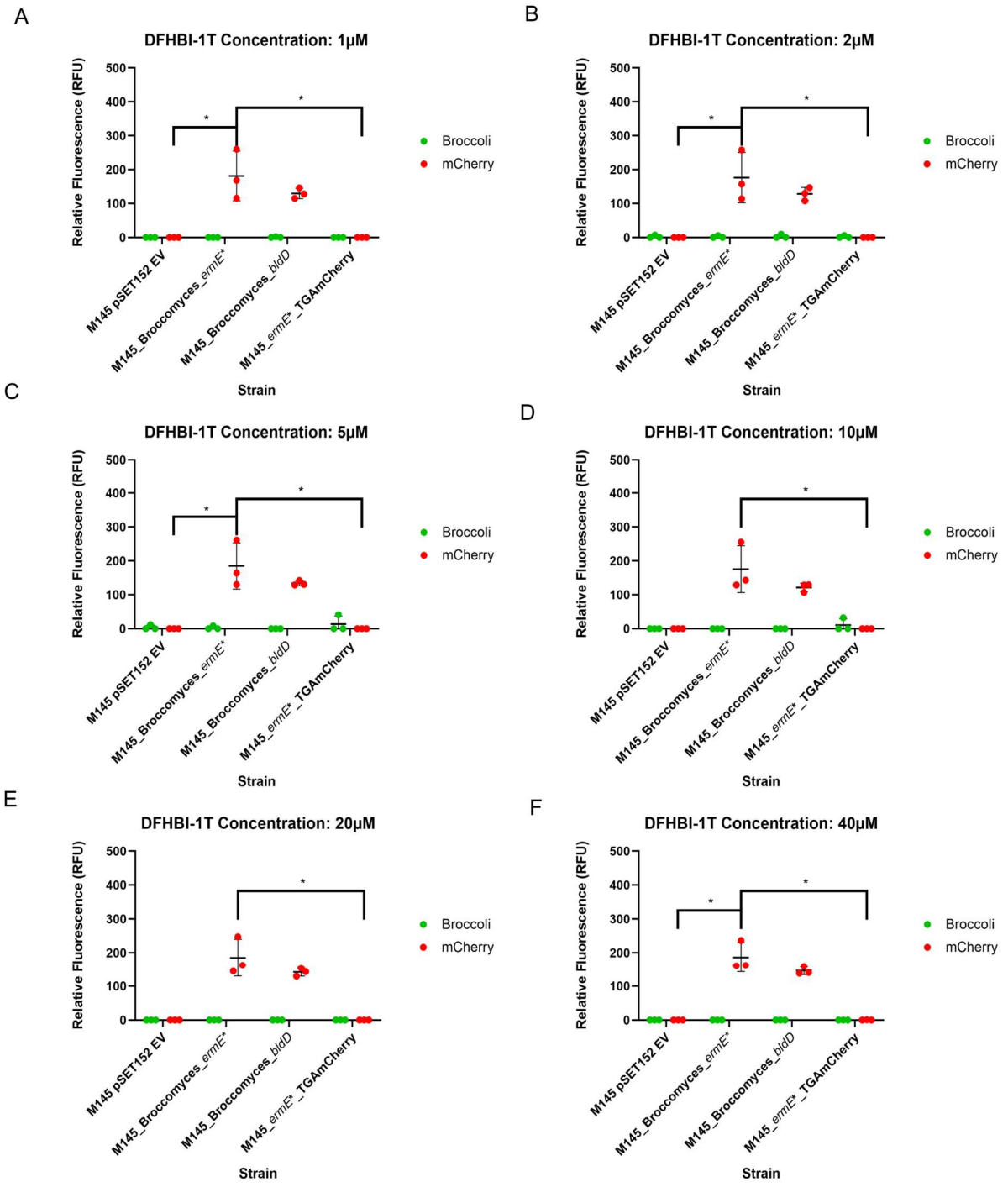

Fig. 3.17: DFHBI-1T fluorophore concentration and its impact on Broccoli aptamer fluorescence in *S. coelicolor* M145. Fluorescence output from the Broccoli RNA aptamer was measured following incubation with increasing concentrations of DFHBI-1T: **(A)** 1 μM, **(B)** 2 μM, **(C)** 5 μM, **(D)** 10 μM, **(E)** 20 μM, and **(F)** 40 μM. Data was analysed with Kruskal-Wallis tests (*p*-values: **A**:0.0026, **B**:0.0026, **C**:0.0026, **D**:0:0013, **E**: 0.0013, **F**: 0.0009), followed by Dunnett's multiple comparisons tests between strain (*p < 0.05, **p < 0.01)

3.3.10 Increasing the duration of DFHBI incubation does not increase Broccoli fluorescence output

With the Broccoli RNA aptamer system, fluorescence is seen after successful binding of DFHBI to a properly folded aptamer structure (Filonov *et al*, 2014). Understanding this, the next round of optimisation sought to determine whether extending the incubation time with DFHBI-1T was required to enhance the measurability of the Broccoli aptamer in the Broccomyces constructs. The rationale behind these next experiments was that a longer incubation may improve uptake of the DFHBI-1T fluorophore into *Streptomyces* cells, resulting in increased aptamer-fluorophore binding and an increase in fluorescence (Filonov and Jaffrey, 2016).

To test this, *S. coelicolor* M145 cells expressing the Broccomyces constructs were grown and washed with the previously optimized conditions and incubated with 5 μM DFHBI-1T. Broccoli and TTA-mCherry fluorescence were measured at various timepoints following the addition of DFHBI-1T, including immediate detection (<5 minutes after DFHBI-1T addition) and following incubation at 30^{o}C, from 15 minutes up to and including 2 hours of incubation. Fluorescence measurements were normalized to the optical density of each well, to account for varying cell density between replicates.

Contrary to the initial hypothesis, results from this optimisation trial demonstrated that Broccoli fluorescence signal plateaued rapidly post-DFHBI incubation, with no significant increase observed beyond 15-minutes (**Fig. 3.18A, Fig. 3.18B**). Broccoli fluorescence intensity remained consistent across all time conditions, suggesting that DFHBI-binding may occur rapidly, meaning additional incubation time does not result in more aptamer-fluorophore interactions. While TTA-mCherry fluorescence for both Broccomyces- *ermE** and Broccomyces- *bldD* remained consistent regardless of DFHBI-1T incubation time, prolonged incubation with 5μM DFHBI-1T failed to improve Broccoli fluorescence above baseline levels (**Fig. 3.18**). These findings imply that the reason for failing to observe detectable Broccoli

fluorescence in *Streptomyces* species is not fluorophore diffusion or uptake through the *Streptomyces* cell wall. However, this inability to visualize Broccoli fluorescence as a part of a high-throughput assay could potentially be due to a number factors. For example, insufficient Broccoli aptamer expression could be caused through misfolding of the aptamer structure in *Streptomyces*, difficulty traversing the cell membrane, or through poor retention of the fluorophore within the cell due to efflux (Wu *et al,* 2005, Nag and Mehra, 2021, Squire *et al*, 2023). The main result of these findings is that the Broccomyces reporter system required further refinement to achieve detectable Broccoli fluorescence in *Streptomyces* species, focusing on improving aptamer-fluorophore interactions.

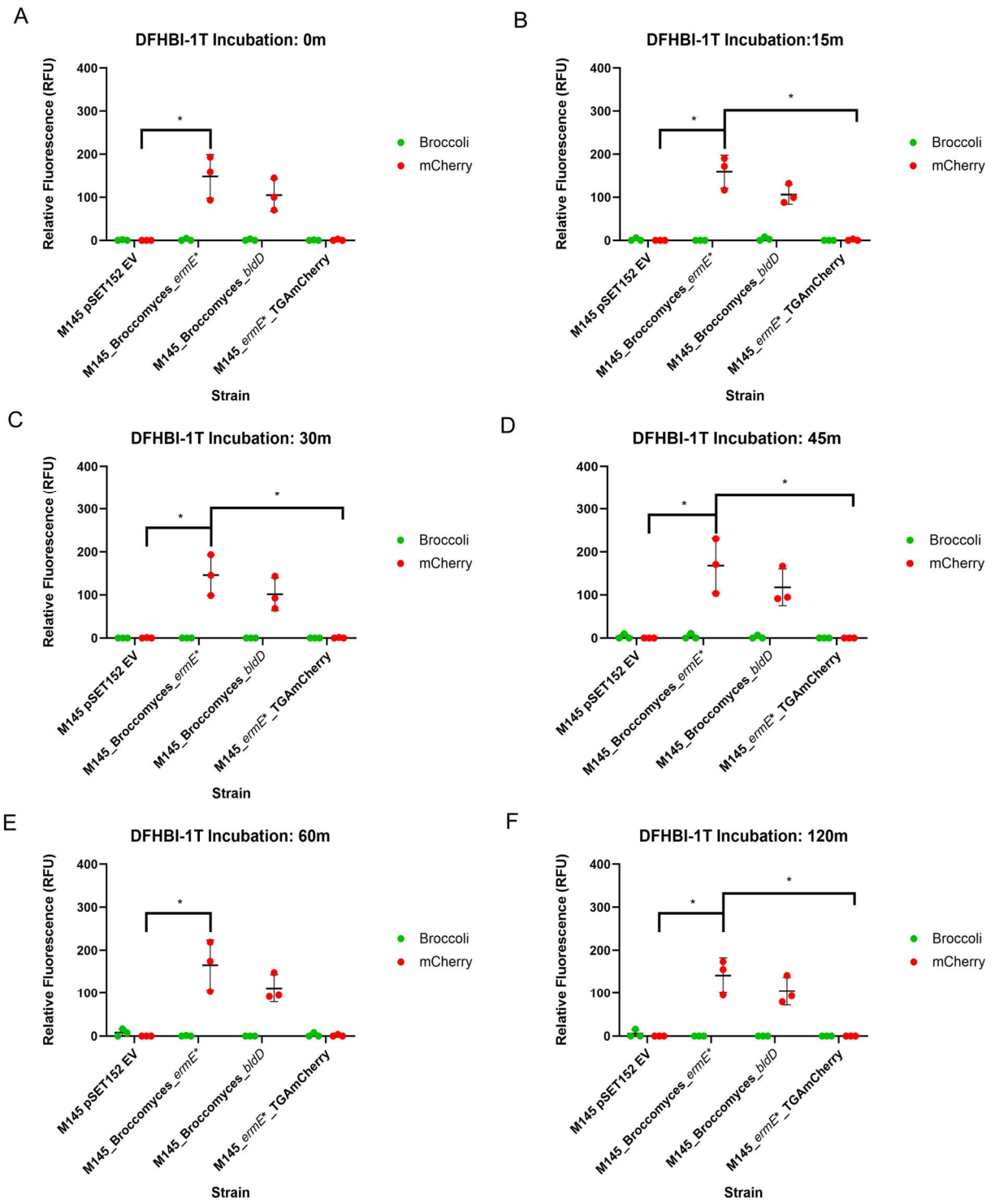

Fig. 3.18: Impact of DFHBI-1T Incubation duration on promoter-driven Broccoli/mCherry fluorescence output in *S. coelicolor* M145. Fluorescence intensity was measured at six timepoints post-DFHBI-1T addition**: (A)** 0 minutes, **(B)** 15 minutes, **(C)** 30 minutes, **(D)** 45 minutes, **(E)** 60 minutes, and **(F)** 120 minutes. Each graph represents the fluorescence distribution across biological replicates (n = 3) normalized to optical density (OD_{600}). Data was analysed with Kruskal-Wallis tests (*p*-values: **A**:0.0032, **B**:0.0021, **C**:0.0033, **D**:0:0013, **E**: 0.0013, **F**: 0.0013), followed by Dunnett's multiple comparisons tests between strain (*p < 0.05, **p < 0.01)

3.3.11 Mitigating DMSO autofluorescence has no effect on Broccoli fluorescence

After working through buffer optimization, the next approach in optimising Broccoli fluorescence in the Broccomyces fluorescence assay was to investigate the effect of dimethyl sulfoxide (DMSO) in the Broccomyces system. The fluorophore DFHBI-1T is commonly dissolved in DMSO, as it lacks solubility in water and previous literature using DMSO as opposed to methanol, or a different solvent (Dao *et al*, 2021., Furuhata *et al*, 2019., Klima *et al,* 2021). In all previous experiments, a final concentration of 1% DMSO was used, to match the final DMSO concentration in wells containing the DFHBI-1T fluorophore. However, since visualization of Broccoli fluorescence in the reporter assay was still negligible, it was decided to investigate whether the presence of DMSO was having an impact on *Streptomyces* cells, and consequently the quantification of Broccoli fluorescence in plate format.

To do this, another gradient experiment was prepared, where the final concentration of DMSO was reduced gradually from 1% down to 0%, in 0.2% increments, providing six conditions in total: 1.0%, 0.8%, 0.6%, 0.4%, 0.2%, and 0.01%. The DFHBI fluorophore was also dissolved in concentrations of DMSO equal to those utilized in the optimisation experiment. All other conditions for the assay, including buffer conditions (Tris at pH 7.5), DFHBI-1T concentration (5μM), fluorophore incubation time (15 minutes), and the fluorescence readout settings were kept consistent to isolate the effect on fluorescence of DMSO alone.

The normalised data highlighted that altering the concentration of DMSO did not improve the detection of Broccoli-based fluorescence (**Fig. 3.19**). Across all six DMSO concentrations, Broccoli fluorescence intensity stayed at or near background levels, similar to data in previous experiments that used 1% DMSO (**Fig. 3.12, Fig. 3.14, Fig. 3.17 and Fig. 3.18**). In some biological replicates, some visualization of Broccoli fluorescence could be detected in *S. coelicolor* M145 Broccomyces-*ermE*p*-TGAmCherry and Broccomyces-*bldDp*, however this was limited to one biological replicate out of three, showing lack of consistency between

replicates (**Fig. 3.19B, Fig. 3.19E, Fig. 3.19F**). There was no consistent indicator that reducing the concentration of DMSO assisted with aptamer/fluorophore binding. As with other previously rested conditions, TTA-mCherry fluorescence was not significantly affected across the entire DMSO concentration range, implying that DMSO concentrations did not having any negative effect on the *S. coelicolor* translational reporter. This also reaffirmed that any issues seen with Broccoli fluorescence were specific to the aptamer system and not due to general toxicity or disruption from DMSO.

Since 1% DMSO proved easy to work with and had no adverse effects on TTA-mCherry fluorescence, it was used in all following experiments. However, it's clear that DMSO is not the limiting factor in successfully visualizing Broccoli fluorescence in *S. coelicolor* high-throughput assays. These results support the idea that further optimization attempts should focus on alternative aspects such as like RNA stability or to trial alternative RNA aptamer systems to Broccoli.

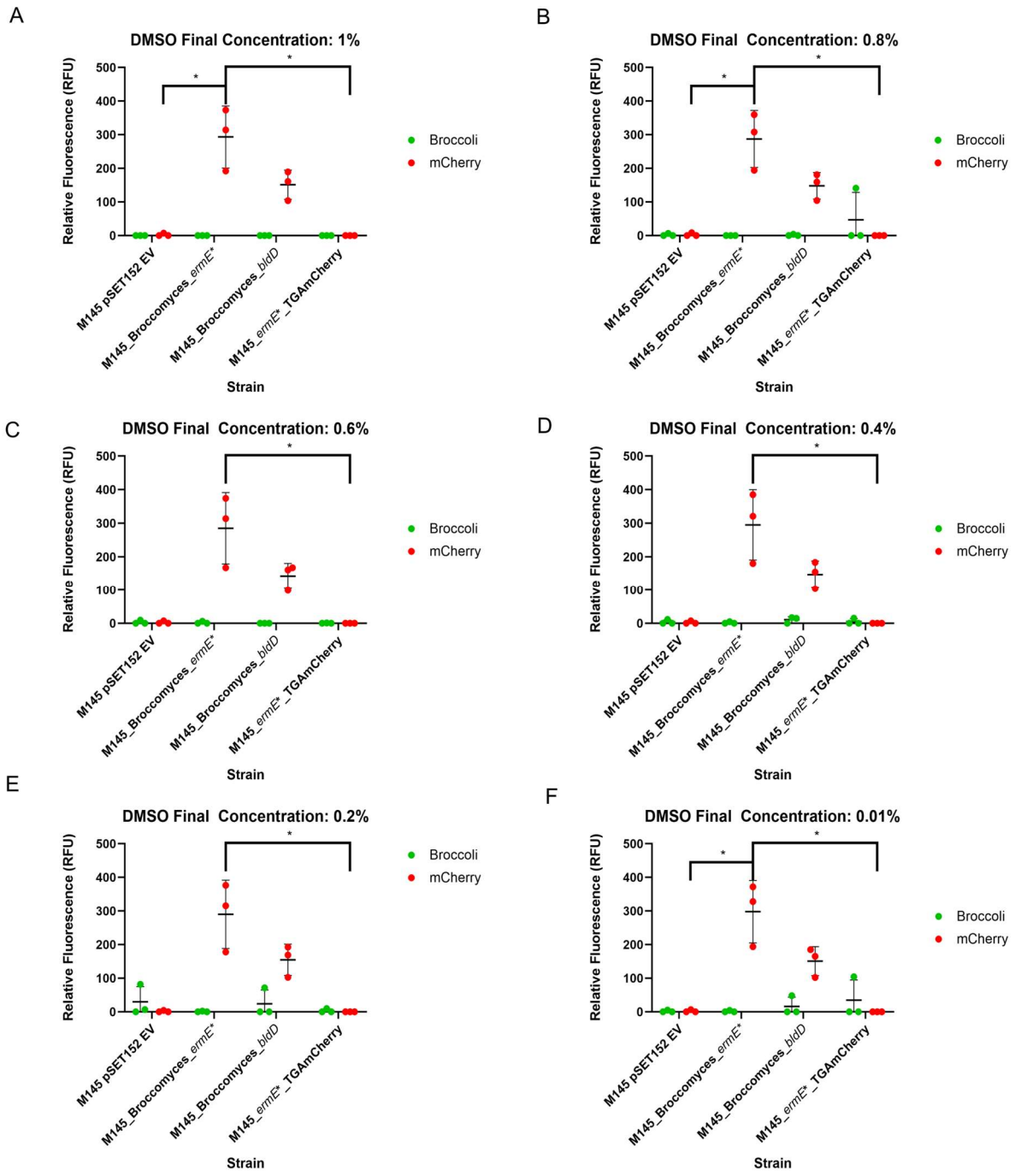

Fig. 3.19: Effect of varying DMSO concentration on Broccoli and TTA-mCherry fluorescence in *Streptomyces coelicolor* M145. DFHBI-1T was dissolved in matching concentrations of DMSO (100%, 80%, 60%, 40%, 20%, and 0%) and added to cultures under otherwise identical conditions. Final concentration of DMSO in each well included **(A):** 1%, **(B):** 0.8%, **(C):** 0.6%, **(D):** 0.4%, **(E):** 0.2%, and **(F):** 0.01%. Data was analysed with Kruskal-Wallis tests (*p*-values: **A**:0.0009, **B**:0.0006, **C**:0.0013, **D**:0:0013, **E**: 0.0013, **F**: 0.0006), followed by Dunnett's multiple comparisons tests between strain (*p < 0.05, **p < 0.01)

3.3.12 The Removal of the Hammerhead Ribozyme to measure localised transcription

The current design of the Broccomyces plasmids contains a hammerhead ribozyme situated between the promoter of interest and the Broccoli aptamer. The hammerhead ribozyme (HHR) is a small, Mg^{2+} -dependant, self-cleaving RNA motif that catalyzes reversible cleavage and ligation reactions at specific sites within an RNA molecule, which has been commonly utilized to release small RNA species from long transcripts and to regulate gene expression post-transcriptionally (Prody *et al,* 1986, Hammann *et al*, 2012). As the Broccoli aptamer is an engineered RNA sequence that also possesses improved stability in the presence of Mg^{2+} (Filonov *et al*, 2014), it was originally decided to include an upstream HHR as the HHR cleaves co-transcriptionally and would assist in signal separation. By cleaving co-transcriptionally, this ensured consistent aptamer folding into its active G-quadruplex conformation, optimizing fluorophore binding and fluorescence. Transcript cleavage with the HHR also produces a standalone Broccoli RNA, distinct from the TTA-mCherry reporter, which allows for more independent assessment of transcriptional versus translational quantification (Banerjee *et al*, 2009). However, the usage of the HHR also came with assay limitations, with previous studies showing HHR usage results in increased RNA instability associated with exonuclease degradation and potent ribonucleases found in *Streptomyces*, as well as potential incomplete transcript cleavage and markedly reduced activity *in vivo* compared to *in vitro* (Bralley *et al*, 2014, Wurmthaler *et al,* 2017).

Given the benefits and drawbacks associated with the HHR, it was hypothesized that removing the ribozyme, hence leaving the Broccoli aptamer attached to the mRNA sequence, may improve Broccoli visualisation, despite potential heterogeneity at the RNA's 5`-end. While the HHR is active, Broccoli aptamer populations are uniform due to accurate cleavage but are more vulnerable to degradation, reducing fluorescence; whereas if the ribozyme is absent, it would help the Broccoli RNA to retain its natural 5`-triphosphate, potentially improving stability

and steady-state fluorescence. To accurately assess these competing effects, an experimental comparison between constructs containing and lacking the HHR is essential

To accomplish this, the HHR was excised from the Broccomyces constructs via restriction digest. The HHR region was flanked by two MfeI restriction sites, facilitating its excision (**Fig. 3.20A**). Successful removal was confirmed through gel electrophoresis of the digested plasmids. Due to the differences in the genetic sequences between the Broccomyces-*ermE*p* and Broccomyces-*bldDp* plasmids, two separate restriction digestions were ran. Both of the Broccomyces plasmids contain an AflII site within the HHR, with no other AflIII sites located elsewhere in the construct, however other available restriction sites differ between the plasmids. For Broccomyces-*ermE*p*, an EcoRV site is located 1kbp downstream of the AflIII site, allowing for easy verification through the presence of absence of this restriction fragment, as a successful deletion mutant would lack the AflII site, resulting in only one restriction fragment at 6.8kbp (**Fig. 3.20B**). Alternatively, for Broccomyces-*bldDp*, the EcoRV site is not present. As such, an XhoI site was chosen as an alternative restriction site, which following digestion with XhoI and AflII, results in two restriction fragments of 2.8kbp and 4kbp in length, with a successful deletion candidate only exhibiting one restriction fragment at 6.8kbp (**Fig. 3.20C**)

The modified plasmids were then sent to Plasmidsaurus for whole plasmid sequencing to confirm both full HHR removal and no impact on the coding sequence following the deletion. Sequencing confirmed the removal of the HHR in both Broccomyces-*ermE*p* and Broccomyces-*bldDp* without impacting the sequence of the adjacent promoters of interest and Broccoli aptamer. Once the HHR was confirmed to have been excised from both Broccomyces constructs, the modified plasmids were transformed into *E. coli* ET12567 pUZ8002 and conjugated into *S. coelicolor* M145 (**Fig. 3.21**).

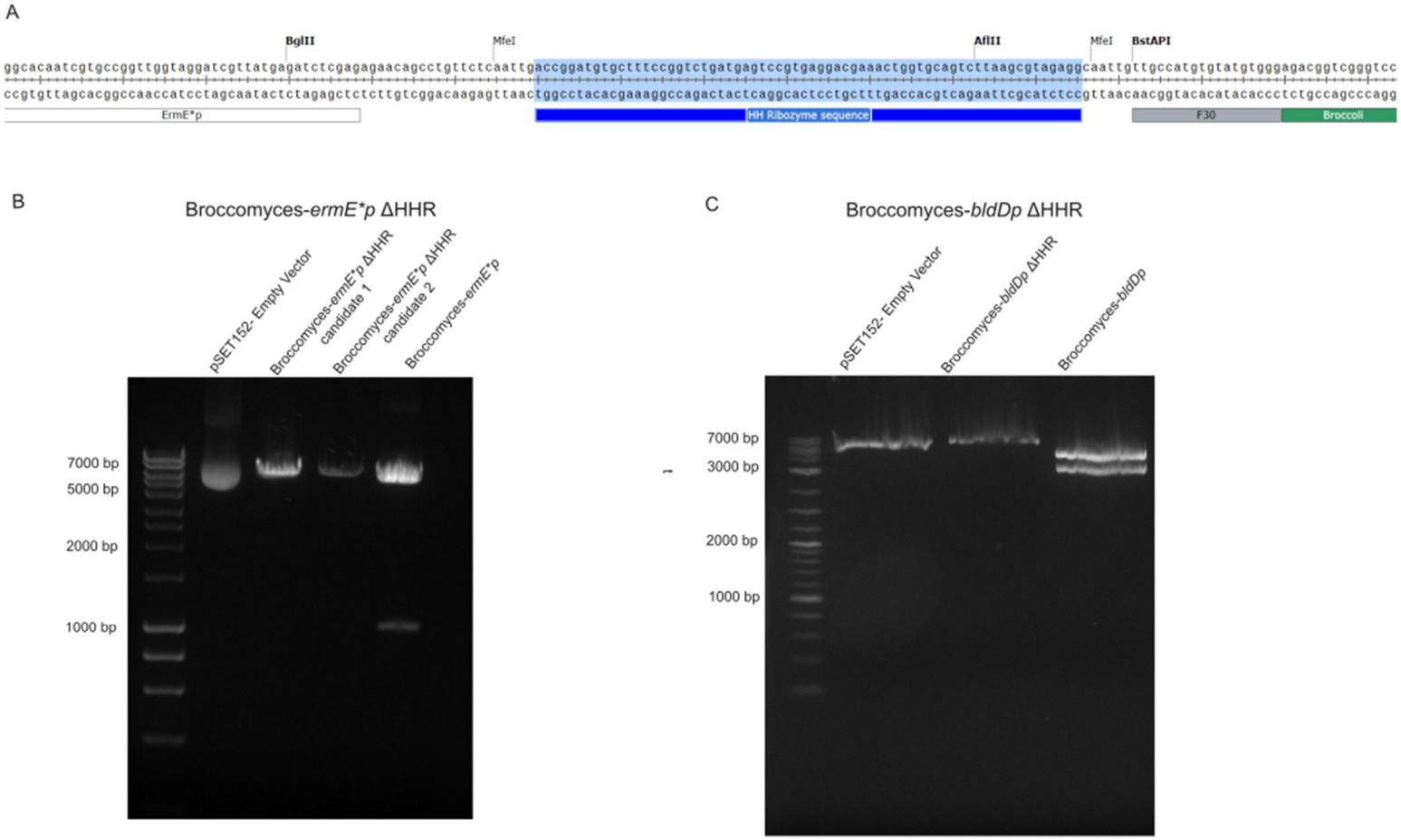

Fig. 3.20: Removal of Hammerhead Ribozyme (HHR) from dual reporter construct. (A) SnapGene visualisation of the Broccomyces-*ermE*p* plasmid, containing the *ermE** promoter, the HHR and the Broccoli aptamer (with its F30 scaffold). The HHR, flanked by two MfeI sites is highlighted **(B)** Agarose gel electrophoresis confirmed HHR removal through restriction digestion analysis for Broccomyces-*ermE*p* ΔHHR and Broccomyces-*bldDp* ΔHHR

A

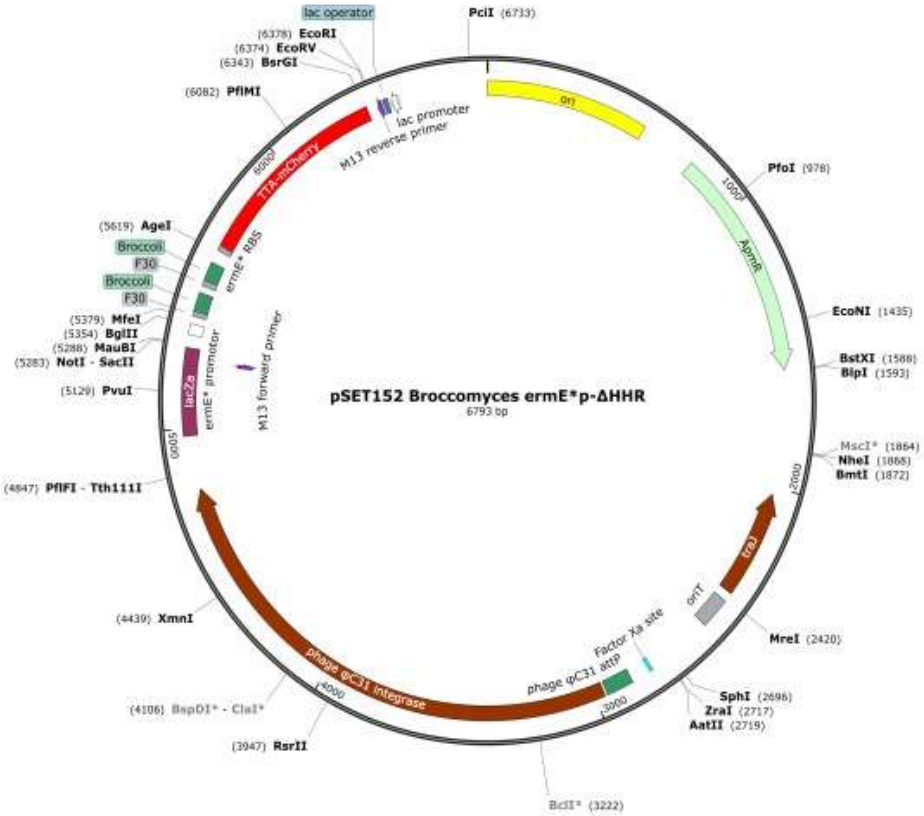

B

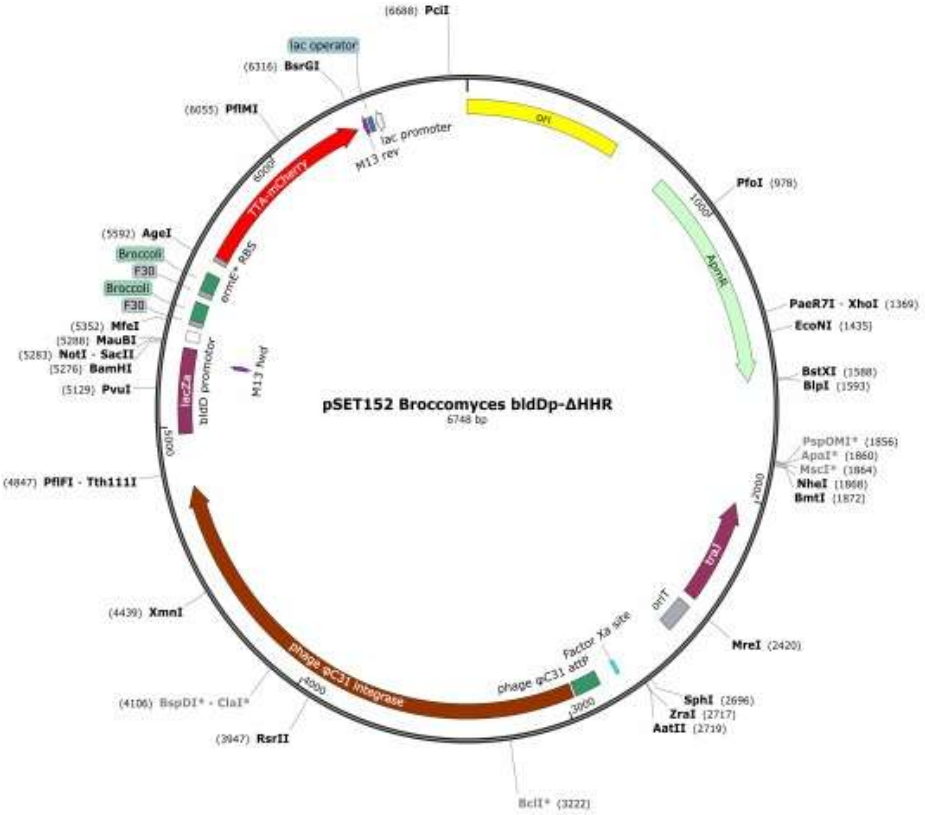

Fig. 3.21: Plasmid maps for the (A) Broccomyces-*ermE*p* ΔHHR and (B) the Broccomyces-*bldDp* ΔHHR.

Plasmid maps were generated by SnapGene TM.

3.3.13 Testing with ΔHHR-Broccoli yields minimal Broccoli-based fluorescence in *Streptomyces coelicolor*

Integration of the modified plasmids did not impact *Streptomyces* morphology or growth, similar to the HHR-containing Broccomyces plasmids. Following successful conjugation, *S. coelicolor* M145 strains possessing the ΔHHR-Broccomyces plasmids were subjected to both fluorescence microscopy (**Fig. 3.22, Fig. 3.23)** and the most optimised version of the 96-well plate assay, to determine whether removal of the HHR resulted in improved Broccoli fluorescence visualisation (**Fig. 3.24**).

Fluorescent microscopy was carried out with the same methodology outlined previously (see **Section 3.3.3**), with grown *Streptomyces* hyphae adhering to angled cover slips in MS media, before being visualised in the presence and absence of 40mM DFHBI-1T. As with the previous microscopy image analysis, microscope slides were imaged using an Olympus Fluorescent microscope, measuring 70% gain and an exposure time of 600ms for both Broccoli and TTA-mCherry fluorescent measurement. Obtained images were then analysed using the program Fiji ImageJ.

Image analysis from widefield fluorescence microscopy showed no noticeable improvement in Broccoli fluorescence with the HHR absent, compared to when the HHR was present, both in Broccomyces-*ermE*p* (**Fig. 3.22**) and Broccomyces-*bldDp* (**Fig. 3.23**), regardless of time point. In some cases, such as at 48 hours of incubation in *S. coelicolor* strains containing the Broccomyces-*bldDp* plasmids, higher levels of Broccoli fluorescence were seen in the strain possessing the HHR, compared to the deletion strain (**Fig. 3.23B, Fig. 3.23E**). However, in most cases, the absence of the HHR has no detectable effect on improving Broccoli fluorescence detection, irrespective of the promoter being tested. These data suggest that leaving the Broccoli aptamer attached to the mRNA sequence does not improve Broccoli aptamer visualization and challenges the initial assumption that the HHR might hinder transcript accumulation or folding and instead points to a potentially stabilizing or expression-

enhancing role. These data also further highlight the functionality and individuality of the TTA-mCherry reporter dependant on the tested promoter, with the *ermE*p* construct detectable at all timepoints, regardless of the presence of the HHR (**Fig. 3.22).** Converserly, TTA-mCherry fluorescence is easily detectable in the *bldDp* construct at both the 24- and 48-hour timepoints, while being undetectable at 72 hours, likely attributable to reduced activity at later growth cycle stages (**Fig. 3.23**). This difference in detectable fluorescence between both reporters indicating signal separation between the two reporters, allowing both reporters to serve as independent readouts for promoter activity without interference from the other.

To determine whether the data from the microscopy findings remains consistent, both the *S. coelicolor* HHR+ and ΔHHR Broccomyces strains were subjected to readout quantification using the most optimised version of the 96-well plate–based fluorescence assay that had been tested that this stage of optimisation (See **Section 3.3.11**). Consistent with the microscopy results, compared to the HHR+ strains (**Fig. 3.24A**), the plasmids exhibited no significant increase in Broccoli fluorescence relative to their HHR+ counterparts (**Fig. 3.24B**). This absence of detectable Broccoli fluorescence is also consistent with the previous optimisation attempts, which could be contributed to the fact that aerial hyphae formation and sporulation is blocked in liquid culture for *S. coelicolor* (Manteca and Yagüe, 2018). Fluorescence levels associated with TTA-mCherry remained relatively consistent with previous data in both Broccomyces HHR+ and ΔHHR, further exemplifying that the HHR plays no role in affecting TTA-mCherry fluorescence, confirming the separation between the two reporter systems. Together, these data reinforce the null hypothesis that the hammerhead ribozyme does not impair Broccoli reporter performance in *S. coelicolor*, with some conditions, such as solid media growth and microscopy, suggesting the presence of the HHR to accurately cleave the aptamer, enhances detectable Broccoli fluorescence.

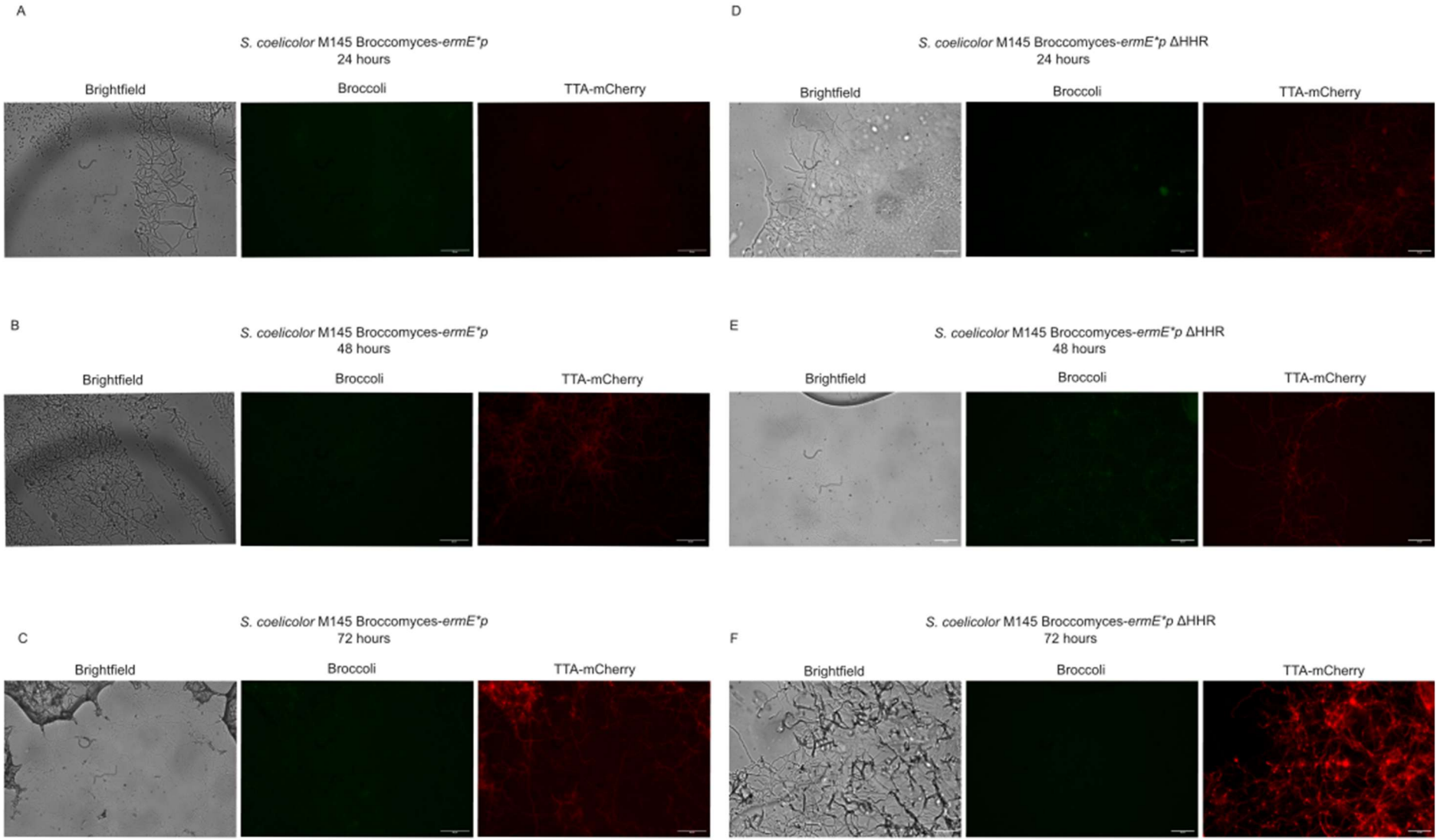

Fig. 3.22 Fluorescence and Brightfield microscopy of *S. coelicolor* Broccomyces- *ermE and *S. coelicolor* + pSET152 Broccomyces-*ermE*p* ΔHHR**. Imaged at 24, 48 and 72 hours after incubation with 40μM DFHBI-1T. No substantial increase in Broccoli fluorescence detected at any timepoint. Scale bar = 25 μm.

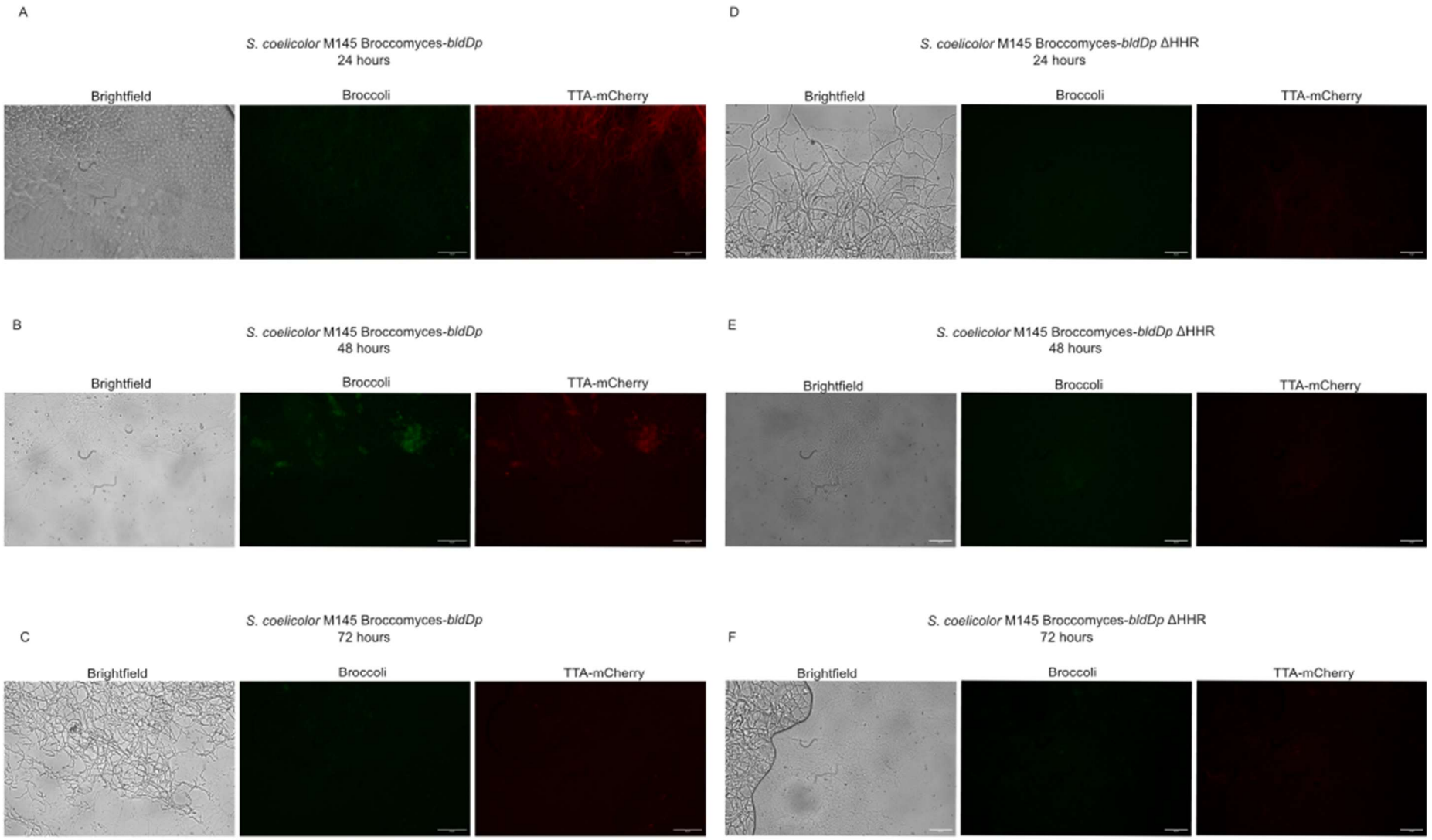

Fig. 3.23: Fluorescence and Brightfield microscopy of *S. coelicolor* Broccomyces- *ermE*p* and *S. coelicolor* + pSET152 Broccomyces-*ermE*p* ΔHHR. Imaged at 24, 48 and 72 hours. Similar to Broccomyces-*ermE**, no substantial increase in Broccoli fluorescence detected at any timepoint following removal of HHR. Scale bar = 25 μm.

A

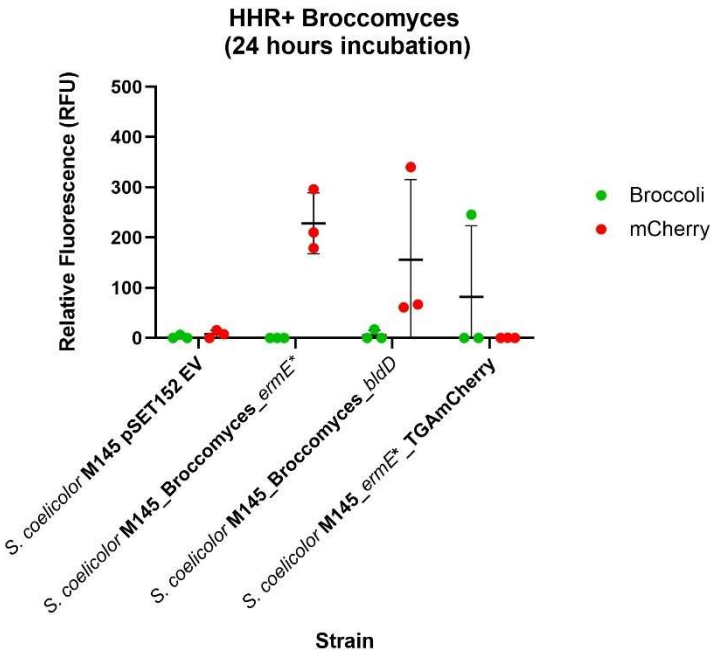

B

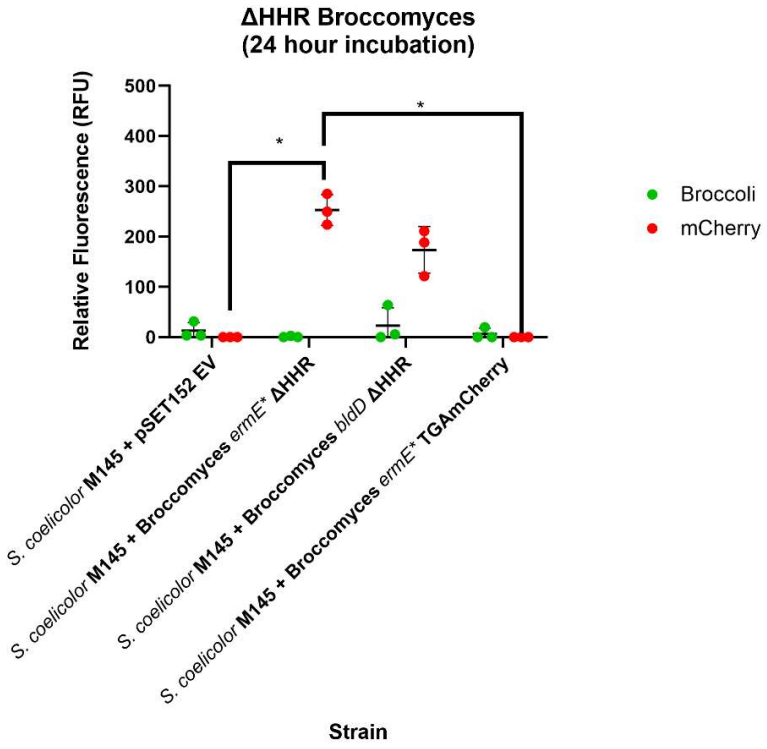

Fig. 3.24: Fluorescence assay analysis of Broccomyces dual-reporter plasmids (HHR+ vs. ΔHHR) in *S. coelicolor* M145. Broccoli and TTA-mCherry signals were measured in strains containing either the wild-type plasmid with the (**A**) hammerhead ribozyme (HHR+) or the (**B**) ribozyme-deleted variant (ΔHHR) under the control of *ermE** or *bldD* promoters. Error bars represent standard deviation from three biological replicates. Data was analysed with Kruskal-Wallis tests (*p*-values: **A**:0.0057, **B**:0.0006), followed by Dunnett's multiple comparisons tests between strain (*p < 0.05, **p < 0.01).

3.4 Summary

The development of the Broccomyces dual reporter system was driven by the aim to create a high-throughput assay capable of simultaneously reporting transcriptional and translational outputs in *Streptomyces coelicolor*. While the protein-based TTA-mCherry fluorescence consistently proved to be reliable, responsive, and promoter-dependent across all optimisation experiments, the RNA-based Broccoli fluorescence reporter presented persistent challenges that, despite numerous optimization attempts, could not be overcome under the current system design. The Broccoli aptamer-DFHBI complex could be visualised in the solid medium system suggesting that the differences in the way that these organisms grow may affect RNA stability and turnover and requires further investigation. Fluorescence microscopy investigation confirmed that Broccoli/DFHBI and Broccoli/DFHBI-1T fluorescence could be visualized, initially suggesting the aptamer-fluorophore complex formed normally within *S. coelicolor* cells. However, current attempts to transition the Broccomyces reporter to a high-throughput 96-well assay format failed to produce Broccoli fluorescence above background levels despite an exhaustive investigation in to optimising the variable of the experiment.

Investigation of the influence of growth phase, washing buffer, the concentration and nature of the fluorophore (DFHBI or DFHBI-1T), solvent, incubation time and hammerhead ribozyme impact on Broccoli fluorescence were all investigated and while the TTA-mCherry-translational reporter of the Broccomyces system remains fully functional and informative for probing translation in *Streptomyces*, suggesting that the system functions, the Broccoli aptamer does not function well in liquid cultures of *Streptomyces*. This could be attributed to several intracellular conditions, including poor aptamer folding, transcript stability, or the high-GC content of *Streptomyces* impacting Broccoli performance, with literature showing the use of these systems in GC-rich bacteria is currently scarce (Henri *et al*, 2019, Jensen *et al*, 2023). As of now, the Broccomyces system can reliably function as a translational reporter, but use as transcriptional reporter in high-throughput *S. coelicolor* assays remains limited. There is also the potential to investigate the use of the system in other *Streptomyces* species.

Chapter 4: Application of the Broccomyces dual-reporter system in *Streptomyces coelicolor* to study *bldA*-dependent gene regulation

4.1 Introduction

Gene expression in *Streptomyces* is regulated at both the transcriptional, post-transcriptional, translational and post-translational levels, with multi-level of control influencing differentiation, metabolism, and specialised metabolite production (Lee *et al*, 2020., McCormick and Flärdh, 2012 Płachetka *et al*, 2021). Developing methods to help visualize these regulatory processes is essential to elucidate the spatial and temporal control of these processes in these bacteria. The previous chapter highlighted the potential use of a Broccoli/mCherry dual-reporter system for the visualisation and quantification of transcriptional and translational output in *Streptomyces coelicolor*. However, while the modified TTA-mCherry continues to provide a visible fluorescence output under both microscopic and high-throughput conditions, attempts to visualize transcriptional output via fluorescence of the Broccoli aptamer have so far been limited, suggesting possible problems in the stability, folding, or maturation of the Broccoli RNA structure in *S. coelicolor* gene expression.

During the early optimisation of the orthogonal Broccoli/mCherry system, expression of the TTA containing mCherry was observed, including at timepoints when the *bldA*-tRNA is reportedly unavailable. To further investigate *bldA*-dependent regulation of gene expression, a more in-depth study of the system was undertaken. Since *bldA* is required for the translation of TTA-containing genes, and *bldD* functions as a transcriptional repressor of *bldA* during vegetative growth, mutants of these genes provide valuable genetic backgrounds to examine gene regulation at both transcriptional and translational levels (den Hengst *et al,* 2010, Hackl and Bechthold, 2015, Yan *et al*, 2019). Investigations into the quantification of transcription and translation in both *bldA* and *bldD* deficient backgrounds will provide further clarity on how *bldA* and *bldD* functionally impact gene expression.

4.2 Aims of this chapter

The aims of this chapter are to study the transcriptional and translational landscape of *bldA*-dependent gene regulation in *Streptomyces* to validate the orthogonal Broccoli/mCherry system, and to understand the observation that TTA containing mCherry appears to be translated at points in the *Streptomyces* lifecycle when *bldA* is not expressed, as seen in the previous chapter.

4.3 Results

4.3.1 TTA containing genes are translated throughout growth in *S. coelicolor* M145

The observation from the Broccomyces dual-reporter system optimisation chapter (see **Chapter 3**), that *bldA*-dependent genes (those containing a TTA codon) are expressed at all stages in the *Streptomyces* lifecycle, even when the *bldA*-tRNA is not available, required further investigation. These data are in contrast to the existing dogma, that UUA codons are not translated in the absence of the $tRNA^{bldA}$ (Chater, 2006., Leskiw *et al,* 1991., Rokytskyy *et al*, 2016). By using confocal microscopy (Leica SP8) in the presence of 40 μM DFHBI in 10% glycerol, it was found that transcription and translation of a TTA codon containing gene in WT *S. coelicolor* from the constitutive *ermE** promoter was apparent, even at 24 hours of growth, prior to initiation of development (**Fig. 4.1A**). Conventional thought, based on the literature is that when $tRNA^{bldA}$ is not expressed at an early-stages in the lifecycle (24 h), translation of TTA containing genes (in this case TTA-mCherry) would not be possible (Leskiw *et al*, 1993., Petterson and Kirsebom, 2011). To further test this, expression of the Broccomyces dual-reporter system was studied at a later point in growth (during aerial hyphae formation and sporulation – 72 h) when *bldA* was likely available for translation of TTA containing genes. At 72 hours of growth, expression of both Broccoli and mCherry were apparent in *S. coelicolor* M145 cells, indicating that *bldA* is available for translation of the TTA containing mCherry (**Fig. 4.1B**). However, this does not fully explain how translation maybe occurring at earlier stages of growth when *bldA* is unavailable.

The availability of *bldA* is dependent on *bldD*, although the role in regulation is not clear, given the atypical binding site of BldD in the *bldA* gene (den Hengst, 2010). If *bldA* is repressed by BldD, and the *bldD* promoter is developmentally regulated, then the expression of the Broccomyces dual-reporter system would be dependent on *bldD* expression (developmentally regulated). To test this, the Broccomyces dual-reporter system was driven from the *bldDp* in *S. coelicolor* M145, and expression examined at 24 hours (prior to *bldA* availability) (**Fig. 4.2A**)

and during development (*bldA* available; **Fig. 4.2B**). At the early time point (24h), *bldDp* dependent transcription of the Broccoli was very low, and this had increased by 72 hours. At both time points translation of the TTA-containing mCherry was apparent in the cells. Again, these data contradict the accepted literature.

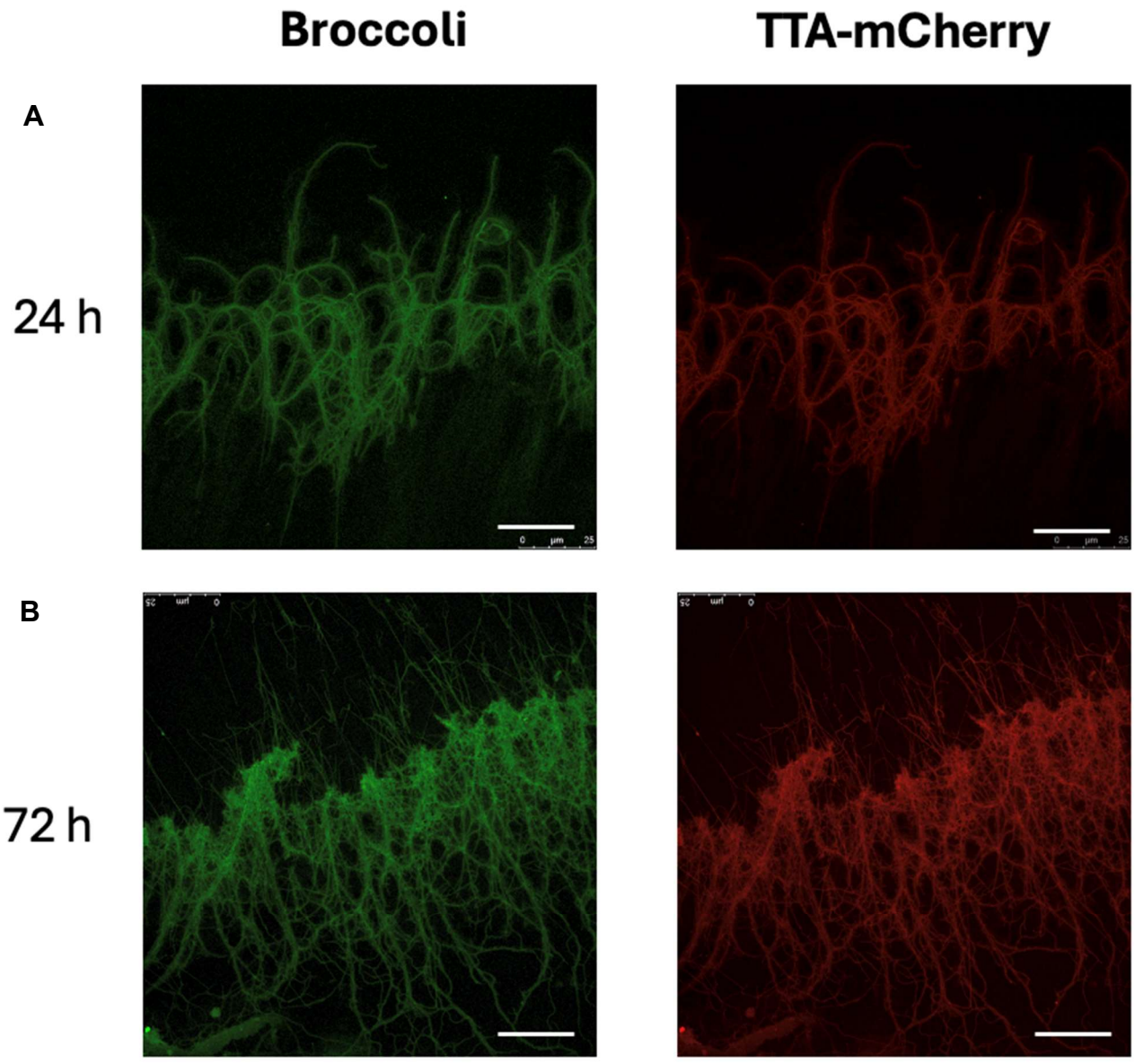

Fig. 4.1 TTA containing genes are translated throughout growth in *S. coelicolor* M145. Confocal Microscopy of *S. coelicolor* M145 coverslip cultures at (**A**) 24 h and (**B**) 72 h of growth showing transcription from the *ermE*p* and translation of the TTA-mCherry at both time points. Scale bar = 25 µm.

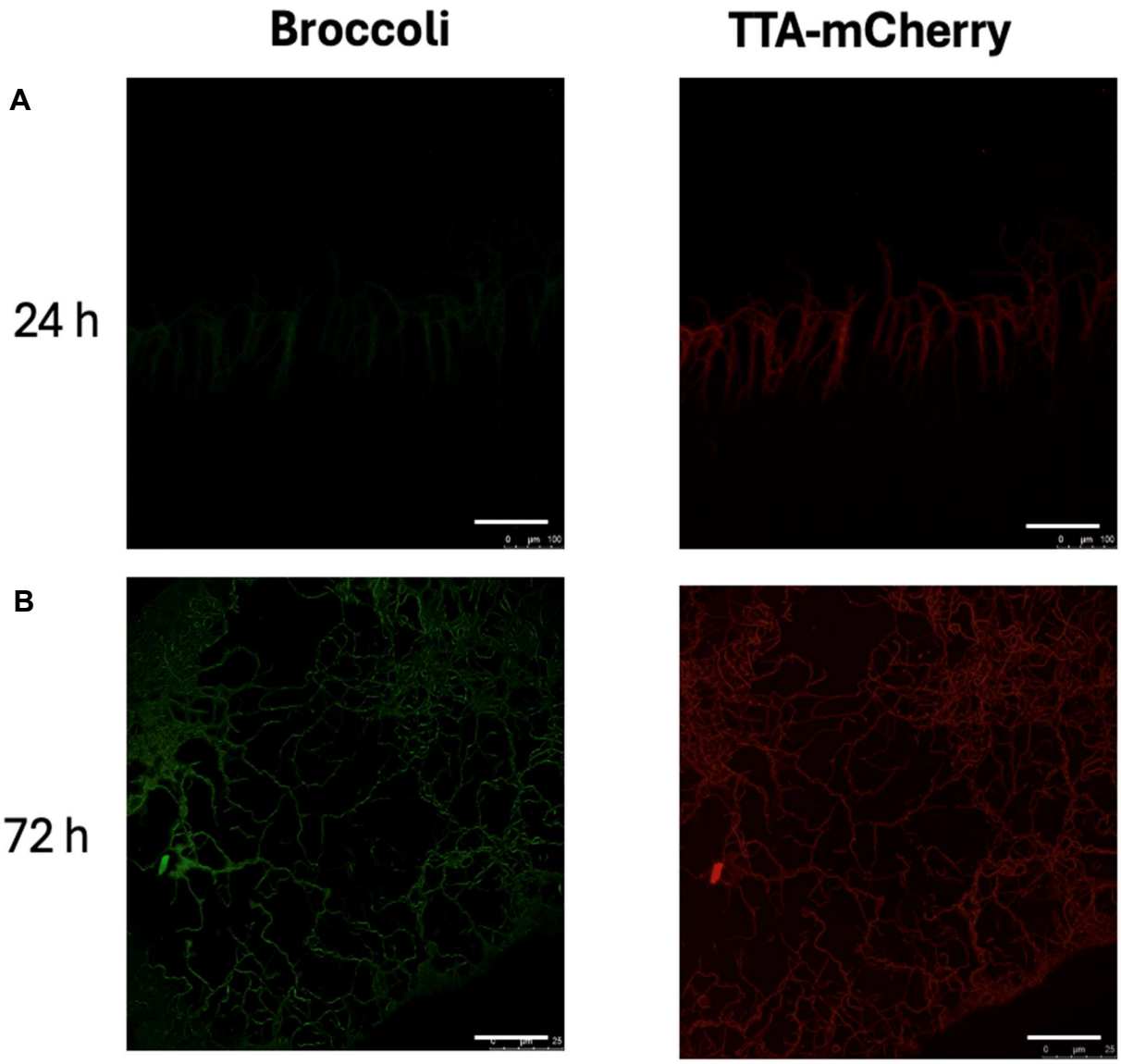

Fig. 4.2 TTA containing genes are translated throughout growth in *S. coelicolor* M145. Confocal Microscopy of *S. coelicolor* M145 coverslip cultures at (**A**) 24 h and (**B**) 72 h of growth showing transcription from the *bldDp* later in growth and translation of the TTA-mCherry at both time points. Scale bar = 25 µm.

4.3.2 TTA containing genes are translated in a *bldA* mutant background

To gain further insight into the possible translation of TTA containing genes in the absence of the *bldA*-tRNA, the Broccomyces dual-reporter system was introduced into the *bldA*-deficient strain *S. coelicolor* J1700 (Leskiw, Bibb and Chater, 1991). The hypothesis to be tested is that if TTA-mCherry translation was possible at supposedly non-permissive stages in the lifecycle of *Streptomyces*, then this could be due to either small amounts of *bldA* being available in the cell, sufficient for translation or through Wobble-Base pairing, where pairings between two nucleotides do not match Watson-Crick base pairs (Crick, 1966).

To test this, the two previously used constructs, Broccomyces-*ermE*p* and Broccomyces-*bldDp* were introduced into *S. coelicolor* J1700. Additionally, the Broccomyces-*ermE*p* TGA-mCherry (L11*) nonsense mutant, which lacks a functional mCherry protein due to a premature stop codon, was included as a TTA-mCherry negative control. The empty vector for pSET152 was also included as a negative control for the pSET152 backbone. Each of the Broccomyces plasmids was introduced into *S. coelicolor* J1700 using standard interspecies conjugation via *E. coli* ET12567/pUZ8002.

Exconjugants were selected on apramycin-containing media and verified by genomic DNA extraction and PCR, using the pSET152 Broccomyces check primers (primer numbers 1 and 2), to confirm successful integration (**Fig. 4.3**). The amplified region in the empty vector for pSET152 was 410bp, while the amplicon for the plasmids containing the Broccomyces reporter system was 1.5kbp. No observable differences in growth, pigmentation, or sporulation were noted between *S. coelicolor* J1700 transformants and the native *S. coelicolor* J1700 strain, as observed in *S. coelicolor* M145.

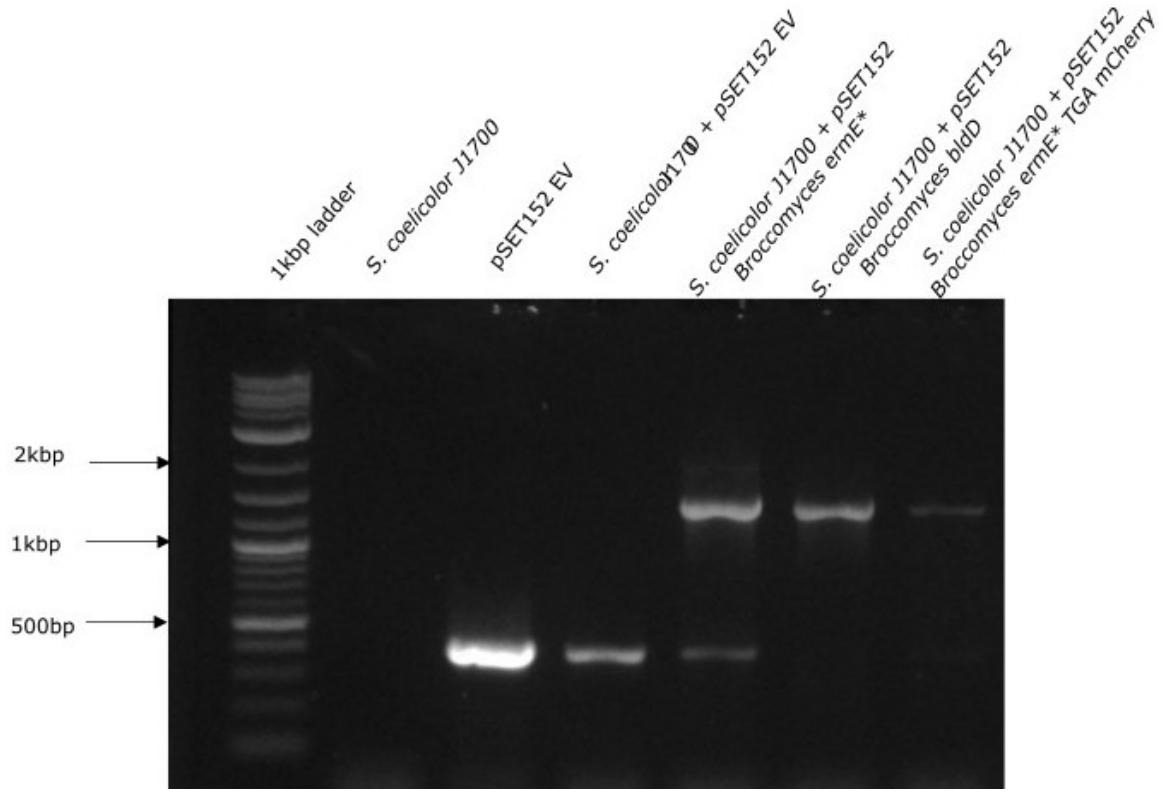

Fig. 4.3: Agarose gel electrophoresis of *S. coelicolor* J1700 candidates, showing successful Broccomyces system conjugation. *S. coelicolor* J1700 was included as a negative control for no inserted plasmid, whereas the pSET152 EV plasmid was included as a positive control for the presence of the amplicon.

When the *S. coelicolor bldA* mutant strain (J1700) was examined at 72 hrs of growth using confocal microscopy (Leica SP8), at a time point when *bldA* is available in WT cultures (Trepanier *et al*, 2002, Petterson and Kirsebom, 2011) transcription (Broccoli) and translation (TTA-mCherry) could clearly be seen in the cells with either the *ermE*p* (**Fig. 4.4A**) or the *bldDp* (**Fig. 4.4B**) Broccomyces constructs, indicating that TTA codon translation is possible, even when driven by developmentally regulated promoters. Imaging was performed under identical exposure conditions to those performed in the *S. coelicolor* M145 in the presence of 40 µM DFHBI in 10% glycerol.

One explanation for translation of the TTA-mCherry in the absence of the *bldA*-tRNA is through Wobble-Base pairing (WBP; Crick, 1966). It has been previously shown in both *E. coli* and *Streptomyces* species that the leucine $tRNA^{CAA}$ is able to read UUA codons when a UUA-reading tRNA is not present (Takai *et al*, 1994., Trepanier *et al*, 2002, Petterson and Kirsebom, 2011). The leucine $tRNA^{CAA}$ also possesses a higher codon usage than the leucine $tRNA^{UAA}$ (0.02 vs 0.00; See **Appendix 2**). Another explanation is the potential for targeted tRNA modification to enable the use of non-canonical tRNAs in translation (Schuntermann *et al*, 2024).

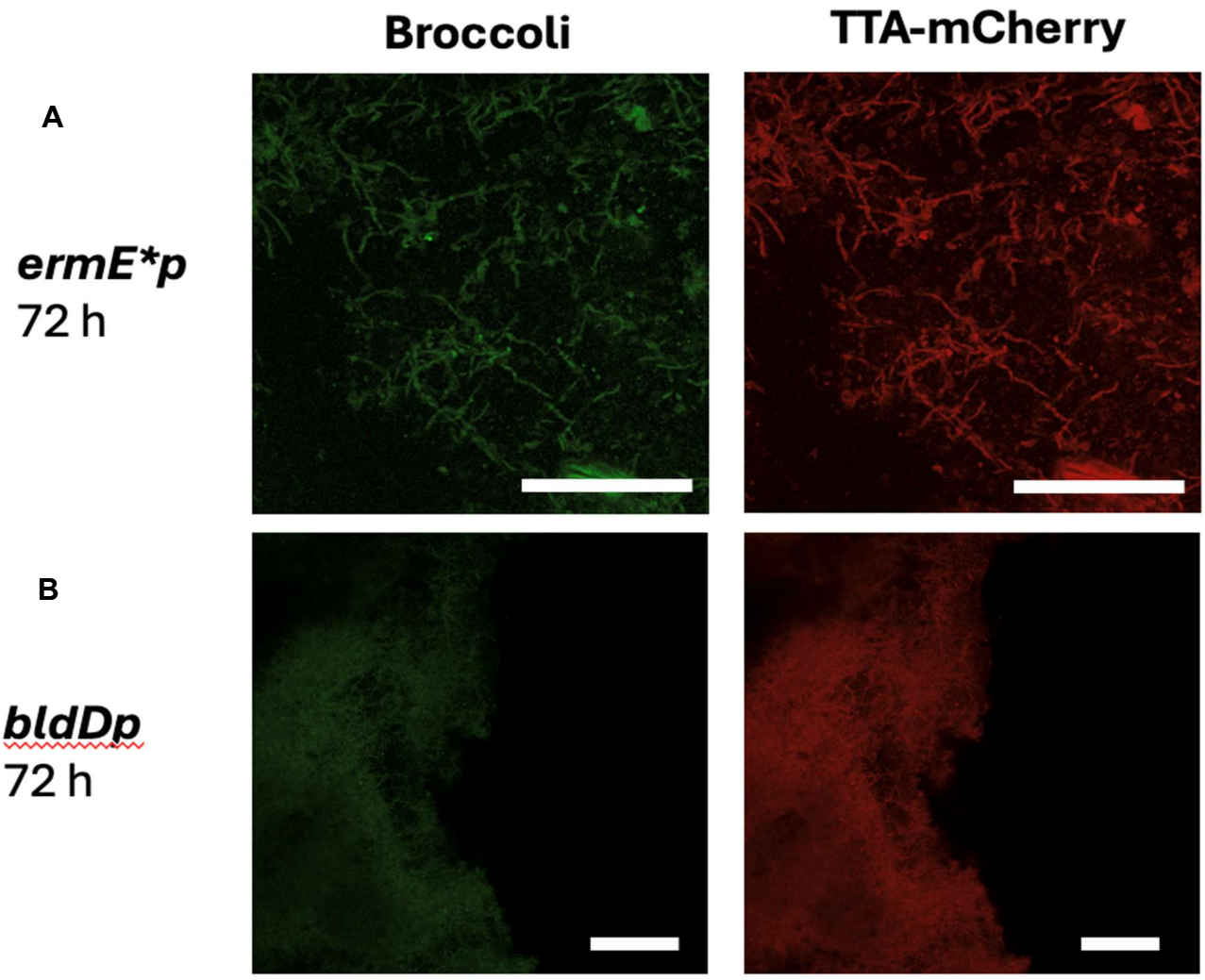

Fig. 4.4 TTA containing genes are translated in a *S. coelicolor bldA* mutant (J1700). A: Confocal Microscopy of *S. coelicolor* J1700 coverslip cultures at 72 h of growth showing transcription from the *ermE*p* showing translation of the TTA-mCherry. **B:** Confocal Microscopy of *S. coelicolor* J1700 coverslip cultures at 72 h of growth showing transcription from the *bldDp* showing translation of the TTA-mCherry. Scale bar = 25 μm.

4.3.3 TTA containing genes are translated in a *bldD* mutant background

To understand if translation of the TTA-mCherry was the result of suppression in the *bldA*-deficient mutant *S.coelicolor* J1700, through WBP or tRNA modification, or via a developmental mechanism, the Broccomyces system was introduced into the *S. coelicolor bldD* mutant (J774) (Merrick, 1976, Hunt *et al*, 2005). The *bldD*-deficient *S. coelicolor* J774 (*cysA15 pheA1 mthB2 bldD53* NF SCP2*) is characterized by a tyrosine to cysteine point mutation at position 62 (Elliot *et al*, 1998). This mutation results in a significant structural change to the BldD dimer, rendering it defective. Given that *bldD* regulates *bldA,* it was reasoned that controlling expression of *bldA*, through using a defective variant of the master regulator of development *bldD*, may offer some insight into how TTA translation may occur. Broccoli and TTA-mCherry fluorescence in the *S.* coelicolor J774 background was visualised using confocal microscopy (Leica SP8). Imaging was performed under identical exposure conditions to those performed in the *S. coelicolor* M145 and *S. coelicolor* J1700 backgrounds, in the presence and absence of 40 µM DFHBI in 10% glycerol (**Fig. 4.5**).

When the *S. coelicolor bldD* mutant strain (J774) was examined at 72 hrs of growth, at a time point when *bldA* should be available in WT cultures (Trepanier *et al*, 2002, Petterson and Kirsebom, 2011), transcription (Broccoli) and translation (TTA-mCherry) could clearly be seen in the cells with either the *ermE*p*-driven (**Fig. 4.5A**) or the *bldDp*-driven (**Fig. 4.5B**) Broccomyces constructs. These data indicate that TTA codon translation is possible, even when protein expression is driven by developmentally regulated promoters. Imaging was performed under identical exposure conditions to those previously.

An explanation for the presence of detectable TTA-mCherry in the absence of *bldD* is that without the global regulator repressing the *bldA* gene. This would allow for unregulated expression of the leucine-tRNA^{BldA}, resulting in an overexpression of *bldA*, which could be detected as an increased presence of TTA-mCherry. Loss of BldD has previously been shown result in precocious hypersporulation, while bypassing aerial hyphae formation (Tschowri *et al,* 2014., Bush *et al*, 2017). According to Bush *et al,* this loss of BldD essentially removes the developmental ‘brake ‘ from *S. coelicolor*, which results in unrepressed development, which may result in increased expression of genes commonly repressed by BldD, including *bldA*, subsequently resulting in increased levels of TTA codon-dependant translation and TTA-mCherry. A different explanation is through the expression of other genes in the absence of BldD. The loss of BldD would impact the wider regulatory network, including other repressors such as BldC and BldO, which represses *whiB* alongside BldD (Bush *et al*, 2017., Bush *et al*, 2019). The loss of BldD may result in a pleiotropic effects on other regulators, indirectly affecting their ability to regulate their targets, leading to the early expression of genes normally repressed until later stages in development, which may in turn influence *bldA* expression.

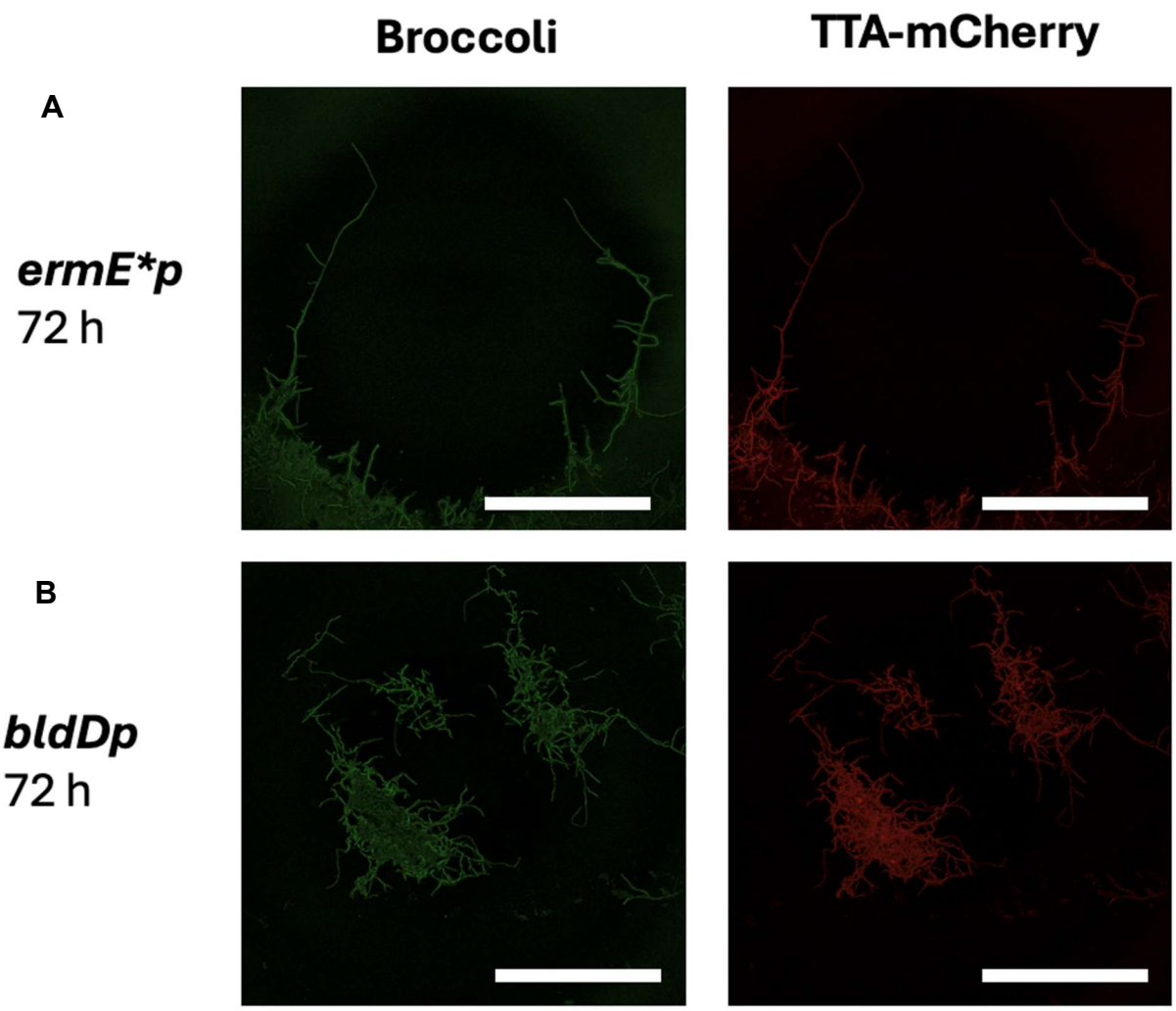

Fig. 4.5 TTA containing genes are translated in a *S. coelicolor bldD* mutant (J774). A: Confocal Microscopy of *S. coelicolor* J774 coverslip cultures at 72 h of growth, showing transcription from the *ermE*p* showing translation of the TTA-mCherry. **B:** Confocal Microscopy of *S. coelicolor* J774 coverslip cultures at 72 h of growth showing transcription from the *bldDp* showing translation of the TTA-mCherry. Scale bar = 25 μm.

4.3.4 Broccomyces reporter 96-well plate assay highlights TTA-mCherry is translated under conditions that were thought to be non-permissive.

Analysis of the confocal microscopy data highlighted that while Broccoli and TTA-mCherry fluorescence could be detected in the *S. coelicolor* M145, J1700 and J774 backgrounds after growth on solid media, the functionality of the Broccomyces constructs in these backgrounds in liquid culture required further investigation. Given that development in *S. coelicolor* is restricted in liquid culture (Schlimpert and Elliot, 2023., Yagüe *et al*, 2013), the strains containing the Broccomyces constructs were grown in spring-containing flasks containing TSB for 24 hours, washed twice in the Tris washing buffer, then transferred to a 96-well plate containing either 5 μM DFHBI-1T (final concentration 1% DMSO), or an equal concentration of DMSO (to serve as a DFHBI negative control). Post-inoculation, the plates were incubated at 30ºC for 15 minutes before being read using a FlexStation3 plate reader (Molecular Devices), measuring fluorescence according to the excitation and emission spectra of the Broccoli/DFHBI-1T aptamer/fluorophore complex (472nm/507nm) and TTA-mCherry (587nm/610nm).

Broccoli fluorescence was measured at background levels for all Broccomyces constructs, with only one biological replicate per construct exhibiting detectable Broccoli fluorescence (**Fig. 4.6**). This inability to visualize Broccoli fluorescence in *Streptomyces* after growth in liquid culture is consistent with previous data seen in *S. coelicolor* M145 (See **Chapter 3**).

Consistent with previous data seen in **Chapter 3**, TTA-mCherry translation was observed in *S. coelicolor* M145 cultures. Conversely, TTA-mCherry fluorescence in the *S. coelicolor* J1700 background was considerably different compared to *S. coelicolor* M145, with substantially reduced TTA-mCherry fluorescence in both Broccomyces-*ermE*p* and Broccomyces-*bldDp* after 24 hours incubation (**Fig. 4.6B**). Compared to relative fluorescence seen in the *S. coelicolor* M145 background, TTA-mCherry fluorescence in both Broccomyces-*ermE*p* and Broccomyces-*bldDp* in the *S. coelicolor* J1700 background was approximately 10-fold lower,

when compared to the respective Broccomyces construct in the *S. coelicolor* M145 background. The reduction in TTA-mCherry output results in insignificance when compared to the empty vector in the *S. coelicolor* J1700 background, compared to significance when utilised in the *S. coelicolor* M145 background. This translational output reduction is consistent with what would be expected due to the absence of a functioning *bldA*-encoded TTA tRNA, however, the presence of some TTA-mCherry fluorescence, as opposed to the complete absence of the translational reporter, implies that some TTA-mCherry transcripts are successfully being translated, even in the absence of *bldA*. These data imply that the TTA codon in the engineered TTA-mCherry is still translated, which could be attributed to WBP. The visualization of TTA-mCherry fluorescence in both microscopy and the 96-well plate assay environments in a background that should result in the absence of mCherry fluorescence, however minor, is worth further investigation.

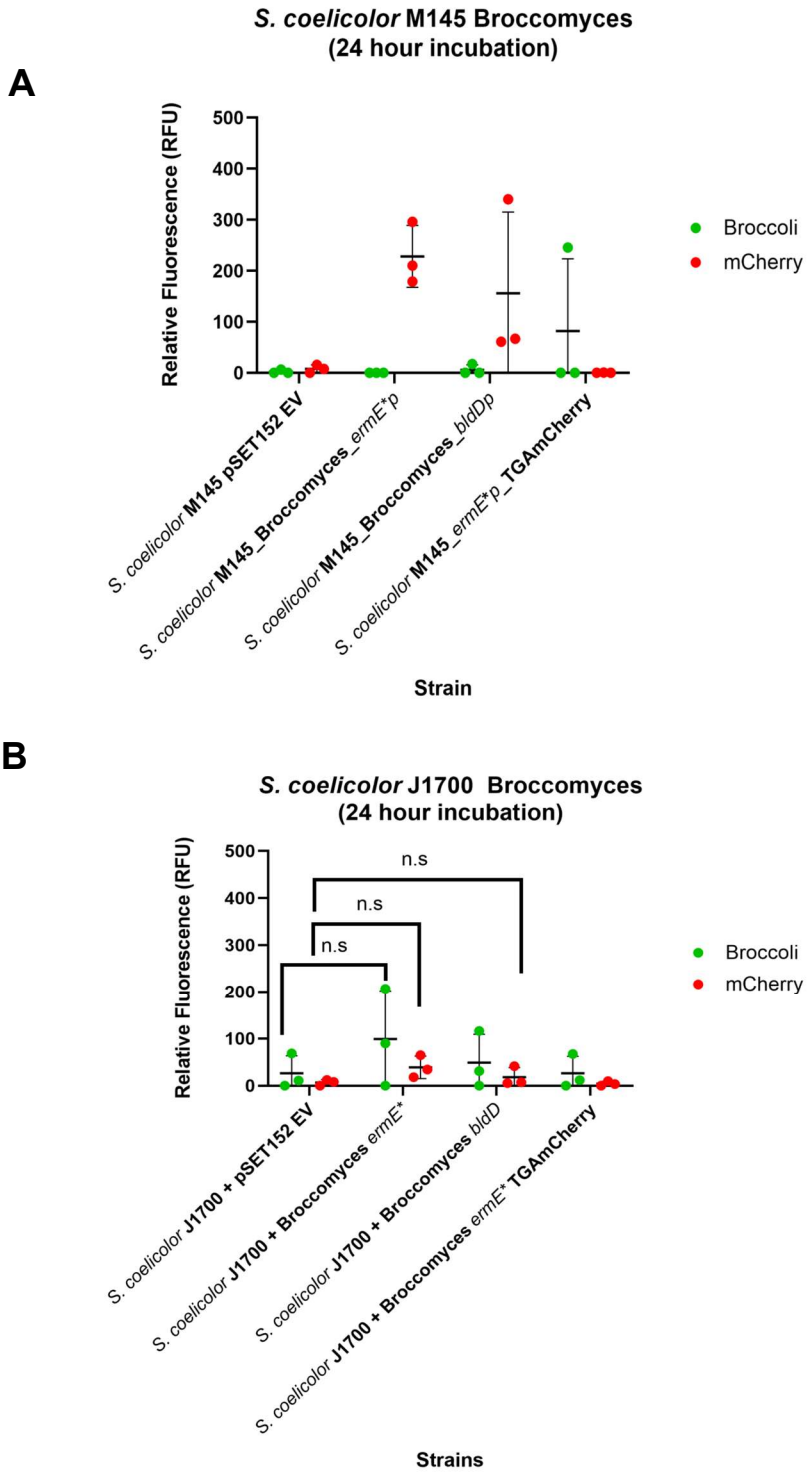

Fig. 4.6: Normalised fluorescence measurements of Broccomyces 96-well plate-based assay in (A) *S.coelicolor* M145 (WT) compared to (B) *S. coelicolor* J1700 (*bldA* mutant). Fluorescence measurements were normalised to cell density (OD_{600}) to account for differences in biomass per well. *S. coelicolor* J1700 Broccoli and TTA-mCherry data was analysed by Kruskal-Wallis test (p= 0.80, p=0.14 respectively), followed by Dunnett's multiple comparisons tests between strains (*p < 0.05, **p < 0.01)

After utilising the Broccomyces system in the *bldA*-deficient *S. coelicolor* J1700, the next step was to examine of the behaviour of Broccomyces constructs in the *bldD*-deficient *S. coelicolor* J774. The global regulator BldD represses a wide set of genes during vegetative growth, including *bldA*. As such, *bldD* indirectly influences the availability of the rare TTA-decoding tRNA by modulating *bldA* transcription (den Hengst *et al*, 2010, Tschowri *et al*, 2014). It was hypothesised that *bldD*- deficiency would lead to unregulated expression of *bldA*, leading to an increase of the leucine-tRNA^{BldA} (and TTA-mCherry translation), compared to WT *S. coelicolor*.

Similar to the *S. coelicolor* M145 and *S. coelicolor* J1700 background, Broccoli fluorescence could not be visualized above background levels in *S. coelicolor* J774 (**Fig. 4.7B**). This consistent inability to visualize Broccoli fluorescence could be explained by certain life cycle developments, such as sporulation, being repressed in liquid media (Manteca and Yagüe, 2018). This would explain to discrepancy between the presence and absence of Broccoli fluorescence visualisation on solid media and in liquid media respectively. Regardless, these data conclude that the Broccoli aptamer is not a reliable fluorescence reporter in liquid *Streptomyces* culture and will require further experimentation for sufficient utilisation.

Translation of the TTA-mCherry in *S. coelcolor* J774 could be detected at 24 hours in both the Broccomyces-*ermE*p* and Broccomyces-*bldDp* mediated constructs (**Fig. 4.7B**). When compared to relative fluorescence detected in the *S. coelicolor* M145 background, overall TTA-mCherry fluorescence was consistently higher in the *S. coelicolor* J774 background across all biological replicates. These findings further support the initial hypothesis that the lack of BldD repressing the *bldA* gene would result increased levels of the leucine-tRNA^{BldA}, , detected as higher TTA-mCherry relative fluorescence compared to the *S. coelicolor* M145 Broccomyces constructs. To conclude, while the Broccomyces system in liquid culture is not suitable as a transcriptional reporter due to the inability to visualize Broccoli-based fluorescence, the system has proven itself repeatedly as a translational reporter, based on the availability of the rare leucine TTA-tRNA, making it an asset for determining gene expression in *S. coelicolor*.

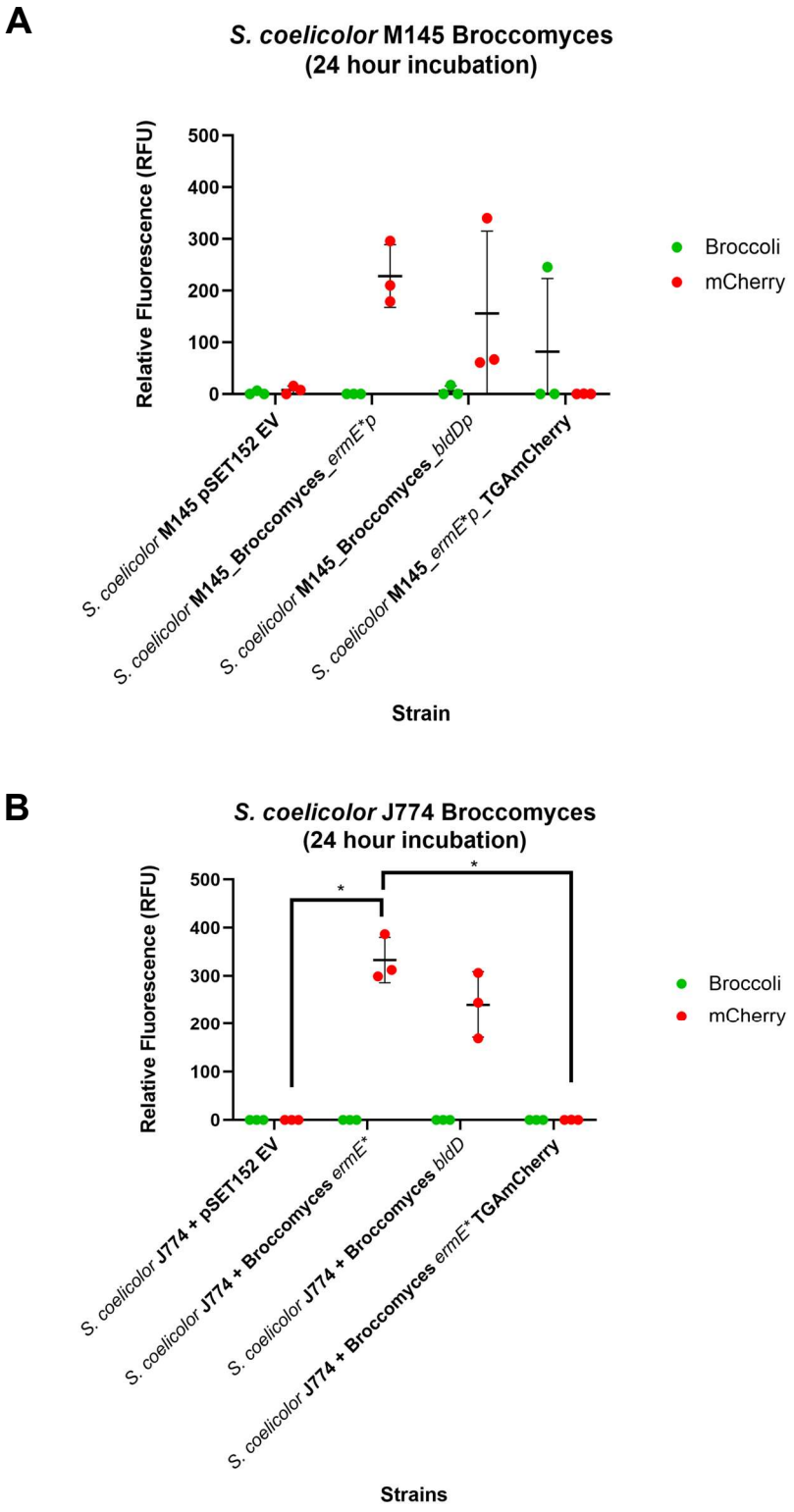

Fig. 4.7: Broccomyces 96-well plate fluorescence reporter output in (A) *S. coelicolor* M145 (WT) and (B) *S. coelicolor* J774 (*bldD* mutant). Fluorescence measurements were normalised to cell density (OD_{600}) to account for differences in biomass per well. TTA-mCherry data was analysed by Kruskal-Wallis test (p= 0.002), followed by Dunnett's multiple comparisons tests between strains (*p < 0.05, **p < 0.01)

4.4 Summary

Following optimisation of the Broccomyces dual-reporter system in *S. coelcolor* M145, the transcriptional and translational landscape of *bldA*-dependent gene regulation warranted further validation. Confocal microscopy of *S. coelicolor* M145 expressing the Broccomyces constructs at 24- and 72-hours confirmed that TTA codons are consistently translated at times and conditions where their translation is not expected, regardless of promoter dependency (**Fig. 4.1A, Fig. 4.2A**). This contradicts existing literature, as expression of *bldA* is minimal at this time in development (Leskiw *et al*, 1993., Petterson and Kirsebom, 2011). These data imply that an alternative mechanism exists for the translation of TTA codons prior to *bldA* expression.

To further investigate the translation of TTA containing genes in the absence of the *bldA*-tRNA, the Broccomyces constructs were conjugated into a *bldA*-deficient strain (*S. coelicolor* J1700) and a *bldD*-deficient strain (*S. coelicolor* J774). Confocal microscopy was repeated in these two mutant backgrounds and confirmed the translation of TTA codons in conditions previously thought to be unlikely, contrasting further against established literature (**Fig. 4.4, Fig. 4.5**). Translation of TTA codons in a *bldA*-deficient background could be attributable to WBP, which has been documented previously in strains lacking a UUA-reading tRNA (Takai *et al*, 1994., Trepanier *et al*, 2002, Petterson and Kirsebom, 2011). In a *bldD*-deficient background, the inability to repress genes usually developmentally regulated may give rise to overexpression of those genes, including *bldA*, resulting in detectable TTA-mCherry as part of the Broccomyces dual-reporter. The Broccoli/DFHBI aptamer-fluorophore complex could be visualized in all backgrounds and conditions, indicating detectable promoter-driven transcription in both wild-type and mutant backgrounds.

The Broccomyces dual-reporter was utilized in the *S. coelicolor* J1700 and *S. coelicolor* J774 backgrounds in liquid media to confirm if differences in background-dependant translational output could be quantified. Across all tests, the relative fluorescence for the Broccoli/DFHBI-1T complex could not be visualized above background levels, consistent with optimisation data from the previous chapter (see **Chapter 3**), concluding that the Broccoli aptamer functions for *Streptomyces* fluorescence microscopy, it is not a reliable transcriptional reporter in liquid *Streptomyces* culture. Relative TTA-mCherry fluorescence in the *S. coelicolor* J1700 background was comparatively lower, when compared to TTA-mCherry output in *S. coelicolor* M145. However, even in the absence of a functional leucine-tRNA^{BldA}, small levels of TTA-mCherry fluorescence were still detected, implying the presence of TTA codon translation and aligning with the previous confocal microscopy (**Fig. 4.6**). Comparatively, in the *S. coelicolor* J774 background after 24 hours of incubation, relative TTA-mCherry fluorescence was consistently higher than in *S. coelicolor* M145, further indicating that loss of BldD may result in unregulated expression of *bldA* (**Fig. 4.7**). Comparing solid media and liquid culture, the fluorescence profiles between conditions are different, however this is expected as much of *Streptomyces* development does not occur in liquid media (Manteca and Yagüe, 2018).

Together, these data suggest that an alternative mechanism, such as WBP or targeted tRNA modification, may result in the detectable translation of TTA codons in the absence of a functional leucine-tRNA^{BldA}, but more investigation is required to test this hypothesis (Crick, 1966., Schuntermann *et al*, 2024). However, before this, the TTA-mCherry fluorescence observed in *S. coelicolor* J1700 could be attributable to additional mechanisms, such as mutations that affect translation of TTA codons. While the genotype for *S. coelicolor* J1700 has been characterized, the wider genetic background is currently unknown, making it possible that additional mutations, beyond the characterized *bldA39* mutation, may influence its translational capacity (Merrick, 1976). To test this hypothesis, the genome of *S. coelicolor* J1700 will be sequenced and the mutational background explored.

Chapter 5: Genomic Characterisation of the *Streptomyces coelicolor bldA* mutant J1700

5.1 Introduction

Morphological development of *Streptomyces coelicolor* bald (*bld*) mutants is halted at an early stage in the lifecycle, preventing the formation of aerial hyphae and the subsequent development of spores (Pope *et al*, 1998). In addition to the loss of aerial mycelium formation, several mutations in the *bld* loci have been found to pleiotropically inhibit specialized metabolite production (Chandra and Chater, 2008; Chandra and Chater 2014). One of the more severe *bld* phenotypes that has been identified to date has been mapped to the *bldA* locus, where mutations result in complete loss of morphological development and specialized metabolite production (Chater and Chandra, 2006; Hackl and Bechthold, 2015). The *bldA* gene encodes the rare leucine (UUA) tRNA in *Streptomyces* species, with mutations in *bldA* abolishing the formation of aerial hyphae, rendering the streptomycetes unable to produce spores, this results in the presence of the vegetative mycelium only. *S. coelicolor* strains lacking a functional *bldA* gene are unable to synthesize specialized metabolites such as actinorhodin and undecylprodigiosin due to the biosynthetic gene clusters that encode them possessing a varying number of TTA codons, which requires a functional Leu-tRNA^{BldA} to be efficiently translated. A non-functional Leu-tRNA^{BldA} has a downstream effect on TTA-containing genes, by stalling translation and halting associated specialized metabolite production, making *bldA* crucial to antimicrobial production in *S. coelicolor*.

The classically studied *bldA* strain in *Streptomyces coelicolor*, J1700 was created using the *bldA39* mutation characterized by Merrick., (1976), which was subsequently phage cloned into the *S. coelicolor* J1501 strain background (*his1A, ura1A, strA1, pgl-1,* SCP1^{-}, SCP2^{-}), a strain historically used for genetic mapping experiments (Guthrie and Chater, 1990). The strain *S. coelicolor* J1700 was later used in studies by Leskiw *et al* to characterize the *bldA* gene (Leskiw *et al*, 1991; Leskiw *et al*, 1991; Leskiw *et al*, 1993). The genetic lesion leading to the

bldA morphological phenotype can be complemented through the addition of a copy of *bldA* gene either on a phage or on an integrating plasmid (Piret and Chater, 1985; Stone, Munnoch & Hoskisson, Unpublished; See **Section 6.2**). Studies of specialized metabolite production by the *S. coelicolor* J1700 (*bldA39*) strain demonstrated that mutants exhibit reduced expression of undecylprodigiosin (RED) BGC (Guthrie and Chater, 1990). Additionally, while actinorhodin (ACT) production appears to be controlled at the level of transcription, translation of the regulatory gene *actII-ORF4* appears to be *bldA*-dependent (Gramajo *et al*, 1993).

Many studies investigating the functionality of *bldA* to date have been conducted in the *S. coelicolor* J1700 (*bldA39*) strain, however the wider genetic background, is currently unknown. There may be underlying mutations in *S. coelicolor* J1700 that have not yet been identified, which have an unknown impact on specialised metabolite production not attributable to a non-functioning Leu-tRNA^{BldA}. This is problematic as these mutations may influence both specialised metabolite production, development, and TTA codon-dependant translation, with regards to the Broccomyces dual-reporter system. Therefore, in this chapter, the genome sequencing of the *Streptomyces coelicolor* J1700 mutant is described, as well as characterisation of additional mutations in that strain background through genome sequencing. The growth rate and specialised metabolite production of *S. coelicolor* M145 and *S. coelicolor* J1700 will also be compared, to understand if comparisons between these two strains are justified.

5.2 Aims

The aims of this chapter are to sequence the genome of the *bldA* mutant *Streptomyces coelicolor* J1700 and explore the wider mutational background of *S. coelicolor* J1700. This will allow for comparisons between underlying mutations and the phenotype observed in *S. coelicolor* J1700. The impact of the mutations in *S. coelicolor* J1700 on growth rate and specialised metabolite production will be investigated and compared to *S. coelicolor* M145.

5.3 Results

5.3.1 Whole Genome Sequencing of *Streptomyces coelicolor* J1700

Streptomyces genomes have several unique features which can result in increased difficulty in obtaining a whole genome sequence, such as high GC content, linear chromosomes and plasmids, and repetitive regions, particularly around polyketide synthase and non-ribosomal peptide synthetase gene clusters. However, *Streptomyces coelicolor* M145 and *Streptomyces coelicolor* J1700 lack the plasmids SCP1 and SCP2, which makes obtaining a genome sequence through genomic DNA extraction easier. As, such, genomic DNA from M145 and J1700 was extracted via phenol-chloroform extraction. For the sequencing of both strains, the Illumina NovoSeq 6000 platform was used, which produces read lengths of 2x250 bases. In the service provided by Novogene Ltd, a minimum of 90x coverage was guaranteed. A schematic summary diagram of the workflow used in this study for sequencing *S. coelicolor* J1700 can be found in **Fig. 5.1**.

Breseq is a computational pipeline that uses uses a combination of bioinformatic packages to find mutations relative to a reference genome and can report single nucleotide polymorphisms (SNPs), point insertions and deletions, as well as large deletions for WGS reads from a screened mutant strain (Deatherage and Barrick, 2014). Breseq mapping analysis of each strain was performed (using default settings, without --predict-polymorphisms) and the output GenomeDiff files were compared (gdtools COMPARE). The use of Breseq analysis reports ‘predicted mutations ‘, including small variants (indels and single nucleotide changes (SNC), and regions of ‘unassigned missing coverage evidence ‘ (typically large deletions). In the instance of this experiment, this was typically caused by deletions with read coverage of the *S. coelicolor* M145 reference sequence also present. Mutations were then transferred to the reference genome (using the gdtools APPLY command), generating a FASTA, GENBANK and GFF3 version of the genome containing the present mutations. This was carried out for all mutations in ‘predicted mutations ‘ while necessary manual edits were made as required.

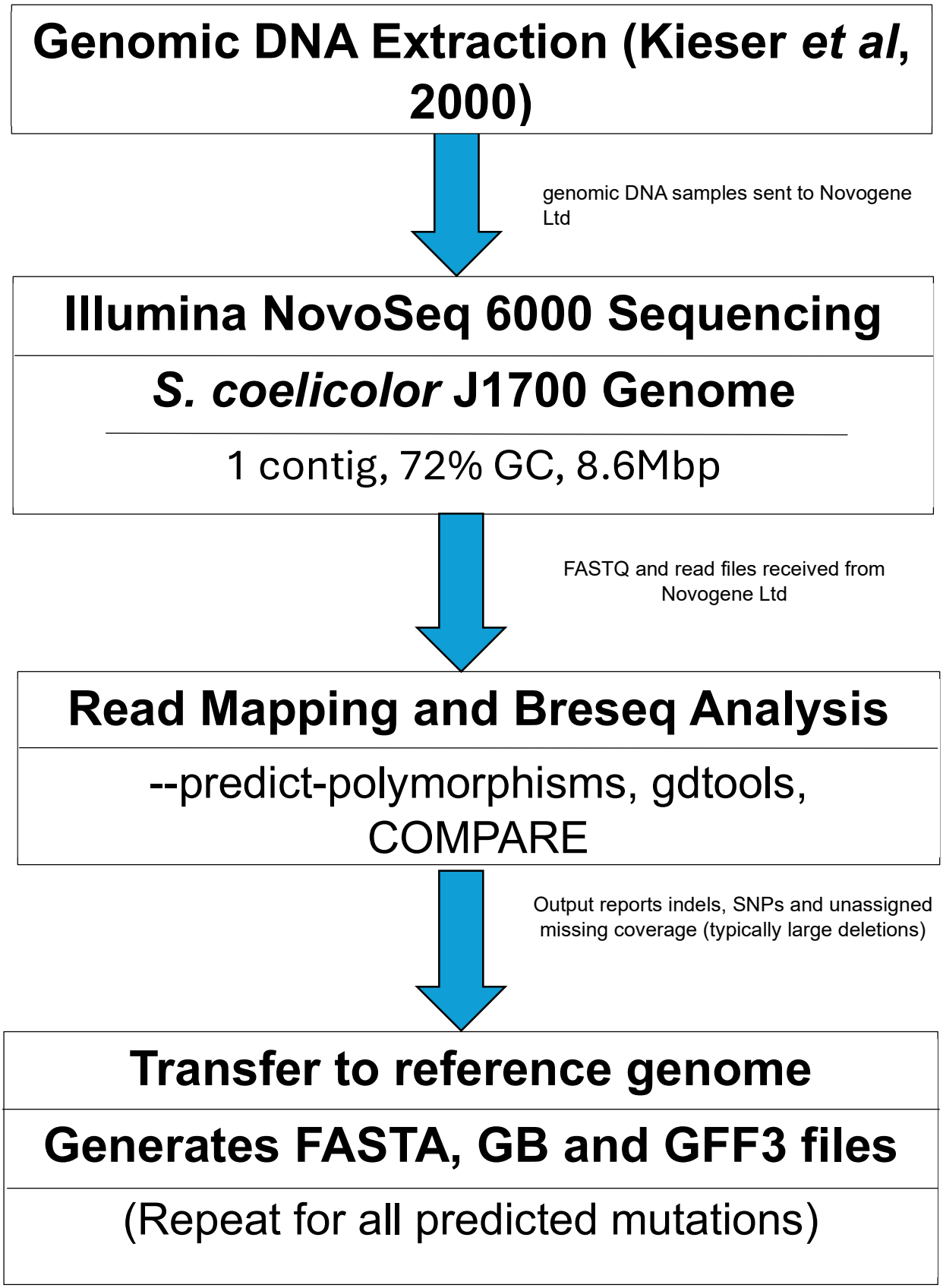

Fig. 5.1: Schematic workflow diagram describing *S. coelicolor* J1700 genome sequencing process, from extraction to bioinformatic analysis

5.3.2 The genome of *S. coelicolor* J1700 has extensive mutations across the genome that likely reflect the parental strain *S. coelicolor* J1501.

The whole genome sequence of *Streptomyces coelicolor* J1700 was determined at 137.6x coverage and was mapped to the wild type *S. coelicolor* M145 strain. The genome of *S. coelicolor* J1700 was determined to be 8,608,660 bp (**Fig. 5.2**), consisting of 7823 CDSs (compared to the 7825 CDSs found in *S. coelicolor* M145 (Bentley *et al*, 2002). **Fig. 5.2** also highlights any clusters of orthologues groups (COGs) found in the *S. coelicolor* J1700 genome, taken from the COG database (Galperin *et al*, 2021). These COGs are proteins found across a wide spectrum of bacteria, such as ribosomal proteins, aminoacyl-tRNA synthases and RNA polymerase subunits, as well as metabolic and signalling enzymes. The presence of tRNAs and rRNAs in *S. coelicolor* are also shown, between the COGs and CDSs on the forward and reverse strands.

Following Breseq analysis, an 'unassigned missing coverage evidence 'region of the *S. coelicolor* J1700 genome was identified, indicating a 53,414 bp deletion between 7,014,046 bp and 7,071,460 bp of the genome. This lack of coverage suggests the loss of genes from *SCO6353-SCO6406* (**Table 5-1**). Several other gene deletions were also detected (**Table 5-1**). Comparison of *S. coelicolor* M145 and J1700 reveals that there are 324 mutations in J1700 (**Appendix 1**). These mutations are characterised as 121 non-synonymous mutations, 78 synonymous mutations, 74 intergenic mutations, 39 coding frameshifts, three pseudogenes (SCO0634, SCO2890 and SCO4318), three deletions of approximately 1kb, (affecting the coding sequences of SCO3991, SCO4697, SCO4698, SCO4699, SCO5630, and SCO5632), three nonsense mutations, two non-coding (including *bldA* and methionine tRNA anticodon CAT) and two nonstop mutations. It is probable that many of these mutations reflect those in the *S. coelicolor* J1501 genetic background, from which J1700 was constructed (Piret and Chater, 1985). To test this hypothesis, additional WGS analysis with the J1501 progenitor strain would need to be performed, which is beyond the scope of this work.

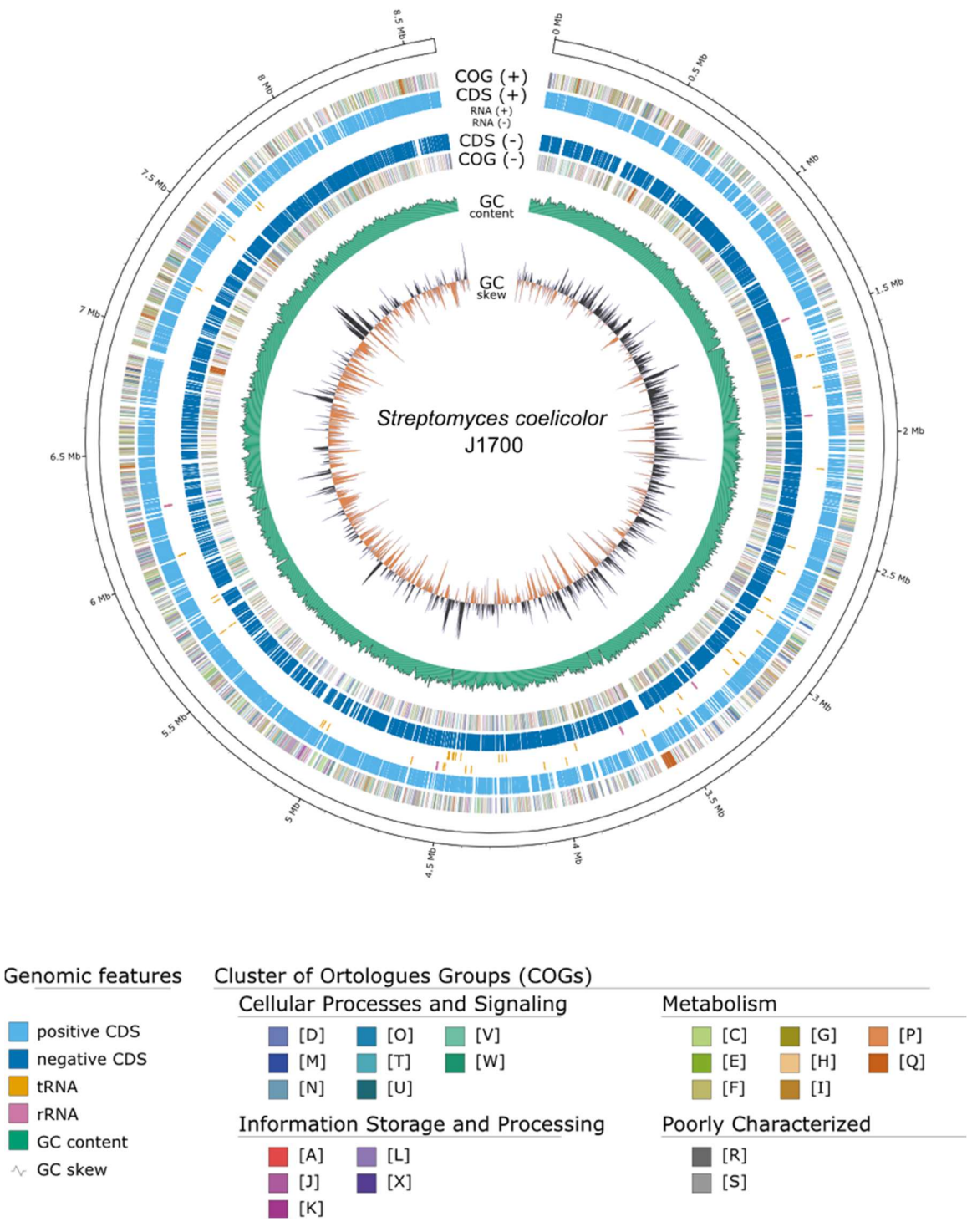

Fig. 5.2: GenoVi visualisation of the *S. coelicolor bldA* mutant (J1700) genome (GenoVi designed by Cumsille *et al*, 2023). Labelling highlights cluster of orthologues groups (COG) and coding sequences (CDS) on forward and reverse strands, along with GC content and skew (Galperin *et al*, 2021).

Table 5-1: Genes affected by the detected deletions in *S. coelicolor* J1700, their function, size and location

Gene	Function	Size (bp)	Location (5`-3`)
SCO3991	Transposase	880	4,388,129-4,389,009
SCO4697	putative integral membrane protein	1,814	5,121,109-5,122,923
SCO4698	putative insertion element IS1652 transposase	1,019	5,122,836-5,123,855
SCO4699	possible Rhs protein	2,783	5,123,855-5,126,638
SCO5630	probable IS1648 transposase	880	6,131,534-6,132,414
SCO5632	hypothetical protein SC6A9.35	242	6,132,437-6,132,679
SCO6353	probable two-component sensor	1,379	7,014,907-7,016,286
SCO6354	probable two-component regulator	614	7,016,283-7,016,897
SCO6355	probable integral membrane protein	818	7,016,899-7,017,717
SCO6356	probable integral membrane protein	605	7,017,714-7,018,319
SCO6357	putative membrane protein	686	7,018,316-7,019,002
SCO6358	conserved hypothetical protein SC3A7.26	389	7,019,120-7,019,509
SCO6359	possible integral membrane protein	929	7,019,506-7,020,435
SCO6360	probable ABC transporter ATP-binding protein	938	7,020,934-7,021,872
SCO6361	probable integral membrane protein	839	7,021,869-7,022,708
SCO6362	probable two-component sensor	1,289	7,022,727-7,024,016
SCO6363	probable two-component regulator	668	7,024,013-7,024,681
SCO6364	probable two-component regulator	791	7,024,745-7,025,536
SCO6365	probable integral membrane protein	2,642	7,025,526-7,028,168
SCO6366	probable ABC transporter ATP-binding protein	689	7,028,165-7,028,854
SCO6367	probable ABC transporter ATP-binding protein	737	7,028,841-7,029,578
SCO6368	probable lipoprotein	770	7,029,575-7,030,195
SCO6369	probable two-component sensor	1,310	7,030,354-7,031,664
SCO6370	probable integral membrane protein	1,034	7,031,672-7,032,706
SCO6371	probable integral membrane protein	839	7,032,798-7,033,637
SCO6372	questionable ORF	233	7,033,729-7,033,962
SCO6373	probable integral membrane protein	1,397	7,034,266-7,035,663
SCO6374	probable sugar transferase	1,436	7,035,788-7,037,224
SCO6375	probable secreted protein	662	7,037,737-7,038,399

SCO6376	probable integral membrane protein	899	7,038,757-7,039,656
SCO6377	probable lipoprotein	1,355	7,039,699-7,041,054
SCO6378	small hydrophobic protein	299	7,041,611-7,041,910
SCO6379	putative membrane protein	683	7,042,054-7,042,737
SCO6380	hypothetical protein SC4A2.16c	356	7,043,084-7,043,440
SCO6381	probable lipoprotein	1,343	7,043,724-7,045,067
SCO6382	possible secreted protein	908	7,046,618-7,047,526
SCO6383	probable integral membrane protein	683	7,048,443-7,049,126
SCO6384	probable integral membrane lysyl-tRNA synthetase	1,769	7,049,382-7,051,151
SCO6385	probable integral membrane protein	1,934	7,051,526-7,053,460
SCO6386	questionable ORF	383	7,053,632-7,054,015
SCO6387	questionable ORF	566	7,054,118-7,054,684
SCO6388	hypothetical protein SC3C8.07c	359	7,054,965-7,055,324
SCO6389	hypothetical protein SC3C8.08c	392	7,055,321-7,055,713
SCO6390	probable integral membrane protein	1,103	7,056,189-7,057,292
SCO6390	probable integral membrane protein	1,103	7,056,189-7,057,292
SCO6391	probable IS110 transposase/integrase	1,217	7,057,809-7,059,026
SCO6392	probable transposase	1,139	7,059,104-7,060,243
SCO6393	probable transposase IS21/IS1162 family	463	7,060,375-7,061,838
SCO6394	probable IS element ATP binding protein (IS21/IS1162 family)	770	7,061,835-7,062,605
SCO6395	probable IS element transposase	2,158	7,063,063-7,065,221
SCO6396	probable transposase for IS1648	880	7,063,621-7,064,501
SCO6399	hypothetical protein SC3C8.18c	515	7,065,214-7,065,729
SCO6400	probable transposase for IS117	1,244	7,066,309-7,067,553
SCO6401	unknown ORF in IS117	527	7,067,605-7,068,132
SCO6402	unknown ORF in IS117	353	7,067,650-7,068,003
SCO6403	hypothetical protein SC3C8.22c	380	7,068,218-7,068,598
SCO6404	hypothetical protein SC3C8.23	179	7,069,255-7,069,434
SCO6405	possible DNA recombinase	2,018	7,069,508-7,071,526
SCO6406	possible secreted protein	395	7,071,396-7,071,791

5.3.3 *bldA39* mutation in *S. coelicolor* J1700 results in an anticodon change from Leu-UAA to Ser-UGA

It was first shown by Lawlor and colleagues that the *bldA39* mutation resulted in a mutation in the anticodon loop of the Leucyl-tRNA^{UAA}, resulting in a putative seryl-anticodon as opposed to a leucyl-tRNA (Lawlor *et al*, 1987). This anticodon loop mutation prevents the leucyl-tRNA^{UAA} from complementary pairing with the UUA mRNA, and consequently, prevents efficient translation of the TTA codon. It is unclear if this mutated tRNA species can be charged with serine by the corresponding aminoacyl-tRNA synthetase (aaRS). Given the selectivity that aaRSs enzymes possess, it is unlikely this mutated tRNA can be charged, given the limited editing mechanisms of aaRSs between serine and leucine tRNAs (Tawfik and Gruic-Sovulj, 2020). The secondary structure impact this mutation has on the leucyl-tRNA^{UAA} is shown in **Fig. 5.3**.

The confirmation of the *bldA39* mutation results in an anticodon disruption means that J1700 represents the only 'classical' *bldA* mutant strain affecting the anticodon. Other documented mutations in the leucyl-tRNA^{UAA} encoded by *bldA* include those affecting the anticodon stem (bldA1 [nt2 8 G-A]) and the tRNA^{bldA} D-arm (*bldA16* [nt 22 C-T], *bldA62* [nt 23 A-C]) (Guthrie and Chater, 1990; Kwak *et al*, 1996). The single nucleotide T-C mutation attributed to the *bldA39* phenotype is found at position 3,380,959 in *S. coelicolor* J1700 chromosome (which equates to position 3,380,943 in *S. coelicolor* M145).

A

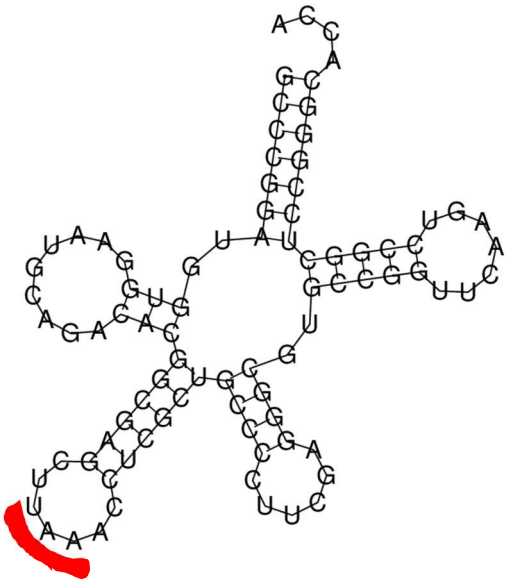

S. coelicolor **M145** ***bldA***

B

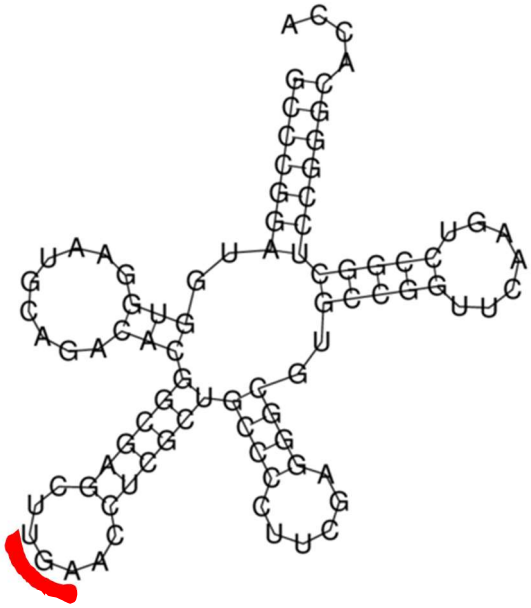

S. coelicolor **J1700** ***bldA***

C

```
M145_bldA   1 GCCCGGATGGTGGAATGCAGACACGGCGAGCTTAAACCTCGCTGCCCCTTCGAGGGCGTGCCGGTTCAAGTCCGGCTCCGGGCACCA  87
              ||||||||||||||||||||||||||||||||.|||||||||||||||||||||||||||||||||||||||||||||||||||||
J1700_bldA  1 GCCCGGATGGTGGAATGCAGACACGGCGAGCTTGAACCTCGCTGCCCCTTCGAGGGCGTGCCGGTTCAAGTCCGGCTCCGGGCACCA  87
```

Fig. 5.3: The secondary structures of the leucyl-tRNA^{UAA} encoded by *bldA*. A: The wild-type copy of the UAA tRNA found in *S. coelicolor* M145, resulting in a correct TTA codon. **B:** The mutated anticodon loop found in the *bldA* mutant J1700 Leucine-tRNA^{UAA} results in a serine-TCA codon, with the anticodon triplet highlighted. Secondary structures were created using the RNAFold Web Server, hosted by the University of Vienna (Gruber *et al*, 2008). **C:** Alignment of *S. coelicolor* M145 and J1700 *bldA* sequences, the tRNA anticodon is highlighted. Alignment carried out with EMBOSS Needle using 5` sequence start.

5.3.4 Absence of undecylprodigiosin expression on *S. coelicolor* J1700 may be the result of an *IS110* insertion located in the biosynthetic gene cluster (*red*)

Identification of biosynthetic gene clusters of the *S. coelicolor* J1700 genome was completed using the antiSMASH software (Blin *et al*, 2023). Analysis of the BGC data revealed the presence of all 24 BGCs known from *Streptomyces coelicolor* M145 (**Table 5-2)**, however, a more detailed investigation into the WGS data indicated the presence of several mutations inside some of these BGCs. It was reported previously by Guthrie & Chater (1990) that reduced RED gene expression was detected in the *S. coelicolor* J1700 strain when using *xylE* transcriptional reporter strains. Examination of *S. coelicolor* J1700 BGCs reveals the presence of a synonymous mutation in the undecylprodigiosin BGC pathway regulator *redD* (Malpartida *et al*, 1990), specifically L150L, the result of a CTC-CTT SNP. This mutation results in a change to a much less frequently used leucine codon, with a reduction in relative frequency from 38% to 2%; however, this synonymous mutation is unlikely to significantly affect RED gene expression as leucine translation is still present.

An additional mutation was detected in the intergenic region between SCO5885, a putative membrane protein and SCO5886 (*redR*), which encodes a -oxoacyl-[acyl-carrier protein] synthase II. WGS analysis revealed the presence of an inserted IS110 element in the intergenic region between SCO5885 and SCO5886 (**Fig 5.4**) (Chater *et al*, 1985). The inserted IS110 sequence contains an open-reading frame (ORF) for a transposase, an enzyme which catalyses the movement of a DNA sequence to a different part of the genome. As the inserted IS110 sequence runs in the same orientation as both SCO5885 and SCO5886, the inserted IS110 element is unlikely to interfere with the translation of SCO5886, however, due to its insertion in the intergenic region between the two genes, the IS110 sequence is more likely to have an impact on undecylprodigiosin production through promoter disruption or premature transcription termination. SCO5886 encodes a homolog of *fabF* (3-ketoacyl-ACP synthase II), in which mutations and deletions have been previously documented to result in substantial decreases in undecylprodiginine production (Mo *et al*, 2008).

Table 5-2: Summary of *S. coelicolor* J1700 Biosynthetic Gene Clusters as predicted by antiSMASH.

Region	Type	Region	Most similar	% similarity
1	hglE-KS	86.694-139,654	leinamycin	2%
2	terpene	166,501-192,008	isorenieratene	100%
3	lanthipeptide-class-i	246,526-271,084	lobophorin CR4	5%
4	NRP-metallophore,NRPS	493,989-552,325	coelichelin	100%
5	RiPP-like	791,584-801,799	informatipeptin	42%
6	T3PKS	1,257,625-1.298.479	flaviolin/1,3,6,8-tetrahydroxynaphthalene	100%
7	ectoine	1,995,500-2,005,898	ectoine	100%
8	melanin	2,939,306-2,949,875	istamycin	4%
9	NI-siderophore	3,024,895-3,054,682	desferrioxamin B/desferrioxamine E	100%
10	NRPS	3,523,335-3,603,988	CDA1b/CDA2a/CDA2b/CDA3a/CDA3b/CDA4a/CDA4b	87%
11	T2PKS	5,494,930-5,567,424	actinorhodin	100%
12	terpene	5,671,088-5,692,101	albaflavenone	100%
13	T2PKS	5,751,945-5,824,487	spore pigment	66%
14	NI-siderophore	6.326.587-6,356,533	kinamycin	19%
15	NRPS-like,T1PKS,prodigiosin	6,429,649-6,476,442	undecylprodigiosin	100%
16	RiPP-like	6,632,343-6,643,659		
17	terpene	6,656,219-6,678,399	geosmin	100%
18	NI-siderophore	6,833,315-6.864.522	enduracidin	10%
19	T1PKS,butyrolactone, hydrogen-cyanide	6,880.898-6,956,537	coelimycin P1	100%
20	thioamide-NRP,NRPS	7,088,264-7,142,447	nogalamycin	40%
21	lanthipeptide-class-iii	7,409,742-7.432.456	SapB	100%
22	terpene	7,506,017-7,532,758	hopene	100%
23	PKS-like,T1PKS	7,570,412-7.618.555	arsono-polyketide	92%
24	lanthipeptide-class-i	7,682,907-7,709,360		
25	other,T3PKS	7,793,470-8,047,475	germicidin	100%
26	indole	8,269,637-8,290,764	5-dimethylallylindole-3-acetonitrile	100%
27	T3PKS,NRP-metallophore,NRPS,terpene	8,475,102-8,549,581	coelibactin	100%

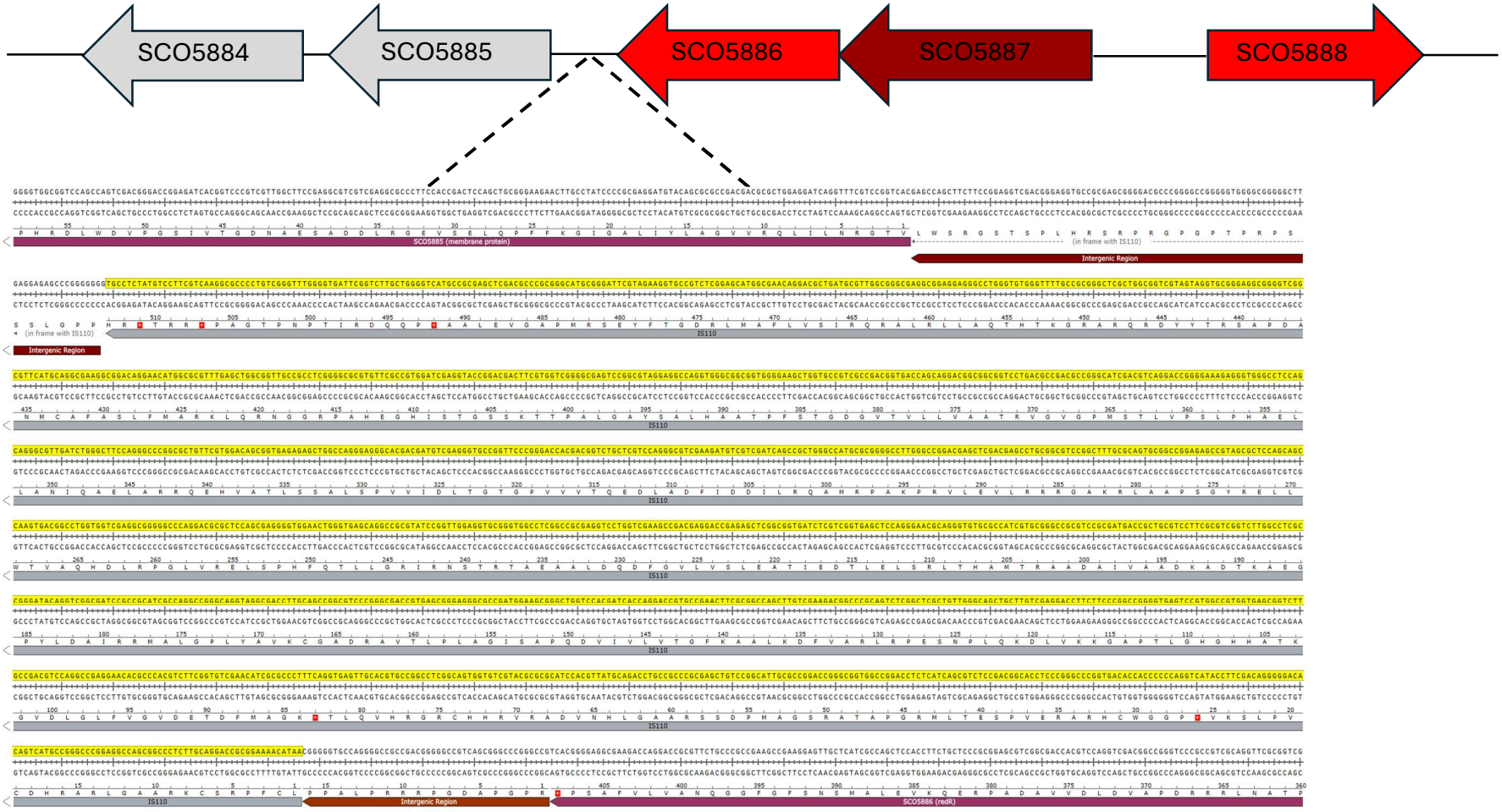

Fig. 5.4 Detailed genomic view of the IS110 insertion in the intergenic region between SCO5885 and SCO5886 in *S. coelicolor* J1700. The inserted IS110 element is highlighted in yellow.

5.3.5 Multiple mutations found across CDA synthase genes, potentially impacts CDA production

Further mutations in BGCs were detected, such as in the coelichelin BGC, with a synonymous mutation in a putative peptide synthetase (SCO0492; TTC-TTT; F2247F). Additional mutations are also present in the coelimycin BGC where two synonymous mutations are present in *cpkP*β (SCO6269: GCG-GCA; A166A; and GCG-GCC; A179A) and two further synonymous mutations in *cpkC* (SCO6273: GGG-GGC; G561G; and AAG-AAA; K562K) (Gomez-Escribano *et al*, 2012). The consequences of all these mutations are unknown; however, the synonymous mutations present in the BGC genes are unlikely to produce significant alterations to the phenotype of *S. coelicolor* J1700. To truly assess the consequences of these mutations, there would need to be extensive work through complementation studies to assess potential effects through mRNA stability of synonymous changes.

Two further missense mutations were also found in the calcium-dependent antibiotic (CDA) BGC, specifically in the CDA peptide synthetase I (SCO3230; CTC-GTC; L3479A; and GCC-GTC; A5927V). Alterations to the amino acid sequence caused by missense mutations are far more likely to positively or negatively impact metabolite production, with missense mutations commonly causing changes in protein structure. Unfortunately, for SCO3230, the impact of these missense mutations cannot currently be modelled due to the size of the SCO3230 CDS, as protein prediction software like AlphaFold 3, cannot model proteins more than 5000 amino acids, whereas the complete structure for SCO3230 reaches 7463 amino acids (Abramson *et al*, 2024). However, given the crucial role of SCO3230 in CDA biosynthesis (Lewis *et al*, 2019), both mutations may provide insight into CDA yield or activity. As such, to confirm this, future work such as replicating the mutations in a clean background, and comparative analysis would be required to determine if these mutations alter CDA yield or are functionally neutral.

A missense mutation was identified in the actinorhodin BGC, within the ActIV bifunctional cyclase (SCO5091; GCG-GAC; A230D) (Taguchi *et al*, 2017). The A230D mutation in the

ActIV cyclase may impact actinorhodin production as the introduction of an aspartic acid in place of an alanine would change the charge at that position, potentially resulting in a disruption to protein folding and stability. Again, inducing the same mutation in a wild-type background, accompanied with complementation experiments, would be required in order to ascertain any differences in metabolite production.

5.3.6 The *hisA1* genotype is a result of mutation in the histinol dehydrogenase gene, *hisD*

One of the genetic markers present in *S. coelicolor* J1501 strain, the progenitor of *S. coelicolor* J1700 is *hisA1*. Strains carrying this mutation are histidine auxotrophs, reliant on external sources of histidine for sufficient growth (Kieser *et al*, 2000). The designation of *hisA1* as a mapping group is well-established, but previous literature is not clear about where the specific mutation resulting in histidine auxotrophy is located. Limauro et al (1990) previously suggested that the so-called *hisA1* gene in *S. coelicolor* was in fact an ortholog of *hisD,* the histidinol dehydrogenase, in *Escherichia coli*. In *S. coelicolor*, *hisD* is encoded by the gene SCO2054.

Histidinol dehydrogenase catalyses the terminal reaction in histidine biosynthesis that oxidises L-histidinol to L-histidine and in *S. coelicolor* is the first gene in a three gene operon (*hisDCB*). Sequencing of *S. coelicolor* J1700 identified a missense mutation in the gene SCO2054 (*hisD*) (T-C) resulting in a E264G missense mutation in the histidinol dehydrogenase sequence. The Chai server's protein structure prediction software was used to determine the effect of the E264G on protein folding, to visualize if the mutation impacts the protein structure of histidinol dehydrogenase, leading to loss of function (**Fig.5.5)** (Chai Discovery Team *et al*, 2024). Protein prediction software such as AlphaFold and Chai use confidence metrics to help judge reliability, including the predicted Local Distance Difference Test (pLDDT) and the predicted TM score (pTM) (Chai Discovery team *et al,* 2024; Jumper *et al*, 2021). The pLDDT provides a score for each protein residue, with higher values indicating reliable backbone and residue placement, whereas the pTM score offers a more global confidence determinator, scored

between 0-1, with higher pTMs predicted to be more accurate to overall protein structures. Chai's protein prediction software indicated pTMs for *S.coelicolor* M145-HisD and *S. coelicolor* J1700-HisD at 0.9272 and 0.9291 respectively, indicating high confidence in the protein structure for both wild-type and mutant HisD, while pLDDTs for both proteins were consistently above 90, signifying high confidence for both residue placement and protein structure. As can be seen from **Fig. 5.5**, the overall structure between wild-type and mutant HisD are incredibly similar, indicating that the E264G mutation does not impact the structure of HisD.

Prediction modelling for both the wild-type histidinol dehydrogenase and the mutated protein found in *S. coelicolor* J1700 exhibited no clear structural changes. To confirm this visualization, PyMOL software was utilized to study the impact of E264G on the structure of HisD. The root mean square deviation (RMSD) between the wild-type and mutated HisD proteins was calculated, as RMSD is commonly used to measure the average distance between two atoms of superimposed structures, to calculate structural similarity. Analysis of protein structure using PyMOL indicated a low root mean square deviation (RMSD) of 0.313, confirming that both proteins were nearly identical in atomic positions, and that E264G did not cause detectable structural shifts (Schrödinger and DeLano, 2020).

Previous literature shows that the E264G mutation maps to the region of the protein that coordinates a catalytic zinc ion, which is needed for substrate binding (Barbosa *et al*, 2002). Glutamate residues are negatively charged and possess a carboxylate group, which allows them them to interact and influence positively charged Zn^{2+} ions. After the E264G mutation mutates this residue to a glycine residue, this causes the loss of both its negative charge and its carboxylate side chain, making the mutated residue incapable of interacting with Zn^{2+} ions in the binding site. This reduces the number of residues interacting with Zn^{2+} at the active site from four to three, suggesting that the mutated histidinol dehydrogenase found in *S. coelicolor* J1700 is likely negatively impacted, or even non-functional (**Fig. 5.5**). This lack of function explains the loss of histidine biosynthesis and reliance on external histidine in *S. coelicolor* J1700.

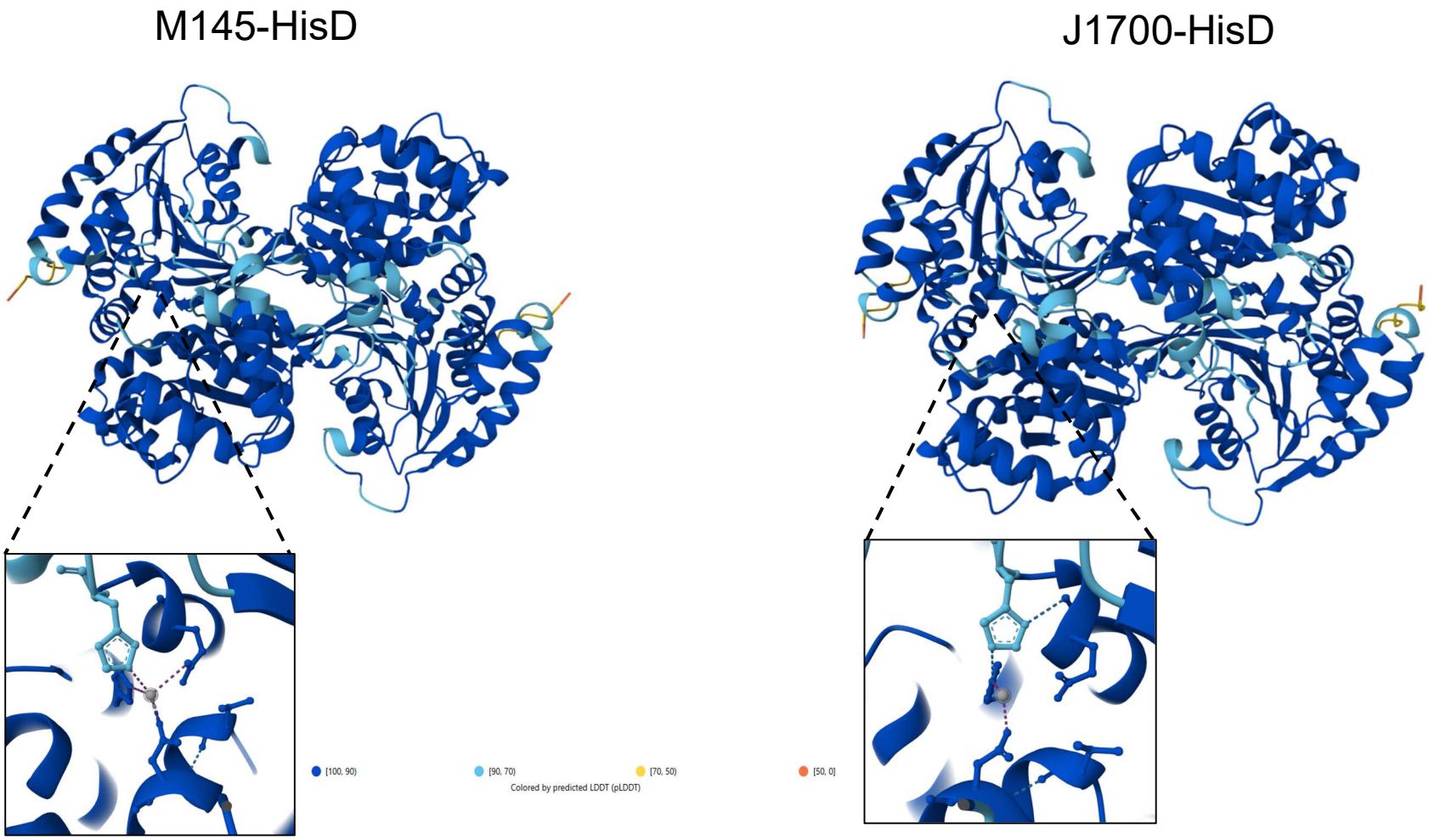

Fig. 5.5: Impact on structure and zinc binding site of E264G mutation in SCO2054 (*hisD*). Chai-predicted structural models of the wild-type and mutant SCO3650 protein, with dotted lines illustrating residue interactions. Further visualization of the zinc-coordinating region, with positive and negatively charged residue interactions showing reduced zinc interaction in J1700-HisD. (M145-HisD pTm = 0.9272, J1700-HisD pTm = 0.9291).

5.3.7 The *uraA1* mutation maps to the putative uridine 5`-monophosphate synthase in *S. coelicolor* J1700

Another widely used, historical genetic marker in *S. coelicolor* J1501 is *uraA1*, where strains exhibit uracil auxotrophy. Analysis of the mutations detected in *S. coelicolor* J1700 revealed that there was no mutation present in the *uraA* gene, suggesting that this may also reflect the use of *uraA* as a group designation. Analysis of the genome mutations in *S. coelicolor* J1700 following Breseq analysis identifies a putative uridine 5-monophosphate synthase (SCO3650: *pyrE*) that possesses a 10bp deletion (99-108/549 nt) towards the 5`-end of the coding sequence. This deletion also results in a frameshift, disrupting the rest of the coding sequence, and potentially impacting the protein structure significantly. Uridine 5'-monohosphate synthase catalyses the formation of uridine monophosphate (UMP) as an initial step in uridine triphosphate biosynthesis and RNA metabolism. This led to the hypothesis that the uracil auxotrophy seen in *S. coelicolor* J1700 is likely the result of the frameshift mutation in *pyrE* of *S. coelicolor*. The *pyrE* gene also maps to the *uraA1* location of the physical map of the *S. coelicolor* chromosome, suggesting this is the mutation that results in uracil auxotrophy in *S. coelicolor* J1700 (Redenbach *et al*, 1996). To investigate whether this 10bp deletion affected the protein structure of SCO3650, protein prediction software was used to model both the wild-type and mutant proteins

The AlphaFold protein folding server was used to predict the impact of the frameshift mutation in SCO3650, clearly demonstrating the loss of protein structure and lack of viability, which provides evidence that the frameshift mutation renders the uridine 5'-monophosphate synthase non-functional **(Fig. 5.6)** (Abramson *et al,* 2024; Jumper *et al*, 2021)**.** To investigate the requirement of *S. coelicolor* J1700 for histidine and uracil auxotrophy, both *S. coelicolor* M145 and *S. coelicolor* J1700 were grown on minimal media in the presence and absence of histidine and uracil. The results (shown in **Fig. 5.7**) confirm the need for both histidine and uracil for *S. coelicolor* J1700 to grow, whereas this is not the case for *S. coelicolor* M145.

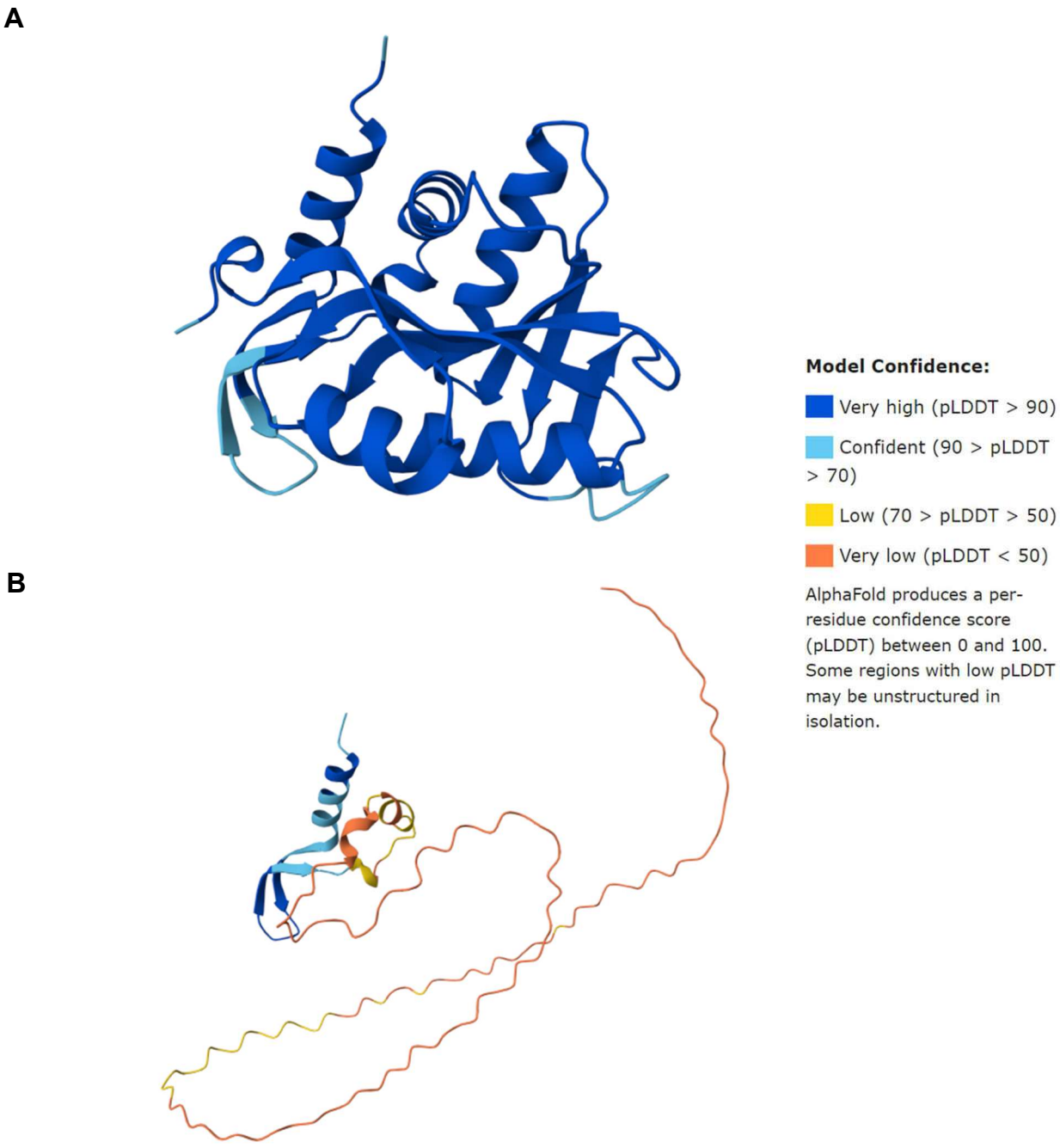

Fig. 5.6: A missense mutation in SCO3650 (*pyrE)* results in complete loss of protein structure. **A:** AlphaFold-predicted structure of the wild-type SCO3650 protein exhibits a high predicted model template (pTM) score of 0.94. **B** AlphaFold-predicted structure of the SCO3650 protein from *S. coelicolor* J1700, illustrating a complete loss of structural integrity (pTm = 0.22).

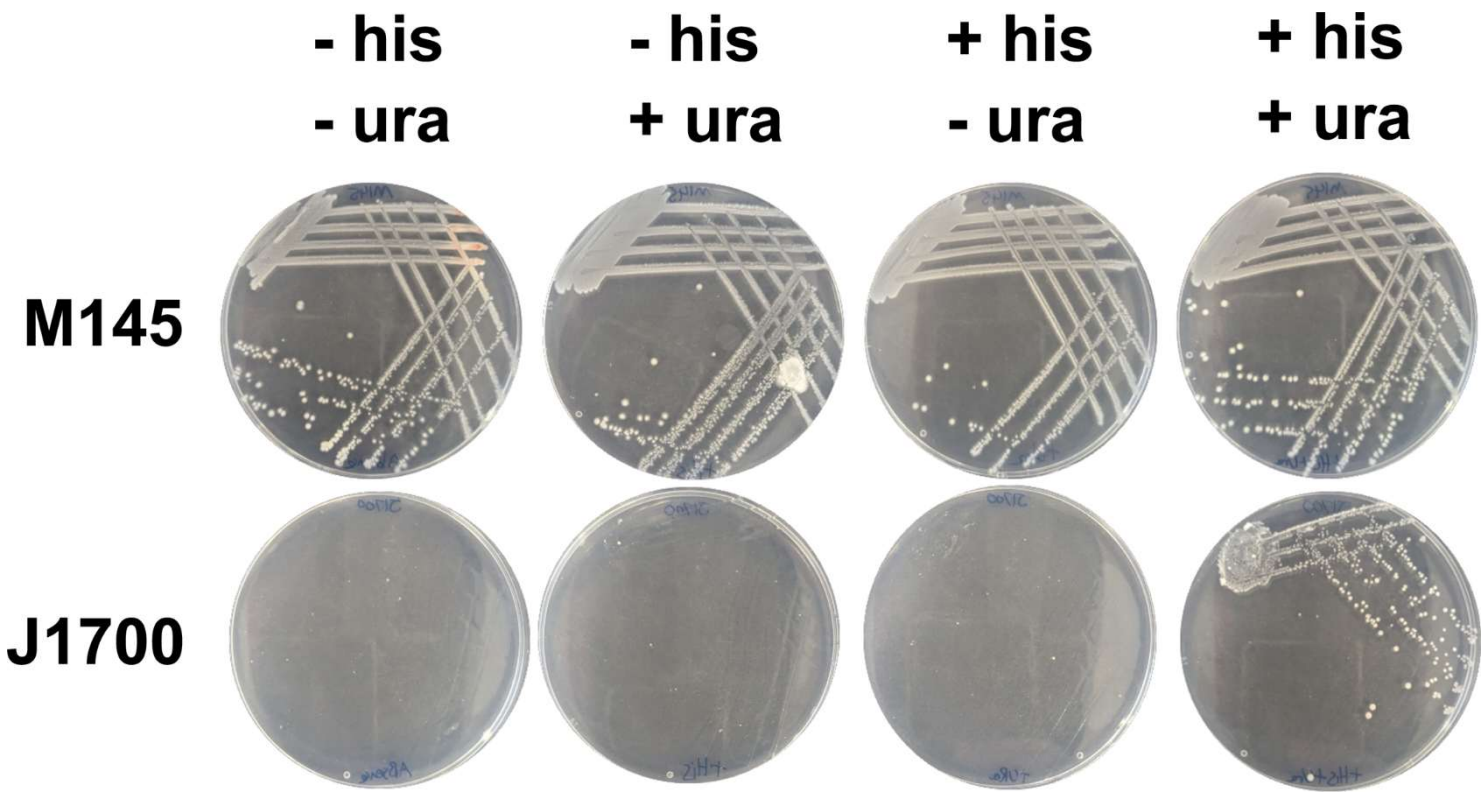

Fig. 5.7: Histidine and Uracil auxotrophic analysis of *S. coelicolor* M145 (WT) and *S. coelicolor* J1700 (*bldA* mutant). Both *S. coelicolor* M145 and J1700 were grown in the presence of histidine (his) or uracil (ura) according to Kieser *et al* to test for auxotrophy based on the genotype of the parental strain *S. coelicolor* J1501 (Kieser *et al*, 2000).

5.3.8 *Streptomyces coelicolor* J1700 exhibits impaired growth compared to *Streptomyces coelicolor* M145

To visualise the morphological differences of *Streptomyces coelicolor* J1700 compared to wild-type *S. coelicolor* M145, both strains were grown on Mannitol soya flour agar (MS) for up to 5 days (**Fig. 5.8**). Following incubation, colonies were imaged using stereomicroscopy. It was observed that growth of *S. coelicolor* J1700 on MS was diminished compared to the growth of *S. coelicolor* M145, noted by the reduction in colony diameter. As expected, compared to *S. coelicolor* M145, *S. coelicolor* J1700 produced no aerial hyphae or specialised metabolites, demonstrated by the lack of actinorhodin pigmentation after five days incubation. Noting the reduced amount of growth of *S. coelicolor* J1700 compared to *S. coelicolor* M145 on solid media, growth kinetics experiments were carried out by gravimetric dry weight calculation over a period of 72 hours in TSB media to confirm if the differences in growth rate between the two strains extends to both solid and liquid media. This method was selected as optical density measurement, which is commonly used for bacterial growth measurements, proved to be unsuitable for *Streptomyces* growth curves*,* attributable to its mycelial growth cycle (Hobbs *et al*, 1989). Dry weight aliquots were taken at eight-hour intervals over a 72-hour period.

From the results of gravimetric dry weight analysis, shown in **Fig. 5.9**, it can be determined that the specific growth rate of J1700 is delayed in comparison to that of M145. To confirm this, the experiment was carried out in biological triplicate, where replication further exemplified the difference between the specific growth rate of the two *S. coelicolor* strains. Cell dry weight quantification revealed that while *S. coelicolor* J1700 eventually matched the dry weight of *S. coelicolor* M145 after 72 hours, the initial growth of J1700 was staggered by comparison, reaching stationary phase after 48 hours compared to 24 hours in *S. coelicolor* M145.

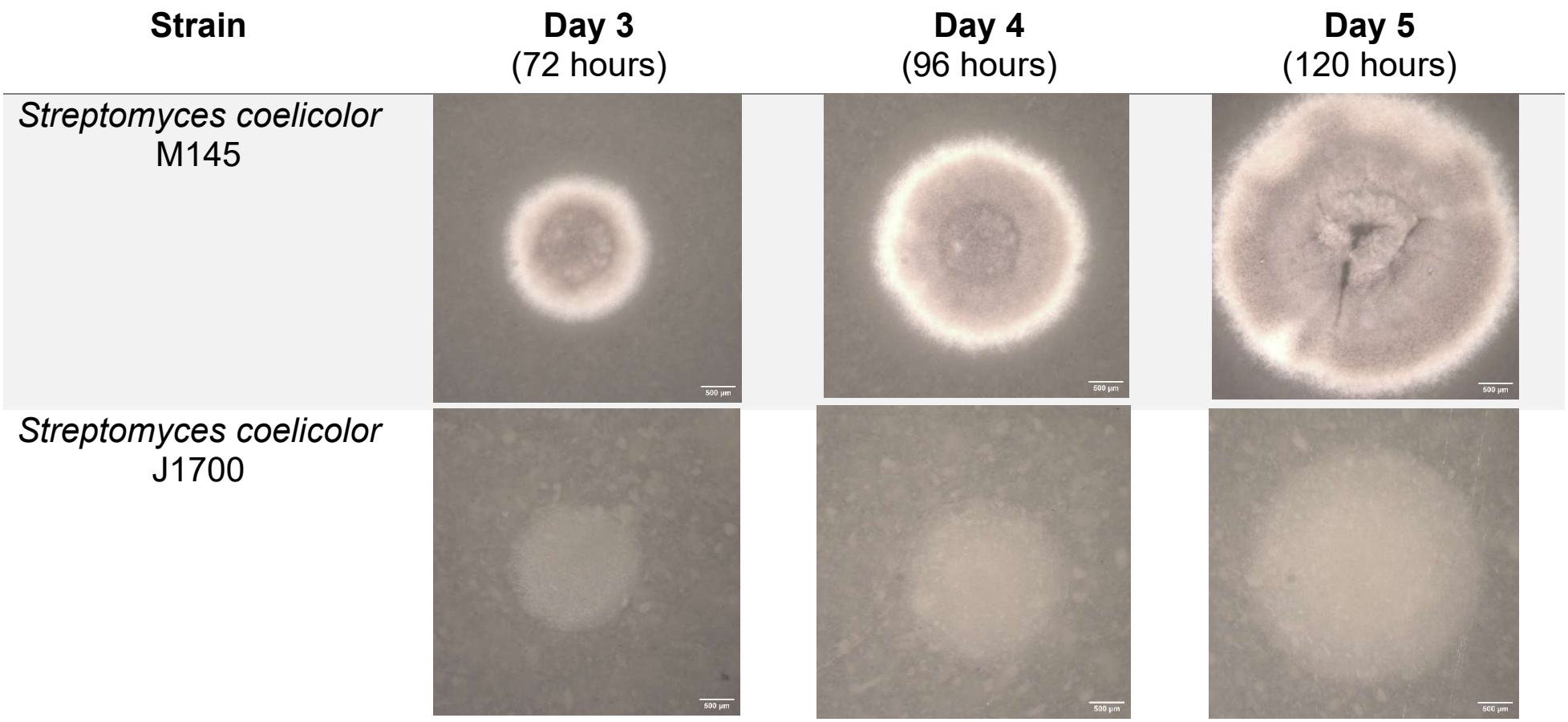

Fig. 5.8 Stereomicroscopic analysis of *S. coelicolor* M145 (WT) and *S. coelicolor* J1700 (*bldA* mutant) at 72-, 96- and 120-hours incubation at 30°C on MS agar. The phenotypic difference between the two strains is highlighted, with the lack of a viable *bldA* tRNA appearing to have a visible impact on colony diameter, metabolite production and aerial hyphae production

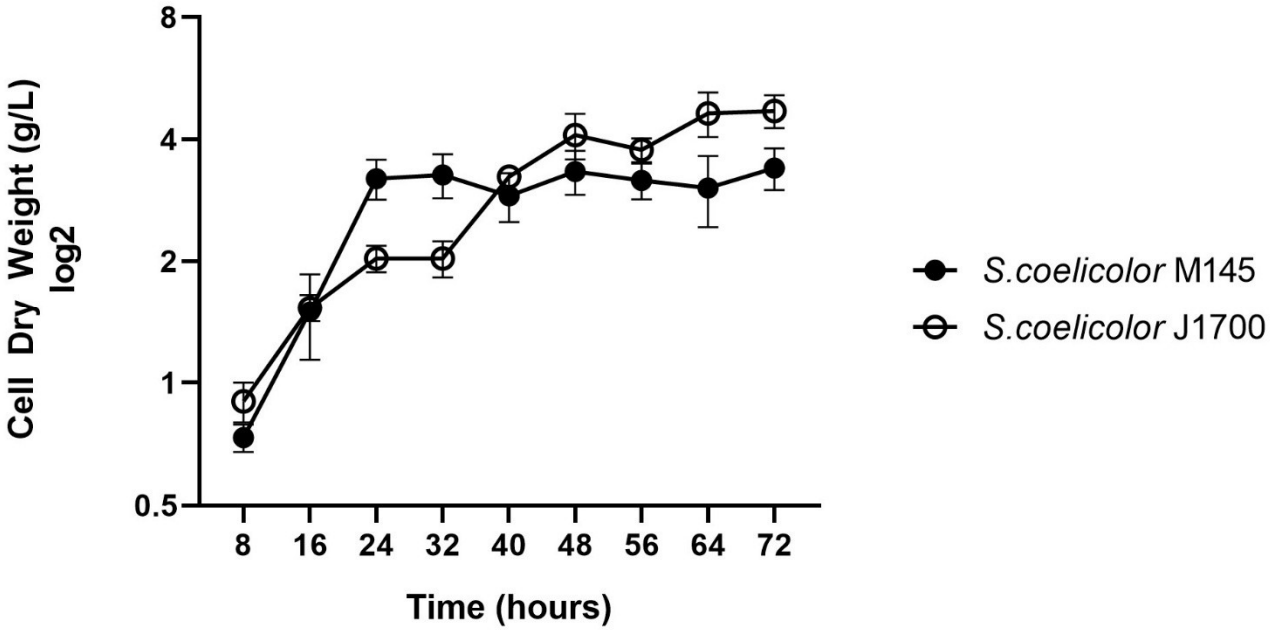

Fig. 5.9: Cell dry weight of *S. coelicolor* M145 (Wild-Type) and *S. coelicolor* J1700 (*bldA* mutant), determined through gravimetric separation of cell mass from media. Experiments were carried out in triplicate and mean dry cell weight was plotted using Graphpad 8. Error bars represent standard deviation from the mean. Specific growth rate was calculated between 8 and 16 hours and was determined as 0.089 h^{-1} for *S. coelicolor* M145 and 0.066 h^{-1} for *S. coelicolor* J1700.

5.3.9 *Streptomyces coelicolor* J1700 exhibits impaired antibiotic production compared to *Streptomyces coelicolor* M145

Actinorhodin (ACT) is an extracellular, blue-pigmented antibiotic produced by *S. coelicolor* A3(2) that has the additional effect of acting as a pH indicator due to its pH-dependant colour change, turning red in the presence of acidic condition, and appearing blue under basic conditions (Bystrykh *et al*, 1996). Undecylprodigiosin (RED) is an alkaloid produced by certain Actinomycetota, including *S. coelicolor* A3(2), which has previously been investigated as a potential anticancer and antimalarial agent (Liu *et al*, 2013; Stankovic *et al*, 2014).

Previous research and observation from self-conducted growth experiments using *S. coelicolor* M145 and *bldA*-deficient strains revealed a distinct difference in ACT and RED production between the two strains (Passatino *et al,* 1991; Gramajo *et al*, 1993; White and Bibb, 1997). To quantify the production, ACT and RED assays were performed in cultures grown in YEME media, which has previously been documented to increase ACT production (Elibol, 2004). Increases in cell biomass can impact on both ACT and RED production, such that cell dry weight measurements were carried out in tandem and the ACT and RED yields per gram of cell dry weight (CDW) were calculated for both strains.

ACT production was first visually noticed after 48-56 hours of incubation into culture for *S. coelicolor* M145, whereas media pigmentation changes never occurred for *S. coelicolor* J1700 for the 120-hour run time of each experiment. This lack of ACT or RED produced was confirmed by differences in extracellular ACT and RED, determined through supernatant absorbance measurements (OD_{633} and OD_{530} respectively) recorded after 120 hours (**Fig. 5.10A, Fig. 5.11A**). Analysis of extracellular ACT production demonstrated that the *S. coelicolor* M145 strain produced significantly more ACT than the J1700 mutant, which is consistent with the understanding from previous literature that *bldA*-deficient *Streptomyces* are unable to produce antibiotics or other secondary metabolites (**Fig. 5.10A**) (Kim *et al*, 2005).

However, measured after 120 hours at the end of the experiment, when ACT and RED yields were determined, however CDW between the two strains did not show any substantial difference in biomass produced between the two strains, which may have given rise to increased ACT or RED production (**Fig. 5.10B, Fig 5.11B**). Undecylprodigisin remains intracellular and requires cell lysis for accurate quantification. This was done through acidification of cell pellets with HCl and extraction of acidified product using methanol before optical density measurement, and quantification using the Beer-Lambert law calculation. Compared to ACT production, RED production appeared markedly lower in *S. coelicolor* M145, to near negligible levels. Production of RED in *S. coelicolor* J1700 was non-existent, which further corroborates historical findings (**Fig. 5.11C**).

Following CDW determination and optical density analysis of both ACT and RED production, ACT and RED per gram of CDW was calculated, with *S. coelicolor* M145 showing considerably increased ACT production compared to J1700 (**Fig. 5.10C**), however RED production was found to be negligible in both strains (**Fig. 5.11C**). This could be attributed to the small-scale nature of the experiments as only 50 mL of YEME was used for each culture replicate; however this does not explain the large differences in RED yield seen between biological replicates. An alternate hypothesis could be made for variant conditions within the incubator, however media production, media pH, spore/mycelium inoculation and springs for aeration remained consistent for each replicate. An argument could be made for RED production decreasing over the 120-hour period due to depleting nutrients or media pH changes over time, with previous literature showing low RED production in *S. coelicolor* is not uncommon, and that RED production plateaus after stationary phase (Kang *et al,* 1998; Jaber *et al*, 2011).

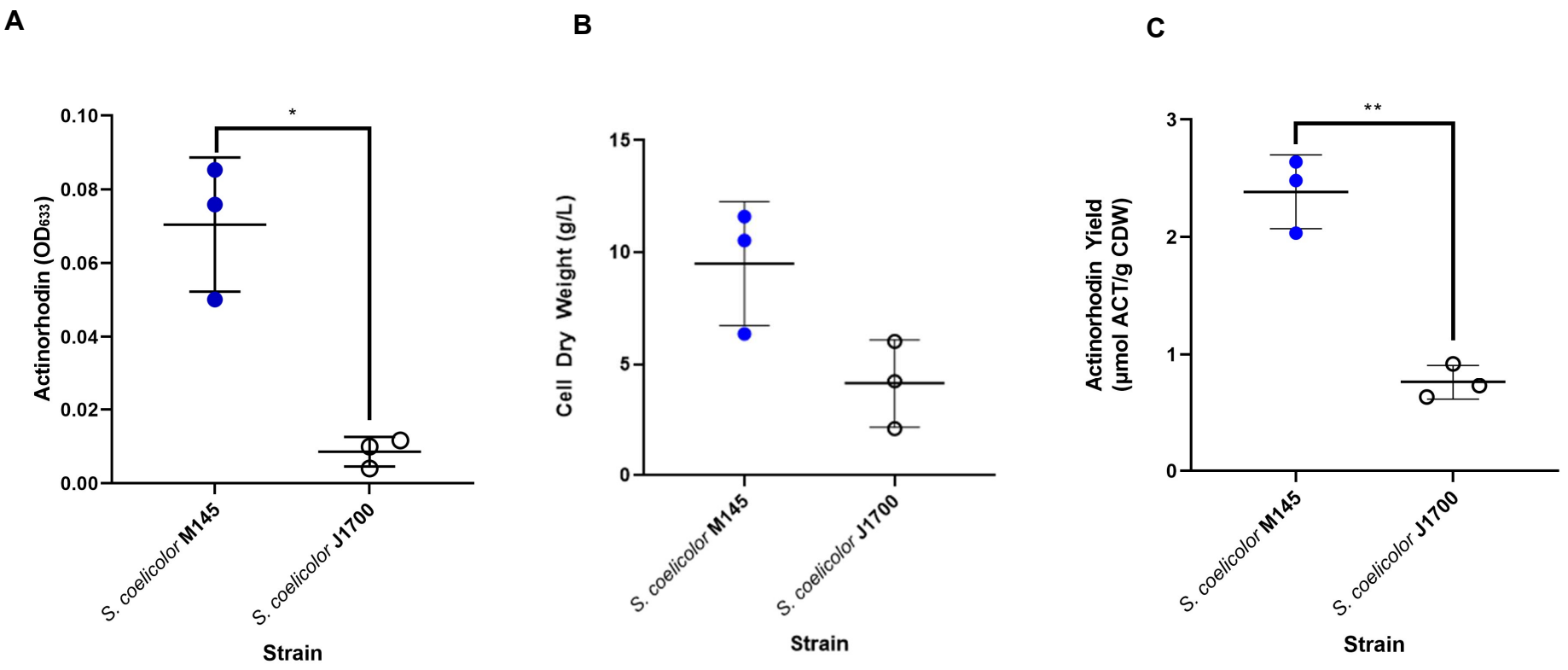

Fig. 5.10: Extracellular actinorhodin production of *S. coelicolor* M145 (Wild-type) and J1700 (*bldA* mutant). A: Extracellular ACT production was measured at OD_{633} (n=3) after 120 hours. **B:** Cell dry weight was measured (n=3) with cell pellet of supernatant used for extracellular ACT quantification at 120 hours**. C:** Actinorhodin yield (µmol) given per gram of CDW for strains after incubation at 30°C for 120 hours. Data was analysed using unpaired t-test, finding that ACT yield per gram of cell dry weight between *S. coelicolor* M145 and *S. coelicolor* J1700 was significant. (p= 0.0048).

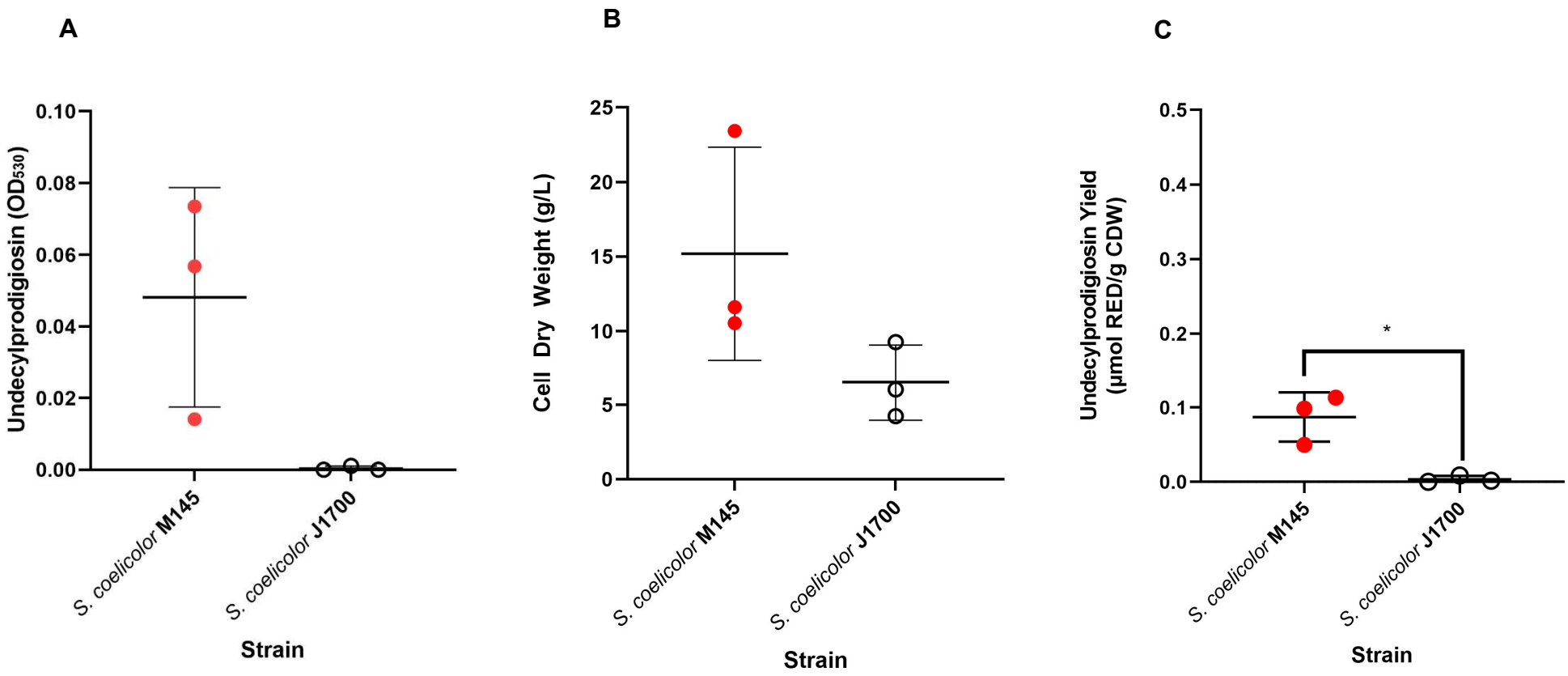

Fig. 5.11: Intracellular undecylprodigiosin production of *S. coelicolor* M145 (Wild-type) and J1700 (*bldA* mutant). A: Intracellular RED production was measured at OD_{530} (n=3) after 120 hours. **B:** Cell dry weight was measured (n=3) with cell pellet from homogenous *S. coelicolor* culture after 120 hours incubation. **C:** Undecylprodigiosin yield (µmol) given per gram of CDW for strains after incubation at 30°C for 120 hours. Data was analysed using unpaired t-test, finding that RED yield per gram of cell dry weight between *S. coelicolor* M145 and *S. coelicolor* J1700 was significant (p= 0.0460).

ACT and RED production are closely associated with *Streptomyces* growth, with production shown to be growth phase dependant, both on solid and in liquid culture (Bibb, 2005; Hoskisson and Fernández-Martínez, 2018). Previous work on this topic has shown that culture conditions can greatly impact both the timing and quantity of ACT and RED production (McArthur and Bibb, 2008; Nieselt et al., 2010). From the data presented in **Fig. 5.10** and **Fig. 5.11**, there is a clear established connection between the production of ACT and RED in *Streptomyces coelicolor* and the presence of a functioning leucine-tRNA^{BldA}, which is consistent with previous established literature (Fernández-Moreno *et al*, 1991; White and Bibb, 1997; Chater, 2013). Physiological stress has been shown to impact ACT and RED production, as has nutrient limitations (Bibb, 2005). Both the ACT and RED biosynthetic gene clusters have been documented to contain TTA codons in either response regulators, transporter genes or activator genes found in both BGCs. Without a functional *bldA* tRNA, these genes are likely not translated properly, leading to the failure to initiate biosynthesis, explaining the absence of ACT and RED production in *S. coelicolor* J1700.

However, a major limitation to using *S. coelicolor* J1700 as a leucine-tRNA^{BldA} negative control is the presence of the additional mutations detected through whole genome sequencing and Breseq analysis to highlight those mutations (see **Section 5.3.1** to **Section 5.3.7**). It has been shown throughout that these mutations may influence specialised metabolism or other pathways independent of *bldA*, complicating the interpretation of experiment results as the results seen may be attributable to the additional mutation, rather than solely caused by a non-functional leucine-tRNA^{BldA}. Therefore, it was hypothesized that constructing a precise *bldA* deletion in *S. coelicolor* M145 would provide a cleaner genetic background to assess the effects of how the *bldA* tRNA influences gene expression and specialised metabolism in *S. coelicolor.*

5.4 Summary

In this chapter, the classical *bldA* mutant of *S. coelicolor* J1700 was sequenced and previously uncharacterized mutations within the genetic background were identified and documented. Sequencing of the *S. coelicolor* J1700 genome was completed through the use of the Illumina platform. Breseq analysis of the resultant reads highlighted the presence of nearly 300 undocumented mutations, as well as several deletions, including a large-scale deletion of 53,414 bp between 7,014,046 bp and 7,071,460 bp. From the analysis of the reads, these deletions have had an impact on the coding sequences of 59 genes, ranging from short indels to full gene deletions (**Table 5-1**). Further analysis of the sequencing reads also highlighted the SNP negating the function of the *bldA* tRNA, a T>C mutation at the second nucleotide in the anticodon loop, making *S. coelicolor* J1700 the sole *bldA* mutant that possesses a direct mutation effecting the anticodon sequence, rather than other segments of the tRNA such as the D-arm and the stem (**Fig. 5.3).**

Other mutations were detected in other BGCs, including the *act, red*, *cda*, coelichelin and coelimycin BGCs. Of particular note is the 1.5kb IS110 insert in the intergenic regions between SCO5885 and SCO5886 in the RED BGC (**Fig. 5.4**). Insertion of IS110 into this intergenic region is likely to have disrupted potential promotor regions or read through transcription from the upstream gene resulting in polar effects on expression of genes in the BGC. IS110 encodes a transposase, which itself could affect transcription of neighbouring genes.

The genotypic markers found in the ancestral J1501 strain, namely *his1a* and *ura1a*, conferring histidine and uracil auxotrophy respectively, were explored due to notable mutations in the histidinol dehydrogenase (*hisD*) and uridine 5'-monophosphate synthase (*pyrE*) genes. Protein prediction and structural analysis confirmed complete structural collapse of the *pyrE* protein, contributable to a 10bp frameshift deletion early in the coding sequence (**Fig. 5.6**). Structural analysis of the mutated histindinol dehydrogenase revealed no obvious structural impact, however the mutation (E264G) was known to map to a Zn^{2+} active site, previously documented as essential for enzymatic functionality (Barbosa *et al*, 2002).

Experiments focused on the *S. coelicolor* J1700 growth compared to the wild-type *S. coelicolor* M145 **(Fig. 5.8** and **Fig. 5.9)** confirmed the bald phenotype linked to characteristic *bld*-deficient strains and confirmed the presence of a reduced growth rate in the *S. coelicolor* J1700 strain respectively and consistent with the literature (Hesketh *et al*, 2007).

The differences between *S. coelicolor* M145 and *S. coelicolor* J1700 in regard to specialised metabolite production was investigated through the quantification of ACT and RED via metabolite production assays (**Fig. 5.10** and **Fig. 5.11**). These data confirmed the presence of ACT and RED production in a strain with a functional *bldA* tRNA and depleted ACT and RED production in a *bldA*-deficient strain, where key mutations have abolished normal sporulation and metabolite production, with these data consistent with those seen in previous literature (Fernández-Moreno *et al*, 1991; White and Bibb, 1997; Yan *et al*, 2020. There are known associations between specialised metabolite production, physiological development, and bacterial stress, the first two clearly linked to phenotypes seen in the *bldA39* mutant (Bibb, 2005; Yoon and Nodwell, 2014). However, while previous research is consistent with the data determined through these experiments (Fernández-Moreno *et al*, 1991; White and Bibb, 1997), it is not enough to simply assume the deficiency in ACT and RED production are the result of solely the *bldA39* mutation, due to the presence of the other previously undocumented mutations found in the *act* and *red* biosynthetic gene clusters, brough to light through whole genome sequencing and Breseq analysis performed earlier in this chapter (**Fig**. **5.4**; **Appendix 1**)

To fully understand the impact a deficient *bldA* tRNA has on *S. coelicolor* species, an investigation into complementation studies and the prospect of novel tRNA knockouts in the *S. coelicolor* M145 background is required. The next chapter investigates the impact of *S. coelicolor* J1700 tRNA overexpression, tRNA complementation and the effect of a complete *bldA* deletion on metabolite production, secondary mutations resulting from *bldA* removal and transcriptomic impact of the removal of a rare leucine tRNA.

Chapter 6: Construction of an isogenic *bldA* deletion mutant and its characterisation.

6.1 Introduction

In the previous chapter, WGS of the *Streptomyces coelicolor* J1700 genome, along with subsequent morphology and specialized metabolite yield studies revealed additional, previously undocumented, mutations. These mutations are a result of repeated exposure to mutagens (Merrick, 1976) and the genetic background of *S. coelicolor* J1501, the background in which the *bldA39* mutation was first cloned (Piret and Chater, 1985). Historical studies of *S. coelicolor* J1700 suggested that incomplete complementation of undecylprodigiosin occurred, which may be linked to the presence of an IS110 element within the biosynthetic gene cluster in that strain (see **Section 5.3.4**). To further understand the impact of the *bldA39* mutation in *S. coelicolor* J1700, genetic complementation and functional analysis was undertaken, along with construction of an isogenic *bldA*-tRNA deletion in *S. coelicolor* M145. The isogenic *bldA* mutant can then be used for more reliable studies of gene function and complementation and to study potential complementation with alternative tRNAs.

The central aim of this chapter is to investigate complementation of *S. coelicolor* J1700 for recovery of the sporulation phenotype and specialised metabolite production. Creation of an isogenic *bldA* Leu-tRNA^{UAA} deletion in *Streptomyces coelicolor* M145 using CRISPR will be used to test if full complementation is possible. Given the close nature of a previously unpredicted wobble-base pairing tRNA, CRISPR will also be used to delete this Leu-tRNA^{CAA}, decoding the TTG codon. This will be followed by the attempt to make a *bldA*/Leu-tRNA^{CAA} double deletion mutant, and to characterise the effects of these mutations on growth and nutrient usage using Biolog phenotypic microarrays. Finally, the global transcriptome of the *bldA* deletion will be compared to the *S. coelicolor* M145 strain to understand any global transcriptional changes as a result of *bldA* deletion.

Whilst TTA codons (decoded by Leu-tRNA^{BldA}) are present in <2% of all *Streptomyces coelicolor* genes (Li *et al*, 2007), the impact of a *bldA* mutation on *Streptomyces* colonies cannot be understated and has been well documented in previous studies, although there are some inconsistencies within the literature between species and when studies have been conducted with non-isogenic strains (Hackl and Bechthold, 2015., Hesketh *et al,* 2007., Kim *et al*, 2005., Koshla *et al*, 2019., Leskiw *et al,* 1991., Leskiw *et al*, 1993., Leskiw and Mah, 1995). Therefore, it was hypothesised that the deletion of the *bldA* tRNA would result in quantifiable delays in growth, effects of sporulation and antibiotic production, in addition to the upregulation of a multitude of transcripts to suppress or mitigate the effects that the tRNA deletion may have on the strain.

6.2 Aims

The aims of this chapter were to investigate complementation and tRNA overexpression of *S. coelicolor* J1700 to understand how it may influence growth and specialized metabolite production. Following this, isogenic Δ*bldA*, ΔLeu-tRNA^{CAA}, and double Leu-tRNA$^{BldA/CAA}$ deletion mutants will be made in the *S. coelicolor* M145 background and the effects of complementation on these isogenic deletion strains will be investigated. After complementation studies, the effects of tRNA deletions on Actinorhodin (ACT) and undecylprodigiosin (RED) production, as well as the effect of tRNA deletion on growth rate and the transcriptome will be explored

6.3 Results

6.3.1 Investigation into *S. coelicolor* leucine codon usage

In *Streptomyces* species, as well as being used in protein synthesis, leucine is also used as a polyketide precursor and an alternative energy source (Hafner *et al*, 1991., Li *et al*, 2009., Li *et al*, 2021), There are six leucine codons in the standard genetic code, only five of the associated tRNAs are detected across the genome of *Streptomyces coelicolor*. The tRNA for the CUU codon is noticeably absent from the genome of *S. coelicolor* (Bentley *et al*, 2002., Fan *et al*, 2019). This indicates one of two possibilities: that the CUU codon is a rarity in the *S. coelicolor* genome, or that any CUU codons present in reading frames are reliant on WBP of other neighbouring tRNAs, such as CUC, to be successfully decoded. Previous research has shown that both the CUU and CUC leucine codons can successfully be decoded by the Leu-tRNA^{GAG} (Crick, 1966., Agris, 2004., McFeely *et al*, 2023). As such, a WBP match between the *bldA* tRNA (Leu-tRNA^{UAA}) and the Leu-tRNA^{CAA} may be possible, which may suggest that overexpression of the Leu-tRNA^{CAA} may suppress the *bldA* phenotype.

Initially, the genome of *S. coelicolor* was analysed and the genomic positions of all leucine tRNAs were identified (**Fig. 6.1A**). Genomic analysis revealed the presence of single copies of leucine tRNAs for four of the six leucine tRNAs (Leu-tRNA^{CAA}, Leu-tRNA^{UAA}, Leu-tRNA^{UAG} and Leu-tRNA^{CAG}), while Leu-tRNA^{GAG} notably had two copies across the genome. The Leu-tRNA^{AAG} (which decodes CUU codons) was notably absent from the genome. Following this, the tRNA anticodon loops were matched to their mRNA codon counterparts, with WBP matches highlighted, along with the historical relative codon frequency across the genome (**Fig 6.1B;** Kieser *et al*, 2000). These data underscore the potential for non-canonical interactions that expand codon recognition and suggests a flexible decoding system that may enhance translational efficiency under varying cellular conditions.

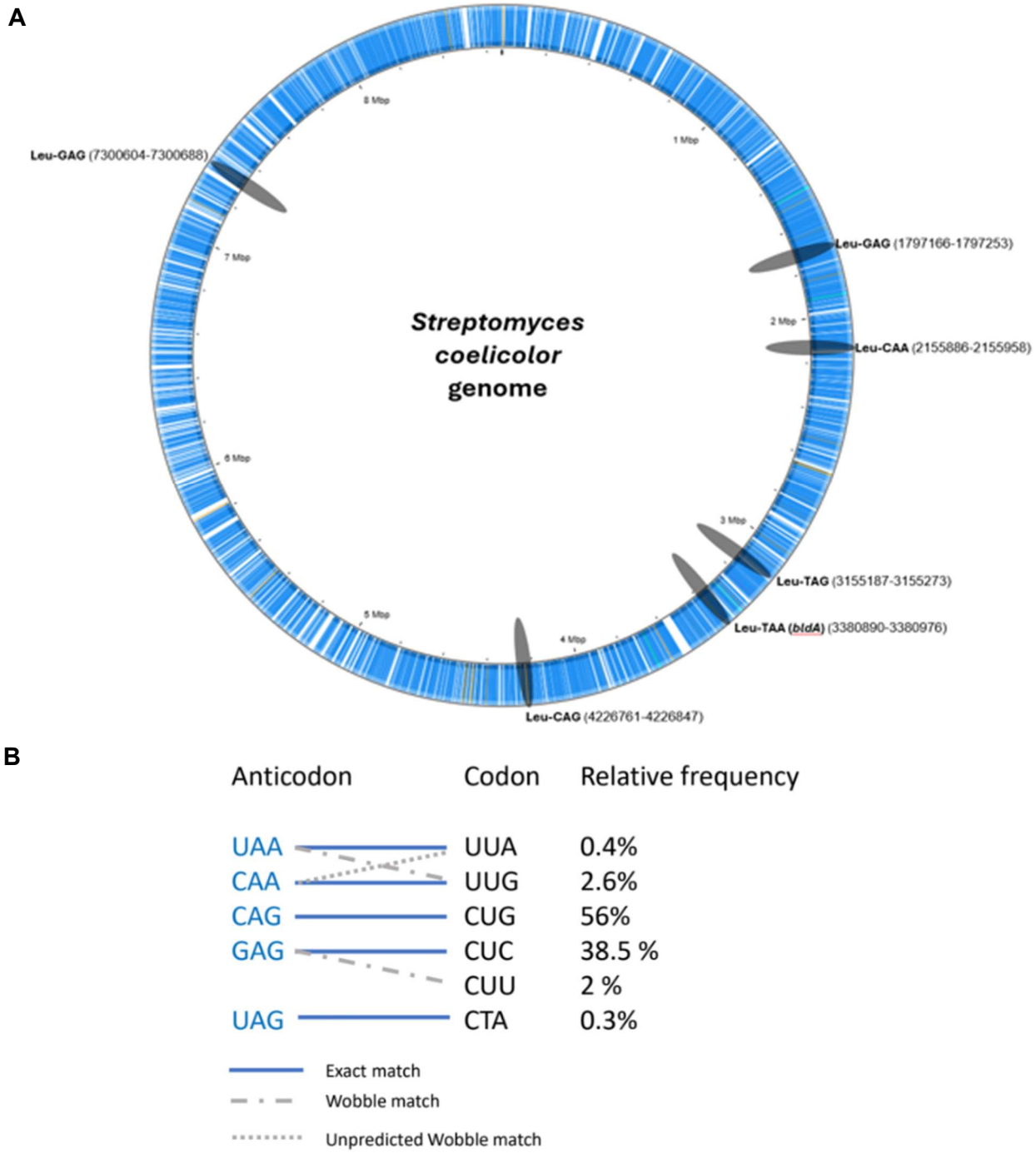

Fig. 6.1 Genomic Distribution and Wobble Base Pairing of Leucine tRNAs in *Streptomyces*. **A:** Schematic representation of the *Streptomyces* genome highlighting the positions of all identified leucine tRNA genes. Each gene is annotated with its genomic coordinates and corresponding anticodon sequence. Figure created using Prokka (Seemann, 2014). **B:** Leucine codon-anticodon matches, based on presence in the *Streptomyces coelicolor* genome, with corresponding codon relative frequencies. Solid lines indicate confirmed wobble base pairing between codons and dashed lines indicate predicted wobble base pairing between the anticodons and leucine codons. Relative frequencies were obtained from Kieser *et al*, 2000.

To date, the codon frequencies quoted are based on Kieser et al., (2000) which were based on 100 genes that were sequenced to that point. A full analysis has not been systematically undertaken to date in terms of the leucine-tRNA landscape. To study the frequency of use of all leucine codons in the 7825 coding sequences in the *S. coelicolor* genome, the frequency of leucine codons was determined using Python script (see **Appendix 6**) to analyse all coding sequences (CDS) in the *S. coelicolor* M145 genome, find any sequences with leucine codons within their sequence (**Table 6-1**), and extracting the gene names that contain a leucine codon and the consequent nucleotide arrangement. A detailed breakdown of leucine codon usage and frequency in *S. coelicolor* can be seen in **Appendix 3.**

These data showed that 145 genes in *S. coelicolor* possess a TTA codon (corresponding to Leu-tRNA^{BldA}), matching bioinformatic analysis from previous literature (Li *et al*, 2007, Kalan *et al*, 2013). Another publication suggests that there are 152 TTA-containing codons in *S. coelicolor*, however this is in contrast to previous historical literature (Silov *et al*, 2020). These data also indicate that the TTA codon is present in 1.8% of all *S. coelicolor* genes. The Leu-tRNA^{UAA} is clearly important for the lifecycle of *S. coelicolor*, given the severe phenotype of a *bldA* mutant (Leskiw *et al*, 1993, Hesketh *et al*, 2007, Petterson and Kirsebom, 2011). The Leucine-tRNA^{CAA} is much more frequent, with 3322 of the 7825 CDS in the *S. coelicolor* genome possessing a TTG codon. This equates to 42.5% of all *S. coelicolor* CDS, emphasizing the increased usage of the TTG leucine codon over the TTA leucine codon (encoded by *bldA*). As the Leu-tRNA^{CAA} is the closest potential WBP match for the Leu-tRNA^{BldA}, it was hypothesized that overexpression of the Leu-tRNA^{CAA} may compensate for a defective Leu-tRNA^{BldA}.

Table 6-1: Leucine codon usage and frequency in *S. coelicolor*

Leucine Codon	Matching tRNA	Number of CDS containing Leucine codon	Percentage of *S. coelicolor* CDS containing Leucine codon	Average number of codons per CDS
TTA	UAA (*bldA*)	145	1.8%	1.08
TTG	CAA	3322	42.5%	1.85
CTG	CAG	7751	99.1%	20.50
CTC	GAG	7709	98.5%	12.23
CTA	UAG	629	8.0%	1.32

6.3.2 Complementation of *S. coelicolor* J1700 only partially restores sporulation and metabolite producing phenotype

The whole genome sequence of *S. coelicolor* J1700 revealed a myriad of undocumented mutations that were likely associated with the *S. coelicolor* J1501 genetic background in which J1700 was created. *S. coelicolor* J1501 is a historical strain that was originally used in genetic mapping experiments and has a complex, largely undocumented genotype (Keiser et al., 2000), that was shown in the previous chapter to be even more extensive than previously thought (**Chapter 5**). To complement *S. coelicolor* J1700 with a WT allele of the *bldA*-tRNA, plasmids were designed in the pIJ10257 background, one functioning as an empty vector control (**Fig. 6.2**), one expressing the leucine-tRNA^{BldA} to determine whether restoration of the impacted tRNA could restore sporulation and antibiotic production (**Fig. 6.3**), and one expressing the leucine-tRNA^{CAA} (**Fig. 6.4**). The rationale behind creating the pIJ10257-Leu-tRNA^{CAA} plasmid is that the leucine-tRNA^{CAA} decodes the TTG codon, which is the closest natural Wobble-Base Pairing match to the TTA codon found in the *S. coelicolor* genome, translated by the *bldA* Leu-tRNA^{UAA} anticodon (See **Section 6.3.1**). By creating a plasmid that encodes an additional copy of the leucine-tRNA^{CAA}, it was hypothesised that overexpression of the leucine-tRNA^{CAA} may be sufficient to suppress the *bldA* phenotype if wobble-base pairing was occurring. The pIJ10257-Leu-tRNA^{CAA} and pIJ10257-*bldA* plasmids were synthesized by GenScript (**Fig. 6.2, Fig. 6.3, Fig. 6.4**), and then the non-methylating *E. coli* strain ET12567/pUZ8002 was transformed with each plasmid to facilitate intergeneric conjugation to *Streptomyces*. These plasmids were then introduced into *S. coelicolor* M145 and *S. coelicolor* J1700 with selection on hygromycin (50 µg/ml).

Genomic DNA extraction of the *S. coelicolor* M145 and *S. coelicolor* J1700 exconjugants was followed by PCR using the pIJ10257 check primers (primer numbers 7 and 8), and agarose gel electrophoresis using the extracted gDNA as a template. Agarose gel electrophoresis shows successful conjugation of the pIJ10257 vectors into both the *S. coelicolor* M145 and *S. coelicolor* J1700 backgrounds (**Fig. 6.5A**). PCR amplification of wild-type gDNA with no

integrated construct yielded no amplicon and functioned as a negative control for the experiment, whereas the integrated pIJ10257 empty vector (EV) containing strains possessed an amplicon of 232bp. *S. coelicolor* M145 and J1700 strains possessing the Leu-tRNA^{CAA} overexpression plasmid exhibited an amplicon at 376bp, and strains possessing the *bldA* complementation plasmid exhibited a 434bp amplicon..

Overexpression of the leucine-tRNA^{CAA} and leucine-tRNA^{BldA} -containing pIJ10257 derivatives have little impact on colony morphology in *S. coelicolor* M145 (**Fig. 6.5B)**. When the plasmids were introduced into *S. coelicolor* J1700, *bldA* complementation of *S. coelicolor* J1700 was found to restore sporulation and production of the pigmented antibiotic production (**Fig. 6.5B**). Overexpression of the potential wobble-base pair leucine-tRNA^{CAA} does not appear to complement the *S. coelicolor* J1700 strain, with no restoration of sporulation or antibiotic production (**Fig. 6.5B**).

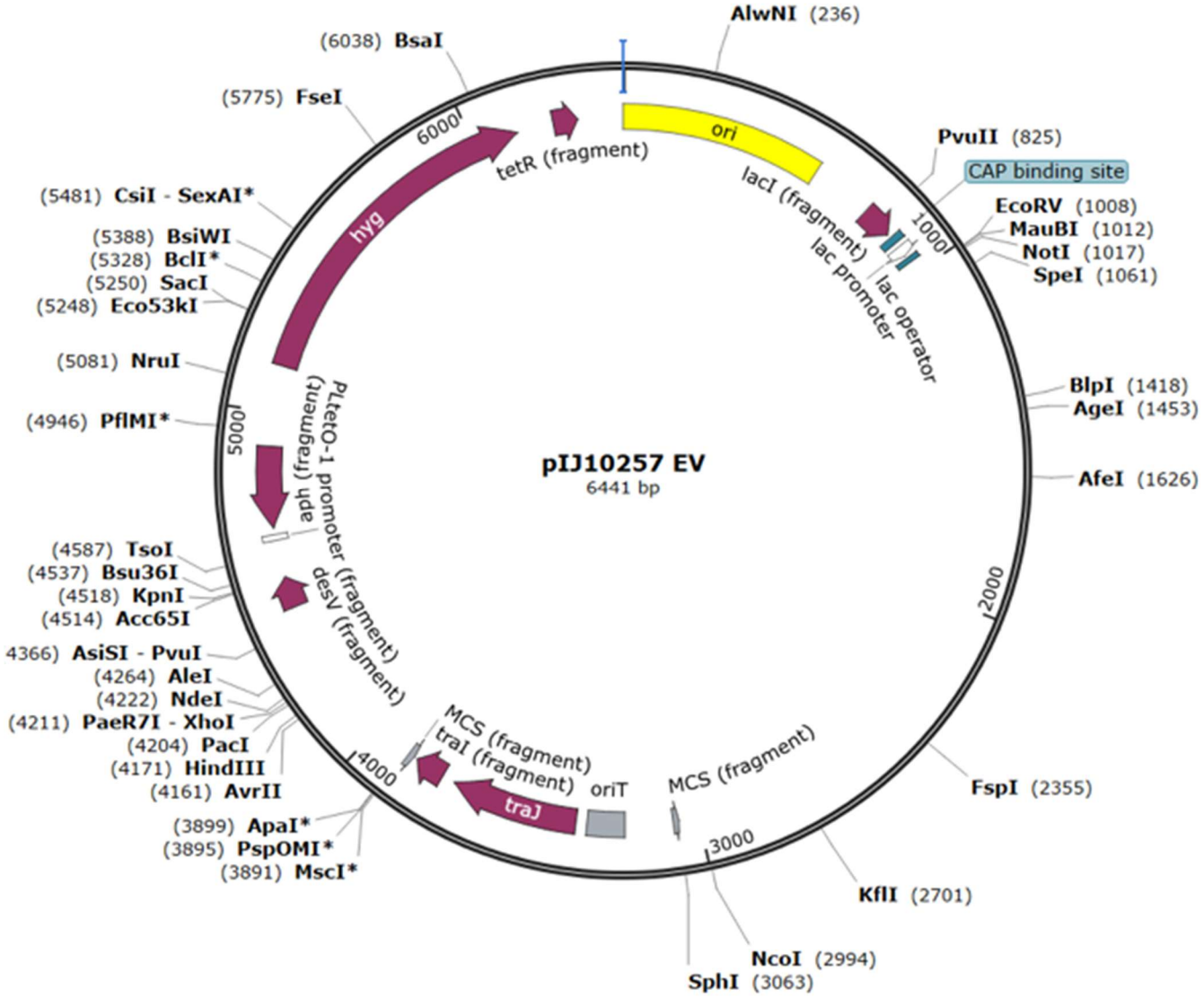

Fig. 6.2: Plasmid construct used as an empty vector (EV) for Leucine-tRNA overexpression and complementation studies in *S. coelicolor*. All plasmid maps were created using SnapGene™.

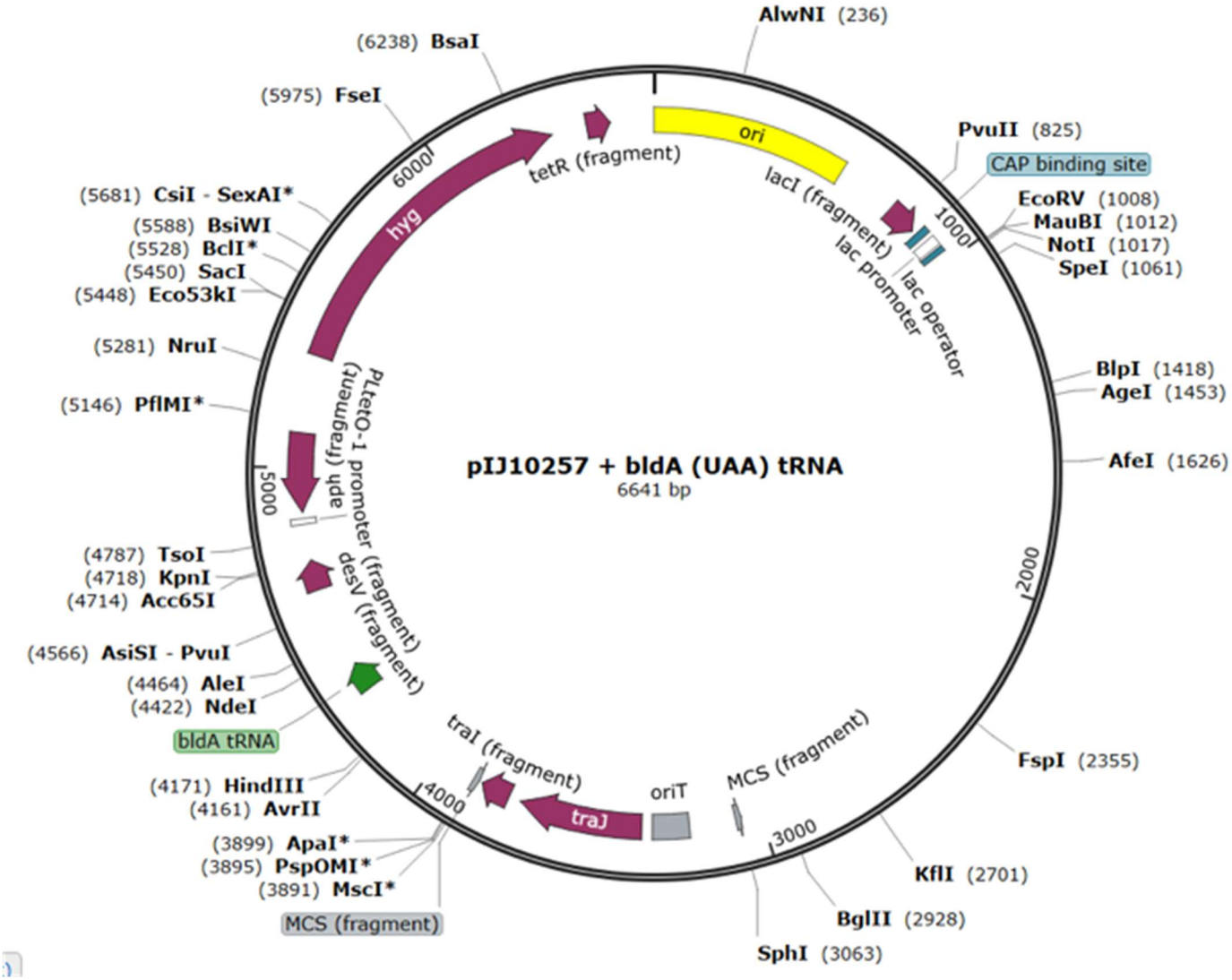

Fig. 6.3: Plasmid construct used for overexpression of the Leucine-tRNA^{BldA} for Leucine-tRNA overexpression and complementation studies in *S. coelicolor*. All plasmid maps were created using SnapGene™.

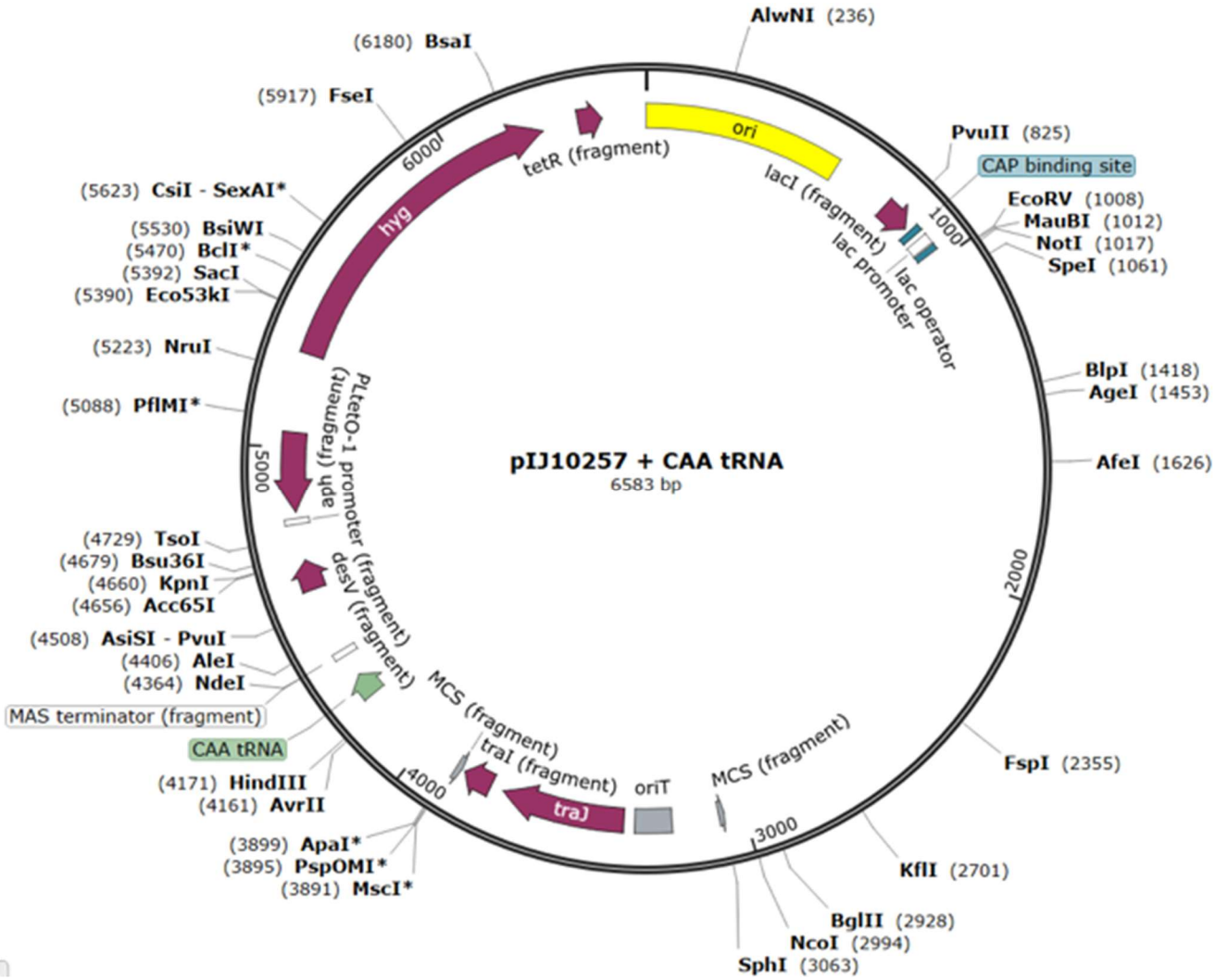

Fig. 6.4: Plasmid construct used for overexpression of the Leucine-tRNA^{CAA} for Leucine-tRNA overexpression and complementation studies in *S. coelicolor*. All plasmid maps were created using SnapGene™.

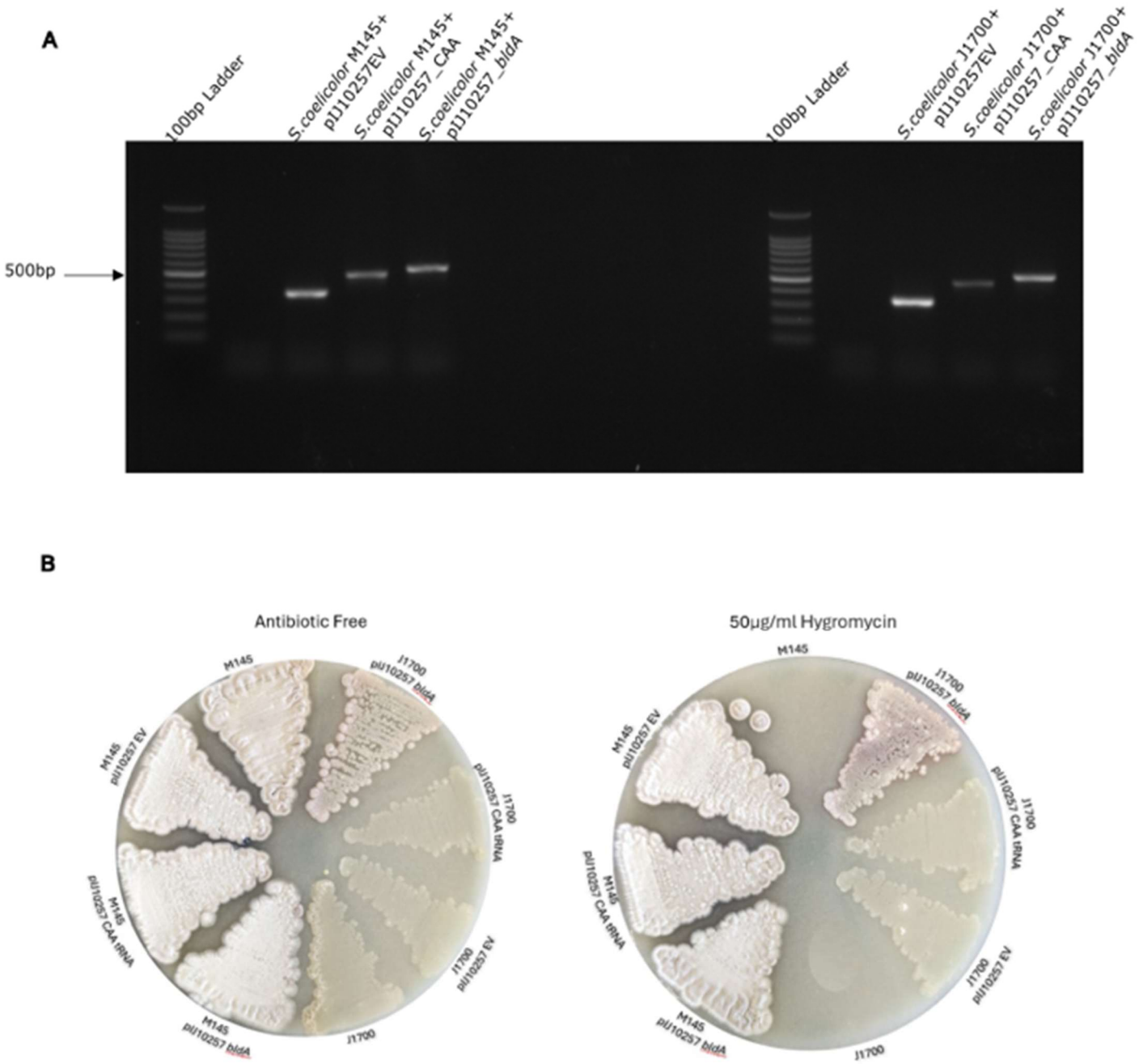

Fig. 6.5: Complementation of the historical *bldA39* mutation in *S. coelicolor.* A: Confirmation of pIJ10257 plasmid derivatives in the appropriate strains *S. coelicolor* M145 and *S. coelicolor* J1700. PCR amplification of wild-type gDNA with no integrated construct (no product, negative control), intergrated pIJ10257 empty vector (EV) from gDNA (predicted product 232bp) CAA tRNA (predicted product 376bp) and *bldA* gene (predicted product 434bp).. **B: Complementation of *S. coelicolor* M145 (Wild-type) and *S. coelicolor* J1700 (*bldA* mutant), with tRNA-expressing plasmids on MS agar.** *S. coelicolor* M145 morphology remains consistent regardless of plasmid insertion (empty vector, Leucine-tRNA^{BldA} or Leucine-tRNA^{CAA} overexpression). Complementation of *S. coelicolor* J1700 with the wild-type *bldA* gene partially restores sporulation and pigmented antibiotic production.

6.3.3 Complementation of *S. coelicolor* J1700 does not restore secondary metabolite production in liquid media

To further investigate the restoration of antibiotic production in *S. coelicolor* J1700 observed on solid media. The production of actinorhodin (ACT) and undecylprodigiosin (RED) was characterised in liquid culture as previously conducted (**Chapter 5)**. Testing of specialised metabolite production was conducted using the wild-type strain *S. coelicolor* M145 and historical *bldA39* mutant *S. coelicolor* J1700, both of which were accompanied with *bldA* complemented *S. coelicolor* M145 and J1700 strains, and Leu-tRNA^{CAA} overexpression *S. coelicolor* M145 and J1700 strains. An empty vector version of each parental strain containing pIJ10257 alone as a control.

Although not observed on solid media, ACT production assays in liquid YEME medium indicate that an additional copy of the Leu-tRNA^{UAA} (*bldA*) increases ACT production in *S. coelicolor* M145 (**Fig 6.6.A, B and C**). Two genes in the *act* BGC *act*II-ORF2 and *act*II-ORF4 (encoded by SCO5083 and SCO5085 respectively) both possess a TTA leucine codon at early points in their coding sequences (Hackl and Bechthold, 2015). The additional copy of the Leu-tRNA^{UAA} (*bldA*) from the complementation plasmid is under the control of a control of a constitutive promoter, suggesting that overexpression of the tRNA permits translation of the TTA codon containing genes, consequently improving ACT production. A small increase in RED production can also be observed in both the Leu-tRNA^{BldA} complementation strain and the Leu-tRNA^{CAA} overexpression strain (**Fig 6.7.A, B and C**). This increase could be attributable to increased translation, as the *red* BGC response regulator *redZ* (encoded by SCO5881) contains a TTA codon.

In *S. coelicolor* J1700, ACT and RED production is reduced compared to *S. coelicolor* M145 as expected (**Fig. 6.6, Fig. 6.7**). Once *S. coelicolor* J1700 is *bldA* complemented, a slight restoration in ACT production is detected, however this complementation does not restore ACT production to WT *S. coelicolor* levels (**Fig. 6.6A, B and C**). This lack of complete

specialised metabolite restoration could be contributed to the additional mutations previously detected in *S. coelicolor* J1700, particularly those affected the *act* BGC (see **Chapter 5**). Leu-tRNA^{CAA} overexpression in *S. coelicolor* J1700 has minimal impact on ACT production, which is consistent with data seen when the Leu-tRNA^{CAA} is overexpressed in *S. coelicolor* M145 (**Fig. 6.6A, B and C**)

Conversely, RED production is completely unaffected by *bldA* complementation in *S. coelicolor* J1700 (**Fig 6.7A, B and C**). These data suggest that *bldA* complementation is not sufficient to restore RED production in the mutated *S. coelicolor* J1700 background, with the previously detected IS110 element insertion within the *red* BGC (between SCO5885 and SCO5886) as the likely reason for disrupted RED production (see **Section 5.3.4**). The inserted IS110 sequence likely impacts RED production through either promoter disruption or premature transcription termination, resulting in an inability to produce RED.

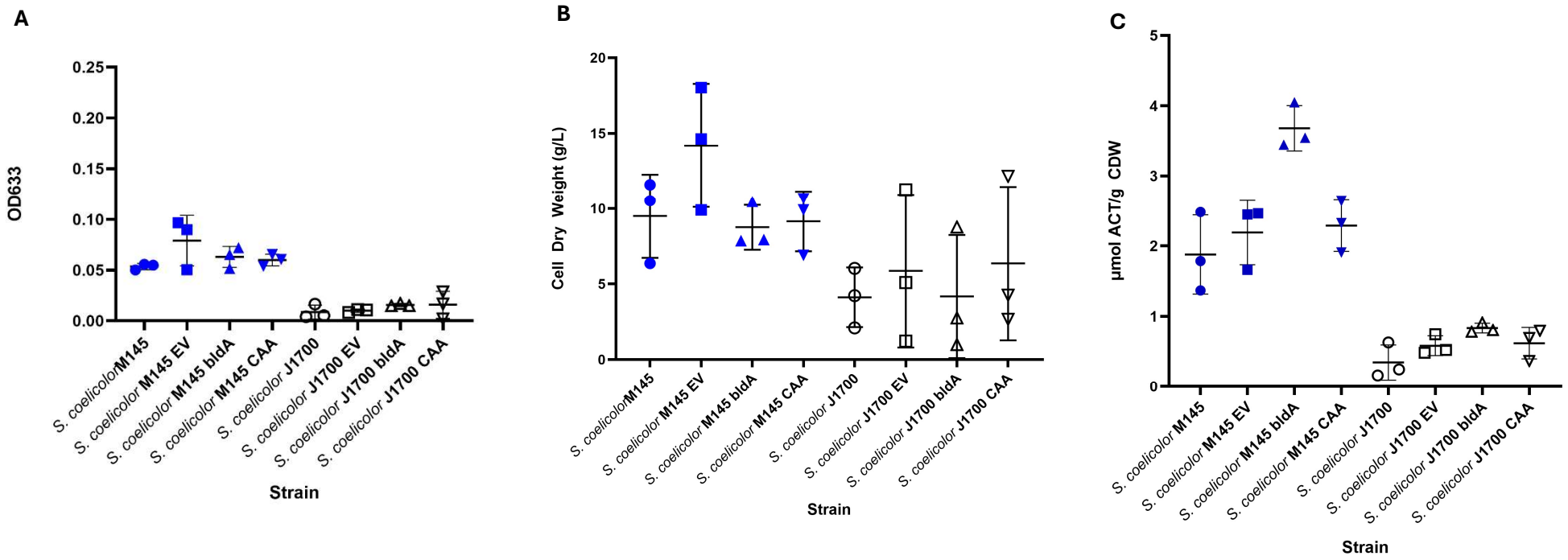

Fig. 6.6: Extracellular ACT production in *S. coelicolor* M145 (Wild-Type) and J1700 complements (*bldA* mutant). A): ACT levels are slightly increased in the M145 empty vector and *bldA* complement strains (N=3). **B:** Cell dry weight was measured (N=3) after 120 hours incubation. **C:** Normalization reveals key differences in production efficiency. Data was analysed using an Ordinary one-way ANOVA, highlighting significant difference in ACT production between strains ($F(7,16) = 35.53$, $P=<0.0001$). Welch's correction unpaired t-test shows *bldA* overexpression in M145 is statistically relevant ($p=0.0148$)

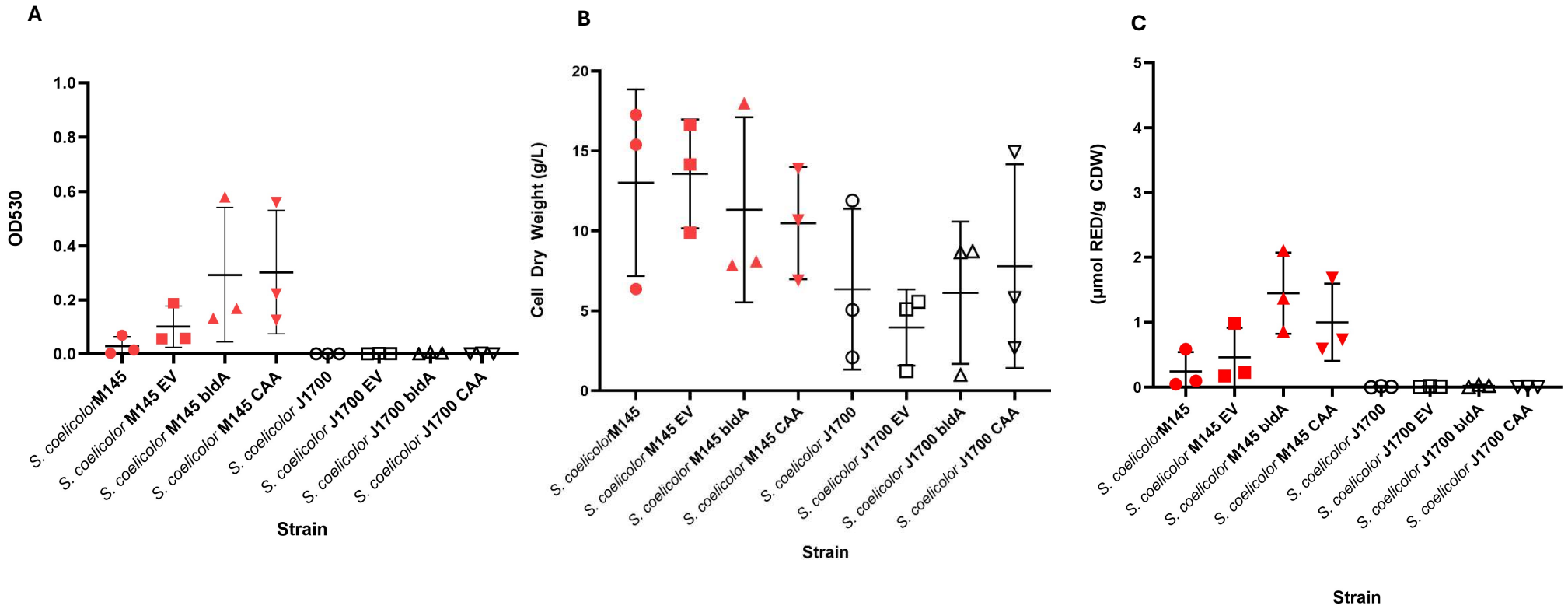

Fig. 6.7: Intracellular RED production in *S. coelicolor* M145 (Wild-Type) and J1700 (*bldA* mutant) complements. A): RED levels are near zero for all strains of *S. coelicolor* J1700, with increases seen in complemented M145 cultures (N=3). **B:** Cell dry weight was measured (N=3) after 120 hours incubation. **C:** Normalization to CDW reveals low amount of RED produced in both *S. coelicolor* M145 and J1700. Data was analysed using an Ordinary one-way ANOVA showing RED yield between strains to be significant ($F(7,16) = 6.884$, $P=0.0007$).

6.3.4 Construction of an isogenic *bldA* knockout in *S. coelicolor* M145 using CRIPSR

In **Chapter 5**, it was shown that the *bldA39* mutant *S. coelicolor* J1700 possesses over 300 previously unknown mutations, including those found in BGC for the two prominent pigmented antibiotics produced by *S. coelicolor*. Complementation of *S. coelicolor* J1700 with a wild-type copy of *bldA* is incomplete with phenotypes not being restored to WT (**Fig 6.5-Fig 6.7**). Overexpression of the closest Wobble-Base pairing tRNA match (Leu-tRNA^{CAA}) also failed to supress the sporulation and antibiotic-deficient phenotype of *S. coelicolor* J1700. These data suggest that *bldA*-associated phenotypes seen in *S. coelcolor* J1700 may not be fully explained by the mutation of the Leu-tRNA^{BldA} alone. This suggests the complex genetic background of *S. coelicolor* J1700 may result in the incomplete complementation of the *bldA39* mutation. This hypothesis is supported by the whole genome sequencing (WGS) analysis of *S.coelicolor* J1700 (**Chapter 5**), To fully test this hypothesis, an isogenic *bldA* mutant would be required.

To address this, CRISPR-Cas9-mediated genome editing was employed to create a precise *bldA* tRNA knockout in *S. coelicolor* M145. The use of CRISPR-Cas9 allowed for targeted deletion of the *bldA* gene in an otherwise clean genetic background, eliminating the effects of background mutations seen in *S. coelicolor* J1700 (Merrick, 1976). The resulting Δ*bldA* mutant in *S. coelicolor* M145 background will provide a more robust platform for dissecting *bldA* function. To construct a plasmid to delete the *bldA* tRNA encoding region, the CRISPR-dCas9 (pCRISPR-Cas9 (Addgene plasmid #125686)) vector requires four components: an encoded Cas9, a sgRNA, a 20 bp spacer that targets the *bldA* encoding region in *S. coelicolor* M145 and two homologous regions adjacent to the gene of interest - upstream and downstream sequences (Tong *et al*, 2020). The Δ*bldA* CRISPR-Cas9 knockout vector including all four components was created through a multi-step restriction enzyme cloning process, resulting in pCRISPR_Δ*bldA* (with a pSET152 backbone). An overview of the process is shown in **Fig. 6.8**.

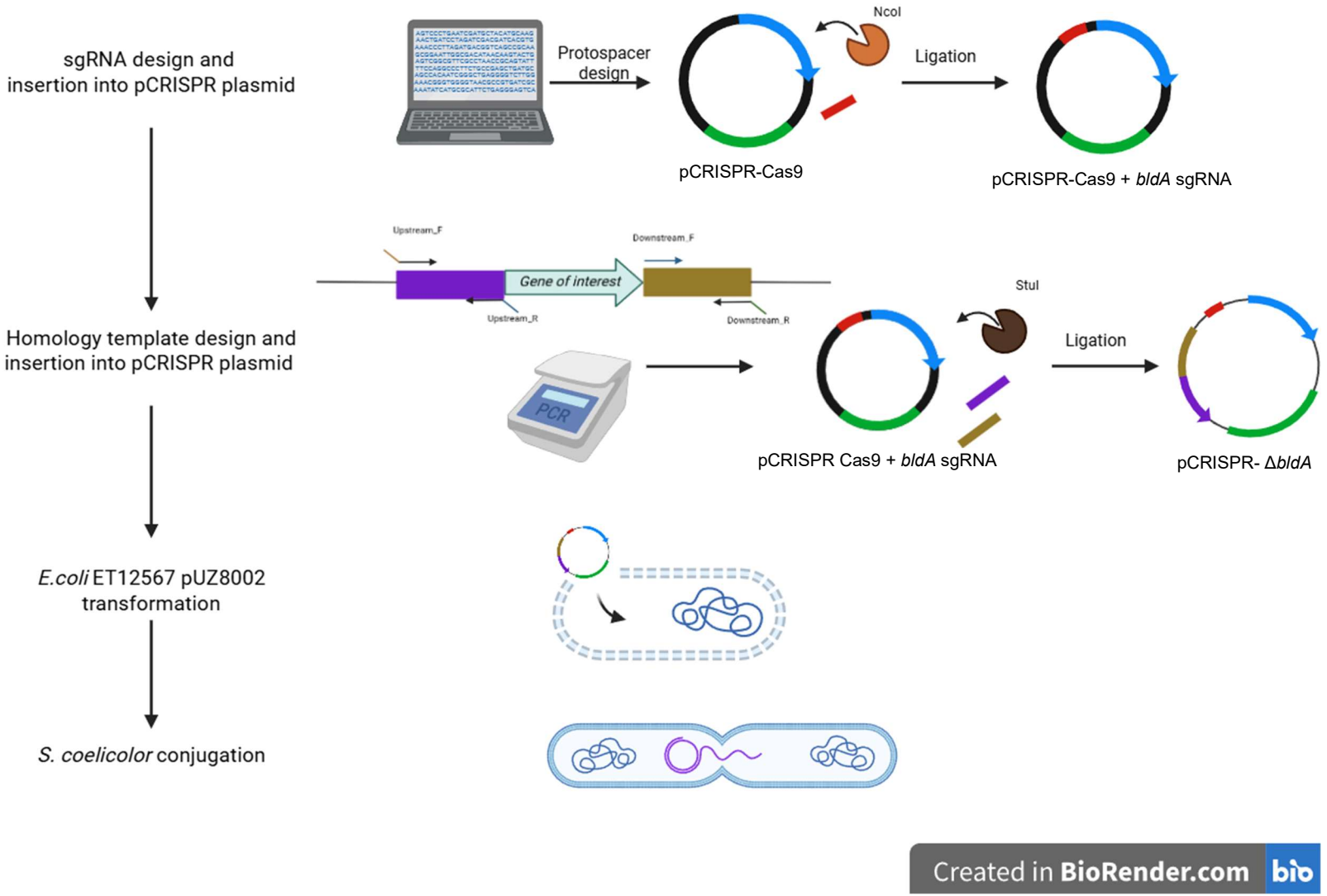

Fig. 6.8. Schematic illustrating the CRISPR-Cas9–mediated construction of a novel Δ*bldA* knockout in *S. coelicolor* M145. First, a CRISPR-Cas9 plasmid was constructed containing a small-guide RNA (sgRNA) designed by CRISPY-web (Blin *et al,* 2016), targeting the desired gene. The plasmid also contained adjacent upstream and downstream sequences adjacent for homologous recombination. The plasmid was introduced into *S. coelicolor* M145 via conjugation with *E. coli* ET12567 pUZ8002. Mutants were screened by PCR to determine *bldA* deletion and confirmed by sequencing to validate successful *bldA* deletion. Created with Biorender (Biorender, 2025).

6.3.5 Construction and integration of the pCRISPR_Δ*bldA* plasmid

The initial step in the construction of the pCRISPR_Δ*bldA* plasmid requires the creation of the sgRNA specific to the *bldA* region on the *S. coelicolor* M145 genome and for primer design of the editing temples required for homologous recombination. To design sgRNA the identification program CRISPy-web (Blin *et al*., 2018) was used. This tool allows interactive selection of regions of interest and then scans for potential sgRNA sites, identifying potential mismatch sites in the genome that could cause off target effects (Blin *et al*, 2018). The genome of *S. coelicolor* M145 was retrieved from NCBI (Accession number: AL645882) and uploaded to CRISPy-web, followed by selection of the *bldA* locus. CRISPy-web identified potential 20bp protospacer sgRNA sites, the protospacer with the fewest off-target sites was selected **(Fig. 6.9A)**. This protospacer was then used to design a 60bp sgRNA for insertion into the pCRISPR-Cas9 plasmid (Tong *et al*, 2020). The 60bp sgRNA was comprised of two 20bp regions that are homologous to regions upstream and downstream of the *bldA* gene and the 20bp protospacer designed by CRISPy-web inbetween them. The template below highlights the different components of the desired sgRNA within the pCRISPR-Cas9 plasmid:

CGGTTGGTAGGATCGACGGC-**CGGATGGTGGAATGCAGACA**-GTTTTAGAGCTAGAAATAGC

Key

Text- Plasmid homology arms

Bold Text- sgRNA protospacer

The 60bp sgRNA encoding fragment was designed and ordered from IDT, where the desalted sgRNA encoding fragment was resuspended with sterile distilled water (100μM stock concentration) (primer number 9). To prepare the regions of homology, a set of primers were designed that amplified two 1kb DNA fragments which flanked either side of the *bldA* tRNA coding sequence, with each primer possessing a 20-nt overhang at each end of the desired fragment to facilitate Gibson assembly into the pCRISPR-Cas9 plasmid **(Fig. 6.9B)**. Genomic *S. coelicolor* M145 DNA was used to amplify the fragments by PCR. The PCR protocol followed for the amplification of the homology fragments is outlined in **Section 2.6.4.** Each fragment was amplified separately and resolved using electrophoresis on a 1% agarose gel, enabling visualisation of the desired product, using primer numbers 12 and 13 for the upstream fragment, and primer numbers 14 and 15 for the downstream fragment. **(Fig. 6.9C)**. The amplified upstream and downstream fragments were purified by gel extraction, quantified using a NanoDrop 2000c spectrophotometer and stored at -20°C until required.

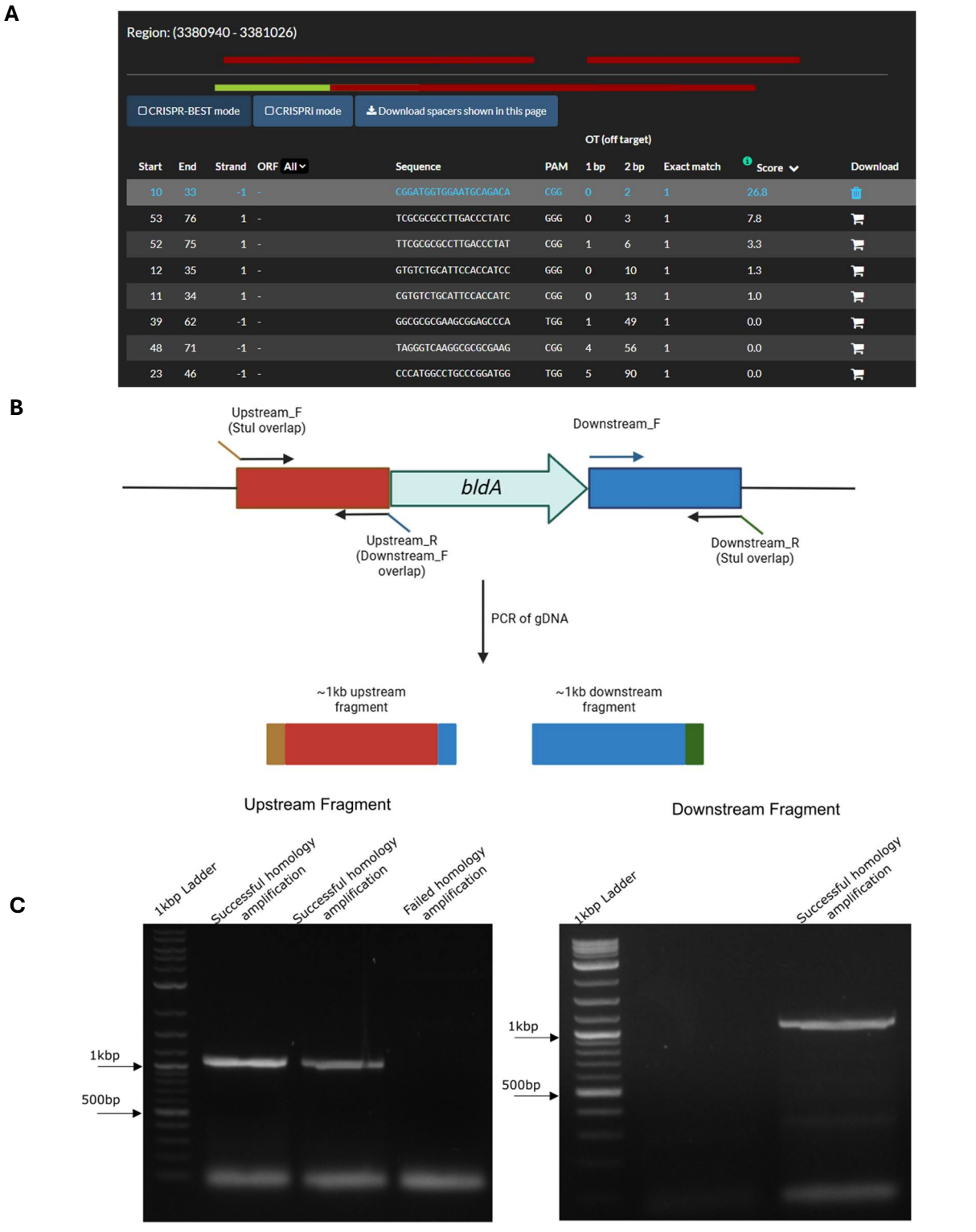

Fig. 6.9. Design of the pCRISPR_ΔbldA sgRNA sgRNA and editing templates. A: Selection of the optimal 20 bp sgRNA protospacer targeting the *bldA* gene in *S. coelicolor* M145 using CRISPy-web, to minimize off-target effects. **B**: Schematic of primer design for amplification of ~1 kb upstream and downstream homology arms flanking the *bldA* locus, with 20-nt overhangs for Gibson assembly. **C**: Electrophoresis of PCR-amplified homology arms on a 1% agarose gel, showing successful amplification of expected ~1 kb fragments.

With the sgRNA encoding fragment and editing templates prepared, restriction enzyme cloning was used to insert each fragment into the pCRISPR-Cas9 vector. The pCRISPR-Cas9 plasmid was digested with NcoI for 1 hour before treatment with FastAP alkaline phosphatase for a further 15 minutes, to prevent relegation of the vector. The linearized plasmid was purified through gel extraction following resolution in a 1% agarose gel. The sgRNA encoding fragment was then cloned into the linear pCRISPR-Cas9 plasmid and ligated with NEBuilder HiFi DNA Assembly Master Mix at 50°C for 1 hour before the ligated plasmid where it was used to transform chemically competent *E. coli* DH5α.

The pCRISPR_Δ*bldA* plasmid was verified through PCR and whole plasmid sequencing. Colonies were picked after 18 hours incubation on apramycin containing LB plates (50 μg/ml^{-1}) with sterile toothpicks and transferred into a 96-well plate containing LB supplemented with 50 μg/mL apramycin. The selected colonies were then incubated at 37°C for 2 hours before 1μL from each culture was used as a template for colony PCR, using specific *bldA* sgRNA-TEST primers to determine the presence of the protospacer (primer numbers 10 and 11). Due to a size difference of only 20bp, this proved difficult to visualize on 1% agarose gel. As such, a 3% agarose gel was used to visualize positive clones. Candidate clones were inoculated into fresh LB media containing 50 μg/mL apramycin and grown overnight before isolating the plasmid. Putative clones were sent for Sanger sequencing, performed by the Eurofins Sequencing service, to confirm accurate protospacer insertion, using the M13_reverse primer to sequence the region containing the modified sgRNA (primer number 6). Sequencing results were analysed on SnapGene and assembled via the CAP3 Sequence Assembly Program **(Fig. 6.10A)**. Positive clones were stored at -20°C.

To insert the homology arms, a positive pCRISPR_ Δ*bldA* plasmid, already containing the *bldA* sgRNA, was digested with StuI. The linearized plasmid was separated using agarose gel electrophoresis, and the appropriate band was extracted and quantified. The two previously extracted homology templates were then cloned into the linearized pCRISPR_*bldA* candidate using Gibson assembly, with the required fragment volume calculated and matching a molar

ratio of 3:1 (insert/vector). The ligation reaction was incubated and *E. coli* DH5α was transformed as previously described. Colonies obtained after overnight growth were screened by colony PCR, using the StuI primer set (primer numbers 16 and 17) to amplify flanking regions of the StuI site, indicating insertion of both upstream and downstream homology fragments resulting in an amplicon of ~2kb on an agarose gel for positive clones (**Fig. 6.10B**). Positive clones possessing a ~2kb amplicon were grown overnight in fresh LB media containing apramycin 50 $\mu g ml^{-1}$). Plasmids extracted using a NEB Monarch Miniprep Kit and submitted for the whole plasmid sequencing service (Plasmidsaurus). Whole plasmid sequencing was chosen over Sanger sequencing for this experiment due to the larger size of the cloned insert and to check for any mutations within the pCRISPR-*bldA* plasmid prior to final transformation and conjugation into *S. coelicolor* M145 **(Fig. 6.11**). Sequencing results were analysed on SnapGene™.

A

B

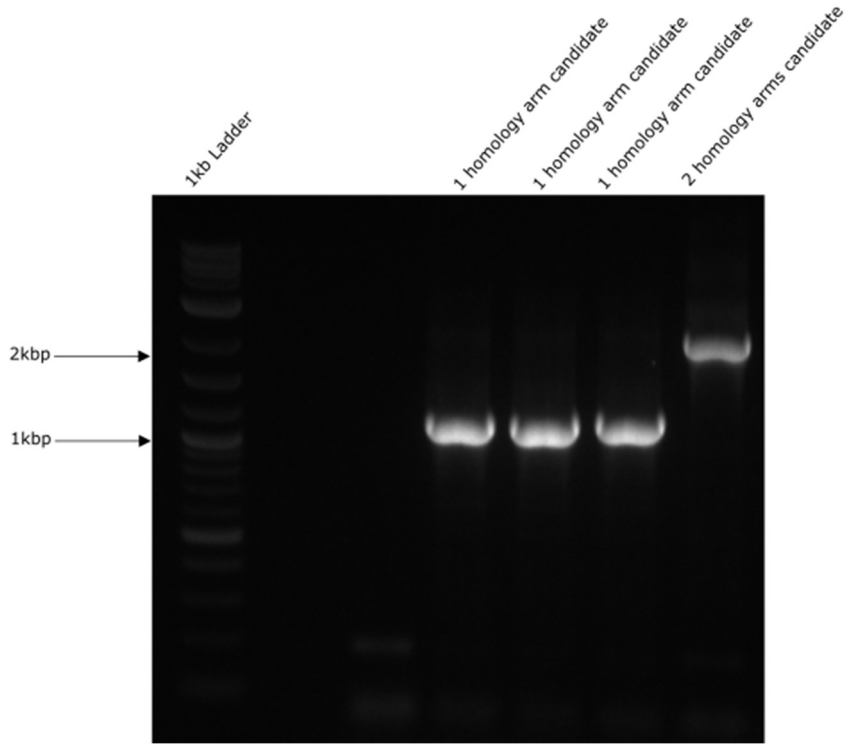

Fig. 6.10: Insertion of sgRNA and construction of homology regions for the pCRISPR_Δ*bldA* plasmid. A: Plasmid sequencing confirms cloning of 20 bp *bldA* spacer sequence required for Cas9 to create a double stranded break at the complementary location**. B:** Insertion of upstream and downstream homology arms into the validated pCRISPR_*bldA* plasmid. Colony PCR targeting the flanking regions of the insertion site confirmed successful ~2 kb insertions, indicating presence of both homology arms.

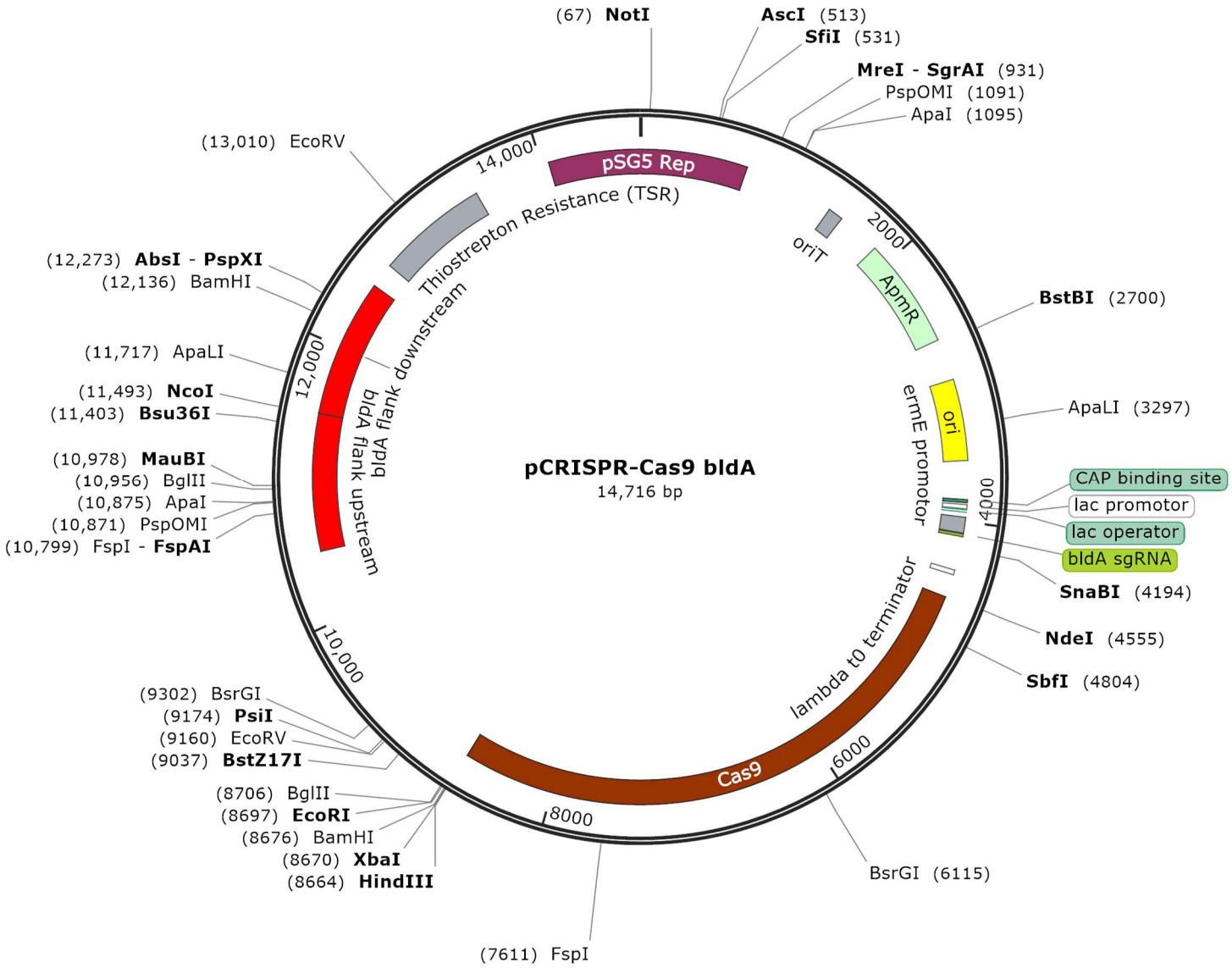

Fig. 6.11 Plasmid construct of the completed pCRISPR_Δ*bldA* plasmid, with sgRNA and completed homology arms. Plasmid maps were created using SnapGene™.

S. coelicolor JWS-Δ*bldA* candidate colonies were confirmed by patching colonies onto fresh MS agar plates containing apramycin (50 μgml^{-1}) and nalidixic acid (25μg/ml^{-1}). Apramycin resistant patches were further streaked on to fresh MS agar plates containing apramycin (50 μg/ml^{-1}) and nalidixic acid (25μg/ml^{-1}) and grown for 5 days at 30^{o}C, which is sufficient time for *S.coelicolor* to fully sporulate. Candidates that exhibited the classical *bldA* phenotype were grown up and genomic DNA was extracted, then subjected to PCR using the *bldA* tRNA knockout confirmation check primers (primer numbers 18 and 19). In *S. coelicolor* M145, these primers yield a 428bp amplicon, which includes the *bldA* gene, in deletion mutants the amplicon is reduced by 87bp, such that *S. coelicolor* JWS-Δ*bldA* mutants would give rise to a 341bp fragment (**Fig. 6.12A).** To further verify the *bldA* deletion strains, the respective amplicons were gel purified and sequenced (Eurofins) to confirm the deletion of the 87bp *bldA* gene. To confirm the mutation and the absence of any potential off-target mutations, three putative *S. coelicolor* JWS-Δ*bldA* candidates had their whole genome sequenced (supplied by Novogene Ltd), using the Illumina sequencing platform. All three candidates were confirmed as *S. coelicolor* JWS-Δ*bldA* strains. To cure the pCRISPR plasmid following confirmation of the deletion of *bldA* and to ensure no future off-target effects, the *S. coelicolor* JWS-Δ*bldA* strains were passaged several times on to fresh MS medium, with and without apramycin (50 μg/ml^{-1}) to screen for the loss of the plasmid (apramycin sensitivity) and retention of the *bldA* phenotype. The *S. coelicolor* JWS-Δ*bldA* strain exhibits extreme changes in colony morphology compared to *S. coelicolor* M145 after five days incubation at 30^{o}C, characterized by a lack of aerial hyphae and sporulation (**Fig 6.12B**).

Next, the impacts that *bldA* deletion had on growth rate was investigated by comparing cell dry weights of *S. coelicolor* strains, including *S. coelicolor* M145 (wild-type strain), *S. coelicolor* J1700 (a strain where the Leu-tRNA^{BldA} is mutated but not removed entirely), and *S. coelicolor* JWS-Δ*bldA* (where the entire tRNA encoding sequence has been excised). Compared to *S. coelicolor* M145 and *S. coelicolor* J1700, *S. coelicolor* JWS- Δ*bldA* possesses stunted growth in comparison, observed by only reaching exponential phase after 32 hours of growth in TSB,

compared to *S. coelicolor* M145 and J1700 reaching exponential phase after 16 hours (**Fig. 6.13**). Calculations of the specific growth rate (h^{-1}) for all three strains further exemplified this finding, with the specific growth rate of *S. coelicolor* JWS- Δ*bldA* (0.0437 h^{-1}) being reduced when compared to both *S. coelicolor* M145 and *S. coelicolor* J1700 (0.0513 h^{-1} and 0.0660h^{-1} respectively). This deficient growth rate cannot be attributed to different starting inoculums as both *S. coelicolor* J1700 and *S. coelicolor* JWS- Δ*bldA* both used the equivalent of $1x10^6$ CFU/ml, while for *S. coelicolor* M145, $1x10^6$ spores/ml was used. This reduction in growth rate is unlikely to be due to additional mutations, due to the reduced number of mutations in *S. coelicolor* JWS- Δ*bldA* compared to *S. coelicolor* J1700, however, as the leucine-$tRNA^{BldA}$ is an important regulator in *Streptomyces coelicolor*, it is possible that the cause of this reduced level may be linked to the transcriptional background of *S. coelicolor* JWS- Δ*bldA*. Overall, these data indicate that the deletion of *bldA* has a measurable impact on the growth of *S. coelicolor*, whereas the additional mutations in *S. coelicolor* J1700 may suppress this stunted growth phenotype (see **Chapter 5** and **Appendix 1**).

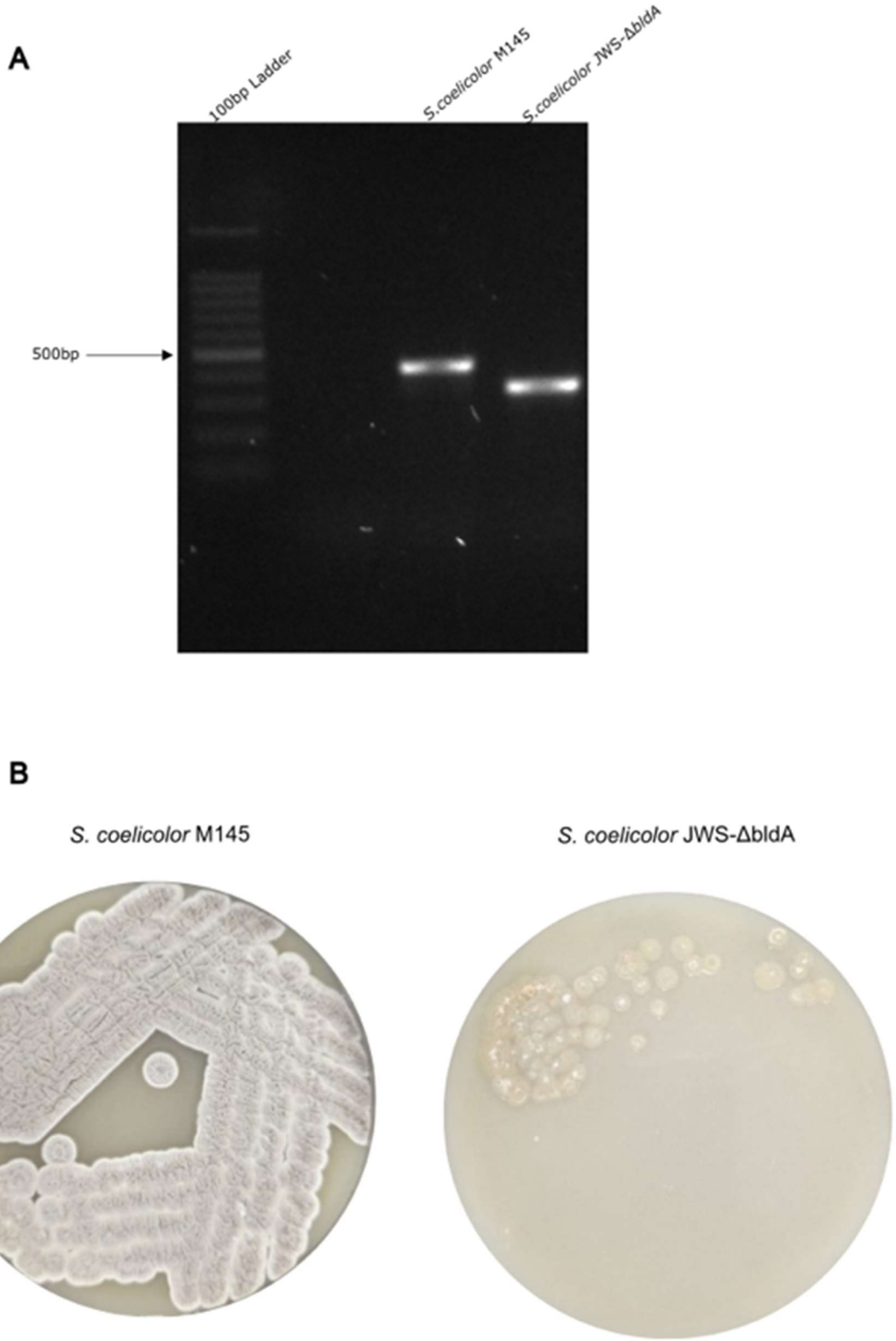

Fig. 6.12: Confirmation and phenotypic analysis of *S. coelicolor* JWS-Δ*bldA*. A: PCR amplification of the *bldA* locus from candidate *S. coelicolor* JWS-Δ*bldA* mutants. Successful knockouts produce an 87bp smaller amplicon due to the removal of the 87 bp *bldA* encoding sequence. **B:** Colony morphology comparison after 5 days growth on MS agar at 30°C, showing the characteristic bald phenotype of *S. coelicolor* JWS-Δ*bldA* colonies compared to wild-type *S. coelicolor* M145.

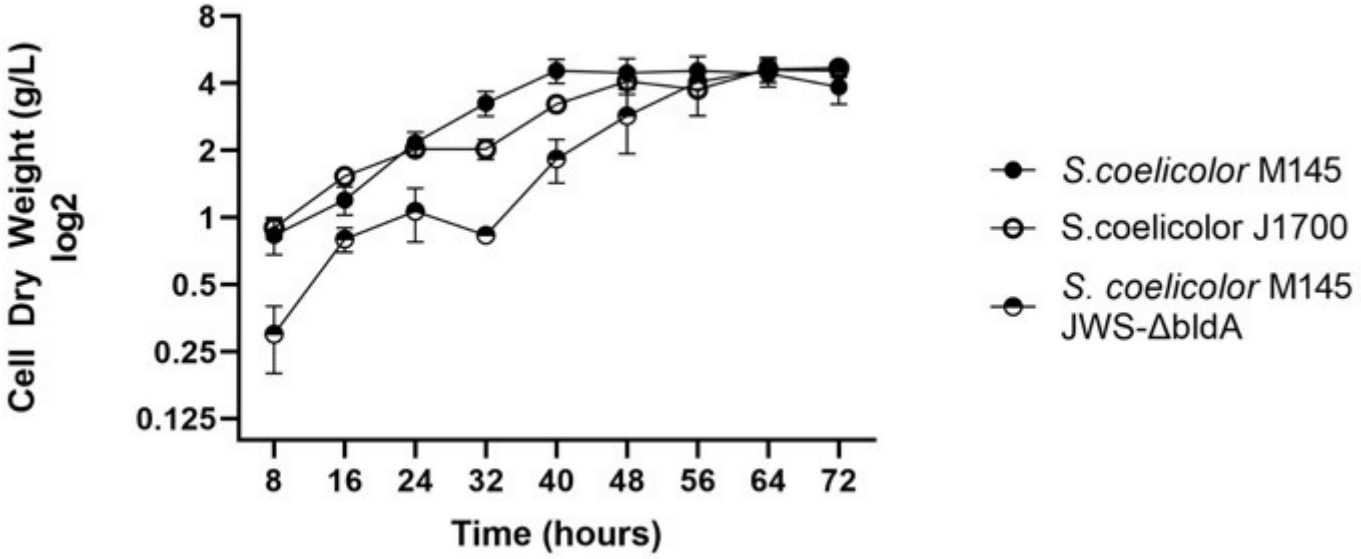

Strain	Specific Growth Rate (h^{-1})
S. coelicolor M145	0.0513
S. coelicolor J1700	0.066
S. coelicolor JWS- Δ*bldA*	0.0437

Fig. 6.13: Comparative cell dry weights of *S. coelicolor* M145, *S. coelicolor* J1700 and *S. coelicolor* JWS-Δ*bldA* in TSB. Experiments were carried out in triplicate and mean dry cell weight was plotted using Graphpad 8. Specific growth rate was calculated using the exponential growth phase for each strain.

6.3.6 The Leu-tRNA^{CAA} is essential in *S. coelicolor*

Deletion of the *bldA* gene in *S. coelicolor* M145 resulted in the classical '*bldA*-phenotype' as expected. Given that the closest Wobble-Base Pairing match in the *S. coelicolor* genome was the Leu-tRNA^{CAA} gene, that decodes UUG codons, it was hypothesized that overexpression of the Leu-tRNA^{CAA} may suppress the *bldA* phenotype. Previous work has suggested that the Leu-tRNA^{CAA} gene is able to suppress the *bldA* phenotype, even though the Leu-tRNA^{CAA} isoacceptor is a type I tRNA, compared to the other Leu-tRNAs possessing a type II structure (Petterson and Kirsebom, 2011., Fan *et al*, 2019). It was hypothesized that generating a Leu-tRNA^{CAA} knockout strain would allow greater clarity of function and potential for Wobble-Base Pairing.

The same methodology for the creation of *S. coelicolor* JWS-Δ*bldA* was used to create the pCRISPR-Cas9 plasmid utilized in the attempted deletion of Leu-tRNA^{CAA}. The 60bp sgRNA, containing the specific Leu-tRNA^{CAA} coding sequence for accuracy was designed and ordered from IDT^{TM} (primer number 20 for sgRNA, primer numbers 21 and 22 for sgRNA insertion confirmation). However, after several attempts at restriction digestion and ligation of the sgRNA into the plasmid backbone, the initially designed sgRNA was deemed unsuitable due to an inability to achieve success ligation. As such, a further three sgRNA specific to the Leu-tRNA^{CAA} coding sequence were designed (primer numbers 23, 26 and 29), using the respective sgRNA confirmation primers (see **Table 2-5**). The sgRNA designed as primer number 26 was successfully ligated into the pCRISPR-Cas9 plasmid backbone as the following protospacer:

CGGTTGGTAGGATCGACGGC-**GAGCAACGTGTCTCTACCGC**-GTTTTAGAGCTAGAAATAGC

Key
Text- Plasmid homology arms
Bold Text- sgRNA protospacer

Homology arms for the pCRISPR Leu-tRNA^{CAA} plasmid were designed in the same manner as outlined previously (see **Section 6.3.5**), with *S. coelicolor* M145 gDNA used as a template for homology arm amplification for both upstream (primer numbers 32 and 33) and downstream (primer numbers 34 and 35) fragments. A complete assembly of the pCRISPR_ΔLeu-tRNA^{CAA} can be seen in **Fig. 6.14**.

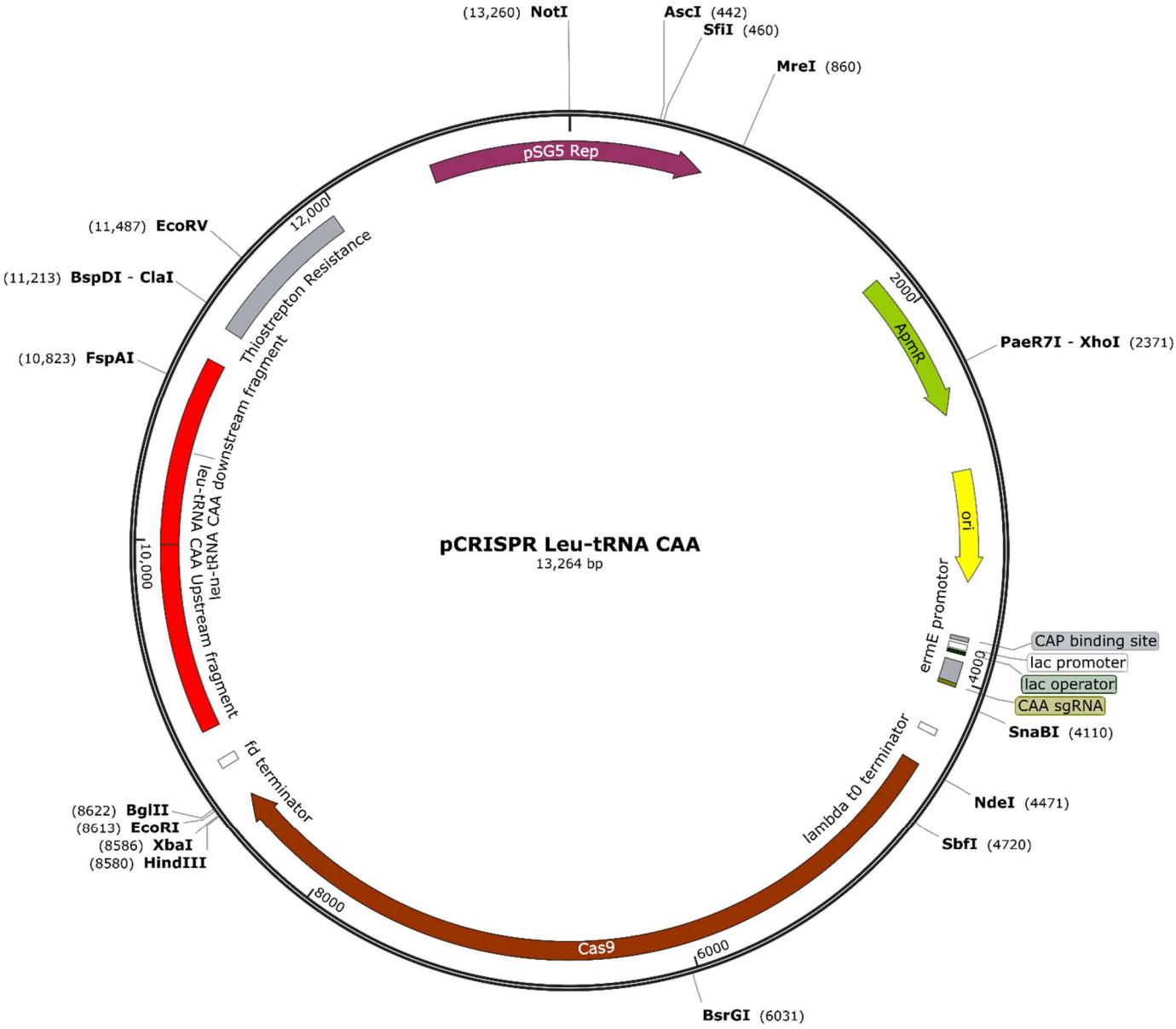

Fig. 6.14 Plasmid construct of the completed pCRISPR_ΔLeu-tRNA^{CAA} plasmid, with sgRNA and completed homology arms. Plasmid maps were created using SnapGene™.

However, while the construction of the pCRISPR_ΔLeu-tRNA^{CAA} plasmid was successful, conjugation of the pCRISPR_ΔLeu-tRNA^{CAA} plasmid into *S. coelicolor* M145 proved to be a considerable challenge. This is highlighted in **Fig 6.15**, where comparative candidates between *S. coelicolor* JWS-Δ*bldA* exconjugants (**Fig. 6.15A**), and potential *S. coelicolor* JWS-ΔLeu-tRNA^{CAA} exconjugants (**Fig. 6.15B**), show that the conjugational efficiency with the pCRISPR-LeuCAA plasmid is reduced. The conjugation efficiency was calculated based on the number of recipient cells, as the number of recipient spores were used between a range of 10^5, 10^6, 10^7 and 10^8 spores, with the number of donor *E. coli* ET12567/pUZ8002 cells kept constant for each conjugation experiment (500µL of *E. coli* cells grown to an OD_{600} of 0.5, roughly equal to 4 x 10^8 cells). Recipient spores were previously quantified through CFU serial dilution plating.

This challenge is further highlighted in **Fig 6.16A,** where an agarose gel of conjugation candidates reveals that many candidates failed to fully delete the Leu-tRNA^{CAA} coding sequence, evident by the absence of an amplicon at the expected deletion size or by the presence of both the wild-type (500bp) and deletion-sized amplicons (427bp), indicating incomplete or mixed populations (determined by PCR using the Leu-tRNA^{CAA} removal confirmation primers (numbers 36 and 37)). Overall, 90 potential deletion candidates were screened, with none of the tested candidates possessed solely the deletion amplicon, whereas seven total candidates exhibited a mixed population of both WT and deletion-length amplicons. Attempts to remove mixed populations by antibiotic selection were unsuccessful, despite selection pressure, and once selection pressure was removed, full reversions to WT-Leu^{CAA} were seen (through the absence of the pre-existing deletion-sized amplicon) (**Fig. 6.16B**). To confirm the correct genomic sequence was targeted, a WT amplicon and a deletion sized amplicon were gel extracted, purified and sent for Sanger sequencing, performed by Eurofins^{TM}. Analysis of both amplicons highlighted the Leu-tRNA^{CAA} was indeed being deleted, characterised by the deletion of a 73bp region mapping to the Leu-tRNA^{CAA} (**Fig 6.17**).

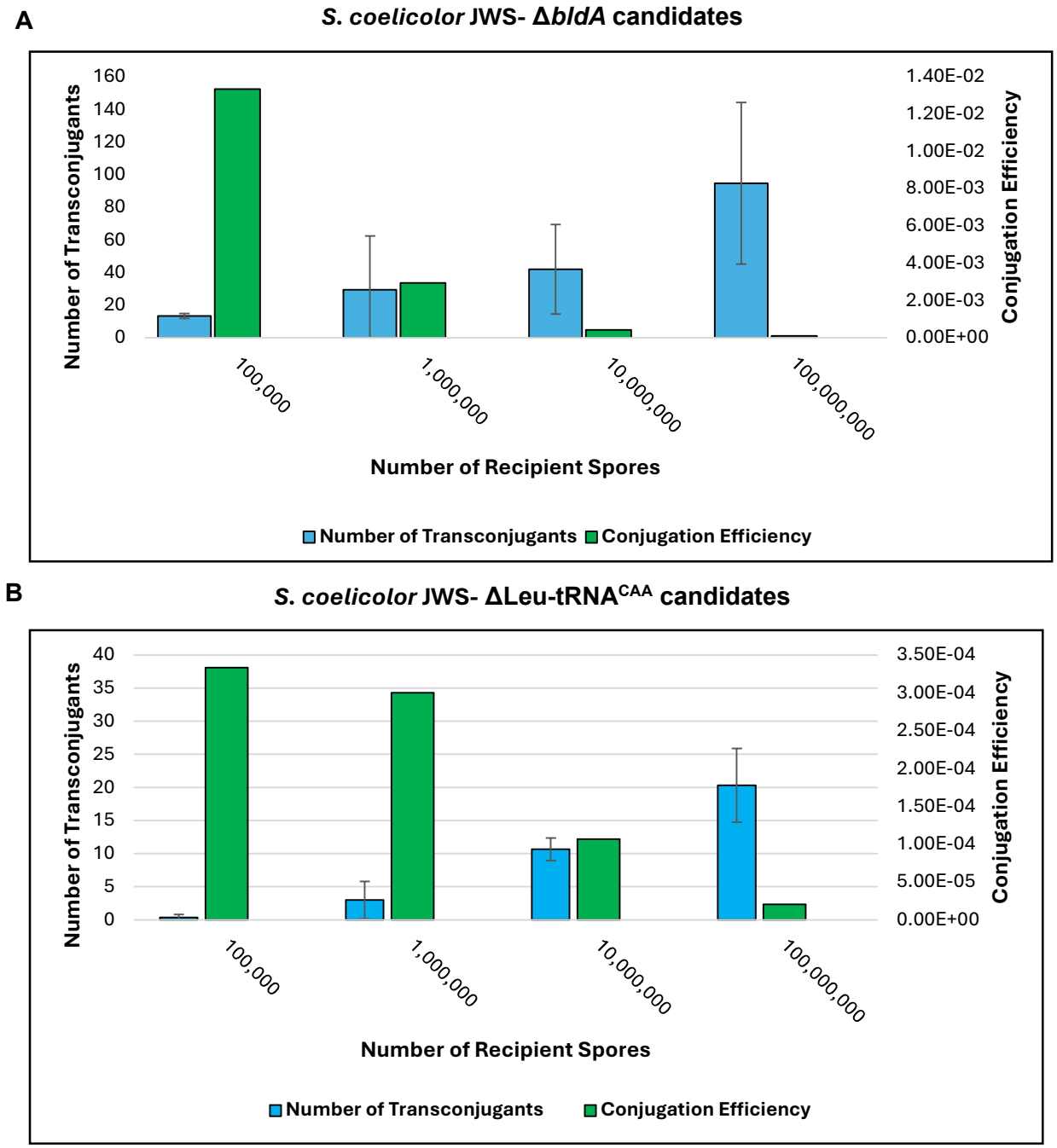

Fig. 6.15: Conjugation efficiency between *S. coelicolor* JWS-Δ*bldA* candidates and potential *S. coelicolor* JWS-ΔLeu-tRNA^{CAA} candidates. A: *S. coelicolor* JWS- Δ*bldA* number of exconjugant colonies increases and conjugation efficiency decreases as recipient spore number increases. B: *S. coelicolor* JWS- ΔLeu-tRNA^{CAA} number of exconjugant colonies increases and conjugation efficiency decreases as recipient spore number increases. Exconjugant count and conjugation efficiency in *S. coelicolor* JWS- ΔLeu-tRNA^{CAA} candidates is notably lower than in *S. coelicolor* JWS- Δ*bldA* candidates.

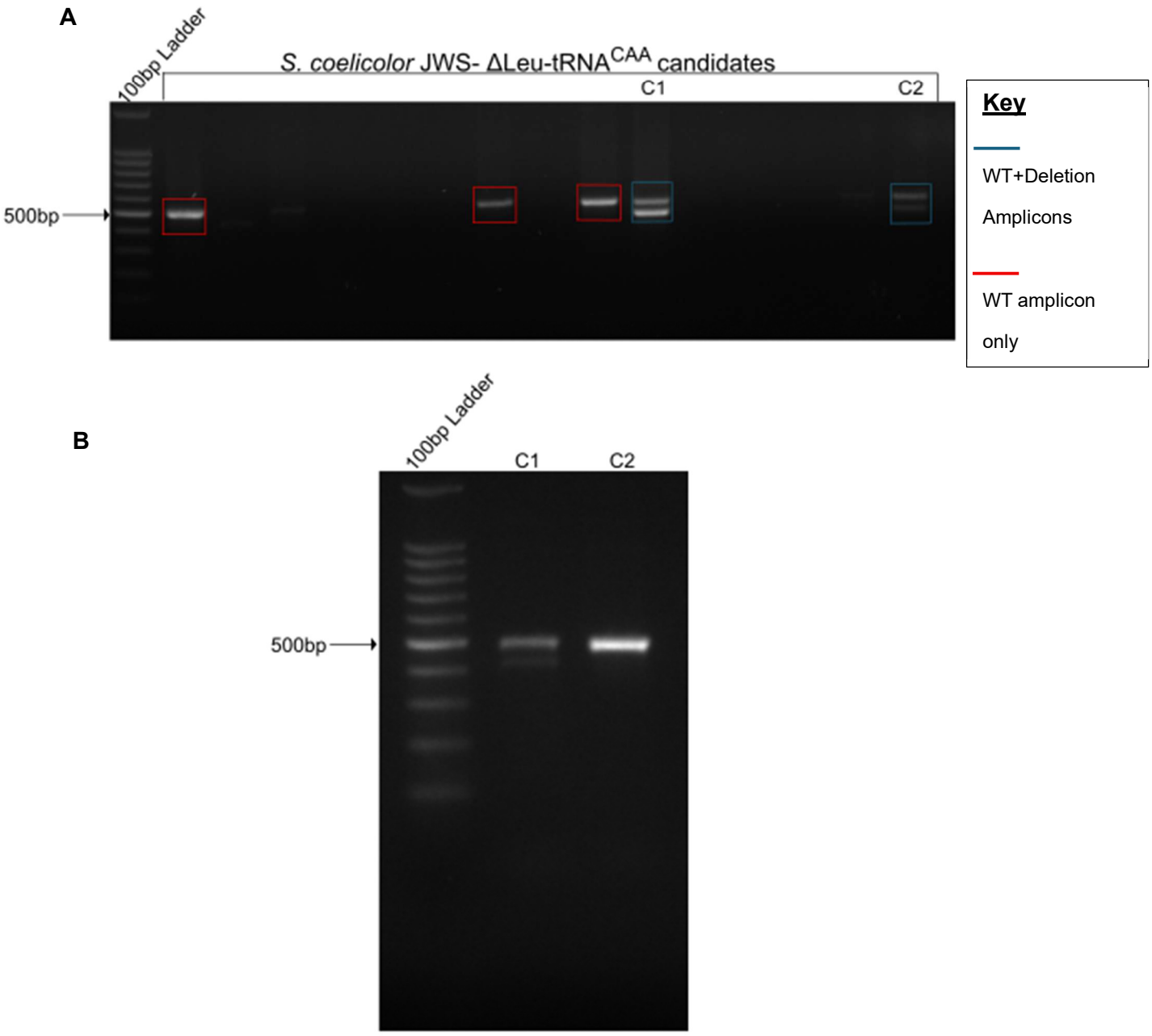

Fig. 6.16: Successful *S. coelicolor* JWS-ΔLeu-tRNA^{CAA} candidates revert to wild-type over time. A: Agarose gel of *S. coelicolor* JWS-ΔLeu-tRNA^{CAA} candidates highlights either failed amplification, wild-type amplicons only (red) or mixed populations of wild-type and deletion amplicons (blue). Candidates containing both wild-type and deletion amplicons (C1 and C2) were carried forward. **B:** Agarose gel of *S. coelicolor* JWS-ΔLeu-tRNA^{CAA} candidates C1 and C2 after restreaking. Candidates lose deletion amplicon, indicating full reversion to wild-type coding sequence.

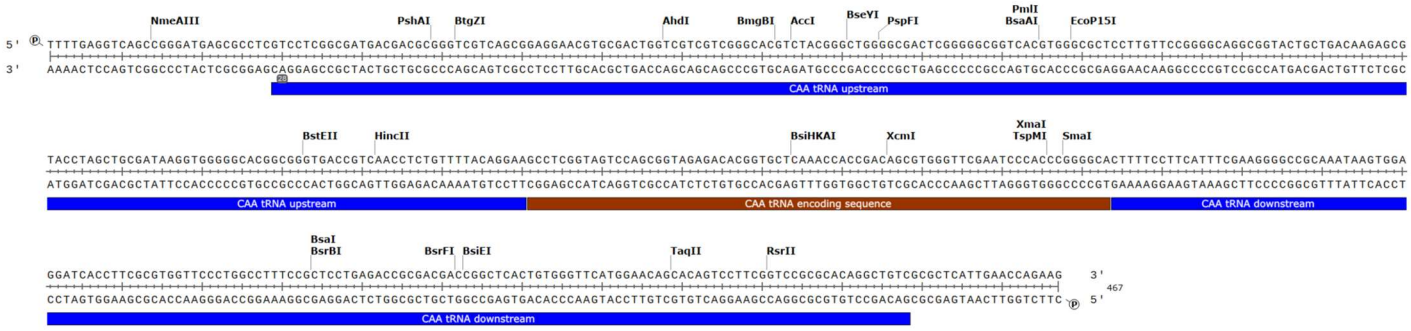

***S. coelicolor* JWS-ΔLeu-tRNA^{CAA}: WT band**

***S. coelicolor* JWS-ΔLeu-tRNA^{CAA} : Deletion band**

Fig. 6.17: Sanger sequencing of gel-extracted wild-type and Leu-tRNA^{CAA} deletion amplicons from a *S. coelicolor* JWS-ΔLeu-tRNA^{CAA} candidate. Sequencing confirming successful deletion of the 73 bp Leu-tRNA^{CAA} coding region in the selected candidate before reversion takes place. Sequencing was performed by Eurofins and validated the targeted genomic region.

These data suggest that the Leu-tRNA^{CAA} gene in *S. coelicolor* is essential. Comparative total exconjugants and conjugation efficiency was low compared to a successful pCRISPR-mediated knockout (*S. coelicolor* JWS-Δ*bldA*), with a 100-fold decrease in efficiency detected between the two strain (**Fig. 6.15**). Additionally, while the targeted sequence for the pCRISPR-Leu-tRNA^{CAA} plasmid was accurate, repeat streaking of potential *S. coelicolor* JWS-ΔLeu-tRNA^{CAA} candidates resulted in reversion, as evidenced through agarose gel amplicons (**Fig 6.16**). Sanger sequencing of both amplicons proved that the amplified regions pertained to the site of the Leu-tRNA^{CAA}, indicating the pCRISPR Leu-tRNA^{CAA} plasmid was targeting the correct location (**Fig. 6.17**). The Leu-tRNA^{CAA}, based on the data above, and the presence of TTG codons in 42.5% of *S. coelicolor* CDSs (see **Table 6-1**), is essential to *S. coelicolor* and the absence of this tRNA would result in defective translation of almost half of the *S. coelicolor* genome, which may explain the inability to construct this deletion mutant.

6.3.7 Genome analysis of *S. coelicolor* Δ*bldA* mutants reveal the presence of potential suppressor mutations

Deletion of the *bldA* gene from the *S. coelicolor* M145 genome was confirmed whole genome sequencing. Analysis of the genomes of three independent strains of *S. coelicolor* JWS-Δ*bldA* revealed a small number of mutations that were not present in the isogenic parent strain *S. coelicolor* M145. Two consistent mutations were identified that differed from the Genbank *S. ceolicolor* M145 sequence (Accession No.: AL645882), the deletion of the 87bp *bldA* gene as expected, and an additional mutation found in SCO4635, a 50S ribosomal protein L33, which possesses a putative zinc-binding motif (Shin *et al*, 2007). This mutation was a 7bp contraction of a tandem repeat located at the extreme C-terminus of the protein. Given this mutation was found in all *S. coelicolor* JWS-Δ*bldA* mutants, and the ribosome and its proteins are required for mRNA translation along with tRNAs, this mutation may suppress effects of the *bldA* mutation. This 7bp contraction of the C-terminus could suppress the *bldA* deletion phenotype through increased misreading, which has been shown as a phenotype in other ribosomal proteins with a mutated C-terminus (Kamath *et al,* 2017). As this mutation was not detected during whole genome sequencing of the *S. coelicolor* J1700 genome, which is a point mutation rather than a full gene deletion, further investigation is needed. To determine the impact of this deletion on the structure of the protein and ribosome function, the structure of 50S ribosomal protein L33 was modelled for the wild-type and the mutant 50S ribosomal protein L33 using AlphaFold3 (**Fig. 6.18**).

Whilst the unstructured C-terminal region is truncated; there is no major effect on overall protein structure. There is potential for effects on protein-protein interactions for 50S ribosomal protein L33, or zinc co-ordination could be altered if the binding motif is impacted through the loss of a histidine residue at the C-terminus of the ribosomal protein (Li *et al*, 2022). A comprehensive overview of all additional mutations identified across successful *S. coelicolor* JWS- Δ*bldA* strains can be seen in **Table 6-2**.

Table 6-2: Summary of the mutations detected in the genome of *S. coelicolor* JWS-Δ*bldA* strains

Mutation	*S. coelicolor* JWS-Δ*bldA* (Replicate 1)	*S. coelicolor* JWS-Δ*bldA* (Replicate 2)	*S. coelicolor* JWS-Δ*bldA* (Replicate 3)	Annotation	Gene	Description
+C	Absent	Present	Present	intergenic (-6/+15)	SCO1933-/-SCO1934	Hypothetical protein/putative cytochrome oxidase assembly factor
Δ87 bp	Present	Present	Present	noncoding (1-87/87 nt)	*bldA*	tRNA-Leu
Δ45 bp	Present	Absent	Absent	coding (572-616/1044 nt)	SCO4108	Probable peptidase
$(CACCGCG)_{2\rightarrow1}$	Present	Present	Present	coding (148-154/165 nt)	SCO4635	50S ribosomal protein L33
C→T	Present	Absent	Absent	H159H (CA<u>C</u>→CA<u>T</u>)	SCO6277	Putative epoxide hydrolase

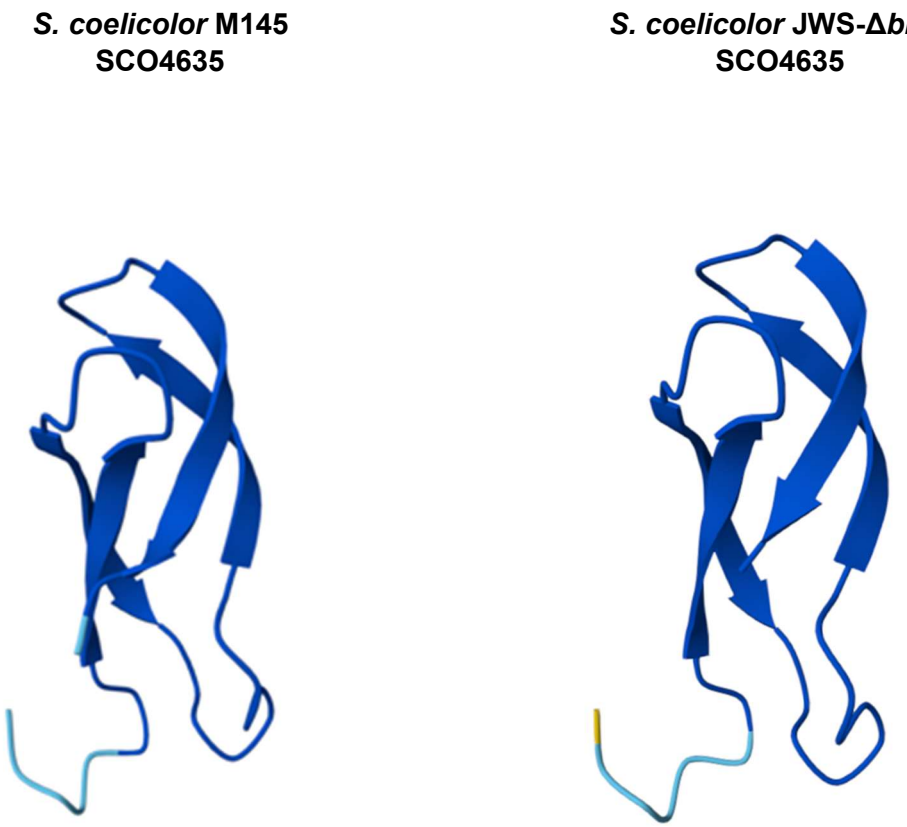

Fig. 6.18. Structural comparison of wild-type and mutant 50S ribosomal protein L33 in *S. coelicolor* M145 and *S. coelicolor* JWS-Δ*bldA*. AlphaFold3-generated models of the wild-type (left) and mutated (right) 50S ribosomal protein L33 are shown. While the overall protein structure remains largely unchanged, the shortened C-terminus in the mutant may influence protein-protein interactions within the ribosome.

6.3.8 *S. coelicolor* JWS-Δ*bldA* is fully complemented with a WT copy of *bldA*

To determine the effect of the potential suppressor mutations observed in the genome sequencing of the *S. coelicolor* JWS-Δ*bldA* strains, complementation studies were performed. If the phenotype of *S. coelicolor* JWS-Δ*bldA* can be fully complemented by a WT copy of *bldA,* this would show genetic linkage of the phenotype to deletion of the *bldA* gene. The previously used pIJ10257-based complementation plasmids were utilized to complement these strains. Three plasmids: pIJ10257_*bldA,* pIJ10257_Leu-tRNA^{CAA} and the pIJ10257 empty vector were all introduced in to *S. coelicolor* JWS-Δ*bldA* via conjugation. Given this is a bald strain, a mycelial suspension was used as the recipient for conjugation due to the deficiency in spore production (Elliot *et al*, 1998, Silov *et al*, 2020). Exconjugants were grown over a period of five days before selection and restreaking onto fresh media to isolate single colony clones.

Phenotypic differences were observed between the parental *S. coelicolor* JWS-Δ*bldA* strain and the resultant exconjugants (**Fig. 6.19**). The empty vector control conjugation resulted in minimal phenotypic changes from the parental strain, with the *bld* phenotype still dominant (**Fig**. **6.19A, Fig. 6.19B**) Unlike observations documented in *S. coelicolor* J1700 *bldA* complementation (see **Fig 6.5**), *bldA* complementation of *S. coelicolor* JWS-Δ*bldA* resulted in complete restoration of both the sporulation and the specialised metabolite-producing phenotype (**Fig. 6.19C**). Interestingly, with overexpression of the Leu-tRNA^{CAA}, while the full wild-type phenotype had not been recovered, partial restoration of sporulation could be seen (**Fig. 6.19D**). This visualization suggests that Leu-tRNA^{CAA} may in part supress the *bldA* sporulation phenotype, which has previously been documented in other *Streptomyces bldA* mutants (Petterson and Kirseborn, 2011, Fan *et al*, 2019). Restoration of the secondary metabolite-producing phenotype was not seen in these exconjugants, indicating the importance of a functioning Leu-tRNA^{bldA} for this phenotype. A comparison between Leu-tRNA^{CAA} overexpression and *bldA* complementation phenotypes in *S. coelicolor* M145, *S. coelicolor* J1700 and *S. coelicolor* JWS- Δ*bldA* can be seen in **Fig. 6.20,** with clear visual distinction observable between *S. coelicolor* J1700 and *S. coelicolor* JWS-Δ*bldA* counterparts.

Stereomicroscopy was used to further observe the phenotypic changes after Leu-tRNA overexpression and complementation in *S. coelicolor* JWS-Δ*bldA* after growth on MS media for five days (**Fig. 6.21**). It was observed that while *S. coelicolor* JWS-Δ*bldA* (**Fig 6.21A**) and *S. coelicolor* JWS-Δ*bldA* pIJ10257 EV (**Fig 6.21B**) exhibit no sporulation, typical of a *bldA* mutant (Hackl and Bechthold, 2015., Lawlor *et al,* 1987., White and Bibb, 1997), *bldA* complementation of *S. coelicolor* JWS-Δ*bldA* restores full sporulation, including restoration of the gray polyketide pigment, indicating complete restoration of the sporulation regulation network governed by *whiG* (**Fig. 6.21C;** Gallagher *et al*, 2024). Overexpression of the Leu-tRNA^{CAA} appears to partially restore sporulation, particularly to the centre of *S. coelicolor* JWS-Δ*bldA* colonies, however sporulation is markedly reduced when compared to *bldA* complementation (**Fig. 6.21D**). These data imply that while overexpression of Leu-tRNA^{CAA} can partially rescue the *bldA* morphological phenotype, it is unable to completely restore sporulation, suggesting a functional copy of *bldA* is essential for full restoration of the wild-type phenotype. After observing the impact of *bldA* complementation and Leu-tRNA^{CAA} overexpression on colony morphology in of *S. coelicolor* JWS-Δ*bldA*, next the impact on specialized metabolite production was investigated in this new *bldA* knockout strain.

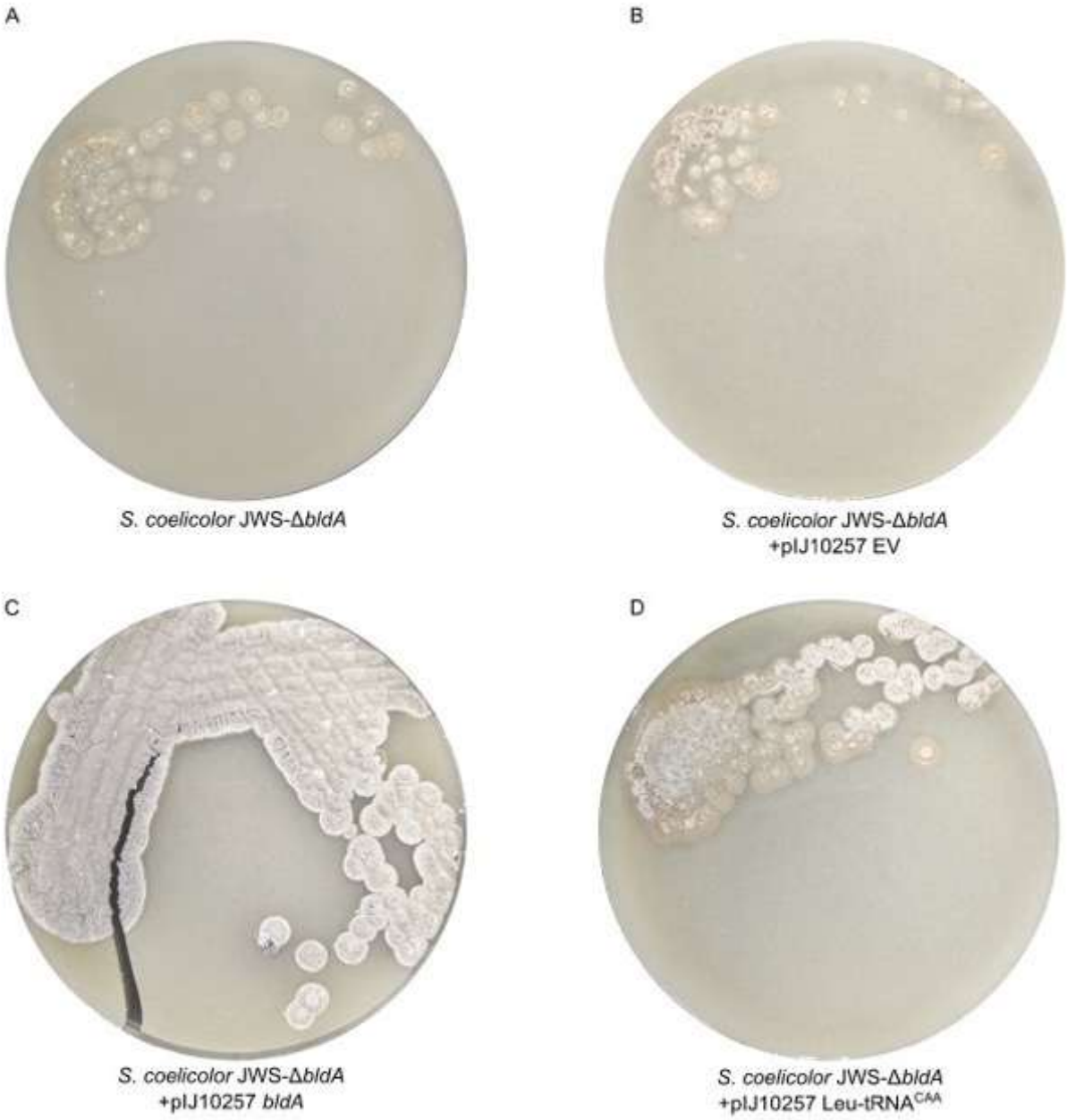

Fig. 6.19. Phenotypic restoration in *S. coelicolor* JWS-Δ*bldA* strain following complementation with *bldA* and overexpression of Leu-tRNA^{CAA}. A: *S. coelicolor* JWS-Δ*bldA* exhibits a *bldA* phenotype, with lack of aerial hyphae and sporulation. **B:** Intergration of pIJ10257 empty vector (EV) has minimal effect on *S. coelicolor* JWS-Δ*bldA* phenotype. **C**: Complementation of *S. coelicolor* JWS-Δ*bldA* fully restores sporulation phenotype. **D:** Overexpression of Leu-tRNA^{CAA} in *S. coelicolor* JWS-Δ*bldA* partially restores sporulation.

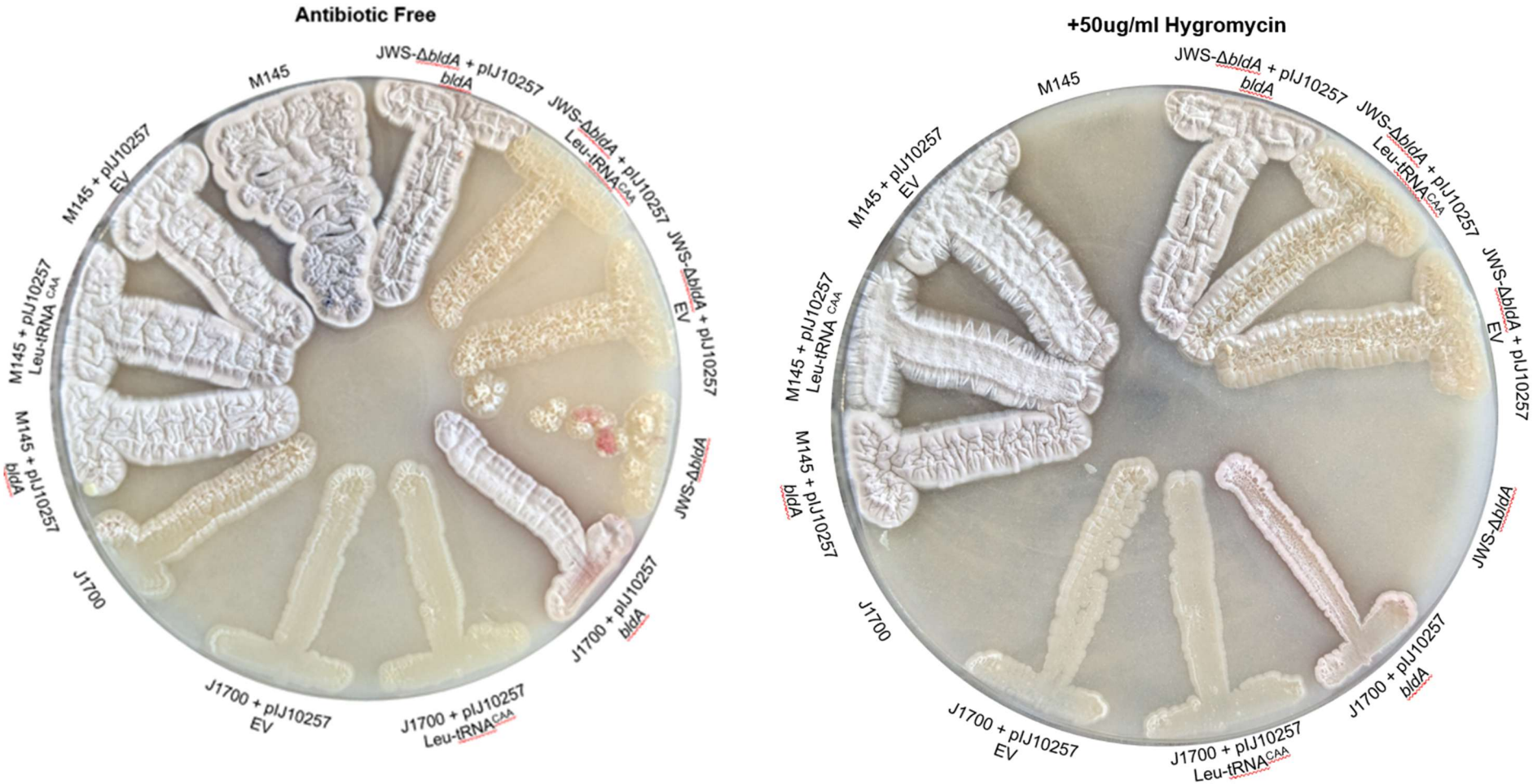

Fig. 6.20: *bldA* complementation and Leu-tRNA^{CAA} overexpression of *S. coelicolor* M145 (Wild-Type), *S. coelicolor* J1700 (*bldA* mutant) and *S. coelicolor* JWS-Δ*bldA* (*bldA* deletion strain). Strains were grown on MS media and incubated at 30ºC for 5 days before imaging.

.

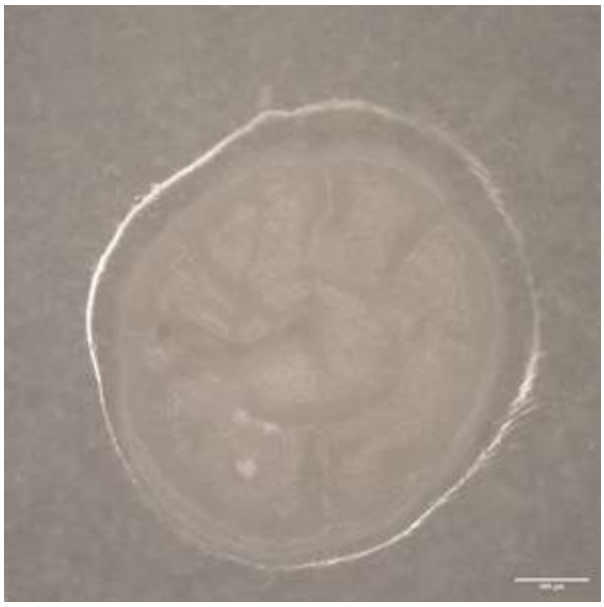

S. coelicolor JWS- Δ*bldA*

S. coelicolor JWS- Δ*bldA* pIJ10257 EV

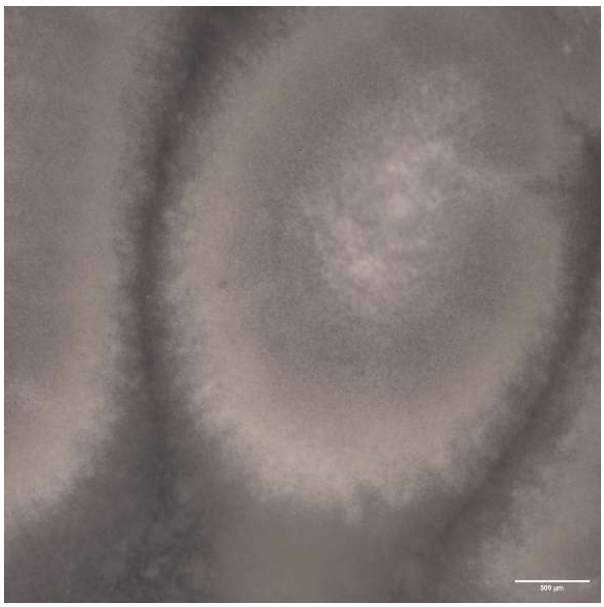

S. coelicolor JWS- Δ*bldA* pIJ10257 *bldA*

S. coelicolor JWS- Δ*bldA* pIJ10257 Leu-tRNA^{CAA}

Fig. 6.21: Stereomicroscopy images of *S. coelicolor* JWS-Δ*bldA* and pIJ10257 complementation strains on MS agar. Images were taken at 2x magnification after five days incubation. An SMZ1500 stereomicroscope coupled with a mercury arc lap was used, and images were acquired using a DFK 33UX264 CMOS camera system. Scale bar = 500µm.

6.3.9 Complementing *ΔbldA* strain fully restores antibiotic production

The *S. coelicolor* JWS-Δ*bldA* strains can be complemented in term of sporulation on solid medium (**Fig. 6.19, Fig. 6.20, Fig. 6.21**). To quantitatively test restoration of specialised metabolite production, ACT and RED yields in liquid cultures are required. *S. coelicolor* M145 is well-known for its ability to produce several natural products, including the pigmented specialised metabolites ACT and RED, both of which are reported to be tightly regulated by *bldA* (White and Bibb, 1997; Trepanier *et al*, 2002). Complementation of the *bldA* lesion in *S. coelicolor* J1700 with a WT copy of *bldA* or Leu-tRNA^{CAA} gene failed to fully restore either ACT or RED production to wild-type levels (**Fig. 6.6** and **Fig. 6.7**). To determine if *bldA* complementation or overexpression of the Leu-tRNA^{CAA} can restore ACT and RED production to wild-type levels in *S. coelicolor* JWS-Δ*bldA,* the wild-type *S. coelicolor* JWS-Δ*bldA*, along with the *bldA* complemented, Leu-tRNA^{CAA} overexpressed and pIJ10257 EV strains were used to investigate ACT and RED production. Cultures were grown in YEME media for two days, standardised to an OD_{600} of 0.1, and then grown for an additional five days, the same as previous experiments in *S. coelicolor* J1700 (See **Section 6.3.3**). ACT and RED production were quantified through the alkaline exposure and methanol extraction methods, followed by spectrophotometric quantification at OD_{633} and OD_{530} respectively.

The complementation of *S. coelicolor* JWS-Δ*bldA* with a WT copy of *bldA* fully restored of both ACT and RED production to wild-type levels (**Fig. 6.22A,B and C**, **Fig. 6.23A, B and C)**, unlike in the *S. coelicolor* J1700 background (**Fig. 6.3** and **Fig. 6.4)**. Moreover, while overexpression of the Leu-tRNA^{CAA} in *S. coelicolor* JWS-Δ*bldA* did result in low-level pigmentation production **(Fig. 6.22A, Fig. 6.23A**), normalisation of these absorbance measurements to cell dry weight (**Fig. 6.22B, Fig. 6.23B**) resulted in negligible difference in ACT or RED production compared to the parent strain *S. coelicolor* JWS-Δ*bldA* (**Fig. 6.22C, Fig. 6.23C**). The empty vector control strain of *S. coelicolor* JWS-Δ*bldA* showed no detectable ACT or RED, demonstrating genetic linkage of the phenotype.

These data demonstrate that full restoration of *bldA*-dependent secondary metabolism is possible in the *S. coelicolor* JWS-Δ*bldA*. These data also indicate that the incomplete complementation of *S. coelicolor* J1700 is likely due to additional mutations that were identified in the strain background (see **Chapter 5**). The complementation of *S. coelicolor* JWS-Δ*bldA* with a WT copy of *bldA* also indicates that the IS110 element identified in the *red* BGC is likely responsible for the incomplete complementation of RED production in *S. coelicolor* J1700 (see **Section 5.3.4** and **Fig 6.7**).

The observation that overexpression of the Leu-tRNA^{CAA} gene can induce a low but reproducible increase in pigmentation further supports the idea that increased tRNA availability can partially suppress the *bldA* phenotype (Petterson and Kirsebom, 2011) likely through WBP. These data show the value of isogenic strain pairs for studying gene function.

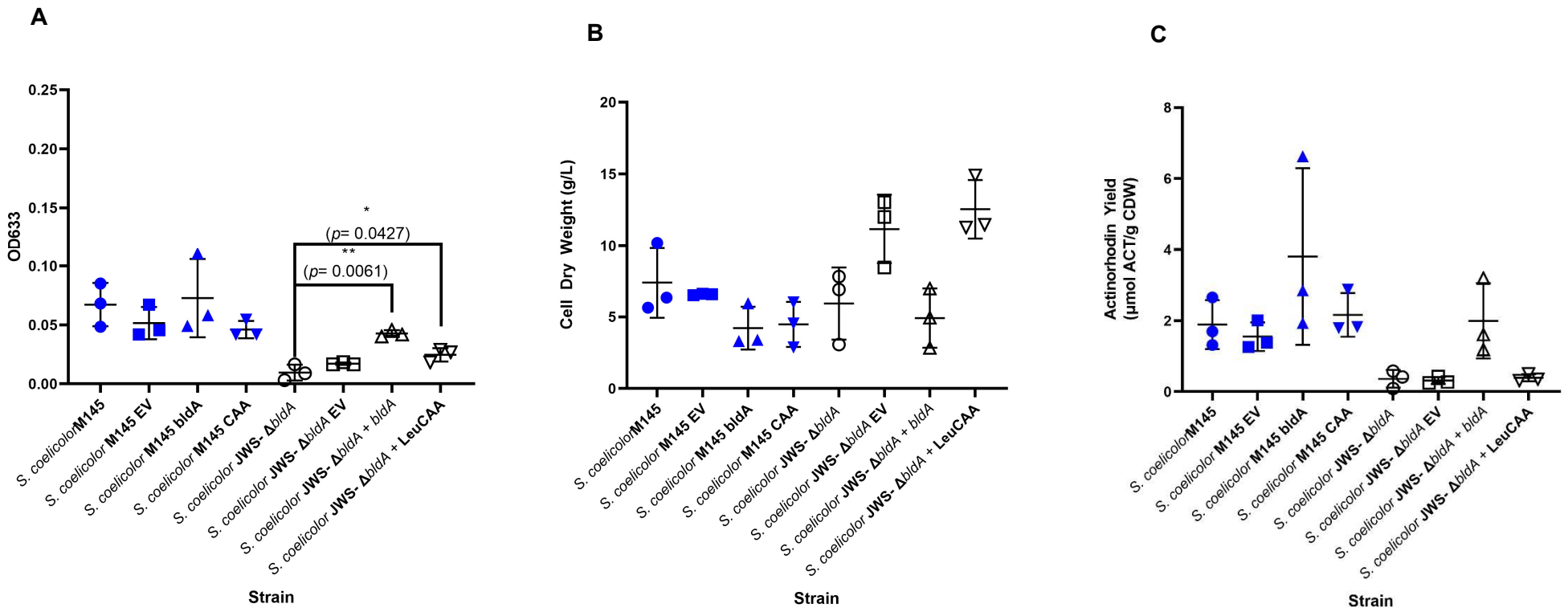

Fig. 6.22. Quantification of ACT production in *S. coelicolor* M145 (Wild-Type) and *S. coelicolor* JWS-Δ*bldA* exconjugants. **A:** Extracellular ACT production was measured at OD_{633} (n=3) after 120 hours. **B:** Cell dry weight was measured (n=3) with cell pellet of supernatant used for extracellular ACT quantification at 120 hours. **C:** ACT yield (µmol) given per gram of CDW for strains after incubation at 30°C for 120 hours. Data was analysed using unpaired t-test with Welch's correction, finding that ACT yield between M145 and JWS-Δ*bldA* was significant (*p*=0.0484), whereas M145 and JWS-Δ*bldA* + *bldA* was not significant (P=0.8905). Data was also analysed using a Kruskal-Wallis test, finding ACT yield between strains to be significant (*p*=0.0120)

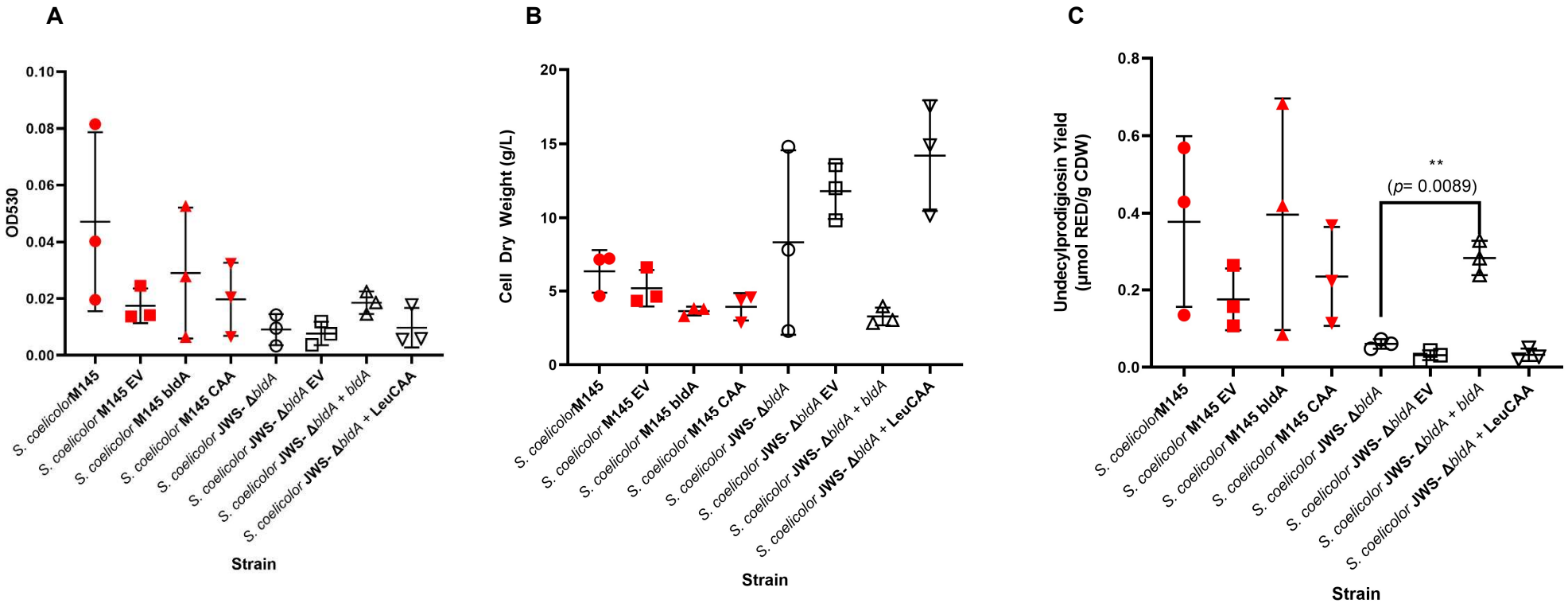

Fig. 6.23. Quantification of RED production in *S. coelicolor* M145 (Wild-Type) and *S. coelicolor* JWS-Δ*bldA* exconjugants. A: Intracellular RED production was measured at OD_{530} (n=3) after 120 hours. **B:** Cell dry weight was measured (n=3) with cell pellet from homogenous *S. coelicolor* culture after 120 hours incubation. **C:** RED yield (µmol) given per gram of CDW for strains after incubation at 30°C for 120 hours. Data was analysed using Kruskal-Wallis test, showing statistical difference across strains (p=0.0122). Unpaired t-test with Welch's correction highlights statistical difference between *S. coelicolor* JWS- Δ*bldA* and its *bldA* complement (p=0.0089), whereas comparison between *S. coelicolor* M145 and *S. coelicolor* JWS- Δ*bldA* + *bldA* was not significant (p=0.5365).

6.3.10 The effect of *bldA* deletion on Carbon and Nitrogen Utilization in *Streptomyces coelicolor*

It has long been known that *bld* mutants of *Streptomyces* are defective in carbon and nitrogen utilisation (Pope *et al*, 1996., Sprusansky *et al*, 2005). To further investigate the physiological consequences of a *bldA* deletion in *Streptomyces coelicolor*, carbon and nitrogen utilization profiles in both *S. coelicolor* M145 (isogenic parent) and the *bldA* deletion strain *S. coelicolor* JWS-Δ*bldA* were determined. Given the broad regulatory role of *bldA* in coordinating both development and specialised metabolite production in *Streptomyces* (Chater, 2013, Hou *et al*, 2018), it was hypothesised that mutation or deletion of *bldA* will affect carbon and nitrogen metabolism. This is important as metabolism is integrated with developmental signalling and antibiotic biosynthesis in *Streptomyces* (Niu *et al*, 2016).

To assess whether the loss of *bldA* influences carbon and nitrogen utilisation, *S. coelicolor* M145 and the isogenic Δ*bldA* strain were compared using BioLog phenotypic microassay plates. These plates test the ability for strains to grow in media containing individual carbon or nitrogen sources as the sole nutrient (Bochner *et al*, 2001). Briefly, single colonies of *S. coelicolor* M145 and *S. coelicolor* JWS-Δ*bldA* were streaked on LB agar and incubated for two days, until colonies had begun to form but had not yet sporulated. Mycelium were then picked and inoculated into BioLog™ minimal growth media and normalised to an OD_{600} of 0.04. The inoculated media was then transferred into BioLog PM1 (specifically designed for carbon utilisation assays) and BioLog PM3b (specifically designed for nitrogen utilisation assays) plates. After inoculation, the plates were loaded into a BioLog plate reader, which quantifies growth through colorimetric detection of cellular respiration (which is detectable through a coloured redox dye, where NADH production increases colourmetric signal) over an 80-hour incubation period (BioLog, 2025). Following incubation, growth kinetics between *S. coelicolor* M145 and *S. coelicolor* JWS-Δ*bldA* were compared to identify substrates that exhibited strain-specific utilization patterns. Due to time constraints, this experiment was only conducted with a single replicate (n=1). As such, these data were interpreted as exploratory and descriptive,

providing a preliminary view into metabolic utilisation phenotypes associated with *bldA* deletion.

6.3.11 Effects of *bldA* deletion on Carbon utilization

Initial observations revealed that the *S. coelicolor* JWS-*ΔbldA* strain exhibited a reduced ability to use a diverse range of carbon sources compared to its parental strain. While *S. coelicolor* M145 showed robust growth across a diverse set of sugars, organic acids, and alcohols, by comparison, *S. coelicolor* JWS-Δ*bldA* knockout possessed reduced specific growth rates for many substrates (**Fig 6.24**). This pattern is also clearly reflected in the comparative heatmap (**Fig. 6.25**), which highlights carbon source-specific growth defects in *S. coelicolor* JWS-Δ*bldA*. The decreased specific growth rates included glucose, rhamnose, fructose and lactulose, with substantial differences in growth seen in Tween-20 and D-Trehalose. Growth in the presence of sucrose was also heavily impacted in *S. coelicolor* JWS-Δ*bldA* when compared to growth in *S. coelicolor* M145, suggesting that core glycolytic functions are impacted by the deletion of *bldA*. Sugar alcohols such as glycerol and mannitol also yielded diminished growth, indicating that the defect is not limited to sugars alone, however using sugar alcohols for carbon utilisation was not as impacted as sugars for carbon utilisation.

The absence of *bldA* also abolished growth on D-Melibiose and L-Fucose when compared to the isogenic parent *S. coelicolor* M145 growth. There are also a few sugar-based carbon sources that retain specific growth rates that match that of the wild-type M145 strain, including maltose and D-galactose, however no sugar-based carbon source improves growth rate in the *ΔbldA* strain. These data predominantly highlight an inability of *S. coelicolor ΔbldA* strains to utilize sugars efficiently, supporting previous work that demonstrated that *bld* mutants are unable to regulate *galP1*, a sugar utilisation promotor (Pope *et al*, 1996).

When organic acids are provided as carbon sources to the *S. coelicolor* JWS-Δ*bldA* mutant, the specific growth rates are similar to the parental *S. coelicolor* M145 **(Fig 6.24, Fig 6.25).** While some organic acids, such as formic acid, result in poor growth when utilized as a carbon source in *S. coelicolor* JWS-*ΔbldA*, many others including succinic acid and L-lactic acid possess growth rates equal to that of the progenitor *S. coelicolor* M145 strain. In three instances, the *S. coelicolor* JWS-Δ*bldA* mutant grew better that the parental strain, on D-malic acid, methyl pyruvate, or Tween-80. A similar trend was seen in amino acids, with several amino acids possessing reduced utilisation in *S. coelicolor* JWS-*ΔbldA* (D-alanine, L-aspartic acid and D-threonine), and some retaining wild-type levels of utilisation (L-proline, L-asparagine and L-threonine. The specific growth rates when utilising different carbon sources was also compared between *S. coelicolor* M145 and *S. coelicolor* JWS-Δ*bldA* (**Fig. 6.26**). These date highlight that the specific growth rate in *S. coelicolor* JWS-Δ*bldA* is reduced for the majority of utilized carbon sources when compared to *S. coelicolor* M145, further emphasising that the deletion of *bldA* has a negative impact of primary metabolism involving carbon utilization

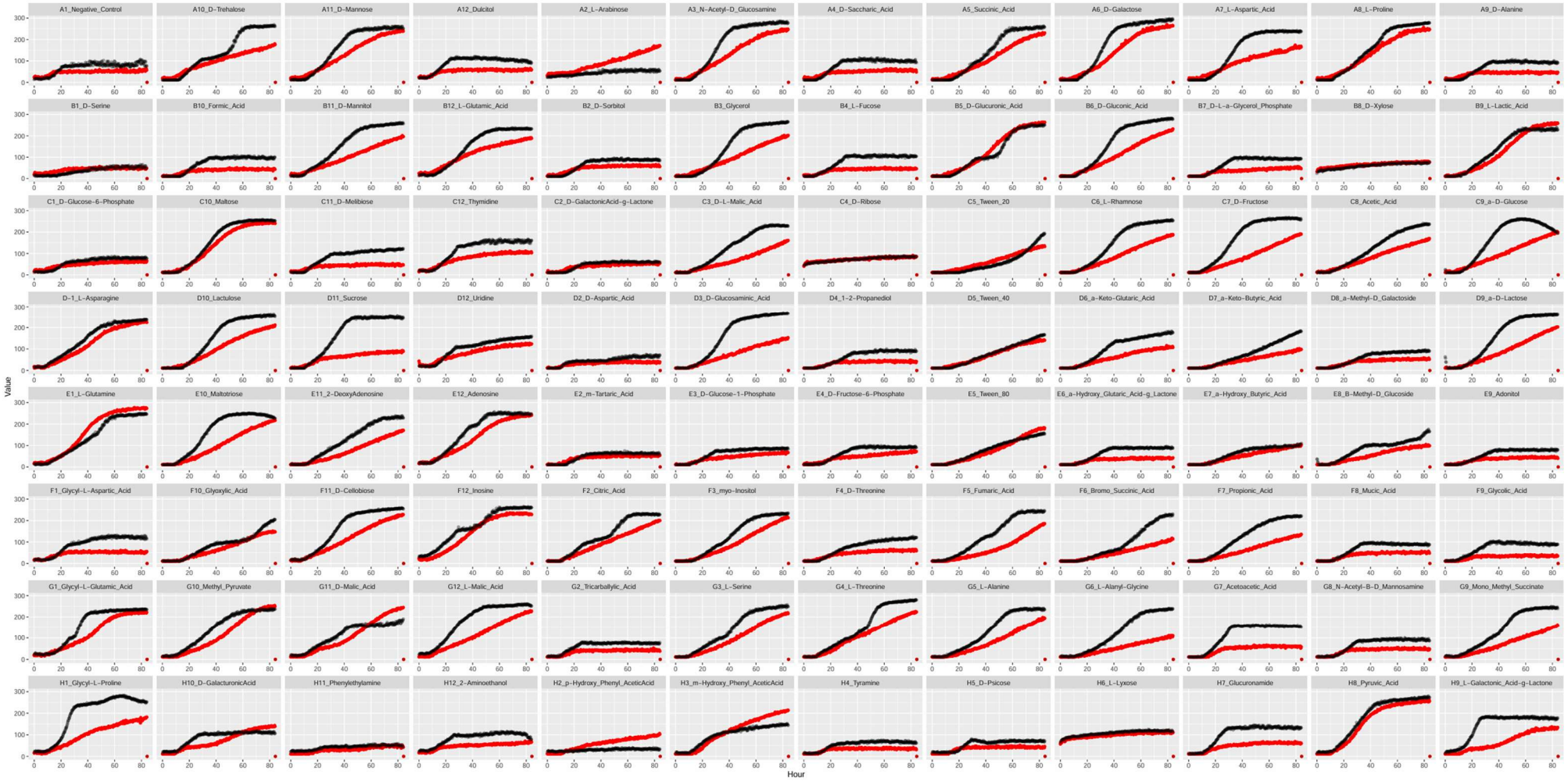

Fig. 6.24. Impact of *bldA* deletion on carbon source utilization in *Streptomyces coelicolor* M145 (Wild-Type) and *S. coelicolor* JWS-Δ*bldA*. Growth curves comparing the carbon utilization profiles of the wild-type *S. coelicolor* M145 (black) and ***S.*** *coelicolor* JWS-Δ*bldA* (red) across a range of individual carbon sources over a period of 80 hours. Each panel represents the optical density of *S. coelicolor* cultures over time for a specific carbon source.

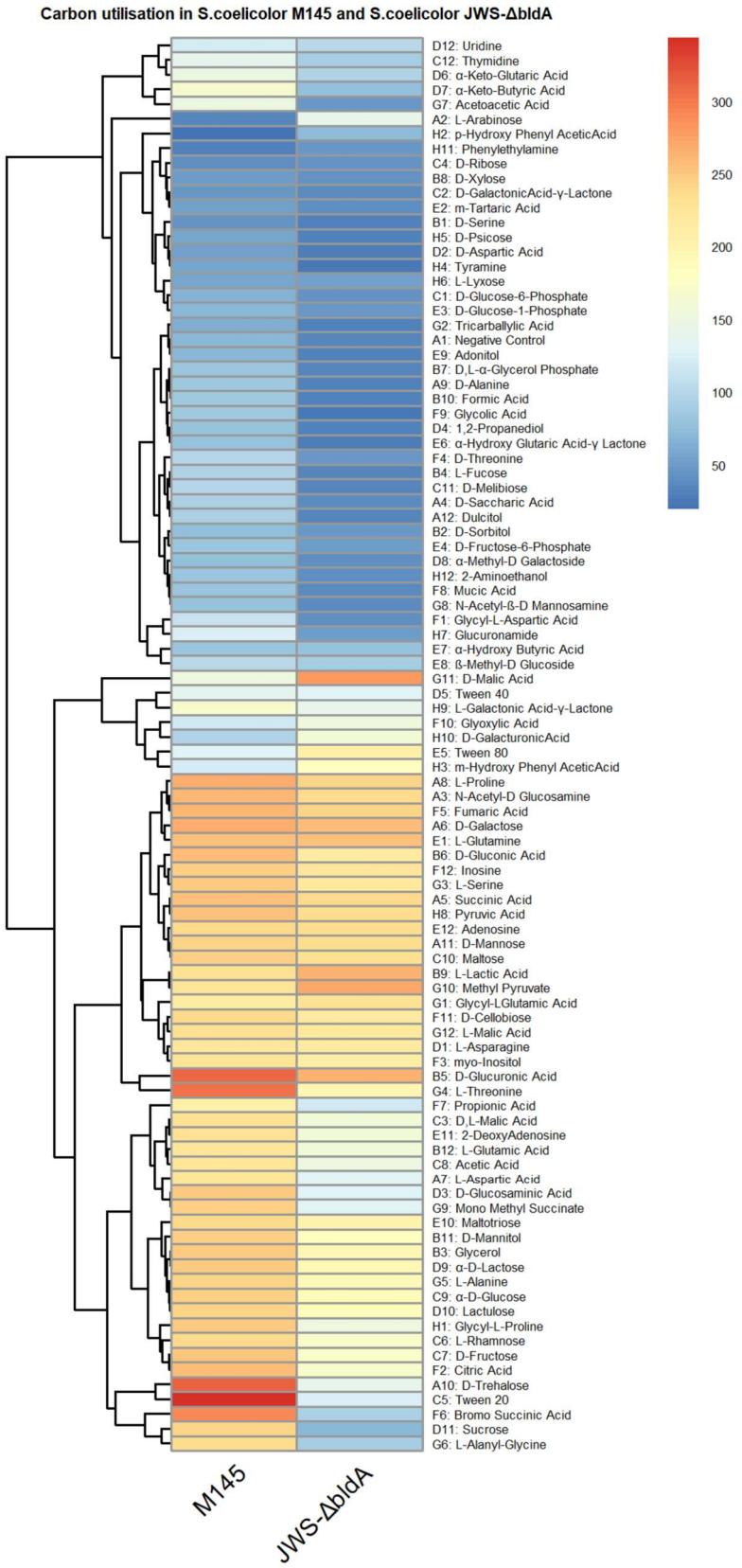

Fig. 6.25: **Heatmap summarizing the relative growth of wild-type *S. coelicolor* M145 (Wild-Type) and *S. coelicolor* JWS-Δ*bldA* across all tested carbon sources**. Colours represent normalized growth intensity, with dark blue shades indicating poor growth and dark red shades indicating high growth.

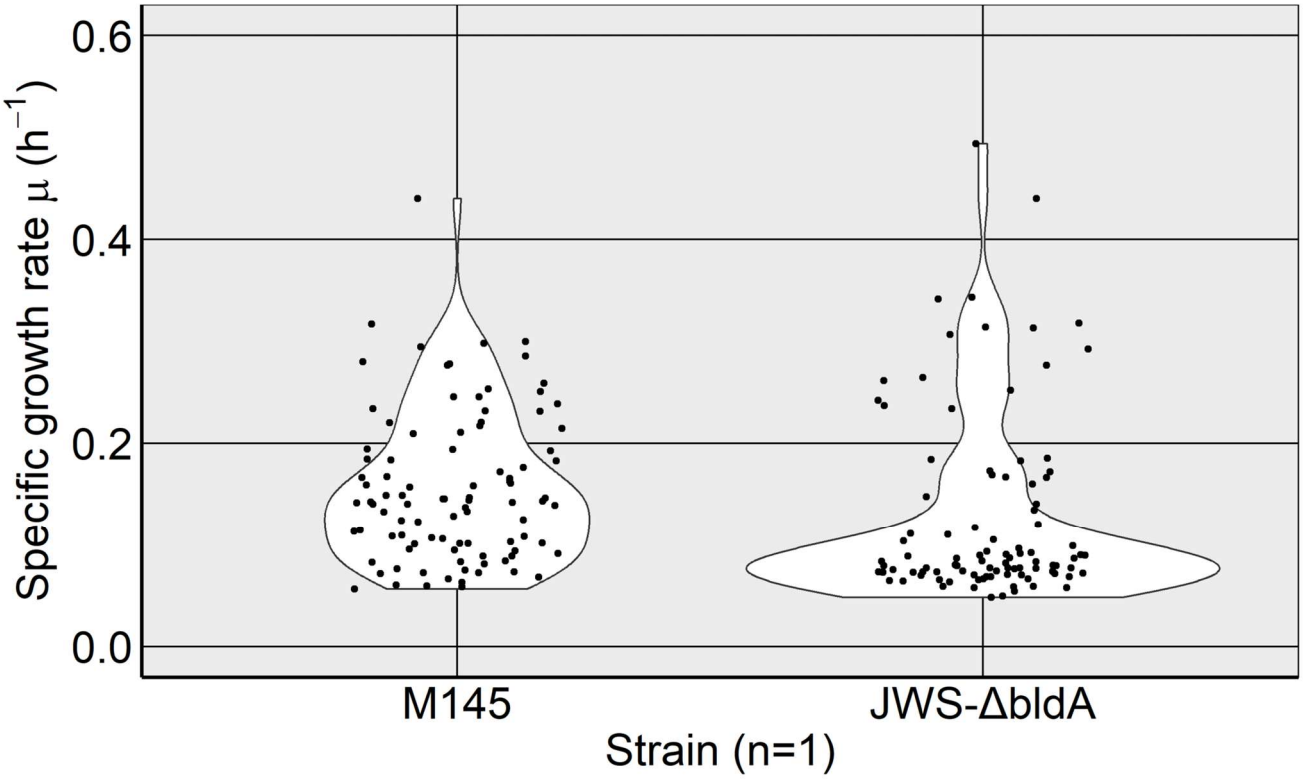

Fig. 6.26: Distribution of carbon source dependant specific growth rates (h^{-1}) in *S. coelicolor* M145 (Wild-Type) and and *S. coelicolor* JWS-Δ*bldA*. Violin plots show the distribution density of specific growth rate for each strain. Each point represents an individual carbon source.

6.3.12 Effects of *bldA* deletion on Nitrogen utilization

A similar trend was observed in nitrogen utilisation across both strains. While both strains were able to utilize a majority of tested amino acids and simple nitrogen compounds, *S. coelicolor* JWS-Δ*bldA* consistently exhibited reduced growth for several nitrogen sources, particularly amino acids and nitrogen-containing nucleotides (**Fig. 6.27**). Growth was notably lower in *S. coelicolor* JWS-Δ*bldA* for the majority of tested L-amino acids, while growth in the presence of D-amino acids was either minimal or completely absent. Several organic amines were also tested, in which growth of both the parental M145 strain and the Δ*bldA* mutant varied from stunted to completely abolished, with growth of the Δ*bldA* mutant consistently inhibited in comparison to its parental strain when growth was detected. Only three of the amino acids or organic amines tested exhibited similar growth rates between the two strains: those being L-aspartic acid, L-cysteine and L-glutamic acid (replicating data from the carbon utilisation plates; **Fig. 6.24, Fig. 6.25**). None of the tested amino acids or organic amines exhibited improved growth in *S. coelicolor* JWS-Δ*bldA* compared to the parental strain *S. coelicolor* M145 under the same condition (**Figure 6.27)**. Specific growth rates of nitrogen utilisation in *S. coelicolor* M145 and *S. coelicolor* JWS-Δ*bldA* was also investigated, which, similar to carbon source-determined specific growth rate, highlighted that *S. coelicolor* JWS-Δ*bldA* exhibited consistently reduced specific growth rate compared to *S. coelicolor* M145 (**Fig. 6.28**)

Taking the carbon and nitrogen utilisation data together, these data suggest that there is a role for *bldA* in efficient utilization of many nutrient sources. This could be due to its role in translation of TTA-codon-containing regulatory genes, yet the improved or retained growth in the presence of certain organic acids suggests metabolic flexibility may be partly preserved in these contexts and supports the hypothesis that *bldA* is important for regulating pathways linked to metabolism and nutrient source preference. It has also been reported in previous literature that nutritional status of *S. coelicolor* cells is a key regulator of the global regulator BldD via cyclic-di-GMP and *bldD* is a direct regulator of *bldA* (den Hengst *et al*, 2010). These

data suggest that modulation of *bldD* activity through *Streptomyces* nutritional status is evidenced through *bldA* regulation and downstream effects.

Although limited by replication, these data suggest that the deletion of *bldA* may reduce metabolic adaptability in *S. coelicolor* and prevent it from utilising carbon and nitrogen from common sources, highlighting a potential role for *bldA* in enabling metabolic adaptability, in addition to its already established functions in development and specialised metabolite production. Given the exploratory nature of this study, follow-up experiments with biological replicates and quantitative growth analyses will be necessary to confirm this hypothesis.

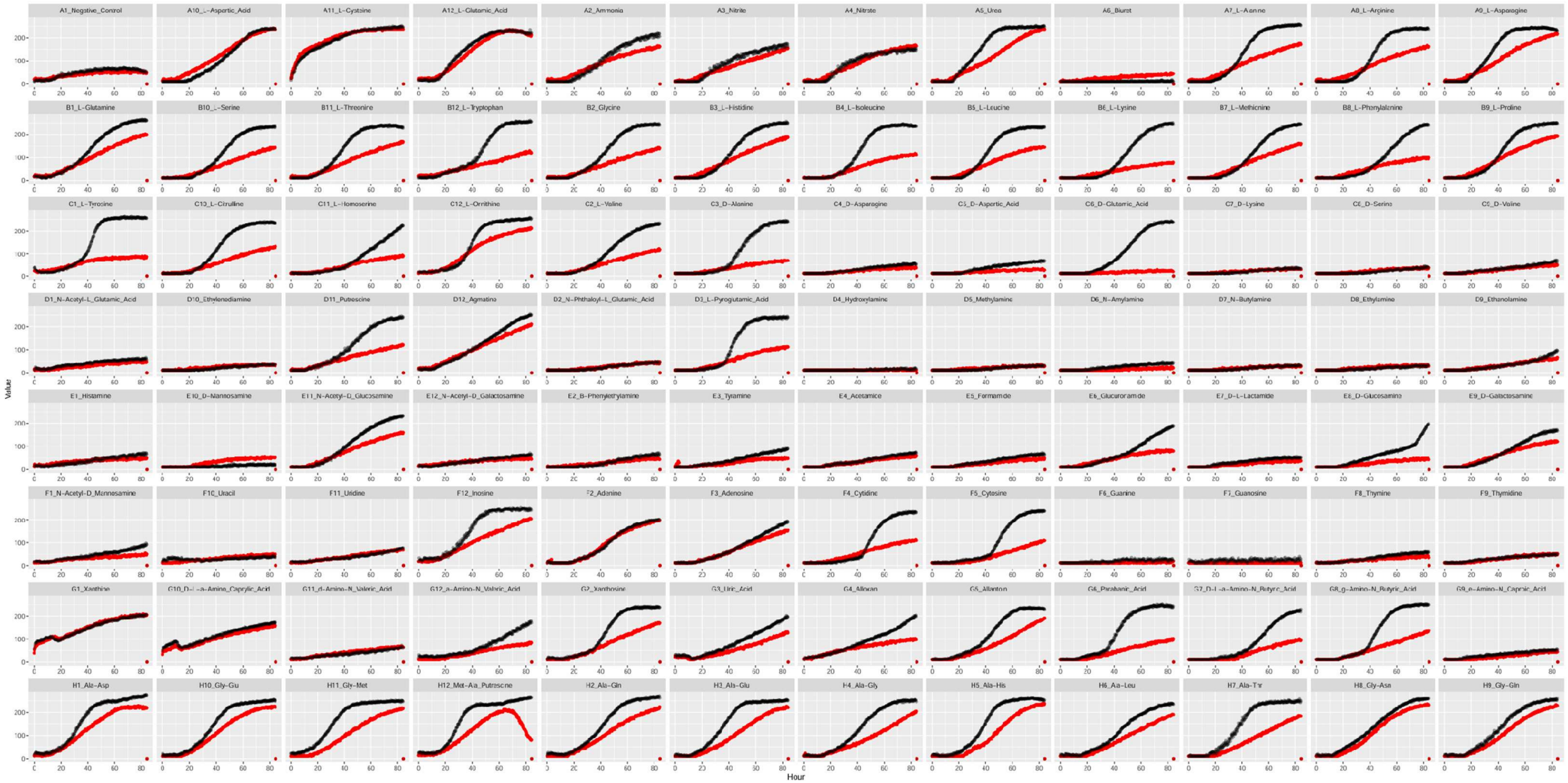

Fig. 6.27. Impact of *bldA* deletion on nitrogen source utilization in *Streptomyces coelicolor* M145 (Wild-Type) and *S. coelicolor* JWS-Δ*bldA*.

Growth curves comparing nitrogen utilization profiles of wild-type *S. coelicolor* M145 (black) and *S. coelicolor* JWS-Δ*bldA* (red**)** across a range of nitrogen sources over a period of 80 hours. Each panel represents optical density over time for a specific substrate.

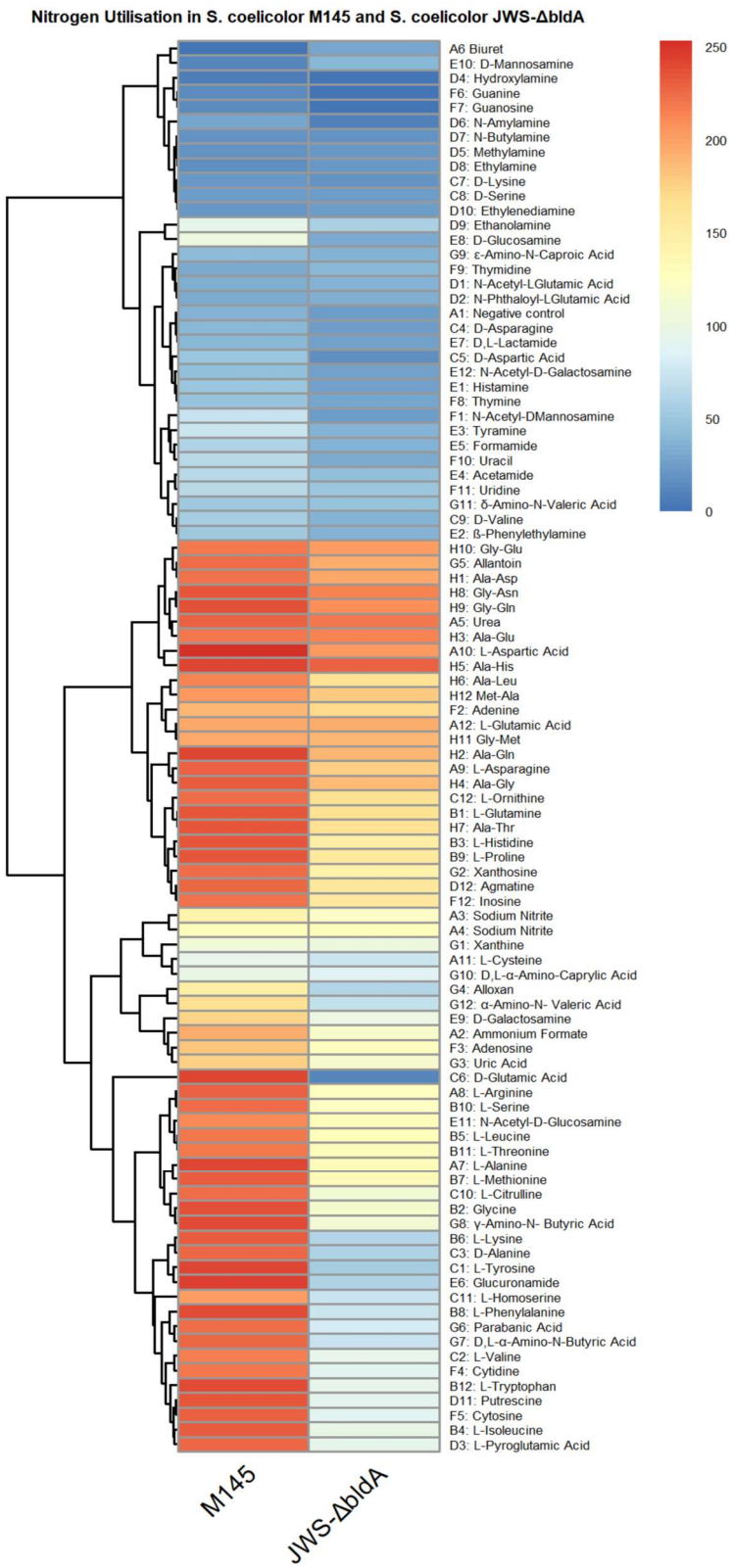

Fig. 6.28: **Heatmap summarizing the relative growth of wild-type *S. coelicolor* M145 (Wild-Type) and *S. coelicolor* JWS-Δ*bldA* across all tested nitrogen sources in the BioLog PM3b plate**. Colours represent normalized growth intensity, with dark blue shades indicating poor growth and dark red shades indicating high growth.

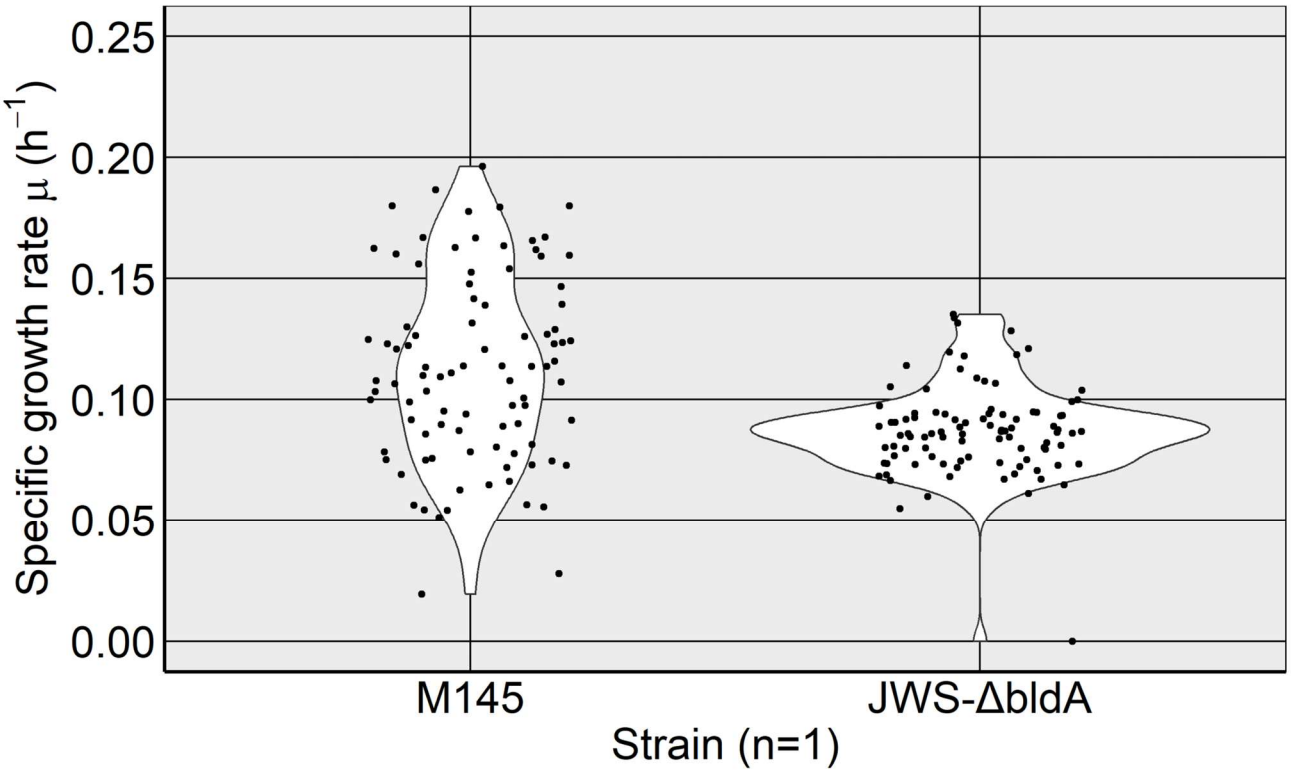

Fig. 6.29: Distribution of nitrogen source dependant specific growth rates (h^{-1}) in *S. coelicolor* M145 (Wild-Type) and and *S. coelicolor* JWS-Δ*bldA*. Violin plots show the distribution density of specific growth rate for each strain. Each point represents an individual nitrogen source**.**

6.3.13 Transcriptomic analysis of the *S. coelicolor* JWS-Δ*bldA* strain reveals tRNA loss impacts on global transcriptional patterns

While *bldA* is likely to mediate much of its activity through reduced translation of TTA containing genes (Leskiw *et al,* 1993., Leskiw and Mah, 1995., Hesketh *et al*, 2007), the downstream effects of reducing translation of TTA containing genes may affect global transcription in a *bldA* mutant. To determine the impact of *bldA* deletion on the *S. coelicolor* gene expression, whole transcriptome analysis was performed. *S. coelicolor* M145 and *S. coelicolor* JWS-Δ*bldA* were grown in TSB media and RNA was extracted from triplicate cultures in exponential phase. Triplicate RNA cultures were sent to Novogene™ for RNA-seq, however, one sample for either culture failed to pass RNA Intergrity Number (RIN) verification, indicating RNA degradation, and as such, only two samples for each strain were carried forward. Transcripts were mapped to the *S. coelicolor* A3(2) reference genome (Accession Number: AL645882) using Salmon (v1.10.1) (Bentley *et al*, 2002., Patro *et al*, 2017). The mean fold change was calculated using DESeq2 (v1.46.0) (Love *et al*, 2014). A total of 641 chromosomal genes and six RNAs had their transcription affected due to *bldA* deletion (**Appendix 4)**. It was found that of these 641 genes, 18 contained TTA codons, of which 14 were downregulated and four were upregulated (*SCO1227, SCO1434, SCO4015* and *SCO4636*) (**Table 6-3)**. A summary of the significantly downregulated and upregulated *S. coelicolor* genes in response to the deletion of *bldA* can be found in **Table 6-4** and **Table 6-5** respectively, organised by fold change. A complete list of all upregulated or downregulated genes (Fold change= >1-<-1) can be found in **Appendix 4**.

In total, 144 chromosomal *S. coelicolor* genes were significantly downregulated in the *S. coelicolor* JWS-Δ*bldA* strain, using the fold change of -1.5 as a cutoff point, accompanied by an EDGE test P value of < 0.05. A further 154 chromosomal genes were downregulated but possessed fold changes of between -1 and -1.5 and were as such omitted. Differentially expressed genes (DEGs) were detected across the entirety of the genome, with the 144 DEGs significantly downregulated accounting for >2% of all *S. coelicolor* genes (Bentley *et al*, 2002).

Regarding the ACT and RED biosynthetic gene clusters, no genes in either BGC were transcriptionally affected by the deletion of *bldA*. However, while the BGCs themselves were unaffected, other genes previously documented to affect specialised metabolite production were notably decreased. While the fold-change was only -1.3, transcription of SCO2792 (*adpA*) was downregulated, which likely affects ACT and RED production due to *adpA* being a direct regulator of *redD* promotor-binding, repression of the antibiotic negative regulator *wblA* and its role encoding a central transcriptional activator (Park *et al*, 2009, Kalan *et al,* 2013, Lee *et al*, 2013). Furthermore, the hypothetical protein SCO5771 was also downregulated, in which previous mutations have been shown to reduce overall ACT yield (Xu *et al*, 2019). In relation to carbon and nitrogen utilisation, several notable downregulated genes were detected, including SCO5578, a sugar transporter and a potential homolog of glucose transport protein, SCO1234-SCO1236 (encompassing three urease subunits), and SCO5977, an amino acid permease. The detected downregulation of each of these genes passed the statistical thresholds for significance, meaning these data could contribute to the detected reduction in sugar-based carbon utilisation, urea nitrogen utilisation, and amino-acid-based nitrogen utilisation in *S. coelicolor* JWS-Δ*bldA* respectively.

In contrast to downregulated genes, 276 chromosomal genes were significantly upregulated in *S. coelicolor* JWS-Δ*bldA*, with a further 73 chromosomal genes possessing a fold-change of between 1 and 1.5. When compared to downregulated genes, the genes upregulated in *S. coelicolor* JWS-Δ*bldA* lacked the rare TTA codons, indicating their expression is independent of *bldA*-regulated translation control. Additionally, genes upregulated in *S. coelicolor* JWS-Δ*bldA* knockout were predominantly associated with antibiotic resistance proteins (SCO0783, SCO3912 and SCO7662), transcriptional regulators (SCO1376, SCO2745 and SCO1289), metabolic enzymes (SCO3006, SCO3197 and SCO5444) and transporter proteins (SCO5448, SCO5451 and SCO6512). Upregulation of a variety of family transcriptional regulators could be the result of compensatory response to the deletion of *bldA*, with the resultant network reprogramming being an attempt to restore homeostasis in the absence of the missing Leu-

$tRNA^{UAA}$ (Tiefenbacher *et al*, 2024). The upregulation of antibiotic resistance proteins, metabolic enzymes, and transporters in *S. coelicolor* JWS-Δ*bldA* could be the result of direct and indirect regulatory consequences or stress responses. While these genes typically lack TTA codons, their expression may be affected due to the disrupted developmental progression commonly associated with *bld* mutants, and compensatory stress responses, consistent with the pleiotropic impact of *bldA* deletion across *Streptomyces* species (Makitrynskyy *et al*, 2013). These data have been plotted to show respective fold change for all upregulated and downregulated genes in **Fig. 6.30**.

The transcriptomics data for *S. coelicolor* JWS-Δ*bldA* corroborates previous transcriptomics data using microarrays focusing on the gene expression of a *bldA* mutant in *S. coelicolor* M600 (a plasmid-free prototrophic strain of *S. coelicolor* A3(2), that was subsequently shown to have a 1 Mbp duplication at a chromosome end (Weaver et al., 2004; Hesketh *et al*, 2007). Of the 144 significantly downregulated DEGs, 10 match downregulated genes detected by the Hesketh data, nine of those DEGs possessing a fold change of <-2. Only one upregulated gene between both datasets matched (SCO3608, a hypothetical protein), however only 17 genes were upregulated in the Hesketh dataset. The differences in the two datasets is likely due to different backgrounds of the strains of *S. coelicolor* used. However, the 11 DEGs shared across both datasets may warrant further investigation as it is apparent that any form of *bldA* interference results in differential gene expression in these 11 genes. In conclusion, the deletion of *bldA* in *S. coelicolor* results in widespread impact on the transcriptome of *S. coelicolor*, with secondary metabolite-associated genes and catabolism-associated genes downregulated, while genes focused on transport, regulation and resistance are upregulated as a compensatory response to the loss of *bldA*.

Table 6-3: Differently expressed genes (DEGs) in *S. coelicolor* JWS- Δ*bldA* that contains a TTA codon

Gene	Function	Upregulated/ Downregulated	Fold Change	p-value
SCO4636	hypothetical protein	Upregulated	4.044144	5.28 e-22
SCO1227	DNA-binding protein	Upregulated	2.734583	1.76 e-3
SCO4015	hypothetical protein	Upregulated	1.675267	1.56 e-3
SCO1434	CbxX/CfqX family protein	Upregulated	1.204636	1.39 e-3
SCO2792	AraC family transcription regulator	Downregulated	-1.30163	2.57 e-4
SCO6717	acyl-ACP desaturase	Downregulated	-1.49086	6.59 e-08
SCO7465	hypothetical protein	Downregulated	-1.49772	2.68 e-06
SCO2524	hypothetical protein	Downregulated	-1.55463	2.21 e-3
SCO3770	cytochrome P450 oxidoreductase	Downregulated	-1.59183	5.57 e-05
SCO4213	hypothetical protein	Downregulated	-1.65217	4.55 e-3
SCO7233	hypothetical protein	Downregulated	-1.75218	1.93 e-06
SCO4431	hypothetical protein	Downregulated	-1.81851	1.50 e-06
SCO4671	LysR family transcriptional regulator	Downregulated	-2.11442	5.56 e-05
SCO3262	hypothetical protein	Downregulated	-2.29678	5.33 e-08
SCO4464	Hydrolase	Downregulated	-2.32173	2.80 e-07
SCO3487	Hydrolase	Downregulated	-2.65907	1.03 e-13
SCO6638	hypothetical protein	Downregulated	-3.07664	7.55 e-10
SCO6623	ATP/GTP binding protein	Downregulated	-5.13678	2.79 e-07

Table 6-4: Summary of *S. coelicolor* genes which are downregulated in response to *bldA* deletion.

Gene	Function	Fold Change	p-value
SCO3664	regulatory protein	-1.50147	2.27 e-4
SCO6109	hydrolase	-1.50494	3.59 e-7
SCO1055	alpha-xylosidase	-1.50636	1.56 e-3
SCO6736	metallopeptidase	-1.51157	3.66 e-6
SCO7147	ketoreductase	-1.51785	3.43 e-3
SCO2397	oxidoreductase	-1.52192	2.83 e-5
SCO1455	hydrolase	-1.52439	5.87 e-6
SCO3128	fatty acid desaturase (membrane)	-1.52678	1.64 e-6
SCO1510	peptidyl-prolyl cis-trans isomerase	-1.52940	9.53 e-8
SCO5573	formamidopyrimidine-DNA glycosylase	-1.53618	1.75 e-3
SCO1777	hypothetical protein	-1.54139	9.92 e-8
SCO2912	hypothetical protein	-1.54208	2.53 e-3
SCO1517	hypothetical protein	-1.54910	6.88 e-9
SCO2524	hypothetical protein	-1.55463	2.21 e-3
SCO6100	phosphoadenosine phosphosulfate reductase	-1.56280	8.19 e-6
SCO2848	hypothetical protein	-1.59119	4.06 e-4
SCO5293	oxygenase subunit	-1.59178	4.49 e-6
SCO3770	cytochrome P450 oxidoreductase	-1.59183	5.57 e-5
SCO7417	cytochrome P450-family protein	-1.60139	1.01 e-5
SCO6593	hypothetical protein	-1.60877	4.71 e-6
SCO2910	cysteine synthase	-1.61355	2.52 e-8
SCO6225	hypothetical protein	-1.61659	2.05 e-5
SCO0494	iron-siderophore binding lipoprotein	-1.61672	5.67 e-6
SCO3767	hypothetical protein	-1.63593	1.00 e-9
SCO2865	regulatory protein	-1.65042	7.16 e-6
SCO4213	hypothetical protein	-1.65217	4.55 e-3
SCO6097	sulfate adenylyltransferase subunit 1	-1.65418	1.59 e-10
SCO7466	ATP/GTP-binding protein	-1.66503	8.71 e-8
SCO7001	hypothetical protein	-1.66693	2.08 e-5
SCO5337	hypothetical protein	-1.67397	2.03 e-4
SCO0888	hypothetical protein	-1.68413	1.55 e-8
SCO7418	cytochrome P450-family protein	-1.69221	4.62 e-4
SCO6093	hypothetical protein	-1.71217	4.67 e-5
SCO2770	agmatinase	-1.71436	5.25 e-6
SCO2383	hypothetical protein	-1.71704	1.65 e-5
SCO6102	nitrite/sulfite reductase	-1.71736	1.62 e-3
SCO0987	hypothetical protein	-1.73824	1.78 e-5
SCO7233	hypothetical protein	-1.75218	9.30 e-6
SCO0498	peptide monooxygenase	-1.75591	1.14 e-3
SCO6676	hypothetical protein	-1.75936	7.17 e-4
SCO3018	regulatory protein	-1.76305	2.25 e-4
SCO5425	phosphate acetyltransferase	-1.76488	3.54 e-4
SCO4670	serine protease	-1.78231	4.03 e-3
SCO3023	adenosylhomocysteinase	-1.78680	1.31 e-9
SCO6098	sulfate adenylyltransferase subunit 2	-1.79431	1.24 e-10
SCO5977	amino acid permease	-1.79598	1.55 e-4
SCO7728	hypothetical protein	-1.80109	2.89 e-4
SCO5468	transmembrane transport protein	-1.80760	1.41 e-6
SCO3206	transmembrane efflux protein	-1.80884	3.79 e-6
SCO5811	transcriptional regulator	-1.81707	1.88 e-4
SCO2525	hypothetical protein	-1.81828	6.69 e-4
SCO4431	hypothetical protein	-1.81851	1.50 e-6
SCO0499	formyltransferase	-1.82137	1.68 e-4
SCO3261	ATP-binding protein	-1.83300	5.11 e-7
SCO7517	hypothetical protein	-1.83503	1.08 e-4
SCO6095	ABC transporter ATP-binding protein	-1.85287	5.51 e-10
SCO5424	acetate kinase	-1.85476	2.92 e-5

SCO4257	hydrolytic protein	-1.86826	1.36 e-3
SCO6592	hypothetical protein	-1.87970	1.92 e-5
SCO5679	aldehyde dehydrogenase	-1.90664	6.55 e-7
SCO4593	hypothetical protein	-1.91203	2.15 e-3
SCO1557	lipoprotein	-1.92055	3.17 e-9
SCO3139	Sodium solute symporter	-1.92481	8.20 e-4
SCO2816	hypothetical protein	-1.92558	1.51 e-5
SCO4544	hypothetical protein	-1.92907	1.97 e-4
SCO6096	lipoprotein	-1.94297	2.35 e-11
SCO4297	oxidoreductase	-1.96710	4.81 e-10
SCO4250	hypothetical protein	-1.97089	1.95 e-3
SCO6671	hypothetical protein	-1.97260	2.83 e-7
SCO2911	hypothetical protein	-1.97387	2.44 e-5
SCO5578	sugar transporter	-1.98113	1.15 e-4
SCO0988	acetyltransferase	-1.99671	1.19 e-4
SCO0575	peptidase E	-2.01492	1.30 e-5
SCO4254	hypothetical protein	-2.02202	2.42 e-5
SCO6591	hypothetical protein	-2.05255	7.67 e-5
SCO1232	urease accessory protein	-2.06739	2.25 e-3
SCO6094	transport system integral membrane protein	-2.07278	9.16 e-13
SCO1236	urease subunit gamma	-2.08575	1.33 e-6
SCO4164	thiosulfate sulfurtransferase	-2.09074	7.22 e-6
SCO4244	hypothetical protein	-2.10396	7.92 e-6
SCO4671	LysR family transcriptional regulator	-2.11442	5.56 e-5
SCO4675	hypothetical protein	-2.12906	1.47 e-11
SCO7141	hypothetical protein	-2.13606	1.33 e-4
SCO0870	two-component system response regulator	-2.13708	1.48 e-7
SCO7199	hypothetical protein	-2.15014	2.01 e-4
SCO7705	oxidoreductase	-2.15022	6.29 e-4
SCO6553	integral membrane efflux protein	-2.16093	3.16 e-6
SCO1235	urease subunit beta	-2.16607	6.32 e-4
SCO6310	cytochrome P450	-2.16655	1.30 e-10
SCO4242	hypothetical protein	-2.22225	1.84 e-5
SCO6590	esterase	-2.23990	3.29 e-5
SCO5676	4-aminobutyrate aminotransferase	-2.24295	3.65 e-14
SCO7200	hypothetical protein	-2.26876	7.94 e-7
SCO4255	hypothetical protein	-2.27142	3.15 e-3
SCO1234	urease subunit alpha	-2.29295	2.71 e-4
SCO3262	hypothetical protein	-2.29678	5.33 e-8
SCO4464	hydrolase	-2.32173	2.80 e-7
SCO7810	oxidoreductase	-2.39254	4.79 e-4
SCO1773	L-alanine dehydrogenase	-2.41467	1.62 e-19
SCO4498	proton transport protein	-2.42305	4.09 e-11
SCO4259	ATPase AAA	-2.42502	2.29 e-6
SCO5436	Sodium dicarboxylate symporter	-2.43313	4.64 e-5
SCO4994	hypothetical protein	-2.47529	1.54 e-6
SCO4587	hypothetical protein	-2.49052	1.02 e-7
SCO1356	iron sulfur protein	-2.62998	1.24 e-3
SCO3452	methyltransferase	-2.64355	3.028 e-3
SCO3487	hydrolase	-2.65907	1.03 e-13
SCO4672	hypothetical protein	-2.67311	7.92 e-9
SCO4260	hypothetical protein	-2.69329	1.23 e-6
SCO1459	amino acid transporter	-2.71335	1.07 e-5
SCO4261	response regulator	-2.72649	1.62 e-11
SCO7657	hypothetical protein	-2.74455	1.49 e-25
SCO2213	regulatory protein	-2.81806	9.31 e-12
SCO4678	hypothetical protein	-2.81958	4.86 e-19
SCO5772	hypothetical protein	-2.98793	1.60 e-6
SCO4245	hypothetical protein	-3.00982	2.11 e-3
SCO4681	short chain dehydrogenase	-3.04039	1.35 e-10
SCO4243	hypothetical protein	-3.06558	2.12 e-3
SCO6638	hypothetical protein	-3.07664	7.55 e-10
SCO2217	hypothetical protein	-3.09583	4.10 e-13
SCO1617	hypothetical protein	-3.17319	4.02 e-5

SCO5771	hypothetical protein	-3.17946	8.94 e-7
SCO4679	hypothetical protein	-3.24153	2.99 e-21
SCO0762	protease inhibitor protein	-3.31889	4.74 e-7
SCO4256	hydrolytic protein	-3.33324	3.16 e-8
SCO0930	lipoprotein	-3.36018	1.02 e-4
SCO1454	amino oxidase	-3.41006	1.07 e-28
SCO4682	tautomerase	-3.45084	1.14 e-8
SCO6623	ATP/GTP binding protein	-3.45361	2.79 e-7
SCO0300	monooxygenase	-3.49156	3.28 e-3
SCO0644	hypothetical protein	-3.51814	7.34 e-7
SCO6637	hypothetical protein	-3.56967	2.81 e-20
SCO0248	hypothetical protein	-3.64913	1.81 e-3
SCO4258	hydrolytic protein	-3.94753	2.80 e-21
SCO6456	hydrolytic protein	-3.99156	9.09 e-14
SCO4246	hypothetical protein	-4.26285	2.02 e-13
SCO0752	protease	-4.41611	7.24 e-4
SCO4248	hypothetical protein	-5.16487	1.65 e-4
SCO4251	hypothetical protein	-5.27099	1.34 e-27
SCO4247	hypothetical protein	-6.57907	6.46 e-08
SCO6055	carbonic anhydrase	-6.62336	5.64 e-4
SCO4252	hypothetical protein	-7.21075	7.52 e-37
SCO4253	hypothetical protein	-7.36917	3.46 e-59
SCO4698	IS1652 transposase	-8.22762	2.54 e-6

Table 6-5: Summary of *S. coelicolor* genes which are upregulated in response to *bldA* deletion.

Gene	Function	Fold Change	p-value
SCO6006	transmembrane transport protein	1.50129	3.89 e-3
SCO4208	integral membrane transport protein	1.51659	3.82 e-3
SCO5530	hypothetical protein	1.52179	4.29 e-3
SCO3712	hydrolase	1.52181	3.13 e-4
SCO3000	phosphatase	1.52679	4.12 e-4
SCO2672	hypothetical protein	1.52871	1.67 e-5
SCO4588	hypothetical protein	1.53076	2.08 e-5
SCO5444	glycogen phosphorylase	1.53175	4.61 e-4
SCO5264	hypothetical protein	1.53455	2.74 e-4
SCO1661	glycerol-3-phosphate dehydrogenase	1.53738	4.36 e-4
SCO7295	LuxR family transcriptional regulator	1.53839	9.45 e-4
SCO4639	hypothetical protein	1.55274	1.14 e-5
SCO3197	1-phosphofructokinase	1.56036	6.58 e-7
SCO4867	hypothetical protein	1.56621	1.49 e-3
SCO4872	hypothetical protein	1.56778	3.76 e-3
SCO5045	hypothetical protein	1.58847	9.61 e-6
SCO3369	large ATP-binding protein	1.58937	1.19 e-4
SCO5285	ATP-dependent protease	1.59760	6.81 e-7
SCO4408	hypothetical protein	1.60129	5.81 e-4
SCO4069	hypothetical protein	1.60319	1.28 e-4
SCO4409	RNA polymerase sigma factor	1.61803	1.8 e-4
SCO5184	ATP-dependent DNA helicase	1.62194	4.39 e-3
SCO0714	oxidoreductase	1.62265	3.27 e-3
SCO3633	ABC transporter ATP-binding protein	1.62382	1.89 e-3
SCO0609	hypothetical protein	1.62993	4.17 e-3
SCO4024	integral membrane efflux protein	1.63914	2.99 e-4
SCO5218	hypothetical protein	1.64938	1.70 e-6
SCO4805	hypothetical protein	1.65413	2.65 e-3
SCO3999	lipoprotein	1.67158	4.54 e-3
SCO3952	hypothetical protein	1.67447	2.38 e-4
SCO4015	hypothetical protein	1.67527	1.56 e-3
SCO3971	hypothetical protein	1.67611	7.88 e-6
SCO3230	CDA peptide synthetase I	1.68477	2.51 e-3
SCO3749	hypothetical protein	1.69047	4.23 e-3
SCO6517	uvrA-like protein	1.69484	1.70 e-6
SCO1989	aminopeptidase	1.71642	1.85 e-6
SCO4778	Ser/Thr protein kinase	1.72350	8.85 e-5
SCO1320	hypothetical protein	1.73717	4.64 e-4
SCO4908	RNA polymerase sigma factor	1.73836	3.53 e-8
SCO4790	hypothetical protein	1.73884	3.63 e-4
SCO3006	acetyltransferase	1.75872	1.53 e-4
SCO2939	hypothetical protein	1.77665	3.26 e-8
SCO1366	hypothetical protein	1.78173	4.12 e-4
SCO1406	hypothetical protein	1.78764	2.04 e-7
SCO4316	ATP/GTP binding protein	1.78798	1.59 e-6
SCO0733	hypothetical protein	1.78805	1.26 e-5
SCOs02	RNA	1.80037	3.40 e-8
SCO3672	cell surface biosynthesis associated protein	1.80619	1.84 e-3
SCO3973	hypothetical protein	1.80794	3.84 e-4
SCO4896	transport integral membrane protein	1.81697	4.79 e-4
SCO5160	hypothetical protein	1.82774	2.42 e-3
SCO0798	hypothetical protein	1.83711	4.492 e-3
SCO5056	exodeoxyribonuclease VII large subunit	1.84782	7.0 e-4
SCO4895	RNA polymerase factor sigma-70	1.85031	4.26 e-6
SCO1969	DNA-methyltransferase	1.85336	3.82 e-3
SCO5665	hypothetical protein	1.85396	2.74 e-3
SCO4638	hypothetical protein	1.86556	2.76 e-6

SCO4103	peptidase	1.87485	7.94 e-4
SCO2259	multidomain-containing protein family	1.89692	2.31 e-10
SCO4684	cold shock protein	1.91432	3.18 e-6
SCO3050	hypothetical protein	1.92345	2.17 e-7
SCO1469	hypothetical protein	1.92925	2.44 e-3
SCO6172	oxidoreductase	1.93293	1.43 e-3
SCO1841	hypothetical protein	1.95507	3.02 e-4
SCO3940	transmembrane protein	1.96414	6.85 e-9
SCO6090	antibiotic resistance macrolide glycosyltransferase	1.96981	8.67 e-4
SCO4954	hypothetical protein	1.97004	8.65 e-7
SCO2211	hypothetical protein	1.97635	2.92 e-4
SCO4223	AraC family transcription regulator	1.98095	5.90 e-6
SCO4802	hypothetical protein	1.99003	2.36 e-3
SCO3608	hypothetical protein	1.99553	3.13 e-8
SCO1256	hypothetical protein	2.01933	9.22 e-4
SCO3814	DNA-binding protein	2.02195	7.70 e-6
SCO1376	LacI family transcriptional regulator	2.05294	1.60 e-3
SCO2745	LacI family transcriptional regulator	2.05946	1.70 e-4
SCO1289	GntR family transcriptional regulator	2.07260	7.03 e-6
SCO1113	hypothetical protein	2.07681	2.08 e-4
SCO5921	cold-shock domain-containing protein	2.07998	2.71 e-5
SCO1868	hypothetical protein	2.08855	9.04 e-7
SCO4268	hypothetical protein	2.09136	2.75 e-4
SCO4804	hypothetical protein	2.09803	3.32 e-3
SCO0635	hypothetical protein	2.10855	3.39 e-4
SCO4265	transport integral membrane protein	2.11108	2.48 e-3
SCO0527	cold shock protein	2.13117	7.47 e-5
SCO2354	hypothetical protein	2.15458	1.92 e-4
SCO1991	hypothetical protein	2.16478	7.94 e-6
SCO2353	hypothetical protein	2.17687	3.22 e-4
SCO4055	alcohol dehydrogenase	2.19179	1.14 e-4
SCO3434	DNA polymerase I	2.19915	5.01 e-5
SCO6077	transferase	2.20044	1.66 e-3
SCO4976	hypothetical protein	2.20356	2.11 e-8
SCO3387	transcriptional regulator	2.20501	7.73 e-9
SCO6150	ADA-like regulatory protein	2.20961	1.20 e-3
SCO1027	hypothetical protein	2.21660	3.56 e-3
SCO3296	oxidoreductase	2.22118	6.62 e-4
SCO4224	hypothetical protein	2.22446	2.55 e-11
SCO2224	hypothetical protein	2.24386	1.59 e-6
SCO3164	hypothetical protein	2.24625	1.15 e-6
SCO6044	hypothetical protein	2.26159	4.30 e-4
SCO4904	hypothetical protein	2.26283	7.79 e-8
SCO1727	hypothetical protein	2.26876	4.79 e-4
SCO7367	membrane efflux protein	2.28160	1.62 e-3
SCO3771	penicillin binding protein	2.29728	3.63 e-6
SCO1380	DNA polymerase IV	2.30787	2.66 e-4
SCO6805	integral membrane efflux protein	2.31461	1.58 e-5
SCO1497	hypothetical protein	2.32815	1.44 e-6
SCO1731	hypothetical protein	2.33848	2.00 e-4
SCO2767	ATP/GTP-binding protein	2.34371	4.31 e-5
SCO6284	decarboxylase	2.35350	2.15 e-3
SCO3772	hypothetical protein	2.35705	6.92 e-4
SCO3217	transcriptional regulator	2.36708	1.02 e-4
SCO5265	hypothetical protein	2.36725	5.20 e-10
SCO1724	Ser/Thr protein kinase	2.38469	3.13 e-4
SCO2587	gamma-glutamyl kinase	2.38470	2.88 e-8
SCO2309	transmembrane transport protein	2.38547	5.41 e-8
SCO6973	hypothetical protein	2.38628	1.25 e-3
SCO3917	hypothetical protein	2.38669	9.18 e-6
SCO2472	hypothetical protein	2.39746	7.30 e-4
SCO4803	hypothetical protein	2.40833	1.07 e-4
SCO0901	hypothetical protein	2.40835	3.52 e-5
SCO0907	dehydrogenase	2.44290	2.98 e-6

SCO2877	hypothetical protein	2.47998	1.94 e-8
SCO4979	phosphoenolpyruvate carboxykinase	2.48356	4.34 e-9
SCO1413	hypothetical protein	2.48393	1.25 e-20
SCO4866	ECF sigma factor	2.49134	3.66 e-4
SCO5506	regulatory protein	2.52820	3.96 e-9
SCO1149	hypothetical protein	2.52971	8.21 e-7
SCO3912	beta-lactamase	2.53530	4.37 e-15
SCO0409	spore-associated protein	2.54436	4.63 e-3
SCO1733	acetyltransferase	2.56560	6.61 e-5
SCO1927	AAC(3) family N-acetyltransferase	2.58216	6.57 e-13
SCO1545	acetyltransferase	2.60314	5.12 e-11
SCO1904	transcriptional regulator	2.60836	2.20 e-9
SCO2729	acetyltransferase	2.60997	2.85 e-5
SCO0500	hypothetical protein	2.62294	7.73 e-5
SCO6446	hypothetical protein	2.62449	1.44 e-12
SCO1457	transporter	2.65364	1.93 e-3
SCO1767	DNA hydrolase	2.68200	5.40 e-5
SCO2895	integral membrane transport protein	2.70543	3.01 e-5
SCO5189	hypothetical protein	2.72090	1.37 e-6
SCO7722	hypothetical protein	2.72478	3.54 e-4
SCO4903	hypothetical protein	2.72743	2.62 e-4
SCO1227	DNA-binding protein	2.73458	1.76 e-3
SCO6719	UvrA-like ABC transporter	2.77572	5.97 e-5
SCO2873	hypothetical protein	2.77804	1.35 e-5
SCO5026	hypothetical protein	2.77970	1.83 e-6
SCO5449	ABC transporter	2.78538	3.02 e-12
SCO5228	acetyltransferase	2.80203	3.85 e-9
SCO2496	hypothetical protein	2.80588	2.24 e-5
SCO0558	hypothetical protein	2.81532	1.39 e-3
SCO5219	lipoprotein	2.83844	3.85 e-3
SCO3165	hypothetical protein	2.84397	3.22 e-14
SCO5190	DNA-binding protein	2.84606	2.20 e-7
SCO2465	RNA polymerase principal sigma factor	2.85820	3.99 e-3
SCO5191	hypothetical protein	2.87866	2.44 e-6
SCO3385	L-allo-threonine aldolase	2.88751	7.95 e-18
SCO6952	hypothetical protein	2.89122	6.56 e-9
SCO1585	hypothetical protein	2.91281	1.07 e-5
SCO5450	ABC transporter	2.92476	1.47 e-10
SCO7710	phosphotransferase	2.92541	6.73 e-6
SCO1550	small membrane protein	2.94107	2.97 e-3
SCO4369	hypothetical protein	2.95069	2.40 e-11
SCO4125	acetyltransferase	2.95227	4.12 e-8
SCO1912	4-hydroxy-tetrahydrodipicolinate synthase	2.97127	5.69 e-4
SCO5451	ABC transporter	2.97648	4.89 e-9
SCO5448	ABC transporter	2.97965	6.73 e-12
SCO0516	lipoprotein	2.98390	5.72 e-4
SCO6171	oxidoreductase	2.9866	2.20 e-3
SCO6149	ribosome-associated GTPase	2.99088	4.60 e-6
SCO1764	hypothetical protein	3.00367	1.71 e-7
SCO1362	hypothetical protein	3.03674	5.08 e-5
SCO4186	hypothetical protein	3.04042	3.02 e-15
SCO2896	hypothetical protein	3.04109	1.57 e-4
SCO3277	phosphotransferase	3.04191	1.46 e-6
SCO7724	hypothetical protein	3.10265	3.05 e-6
SCOr06	RNA	3.11507	1.51 e-20
SCO7265	hypothetical protein	3.13286	7.69 e-8
SCO7731	hypothetical protein	3.20145	2.80 e-9
SCO5972	3' terminal RNA ribose 2'-O-methyltransferase Hen1	3.21221	1.14 e-14
SCO5973	phosphatase	3.23418	2.38 e-14
SCO2586	hypothetical protein	3.24775	3.87 e-3
SCO1795	hypothetical protein	3.26447	7.21 e-11
SCO6295	ABC transporter ATP-binding protein	3.26926	8.87 e-7
SCO4963	ABC transporter ATP-binding protein	3.28773	4.06 e-22
SCO4311	hypothetical protein	3.29856	2.81 e-14

SCO5025	transcriptional regulator	3.30096	2.42 e-21
SCO6530	hypothetical protein	3.30111	5.29 e-4
SCO6464	SIR2 family transcriptional regulator	3.31820	1.28 e-7
SCO6529	ATP/GTP binding protein	3.36832	1.25 e-5
SCO6512	ABC transporter ATP-binding protein	3.38609	8.55 e-9
SCO3295	oxidoreductase	3.42533	2.05 e-4
SCO0854	hypothetical protein	3.45357	1.11 e-12
SCOr03	RNA	3.46190	2.94 e-23
SCO6277	epoxide hydrolase	3.46351	3.87 e-3
SCO6720	ABC transporter	3.46507	3.35 e-8
SCO2258	ABC transporter	3.47290	2.85 e-11
SCO3788	hypothetical protein	3.49865	7.99 e-4
SCO4964	integral membrane transport protein	3.49961	6.68 e-19
SCO2379	acetyltransferase	3.51109	1.94 e-8
SCO1586	hypothetical protein	3.54933	7.04 e-10
SCO4637	hypothetical protein	3.55303	7.10 e-20
SCO2257	ABC transporter ATP-binding protein	3.56147	1.70 e-12
SCO2755	acetyltransferase	3.58266	8.81 e-13
SCO2467	hypothetical protein	3.60728	2.75 e-12
SCO2894	ABC transporter ATP-binding protein	3.62341	3.29 e-9
SCO1340	hypothetical protein	3.62437	2.84 e-19
SCO1341	lipoprotein	3.67420	3.71 e-19
SCO4765	hypothetical protein	3.68124	1.17 e-25
SCO1739	DNA polymerase III subunit alpha	3.68625	5.96 e-5
SCO3789	hypothetical protein	3.68933	6.70 e-11
SCO0795	hypothetical protein	3.71210	4.17 e-7
SCO1726	ATPase	3.76466	9.06 e-14
SCO7806	DNA-binding protein	3.76719	8.03 e-7
SCO7721	hypothetical protein	3.77914	1.74 e-9
SCO5024	oxidoreductase	3.79448	1.29 e-23
SCO6399	hypothetical protein	3.79565	9.95 e-5
SCO2343	acetyltransferase	3.85759	6.48 e-12
SCO2878	hypothetical protein	3.85941	4.78 e-14
SCO1321	elongation factor Tu	3.86004	3.21 e-14
SCO4222	hypothetical protein	3.92605	1.37 e-13
SCO0607	lipoprotein	3.92967	2.23 e-5
SCO7653	hypothetical protein	3.95372	2.14 e-11
SCO3631	hypothetical protein	4.01457	1.29 e-13
SCO4636	hypothetical protein	4.04414	5.28 e-22
SCO7366	hypothetical protein	4.06460	2.67 e-18
SCO7606	amino acid binding protein	4.07962	5.45 e-13
SCO2248	hypothetical protein	4.11392	3.22 e-6
SCO7478	phosphotransferase	4.14527	2.68 e-10
SCO2876	acetyltransferase	4.18755	7.19 e-17
SCO2466	hypothetical protein	4.20279	1.25 e-15
SCO3778	threonyl tRNA	4.24263	1.83 e-11
SCO2625	hypothetical protein	4.27788	3.21 e-37
SCO2697	hypothetical protein	4.30465	1.84 e-25
SCO1986	hypothetical protein	4.32229	2.89 e-15
SCO1624	acetyltransferase	4.35718	1.11 e-24
SCO3825	ABC-transporter transmembrane protein	4.38093	4.41 e-20
SCO3360	hypothetical protein	4.38630	1.05 e-24
SCO3386	hypothetical protein	4.40109	1.59 e-4
SCO2264	hypothetical protein	4.42008	2.48 e-21
SCO3299	hypothetical protein	4.45953	2.48 e-22
SCO6228	hypothetical protein	4.45994	2.82 e-10
SCO7445	hypothetical protein	4.49609	9.19 e-5
SCO0784	hypothetical protein	4.51096	8.79 e-7
SCO3953	RNA 2'-phosphotransferase-like protein	4.58502	8.29 e-11
SCO1905	hypothetical protein	4.59635	1.16 e-33
SCO1988	hypothetical protein	4.64636	2.67 e-17
SCO0783	tetracycline resistance protein	4.692863	5.36 e-15
SCO4278	peptidyl-tRNA hydrolase domain-containing protein	4.704694	2.78 e-21
SCO7613	hypothetical protein	4.804804	1.88 e-16

SCO7447	acetyltranferase	4.85536	1.72 e-9
SCO1729	hypothetical protein	4.90990	3.14 e-31
SCO3824	ABC transporter ATP-binding protein	4.95773	6.09 e-39
SCO1147	ABC transporter transmembrane subunit	5.02627	3.32 e-46
SCO1148	ABC transporter	5.05229	1.53 e-34
SCO7460	lipoprotein	5.18958	1.36 e-7
SCO0909	hypothetical protein	5.20401	7.58 e-52
SCO4011	hypothetical protein	5.27184	3.67 e-11
SCO4264	aminoglycoside phosphotransferase	5.43341	2.47 e-37
SCO1730	hypothetical protein	5.45074	4.01 e-22
SCO1987	hypothetical protein	5.55309	2.89 e-15
SCO6285	hypothetical protein	5.56436	9.11 e-5
SCO4225	hypothetical protein	5.61462	1.41 e-29
SCO1306	hypothetical protein	5.82957	5.51 e-4
SCO6728	hypothetical protein	5.94643	1.02 e-3
SCO0408	methyltransferase	5.99172	1.02 e-48
SCO6589	elongation factor G	6.04160	6.83 e-21
SCO7514	hypothetical protein	6.62106	6.16 e-4
SCO6463	hypothetical protein	6.62262	1.566 e-3
SCO1307	hypothetical protein	6.66365	6.15 e-5
SCO7662	chloramphenicol resistance protein	6.83466	7.23 e-4
SCO4370	transposase	7.26669	3.12 e-5
SCO1700	hypothetical protein	8.12913	2.60 e-7
SCO7515	hypothetical protein	8.54050	3.19 e-3
SCO6282	3-oxoacyl-ACP reductase	8.80910	1.61 e-3
SCOr13	RNA	23.92240	5.75 e-7
SCOr12	RNA	23.92240	5.75 e-7

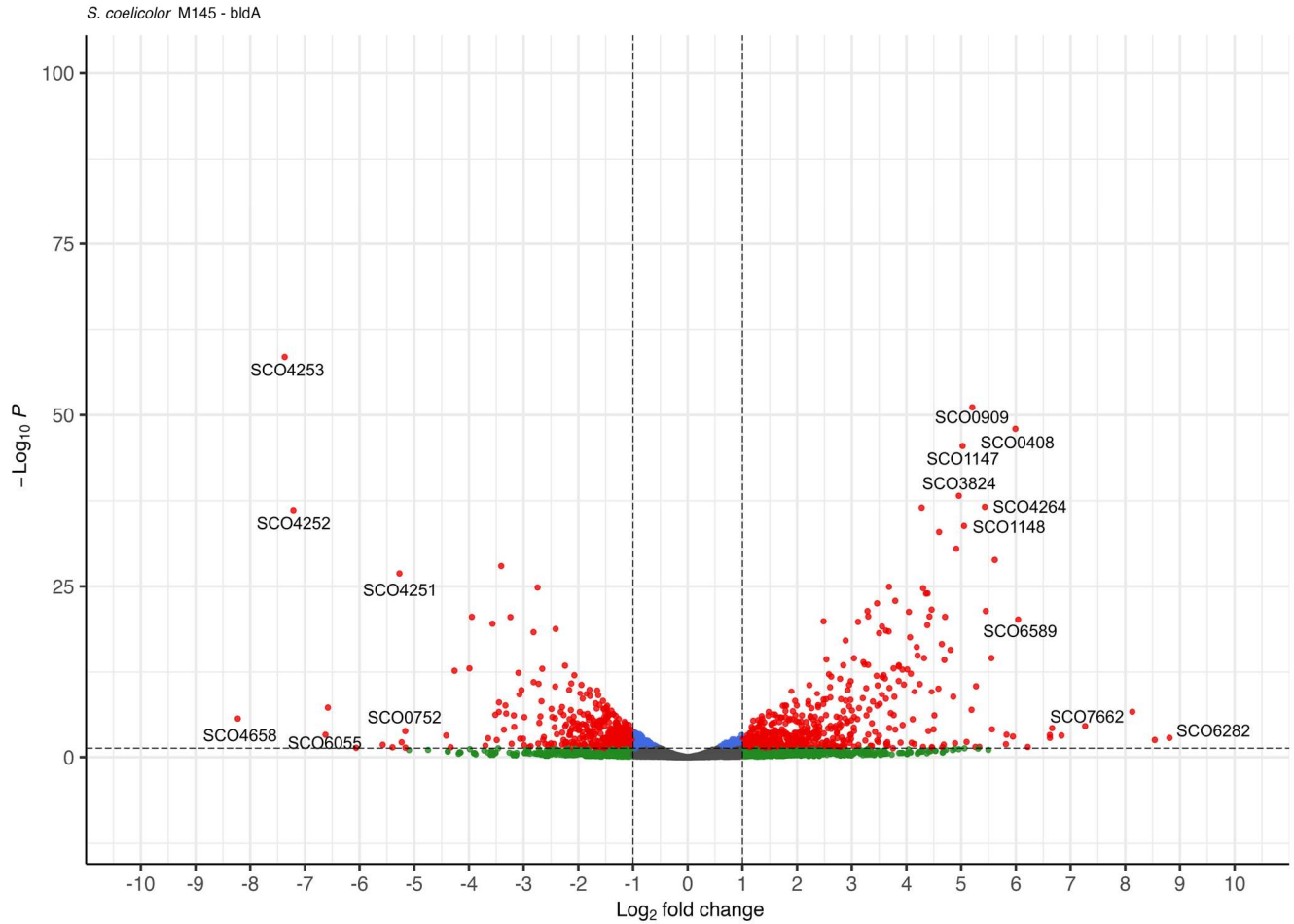

Fig 6.30: Transcriptomic impact of *bldA* deletion in *Streptomyces coelicolor*.

Volcano plot illustrating differential gene expression in *S. coelicolor* JWS-Δ*bldA* compared to the parental *S. coelicolor* M145 strain. Genes significantly upregulated in *S. coelicolor* JWS-Δ*bldA* appear in the right upper quadrant, while significantly downregulated genes appear in the left upper quadrant, with gene identities annotated.

6.4 Summary

The role of *bldA* in *Streptomyces coelicolor* was explored to assess the influence over development, metabolite production, and nutrient utilization. Genetic complementation of the *bldA*-deficient strain *S. coelicolor* J1700 partially restored sporulation on solid medium but it failed to restore wild-type levels of specialised metabolite synthesis in liquid culture. The extensive mutations present in the *S. coelicolor* J1700 genetic background are the likely cause of this discrepancy (See **Chapter 5).** Overexpression of the Leu-tRNA^{CAA} gene, which provides a potential Wobble-Base Pair candidate failed to significantly impact both morphological development and ACT/RED production in *S. coelicolor* J1700. These observations the additional mutations present in the genome of *S. coelicolor* J1700 impact the strain further than previously thought.

To study *bldA* function in an isogenic background, the *bldA* gene was deleted in *S. coelicolor* M145 using CRISPR-Cas9 genome editing. Multiple mutants were isolated and validated through PCR screening and sequencing. Attempts to replicate this process to abolish the Leu-tRNA^{CAA} were unsuccessful, resulting in reversion of any mutants that exhibited the antibiotic resistance phenotype. This indicates that the Leu-tRNA^{CAA} is essential to *S. coelicolor*

The CRISPR-derived Δ*bldA* strain was subjected to the same phenotypic analysis as *S. coelicolor* J1700. Consistent with previous studies and observations seen in *S. coelicolor* J1700, the deletion mutant was unable to form aerial mycelium or spores and presented complete loss of specialised metabolite production exhibiting the ‘classical *bldA* phenotype’ of Merrick, (1976), Takano *et al*, (2003), Silov *et al*, (2020). Complementation of *S. coelicolor* JWS-Δ*bldA* fully restored sporulation and specialised metabolite production, whereas overexpression of the closest WBP match (Leu-tRNA$^{CAA)}$ restored sporulation but was unable to complement antibiotic production. Complementation of *S. coelicolor* JWS-Δ*bldA* demonstrates genetic linkage of the phenotype to the *bldA* gene, whereas partial phenotype restoration as a result of Leu-tRNA^{CAA} overexpression indicates that even in the complete

absence of the Leu-tRNA^{UAA}, Wobble-Base pairing of adjacent tRNAs can recover some aspects of the *bldA* phenotype. These findings reinforce the role of *bldA* role as an important regulatory gene in the *Streptomyces* lifecycle progression.

Given *bld* mutations have a well-established link to nutrient utilisation the use of BioLog-based growth profiling showed that *S. coelicolor* JWS- Δ*bldA* mutant exhibited significantly reduced specific growth rates on a number of carbon and nitrogen sources, especially sugars and sugar alcohols. These growth rate limitations suggest *bldA* plays a significant role in integrating catabolism and development (Villafán *et al*, 2021) especially during nutrient limitation (Claessen *et al*, 2003, Jones and Elliot, 2018).

Investigation of the transcriptome of the *bldA* deletion strain, *S. coelicolor* JWS- Δ*bldA,* revealed significant transcriptional reprogramming in the absence of *bldA*. Many genes involved in secondary metabolism, stress response, and nutrient uptake were downregulated, while a smaller set of genes were upregulated, possibly reflecting compensatory or stress-induced responses. Remarkably, 18 TTA-codon-containing genes were among those affected by the absence of the functional Leu-tRNA^{bldA}*,* including master regulators of antibiotic biosynthesis (e.g., *actII-ORF4*) and pleiotropic developmental regulators such as *adpA*, which themselves control large regulons. The remaining 127 TTA-codon containing genes have previously not been documented as being targets of *bldA*. The transcriptomic data provides strong molecular support for the pleiotropic defects observed in the Δ*bldA* strain and illustrates the extent to which *bldD* likely integrates environmental sensing with developmental and metabolic programs via *bldA*. In conclusion, these data reinforce the role of *bldA* for a number of cellular processes, in morphological differentiation and metabolite production but also provides further insight into its requirement for effective nutrient utilization and its role as a central translation regulator for *S. coelicolor*.

Chapter 7: Application of the Broccomyces reporter system to investigate its use in the study of 5`-UTRs in *Streptomyces clavuligerus*

7.1 Introduction

In bacteria, transcription and translation are coupled and mechanisms of post-transcriptional regulation are known to significantly influence gene expression (Liu *et al*, 2025). The 5`-untranslated regions (UTRs) often harbour diverse mechanisms and specific regions to control translation of mRNAs (Belasco *et al*, 1986., Hwang *et al*, 2022., Yi *et al*, 2017). Moreover, the sequence of the 5`-UTR is known to affect subsequent translation of mRNAs by affecting stability of the mRNA (Arnold *et al*, 1998).

To expand the applicability of the dual-reporter system beyond model species such as *S. coelicolor* and to understand if there is utility of the system to study other aspects of *Streptomyces* biology, the functionality of Broccomyces was explored using *Streptomyces clavuligerus* (Higgens and Kastner, 1971, Tahlan *et al*, 2004, Ríos-Fernández *et al*, 2024). Specifically, the modified TTA-mCherry construct was leveraged to study translational effects linked to the 5`-UTR of mRNAs. The *ccaR* gene encodes a critical regulatory protein that governs production of clavulanic acid and cephamycin in *S. clavuligerus* (Fu *et al*, 2019., Paradkar, 2013., Pérez-Llarena *et al*, 1997). Specific mutations have been identified in the promotor of *ccaR,* the 5`UTR and coding sequence that increased clavulanic acid titre yield (GlaxoSmithKline, 2021). Engineering these key mutations into the 5`UTR of the Broccomyces construct would provide proof of concept data that the system could be used for the study of 5`-UTR functionality.

7.2 Aims of this chapter

The aims of this chapter are to examine the functionality of the Broccomyces system in another species of *Streptomyces*, and to investigate the use of the TTA-mCherry reporter as a tool for analysing translational effects of 5` UTRs in *S. clavuligerus*.

7.3 Results

7.3.1 Testing the orthogonal Broccomyces system as a 5`UTR reporter system

To test the utility of the Broccomyces system for reporting on 5`UTR sequence modifications, the promotor modifications identified by GSK in *ccaR* that are believed to enhance production of clavulanic acid in *S. clavuligerus* were exploited. This species is industrial significant as the major commercial clavulanic acid producer (Paradkar, 2013, López-Agudelo *et al*, 2021). Clavulanic acid (CA) is a β-lactamase inhibitor, commonly used in tandem with β-lactam antibiotics to overcome β-lactamase-associated AMR (Saudagar *et al*, 2008). Previous investigation into clavulanic acid synthesis and regulation has highlighted the regulatory gene, *ccaR*is required for biosynthesis (Pérez-Llarena *et al*, 1997). Later work showed that CcaR binds to the promotor for *claR*, a gene that positively regulates CA production and is integral to the final stages of CA biosynthesis (Martínez-Burgo *et al*, 2015). Understanding how the mutations in the 5`UTR of *ccaR* gene lead to increased CA is crucial for a better understanding of CA production in *S. clavuligerus*.

Given the clinical importance of CA, the BGC, regulation and promotors, including *ccaRp*, have been extensively researched (Jensen, 2012., AbuSara *et al*, 2019., López-Agudelo *et al*, 2021). A patent was filed by GlaxoSmithKline, identifiying two point-mutations in the *ccaR* promotor region, that result in a higher titre of CA when compared to the WT- promotor (GSK, 2021). Examining the data, it was proposed that the two mutations displayed synergy when combined, increasing the CA titre beyond that of the individual mutations. This finding provided the hypothesis that the mutations function to stabilise the mRNA, and whether this could be tested using the Brocomyces system. To test the promotor region of *ccaR* and if the mutations can improve the mCherry production when the individual 5`UTR mutations are present or when they are combined. The patent indicates that the mutations are additive in nature, but the mechanism underpinning this is not clear. It was hypothesised that each mutation may alter stability of the mRNA and combining these mutations further stabilises mRNA stability. To

test this the Broccomyces system was employed such that the Broccoli fluorescence may be enhanced in the presence of the mutations and/or there will be a concomitant increase in mCherry production.

Four plasmids were designed and synthesised (GenScript) based on the previous Broccomyces plasmids: one containing the wild-type *ccaR* promotor found in *S. clavuligerus*, one containing a C48T nucleotide mutation in the *ccaR* promotor (henceforth known as M1), one containing a G143A nucleotide mutation (henceforth known as M2), and one that contained both mutations (henceforth known as M1M2; **Fig. 7.1**). The plasmid maps for the four newly synthesised Broccomyces-*ccaRp* plasmids, which are shown in **Fig. 7.2** (Broccomyces-*ccaRp* WT), **Fig. 7.3** (Broccomyces-*ccaRp* M1), **Fig 7.4** (Broccomyces-*ccaRp* M2), and **Fig. 7.5** (Broccomyces-*ccaRp* M1M2). A condensed version of these plasmids can be seen in **Table 7-1**, detailing the appropriate strain and plasmid, along with the relevant *ccaR* promotor mutations.

Fig. 7.1: Alignment of Wild-Type and mutant *ccaR* promoter sequences for *S. clavuligerus* Broccomyces constructs. Alignment was carried out in Clustal Omega on entire promotor sequence, ending before start codon for the ccaR protein. M1 mutation (green) and M2 mutation (red) are highlighted.

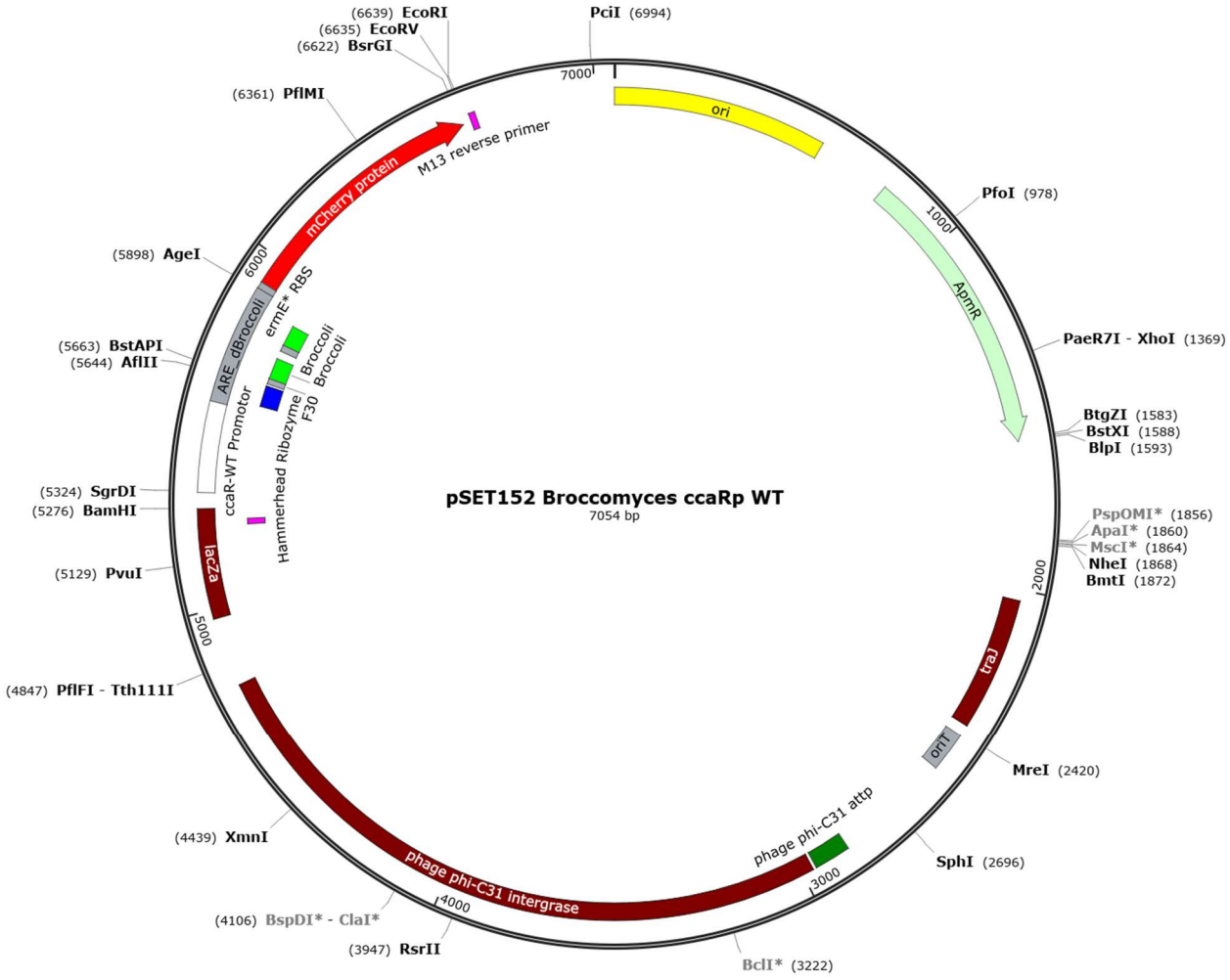

Fig. 7.2: Plasmid map of the Broccomyces-*ccaRp* WT construct, created by GenScript. The plasmid contains a wild-type allele of the *ccaR* promoter, for use as a *ccaR* driven control for Broccomyces experiments in the *S. clavuliverus* background. All plasmid maps were created using SnapGene™.

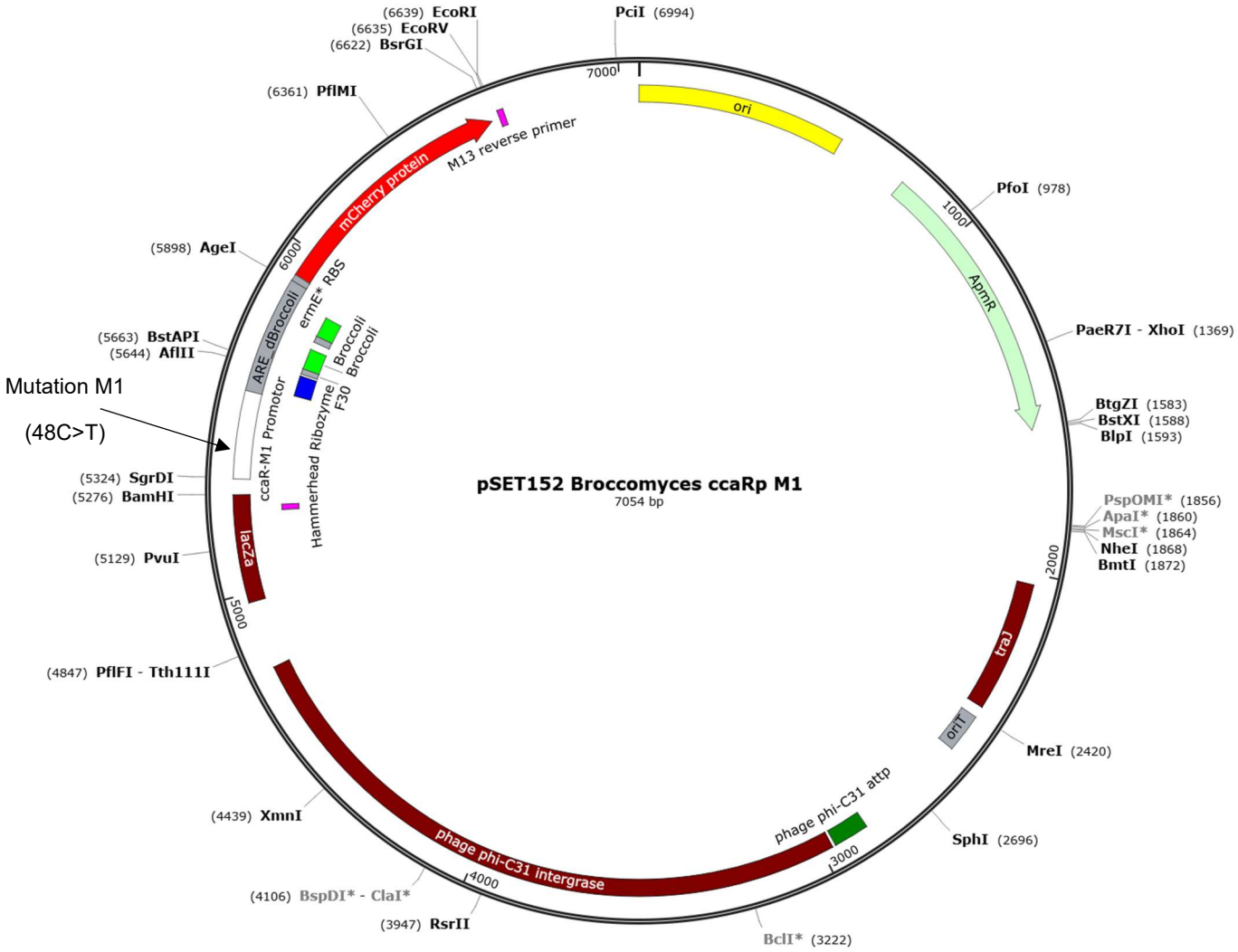

Fig. 7.3 Plasmid map of the Broccomyces-*ccaRp* M1 construct, created by GenScript. C48T nucleotide mutation in the *ccaR* promotor. All plasmid maps were created using SnapGene™.

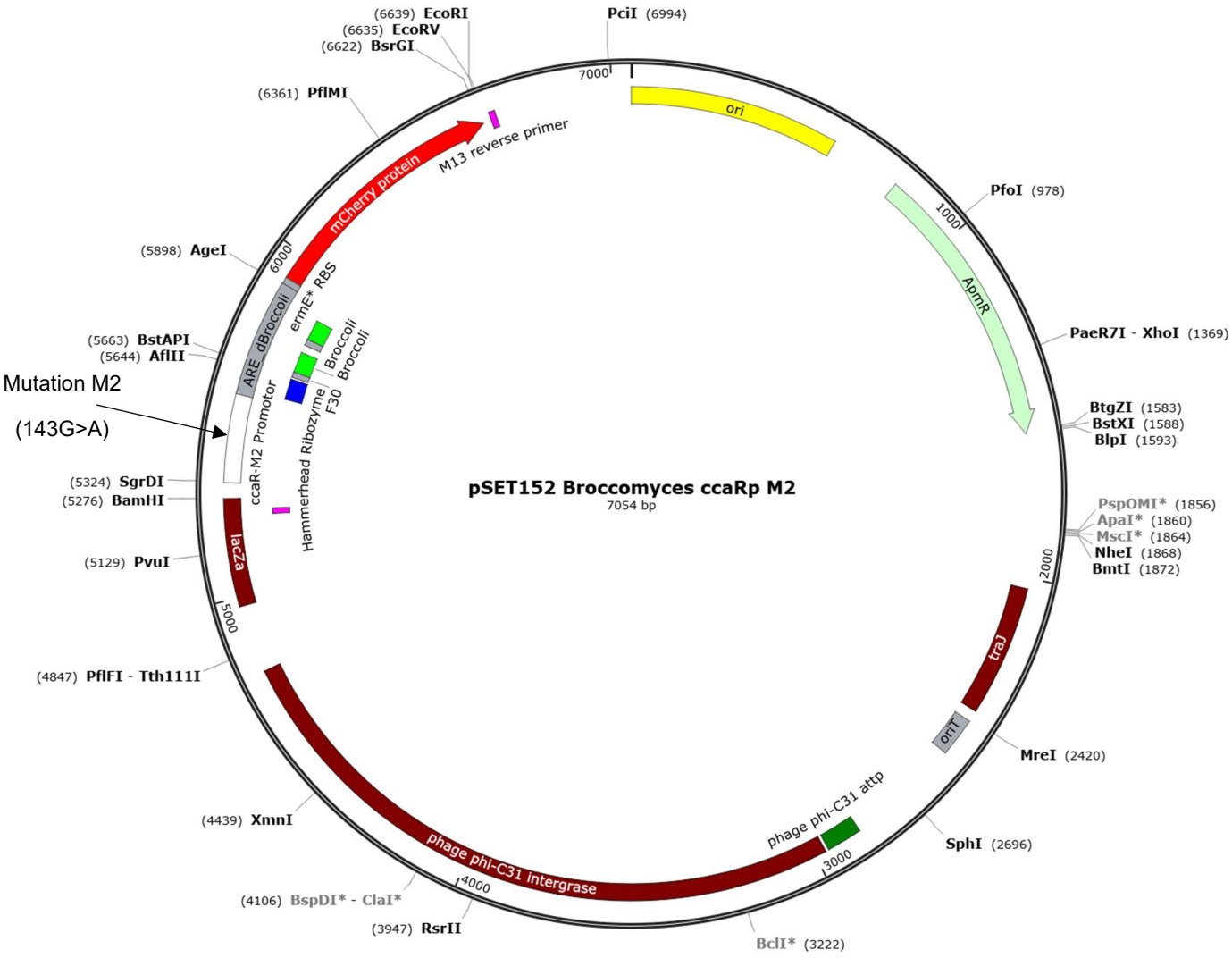

Fig. 7.4 Plasmid map of the Broccomyces-*ccaRp* M2 construct, created by GenScript. G143A nucleotide mutation in the ccaR promoter. All plasmid maps were created using SnapGene™.

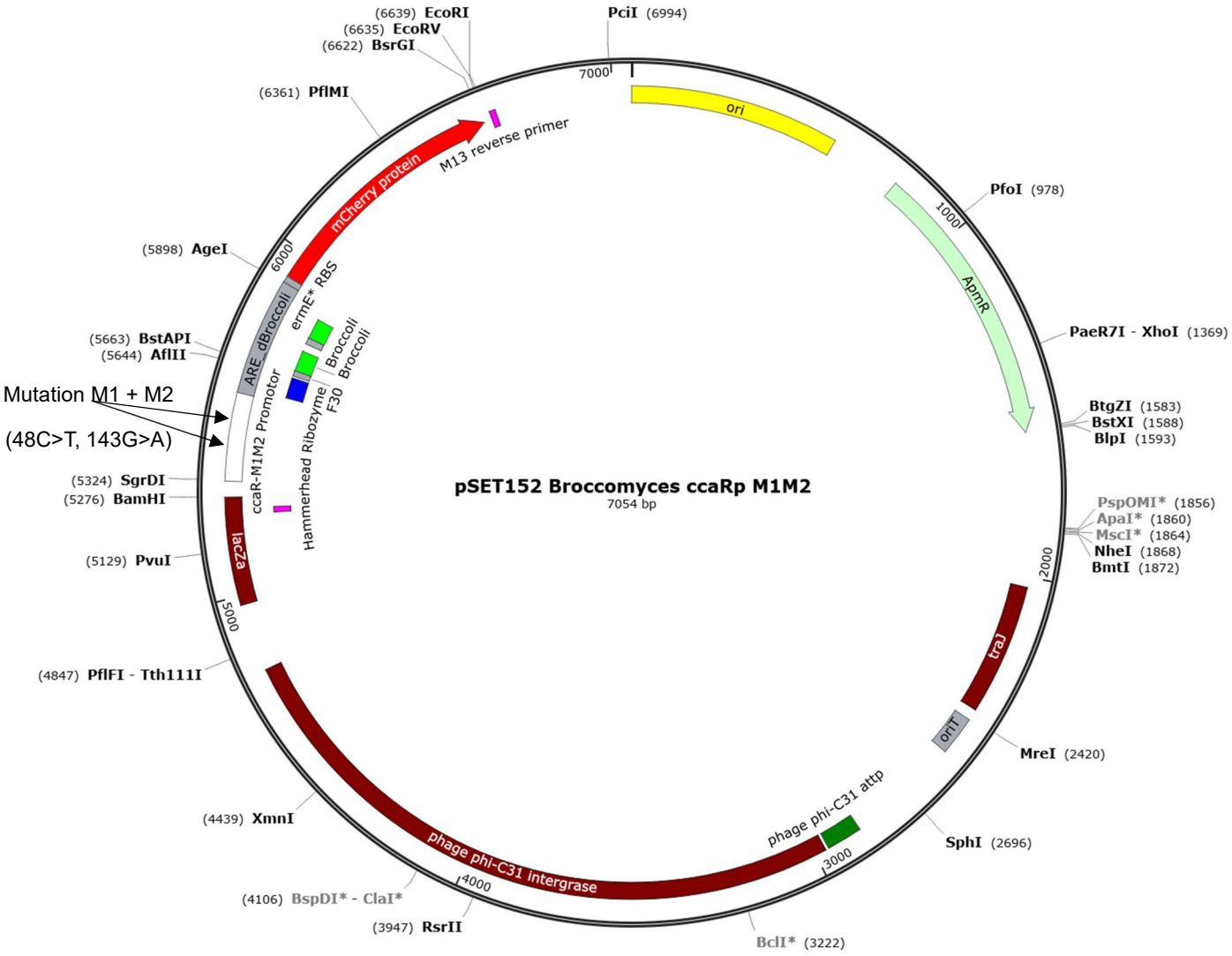

Fig. 7.5 Plasmid maps of the Broccomyces-*ccaRp* M1M2 construct, created by GenScript. C48T and G143A nucleotide mutations in the *ccaR* promotor. All plasmid maps were created using SnapGene™.

Table 7-1: Summary of Broccomyces-*ccaRp* plasmids and *ccaR* promotor characterisation

***S. clavuligerus* Strain**	**Plasmid**	***ccaR* promotor description**
S. clavuligerus SC6- Broccomyces *ccaRp* WT	pSET152-Broccomyces *ccaRp*-WT (Apramycin resistant)	Wild Type *ccaR* promotor
S. clavuligerus SC6- Broccomyces *ccaRp* M1	pSET152-Broccomyces *ccaRp*-M1 (Apramycin resistant)	Single Promoter Point Mutation (48 C>T)
S. clavuligerus SC6- Broccomyces *ccaRp* M2	pSET152-Broccomyces *ccaRp*-M2 (Apramycin resistant)	Single Promoter Point Mutation (143 G>A)
S. clavuligerus SC6- Broccomyces *ccaRp* M1M2	pSET152-Broccomyces *ccaRp*-M1M2 (Apramycin resistant)	Double Promoter Point Mutation (143 G>A,48 C>T)

The Broccomyces-*ccaRp* plasmids were conjugated into the *S. clavuligerus* SC6, a strain of *S. clavuligerus* produced by GSK as a part of their early CA production lineage. Conjugation plates of *S. clavuligerus* were grown for 10 days on L3M9 media to allow for the formation of exconjugants (GSK, 2021), before selection and patching onto fresh L3M9 plates and grown for a further 10 days to allow sporulation. Candidate colonies were checked for the presence of the plasmid following genomic DNA extraction and the presence of the plasmid in the *S. clavuligerus* SC6 background by PCR using the pSET152 Broccomyces check primers (primer numbers 1 and 2) (**Fig 7.6A**). The Broccomyces plasmids were also tested to ensure the plasmids did not alter the physiology of *S. clavuligerus* SC6. As seen in *S. coelicolor* M145 (see **Chapter 3**), the presence of the Broccomyces plasmids had no phenotypic effect on *S. clavuligerus* physiology (**Fig 7.6B**).

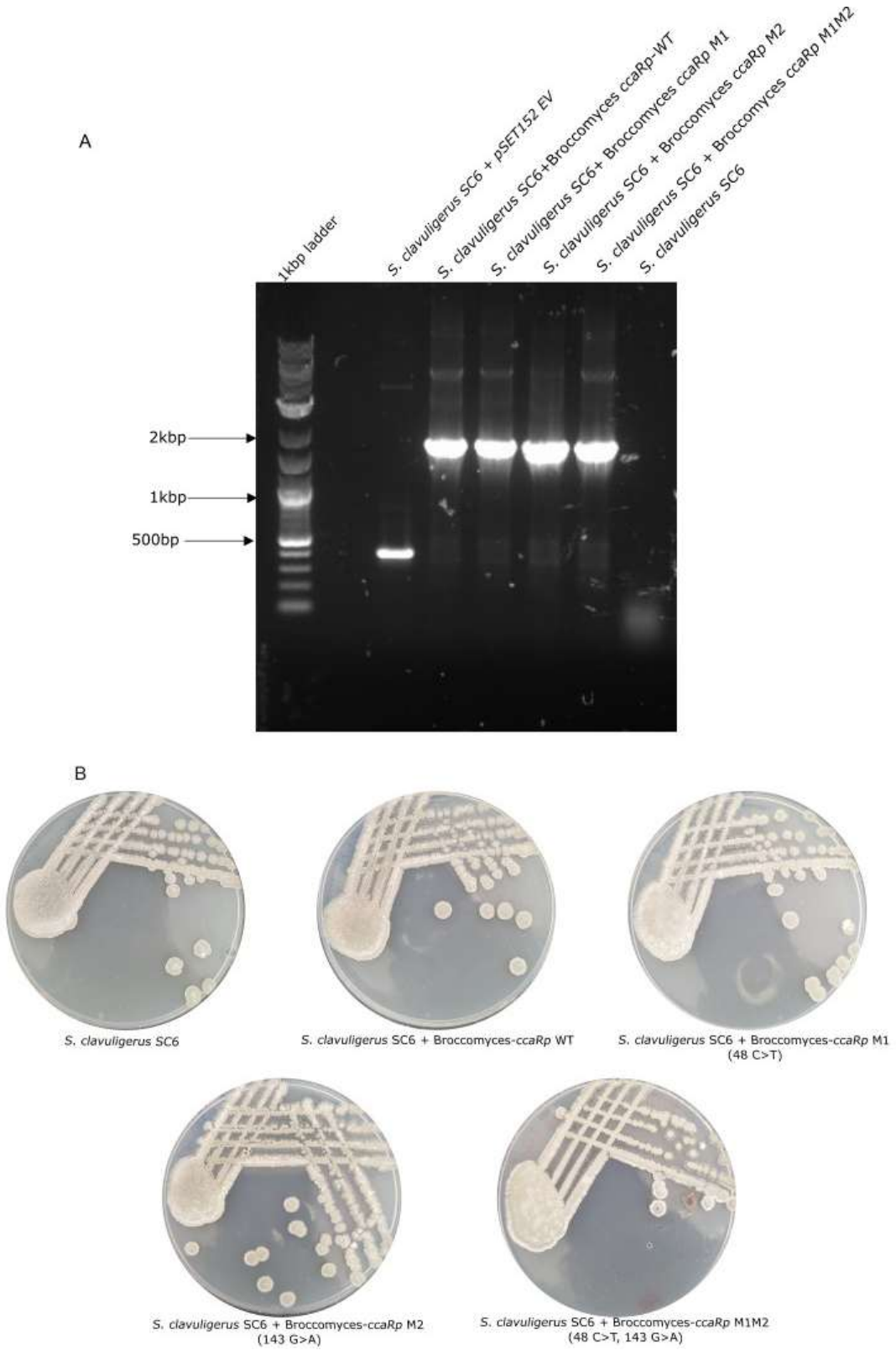

Fig. 7.6: Validation of plasmid integration and phenotypic analysis of *S. clavuligerus* SC6 Broccomyces exconjugants. A: Agarose gel of extracted gDNA for successful Broccomyces plasmid conjugation. Amplicon of pSET152 empty vector: 410bp. Amplicon of Broccomyces inserted region: 1.7kbp. *S. clavuligerus* SC6 used as a negative control for no plasmid conjugation. **B:** Colony morphology of *S. clavuligerus* SC6 and Broccomyces-*ccaRp* strains. Plates incubated at 26°C for 10 days.

7.3.2 Broccomyces-*ccaRp* and other Broccomyces constructs have minimal impact on *S. clavuligerus* SC6 growth.

After successful conjugation of the Broccomyces-*ccaRp* plasmids into *S. clavuligerus* SC6, the Broccomyces-*ermE** and Broccomyces-*ermE**TGA_mCherry constructs were also conjugated to act as a Broccomyces standard and mCherry fluorescence negative control respectively. Before progress on microscopy could begin, the impact of the Broccomyces plasmids on growth in *S. clavuligerus* SC6 was first investigated. Similar to growth experiments previously performed in *S. coelicolor* M145, dry cell weight growth analysis was carried out, with timepoints taken every 24 hours for 168 hours, over three biological replicates.

From the results of this experiment, shown in **Fig. 7.7**, it can be determined that in TSB media, *S. clavuligerus* reaches the stationary phase of growth after 72 hours of incubation at 26^{o}C. **Fig. 7.7** shows that both wild-type *S. clavuligerus* SC6 and the Broccomyces-containing strains possess similar growth curves, indicating the Broccomyces plasmids have minimal impact on growth rate in *S. clavuligerus,* emphasising the dual-reporter's use as accurate readout tools at specific time points in the *Streptomyces* life cycle, without impacting growth. Each strain exhibits a growth curve with exponential phase starting after 48 hours incubation, followed by a stationary phase (starting at 72-96 hours incubation). The growth of *S. clavuligerus* SC6 is concluded with a phase resembling decreased growth, suggesting the cells in the flasks had begun to lyse after 144 hours of incubation. Examination of the growth curves indicate that the Broccomyces plasmids have no impact on the growth of *S. clavuligerus* SC6, indicating that future microscopy and plate reader assay time points are representative of *S. clavuligerus* SC6 growth.

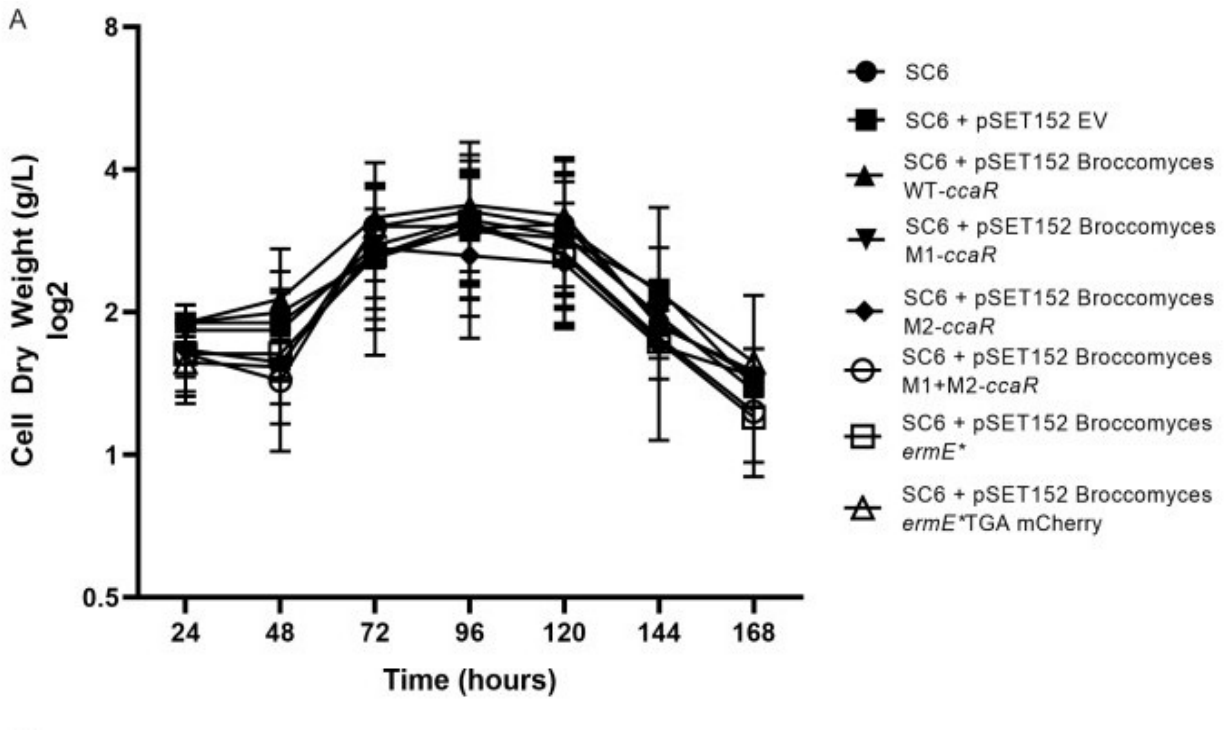

Fig. 7.7: Broccomyces-*ccaRp* constructs have minimal impact on *S. clavuligerus* SC6 growth in liquid media. Growth of *S. clavuligerus* SC6 and Broccomyces strains over a period of 168 hours in TSB media. Strains were measured in biological triplicates and cell dry weight (g) was used as an indicator of growth. Error bars show standard deviation.

7.3.3 Epifluorescence microscopy of *S. clavuligerus* SC6 Broccomyces strains indicates TTA-mCherry may be an effective tool for analysing translational effects of mutations in 5`UTRs

Given the Broccomyces constructs has minimal impact on growth in *S. clavuligerus* SC6, (**Fig. 7.7**), the Broccomyces-containing strains were subjected to widefield epifluorescence microscopy, using 40 μM DFHBI-1T to acquire visualisation of Broccoli-based fluorescence. Wild-type *S. clavuligerus* SC6, as well as *S. clavuligerus* SC6 with the Broccomyces-*ccaRp* plasmids were grown on L3M9 agar against angled cover slips for a period of either three days (to visualize Broccoli and TTA-mCherry production early in the *S. clavuligerus* life cycle) or at seven days (to visualize Broccoli or TTA-mCherry fluorescence when maturation and sporulation are underway). The CA regulator CcaR is also a TTA containing gene and reportedly subject to *bldA*-dependent translation (Trepanier *et al*, 2002).

After three days of incubation, Broccoli fluorescence in the *S. clavuligerus* SC6 Broccomyces-*ccaRp* strains is partially detectable but is not as pronounced as images taken in any of the *S. coelicolor* backgrounds (**Fig. 7.8**). Similar to each of the *S. coelicolor* background, wild-type *S. clavuligerus* SC6 demonstrated no detectable fluorescence for both Broccoli and TTA-mCherry channels (**Fig. 7.8A**). TTA-mCherry fluorescence, on the other hand, is detectable in all four Broccomyces-*ccaRp* strains, with increased TTA-mCherry fluorescence intensity detected in both *S. clavuligerus* SC6 Broccomyces-*ccaRp* M2 and *S. clavuligerus* SC6 Broccomyces-*ccaRp* M1M2 (**Fig. 7.8D, Fig. 7.8E**). This data suggests that M2 and the M1M2 combination in the *ccaR* promotor sequence may result in increased translation. These data also suggests that the TTA-mCherry reporter may serve as a tool for quantifying how mutations in 5` UTRs could impact translation in *Streptomyces*.

After seven days of incubation, Broccoli-based fluorescence is slightly improved in the Broccomyces-*ccaRp* constructs, however due to the intensity detected in TTA-mCherry fluorescence at this time point, this improvement could be contributable to either fluorescence

bleed through or ghosting (**Fig. 7.9**). TTA-mCherry fluorescence output in Broccomyces-*ccaRp* WT and Broccomyces-*ccaRp* M1 is reduced compared to the output at three days incubation, implying the *ccaR* promotor in these strains is downregulated (**Fig. 7.9B, Fig. 7.9C)**. In Broccomyces-*ccaRp* M2 and Broccomyces-*ccaRp* M1M2, TTA-mCherry fluorescence after ten days incubation appears significantly increased compared to fluorescence detected after three days incubation (**Fig. 7.9D, Fig. 7.9E**). These findings indicate that the *ccaR* promotor, M2 and M1M2 result in increased TTA-mCherry translation. These findings highlight that while the *ccaRp*-M1 mutation may not have a significant impact on translational output, *ccaRp*-M2 and the combination of both mutations (*ccaRp*-M1M2) results in improved translation of mCherry. These data also correlate well with the data at 3 days. To quantify if these 5`-UTR mutational effects can be quantified, the *S. clavuligerus* SC6 Broccomyces-*ccaRp* strains were tested using the 96-well plate fluorescence reporter assay.

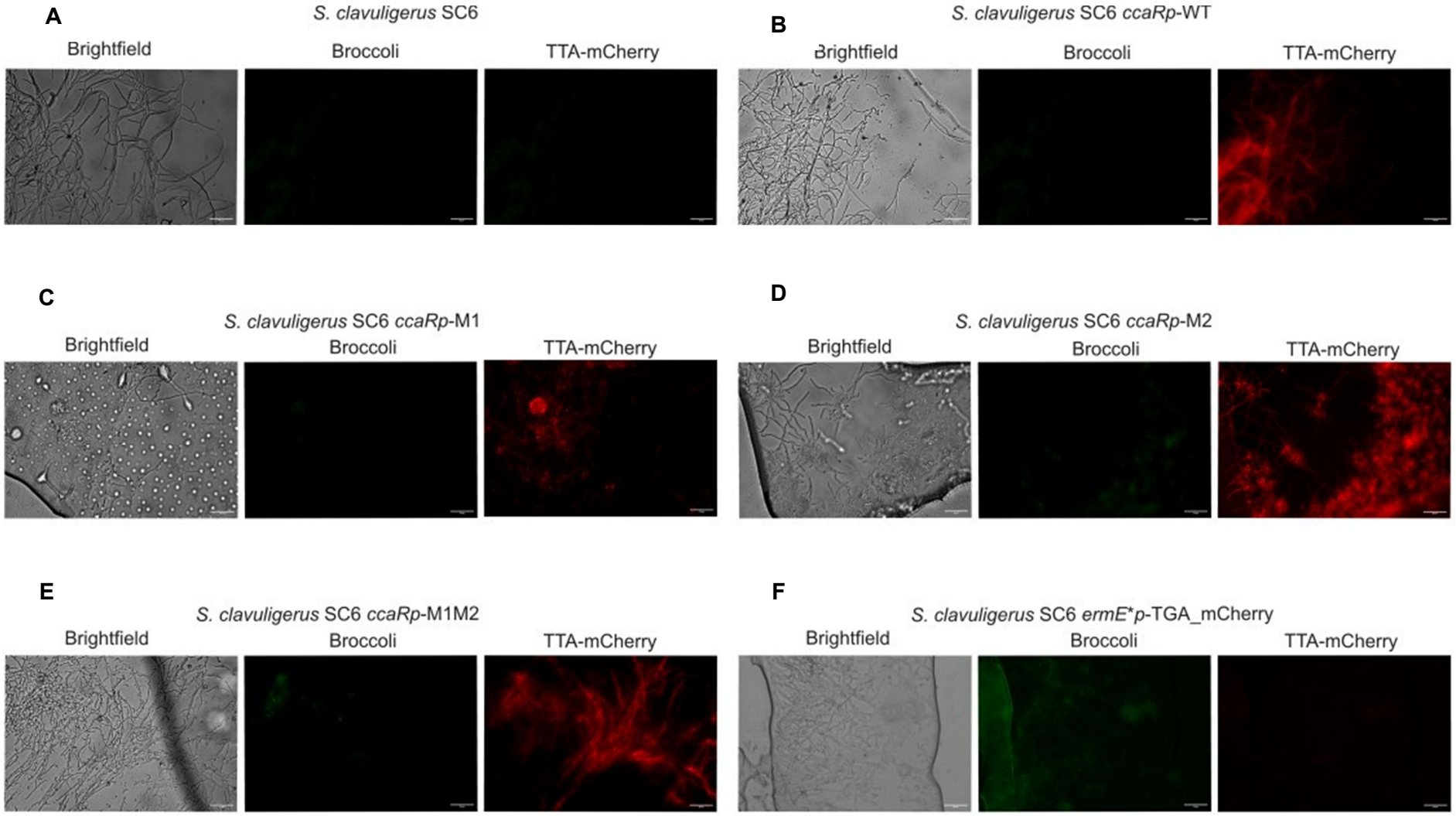

Fig. 7.8: **Widefield Epifluorescence Microscopy Images of *S. clavuligerus* SC6 Broccomyces strains after three days growth on L3M9 agar.** Images were acquired using an Olympus BX51 Upright Fluorescent Mechanical Microscope fitted with FITC and Texas Red filter sets. Images were acquired with a 40x objective lens at 475nm/530nm and 560nm/630nm for Broccoli and TTA-mCherry fluorescence respectively. ImageJ was used to analyse and scale the images. Scale Bar= 25μm

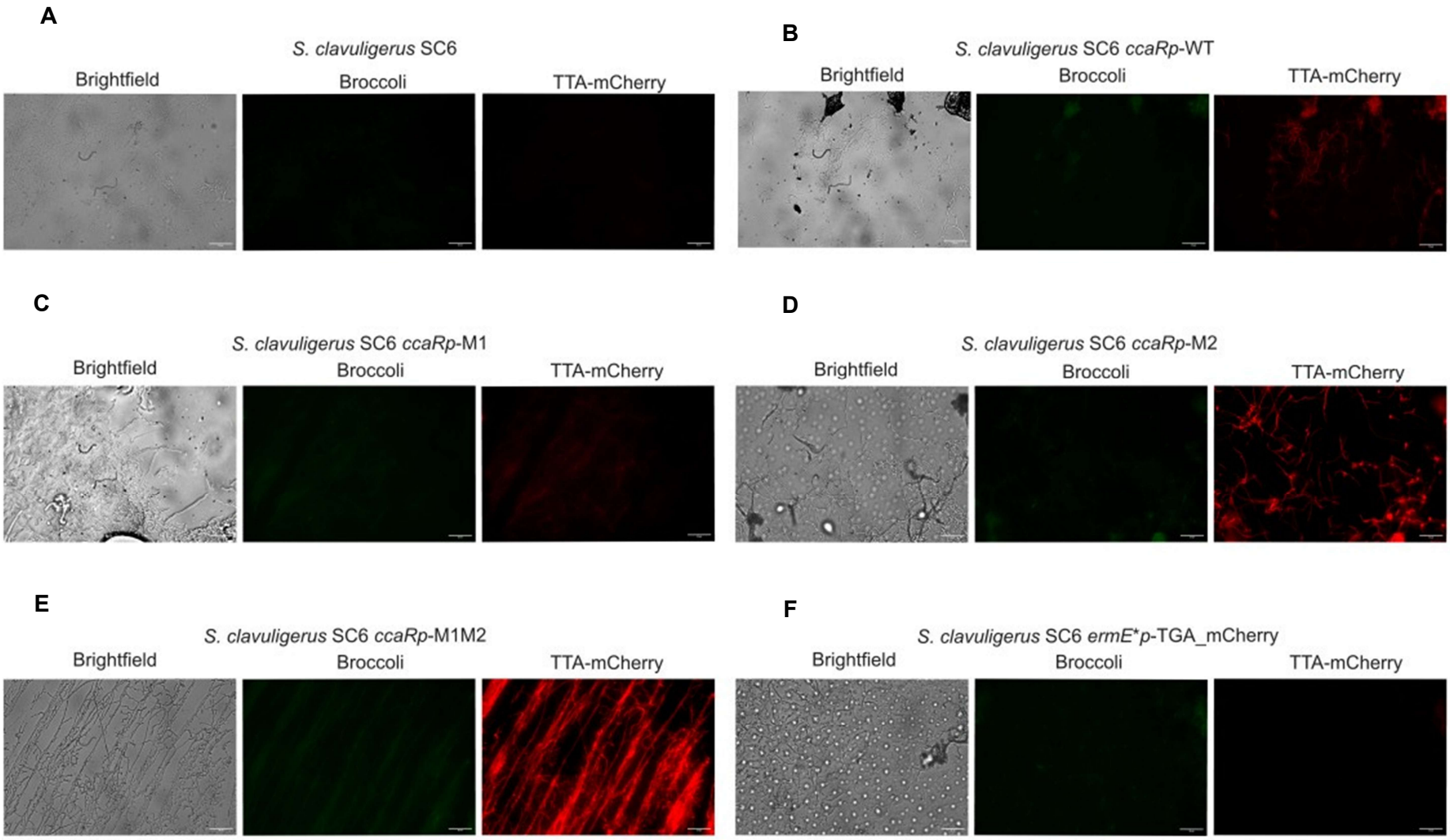

Fig. 7.9: **Widefield Epifluorescence Microscopy Images of *S. clavuligerus* SC6 Broccomyces strains after seven days growth on L3M9 agar.** Images were acquired using an Olympus BX51 Upright Fluorescent Mechanical Microscope fitted with FITC and Texas Red filter sets, with an 40x objective lens at 475nm/530nm and 560nm/630nm for Broccoli and TTA-mCherry fluorescence respectively. ImageJ was used to analyse and scale the images. Scale Bar= 25µm

7.3.4 Broccomyces plate reader assay confirms *ccaRp*-M2 and *ccaRp*-M1M2 result in improved translational output

To quantify the change in translation due to 5`UTR mutations identified through widefield epifluorescence microscopy in *S. clavuligerus* SC6 (**Fig. 7.8, Fig. 7.9**), the mutations in the *ccaR* promotor were quantified using the Broccomyces 96-well plate fluorescence assay over the course of seven days at 24-hour intervals. Cultures of *S. clavuligerus* SC6 containing the Broccomyces reporter system were grown in 250ml flasks with springs in TSB medium at 26ºC, shaking at 200rpm. At each time point, 20ml aliquots were removed and the aliquots were processed as optimised in **Chapter 3**, with 5µM DFHBI-1T used for Broccoli output quantification or DMSO for use as a negative control. In this experiment, wild-type *S. clavuligerus* SC6 was used as a control for autofluorescence, and *S. clavuligerus* SC6 pSET152 empty vector was used as a plasmid control strain. *S. clavuligerus* SC6 Broccomyces-*ermE*p* and *S. clavuligerus* SC6 Broccomyces-*ermE*p* TGA-mCherry were used as a positive control and negative TTA-mCherry control respectively.

A time course of Broccomyces-related fluorescence in *S. clavuligerus* SC6 (**Fig. 7.10)** was performed over 168 hours incubation. At both 24-hours and 48-hours, both Broccoli and TTA-mCherry fluorescence for all tested strains was negligible (**Fig. 7.10A, Fig. 7.10B**). At 72 hours incubation, TTA-mCherry in both the Broccomyces-*ccaRp* and Broccomyces-*ermE** backgrounds could be detected, with *ccaRp*-M2 and *ccaRp*-M1M2 displaying approximately four-fold the relative fluorescence of both Broccomyces-*ccaRp* WT and Broccomyces-*ccaRp* M1 (**Fig 7.10C**). This trend of increased relative fluorescence in Broccomyces-*ccaRp* M2 and Broccomyces-*ccaRp* M1M2 persists at the 96- hour incubation time point, with *ccaRp*-M1M2 fluorescence increasing to match the output detected into Broccomyces-*ccaRp* M2. Interestingly, at both the 120-hour and 144-hour time points, overall relative fluorescence for Broccomyces-*ccaRp* M1M2 begins to surpass that of Broccomyces-*ccaRp* M2 (**Fig. 7.10E, Fig. 7.10F**). While Kruskal-Wallis statistical analysis between the two strains indicates this increase was not significant (p=>0.99), it could indicate that the combination of *ccaRp* M1 and

ccaRp M2 may have a synergistic effect on TTA-mCherry output, and consequently, translational output for CcaR. At 144-hour, overall relative fluorescence for all Broccomyces strains begins to decrease, with minimal fluorescence for both Broccoli and TTA-mCherry being detectable at 168-hour incubation, likely due to cessation of growth and cell lysis, which was also observed in the dry weight analysis (**Fig. 7.7** & **Fig. 7.10G**).

These data further support the hypothesis that when compared to *ccaRp*- WT and *ccaRp*- M1, the presence of the mutations *ccaRp*-M2 and *ccaRp*-M1M2 improve translational output of TTA-mCherry, as well as likely improving the translation of its native protein, ccaR. These data also support the hypothesis that the TTA-mCherry fluorescence construct can serve as both a translational reporter and a reporter for 5`UTR mutation assessment.

The same data was also plotted as a time series to illustrate the temporal profiles of expression of Broccoli/mCherry as a function of the promoter (**Fig 7.11**). While relative TTA-mCherry fluorescence can be detected in Broccomyces-*ccaRp* WT and Broccomyces-*ccaRp* M1 (**Fig. 7.11A, Fig. 7.11B**), these relative values are muted when compared to both Broccomyces-*ccaRp* M2 and Broccomyces-*ccaRp* M1M2 during exponential and stationary phase, further highlighting that *ccaRp*-M2 and *ccaRp*-M1M2 are beneficial promotor mutations for enhancing *ccaRp*-driven expression (**Fig. 7.11C, Fig. 7.11D**).

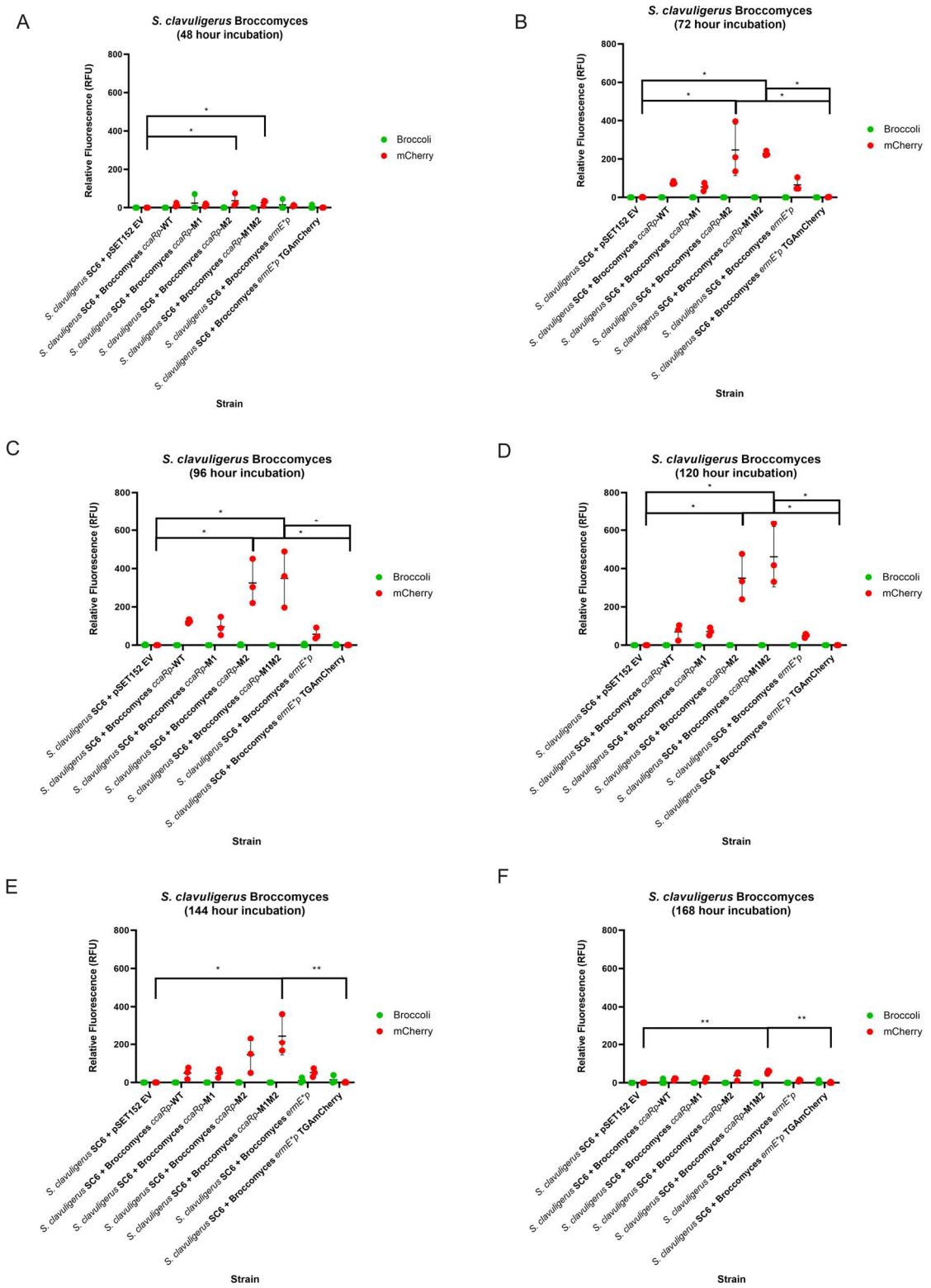

Fig 7.10: Time Course Fluorescence assay data of Broccoli and TTA-mCherry in *S. clavuligerus* SC6 Broccomyces plasmids. Readings were taken every 24 hours over a period of seven days (168 hours). The 24-hour time point was omitted due to negligible differences between 24 and 48 hours. Data was analysed by Kruskal-Wallis test (48-hour p=0.026, 72-hour p=0.007, 96-hour p=0.006, 120-hour p=0.007, 144-hour p=0.013, 168-hour p=0.012), followed by Dunnett's multiple comparisons tests between strains (*p < 0.05, **p < 0.01)

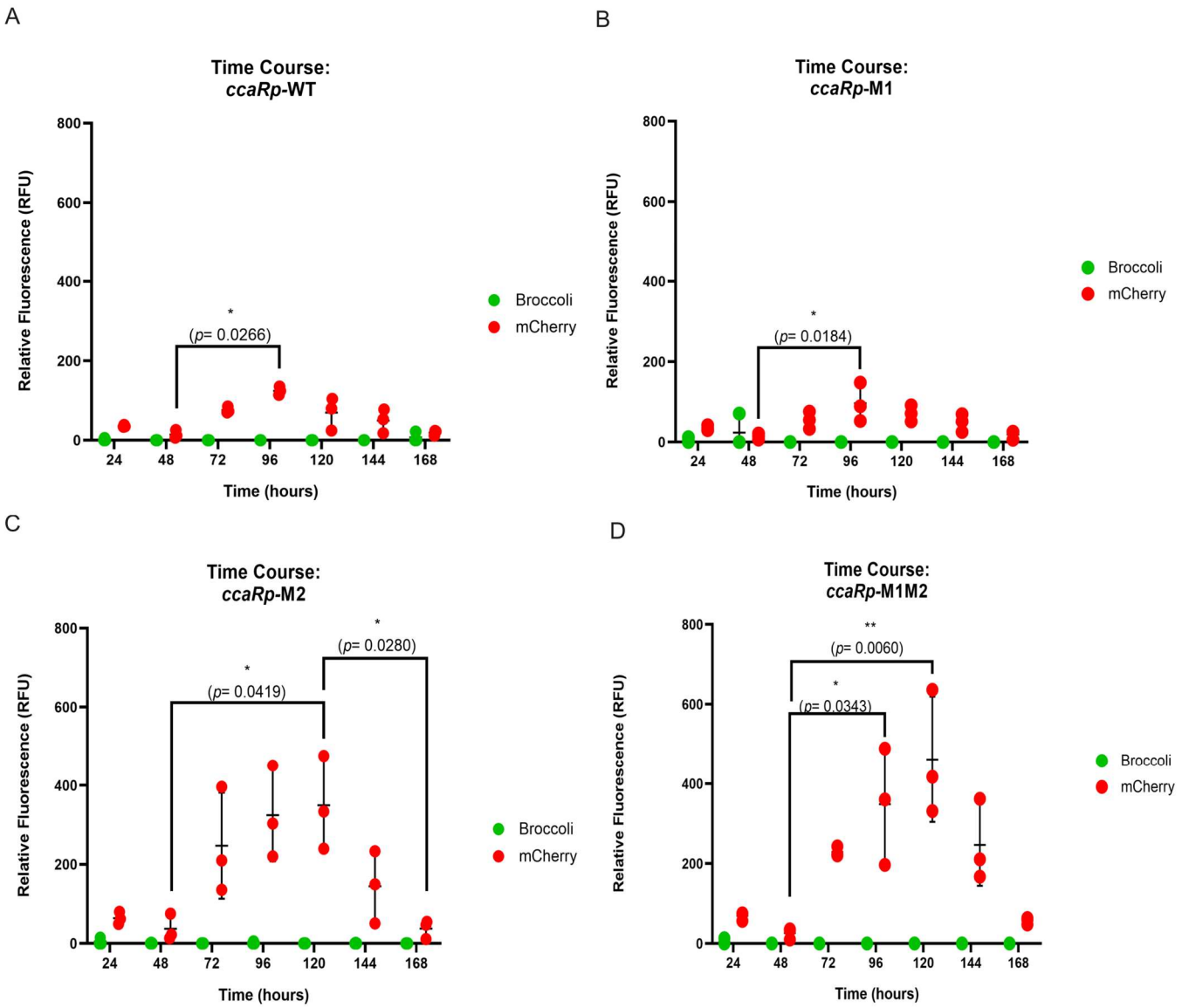

Figure 7.11: Analysis of Broccoli and TTA-mCherry relative fluorescence plotted over time for *S. clavuligerus* SC6 Broccomyces-*ccaRp* reporters. Error bars correspond to standard deviation from the mean (N=3).

7.3.5 Mutations in *ccaRp* result in improved *ccaRp* stability and CA production.

Microscopy and the Broccomyces fluorescence assay provided evidence to suggest that the presence of the M2 or the combination of M1M2 in the 5`-UTR of *ccaRp* has a positive effect on translational of the mCherry reporter gene. To further understand what is driving this increase in gene expression, the effect of the *ccaRp* mutations on mRNA structure and positional entropy in the mRNA were investigated.

Using the RNAFold WebServer, the sequence of the *ccaR* promotor was used to generate a secondary structure prediction for the wild-type promotor and all three *ccaRp* mutant alleles (M1, M2, M1M2; **Fig 7.12**). The wild-type *ccaRp* allele exhibited high levels of positional entropy, denoted by green and blue colours for each nucleotide in **Fig. 7.12A**. The presence of M1 in *ccaRp*-M1 has minimal effect on the overall positional entropy of the *ccaR* promotor but does slightly impact the structure of one of the hairpins formed by the promotor structure (**Fig 7.12B**). Conversely, the presence of M2 in the *ccaR* promotor has a significant impact on overall positional entropy, with the mutation substantially reducing overall positional entropy (**Fig 7.12C**). This reduced positional entropy results in a more ordered nucleotide arrangement, leading to increased structural stability of the 5`UTR region. A similar improvement to promotor stability was detected in the combined mutation *ccaRp*-M1M2, which also retained the impact to the hairpins affected by the M1 mutation (**Fig 7.12D**). Stability improvements and conformational changes induced by the presence of M1 and M2 in the *ccaR* promotor together is likely responsible for the improved translational output detected in the presence of the *ccaRp*-M1 and *ccaRp*-M1M2 over the wild-type *ccaR* promotor. These changes to *ccaRp* 5`-UTR conformationn may increase structural consistency and improve ribosome access of the mRNA (Garcia-Martin and Clote, 2015, Cholewa and Placzek, 2020).

These data based on the Broccoli/mCherry reporter system and the computational assessment of the *ccaR* promotor provide mechanistic support for the data presented by GSK in the patent (**Fig 7.13**) that shows *ccaRp*-M2 in particular has a positive impact on CA titre in *S. clavuligerus* SC2 (an early production strain). Results from a time-course experiment of CA

titre profiles in *S. clavuligerus* SC2 containing *ccaRp* mutations M1, M2, as well as a third mutation M3 (which affects the coding sequence of the *ccaR* gene) highlights that *ccaRp*-M1 and *ccaR*-M3 alone have minimal impact on CA yield (**Fig. 7.13**). This small improvement to CA production is also seen in the combined M1+M3 strain. The presence of the mutations *ccaRp*-M2 and *ccaRp*-M1M2M3 consistently result in improved CA production in *S. clavuligerus* SC6 (**Fig 7.13)**. The improved translational efficiency seen in *ccaRp*-M2 and *ccaRp*-M1M2 can be attributed to the improved 5`UTR stability, identified through reduced overall positional entropy and increased reporter activity.

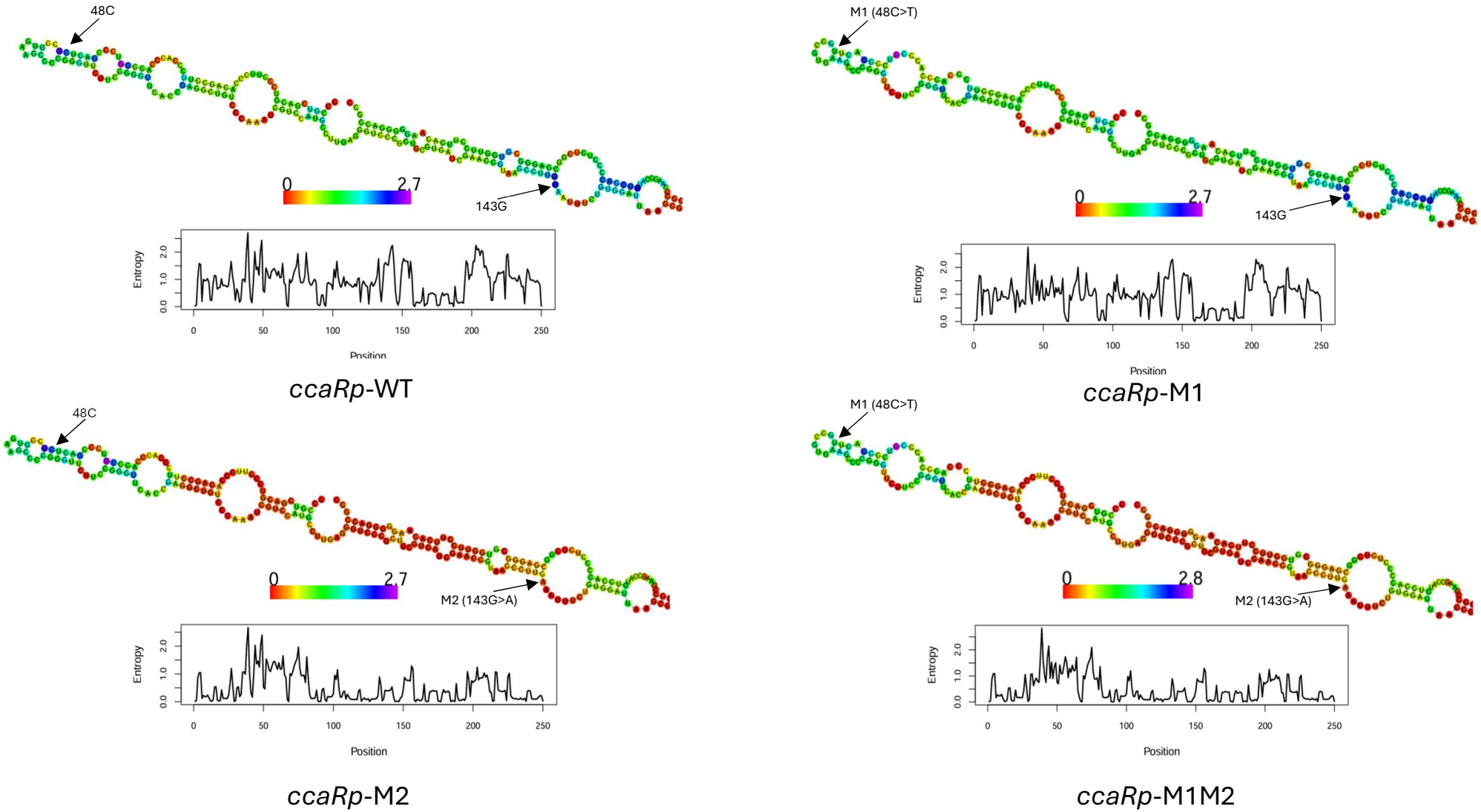

Figure 7.12: Promotor structures of *S. clavuligerus ccaRp* and mutated variations. Structures and graphs were generated through the University of Vienna RNAfold WebServer (Gruber *et al,* 2008). Positional entropy is denoted with different colours; red depicts the lowest, while purple represents the highest positional entropy. Graphs represent positional entropy at each nucleotide position.

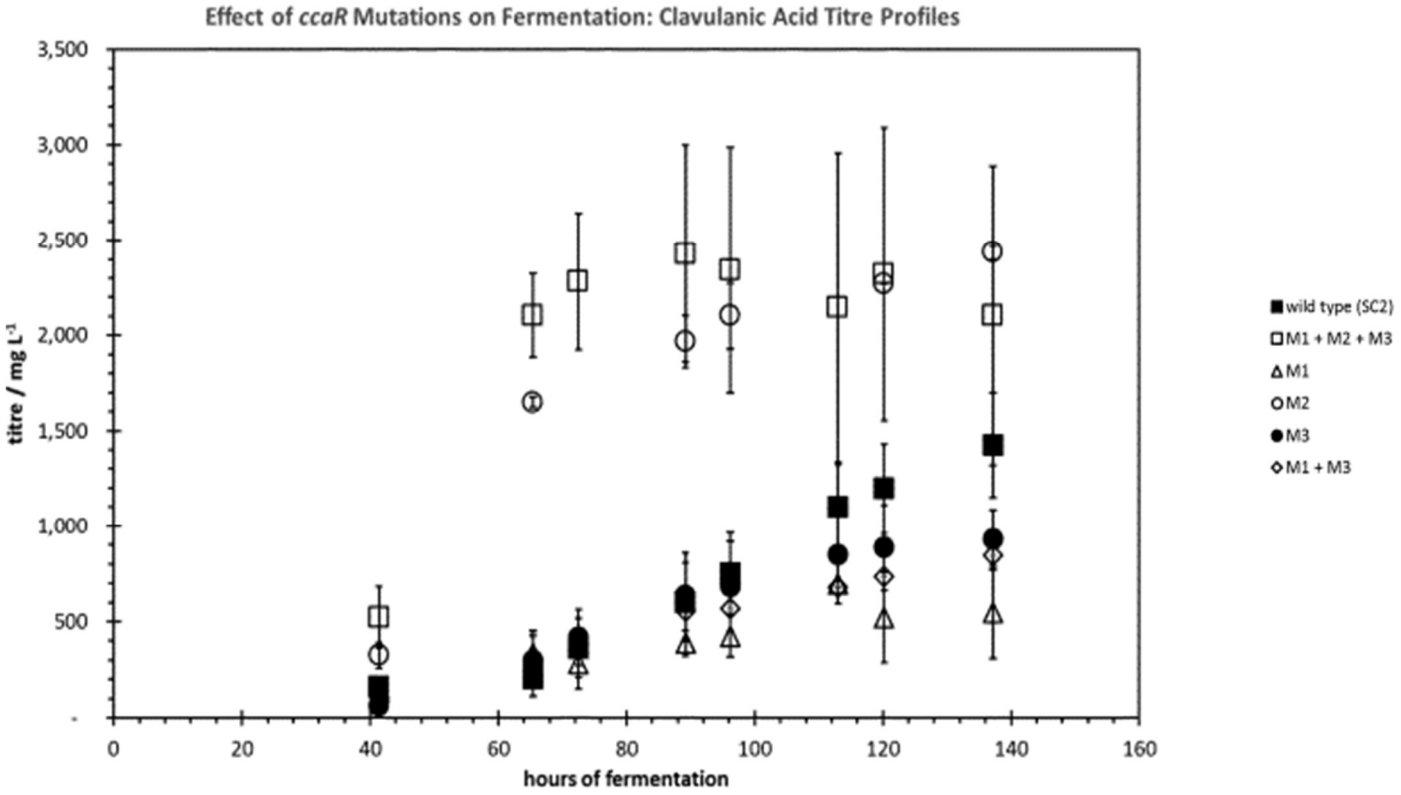

Figure 7.13: Impact of *ccaR* promotor region mutations on CA titre in *S. clavuligerus* SC2 (Adapted from GlaxoSmithKline, 2021). Following pre-culture for 52 hours, 3% volume was inoculated into 2L micro-fermenters. At each time point, 1.5mL aliquots were centrifuged, diluted into COBAS cups and ran on a MIRA S PLUS auto analyser to determine CA concentration. Assay was performed in duplicate (N=2). Data points represent mean values with standard deviation error bars.

7.4 Summary

The functionality of the Broccomyces dual reporter system was explored in *Streptomyces clavuligerus and* as a means to investigating utility as a reporter for 5`-UTR stability. This was done by creating new constructs with the *ccaR* promotor as the promotor of choice, along with variations of the *ccaR* promotor with mutations previously documented to improve CA production in *Streptomyces clavuligerus* (GSK, 2021). While the Broccoli signal was not strong enough to visualise mRNA localisation and abundance, the system is useful as a reporter for 5`UTR stability. Visualisation of TTA-mCherry in Broccomyces-*ccaRp* M2 and Broccomyces-*ccaRp* M1M2 was substantially greater than what was seen in the wild-type *ccaRp* reporter, indicating those mutations may have a positive effect on translational efficiency. This finding was confirmed quantitatively through the Broccomyces reporter fluorescence assay, with relative TTA-mCherry fluorescence for Broccomyces-*ccaRp* M2 and Broccomyces-*ccaRp* M1M2 being consistently higher than its *ccaRp*-WT and *ccaRp*-M1 counterparts. With prolonged incubation, relative fluorescence in the Broccomyces-*ccaRp* M1M2 double mutant exceeded that of the single *ccaRp* M2 mutant, indicating the two mutations may have a synergistic effect on translational output. Analysis of the mRNA structure of the *ccaRp* promotors highlights that the presence of the M2 mutation improves promotor stability, with the double mutant (*ccaRp* M1M2) retaining this improved stability, as well as retaining the impact that M1 has on the hairpin loops in the structure near the M1 mutation site.

These data, combined with data produced by GSK which highlights regarding 5`-UTR mutations having a positive effect on CA titres, indicates that the TTA-mCherry reporter can be used to read out on translational efficiency relating to 5`-UTR function and stability.

8. Discussion

There is an urgent requirement for novel strategies to combat bacterial infections, by either the discovery of new antimicrobial products or the enhanced production of existing molecules. One way to increase production of existing antimicrobials is to gain a deeper understanding of the regulatory mechanisms that underpin their production. Translational control of antimicrobial-producing biosynthetic gene clusters in *Streptomyces* has generally been considered to be under the control of the rare leucine tRNA *bldA* (Liu *et al*, 2013). To fully elucidate the mechanisms of control, new methodologies are required, both for identifying new antimicrobial agents, or methods to investigate how antimicrobials may be regulated, and metabolite yields can be improved. To achieve this, new tools are required to investigate the effects of strain engineering to improve regulation of antimicrobial biosynthetic pathways and consequently, increase yield.

The overall aims of this thesis was two-fold. First was the creation of the Broccomyces system as a promoter-dependant transcriptional and translational reporter, a resource previously unused to *Streptomyces* and other Actinomycetota. By doing this, this raised questions around the accepted literature dogma on *bldA.* These data (as seen in **Chapter 3** and **Chapter 4**) led to an investigation into the biological role of the *bldA* tRNA (Leu-TTA) in *S. coelicolor*, which was the second aim of this thesis. By expanding the understanding of the function and impact of the Leu-tRNA^{BldA}, the impact of *bldA* deletion on primary metabolite utilisation, secondary metabolite production, and transcriptome was investigated.

8.1 The Broccomyces system is a valid translational reporter in *Streptomyces* species.

There is an ever-increasing need for new antimicrobials and techniques to validate and quantify antimicrobial production. With the *Streptomyces* genus accounting for 80% of todays antibiotics, it is a prime target for the design of assays focused on optimising specialised

metabolite output (Watve *et al*, 2001., Procópio *et al*, 2012). To accomplish this quantification of the transcriptional and translational output of genes under the control of specific promoters is required to enable precise monitoring of biosynthetic gene cluster activation, understanding of regulatory mechanisms to facilitate rational engineering of strains for improved metabolite yields

The Broccomyces dual-reporter system was designed and tested using the *bldA* translational control system in *Streptomyces* (see **Chapter 3**). While both aspects of the Broccomyces dual-reporter could be visualized in a qualitative assay, attempts to optimise the Broccoli-based transcriptional reporter in the quantitative assay format were unsuccessful, as no signal was detectable above background levels in liquid cultures. Actinomycetes and *Streptomyces* are GC-rich, spore-forming, Gram-positive bacteria, in which the functionality of the Broccoli aptamer has not been tested in previous literature, with Broccoli aptamer utilisation previously limited to Gram-negative bacteria and mammalian culture (Climent-Catala *et al,* 2023., Chen *et al,* 2025., Filonov and Jaffery, 2016., van der Sijs *et al*, 2024). Recent studies have begun to explore the functionality of the Broccoli aptamer in Gram-positive bacteria; however, instances of this work are minimal compared to Broccoli utilisation in the previously mentioned systems (Bychenko *et al,* 2020., Squire *et al*, 2023).

The inability to visualize Broccoli-based fluorescence in *Streptomyces* liquid culture may be due to multiple factors, including poor Broccoli mRNA stability, the possibility that secondary structures in high-GC transcripts hinder proper folding or ligand binding of the Broccoli aptamer, or that the differences between *Streptomyces* solid and liquid cultures (ie: the lack of sporulation) result in an inability to detect Broccoli-based fluorescence in liquid culture (Litke and Jaffrey, 2019., Hou and Jaffrey, 2023., Yagüe *et al*, 2014., Filonov *et al*, 2015). This hypothesis could explain why the Broccoli aptamer has mainly been shown to function in moderate GC containing organisms such as *E. coli* and *A. baumannii*, as well as mammalian cultures (Filonov *et al,* 2014, Filonov and Jaffery, 2016, Okuda *et al,* 2016, Han *et al*, 2025). An alternative hypothesis for this inability to visualise Broccoli fluorescence in *Streptomyces*

liquid culture is through not capturing the correct time-points for maximum expression. While time-course experiments were completed during Broccoli fluorescence optimisation, it is possible the maximum expression threshold is transient in cultures, with RNA recycling and degradation not well studied in *Streptomyces* (Pepler *et al*, 2025). Future experiments would include completion of Broccomyces-based fluorescence assays between 24- and 36 hours, at every two-hour interval between this time. A further possibility is reduced function of the Broccoli aptamer within the Broccomyces dual-reporter over time, either through the accumulation of mutations in the orthogonal aptamer, or with functionality decreasing between spore stock freeze-thaw cycles (Shepard *et al*, 2010). This possibility could be confirmed through sequencing of plasmids from frequently utilized spore stocks. This could be solved through potential reconjugation of Broccomyces plasmids regularly to ensure no loss of function.

Potential future experiments to improve Broccoli-based output in *Streptomyces* include the testing for Broccoli fluorescence in cell-free conditions; through lysis of *Streptomyces* bacteria expressing the Broccoli aptamer and the addition of DFHBI-1T to the lysate. Alternative aptamer systems could also be pursued; while aptamers such as Mango may function as a single reporter system, its utilisation in Broccomyces is not recommended due to its spectra overlap with mCherry (Bychenko *et al*, 2023). The Pepper aptamer, on the other hand, boasts the advantage of binding to a variety of benzylidene-cyanophenyl (HBC) derivatives, each of which providing different excitation/emission spectra, dependant on the ligand utilized (Rees *et al*, 2022). Using the Pepper aptamer in place of Broccoli, particularly if utilising a HBC ligand that fluoresces cyan (to better distinguish between transcriptional and translational output), may rectify the issues previously seen with the Broccomyces transcriptional reporter.

Conversely, the TTA-mCherry translational reporter consistently showed clear expression, both under qualitative and quantitative assays. The translational output of TTA-mCherry also varies based on Leu-tRNA^{BldA} expression, with TTA-mCherry expression muted in the *bldA*-deficient *S. coelicolor* J1700 background (Merrick, 1976; **Chapter 4**). Partial detection of TTA-

mCherry fluorescence in *S. coelicolor* J1700 may be contributable to modifications of tRNAs that allow for mistranslation, such as Wobble-Base Pairing (WBP) or modifications to the tRNA core region (Bednářová *et al,* 2017., Yared *et al*, 2024). Previous studies have shown that the Leu-tRNA^{CAA} may be able to suppress the *bldA* phenotype, likely through mistranslation of TTA codons through WBP (Fan *et al,* 2019., Petterson and Kirsebom, 2011., Trepanier *et al*, 2002). Utilisation of the TTA-mCherry translational reporter was also shown in a *bldD*-deficient strain, resulting in increased TTA-mCherry output, likely due to unregulated expression of the *bldA* tRNA in the absence of the BldD regulator (Tschowri *et al,* 2014., Bush *et al*, 2017). The robustness of the TTA-mCherry translational reporter highlights a key biological advantage by providing insight into not only successful protein synthesis and stability but also serves as a tool for quantification of promotor-dependent translation. This translational reporter system is also able to provide insights into promoter strengths at various stages of the *Streptomyces* life cycle, which will enable future investigation into translation of BGC expression, allowing for more detailed observation of specialized metabolite production in *Streptomyces* species (Lee *et al*, 2019). Following confirmation of the functionality of the TTA-mCherry translational reporter in *bldA*- and *bldD*- deficient backgrounds (Merrick, 1976), the possibility of utilizing the TTA-mCherry translation reporter as a screen for increased specialised metabolite yield through promotor mutations was investigated (Barriscale *et al*, 2014., Jaganathan *et al*, 2025., Yus *et al*, 2017).

8.2 The Broccomyces translational reporter can be influenced by promotor and 5` UTR mutations.

Following use of the Broccomyces reporter system in *S. coelicolor* backgrounds (**Chapter 3, Chapter 4**), its functionality in other *Streptomyces* species was investigated. Broccomyces use in *S. clavuligerus* was investigated due its importance as a producer of β-lactam antibiotics, including clavulanic acid (CA) (López-Agudelo *et al*, 2021, Shin *et al*, 2021;

Chapter 7). Previously published data highlighted that mutations made to the *ccaR* promoter resulted in improved CA yield (GSK, 2021., Cazier and Blazeck, 2021), leading to the hypothesis that the TTA-mCherry reporter may be influenced by promoter mutations, allowing it to be used as a comparative tool between mutations in 5′-UTR regions and metabolite yield. Two previously documented mutations were investigated (*ccaRp*-M1 and *ccaRp*-M2) along with a double mutant previously shown to result in increased CA production (GSK, 2021). Both fluorescence microscopy and the Broccomyces high-throughput assay indicated that the mutations *ccaRp*-M2 and *ccaRp*-M1M2 resulted in increased TTA-mCherry production, which reinforces data from GSK that these mutations increase CA production (**Fig. 7.7, Fig. 7.8, Fig. 7.9**). Furthermore, the effects these mutations had on promoter structure were investigated, with *ccaRp*-M2 resulting in universally reduced positional entropy, increasing the overall stability of the promoter (Garcia-Martin and Clote, 2015; **Fig 7.11**). The *ccaR*-M1 mutation was shown to introduce a small hairpin structure in the promoter sequence (Bikard *et al*, 2010), however this had no effect on improving TTA-mCherry yield, which is consistent with CA yield data previously reported (GSK, 2021; **Fig. 7.13**), however hairpin loops have been shown previously to impact translation, both positively and negatively, dependant on the location in the 5`-UTR (Georgakopoulos-Soares *et al*, 2022). Additionally, the formation of the *ccaRp*-M1 hairpin early in the UTR sequence may also impact attenuation through interference of hairpin formations required for transcription termination (Yanofsky, 1981., Henkin and Yanofsky, 2002). This may explain why *ccaRp*-M1M2 exhibits a synergistic effect on improved translational output compared to *ccaRp*-M2 alone, especially after substantial incubation (**Fig 7.9**). Comparison of these data to the preliminary results by GSK indicates that these mutations affect either the structure of stability of the *ccaR* promoter, resulting in the increase of CA production, and this effect can be measured in the form of increased TTA-mCherry fluorescence.

The Broccomyces TTA-mCherry reporter responded in a consistent, repeatable way to each of these promoter mutations, supporting the hypothesis that the system is sensitive to

upstream regulatory effects, and can be used to measure how mutations in 5`-UTRs may influence translation (Pickering and Willis, 2005., Steri *et al*, 2019). This means the system can also be utilized to investigate whether mutations to 5`-UTRs of BGCs influence overall translation and metabolite production (Chen *et al,* 2022., Zhao *et al*, 2019). Aside from this study, previous literature has shown consistently that mutations to 5`-UTR regions can have positive or negative effects on translational output, whether by influencing the availability of ribosome-binding sites (Ray *et al*, 2022), formation of 'standby sites ' to facilitate rapid ribosome positioning (de Smit and van Duin, 2003., Liu *et al*, 2025) or through secondary structure influence (Evfratov *et al*, 2016., Tietze and Lale, 2021). This highlights the potential for the Broccomyces dual-reporter to find use as a tool for the dissection of regulatory elements in BGCs. These data supporting this observation (**Chapter 7**) with potential to use the Broccomyces translational reporter as a baseline for a *Streptomyces* toolkit to measure customized 5`-UTR expression systems, which will prove valuable in optimising 5`-UTRs for specialized metabolite production.

8.3 Undocumented mutations in *S. coelicolor* J1700 led to the creation of a novel isogenic *bldA* deletion strain.

Following confirmation of detectable TTA-mCherry fluorescence in a *bldA*-deficient strain (**Chapter 4**), detailed whole genome sequencing of the strain was performed to elucidate the genetic background of *S. coelicolor* J1700, as well as reveal information on affected genes that give it its genotype (**Chapter 5**). It was hypothesised that a high-quality genome sequence could provide essential information regarding mutations that could be influencing the Broccomyces translational reporter. Therefore, Illumina sequencing technology was used to sequence the genome of *S. coelicolor* J1700, followed by Breseq pipeline analysis, constructed by the Barrick lab, to highlight genome-wide mutations (Deatherage and Barrick, 2014). Analysis of sequencing data highlighted the presence of nearly 300 previously unknown mutations in *S. coelicolor* J1700 when compared to wild-type *S. coelicolor* M145, which has

since been published (Stone *et al*, 2025) (See **Chapter 5**). These data challenge previous assumptions regarding how clean this commonly used *bldA*$^{-}$ strain really is.

Aside from previously understood mutations, including a missense mutation that renders *bldA* ineffective (**Section 5.3.3**), and further characterisation of histidine and uracil auxotrophy markers (**Section 5.3.6 and 5.3.7**), additional mutations were found within BGC intergenic regions and coding sequences, as well as transporter proteins and two-component systems (**Section 5.3.4, Section 5.3.5, Appendix 1**). It was hypothesized the mutations found in the *S. coelicolor* J1700 genome may contribute to deficiencies seen in metabolism and phenotype, which may lead to misinterpreting results previously attributed to the loss of *bldA* alone. In previous literature, RED production has been noted to be minimal and could be attributed to the loss on *bldA* in comparison to *bldA*$^{+}$ strains (Guthrie and Chater, 1990, Guthrie *et al*, 1998). However, the presence of an IS110 element, impacting the intergenic space between SCO5885-SCO5886 (which forms part of the *red* BGC), may also be impacting RED production in *S. coelicolor* J1700 through promotor disruption, providing an alternative explanation for the reduced RED production seen in *S. coelicolor* J1700. Mutations or interference within promoter sequences has previously been shown to improve or reduce ACT production in *S. coelicolor* by Sohoni *et al,* 2014, suggesting this IS110 insertion may be producing a similar effect in the *red* BGC of *S. coelicolor* J1700. Mutations were also detected within various other BGCs responsible for the production of specialized metabolites, including important genes within the *act* and *cda* BGCs (Lewis *et al,* 2019., Taguchi *et al*, 2017), making it difficult to solely ascribe the loss of all secondary metabolite production to the *bldA39* mutation alone. As such, an isogenic Δ*bldA* strain was deemed necessary for further investigation into *bldA* function

The deletion of *bldA* in the *S. coelicolor* M145 background has been attempted in the past using older gene-editing techniques, but previous literature has shown that *bldA* mutants in *S. coelicolor* M145 cannot be easily constructed (Gehring *et al,* 2004, Hesketh *et al*, 2007). Newer gene-editing techniques, such as the CRISPR-Cas system allow for higher precision,

flexibility and the ability to target multiple genes simultaneously, depending on the technique used (Quandt and Hynes, 1993, Tong *et al*, 2020, Xu and Li, 2020). CRISPR-Cas systems possess an advantage over older gene-editing techniques as they enable programmable, site-specific cuts, leading to more efficient gene editing, and have previously been successful in activating silent gene clusters and improving metabolite production (Zhang *et al,* 2017, Kim *et al*, 2025).

The successful deletion of *bldA* in the *S. coelicolor* M145 background using a CRISPR-Cas9 system demonstrates that modern gene-editing tools can overcome the challenges associated with historical mutagenesis methods (Lone *et al,* 2018., Tavakoli *et al*, 2021). Whole genome sequencing of the newly created *S. coelicolor* JWS-Δ*bldA* revealed it possessed only two consistent suppressor mutations, including a mutation in the 50S ribosomal subunit L33, previously characterized as a zinc-dependant ribosomal protein (Owen *et al*, 2007; **Chapter 6**). The cleaner genetic background of *S. coelicolor* JWS-Δ*bldA*, together with its ability to be fully complemented, further suggest many of the phenotypic traits seen with *S. coelicolor* J1700 may be partially attributable to its additional mutations (**Chapter 5**), highlighting the importance of genetic background checks and the utilisation of precise tools for genetic manipulation to confirm genetic impacts attributable to intended mutations.

This also opens new possibilities for understanding regulatory networks, secondary metabolism, and development in *Streptomyces* (Lee *et al,* 2020., McCormick and Flärdh, 2012., van Wezel and McDowall, 2011). CRISPR-mediated deletions can assist in determining gene essentiality and function of putative genes, while reducing the risk of unknown genome changes (Bock *et al*, 2022). This work contributes to the role of CRISPR and newer gene-editing systems in natural product research (Tong *et al*, 2020, Ameruso *et al*, 2022, Lee *et al*, 2024); and data from this project highlights its capabilities in the deletion of important DNA sequences such as *bldA*. In future experiments, CRISPR and similar gene-editing technologies could be used to construct a library of cleaner deletion mutants to supercede the historical strains (Tavakoli *et al*, 2021). The construction of this new line of *Streptomyces*

CRISPR mutants would provide greater insight into investigating gene function in both life cycle and metabolite production, as well as impacts beyond the scope of this project.

8.4 The Leucine tRNA^{CAA} is essential to viable *S. coelicolor* M145.

While utilisation of CRISPR-Cas9 was successful in the deletion of *bldA* from *S. coelicolor* M145, the Leucine-tRNA^{CAA} was not readily deleted in the same manner (**Section 6.3.6**). Over multiple attempts to construct a double-strand break in the Leu-tRNA^{CAA} coding sequence resulted in either only single-stranded breaks or failure to replicate the double-stranded break in all copies of the genome each *Streptomyces coelicolor* cell possessed (Chandra and Chater, 2014., Zhao *et al*, 2020). Sequencing confirmed CRISPR targeting was in the correct location, but a successful knockout could not be generated, indicating complete deletion of the Leu-tRNA^{CAA} is not tolerated and may be lethal, as retention of the wild-type gene band has been previously documented in other species is indicative of essentiality (Zhang and Matlashewski, 2024; **Fig. 6.16, Fig. 6.17**).

Investigations into the Leu-tRNA^{CAA} in previous literature are limited but has been shown previously by Petterson and Kirsebom (2011), to suppress the phenotype seen in other *bldA* mutants, and previous work by Fan and colleagues (2019), highlighted similarities between both the Leu-tRNA^{BldA} and the Leu-tRNA^{CAA}. The work completed by Fan *et al* (2019) also attempted to construct a Leu-tRNA^{CAA} deletion mutant but were also unsuccessful, attributing the inability to construct the deletion mutation down to the higher codon usage of the TTG codon compared to the TTA codon. This finding was also confirmed in this study through codon usage analysis, suggesting its criticality for translation of a large portion of the *S. coelicolor* proteome. Higher TTG usage is likely due to evolutionary optimisation , due to the high GC content of *Streptomyces* genomes (Di Salvo *et al,* 2018., Wright and Bibb, 1992), which would also explain the reason why TTA codons are exceedingly rare by comparison (Leskiw *et al,* 1991., Silov *et al*, 2021). The work performed by Fan and colleagues (2019) also hypothesized

that the Leu-tRNA^{BldA} and the Leu-tRNA^{CAA} had similar functions, which would collaborate with the hypothesis that in the absence of the Leu-tRNA^{BldA}, the Leu-tRNA^{CAA} may mistranslate TTA codons through WBP, further supporting the hypothesis outlined in this thesis, and providing an explanation for the visualisation of TTA-mCherry in a *bldA*-deficient background (**Chapter 4**).

The combination of increased frequency and usage (compared to Leu-tRNA^{BldA}), an inability to maintain the deletion after removal of selective pressure, and confirmation that the right genetic sequence is being targeted reinforce the hypothesis that the Leu-tRNA^{CAA} is essential to *S. coelicolor*. The essentiality of the Leu-tRNA^{CAA}, hypothesized by this study and data from previous literature (Fan *et al*, 2019), poses a barrier for attempts to understand the importance of this tRNA for potential Wobble-Base pairing analysis. While the Leu-tRNA^{CAA} may not be able to be deleted, CRISPR interference (CRISPRi) could be used to examine how repressing expression of the Leu-tRNA^{CAA} affects *S. coelicolor* (Larson *et al*, 2013, Zhang *et al*, 2021). This approach silences gene expression rather than complete gene deletion, by blocking RNA polymerase from initiating transcription (Tong *et al*, 2020), and has been used to investigate silencing of essential genes in both *Streptomyces* and other species in recent studies (Ameruoso *et al*, 2022, Sun *et al*, 2023) and could provide a gateway for new studies and projects to study the effects of reducing expression of *S. coelicolor* genes.

8.5 Removal of the *bldA* encoding sequence results in widespread gene upregulation and diminished metabolite utilization and production.

Deletion of *bldA* in the *S. coelicolor* M145 background impacted nearly every aspect investigated, including phenotype, growth, metabolite production and utilization, but also had a substantial effect on the wider transcriptome (**Chapter 6**). The complete loss of spores and aerial hyphae, as well as minimal specialised metabolite production for both ACT and RED were seen in the absence of *bldA*, indicating the Leu-tRNA^{BldA} is indeed crucial for successful specialised metabolite production in *S. coelicolor*, and corroborates previous literature using

older *bldA*$^{-}$ control strains (Hesketh *et al*, 2007., Merrick, 1976., Takano *et al*, 2003). Successful complementation *of S. coelicolor* JWS-Δ*bldA* emphasizes the important role of TTA-containing regulatory genes in controlling antibiotic biosynthesis and morphological development (Chater, 2006., den Hengst *et al*, 2010, Hackl and Bechthold, 2015). The construction of the *S. coelicolor* JWS-Δ*bldA* will serve as a crucial strain for future investigations into *bldA*, as it allows for more controlled analysis of the specific effects of *bldA* in a commonly utilized background, without excessive suppressor mutations influencing activity (See **Chapter 5**).

The combined specialised metabolite yield quantification in *S. coelicolor* JWS- Δ*bldA* and its complemented counterparts, as well as phenotypic and transcriptomic analysis in *S. coelicolor* JWS-Δ*bldA* provides a multi-dimensional view of *bldA*'s function (see **Chapter 6**). RNA-seq revealed widespread gene upregulation, including in genes that do not possess TTA codons, suggesting that the removal of *bldA* also has indirect regulatory effects, affecting the wider transcriptome, which has been seen previously in other transcriptomic experiments in other *bldA* deletion strains (Hesketh *et al*, 2007). Many upregulated genes belonged to two-component systems (Sánchez de la Nieta *et al*, 2022), antibiotic resistance (Vecchione *et al*, 2009), and a variety of transcriptional regulators, triggered by the disruption caused by the removal of *bldA* (Fink *et al*, 2002, Romero-Rodríguez *et al*, 2015). Hesketh and colleagues in 2007 also demonstrated how the removal of *bldA* affects the wider transcriptome, however their study was performed in *S. coelicolor* M600, a plasmid-free derivative of *S. coelicolor* A3(2) . Comparisons between the Hesketh experiment and data generated as a part of this study reveals that while more genes in total were differentially affected by the removal of *bldA* in *S. coelicolor* JWS-Δ*bldA*, there was noticeable overlap between which genes were affected in both studies, with 11 compared genes being found in both sets of results (**Section 6.3.12**).

While its deletion caused stalled translation of integral TTA-containing regulatory genes (ie., *adpA*, *redZ*, etc) (White and Bibb, 1997, Takano *et al*, 2003), its deletion also appeared to have a minimal effect on transcription in genes found in BGCs, including the *act* BGC, as no

genes within the BGC were transcriptionally affected (Fernández-Moreno *et al*, 1994; **Section 6.3.13, Appendix 4**). This was in contrast to the findings from Hesketh *et al,* (2007), where three of the 22 genes within the *act* BGC were found to be downregulated (SCO5073, SCO5074 and SCO5079), however other research in an *S. clavuligerus ΔbldA* mutant suggests proteins encoded by a TTA codon are still present at regular levels, suggesting the link between *bldA* and TTA dependence may need reinvestigating (Ferguson *et al*, 2016). These data imply a disconnect between transcript levels and protein output, reinforcing that *bldA* has a role as a translational bottleneck (Hackl and Bechthold, 2015). In order to confirm this hypothesis, proteomic analysis of *S. coelicolor* JWS-Δ*bldA* would be required, which could be subsequently compared to the respective transcriptomic analysis to highlight which upregulated genes are also translated more frequently.

The data presented within this thesis represent only the start of possible explorations into complex regulatory networks governed by translational control, and the broader consequences of rare codon usage in development and metabolism in *Streptomyces*. Utilizing *S. coelicolor* JWS-Δ*bldA*, future tests could be performed to assess several factors in regard to the importance of *bldA*. These include assessing if TTA codon usage acts as a temporal regulation mechanism (Leskiw *et al*, 1993., Hesketh *et al*, 2007), through the construction of mutants containing TTA-free variants of TTA-containing key regulators (*adpA*, *redZ*) and using reporter constructs, such as a modified version of Broccomyces, or fluorescent reporters fused to native or altered genes (Kataoka *et al*, 1999, Haiser *et al*, 2008) Additionally, investigations into codon optimisation to bypass *bldA* dependence through substitution with synonymous leucine codons could be tested to assess metabolite production, protein expression, and regulatory behaviour in a Δ*bldA* background, which has been investigated previously in *S. coelicolor* A3(2) (Leskiw *et al*, 1991). These experiments could provide groundwork for industrial research and the optimisation of specialised metabolite production, as dependence on *bldA* expression can limit pathway expression and translation, as seen in this study and previous work (Ferguson *et al,* 2016., Makitrynskyy *et al*, 2013, Ünsaldı *et* al, 2016., White

and Bibb, 1997). Overall, the *S. coelicolor* JWS-Δ*bldA* system presents a new valuable platform and these findings underscore the broader implications of translational control in actinomycete biology.

8.6 Rethinking *bldA* regulation in *Streptomyces*

The traditional model for *bldA* in *Streptomyces* is that it encodes the only tRNA for the rare TTA leucine codon (Li *et al*, 2007, Silov *et al*, 2020), with its expression developmentally regulated (Yan *et al*, 2020) and its importance for morphological differentiation and specialized metabolite production (Hackl and Bechthold, 2015). Previous work has also characterized *bldA* to be tightly controlled at the transcriptional level by global regulators such as BldD (den Hengst *et al*, 2010), leading to regulated translation of TTA-containing genes earlier in the *Streptomyces* lifecycle. However, data presented within this thesis provides fresh insight into *bldA* regulation in *Streptomyces*.

First, the Broccomyces TTA-mCherry translational reporter yielded detectable fluorescence in stages of *S. coelicolor* growth before canonical *bldA* expression is thought to occur (See **Chapter 4**), suggesting either an alternative decoding mechanism exists for TTA codons, such as WBP (Crick, 1966), or basal *bldA* levels may be present early in the *Streptomyces* lifecycle. Additionally, in a *bldD*-deficient background, overall quantitative TTA-mCherry fluorescence was increased compared to *S. coelicolor* M145, indicating BldD does limit *bldA*, and links *bldA* to the *Streptomyces* global regulatory network, which has been previously documented (Bush *et al,* 2013., Zacharia *et al*, 2021; **Fig. 4.7**). Next, while the novel isogenic *bldA* deletion strain does reproduce the expected phenotype, overexpression of the Leu-tRNA^{CAA} partially rescues the sporulation-deficient phenotype, implying leucine codon plasticity in *Streptomyces* and questioning the absolute dependence on *bldA* for translation of TTA codons (Rokytskyy *et al*, 2016; **Fig. 6.19, Fig. 6.20, Fig. 6.21**). Full *bldA* complementation restored the WT phenotype to *S. coelicolor* JWS-Δ*bldA*, but not in the historical *S. coelicolor* J1700 strain (**Fig. 6.5, Fig.**

6.19), indicating that background mutations are able to influence the regulatory role of *bldA* (see **Chapter 5**). Finally, transcriptomic analysis and primary metabolite utilisation in *S. coelicolor* JWS-Δ*bldA* suggested that the influence of *bldA* extends further than development and specialized metabolite production as global metabolism and transcriptional networks were shown to be deeply affected by its absence (**Section 6.3.11, Section 6.3.12, Section 6.3.13**).

These data argue against the existing model of *bldA*, where its tightly regulated presence is necessary for any TTA codon translation (Tschowri, 2016). The combination of fluorescent reporter data, phenotypic characterisation of the complemented isogenic Δ*bldA* strain and analysis of carbon/nitrogen utilisation and transcriptomic data give rise to a proposal for a new model of *bldA* regulation. This new hypothesis views *bldA* not as transcriptionally repressed tRNA that acts as a bottleneck for effective TTA codon translation, but as a multi-input integrator of developmental, metabolic and translational signals, with its presence influenced by not only developmental control (ie BldD regulation), but also the metabolic state and genetic background of *Streptomyces*. This model also suggests the presence of a potential early basal supply of the Leu-tRNA^{UAA} which is later amplified after conditions are met (ie BldD derepression, developmental cues and metabolic activity) (Higo *et al*, 2011., Zacharia *et al*, 2021). This hypothesis also suggests *bldA* has a function during metabolic sensing and developmental progression as the loss of *bldA* has been shown to alter global transcription and nutrient utilization. To sustain this hypothesis, future work is required to confirm the presence of the proposed basal level of *bldA,* which could be achieved through tRNA-seq or Ribo-seq at early lifecycle stages (Kim *et al*, 2020). This proposed model reconceptualizes *bldA* as a central node co-ordinating translation, development, and general metabolism, as opposed to a developmental checkpoint. This proposed model also explains why deletion of *bldA* affects more than just genes containing TTA codons

9. Conclusions and Future Work.

The work within this thesis contributes to the wider issue of AMR, as the creation and implementation of a translational reporter that produces quantifiable outputs based on promotor-driven transcription and translation provides more information on antibiotic regulation in *Streptomyces* species. This also allows for translational control in new strains to be understood much faster. This thesis also advances understanding of *bldA* in *S. coelicolor*, both through whole genome sequencing to identify previously undocumented mutations in a historical *bldA*-deficient strain, as well as the creation and characterisation of *S. coelicolor* JWS-Δ*bldA* mutant, which allows for further investigations into the impact of the removal of *bldA* within minimal suppressor mutations.

The central aim of this work was the construction of a dual-reporter system for the quantification of transcriptional and translational output in *Streptomyces* strain, a system which, if successfully implemented, would provide functional insight into TTA codon regulation and become a versatile instrument for investigating gene expression in relation to natural product biosynthesis in *Streptomyces*. This objective was partially met through the validation of the TTA-mCherry translational reporter, however the Broccoli-based transcriptional reporter failed to produce measurable signal in a quantitative assay format, leaving only the TTA-mCherry translational reporter functional. Therefore, the Broccomyces system, in its current form functions reliably only as a translational reporter system in liquid media, which has been robustly confirmed through TTA-mCherry fluorescence quantification in leucine-tRNA^{BldA} abundant and deficient strains, as well as exploring the influence of promotor mutations on translational output through comparison between quantifiable translational output via plate assay and historical clavulanic acid titres (GlaxoSmithKline, 2021). These results underpin the importance of translational regulation, particularly through codon usage and promotor structure, in *Streptomyces* gene expression.

Expansion of the Broccomyces reporter system to improve the transcriptional reporter aspect should be prioritized to increase the functionality of the Broccomyces system to its original intended purpose. The functionality of the Broccoli aptamer in a GC-rich Gram-positive background appears limited, potentially due to the high-GC environment disrupting aptamer folding. Tests involving an *in vitro* environment as opposed to *in vivo* testing may confirm this hypothesis. Alternatively, an entirely different aptamer could be used in place of Broccoli. Aptamers such as Mango or Corn, which use red-shifted fluorophores, should be omitted from testing due to their higher excitation and emission spectra, which may interfere with measurements for the TTA-mCherry translational reporter, however utilisation of TO1-Biotin as a fluorophore, which when bound to Mango emits a 505/535nm spectra, could potentially find use (Dolgosheina *et al*, 2014, Song *et al,* 2018). Alternatively, Pepper fluorescent RNAs are brighter and more stable than the Broccoli aptamer and possess the added benefit of binding to (4-((2-hydroxyethyl)(methyl)amino)-benzylidene)-cyanophenylacetonitrile (HBC) fluorophore analogs (Chen *et al*, 2019, Chen *et al*, 2023). Dependant on the analog used, the Pepper-HBC complex allows for multi-colour imaging, ranging from cyan to orange fluorescence. Utilising the Pepper-HBC combination that yields blue-shifted fluorescence may cause fluorescence that is detectable above background levels in *Streptomyces* strains when utilized in liquid media.

This work also provides a framework for further investigation into *bldA*. Whole genome sequencing, seen in **Chapter 5**, highlights the presence of nearly 300 previously unidentified mutations in *S. coelicolor* J1700, many of which have not been studied in-depth, including mutations within BGC. These mutations make it unclear whether the abolishment of *bldA* is solely contributable to diminished specialized metabolite production in *S. coelicolor* J1700 and are worth further investigation by inducing the same mutations in a clean, genetic background. It was the discovery of these mutations and an inability to rescue the *bldA* phenotype through complementation that led to the creation of the novel *S. coelicolor* JWS-Δ*bldA* mutant, which possesses far fewer suppressor mutations compared to *S. coelicolor* J1700. The construction

of this mutant opens up new possibilities for investigating the importance of *bldA* in the most commonly utilized *S. coelicolor* genetic background (Gehring *et al*, 2004, Hesketh *et al*, 2007). Complementation experiments have shown this deletion mutant can be fully complemented; while the impact of the deletion of *bldA* on primary metabolite utilization, secondary metabolite production and effects on the transcriptomic level have all been investigated. The successful removal of the *bldA* tRNA poses many wider questions on the importance of *bldA*, including how its removal may impact the proteome or metabolome, as it has been shown both in this study and previous literature to impact both primary and secondary metabolism (Leskiw *et al,* 1993, Kim *et al,* 2005, Bibb, 2005, Schlimpert and Elliot, 2023). Additionally, ribosome profiling could be utilized to measure the impact of *bldA* deletion on translational efficiency, which could be useful in confirming if gene upregulation or Wobble-Base pairing is able to partially compensate for the loss of *bldA*. However, due to resource costs and the large amount of work required to process this data, it likely falls outside the remaining scope of this project.

In summary, this thesis addresses two main aspects for *Streptomyces*: the construction of a functioning translational reporter that can be influenced by the availability of the rare TTA codon, and the impact of *bldA* deletion from *S. coelicolor* M145 on physiological, metabolic and genetic levels. This body of work provides a basis for future optimisation of the Broccomyces system, a basis for new reporter systems in *Streptomyces*, and further develops our current understanding of the importance of the rare TTA-codon in *Streptomyces.*

Chapter 10: References

Abramson J., Adler J., Dunger J., Evans R., Green T., Pritzel A., Ronneberger O., Willmore L., Ballard AJ., Bambrick J., Bodenstein SW., Evans DA., Hung CC., O'Neill M., Reiman D., Tunyasuvunakool K., Wu Z., Zemgulyté A., Arvaniti E., Beattie C., Bertolli O., Bridgland A *et al* (2024). Accurate structure prediction of biomolecular interactions with AlphaFold 3. *Nature*. 630: 493-500.

AbuSara NF., Piercey BM., Moore MA., Shaikh AA., Nothias LF., Srivastava SK., Cruz-Morales P., Dorrestein PC., Barona-Gómez F and Tahlan K (2019). Comparative Genomics and Metabolomics Analyses of Clavulanic Acid-Producing *Streptomyces* Species Provides Insight Into Specialized Metabolism. *Front Microbiol*. 10:2550.

Ageely, E, A., Kartje, Z, J., Rohilla, K, J., Barkau, C, L., and Gagnon, K, T (2016). Quadruplex-flanking stem structures modulate the stability and metal ion preference of RNA mimics of GFP. *ACS Chem Biol*. 11:2398-2406.

Agris PF (2004). Decoding the genome: a modified view. *Nucleic Acids Res*. 32(1):223-38.

Aigle B and Corre C (2012). Chapter Seventeen - Waking up *Streptomyces* Secondary Metabolism by Constitutive Expression of Activators or Genetic Disruption of Repressors. *Methods in Enzymology*. 517: 343-366

Alam K., Mazumder A., Sikdar S., Zhao YM., Hao J., Song C., Wang Y., Sarkar R., Islam S., Zhang Y and Li A (2022). *Streptomyces*: The biofactory of secondary metabolites. *Frontiers in Microbiology*. 13:968053

Alam, K, K., Tawiah, K, D., Lichte, M, F., Porciani, D., and Burke, D, H (2017). A Fluorescent Split Aptamer for Visualizing RNA-RNA Assembly *In Vivo*. *ACS Synth Biol.* 6(9): 1710-1721.

Alduina R and Gallo G (2012). Artificial Chromosomes to Explore and to Exploit Biosynthetic Capabilities of Actinomycetes. *J Biomed Biotechnol.* 2012:462049

Ameruoso A., Kcam MCV., Cohen KP and Chappell J (2022). Activating natural product synthesis using CRISPR interference and activation systems in *Streptomyces*. 50(13): 7751-7760.

Aminov, R, I (2009). The role of antibiotics and antibiotic resistance in nature. *Environmental Microbiology*. 11(12): 2970-2988.

Anderson, A, S., and Wellington, E, M, H (2001). The taxonomy of *Streptomyces* and related genera. *International Journal of Systematic and Evolutionary Microbiology*. 51: 797-814.

Arnold TE., Yu J and Belasco JG (1998). mRNA stabilization by the ompA 5` untranslated region: two protective elements hinder distinct pathways for mRNA degradation. *RNA*. 4(3):319-30

Arora, A., Sunbul, M., and Jaschke, A (2015). Dual-colour imaging of RNAs using quencher and fluorophore-binding aptamers. *Nucleic Acid Research*. 43:e144.

Ausländer, S., Fuchs, D., Hürlemann, S., Ausländer, D and Fussenegger M (2016). Engineering a ribozyme cleavage-induced fluorescent aptamer complementation assay. *Nucleic Acid Research*. 44(10): e94.

Ausmees, N., Wahlstedt, H., Bagchi, S., Elliot, M.A., Buttner, M.J. and Flardh, K. (2007) SmeA, a small membrane protein with multiple functions in *Streptomyces* sporulation including targeting of a SpoIIIE/FtsK-like protein to cell division septa. *Molecular Microbiology*, 65, 1458–1473.

Avramova MM., Stevensen CEM., Chandra G., Holmes NA., Bush MJ., Findley KC and Buttner MJ (2023). Global Effects of the Developmental Regulator BldB in *Streptomyces venezuelae*. *Journal of Bacteriology*. 205(6): e00135-23.

Banerjee A., Sammarco MC., Ditch S., Wang J and Grabczyk E (2009). A Novel Tandem Reporter Quantifies RNA Polymerase II Termination in Mammalian Cells. *PLOS One*. 4(7): e6193.

Barbosa JARG, Sivaraman J, Li Y, Larocque R, Matte A *et al* (2002) Mechanism of action and NAD+-binding mode revealed by the crystal structure of L-histidinol dehydrogenase. *Proc Natl Acad Sci USA*; 99:1859–1864

Barka EA, Vatsa P, Sanchez L, Gaveau-Vaillant N, Jacquard C, Meier-Kolthoff JP, Klenk HP, Clément C, Ouhdouch Y and van Wezel GP (2015). Taxonomy, Physiology, and Natural Products of *Actinobacteria*. *Microbiol Mol Biol Rev*. 80(1):1-43.

Baggaley, K., Brown, A, G., and Schofield, C, J (1997). Chemistry and Biosynthesis of Clavulanic Acid and Other Clavams. *Natural Product Reports*. 14(4): 309-333.

Baggett NE, Zhang Y and Gross CA (2017). Global analysis of translation termination in *E. coli. PLoS Genet*. 13(3):e1006676.

Barriscale KA., O'Sullivan SA and McCarthy TV (2014). A single secreted luciferase-based gene reporter assay. *Analytical Biochemistry*. 453: 44-49.

Becher, P, G., Verschut, V., Bibb, M, J., Bush, M, J., Molnár, B, P., Barane, E., Al-Bassam, M, M., Chandra, G., Song, L., Challis, G, L., Buttner, M, J., and Flärdh, K (2020). Developmentally regulated volatiles geosmin and 2-methylisoborneol attract a soil arthropod to *Streptomyces* bacteria promoting spore dispersal. *Nature Microbiology*. 5(6):821-829.

Bednářová A., Hanna M., Durham I., VanCleave T., England A., Chaudhuri A and Krishnan N (2017). Lost in Translation: Defects in Transfer RNA Modifications and Neurological Disorders. *Front. Mol. Neurosci*. 10: 135

Bednarz B., Millan-Oropeza A., Kotowska M., Świat M., Quispe Haro JJ., Henry C and Pawlik K (2021). Coelimycin Synthesis Activatory Proteins Are Key Regulators of Specialized Metabolism and Precursor Flux in *Streptomyces coelicolor* A3(2). *Front Microbiol.* 12:616050.

Belasco JG., Nilsson G., von Gabain A and Cohen SN (1986). The stability of *E. coli* gene transcripts is dependent on determinants localized to specific mRNA segments. *Cell.* 46(2): P245-251

Bennett JA., Kandell GV., Kirk SG and McCormick JR (2018). Visual and Microscopic Evaluation of *Streptomyces* Developmental Mutants. *J. Vis. Exp*. 139: e57373

Bentley, S, D., Brown, S., Murphy, L, D., Harris, D, E., Quail, M, A., Parkhill, J., Barrell, B, G., McCormick, J, R., Santamaria, R, I., and Losick, R (2004). SCP1, a 356 023 bp linear plasmid adapted to the ecology and developmental biology of its host, *Streptomyces coelicolor* A3(2). *Molecular Microbiology*. 51(6): 1615–1628.

Bentley SD, Chater KF, Cerdeño-Tárraga AM, Challis GL, Thomson NR, James KD, Harris DE, Quail MA, Kieser H, Harper D, Bateman A, Brown S, Chandra G, Chen CW, Collins M, Cronin A, Fraser A, Goble A, Hidalgo J, Hornsby T, Howarth S, Huang CH, Kieser T, Larke L, Murphy L, Oliver K, O'Neil S, Rabbinowitsch E, Rajandream MA, Rutherford K, Rutter S, Seeger K, Saunders D, Sharp S, Squares R, Squares S, Taylor K, Warren T, Wietzorrek A, Woodward J, Barrell BG, Parkhill J and Hopwood DA (2002). Complete genome sequence of the model actinomycete S*treptomyces coelicolor* A3(2). *Nature*. 417(6885):141-7.

Berdy, J (2005). Bioactive microbial metabolites. *J Antibiot (Tokyo.).* 58: 1–26.

Berg MD and Brandl CJ (2020). Transfer RNAs: diversity in form and function. *RNA Biol*. 18(3):316-339.

Bertani, G. (1951) Studies on lysogenesis I.: the mode of phage liberation by lysogenic *Escherichia coli*. *Journal of Bacteriology*. 62(3): 293.

Bervoets I and Charlier D (2019). Diversity, versatility and complexity of bacterial gene regulation mechanisms: opportunities and drawbacks for applications in synthetic biology. *FEMS Microbiol Rev.* 43(3): 304-339.

Bhatti AA., Haq S and Bhat RA (2017). Actinomycetes benefaction role in soil and plant health. *Microbial Pathogenesis*. 111: 458-467.

Bibb, M, J (2005). Regulation of secondary metabolism in Streptomycetes. *Current Opinion in Microbiology*. 8(2): 208–215

Bibb MJ, Domonkos A, Chandra G and Buttner MJ (2012). Expression of the chaplin and rodlin hydrophobic sheath proteins in *Streptomyces venezuelae* is controlled by σ(BldN) and a cognate anti-sigma factor, RsbN. *Mol Microbiol*. 84(6):1033-49.

Bibb MJ., Janssen GR and Ward JM (1985). Cloning and analysis of the promoter region of the erythromycin resistance gene (*ermE*) of *Streptomyces erythraeus*. *Gene*. 38(1-3): 215-226.

Bibb, M, J., Molle, V., and Buttner M, J (2000). σ^{BldN}, an Extracytoplasmic Function RNA Polymerase Sigma Factor Required for Aerial Mycelium Formation in *Streptomyces coelicolor* A3(2). *Journal of Bacteriology*. 182(16): 4606-4616.

Biermann M., Logan R., O'Brien K., Seno ET., Rao RN and Schoner BE (1992). Plasmid cloning vectors for the conjugal transfer of DNA from *Escherichia coli* to *Streptomyces* spp. *Gene*. 116: 43-49.

Bikard D., Loot C., Baharoglu Z and Mazel D (2010). Folded DNA in Action: Hairpin Formation and Biological Functions in Prokaryotes. *Microbiol Mol Biol Rev*. 74(4): 570-588.

Bishop A, Fielding S, Dyson P, Herron P (2004). Systematic insertional mutagenesis of a streptomycete genome: a link between osmoadaptation and antibiotic production. *Genome Res*. 14(5):893-900.

Blin K., Pedersen LE., Weber T and Lee SY (2016). CRISPy-web: An online resource to design sgRNAs for CRISPR applications. *Synthetic and Systems Biotechnology*. 1(2): 118-121

Blin K., Shaw S., Augustijn HE., Reitz ZL., Biermann F., Alanjary M., Fetter A., Terlouw BR., Metcalf WW., Helrich EJN., van Wezel GP., Medema MH and Weber T (2023). antiSMASH 7.0: new and improved predictions for detection, regulation, chemical structures and visualisation. *Nucleic Acids Research.* 51(W1): W46-W50.

BioLog (2025). https://www.biolog.com/lab-services/. Accessed on 18/06/2025.

BioRender (2025). https://biorender.com. Accessed on 21/08/2025

Bock C., Datlinger P., Chardon F., Coelho MA., Dong MB., Lawson KA., Lu T., Maroc L., Norman TM., Song B., Stanley G., Chen S., Garnett M., Li W., Moffat J., Qi LS., Shapiro RS., Shendure J., Weissman JS and Zhuang X (2022). High-content CRISPR screening. *Nat Rev Methods Primers.* 2(1):9.

Boulin T., Etchberger JF and Hobert O (2006). Reporter Gene Fusions. WormBook: The Online Review of *C. elegans* Biology. Pasadena (CA): WormBook; 2005-2018. Available from: https://www.ncbi.nlm.nih.gov/books/NBK19738/

Bralley P, Aseem M and Jones GH (2014). SCO5745, a bifunctional RNase J ortholog, affects antibiotic production in *Streptomyces coelicolor. J Bacterio*l. 196(6):1197-205.

Brennan CK., Ornelas MY., Yao ZW and Prescher JA (2021). Multicomponent Bioluminescence Imaging with Naphthylamino Luciferins. *Chembiochem*. 22(16):2650–2654.

Brown AG., Butterworth D., Cole M., Hanscomb G., Hood JD., Reading C and Rolinson GN (1976). NATURALLY-OCCURRING β-LACTAMASE INHIBITORS WITH ANTIBACTERIAL ACTIVITY. *The Journal of Antibiotics*. 29(6): 668-669

Bucca G, Pothi R, Hesketh A, Möller-Levet C, Hodgson DA, Laing EE, Stewart GR and Smith CP (2018). Translational control plays an important role in the adaptive heat-shock response of *Streptomyces coelicolor*. *Nucleic Acids Res*. 46(11):5692-5703.

Bum Kim H., Smith CP., Micklefield J and Mavituna F (2004). Metabolic flux analysis for calcium dependent antibiotic (CDA) production in *Streptomyces coelicolor*. *Metabolic Engineering*. 6(4): 313-325.

Bush K and Bradford PA (2016). β-Lactams and β-Lactamase Inhibitors: An Overview. *Cold Spring Harb Perspect Med*. 6(8): a025247

Bush MJ., Bibb MH., Chandra G., Findlay KC and Buttner MJ (2013). Genes Required for Aerial Growth, Cell Division, and Chromosome Segregation Are Targets of WhiA before Sporulation in *Streptomyces venezuelae*. *mBio*. 4(5):e00684-13

Bush MJ, Chandra G, Findlay KC and Buttner MJ (2017). Multi-layered inhibition of *Streptomyces* development: BldO is a dedicated repressor of *whiB*. *Mol Microbiol*. 104(5):700-711

Bush MJ., Chandra G., Al-Bassam MM., Findlay KC and Buttner MJ (2019). BldC Delays Entry into Development To Produce a Sustained Period of Vegetative Growth in *Streptomyces venezuelae*. *mBio*. 10(1):e02812-18

Bychenko OS., Skvortsova YV., Grigorov AS and Azhikina TL (2020). Use of Genetically Encoded Fluorescent Aptamers for Visualization of *Mycobacterium tuberculosis* Small RNA MTS1338 in Infected Macrophages. *Doklady Biochemistry and Biophysics*. 493: 185-189.

Bychenko O., Khrulev, AA., Svetlova JI Tsvetko V., Kamzeeva PN., Skvortsova YV., Tupertsev, BS., Igor I., Aseev LV., Khodarovich Y., Belyaev ES., Kozlovskaya L., Zatsepin T., Azhikina, T Varizhuk A and Aralov A (2023). Red light-emitting short Mango-based system enables tracking a mycobacterial small noncoding RNA in infected macrophages. *Nucleic Acids Research*. 51. 10.1093/nar/gkad100.

Bystrykh LV., Fernádez-Moreno MA., Herrema JK., Malpartida F., Hopwood DA and Dijkhuizen L (1996). Production of Actinorhodin-Related 'Blue Pigments ' by *Streptomyces coelicolor* A3(2). *Journal of Bacteriology*. 178(8): 2238-2244.

Capstick, D, S., Willey, J, M., Buttner, M, J., and Elliot, M, A (2007). SapB and the chaplins: connections between morphogenetic proteins in *Streptomyces coelicolor. Molecular Microbiology*. 64(3): 602-613.

Cazier AP and Blazeck J (2021). Advances in promoter engineering: Novel applications and predefined transcriptional control. *Biotechnol J*. 16 (10): 2100239.

Cerdeño AM., Bibb MJ., Challis GL (2001). Analysis of the prodiginine biosynthesis gene cluster of *Streptomyces coelicolor* A3(2): new mechanisms for chain initiation and termination in modular multienzymes. *Chemistry and Biology*. 8 (8): 817-829.

Cha, J, H., and Stewart, G, C (1997). The divIVA minicell locus of Bacillus subtilis. Journal of Bacteriology. 179(5): 1671–1683.

Chai Discovery Team., Boitreaud J., Dent J., McPartlon M., Meier J., Reis V., Rogozhonikov A and Wu K (2024). Chai-1: Decoding the molecular interactions of life. *bioRxiv.* 2024.10.10.615955; doi: https://doi.org/10.1101/2024.10.10.615955

Chater KF (2013). Curing Baldness Activates Antibiotic Production. *Chemistry and Biology*. 20: 1199-1200

Chater, K, F (2001). Regulation of sporulation in *Streptomyces coelicolor* A3(2): a checkpoint multiplex? *Current Opinion in Microbiology*. 4(6): 667-673.

Chater KF (2006). *Streptomyces* inside-out: a new perspective on the bacteria that provide us with antibiotics. *Philos Trans R Soc Lond B Biol Sci*. 361(1469): 761-768

Chater KF and Chandra G (2006). The evolution of development in *Streptomyces* analysed by genome comparisons. *FEMS Microbiol Rev*; 30:651–672

Chandra G and Chater KF (2008) Evolutionary flux of potentially *bldA*-dependent *Streptomyces* genes containing the rare leucine codon TTA. *Antonie van Leeuwenhoek*; 94:111–126.

Chandra G and Chater KF (2014) Developmental biology of *Streptomyces* from the perspective of 100 actinobacterial genome sequences. *FEMS Microbiol Rev*; 38:345–379

Chater, K, F., Biró, S., Lee, K, J., Palmer, T., and Schrempf, H (2010). The complex extracellular biology of *Streptomyces*. *FEMS Microbiology Reviews*. 34(2010): 171-198.

Chater KF, Bruton CJ, Foster SG and Tobek I (1985). Physical and genetic analysis of IS110, a transposable element of *Streptomyces coelicolor* A3(2). *Mol Gen Genet*; 200:235–239

Chater, K, F., Bruton, C, J., Plaskitt, K, A., Buttner, M, J., Méndez, C., and Helmann, J, D (1989). The developmental fate of *S. coelicolor* hyphae depends upon a gene product homologous with the motility σ factor of *B. subtilis*. *Cell*. 59(1): 133–143.

Chater KF and Chandra G (2008). The use of the rare UUA codon to define 'Expression Space ' for genes involved in secondary metabolism, development and environmental adaptation in *Streptomyces*. *The Journal of Microbiology*. 46: 1-11.

Chen Z., Chen W., Reheman Z., Jiang H, Wu J and Li X (2023). Genetically encoded RNA-based sensors with Pepper fluorogenic aptamer. *Nucleic Acids Research*. 51(16): 8322-8336.

Chen F., Cocaign-Bousquet M., Girbal L and Nouaille S (2022). 5`UTR sequences influence protein levels in *Escherichia coli* by regulating translation initiation and mRNA stability*. Front Microbiol.* 13:1088941.

Chen Z., Chen W., Xu C., Song H., Ji X., Jiang H., Duan H., Li Z., Gao W., Yao T., Zhang Z., He L., Yin Y., Yang N., Tian W., Wu J and Li X (2025). Near-infrared fluorogenic RNA for in vivo imaging and sensing. *Nat Commun* 16: 518

Chen X., Li S., Zhang B., Sun H., Wang J., Zhang W., Meng W., Chen T., Dyson P and Liu G (2022). A new bacterial tRNA enhances antibiotic production in *Streptomyces* by circumventing inefficient wobble base-pairing. *Nucleic Acids Res*. 50(12): 7084-7096.

Chen X., Zhang D., Su N., Bao B., Xie X., Zuo F., Yang L., Wang H., Jiang L., Lin Q., Fang M., Li N., Hua X., Chen Z., Bao C., Xu J., Du W., Zhang L., Zhao Y., Zhu L., Loscalzo J and Yang Y (2019). Visualizing RNA dynamics in live cells with bright and stable fluorescent RNAs. *Nature Biotechnology*. 37: 1287-1293

Cholewa M and Placzek B (2020). Application of Positional Entropy to Fast Shannon Entropy Estimation for Samples of Digital Signals. *Entropy (Basel)*. 22(10): 1173.

Chudakov DM., Matz MV., Lukyanov S and Lukyanov KA (2010). Fluorescent Proteins and Their Applications in Imaging Living Cells and Tissues. *Physiological Reviews*. 90(3): 1103-1163.

Claessen, D., de Jong, W., Dijkhuizen, L., and Wösten, H, A, B (2006). Regulation of *Streptomyces* development: reach for the sky! *TRENDS in Microbiology*. 14(7): 313-319.

Claessen D., Rink R., de Jong W., Siebring J., de Vreugd P., Boersma FGH., Dijkhuizen L and Wösten (2003). A novel class of secreted hydrophobic proteins is involved in aerial hyphae formation in *Streptomyces coelicolor* by forming amyloid-like fibrils. *Genes and Dev*. 17:1714-1726.

Climent-Catala A, Casas-Rodrigo I, Iyer S, Ledesma-Amaro R and Ouldridge TE (2023). Evaluating DFHBI-Responsive RNA Light-Up Aptamers as Fluorescent Reporters for Gene Expression. *ACS Synth Biol*. 12(12):3754-3765.

Cobb, R. E., Wang, Y., and Zhao, H. (2015). High-efficiency multiplex genome editing of *Streptomyces* species using an engineered CRISPR/Cas system. *ACS Synth. Biol.* 4, 723–728

Crick FH (1966). Codon—anticodon pairing: The wobble hypothesis. *Journal of Molecular Biology*. 19 (2): 548-555.

Cumsille A, Durán RE, Rodríguez-Delherbe A, Saona-Urmeneta V, Cámara B *et al* (2023). GenoVi, an open-source automated circular genome visualizer for bacteria and archaea. *PLoS Comput Biol*; 19: e1010998

Davies, J (2006). Are antibiotics naturally antibiotics? *J Ind Microbiol Biotechnol*. 33:496-499.

Dao NT., Haselsberger R., Khuc MT., Phan AT., Voityuk AA and Michel-Beryerle ME (2021). Photophysics of DFHBI bound to RNA aptamer Baby Spinach. *Scientific Reports*. 11:7356

Deatherage DE and Barrick JE (2014). Identification of mutations in laboratory evolved microbes from next-generation sequencing data using *breseq*. *Methods Mol Biol*. 1151: 165-188

De Jong, W., Manteca, A., Sanchez, J., Bucca, G., Smith, C, P., Dijkhuizen, L., Claessen, D., and Wösten, H, A, B (2009). NepA is a structural cell wall protein involved in the maintenance of spore dormancy in *Streptomyces coelicolor*. *Molecular Microbiology*. 71(6):1591-1603.

de Kraker, M, E, A., Stewardson, A, J and Harbarth S (2016). Will 10 million people die a year due to antimicrobial resistance by 2050? *PLoS Med.* 13(11): e1002184.

De Simeis D and Serra S (2021). *Actinomycetes*: A Never-Ending Source of Bioactive Compounds-An Overview on Antibiotics Production. *Antibiotics (Basel).* 10(5):483.

Debnath, M., Prasad, G.B., Bisen, P.S. (2009). Reporter Gene. In: Molecular Diagnostics: Promises and Possibilities. Springer, Dordrecht. https://doi.org/10.1007/978-90-481-3261-4_5

Delgadillo-Guevara M., Halte M., Erhardt M and Popp PF (2024). Fluorescent tools for the standardized work in Gram-negative bacteria. *J Biol Eng*. 18:25.

den Hengst CD., Tran NT., Bibb MJ., Chandra G., Leskiw BK and Buttner MJ (2010). Genes essential for morphological development and antibiotic production in Streptomyces coelicolor are targets of BldD during vegetative growth. 78(2): 361-379.

de Smit MH and van Duin J (2003). Translational Standby Sites: How Ribosomes May Deal with the Rapid Folding Kinetics of mRNA. *J Mol Biol*. 331: 737-743.

Díaz-Pérez AL., Díaz-Pérez C and Campos-García J (2015). Bacterial l-leucine catabolism as a source of secondary metabolites. *Reviews in Environmental Science and Biotechnology*. 15: 1-29

Di Salvo M., Pinatel E., Talà A., Fondi M., Peano C and Alifano P (2018). G4PromFinder: an algorithm for predicting transcription promoters in GC-rich bacterial genomes based on AT-rich elements and G-quadruplex motifs. *BMC Bioinformatics*. 19(1):36.

Doherty, G, P., Bailey, K., and Lewis, P, J (2010). Stage-specific fluorescence intensity of GFP and mCherry during sporulation in *Bacillus subtilis*. *BMC Research Notes*. 303(2010).

Drawz SM and Bonomo RA (2010). Three decades of beta-lactamase inhibitors. *Clin Microbiol Rev*. 23(1):160-201

Duval M, Simonetti A, Caldelari I and Marzi S (2015). Multiple ways to regulate translation initiation in bacteria: Mechanisms, regulatory circuits, dynamics. *Biochimie*. 114: 18-29

Eaton, D., and Ensign, J, C (1980). *Streptomyces viridochromogenes* spore germination initiated by calcium ions. *Journal of Bacteriology*. 143(1): 377-382.

Edwards, D, H., and Errington, J (1997). The *Bacillus subtilis* DivIVA protein targets to the division septum and controls the site specificity of cell division. *Molecular Microbiology*. 239 24(5): 905–915.

Ellington, A, D., and Szostak, J, W (1990). In vitro selection of RNA molecules that bind specific ligands. *Nature*. 346(1990): 818-822.

Elliot MA., Bibb MJ., Buttner MJ and Leskiw BK (2001). BldD is a direct regulator of key developmental genes in *Streptomyces coelicolor* A3(2). *Molecular Biology*. 40(1): 257-269.

Elliot M., Damji F., Passatino R., Chater K and Leskiw B (1998). The *bldD* gene of *Streptomyces coelicolor* A3(2): a Regulatory Gene Involved in Morphogenesis and Antibiotic Production. 180(6): 1549-1555

Elliot, M.A. and Flärdh, K (2020). *Streptomycete spores*. *eLS*. John Wiley & Sons.

Elliot MA, Locke TR., Galibois CM and Leskiw BK (2003). BldD from *Streptomyces coelicolor* is a non-essential global regulator that binds its own promoter as a dimer. *FEMS Microbiology Letters*. 225(1): 35-40

Elliot, M, A., Karoonuthaisiri, N., Huang, J., Bibb, M, J., Cohen, S, N, Kao, C, M., and Buttner, M, J (2003). The chaplins: a family of hydrophobic cell-surface proteins involved in aerial mycelium formation in *Streptomyces coelicolor. Genes and Development*. 17: 1727-1740.

Evfratov SA., Osterman IA., Komarova ES., Pogorelskaya AM., Rubtsova MP., Zatsepin TS., Semashko TA., Kostryukova ES., Mironov AA., Burnaev E., Krymova E., Gelfand MS., Govorun VM., Bogdanov AA., Sergiev PV and Dontsova OA (2016). Application of sorting and next generation sequencing to study 5´-UTR influence on translation efficiency in *Escherichia coli. Nucleic Acids Res*. 45(6):3487-3502.

Fan, JY., Huang Q., Ji QQ and Wang ED (2019). LeuRS can leucylate type I and type II tRNALeus in *Streptomyces coelicolor*. *Nucleic Acids Res*. 47(9): 6369-6385.

Fatima A., Abbas M., Nawaz S., Rehman Y., ur Rehman S and Sajid I (2024). Whole genome sequencing (WGS) and genome mining of *Streptomyces* sp. AFD10 for antibiotics and bioactive secondary metabolites biosynthetic gene clusters (BGCs). *Gene Reports*. 37: 102050.

Feitelson JS and Hopwood DA (1983). Cloning of a *Streptomyces* gene for an O-methyltransferase involved in antibiotic biosynthesis. *MGG Molecular & General Genetics*. 190(3): 394–398.

Feitelson J S., Malpartida F., Hopwood DA (1985). Genetic and biochemical characterization of the red gene cluster of *Streptomyces coelicolor* A3(2). *Journal of General Microbiology*. 131:2431-2441.

Ferguson NL., Peña-Castillo L., Moore MA., Bignell DR and Tahlan K (2016). Proteomics analysis of global regulatory cascades involved in clavulanic acid production and morphological development in *Streptomyces clavuligerus. J Ind Microbiol Biotechnol*. 43(4):537-55.

Fernández-Martínez LT., Del Sol R., Evans MC., Fielding S., Herron PR., Chandra G and Dyson PJ (2010). A transposon insertion single-gene knockout library and new ordered cosmid library for the model organism *Streptomyces coelicolor* A3(2). *Antonie van Leeuwenhoek*. 99: 515-522**.**

Fernández-Moreno MA., Caballero, JL., Hopwood DA and Malpartida F (1991). The *act* cluster contains regulatory and antibiotic export genes, direct targets for translational control by the *bldA* tRNA gene of *Streptomyces*. *Cell*. 66(4): 769-780.

Fernández-Moreno MA., Martínez E., Caballero JL., Ichinose K., Hopwood DA and Malpartida F (1994). DNA sequence and functions of the *actVI* region of the actinorhodin biosynthetic gene cluster of *Streptomyces coelicolor* A3(2). *J Biol Chem*. 269(40):24854-63

Filonov GS and Jaffery SR (2016). RNA Imaging with Dimeric Broccoli in Live Bacterial and Mammalian Cells. *Curr Protoc Chem Biol*. 8(1):1-28

Filonov, G, S., Kam, C, W., Song, W., and Jaffrey, S, R (2015). In-Gel Imaging of RNA Processing Using Broccoli Reveals Optimal Aptamer Expression Strategies. *Chemistry and Biology*. 22(5): 649-660.

Filonov, G, S., Moon, J, D., Svensen, N., and Jaffrey, S, R (2014). Broccoli: Rapid Selection of an RNA Mimic of Green Fluorescent Protein by Fluorescence-Based Selection and Directed Evolution. *Journal of the American Chemical Society*. 136: 16299-16308.

Fink D., Weissschuh N., Reuther J., Wohlleben W and Engels A (2002). Two transcriptional regulators GlnR and GlnRII are involved in regulation of nitrogen metabolism in *Streptomyces coelicolor* A3(2). *Mol Microbiol*. 46(2):331-47.

Flärdh, K (2003). Essential role of DivIVA in polar growth and morphogenesis in *Streptomyces coelicolor* A3(2). *Molecular Microbiology*. 49(6): 1523–1536.

Flärdh, K., and Buttner, M. J (2009). *Streptomyces* morphogenetics: dissecting differentiation in a filamentous bacterium. *Nature Reviews Microbiology*, 7(1): 36–49.

Fleming, A (1929). On the antibacterial action of cultures of a penicillium, with special reference to their use in the isolation of *B. influenzae*. *British Journal of Experimental Pathology*. 10(3): 226-236.

Fröjd, M, J., and Flärdh, K (2019). Apical assemblies of intermediate filament-like protein FilP are highly dynamic and affect polar growth determinant DivIVA in *Streptomyces venezuelae. Molecular Microbiology*. 112(1): 47-61.

Fu J., Qin R., Zong G., Zhong C., Zhang P., Kang N., Qi X and Cao G (2019). The two-component system CepRS regulates the cephamycin C biosynthesis in *Streptomyces clavuligerus* F613-1. *AMB Express.* 9: 118.

Fuiji T., Gramajo HC., Takano E and Bibb MJ (1996). *redD* and *actII-ORF4*, Pathway-Specific Regulatory Genes for Antibiotic Production in *Streptomyces coelicolor* A3(2), Are Transcribed In Vitro by an RNA Polymerase Holoenzyme Containing s^{hrdD}. *Journal of Bacteriology*.178(11): 3402-3405.

Fujishima K., Kanai A. (2014). tRNA gene diversity in the three domains of life*. Front. Genet.* 5:142.

Furuhata Y., Kobayashi M., Maruyama R., Sato Y., Makino K., Michiue T., Yui H., Nishizawa S and Yoshimoto K (2019). Programmable RNA detection with a fluorescent RNA aptamer using optimized three-way junction formation. *RNA*. 25(5): 590-599

Gallagher KA, Tschowri N, Brennan RG, Schumacher MA and Buttner MJ (2024). How c-di-GMP controls progression through the *Streptomyces* life cycle. *Current Opinion in Microbiology*. 80: 102516.

Galperin MY, Wolf YI, Makarova KS, Alvarez RV, Landsman D *et al* (2021). COG database update: focus on microbial diversity, model organisms, and widespread pathogens. *Nucleic Acids Res*; 49: D274–D281

Gao B and Gupta RS (2012). Phylogenetic Framework and Molecular Signatures for the Main Clades of the Phylum *Actinobacteria*. *Microbiol Mol Biol Rev*. 76(1): 66-112

Garcia-Martin JA and Clote P (2015). RNA Thermodynamic Structural Entropy. *PLoS One*. 10(11): e0137859.

Gehring AM., Nodwell JR., Beverley SM and Losick R (2000). Genomewide insertional mutagenesis in *Streptomyces coelicolor* reveals additional genes involved in morphological differentiation. *PNAS*. 97(17): 9642-9647.

Gehring, AM., Wang ST., Kearns DB., Storer NY and Losick R (2004). Novel Genes That Influence Development in *Streptomyces coelicolor*. *J Bacteriol*. 186(11): 3570-3577.

Georgakopoulos-Soares I., Parada GE and Hemberg M (2022). Secondary structures in RNA synthesis, splicing and translation. *Comput Struct Biotechnol J*. 20:2871-2884.

Glauert, A, M., and Hopwood, D, A (1961). The Fine Structure of *Streptomyces violaceoruber* (*S. coelicolor*). *The Journal of Biophysical and Biochemical Cytology*. 10(4): 505-516.

GlaxoSmithKline (2021). STREPTOMYCES CLAVULIGERUS improved clavulanic acid production via ccaR mutations. WO Patent 2021/004912 A1. World Intellectual Property Organization.

Goh, E, B., Yim, G., Tsui, W., McClure, J., Surette, M, G. and Davies, J (2002). Transcriptional modulation of bacterial gene expression by subinhibitory concentrations of antibiotics. *Proceedings of the National Academy of Sciences*. 99(26): 17025–17030.

Gomez-Escribano JP, Song L, Fox DJ, Yeo V, Bibb MJ *et al* (2012). Structure and biosynthesis of the unusual polyketide alkaloid coelimycin P1, a metabolic product of the cpk gene cluster of *Streptomyces coelicolor* M145. *Chem Sci*; 3:2716

Gottelt M., Kol S., Gomez-Escribano J. P., Bibb M., Takano E. (2010). Deletion of a regulatory gene within the cpk gene cluster reveals novel antibacterial activity in *Streptomyces coelicolor* A3(2). *Microbiology*. 156: 2343-2353.

Gramajo HC, Takano E and Bibb MJ (1993) Stationary-phase production of the antibiotic actinorhodin in *Streptomyces coelicolor* A3(2) is transcriptionally regulated. *Mol Microbiol*; 7:837–845

Grant, S, G., Jessee, J., Bloom, F, R., and Hanahan, D (1990). Differential plasmid rescue from transgenic mouse DNAs into *Escherichia coli* methylation-restriction mutants. *Proceedings of the National Academy of Sciences*. 87(12): 4645 LP – 4649.

Grimm, J.B and Lavis, L.D (2022). Caveat fluorophore: an insiders' guide to small-molecule fluorescent labels. *Nat Methods* 19: 149–158.

Gruber AR., Lorenz R., Bernhart SH., Neuböck R and Hofacker IL (2008). The Vienna RNA Websuite. *Nucleic Acids Res*. 19;36(Web Server issue):W70–W74.

Guthrie EP and Chater KF (1990). The level of a transcript required for production of a *Streptomyces coelicolor* antibiotic is conditionally dependent on a tRNA gene. *Journal of Bacteriology*. 172(11): 6189-6193.

Guyet, A., Benaroudj, N., Proux C., Gominet, M., Coppée, J-Y., and Madodier, P (2014). Identified members of the *Streptomyces lividans* AdpA regulon involved in differentiation and secondary metabolism. *BMC Microbiology*. 14:81.

Hackl S and Bechthold A (2015). The Gene *bldA,* a regulator of morphological differentiation and antibiotic production in *Streptomyces*. *Arch Pharm (Weinheim)*. 348(7): 455-462.

Hafner EW., Holley BW., Holdom KS., Lee SE., Wax RG., Beck D., McArthur HA and Wernau WC (1991). Branched-chain fatty acid requirement for avermectin production by a mutant of *Streptomyces avermitilis* lacking branched-chain 2-oxo acid dehydrogenase activity. *J Antibiot (Tokyo)*. 44(3):349-56.

Haiser HJ., Karginov FV., Hannon GJ and Elliot MA (2008). Developmentally regulated cleavage of tRNAs in the bacterium *Streptomyces coelicolor*. *Nucleic Acids Research*. 36(3): 732-741.

Haiser, H, J., Yousef, M, R., and Elliot, M, A (2009). Cell Wall Hydrolases Affect Germination, Vegetative Growth, and Sporulation in *Streptomyces coelicolor. Journal of Bacteriology*. 191(21): 6501-6512.

Hamed MB, Vrancken K, Bilyk B, Koepff J, Novakova R, van Mellaert L, Oldiges M, Luzhetskyy A, Kormanec J, Anné J, Karamanou S, and Economou A (2018). Monitoring Protein Secretion in *Streptomyces* Using Fluorescent Proteins. *Front Microbiol*. 9:3019.

Hammann C, Luptak A, Perreault J and de la Peña M (2012). The ubiquitous hammerhead ribozyme. *RNA.* 18(5):871-85.

Han KY., Leslie BJ., Fei J., Zhang J and Ha T (2014). Understanding the Photophysics of the Spinach-DFHBI RNA Aptamer-Fluorogen Complex to Improve Live Cell RNA Imaging. *J Am Chem Soc*. 135(50): 19033-19038.

Han S., Min J., Park Y and Park W (2025). Fine-tuning regulation of (p)ppGpp-driven outer membrane vesicle formation in *Acinetobacter baumannii*. *FEBS J*. 292(14):3696-3717

Hardisson, C., Manzanal, M, B., Salas, J, A., and Suárez, J, E (1978). Fine structure, physiology and biochemistry of arthrospore germination in *Streptomyces antibioticus*. *Microbiology*. 105(2): 203–214.

Haug, I., Weissenborn, A., Brolle, D., Bentley, S., Kieser, T., and Altenbuchner, J (2003). *Streptomyces coelicolor* A3(2) plasmid SCP2*: deductions from the complete sequence. *Microbiology.* 149(2): 505–513.

Heim R and Tsien RY (1996). Engineering green fluorescent protein for improved brightness, longer wavelengths and fluorescence resonance energy transfer. *Current Biology*. 6(2): 178-182.

Hempel, A, M., Wang, S-B., Letek, M., Gil, J, A., and Flärdh, K (2008). Assemblies of DivIVA Mark Sites for Hyphal Branching and Can Establish New Zones of Cell Wall Growth in *Streptomyces coelicolor. J. Bacteriol*. 190(22): 7579-7583.

Hempel, A, M., Cantlay, S., Molle, V., Wang, S-B., Naldrett, M, J., Parker, J, L., Richards, D, M., Jung, Y-G., Buttner, M, J. and Flärdh, K (2012). The Ser/Thr protein kinase AfsK regulates polar growth and hyphal branching in the filamentous bacteria *Streptomyces. Proceedings of the National Academy of Sciences*. 109(35): E2371–E2379

Henri J., Bayat N., Macdonald J and Shigdar S (2019). A guide to using nucleic acid aptamers in cell based assays. *Aptamers*. 3: 4-9

Hesketh A., Bucca G., Laing E., Flett F., Hotchkiss G., Smith CP and Chater KF (2007). New pleiotropic effects of eliminating a rare tRNA from *Streptomyces coelicolor*, revealed by combined proteomic and transcriptomic analysis of liquid cultures. *BMC Genomics*. 8:261.

Higgens, C, E and Kastner, R, E (1971). *Streptomyces clavuligerus* sp.nov., a β-Lactam Antibiotic Producer. *International Journal of Systematic and Evolutionary Microbiology*. 21(4): 326-331.

Higo A., Horinouchi S and Ohnishi Y (2011). Strict regulation of morphological differentiation and secondary metabolism by a positive feedback loop between two global regulators AdpA and BldA in *Streptomyces griseus. Mol Microbiol*. 81(6):1607-22.

Hink, M, A., Griep, R, A., Borst, J, W., van Hoek, A., Eppink, M, H, M., Schots, A., and Visser A, J, W, G (2000). Structural Dynamics of Green Fluorescent Protein Alone and Fused with a Single Chain Fv Protein. *Journal of Biological Chemistry*. 275(23): 17556-17560.

Hobbs, G., Frazer, C, M., Gardner, D, C, J., Cullum, J, A. and Oliver, S, G (1989). Dispersed growth of *Streptomyces* in liquid culture. *Applied Microbiology and Biotechnology*. 31(3): 272–277

Höfer, K., Langejürgen, L, V and Jäschke A (2013). Universal Aptamer-Based Real-Time Monitoring of Enzymatic RNA Synthesis. *J. Am. Chem. Soc.* 135(37): 13692-13694

Hong, H., Hutchings, M. I., Hill, L. M., Buttner, M. J. (2005). The Role of the Novel Fem Protein VanK in Vancomycin Resistance in Streptomyces coelicolor. *Journal of Biological Chemistry*, 280, pp. 13055-13061

Hopwood, D. A. (2007). Streptomyces in nature and medicine: the antibiotic makers. Oxford: Oxford University Press, 2007.

Hopwood DA and Wright HM (1983). CDA is a New Chromosomally-determined Antibiotic from *Streptomyces coelicolor* A3(2). *Journal of General Microbiology*. 129: 3575-3579.

Horwitz JP., Chua J., Curby RJ., Tomson AJ., Darooge MA., Fisher BE., Mauricio J and Klundt I (1964) Substrates for cytochemical demonstration of enzyme activity. I. Some substituted 3-indolyl-β-D-glycopyranosides. *Journal of Medicinal Chemistry.* 7: 574-575

Hoskisson PA, Rigali S, Fowler K, Findlay KC and Buttner MJ (2006). DevA, a GntR-Like Transcriptional Regulator Required for Development in *Streptomyces coelicolor*. *J Bacteriol*. 188(14): 5014-5023.

Hoskisson PA and van Wezel GP (2019). *Streptomyces coelicolor*. *Trends in Microbiology*. 27(5): 468-469.

Hou Q and Jaffrey SR (2023). Synthetic biology tools to promote the folding and function of RNA aptamers in mammalian cells. *RNA Biology*. 20: 198-206.

Hou B., Tao L., Zhu X., Wu W., Guo M., Ye J., Wu H and Zhang H (2018). Global regulator BldA regulates morphological differentiation and lincomycin production in *Streptomyces lincolnensis*. *Appl Microbiol Biotechnol*. 102(9): 4101-4115.

Huang R., Liu H., Zhao W., Wang S., Wang S., Cai J and Yang C (2022). AdpA, a developmental regulator, promotes ε-poly-l-lysine biosynthesis in *Streptomyces albulus*. *Microbial Cell Factories*. 21(60).

Huang H, Suslov NB, Li NS, Shelke SA, Evans ME, Koldobskaya Y, Rice PA and Piccirilli JA (2014). A G-quadruplex-containing RNA activates fluorescence in a GFP-like fluorophore. *Nat Chem Biol*. 10(8):686-91.

Hwang S., Lee N., Choe D., Lee Y., Kim W., Kim JH., Kim G., Kim H., Ahn NH., Lee BH., Palsson BO and Cho BK (2022). System-Level Analysis of Transcriptional and Translational Regulatory Elements in *Streptomyces griseus*. *Front Bioeng Biotechnol*. 10:844200.

Hunt, A, C., Servín-González, L., Kelemen, G, H., and Buttner, M, J (2005). The bldC Developmental Locus of *Streptomyces coelicolor* Encodes a Member of a Family of Small DNA-Binding Proteins Related to the DNA-Binding Domains of the MerR Family. *Journal of Bacteriology*. 187(2): 716-728.

Hutchings, M., Truman, AW and Wilkinson B (2019). Antibiotics: past, present and future. *Current Opinion in Microbiology*. 51: 71-80.

Jaganathan K., Ersaro N., Novakovsky G. Wang Y., James T., Schwartzentruber J., Fiziev P., Kassam I., Cao F., Hawe J., Cavanagh H., Lim A., Png G., McRae J., Banerjee A., Kumar A., Ulirsch J., Zhang Y., Aguet F., Wainschtein P., Sundaram L., Salcedo A., Panagiotopoulou SK., Aghamirzaie D., Padhi E., Weng Z., Dong S., Smedley D., Caulfield M., O'Donnell-Luria A., Rehm HL., Sanders SJ., Kundaje A., Montgomery SB., Ross MT and Farh KK (2025). Predicting expression-altering promoter mutations with deep learning. *Science*. 389(6760):eads7373. doi: 10.1126/science.ads7373

Jauri, P, V., Bakker, M, G., Salomon, C, E., and Kinkel L, L (2013). Subinhibitory Antibiotic Concentrations Mediate Nutrient Use and Competition among Soil *Streptomyces. PLOS One*. 8(12): e81064.

Jensen SE (2012). Biosynthesis of clavam metabolites. *Journal of Industrial Microbiology and Biotechnology*. 39(10): 1407-1419.

Jensen D., Manzano AR., Rector M., Tomko EJ., Record MT and Galburt EA (2023). High-throughput, fluorescent-aptamer-based measurements of steady-state transcription rates for the *Mycobacterium tuberculosis* RNA polymerase. *Nucleic Acids Res*. 51(19):e99.

Jeong Y, Kim JN, Kim MW, Bucca G, Cho S, Yoon YJ, Kim BG, Roe JH, Kim SC, Smith CP and Cho BK (2016). The dynamic transcriptional and translational landscape of the model antibiotic producer *Streptomyces coelicolor* A3(2). *Nat Commun*. 7:11605. doi: 10.1038/ncomms11605.

Jones, S, E., and Elliot, M, A (2017). *Streptomyces* Exploration: Competition, Volatile Communication and New Bacterial Behaviours. *Trends in Microbiology*. 25(7): 522-531.

Jones, S, E., and Elliot, M, A (2018). Exploring' the regulation of *Streptomyces* growth and development. *Current Opinion in Microbiology*. 42: 25-30.

Jumper J, Evans R, Pritzel A, Green T, Figurnov M, Ronneberger O, Tunyasuvunakool K, Bates R, Žídek A, Potapenko A, Bridgland A, Meyer C, Kohl SAA, Ballard AJ, Cowie A, Romera-Paredes B, Nikolov S, Jain R, Adler J, Back T, Petersen S, Reiman D, Clancy E, Zielinski M, Steinegger M, Pacholska M, Berghammer T, Bodenstein S, Silver D, Vinyals O, Senior AW, Kavukcuoglu K, Kohli P and Hassabis D (2021) Highly accurate protein structure prediction with AlphaFold. *Nature*. 596(7873):583-589.

Kaiser, B, K., and Stoddard, B, L (2011). DNA regulation and transcriptional regulation by the WhiA sporulation factor. *Scientific Reports*. 1.. doi:10.1038/srep00156

Kalakoutskii, L, V., and Agre, N, S (1976). Comparative Aspects of Development and Differentiation in Actinomycetes. *Bacteriological Reviews*. 40(2): 469-524.

Kalan L., Gessner A., Thaker MN., Waglechner N., Zhu X., Szawiola A., Bechthold A., Wright GD and Zechel DL (2013). A Cryptic Polyene Biosynthetic Gene Cluster in *Streptomyces calvus* Is Expressed upon Complementation with a Functional *bldA* Gene. *Chemistry and Biology*. 20(10): 1214-1224.

Kaltenpoth M (2009). Actinobacteria as mutualists: general healthcare for insects? *Trends Microbiol.* 17(12):529-35.

Kamath D, Allgeyer BB, Gregory ST, Bielski MC, Roelofsz DM, Sabapathypillai SL, Vaid N and O'Connor M (2017). The C-terminus of ribosomal protein uS4 contributes to small ribosomal subunit biogenesis and the fidelity of translation. *Biochimie*. 138:194-201.

Kang SG., Jin W., Bibb M and Lee KJ (1998). Actinorhodin and undecylprodigiosin production in wild-type and *relA* mutant strains of *Streptomyces coelicolor* A3(2) grown in continuous culture. *FEMS Microbiology Letters*. 168(2): 221-226.

Kartje ZJ., Janis HI., Mukhopadhyay S and Gagnon KT (2021). Revisiting T7 RNA polymerase transcription *in vitro* with the Broccoli RNA aptamer as a simplified real-time fluorescent reporter. *Journal of Biological Chemistry*. 296: 100175.

Kataoka M., Kosono S and Tsujimoto G (1999) Spatial and temporal regulation of protein expression by *bldA* within a *Streptomyces lividans* colony. *FEBS Letters*. 462(3): 425-429.

Kaur, H., and Shorie, M (2019). Nanomaterial based aptasensors for clinical and environmental diagnostic applications. *Nanoscale Advances*. 1: 2123-2138.

Kelemen, G, H., Brown, G, L., Kormanec, J., Potúčková, L., Chater, K, F., and Buttner, M, J (1996). The positions of the sigma-factor genes, *whiG* and *sigF*, in the hierarchy controlling

the development of spore chains in the aerial hyphae of *Streptomyces coelicolor* A3(2). *Molecular Microbiology*. 21(3): 593-603.

Kellenburger, C, A., Wilson, S, C., Sales-Lee, Jade., and Hammond, M, C (2013). RNA-based Fluorescent Biosensors for Live Cell Imaging of Secondary Messengers Cyclic di-GMP and Cyclic AMP-GMP. *J. Am. Chem. Soc.* 135(13): 4906-4909.

Kerr L and Hoskisson PA (2019). Reconciling DNA replication and transcription in a hyphal organism: visualizing transcription complexes in live *Streptomyces coelicolor*. *Microbiology*. 165: 1086-1094.

Kieser, T., Bibb, M., Buttner, M., and Chater, K (2000). Practical *Streptomyces* Genetics.

Khan S, Srivastava S, Karnwal A, and Malik T (2023). *Streptomyces* as a promising biological control agents for plant pathogens. *Front Microbiol.* 14:1285543.

Kim D., Chater KF., Lee KJ and Hesketh A (2005). Effects of growth phase and the developmentally significant *bldA*-specified tRNA on the membrane-associated proteome of *Streptomyces coelicolor*. *Microbiology*. 151(8): 2707-2720

Kim DW., Chater KF., Lee KJ and Hesketh A (2005). Changes in the Extracellular Proteome Caused by the Absence of the *bldA* Gene Product, a Developmentally Significant tRNA, Reveal a New Target for the Pleiotropic Regulator AdpA in *Streptomyces coelicolor*. *Journal of Bacteriology*. 187(9): 2957-2966.

Kim DG., Gu B., Cha Y., Ha J., Lee Y., Kim G., Cho B-K and Oh M-K (2025). Engineered CRISPR-Cas9 for *Streptomyces* sp. genome editing to improve specialized metabolite production. *Nature Communications*. 16: 874.

Kim W., Hwang S., Lee N., Lee Y., Cho S., Palsson B and Cho BK (2021). Transcriptome and translatome profiles of *Streptomyces* species in different growth phases. *Sci Data*. 7(1):138. doi: 10.1038/s41597-020-0476-9. Erratum in: Sci Data. 2021 Feb 26;8(1):75.

Kim, S, B., Lonsdale, J., Seong, C.-N. and Goodfellow, M (2003). *Streptacidiphilus gen. nov., acidophilic actinomycetes* with wall chemotype I and emendation of the family *Streptomycetaceae* (Waksman and Henrici (1943) AL) emend. Rainey et al. 1997. Antonie van Leeuwenhoek. 83(2): 107–116.

Klima JC., Doyle LA., Lee JD., Rappleye M., Gagnon LA., Lee MY., Barros EP., Vorobieva AA., Dou J., Bremner S., Quon JS., Chow CM., Carter L., Mack DL., Amaro RE., Vaughan JC., Berndt A., Stoddard BL and Baker D (2021). Incorporation of sensing modalities into de novo designed fluorescence-activating proteins. *Nat Commun*. 12(1):856.

Klug, WS. Cummings MR, Spencer CA, Palladino MA, Killian D (2019). *Concepts of genetics*. (Twelfth ed.). NY NY.

Koshla, O., Yushchuk, O., Ostash, I., Dacyuk, Y., Myronovskyi, M., Jäger, G., Süssmuth, R.D., Luzhetskyy, A., Byström, A., Kirsebom, L.A. and Ostash, B. (2019), Gene *miaA* for post-transcriptional modification of $tRNA_{XXA}$ is important for morphological and metabolic differentiation in *Streptomyces*. *Mol Microbiol*, 112: 249-265.

Kotowska M., Wenecki M., Bednarz B., Ciekot J., Paslawski W., Buhl T and Pawlik K (2024). Coelimycin inside out — negative feedback regulation by its intracellular precursors. *Applied Microbiology and Biotechnology*. 108:531.

Kutzner HJ and Waksman SA (1959). *Streptomyces coelicolor* Mueller and *Streptomyces violaceoruber* Waksman and Curtis, two distinctly different organisms. *J Bacteriol*. 78(4): 528-538.

Kwak J., McCue LA and Kendrick KE (1996). Identification of *bldA* mutants of *Streptomyces griseus*. *Gene*. 171: 75-78.

Langmead B and Salzberg SL (2012). Fast gapped-read alignment with Bowtie 2. *Nature Methods*. 9: 357-359.

Larcombe DE, Braes RE, Croxford JT, Wilson JW, Figurski DH and Hoskisson PA (2024). Sequence and origin of the *Streptomyces* intergenetic-conjugation helper plasmid pUZ8002. *Access Microbiol*. 6(6):000808.v3.

Larson MH., Gilbert LA., Wang X., Liam WA., Weissman JS and Qi LS (2013). CRISPR interference (CRISPRi) for sequence-specific control of gene expression. *Nature Protocols*. 8: 2180-2196.

Lawlor EJ, Baylis HA and Chater KF (1987). Pleiotropic morphological and antibiotic deficiencies result from mutations in a gene encoding a tRNA-like product in *Streptomyces coelicolor* A3(2). *Genes Dev*; 1:1305–1310.

Lee Y., Hwang S., Kim W., Kim JH., Palsson BO and Cho BK (2024). CRISPR-aided genome engineering for secondary metabolite biosynthesis in *Streptomyces*. *Journal of Industrial Microbiology and Biotechnology*. 51, kuae009.

Lee HN, Kim JS, Kim P, Lee HS, Kim ES. 2013. Repression of antibiotic downregulator WblA by AdpA in *Streptomyces coelicolor*. *Appl Environ Microbiol* 79:4159-4163.

Lee Y., Lee N., Hwang S., Kim K., Kim W., Kim J., Cho S., Palsson BO and Cho BK (2020). System-level understanding of gene expression and regulation for engineering secondary metabolite production in *Streptomyces. Journal of Industrial Microbiology & Biotechnology.* 47:739–752

Lee C, Park JM, Hillman PF, Yoo M, Kim HY, Lee CS and Nam SJ (2024). Anti-Melanogenic Activity of Undecylprodigiosin, a Red Pigment Isolated from a Marine *Streptomyces* sp. SNA-077. *Biomol Ther (Seoul).* 32(4): 492-498

Lee CJ., Won HS., Kim JM., Lee BJ and Kang SA (2007). Molecular domain organization of BldD, an essential transcriptional regulator for developmental process of *Streptomyces coelicolor* A3(2). *Proteins*. 68(1): 344-352

Leskiw BK., Bibb MJ and Chater KF (1991). The use of a rare codon specifically during development? *Molecular Microbiology*. 5(12): 2861-2867

Leskiw B.K, Lawlor E.J, Fernandez-Abalos J.M and Chater K.F (1991). TTA codons in some genes prevent their expression in a class of developmental, antibiotic-negative, *Streptomyces* mutants. *Proc. Natl Acad. Sci. USA.* 88:2461–2465.

Leskiw BK., Mah R., Lawlor EJ and Chater KF (1993). Accumulation of bldA-specified tRNA is temporally regulated in *Streptomyces coelicolor* A3(2). *Journal of Bacteriology*. 175(7): 1995-2005.

Lewis RA, Wahab A, Bucca G, Laing EE, Möller-Levet CS, Kierzek A and Smith CP (2019) Genome-wide analysis of the role of the antibiotic biosynthesis regulator AbsA2 in *Streptomyces coelicolor* A3(2). *PLoS One*.14(4): e0200673.

Li H and Durbin R (2009). Fast and accurate short read alignment with Burrows–Wheeler transform. *Bioinformatics*. 25(14): 1754-1760.

Li X., Han M., Zhang H., Liu F., Pan Y., Zhu J., Liao Z., Chen X and Zhang B (2022). Structures and biological functions of zinc finger proteins and their roles in hepatocellular carcinoma. *Biomarker Research*. 10:2

Li X., Kim H., Litke JL., Wu J and Jaffrey SR (2021). Fluorophore-promoted RNA folding and photostability enable imaging of single Broccoli-tagged mRNAs in live mammalian cells. *Angew Chem Int Ed Engl*. 59(11): 4511-4518.

Li S., Li Z., Pang S., Xiang W and Wang W (2021). Coordinating precursor supply for pharmaceutical polyketide production in *Streptomyces*. *Current Opinion in Biotechnology*. 69: 26-34

Li S., Wang J., Li X., Yin S., Wang W and Yang K (2015). Genome-wide identification and evaluation of constitutive promoters in streptomycetes. *Microbial Cell Factories*. 14: 172.

Li ZL., Wang YH., Chu J., Zhuang YP and Zhang SL (2009). Effect of branched-chain amino acids, valine, isoleucine and leucine on the biosynthesis of bitespiramycin 4'-O-acylspiramycins. *Braz J Microbiol*. 40(4):734-46.

Li W., Wu J., Tao W., Zhao C., Wang Y., He X., Chandra G., Zhou, X., Deng Z., Chater KF and Tao M (2007). A genetic and bioinformatic analysis of *Streptomyces coelicolor* genes containing TTA codons, possible targets for regulation by a developmentally significant tRNA. *FEMS Microbiol Lett.* 266(1): 20-28.

Limauro D, Avitabile A, Cappellano C, Puglia AM and Bruni CB (1990). Cloning and characterization of the histidine biosynthetic gene cluster of *Streptomyces coelicolor* A3(2). *Gene*; 90:31–41

Litke JL and Jaffrey SR (2019). Highly efficient expression of circular RNA aptamers in cells using autocatalytic transcripts. *Nat Biotechnol*. 37:667–675.

Liu G., Chater KF., Chandra G., Niu G and Tan H (2013). Molecular Regulation of Antibiotic Biosynthesis in *Streptomyces*. *Microbiology and Molecular Biology Reviews*. 77(1): 112-143.

Liu M., Xu W., Zhu Y., Cui X and Pang X (2021). The Response Regulator MacR and its Potential in Improvement of Antibiotic Production in *Streptomyces coelicolor*. *Current Microbiology*. 78: 3696-3707.

Liu P., Wang YY., Gu Q., Geng M and Ji L (2013). Undecylprodigiosin induced apoptosis in P388 cancer cells is associated with its binding to ribosome. *PLoS One*. 8(6): e65381

Liu YJ., Wang X., Sun Y and Feng Y (2025). Bacterial 5′ UTR: A treasure-trove for post-transcriptional regulation. *Biotechnology Advances*. 78: 108478.

Liu Z., Zhao Y., Huang C and Luo Y (2021). Recent Advances in Silent Gene Cluster Activation in *Streptomyces*. *Front Bioeng Biotechnol*. 9:632230

Llor C and Bjerrum L (2014). Antimicrobial resistance: risk associated with antibiotic overuse and initiatives to reduce the problem. *Ther Adv Drug Saf*. 5(6):229-41.

Lone BA., Karna SKL., Ahmad F., Shahi N and Pokharel YR (2018). CRISPR/Cas9 System: A Bacterial Tailor for Genomic Engineering. *Genet Res Int*. 2018:3797214.

López-Agudelo VA, Gómez-Ríos D and Ramirez-Malule H (2021). Clavulanic Acid Production by *Streptomyces clavuligerus*: Insights from Systems Biology, Strain Engineering, and Downstream Processing. *Antibiotics (Basel).* 10(1):84..

Lopez-Garcia MT, Santamarta I, Liras P. 2010. Morphological differentiation and clavulanic acid formation are affected in a *Streptomyces clavuligerus* adpA-deleted mutant. Microbiology (Reading) 156:2354–2365. doi: 10.1099/mic.0.035956-0.

Love, MI., Huber, W and Anders, S (2014). Moderated estimation of fold change and dispersion for RNA-seq data with DESeq2. *Genome Biology*, 15:550.

Lu Z., Xie P and Qin Z (2010). Promotion of markerless deletion of the actinorhodin biosynthetic gene cluster in *Streptomyces coelicolor*. *Acta Biochim Biophys Sin*. 42(10): 717-721

Lyons SM., Gudanis D., Coyne SM., Gdaniac Z and Ivanov P (2017). Identification of functional tetramolecular RNA G-quadruplexes derived from transfer RNAs. *Nature Communications*. 8: 1127

MacNeil DJ, Gewain KM, Ruby CL, Dezeny G, Gibbons PH and MacNeil T (1992). Analysis of *Streptomyces avermitilis* genes required for avermectin biosynthesis utilizing a novel integration vector. *Gene.*111(1): 61-68

Mak S and Nodwell JR (2017). Actinorhodin is a redox-active antibiotic with a complex mode of action against Gram-positive cells. *Molecular Microbiology*. 106(4): 597-613.

Makitrynskyy R, Ostash B, Tsypik O, Rebets Y, Doud E, Meredith T, Luzhetskyy A, Bechthold A, Walker S, Fedorenko V (2013). Pleiotropic regulatory genes *bldA, adpA* and *absB* are implicated in production of phosphoglycolipid antibiotic moenomycin. *Open Biol*. 3(10):130121.

Malpartida F, Niemi J, Navarrete R and Hopwood DA (1990). Cloning and expression in a heterologous host of the complete set of genes for biosynthesis of the *Streptomyces coelicolor* antibiotic undecylprodigiosin. *Gene*; 93:91–99

Manteca Á and Yagüe P (2018). *Streptomyces* Differentiation in Liquid Cultures as a Trigger of Secondary Metabolism. *Antibiotics (Basel).* 7(2):41

Martell, R, E., Nevins, J, R., and Sullenger, B, A (2002). Optimizing aptamer activity for gene therapy applications using expression cassette SELEX. *Mol. Ther.* 6: 30-34.

Martínez-Burgo Y, Álvarez-Álvarez R, Rodríguez-García A and Liras P (2015). The Pathway-Specific Regulator ClaR of *Streptomyces clavuligerus* Has a Global Effect on the Expression of Genes for Secondary Metabolism and Differentiation. *Appl Environ Microbiol.* 81(19):6637-48.

McBride, M, J., and Ensign, J, C (1987). Metabolism of endogenous trehalose in *Streptomyces griseus* spores and by spores or cells of other actinomycetes. *J. Bacteriol*. 169(11): 5002-5007.

McCormick, J, R., and Flärdh, K (2012). Signals and regulators that govern *Streptomyces* development. *FEMS Microbiology Reviews*. 36(1): 206–231.

McFeely CAL., Shakya B., Makovsky CA., Haney AK., Ashton Cropp T and Hartman MCT (2023). Extensive breaking of genetic code degeneracy with non-canonical amino acids. *Nat Commun.* 14(1):5008.

McGary K and Nudler E (2013). RNA polymerase and the ribosome: the close relationship. *Current Opinion in Microbiology*. 16(2): 112-117

Melior H, Li S, Madhugiri R, Stötzel M, Azarderakhsh S, Barth-Weber S, Baumgardt K, Ziebuhr J and Evguenieva-Hackenberg E (2019). Transcription attenuation-derived small RNA rnTrpL regulates tryptophan biosynthesis gene expression in *trans. Nucleic Acids Res*. 47(12):6396-6410.

Merrick MJ (1976). A morphological and genetic mapping study of bald colony mutants of *Streptomyces coelicolor*. *J Gen Micro*; 96:299–315

Mo S., Sydor PK., Corre C., Alhamadsheh MM., Stanley AE., Haynes SW., Song L., Reynolds KA and Challis GL (2008). Elucidation of the *Streptomyces coelicolor* Pathway to 2-Undecylpyrrole, a Key Intermediate in Undecylprodiginine and Streptorubin B Biosynthesis. *Chemistry and Biology*. 15(2): 137-148.

Molle, V. and Buttner, M.J. (2000) Different alleles of the response regulator gene *bldM* arrest *Streptomyces coelicolor* development at distinct stages. *Molecular Microbiology*, 36, 1265–1278.

Molle, V., Palframan, W.J., Findlay, K.C. and Buttner, M.J. (2000) WhiD and WhiB, homologous proteins required for different stages of sporulation in *Streptomyces coelicolor* A3(2). *Journal of Bacteriology*, 182: 1286–1295.

Myronovskyi M., Welle E., Fedorenko V and Luzhetskyy A (2011). Beta-glucuronidase as a sensitive and versatile reporter in actinomycetes. *Appl Environ Microbiol*. 77(15):5370-83.

Nag A and Mehra S (2021). A Major Facilitator Superfamily (MFS) Efflux Pump, SCO4121, from *Streptomyces coelicolor* with Roles in Multidrug Resistance and Oxidative Stress Tolerance and Its Regulation by a MarR Regulator. *Appl Environ Microbiol*. 87(7): e02238-20

Narva KE and Feitelson JS (1990). Nucleotide sequence and transcriptional analysis of the *redD* locus of *Streptomyces coelicolor* A3(2). *J. Bacteriol.* 172: 326-333

National Office for Animal Health. NOAH response to final O'Neill AMR review report July 2016. Middlesex: *National Office for Animal Health*, 2016

Naville M and Gautheret, D (2009). Transcription attenuation in bacteria: theme and variations. *Briefings in Functional Genomics.* 9 (2):178-189.

NEB Tm Calculator. New England Biolabs, https://tmcalculator.neb.com/. Accessed: 25/03/2025.

Netzker T., Schroeckh V., Gregory MA., Flak M., Krespach MKC., Leadley PF and Brakhage AA (2016). An Efficient Method To Generate Gene Deletion Mutants of the Rapamycin-Producing Bacterium *Streptomyces iranensis* HM 35. *Appl Environ Microbiol*. 82(12): 3481-3492.

Niu G., Chater KF., Tian Y., Zhang J and Tan H (2016). Specialised metabolites regulating antibiotic biosynthesis in *Streptomyces* spp. *FEMS Microbiology Reviews*. 40(4):554-573.

Nodwell, J, R., McGovern, K., and Losick, R (1996). An oligopeptide permease responsible for the import of an extracellular signal governing aerial mycelium formation *in Streptomyces coelicolor. Molecular Microbiology*. 22(5): 881–893.

Noens, E, E., Mersinias, V., Willemse, J., Traag, B, A., Laing, E., Chater, K, F., Smith, C, P., Koerten, H, K., and van Wezel, G, P (2007). Loss of the controlled localization of growth stage-specific cell-wall synthesis pleiotropically affects developmental gene expression in an ssgA mutant of *Streptomyces coelicolor. Mol. Microbiol*. 64(5): 1244–1259.

Norrander J., Kempe T and Messing J (1983). Construction of improved M13 vectors using oligodeoxynucleotide-directed mutagenesis. *Gene*. 26(1): 101-106.

Nouioui, I., Carro, L., García-López, M., Meier-Kolthoff, JP., Woyke, T., Kyrpides, NC., Pukall, R., Klenk, H, P., Goodfellow, M and Göker, M (2018). Genome-Based Taxonomic Classification of the Phylum *Actinobacteria*. *Front Microbiol*. 9:2007.

Ochi K (2016). Insights into microbial cryptic gene activation and strain improvement: principle, application and technical aspects. *The Journal of Antibiotics*. 70: 25-40

Ohnishi Y, Kameyama S, Onaka H, Horinouchi S (1999). The A-factor regulatory cascade leading to streptomycin biosynthesis in *Streptomyces griseus*: identification of a target gene of the A-factor receptor. *Mol Microbiol*. 34(1): 102-111.

Okuda M., Fourmy D., Yoshizawa S (2017). Use of Baby Spinach and Broccoli for imaging of structured cellular RNAs. *Nucleic Acids Research*. 45(3):1404-1415

Omura, S., Takahashi, Y., Iwai, Y., and Tanaka, H (1982). *Kitasatosporia*, a new genus of the order *Actinomycetales*. *The Journal of Antibiotics*. 35(8): 1013–1019.

O'Neill J (2014). Antimicrobial resistance: tackling a crisis for the health and wealth of nations. London: *Review on Antimicrobial Resistance*, 2014.

Oren, A (2024). On validly published names, correct names, and changes in the nomenclature of phyla and genera of prokaryotes: a guide for the perplexed. *npj Biofilms Microbiomes* 10, 20.

Oren A and Garrity GM (2021). Valid publication of the names of forty-two phyla of prokaryotes. *International Journal of Systematic and Evolutionary Microbiology*. 71 (10): 005056

Ouellet, J (2016). RNA Fluorescence with Light-Up Aptamers. *Front Chem.* 4:29.

Owen GA., Pascoe B., Kallifidas D and Paget MSB (2007). Zinc-Responsive Regulation of Alternative Ribosomal Protein Genes in *Streptomyces coelicolor* Involves Zur and σ^R. *J Bacteriol*. 189(11): 4078-4086.

Pagan-Rodriguez D, Zhou X., Simmons R, Bethel CR, Andrea M., Hujer AM., Helfand MS., Jin Z., Guo B., Anderson VE., Ng LM., and. Bonomo RA (2004). Tazobactam Inactivation of SHV-1 and the Inhibitor-resistant Ser130 3 Gly SHV-1 -Lactamase. *Journal of Biological Chemistry*. 279 (19): 19494-19501

Paget MSB., Chamberlin L., Atrih A., Foster SJ and Buttner MJ (1999). Evidence that the extracytoplasmic function sigma factor ςE is required for normal cell wall structure in *Streptomyces coelicolor* A3(2). *J Bacteriol*. 181:204–211

Paige, J, S., Wu, K, Y., and Jaffery, S, R (2011). RNA mimics of green fluorescent protein. *Science*. 333:642-646.

Paradkar A (2013). Clavulanic acid production by *Streptomyces clavuligerus*: biogenesis, regulation and strain improvement. *The Journal of Antibiotics*. 66:411-420.

Park SS, Yang YH, Song E, Kim EJ, Kim WS, Sohng JK, Lee HC, Liou KK, Kim BG. 2009. Mass spectrometric screening of transcriptional regulators involved in antibiotic biosynthesis in Streptomyces coelicolor A3(2). *J Ind Microbiol Biotechnol* 36:1073-1083.

Parte, A. C. (2014) LPSN - List of prokaryotic names with standing in nomenclature. *Nucleic Acids Research*. doi: 10.1093/nar/gkt1111

Passot F, M., Cantlay, S., and Flärdh, K (2021). Protein phosphatase SppA regulates apical growth and dephosphorylates cell polarity determinant DivIVA in Streptomyces coelicolor. Molecular Microbiology. 117(2): 411-428.

Patro R., Duggal G., Love MI., Irizarry RA and Kingsford C (2017). Salmon provides fast and bias-aware quantification of transcript expression. *Nat Methods*.14(4):417-419.

Pauff, S., Withers, J, M., McKean, I, J, W., Mackay, S, P., and Burley, G, A (2017). Synthetic Biological Approaches for RNA Labelling and Imaging: Design Principles and Future Opportunities. *Current Opinion in Biotechnology*. 48: 153-158.

Pawlik K., Kotowska M and Kolesiński P (2010). *Streptomyces coelicolor* A3(2) Produces a New Yellow Pigment Associated with the Polyketide Synthase Cpk. *Journal of Molecular Microbiology and Biotechnology*. 19 (3): 147-151.

Pepler MAD., Mulholland EL., Montague FR and Elliot MA (2025). Defining the networks that connect RNase III and RNase J-mediated regulation of primary and specialized metabolism in *Streptomyces venezuelae*. *J Bacteriol*. 207:e00024-25.

Pérez-Llarena FJ., Liras P., Rodríguez-García A and Martín JF (1997). A regulatory gene (ccaR) required for cephamycin and clavulanic acid production in *Streptomyces clavuligerus*: amplification results in overproduction of both beta-lactam compounds. *J Bacteriol*. 179(6):2053-2059.

Petterson BMF and Kirsebom LA (2011). tRNA accumulation and suppression of the *bldA* phenotype during development in *Streptomyces coelicolor*. *Molecular Microbiology*. 79(6): 1602-1614.

Pickering BM and Willis AE (2005). The implications of structured 5′ untranslated regions on translation and disease. *Seminars in Cell and Developmental Biology*. 16: 39-47

Piret JM and Chater KF (1985). Phage-mediated cloning of *bldA*, a region involved in *Streptomyces coelicolor* morphological development, and its analysis by genetic complementation. *Journal of Bacteriology*. 163(3): 965-972.

Płachetka M., Krawiec M., Zakrzewska-Czerwińska J and Wolański M (2021). AdpA Positively Regulates Morphological Differentiation and Chloramphenicol Biosynthesis in *Streptomyces venezuelae*. *Microbiol Spectr.* 9 (3): e01981-21.

Pope MK., Green BD and Westpheling J (1996). The *bld* mutants *of Streptomyces coelicolor* are defective in the regulation of carbon utilization, morphogenesis and cell--cell signalling. *Mol Microbiol*.19(4):747-56.

Pope, MK., Green B and Westpheling J (1998). The *bldB* Gene Encodes a Small Protein Required for Morphogenesis, Antibiotic Production, and Catabolite Control in *Streptomyces coelicolor*. *Journal of Bacteriology*. 180(6): 1556-1562.

Pothoulakis, G., Ceroni, F., Reeve, B., and Ellis, T (2014). The spinach RNA aptamer as a characterization tool for synthetic biology. *ACS Synth Biol*. 3(3): 182-187,

Prestinaci, F., Pezzotti, P., and Pantosti, A (2015). Antimicrobial resistance: a global multifaceted phenomenon. *Pathog Glob Health.* 109(7): 309–18

Procópio REdL., da Silva IR., Martins MK., de Azevedeo JL and Araújo JM (2012). Antibiotics produced by *Streptomyces*. *The Brazillian Journal of Infectious Diseases*. 16(5): 466-471.

Prody GA, Bakos JT, Buzayan JM, Schneider IR and Bruening G (1986). Autolytic processing of dimeric plant virus satellite RNA. *Science.* 231: 1577–1580

Purssell, E (2019). Antimicrobials*. Understanding Pharmacology in Nursing Practise.* 4: 147-165.

Quainoo S., Coolen JPM., van Hijum SAFT., Huynen MA., Melchers WJK., van Schaik W and Wertheim HFL (2017). Whole-Genome Sequencing of Bacterial Pathogens: the Future of Nosocomial Outbreak Analysis. *Clin Microbiol Rev.* 30(4): 1015-1063.

Quandt J and Hynes MF (1993). Versatile suicide vectors which allow direct selection for gene replacement in gram-negative bacteria. 127(1): 15-21.

Quirós, L, M., Hardisson, C., and Salas, J, A (1986). Isolation and Properties of *Streptomyces* Spore Membranes. *Journal of Bacteriology*. 165(3): 923-928.

Raina M., Ibba M. (2014). tRNAs as regulators of biological processes. *Front. Genet.* 5:171.

Rabyk, M., Yushchuk, O., Rokytskyy, I., Anisimova, M., and Ostash, B (2018) Genomic Insights into evolution of AdpA family master regulators of morphological differentiation and secondary metabolism in *Streptomyces*. *J Mol Evol*. 86: 204–15.

Ray S., Dandpat SS., Chatterjee S and Walter NG (2022). Precise tuning of bacterial translation initiation by non-equilibrium 5′-UTR unfolding observed in single mRNAs. *Nucleic Acid Research*. 50 (15): 8818-8833.

Raynal A., Karray F., Tuphile K., Darbon-Rongère E and Pernodet J-C (2006). Excisable Cassettes: New Tools for Functional Analysis of *Streptomyces* Genomes. *Appl Environ Microbiol*. 72(7): 4839-4844.

Redenbach M, Kieser HM, Denapaite D, Eichner A, Cullum J, Kinashi H and Hopwood DA (1996). A set of ordered cosmids and a detailed genetic and physical map for the 8 Mb *Streptomyces coelicolor* A3(2) chromosome. *Mol Microbiol*; 21:77–96.

Rees HC., Gogacz W., Li NS., Koirala D and Piccirilli JA (2023). Structural basis for fluorescence activation by Pepper RNA. *ACS Chem Biol*. 17(7):1866–1875.

Ríos-Fernández P., Caicedo-Montoya C and Ríos-Estepa R (2024). Genomic Diversity of *Streptomyces clavuligerus*: Implications for Clavulanic Acid Biosynthesis and Industrial Hyperproduction. *Int J Mol Sci*. 25(20): 10992.

Reygaert, W, C (2018). An overview of the antimicrobial resistance mechanisms of bacteria. *AIMS Microbiol.* 4(3): 482-501.

Rokytskyy, I., Koshla, O., Fedorenko, V and Ostash B (2016). Decoding options and accuracy of translation of developmentally regulated UUA codon in *Streptomyces*: bioinformatic analysis. *SpringerPlus*. 5: 982.

Romeo T, Vakulskas CA and Babitzke P (2013). Post-transcriptional regulation on a global scale: form and function of Csr/Rsm systems. *Environmental Microbiology*. 15(2): 313-324.

Romero-Rodríguez A., Robledo-Casados I and Sánchez S (2015). An overview on transcriptional regulators in *Streptomyces. Biochim Biophys Acta*. 1849(8):1017-39

Ruban-Ośmiałowska, B., Jakimowicz, D., Smulczyk-Krawczyszyn, A., Chater, K, F., and Zakrzewska-Czerwińska, J. (2006) Replisome localization in vegetative and aerial hyphae of *Streptomyces coelicolor. Journal of Bacteriology*. 188(20): 7311–7316.

Ruiz-Villafán B., Cruz-Batista R., Mango-Ruiz M., Passari AK., Villareal-Gómez K., Rodríguez-Sanoja R and Sánchez S (2021). Carbon catabolite regulation of secondary metabolite formation, an old but not well-established regulatory system. *Microbial Biotechnology*. 15(4): 1058-1072.

Ryding NJ., Anderson TB and Champness WC (2002). Regulation of the *Streptomyces coelicolor* calcium-dependent antibiotic by *absA*, encoding a cluster-linked two-component system. *J Bacteriol*. 184(3):794-805.

Ryding, N, J., Kelemen, G, H., Whatling, C, A., Flärdh, K., Buttner, M, J., and Chater, K, F (1998). A developmentally regulated gene encoding a repressor-like protein is essential for sporulation in *Streptomyces coelicolor* A3(2). *Mol Microbiol*. 29: 343–357.

Salam MA, Al-Amin MY, Salam MT, Pawar JS, Akhter N, Rabaan AA and Alqumber MAA (2023) Antimicrobial Resistance: A Growing Serious Threat for Global Public Health. *Healthcare (Basel).* 11(13):1946.

Salas, J, A., Guijarro, J, A., and Hardisson, C (1983). High calcium content in *Streptomyces* spores and its release as an early even during spore germination. *J. Bacteriol*. 155(3): 1316-1323.

Salas, J, A., Quiros, L, M., and Hardisson, C (1984). Pathways of glucose catabolism during germination of *Streptomyces* spores. *FEMS Microbiology Letters*. 22(3): 229-233.

Sambrook, J., Fritsch, E. R., & Maniatis, T. (1989). Molecular Cloning: A Laboratory Manual (2nd ed.). Cold Spring Harbor, NY: Cold Spring Harbor Laboratory Press.

Sánchez de la Nieta R., Santamaría RI and Díaz M (2022). Two-Component Systems of *Streptomyces coelicolor*: An Intricate Network to Be Unraveled. *Int J Mol Sci*. 23(23):15085

Santra, K., Geraskin, I., Nilsen-Hamilton, M., Kraus, G, A., and Petrich, J, W (2019). Characterization of the Photophysical Behaviour of DFHBI Derivatives: Fluorogenic Molecules that Illuminate the Spinach RNA Aptamer. *J. Phys. Chem. B*. 123(11): 2536-2545.

Saudagar PS., Survase SA and Singhal RS (2008). Clavulanic acid: a review. *Biotechnology Advances*. 26(4): 335-351.

Schlimpert S and Elliot MA (2023). The Best of Both Worlds—*Streptomyces coelicolor* and *Streptomyces venezuelae* as Model Species for Studying Antibiotic Production and Bacterial Multicellular Development. *Journal of Bacteriology*. 205(7): e00153-23

Schrempf, H (2001). Recognition and degradation of chitin by streptomycetes. *Antonie van Leeuwenhoek*. 79(3): 285–289.

Schrödinger, L. & DeLano, W., 2020. *PyMOL*, Available at: http://www.pymol.org/pymol.

Schumacher, M, A., den Hengst, C, D., Bush, M, J., Le, T, B, K., Trah, N, T., Chandra, G., Zeng, W., Travis, B., Brennen, R, G., and Buttner, M, J (2018). The MerR-Like protein BldC binds DNA direct repeats as cooperative multimers to regulate *Streptomyces* development. *Nature Communications*. 9: 1139

Schuntermann DB, Jaskolowski M, Reynolds NM and Vargas-Rodriguez O (2024). The central role of transfer RNAs in mistranslation. *J Biol Chem*.300(9):107679.

Seemann T (2014). Prokka: rapid prokaryotic genome annotation. *Bioinformatics*. 30(14): 2068-2069.

Seipke, R, F., Kaltenpoth, M., and Hutchings, M, I (2012). *Streptomyces* as symbionts: an emerging and widespread theme?. *FEMS Microbiology Reviews*. 36(4): 862-876.

Seo PW., Kim GJ and Kim JS (2024). A short guide on blue fluorescent proteins: limits and perspectives. *Appl Microbiol Biotechnol*. 108(1): 208

Servin JA., Herbold CW., Skophammer RG and Lake JA (2008). Evidence Excluding the Root of the Tree of Life from the Actinobacteria. *Molecular Biology and Evolution*, 25 (1): 1–4

Seshadri R, Roux S, Huber KJ, Wu D, Yu S, Udwary D, Call L, Nayfach S, Hahnke RL, Pukall R, White JR, Varghese NJ, Webb C, Palaniappan K, Reimer LC, Sardà J, Bertsch J, Mukherjee S, Reddy TBK, Hajek PP, Huntemann M, Chen IA, Spunde A, Clum A, Shapiro N, Wu ZY, Zhao Z, Zhou Y, Evtushenko L, Thijs S, Stevens V, Eloe-Fadrosh EA, Mouncey NJ, Yoshikuni Y, Whitman WB, Klenk HP, Woyke T, Göker M, Kyrpides NC and Ivanova NN (2022). Expanding the genomic encyclopedia of *Actinobacteria* with 824 isolate reference genomes. *Cell Genom*. 2(12):100213.

Sevcikova B., Rezuchova, B., Homerova, D., and Kormanec, J (2010). The Anti-Anti-Sigma Factor BldG Is Involved in Activation of the Stress Response Sigma Factor σH in *Streptomyces coelicolor* A3 (2). *J Bacteriol*. 192(21): 5674-5681

Shanaa OS., Rumyantsev A., Sambuk E and Padkina M (2021). In Vivo Production of RNA Aptamers and Nanoparticles: Problems and Prospects. *Molecules*. 26:1422.

Shaner, N, C., Campbell, R, E., Steinbach, P, A., Giepmans, B, N, G., Palmer, A, E., and Tsien, R, Y (2004). Improved monomeric red, orange and yellow fluorescent proteins derived from *Discosoma* sp. red fluorescent protein. *Nature Biotechnology*. 22: 1567-1572.

Shaner, N, C., Steinbach, P, A., and Tsien, R, Y (2005). A guide to choosing fluorescent proteins. *Nature Methods*. 2(12): 905-909.

Shepard MD., Kharel MK., Bosserman MA and Rohr J (2010). Laboratory Maintenance of *Streptomyces* species. *Current Protocols in Microbiology*. https://doi.org/10.1002/9780471729259.mc10e01s18

Shimomura O., Johnson FH and Saiga Y (1962). Extraction, purification and properties of aequorin, a bioluminescent protein from the luminous hydromedusan, *Aequorea*. *J Cell Comp Physiol*. 59:223-239.

Shin CH., Cho HS., Won HJ., Kwon HJ., Kim CW and Yoon YJ (2021). Enhanced production of clavulanic acid by improving glycerol utilization using reporter-guided mutagenesis of an industrial *Streptomyces clavuligerus* strain. *J Ind Microbiol Biotechnol*. 48(3-4):kuab004. doi: 10.1093/jimb/kuab004.

Shin J., Oh S., Kim S and Roe J (2007). The Zinc-Responsive Regulator Zur Controls a Zinc Uptake System and Some Ribosomal Proteins in *Streptomyces coelicolor* A3(2). *Journal of Bacteriology*. 189(11): 4070-4077

Shu, X., Shaner, N, C., Yarbrough, C, A., Tsien, R Y., and Remington, S, J (2006). Novel Chromophores and Buried Charges Control Color in mFruits. *Biochemistry*. 45(32): 9639-9647.

Siegel, A, P., Baird, M, A., Davidson, M, W., and Day, R, N (2013). Strengths and Weaknesses of Recently Engineered Red Fluorescent Proteins Evaluated in Live Cells Using Fluorescence Correlation Spectroscopy. *Int. J. Mol. Sci*. 14(10): 20340-20358.

Silov S., Zaburannyi N., Anisimova M and Ostash B (2020). The Use of the Rare TTA Codon in *Streptomyces* Genes: Significance of the Codon Context? *Indian Journal of Microbiology*. 61(1): 24-30.

Sohoni SV., Fazio A., Workman CT., Mijakovic I and Lantz AE (2014). Synthetic Promoter Library for Modulation of Actinorhodin Production in *Streptomyces coelicolor* A3(2). *PLoS One*. 9(6):e99701.

Song W, Filonov GS, Kim H, Hirsch M, Li X, Moon JD and Jaffrey SR (2017). Imaging RNA polymerase III transcription using a photostable RNA-fluorophore complex. *Nat Chem Biol*.13(11):1187-1194.

Song, J, Y., Jeong, H., Yu, D, S., Fischbach, M, A., Park, H, S., Kim, J, J., Seo, J, S., Jensen, S, E., Oh, T, K., Lee, K, J., & Kim, J, F (2010). Draft genome sequence of *Streptomyces clavuligerus* NRRL 3585, a producer of diverse secondary metabolites. *Journal of Bacteriology*. 192(23): 6317–6318.

Song, W., Strack, R, L., Svensen, N., and Jaffrey, S, R (2014). Plug-and-Play Fluorophores Extend the Spectral Properties of Spinach. *J Am Chem Soc*. 136(4): 1198-1201.

Souque C., Ojeda IG and Baym M (2024): From Petri Dishes to Patients to Populations: Scales and Evolutionary Mechanisms Driving Antibiotic Resistance. *Annual Review of Microbiology*. 78: 361-382.

Sprusansky O., Stirrett K., Skinner D., Denoya C and Westpheling J (2005). The *bkdR* Gene of *Streptomyces coelicolor* Is Required for Morphogenesis and Antibiotic Production and Encodes a Transcriptional Regulator of a Branched-Chain Amino Acid Dehydrogenase Complex. *J Bacteriol* 187 (2): 664-671.

Squire SO., Sebghatti S and Hammond MC (2023). Cytoplasmic Accumulation and Permeability of Antibiotics in Gram Positive and Gram Negative Bacteria Visualized in Real-Time via a Fluorogenic Tagging Strategy. *ACS Chemical Biology*. 19(1): 3-8

Stackebrandt, E., Rainey, F, A., and Ward-Rainey, N, L (1997). Proposal for a New Hierarchic Classification System, *Actinobacteria* classis nov.. *International Journal of Systematic Bacteriology*. 47(2): 479–491.Waksman, S, A., and Henrici, A, T (1943). The Nomenclature and Classification of the Actinomycetes. *Journal of Bacteriology*. 46(4): 337–41

Stanier, R. Y (1942). Agar-decomposing strains of the *Actinomyces coelicolor* species-group. *Journal of Bacteriology*: 44(5): 555.

Stankovic N, Senerovic L, Ilic-Tomic T, Vasiljevic B, and Nikodinovic-Runic J (2014). Properties and applications of undecylprodigiosin and other bacterial prodigiosins. *Applied Microbiology and Biotechnology*. 98 (9): 3841–3858.

Steri M., Idda ML., Whalen MB and Orrù V (2018). Genetic variants in mRNA untranslated regions. *Wiley Interdiscip Rev RNA*. 9(4):e1474.

Stone JW., Munnoch JT and Hoskisson PA (2025). Whole-genome sequencing of the *Streptomyces coelicolor* bldA39 mutant (J1700) reveals hundreds of previously unknown mutations. *Access Microbiology*. 7:000958.v3

Stovall GM., Cox JC and Ellington AD (2004). Automated Optimization of Aptamer Selection Buffer Conditions. *SLAS Technology*. 9(3): 117-122.

Strack, R, L., Disney, M, D., and Jaffery, S, R (2014). A superfolding Spinach2 reveals the dynamic nature of trinucleotide repeat RNA. *Nat Methods*. 10(12): 1219-1224.

Strack, R, L., Song, W., and Jaffery S, R (2014). Using Spinach-based sensors for fluorescence imaging of intracellular metabolites and proteins in living bacteria. *Nat. Protoc*. 9: 146-155.

Strakova, E., Bobek, J., Zikova, A., Rehulka, P., Benada O., Rehulkova, H., Kofronova, O., and Vohradsky J (2012). Systems Insight into the Spore Germination of *Streptomyces coelicolor. J. Proteome Res*. 12:525-536.

Strakova, E., Bobek, J., Zikova, A., and Vohradsky, J (2013). Global features of gene expression on the proteome and transcriptome levels in *S. coelicolor* during germination. *PLOS ONE*. 8(9): e72842.

StrepDB. StrepDB: The Streptomyces Annotation Server. Available from: https://strepdb.streptomyces.org.uk/cgi-bin/dc3.pl?accession=AL645882&start=4291472&end=4302043&iorm=map&width=1200. Accessed: 25/03/2025

Subramaniam, G., Thakur, V., Saxena, R, K., Vadlamudi, S., Purohit, S., Kumar, V., Rathore, A., Chitikieni, A., and Varshney RK (2020). Complete genome sequence of sixteen plant growth promoting *Streptomyces* strain. *Nature Scientific Reports*. 10, Article Number:10924 (2020).

Sulton D., Pagan-Rodriguez D., Zhou X., Liu Y., Hujer AM., Bethel CR., Helfand MS., Thomson JM., Anderson VE., Buynak JD., Ng LM and Bonomo RA (2005). Clavulanic Acid Inactivation of SHV-1 and the Inhibitor-resistant S130G SHV-1 β-Lactamase: *INSIGHTS INTO THE MECHANISM OF INHIBITION*. *Journal of Biological Chemistry*. 280 (42): 35528-35536.

Sun L., Zheng P., Sun J., Wendisch VF and Wang Y (2023). Genome-scale CRISPRi screening: A powerful tool in engineering microbiology. *Engineering Microbiology*. 3(3): 100089.

Svensen, N., and Jaffrey, S, R (2016). Fluorescent RNA Aptamers as a Tool to Study RNA-Modifying Enzymes. *Cell Chemical Biology*. 23(3): 415-425.

Sydor PK., Barry SM., Odulate OM., Barona-Gomez F., Haynes SW., Corre C., Song L and Challis GL (2011). Regio and Stereodivergent Antibiotic Oxidative Carbocyclizations Catalyzed by Rieske Oxygenase-Like Enzymes. *Nat Chem*. 3(5): 388-392.

Taguchi T, Awakawa T, Nishihara Y, Kawamura M, Ohnishi Y *et al* (2017). Bifunctionality of ActIV as a cyclase-thioesterase revealed by *in vitro* reconstitution of actinorhodin biosynthesis in *Streptomyces coelicolor* A3(2). *Chembiochem*; 18:316–323

Taguchi T., Okamoto S., Lezhava A., Li A., Ochi K., Ebizuka Y and Ichinose K (2007). Possible involvement of ActVI-ORFA in transcriptional regulation of *act*VI tailoring-step genes for actinorhodin biosynthesis. *FEMS Microbiology Letters*. 269(2): 234-239.

Tahlan K., Anders C and Jensen SE (2004). The Paralogous Pairs of Genes Involved in Clavulanic Acid and Clavam Metabolite Biosynthesis Are Differently Regulated in *Streptomyces clavuligerus*. *Journal of Bacteriology*. 186(18): 6286-6297.

Takai K., Horie N., Yamaizumi Z., Nishimura S., Miyazawa T and Yokoyama S (1994). Recognition of UUN codons by two leucine tRNA species from *Escherichia coli*. *FEBS Letters*. 344(1): 31-34

Takano, E., Tao, M., Long., F., Bibb, M, J., Wang, L., Li, W., Buttner, M, J., Bibb, Deng, Z, X., and Chater, K, F (2003). A rare leucine codon in *adpA* is implicated in the morphological defect of *bldA* mutants of *Streptomyces coelicolor*. *Mol. Microbiol*. 50: 475–486.

Tavakoli K., Pour-Aboughadareh A., Kianersi F., Poczai P., Etminan A and Shooshtari L (2021). Applications of CRISPR-Cas9 as an Advanced Genome Editing System in Life Sciences. *BioTech (Basel).* 10(3):14.

Tawfik DS and Gruic-Sovulj I (2020). How evolution shapes enzyme selectivity - lessons from aminoacyl-tRNA synthetases and other amino acid utilizing enzymes. *FEBS J*; 287:1284–1305

Thoma L., Vollmer B and Muth G (2016). Fluorescence microscopy of Streptomyces conjugation suggests DNA-transfer at the lateral walls and reveals the spreading of the plasmid in the recipient mycelium. *Environ Microbiol*. 18(2): 598-608.

Tiefenbacher S., Pezo V., Marlière P., Roberts TM and Panke S (2024). Systematic analysis of tRNA transcription unit deletions in *E. coli* reveals insights into tRNA gene essentiality and cellular adaptation. *Scientific Reports*. 14:24102.

Tietze L and Lale R (2021). Importance of the 5′ regulatory region to bacterial synthetic biology applications. *Microbial Biotechnology*. 14(6): 2291-2315.

Tong Y., Whitford CM., Blin K., Jorgensen TS., Weber T and Yup Lee S (2020). CRISPR–Cas9, CRISPRi and CRISPR-BEST-mediated genetic manipulation in streptomycetes. *Nature Protocols*. 15: 2470-2502.

Trepanier NK., Jensen SE., Alexander DC and Leskiw BK (2002). The positive activator of cephamycin C and clavulanic acid production in *Streptomyces clavuligerus* is mistranslated in a *bldA* mutant. *Microbiology*. 148 (3): 643-656.

Tschowri N (2016). Cyclic Dinucleotide-Controlled Regulatory Pathways in *Streptomyces* Species. *J Bacteriol.*198(1):47-54.

Tschowri, N., Schumacher, M, A., Schlimpert, S., babu Chinnam, N., Findlay, K, C., Brennan, R, G., and Buttner, M, J (2014). Tetrameric c-di-GMP mediates effective transcription factor dimerization to control *Streptomyces* development. *Cell.* 158(5): 1136–1147.

Tsien RY (1998). The green fluorescent protein. *Annual Review of Biochemistry*. 67: 509–44.

Tuerk, C., and Gold, L (1990). Systematic evolution of ligands by exponential enrichment: RNA ligands to bacteriophage T4 DNA polymerase. *Science*. 249(4968): 505-510.

Ünsaldı E., Kurt-Kızıldoğan A., Voigt B., Becher D and Özcengiz G (2014). Proteome-wide alterations in an industrial clavulanic acid producing strain of *Streptomyces clavuligerus*. S*ynth Syst Biotechnol.* 2(1):39-48.

US Centers for Disease Control and Prevention. Antibiotic resistance threats in the United States, 2019. Atlanta, GA: US Department of Health and Human Services, 2019

van der Sijs A., Visser T., Moerman P., Folkers G., Kegel W (2024). Broccoli aptamer allows quantitative transcription regulation studies *in vitro*. *PLoS ONE* 19(6): e0304677.

van Wezel GP and McDowall KJ (2011). The regulation of the secondary metabolism of *Streptomyces*: new links and experimental advances. *Nat. Prod. Rep*. 28: 1311

Varani G and McClain WH (2000). The G.U wobble base pair. *EMBO Reports*. 1(1): 18-23.

Vecchione JJ., Alexander B Jr and Sello JK (2009). Two distinct major facilitator superfamily drug efflux pumps mediate chloramphenicol resistance in *Streptomyces coelicolor. Antimicrob Agents Chemother*. 53(11):4673-7.

Ventura M, Canchaya C, Tauch A, Chandra G, Fitzgerald GF, Chater KF and van Sinderen D (2007). Genomics of Actinobacteria: tracing the evolutionary history of an ancient phylum. *Microbiol Mol Biol Rev*. 71(3):495-548

Waksman, S, A (1950). The Actinomycetes: Their Nature, Occurance, Activities and Importance. Waltham, MA: Chronica Botanica Co.

Waksman, S, A (1961). The role of antibiotics in nature. *Perspectives in Biology and Medicine*. 4(3): 271–287.

Wang W., Li X., Xiang S., Feng X and Yang K (2013). An Engineered Strong Promoter for Streptomycetes. *Applied and Environmental Microbiology*. 79(14): 4484-4492.

Watve MG., Tickoo T., Jog MM and Bhole BD (2001). How many antibiotics are produced by the genus *Streptomyces*? *Archives of Microbiology*. 176: 386-390.

White J and Bibb MJ (1997). *bldA* dependence of undecylprodigiosin production in *Streptomyces coelicolor* A3(2) involves a pathway-specific regulatory cascade *J. Bacteriol*. 179: 627-633

WHO. Antimicrobial resistance. 2021. https://www.who.int/newsroom/fact-sheets/detail/antimicrobial-resistance (accessed May 08, 2022).

World Health Organization (2013) *WHO model list of essential medicines – 18th list*. Geneva: World Health Organization. (Accessed: 03/08/2025).

Williamson NR, Fineran PC, Gristwood T, Leeper FJ, Salmond GP (2006). The biosynthesis and regulation of bacterial prodiginines. *Nature Reviews Microbiology*. 4 (12): 887–899.

Willey, J, M., Santamaria, R., Guigarro, J., Geistlich, M., and Losick, R (1991). Extracellular complementation of a developmental mutation implicates a small sporulation protein in aerial mycelium formation in *S. coelicolor. Cell*. 65: 641:650.

Wittmann, A., and Suess, B (2012). Engineered riboswitches: expanding researcher's toolbox with synthetic RNA regulators. *FEBS Lett*. 586: 2076-2083.

Woese C (1987) Bacterial evolution. *Microbiol Rev*. 51(2):221–71.

Woese CR and Fox GE (1977) Phylogenetic structure of the prokaryotic domain: the primary kingdoms. *Proc Natl Acad Sci U S A*. 74(11):5088–90.

Wolański, M., Donczew, R., Kois-Ostroska, A., Masiewicz, P., Jakimowicz, D., and Zakrzewska-Czerwińska, J (2011). The Level of AdpA Directly Affects Expression of Developmental Genes in *Streptomyces coelicolor*. *J Bacteriol*. 193(22): 6358-6365.

Wolánski, M., Wali, R., Tilley, E., Jakimowicz, D., Zakrzewska-Czerwinska, J., and Herron, P (2011). Replisome Trafficking in Growing Vegetative Hyphae in *Streptomyces coelicolor* A3(2). *J. Bacteriol*. 193(5): 1273-1275.

Wright, F., and Bibb, M, J (1992). Codon usage in the G+C rich *Streptomyces* genome. *Gene.* 113(1): 55-65.

Wu G., Culley DE and Zhang W (2005). Predicted highly expressed genes in the genomes of *Streptomyces coelicolor* and *Streptomyces avermitilis* and the implications for their metabolism. *Microbiology*. 151: 2175-2187.

Wurmthaler LA, Klauser B and Hartig JS (2017). Highly motif- and organism-dependent effects of naturally occurring hammerhead ribozyme sequences on gene expression. *RNA Biol*. 15(2):231-241.

Xu Y and Li Z (2020). CRISPR-Cas systems: Overview, innovations and applications in human disease research and gene therapy. *Comput Struct Biotechnol J*. 18: 2401-2415

Xu Z., Wang Y., Chater KF., Ou HY., Xu HH., Deng Z and Tao M (2017). Large-Scale Transposition Mutagenesis of *Streptomyces coelicolor* Identifies Hundreds of Genes Influencing Antibiotic Biosynthesis. *Appl Environ Microbiol*. 83(6): e02889-16

Xu Z., Li Y., Wang Y., Deng Z and Tao M (2019). Genome-Wide Mutagenesis Links Multiple Metabolic Pathways with Actinorhodin Production in *Streptomyces coelicolor*. *Appl Environ Microbiol*. 85(7): e03005-18

Xu Z, Ji L, Tang W, Guo L, Gao C, Chen X, Liu J, Hu G and Liu L (2022). Metabolic engineering of *Streptomyces* to enhance the synthesis of valuable natural products. *Eng Microbiol*. 2(2):100022.

Yagüe P., López-García MT., Rioseras B., Sánchez J and Manteca A (2013). Pre-sporulation stages of *Streptomyces* differentiation: state-of-the-art and future perspectives. *FEMS Microbiol Lett*. 342(2):79-88.

Yagüe P., Rodríguez-García A., López-García MT., Rioseras B., Martín JF., Sánchez J and Manteca A (2014). Transcriptomic analysis of liquid non-sporulating *Streptomyces coelicolor* cultures demonstrates the existence of a complex differentiation comparable to that occurring in solid sporulating cultures. *PLoS One*. 9(1): e86296.

Yamazaki, H., Takano, Y., Ohnishi, Y., and Horinouchi, S (2003). *amfR*, an essential gene for aerial mycelium formation, is a member of the AdpA regulon in the A-factor regulatory cascade in *Streptomyces griseus*. *Mol Microbiol*. 50:1173–87.

Yan H., Lu X., Sun D., Zhuang S., Chen Q., Chen Z., Li J and Wen Y (2020). BldD, a master developmental repressor, activates antibiotic production in two *Streptomyces* species. *Molecular Microbiology*. 113(1): 123-142.

Yanofsky C (1981). Attenuation in the control of expression of bacterial operons. *Nature*. 289: 751-758.

Yanofsky C (2000). Transcription attenuation: once viewed as a novel regulatory strategy. *J Bacteriol*. 182(1):1-8.

Yared MJ., Marcelot A and Barraud P (2024). Beyond the Anticodon: tRNA Core Modifications and Their Impact on Structure, Translation and Stress Adaptation. *Genes (Basel).* 15(3):374.

Yi JS., Kim MW., Kim M., Jeong Y., Kim EJ., Cho BK and Kim BG (2017). A Novel Approach for Gene Expression Optimization through Native Promoter and 5` UTR Combinations Based on RNA-seq, Ribo-seq, and TSS-seq of *Streptomyces coelicolor*. *ACS Synth Biol*. 6(3):555-565.

Yus E., Yang JS., Sogues A and Serrano L (2017). A reporter system coupled with high-throughput sequencing unveils key bacterial transcription and translation determinants. *Nat Commun*. 8(1):368.

Zacharia VM, Ra Y, Sue C, Alcala E, Reaso JN, Ruzin SE and Traxler MF (2021). Genetic Network Architecture and Environmental Cues Drive Spatial Organization of Phenotypic Division of Labor in *Streptomyces coelicolor. mBio* 12 (3): e00794-21.

Zhao Y., Li G., Chen Y and Lu Y (2020). Challenges and Advances in Genome Editing Technologies in *Streptomyces*. *Biomolecules.* 10(5):734.

Zhao M., Wang SL., Tao XY., Zhao GL., Ren YH., Wang FQ and Wei DZ (2019). Engineering Diverse Eubacteria Promoters for Robust Gene Expression in *Streptomyces lividans. J. Biotechnol.* 289:93–102.

Zhang, Z., Wang, Y., and Ruan, J (1997). A Proposal To Revive the Genus *Kitasatospora* (Omura, Takahashi, Iwai and Tanaka, 1982). *International Journal of Systematic Bacteriology*. 47(4): 1048-1054.

Zhang WW and Matlashewski G (2024). Evidence for gene essentiality in *Leishmania* using CRISPR. *PLoS One*. 19(12):e0316331.

Zhang MM., Wong FT., Wang Y., Luo S., Lim YH., Heng E., Yeo WL., Cobb RE., Enghiad B., Ang EL and Zhao H (2017). CRISPR-Cas9 strategy for activation of silent *Streptomyces* biosynthetic gene clusters. *Nat Chem Biol*. 10.1038/nchembio.2341.

Zhang R., Xu W., Shao S and Wang Q (2021). Gene Silencing Through CRISPR Interference in Bacteria: Current Advances and Future Prospects. *Front Microbiol*. 12:635227.

Zhi, X. Y., Li, W. J. and Stackebrandt, E. (2009). An update of the structure and 16S rRNA gene sequence-based definition of higher ranks of the class Actinobacteria, with the proposal of two new suborders and four new families and emended descriptions of the existing higher taxa. *International Journal of Systematic and Evolutionary Microbiology*. doi: 10.1099/ijs.0.65780-0.

Appendix 1: Predicted mutations detected in *S. coelicolor* J1700 through whole genome sequencing

Uploaded to FigShare under DOI: https://figshare.com/s/ecf2c09cced260423b3d

See associated excel spreadsheet of predicted mutations and unassigned coverage evidence found in *S. coelicolor* J1700 after whole genome sequencing

Appendix 2: Codon usage in *Streptomyces.*

Triplet	Amino acid	Fraction	Frequency/ Thousand	Triplet	Amino acid	Fraction	Frequency/ Thousand
TTT	F	0.02	0.4	**TCT**	S	0.01	0.6
TTC	F	0.98	25.9	**TCC**	S	0.41	20.2
TTA	L	0.00	0.1	**TCA**	S	0.02	1.1
TTG	L	0.02	2.4	**TCG**	S	0.28	13.7
TAT	Y	0.05	1.0	**TGT**	C	0.09	0.7
TAC	Y	0.95	19.5	**TGC**	C	0.91	7.1
TAA	*	0.03	0.1	**TGA**	*	0.80	2.4
TAG	*	0.17	0.5	**TGG**	W	1.00	15.1
CTT	L	0.02	1.6	**CCT**	P	0.02	1.5
CTC	L	0.36	36.6	**CCC**	P	0.41	25.4
CTA	L	0.00	0.4	**CCA**	P	0.02	1.3
CTG	L	0.60	60.9	**CCG**	P	0.54	33.3
CAT	H	0.07	1.7	**CGT**	R	0.07	5.5
CAC	H	0.93	21.8	**CGC**	R	0.47	39.2
CAA	Q	0.05	1.4	**CGA**	R	0.03	2.6
CAG	Q	0.95	25.3	**CGG**	R	0.38	31.8
ATT	I	0.02	0.6	**ACT**	T	0.02	1.2
ATC	I	0.96	27.6	**ACC**	T	0.65	39.8
ATA	I	0.02	0.7	**ACA**	T	0.03	1.6
ATG	M	1.00	15.8	**ACG**	T	0.31	18.9
AAT	N	0.04	0.7	**AGT**	S	0.03	1.5
AAC	N	0.96	16.3	**AGC**	S	0.25	12.4
AAA	K	0.05	1.1	**AGA**	R	0.01	0.8
AAG	K	0.95	19.7	**AGG**	R	0.04	3.7
GTT	V	0.02	1.5	**GCT**	A	0.02	3.1
GTC	V	0.55	46.9	**GCC**	A	0.57	78.4
GTA	V	0.03	2.7	**GCA**	A	0.04	5.6
GTG	V	0.41	34.9	**GCG**	A	0.36	49.4

Appendix 3: Leucine codon usage in *S. coelicolor*

Uploaded to FigShare under DOI: https://figshare.com/s/501d15b6665350c643db

See attached excel spreadsheet of Leucine codon usage per *S. coelicolor* genes (TTA, TTG, CTG, CTC, CTA)

Appendix 4: Transcriptome analysis of *S. coelicolor* JWS-Δ*bldA*

Uploaded to FigShare under DOI: https://figshare.com/s/7cdcf045e9cb2ba2e00c

See associated excel spreadsheet containing all upregulated and downregulated genes detected in *S. coelicolor* JWS-Δ*bldA* following RNA-seq (Fold change <-1 1<)

Appendix 5: Published paper on Whole Genome Sequencing in *S. coelicolor* J1700

ACCESS MICROBIOLOGY
an open research platform

RESEARCH ARTICLE
Stone *et al.*, *Access Microbiology* 2025;7:000958.v3
DOI 10.1099/acmi.0.000958.v3

MICROBIOLOGY SOCIETY
OPEN DATA OPEN ACCESS

Whole-genome sequencing of the *Streptomyces coelicolor bldA39* mutant (J1700) reveals hundreds of previously unknown mutations

Jack W. Stone†, John T. Munnoch and Paul A. Hoskisson*

Abstract

We report the genome sequence of the *bldA39* (J1700) mutant of *Streptomyces coelicolor*, a historically important strain that is deficient in sporulation and antimicrobial production. The *S. coelicolor* J1700 strain was used extensively from the 1980s onwards to underpin important discoveries in development and antibiotic production in *Streptomyces*. The *bldA* gene encodes a leucyl tRNA, required for the translation of the rare TTA codon found in ~2% of genes in *Streptomyces*. The whole genome of *S. coelicolor* J1700 was obtained via Illumina sequencing and mapped to the *S. coelicolor* M145 reference genome. Analysis of the genome sequence compared to *S. coelicolor* M145 identified the known *bldA39* mutation (T>C) and revealed more than 300 further mutations, likely associated with the *S. coelicolor* J1501 genetic background the strain was created in, including the nature of the *hisA1* and *uraA1* alleles used extensively in genetic mapping experiments and several mutations in natural product biosynthetic gene clusters. This work highlights the importance of whole-genome sequencing of historically important strains.

DATA SUMMARY

This whole-genome sequencing project has been deposited in NCBI under the Bioproject PRJNA1186139. The WGS reads used can be accessed in the NCBI's SRA under the accession number SAMN44744323. Table S1 is available on Figshare 10.6084/m9.figshare.27798405[1].

INTRODUCTION

The bacterial genus *Streptomyces* has long been studied as a model for morphological differentiation and the production of natural products such as antibiotics [2]. Decades of genetic analysis of *Streptomyces* bacteria have enabled the identification of regulatory mechanisms that are essential for morphological development (formation of unigenomic spores on reproductive structures called aerial hyphae) and antibiotic production [3–5]. During these studies, numerous mutants have been isolated that are blocked at distinct stages of development, and these fall into two main classes: the so-called white (*whi*) mutants, which are able to form aerial mycelium but are unable to complete development into mature spores. The second class are the so-called bald (*bld*) mutants, which are blocked at an earlier stage of development, which prevents the erection of the aerial hyphae and subsequent development of spores. In addition to causing the loss of aerial mycelium, several mutations in *bld* loci have been found to pleiotropically block antibiotic production [6, 7].

Amongst the most severe *bld* phenotypes that have been identified to date were associated with the *bldA* locus, where mutations result in complete loss of morphological development and natural product production [8, 9]. The *bldA* locus was the first morphological mutant mapped by Hopwood [10] as *bldA1* (S48), with further mapping efforts of Merrick [11] characterizing 12 *bld* mutants into 4 mapping groups, 5 of which were *bldA* alleles. The *bldA* locus was cloned by Piret and Chater [12] and subsequently shown to encode a leucyl tRNA, required for the translation of the rare TTA

Access Microbiology is an open research platform. Pre-prints, peer review reports, and editorial decisions can be found with the online version of this article.
Received 19 November 2024; Accepted 08 January 2025; Published 14 February 2025
Author affiliations: †Strathclyde Institute of Pharmacy and Biomedical Sciences, University of Strathclyde, Glasgow, 161 Cathedral Street, G4 0RE, UK.
***Correspondence:** Paul A. Hoskisson, paul.hoskisson@strath.ac.uk
Keywords: antibiotic; *bldA*; development; morphological mutant; sporulation; *Streptomyces*.
Abbreviations: aaRS, aminoacyl-tRNA synthetase; BGC, biosynthetic gene cluster; CDA, calcium-dependent antibiotic; TSB, tryptone soy broth.
†Present address: School of Life Sciences, Gibbet Hill Campus, University of Warwick, Coventry, CV4 7AL, UK.

codon found in ~2% of genes in *Streptomyces* [13, 14]. The Leu-tRNA^{UUA} accumulates late in growth [13, 15, 16], with much of the *bldA*-associated phenotype believed to be mediated via the highly conserved, TTA-codon containing global transcriptional regulator, AdpA [7, 17]. The effect that *bldA* disruption has on the control of antibiotic production has also been attributed to TTA codons present in biosynthetic gene cluster (BGC) situated regulators such as *actII-ORF4*, *redD* (in *Streptomyces coelicolor* [18, 19]) and *ccaR* (in *Streptomyces clavuligerus* [20]).

Amongst the original *bldA* mutants characterized by Merrick [11] was the *bldA39*, a mutation that was subsequently used in phage cloning experiments to transfer the mutation [12] to the *S. coelicolor* J1501 strain background (*his1A*, *ura1A*, *strA1*, *pgl-1*, SCP1$^-$, SCP2$^-$ [21]) that was historically used for genetic mapping experiments. This created the *S. coelicolor* J1700 (*bldA39*) strain that was subsequently used in studies by Leskiw *et al.* [14–16] to characterize the *bldA* gene. The genetic lesion leading to the *bldA* morphological phenotype can be complemented through the addition of a copy of the *bldA* gene on a phage [12] and by integrating plasmids (Stone, Munnoch and Hoskisson, unpublished). Studies of antibiotic production in the *S. coelicolor* J1700 (*bldA39*) strain found that there is reduced expression of genes in the undecylprodigiosin (*red*) BGC [21]. Actinorhodin (*act*) production appears to be predominantly regulated at the level of transcription, although translation fusions of the 5′ end of *actII-ORF4* containing a single UUA codon to an *ermE* gene demonstrated that the *bldA* tRNA is present and functional early in growth [22].

Many of the studies to date on *bldA* have been conducted in the *S. coelicolor* J1700 (*bldA39*) strain; however, the wider genetic background of this strain is currently unknown. Here, we describe the genome sequencing of the *S. coelicolor* J1700 mutant and provide further information on additional mutations in that strain background. These data are deposited in NCBI under the Bioproject PRJNA1186139. The WGS reads (paired-end Illumina data) used can be accessed in the NCBI's SRA under the accession number SAMN44744323.

METHODS

S. coelicolor J1700 was grown for 24 h in Tryptone Soy Broth (TSB) media at 30 °C, shaking at 200 r.p.m. The genomic DNA of the strain was extracted according to Kieser *et al.* [23], and modifications were provided in Actinobase [24]. Sequencing was performed by Novogene using the Illumina NovaSeq 6000 platform. DNA sequence analysis enabled the mapping of the reads to the *S. coelicolor* M145 chromosome [25]. Breseq [26] mapping analysis of each strain was performed (using default settings, without predict-polymorphisms) and the output GenomeDiff files were compared (gdtools COMPARE). The analysis reports 'predicted mutations', including small variants (indels and single nucleotide changes), regions of 'unassigned missing coverage evidence' (typically large deletions) and 'unassigned new junction evidence' where multiple forms of the same sequence are suggested by the data (typically deletions with read coverage of the *S. coelicolor* M145 reference sequence also present). Mutations were then transferred to the reference genome (using gdtools APPLY) generating a FASTA, GENBANK and GFF3 version of the genome. This was carried out for all mutations in 'predicted mutations' while necessary manual edits were made as required. Auxotroph analysis was carried out according to Kieser *et al.* [23].

RESULTS & DISCUSSION

S. coelicolor J1700 has extensive mutations across the genome that likely reflect the genotype of the parental strain J1501

The whole-genome sequence of *S. coelicolor* J1700 was determined at 137.6× coverage and was mapped to the wild-type *S. coelicolor* M145 strain (NC_003888.3) [22] (Fig. 1). The *S. coelicolor* J1700 strain was originally constructed in the *S. coelicolor* J1501 genetic background (*his1A, ura1A, strA1, pgl-1,* SCP1$^-$, SCP2$^-$) that was historically used for genetic mapping experiments [23]. The *S. coelicolor* J1700 strain was created through phage-mediated transfer of the *bldA39* mutation [12] to *S. coelicolor* J1501, although the overall genetic background of the strain remains unknown.

The genome of *S. coelicolor* J1700 was found to be 8 608 660 bp (Fig. 1), consisting of 7823 CDSs (compared to the 7846 CDSs in *S. coelicolor* M145 [25]). Following the Breseq analysis, an 'unassigned missing coverage evidence' region of the *S. coelicolor* J1700 genome was identified, which indicates a 53 414 bp deletion between 7 014 046 bp and 7 071 460 bp of the genome. This deletion results in the loss of the *SCO6353-SCO6406* genes. Comparison with *S. coelicolor* M145 reveals that there are 324 mutations in J1700 (Fig. 1 and Table S1: 10.6084/m9.figshare.27798405, available in the online Supplementary Material). The mutations in *S. coelicolor* J1700 are characterized as 121 non-synonymous mutations, 78 synonymous mutations, 74 intergenic mutations, 39 coding frameshifts, 3 pseudogenes (SCO0634, SCO2890 and SCO4318), 3 deletions of ~1 kb (affecting SCO3991–SCO3991, [SCO4697]–[SCO4699] and SCO5630–[SCO5632], where the square brackets indicate a potential polar affect on that gene), 3 non-sense, 2 non-coding (including *bldA* and methionine tRNA anticodon CAT) and 2 non-stop mutations. It is likely that many of these mutations reflect those in the *S. coelicolor* J1501 genetic background in which J1700 was constructed [12].

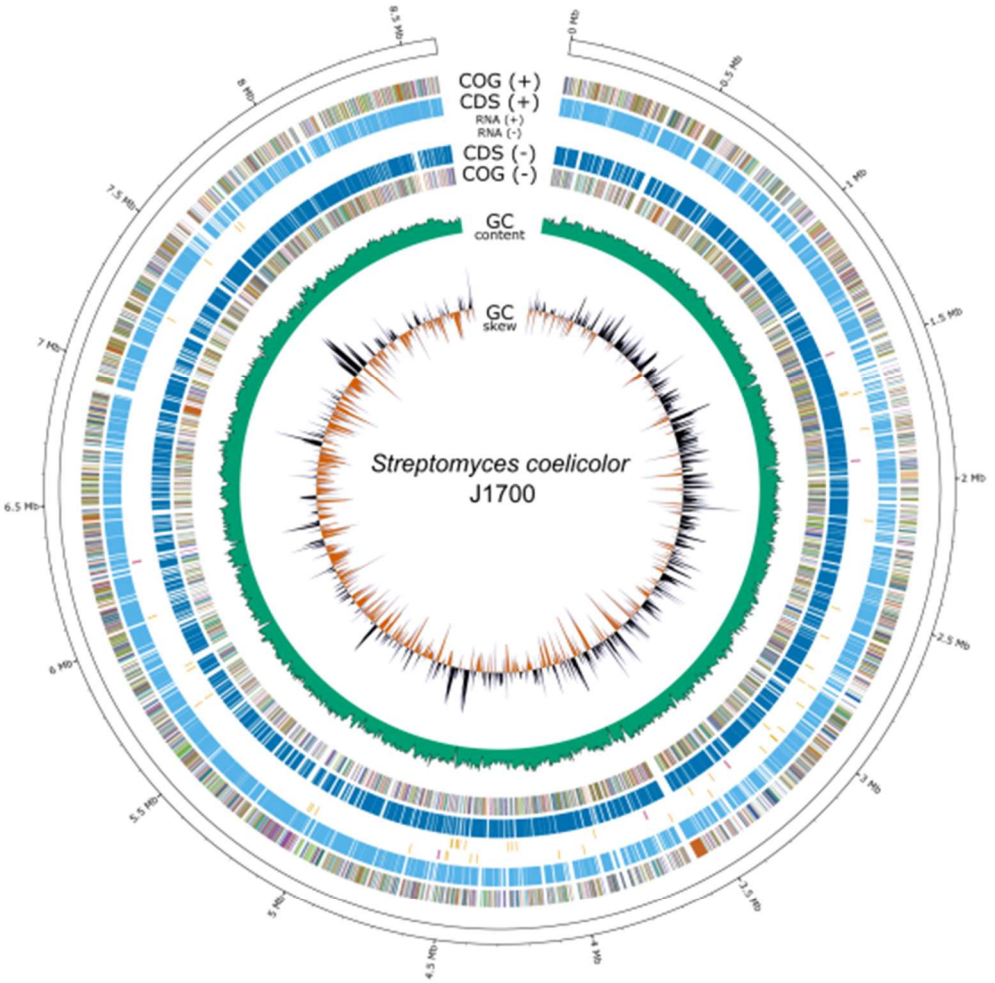

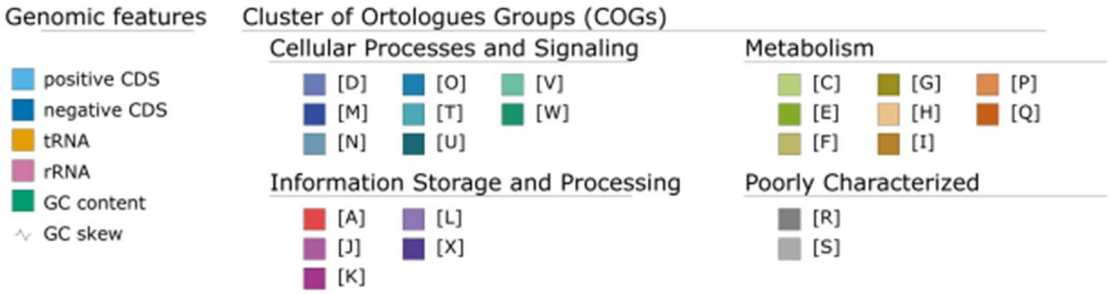

Fig. 1. GenoVi visualization of the *S. coelicolor* J1700 genome [35]. Labelling from outside to the inside: COGs [36] (forward strand); CDS, tRNAs and rRNAs (forward strand); CDS, tRNAs and rRNAs (reverse strand); COGs (reverse strand); Genome G+C content; Genome GC skew.

The *bldA39* mutation in *S. coelicolor* J1700 results in an anticodon change from Leu-UAA to Ser-UGA

Lawlor *et al.* [13] first showed that the *bldA39* mutation results in a mutation in the anticodon loop of the Leucyl-tRNA^{UUA}, which generates a putative seryl-anticodon. It is currently unclear if this tRNA species can be charged with serine by the cognate aminoacyl-tRNA synthetase (aaRS). Given the selectivity of aaRSs enzymes, this is unlikely as there are limited editing mechanisms in the aaRSs between the cognate tRNAs for serine and leucine [27]. The *bldA39* mutant represents the only 'classical' *bldA* mutant strain that disrupted the tRNA anticodon, with other mutations affecting the anticodon stem of the tRNA^{bldA} (*bldA1* [nt 28 G-A]) and the tRNA^{bldA} D-arm (*bldA16* [nt 22 C-T], *bldA62* [nt 23 A-C]) [21]. The single nucleotide T-C mutation attributed to the *bldA39* phenotype is found at position 3 380 959 in *S. coelicolor* J1700 chromosome (position 3 380 943 in *S. coelicolor* M145).

Discrepancies in undecylprodigiosin expression on *S. coelicolor* J1700 may be the result of *IS110* located in the BGC (*red*)

AntiSMASH [28] of the *S. coelicolor* J1700 genome revealed the presence of all 24 BGCs known from *S. coelicolor* M145. A detailed investigation of the BGCs indicated that there are several mutations within these gene clusters.

Guthrie and Chater [21] reported reduced *red* gene expression in the *S. coelicolor* J1700 strain using *xylE* transcriptional reporter strains. Examination of the *S. coelicolor* J1700 reveals the presence of a synonymous mutation in the undecylprodigiosin BGC pathway-specific regulator *redD* [19] (SCO5877: CTC-CTT; L150L). This reflects a change to a much less frequently used codon, but which is unlikely to impact significantly on *red* gene expression. More likely to affect transcription of the *red* cluster in *S. coelicolor* J1700 is the presence of an *IS110* element [29] in the intergenic region between SCO5885 (putative membrane protein) and SCO5886 (*redR*, which encodes a 3-oxoacyl-[acyl-carrier protein] synthase II) at position 6 442 702 bp in the genome.

Further mutations in BGCs were noted, such as in the coelichelin BGC, with a synonymous mutation in a putative peptide synthetase (SCO0492; TTC-TTT; F2247F). Two non-synonymous mutations were noted in the calcium-dependent antibiotic (CDA) BGC in the CDA peptide synthetase I (SCO3230; CTC-GTC; L3479A; and GCC-GTC; A5927V). A non-synonymous mutation was also identified in the actinorhodin (*act*) BGC, in the ActIV bifunctional cyclase [second ring] thioesterase [30] (SCO5091; GCG-GAC; A689D). Additional mutations are also present in the coelimycin BGC [31], where two synonymous mutations are present in *cpkPβ* (SCO6269: GCG-GCC; A179A; and GCG-GCA; A166A) and two further synonymous mutations in *cpkC* (SCO6273: AAG-AAA; K562K; and GGG-GGC; G561G).

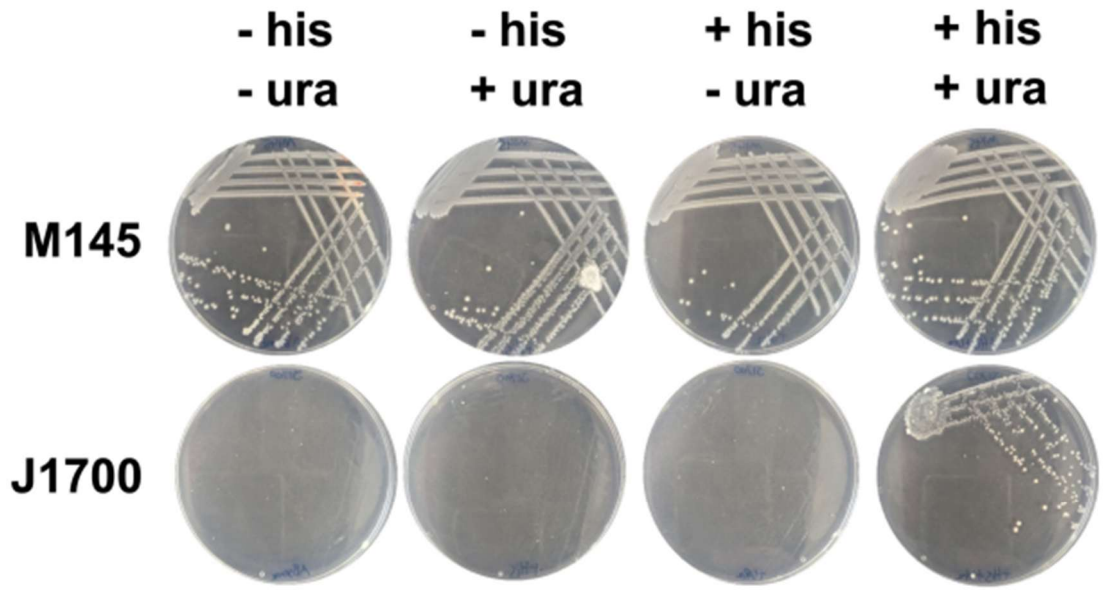

Fig. 2. Auxotrophic analysis of the *S. coelicolor* J1700 strain. The *S. coelicolor* wild-type (M145) and *bldA39* (J1700) strain were grown in the presence of histidine (his) or uracil (ura) according to Kieser *et al.* [23] to test for auxotrophy based on the genotype of the parental strain *S. coelicolor* J1501.

The consequences of these mutations are unknown; however, with mostly synonymous mutations present in the BGC genes, there are unlikely to be significant effects on the phenotype of *S. coelicolor* J1700, with extensive complementation studies required to assess potential effects on phenotype and through mRNA stability where synonymous changes are present.

The *hisa1* genotype is a result of mutation in the histidinol dehydrogenase gene, *hisD*

One of the genetic markers present in *S. coelicolor* J1501 strain, the progenitor of the *bldA*39 strain J1700, is *hisA1*. Strains carrying this mutation are histidine auxotrophs [23]. The designation of *hisA1* as a mapping group is well established, but the literature is not clear about where the mutation that results in histidine auxotrophy is situated. This may reflect the use of '*hisA*' a complementation group in older work on *S. coelicolor* genetics. Work from Limauro *et al.* [32] suggests that the so-called *hisA* gene in *S. coelicolor* was in fact an ortholog of *hisD*, the histidinol dehydrogenase in *Escherichia coli*. Histidinol dehydrogenase catalyses the terminal reaction in histidine biosynthesis that oxidizes L-histindol to L-histidine and in *S. coelicolor* is the first gene in a three-gene operon (*hisDCB*). Sequencing of *S. coelicolor* J1700 identified a missense mutation in the gene *hisD* (T-C) resulting in an E264G change in histidinol dehydrogenase. This mutation maps to the region of the protein that coordinates a catalytic zinc ion that is required for substrate binding [33]. To confirm the requirement of *S. coelicolor* J1700 for histidine, growth on minimal media was tested for its ability to support *S. coelicolor* J1700 in the presence and absence of histidine, confirming auxotrophy (Fig. 2).

The *uraA1* mutation maps to the putative uridine 5′-monophosphate synthase in *S. coelicolor* J1700

A further historic and widely used genetic marker in *S. coelicolor* J1501 is *uraA1*, where strains exhibit uracil auxotrophy. Analysis of the mutations detected in *S. coelicolor* J1700 revealed that there was no mutation present in the *uraA* gene, suggesting that this may also reflect the use of *uraA* as a complementation group designation rather than a gene designation. Auxotrophy analysis of the strain revealed *S. coelicolor* J1700 is auxotrophic for uracil (Fig. 2). Analysis of the genome mutations in *S. coelicolor* J1700 identified a putative uridine 5′-monophosphate synthase (SCO3650: *pyrE*) that possesses a frameshift mutation resulting in a 10 bp deletion (99–108/549 nt) towards the 5′ end of the CDS. The *pyrE* gene also maps to the *uraA1* location of the physical map of the *S. coelicolor* chromosome [34], suggesting that it is this mutation that results in uracil auxotrophy in *S. coelicolor* J1700. Uridine 5′-monophosphate synthases catalyse the formation of uridine monophosphate as an initial step in uridine triphosphate biosynthesis and RNA metabolism. This led us to conclude that uracil auxotrophy is likely the result of a frameshift in *pyrE* of *S. coelicolor*.

SUMMARY

The whole-genome sequencing of bacterial strains has revolutionized the way microbiology is conducted. The sequencing of historical strains that have underpinned significant discoveries in particular fields can help to shed light on discrepancies in older literature, such as here around discrepancies in *red* gene expression in *S. coelicolor* J1700, that could be attributed to the presence of a previously discovered insertion element. Furthermore, the clarification of genetic markers that were historically used to map mutations can help clarify the literature for researchers who may never have undertaken genetic mapping experiments. Overall, the sequencing of the historically important *S. coelicolor* J1700 *bldA39* strain will provide a resource for researchers to use in studying development and antibiotic production in *Streptomyces*.

Funding information
PAH would also like to acknowledge funding from Leverhulme Trust (RPG-2023-128 supporting JTM) and the Royal Academy of Engineering Research Chair Scheme for long term personal research support (RCSRF2021\11\15).

Acknowledgements
The authors would like to thank Dr Neil Holmes (John Innes Centre jic.strepstrains@jic.ac.uk) for searching out the earliest lyophil available of J1700 in the John Innes Collection and Professor Mark J. Buttner (John Innes Centre) for helpful discussions.

Author contributions
J.W.S. – Investigation, Formal Analysis, Writing – Original Draft. J.T.M. – Formal Analysis, Writing – Original Draft. P.A.H. – Conceptualization, Funding Acquisition, Writing – Review and Editing, Supervision, Project Administration.

Conflicts of interest
The authors declare that there are no conflicts of interest.

References

1. **Stone J, Munnoch J, Hoskisson PA.** Whole-genome sequencing of the streptomyces coelicolor blda39 mutant (J1700) of reveals hundreds of previously unknown mutations. figshare. *Figshare*. 2024. . DOI: 10.6084/m9.figshare.27798405.v1https://doi.org/10.6084/m9.figshare.27798405.v1
2. **Schlimpert S, Elliot MA.** The best of both worlds—*Streptomyces coelicolor* and *Streptomyces venezuelae* as model species for studying antibiotic production and bacterial multicellular development. *J Bacteriol* 2023;205:e0015323.
3. **Chater KF.** Taking a genetic scalpel to the *Streptomyces* colony. *Microbiology* 1998;144:1465–1478.

4. **Bush MJ**, **Tschowri N**, **Schlimpert S**, **Flärdh K**, **Buttner MJ**. c-di-GMP signalling and the regulation of developmental transitions in streptomycetes. *Nat Rev Microbiol* 2015;13:749–760.
5. **Flärdh K**, **Buttner MJ**. *Streptomyces morphogenetics*: dissecting differentiation in a filamentous bacterium. *Nat Rev Microbiol* 2009;7:36–49.
6. **Chandra G**, **Chater KF**. Developmental biology of *Streptomyces* from the perspective of 100 actinobacterial genome sequences. *FEMS Microbiol Rev* 2014;38:345–379.
7. **Chandra G**, **Chater KF**. Evolutionary flux of potentially bldA-dependent *Streptomyces* genes containing the rare leucine codon TTA. *Antonie van Leeuwenhoek* 2008;94:111–126.
8. **Chater KF**, **Chandra G**. The evolution of development in Streptomyces analysed by genome comparisons. *FEMS Microbiol Rev* 2006;30:651–672.
9. **Hackl S**, **Bechthold A**. The gene bldа, a regulator of morphological differentiation and antibiotic production in *Streptomyces*. *Arch Pharm* 2015;348:455–462.
10. **Hopwood DA**. Genetic analysis and genome structure in *Streptomyces coelicolor*. *Bacteriol Rev* 1967;31:373–403.
11. **Merrick MJ**. A morphological and genetic mapping study of bald colony mutants of *Streptomyces coelicolor*. *J Gen Micro* 1976;96:299–315.
12. **Piret JM**, **Chater KF**. Phage-mediated cloning of bldA, a region involved in *Streptomyces coelicolor* morphological development, and its analysis by genetic complementation. *J Bacteriol* 1985;163:965–972.
13. **Lawlor EJ**, **Baylis HA**, **Chater KF**. Pleiotropic morphological and antibiotic deficiencies result from mutations in a gene encoding a tRNA-like product in *Streptomyces coelicolor* A3(2). *Genes Dev* 1987;1:1305–1310.
14. **Leskiw BK**, **Bibb MJ**, **Chater KF**. The use of a rare codon specifically during development? *Mol Microbiol* 1991;5:2861–2867.
15. **Leskiw BK**, **Mah R**, **Lawlor EJ**, **Chater KF**. Accumulation of bldA-specified tRNA is temporally regulated in *Streptomyces coelicolor* A3(2). *J Bacteriol* 1993;175:1995–2005.
16. **Leskiw BK**, **Lawlor EJ**, **Fernandez-Abalos JM**, **Chater KF**. TTA codons in some genes prevent their expression in a class of developmental, antibiotic-negative, *Streptomyces* mutants. *Proc Natl Acad Sci USA* 1991;88:2461–2465.
17. **Takano E**, **Tao M**, **Long F**, **Bibb MJ**, **Wang L**, ***et al.*** A rare leucine codon in adpA is implicated in the morphological defect of bldA mutants of *Streptomyces coelicolor*. *Mol Microbiol* 2003;50:475–486.
18. **Liu G**, **Chater KF**, **Chandra G**, **Niu G**, **Tan H**. Molecular regulation of antibiotic biosynthesis in *Streptomyces*. *Microbiol Mol Biol Rev* 2013;77:112–143.
19. **Malpartida F**, **Niemi J**, **Navarrete R**, **Hopwood DA**. Cloning and expression in a heterologous host of the complete set of genes for biosynthesis of the *Streptomyces coelicolor* antibiotic undecylprodigiosin. *Gene* 1990;93:91–99.
20. **Trepanier NK**, **Jensen SE**, **Alexander DC**, **Leskiw BK**. The positive activator of cephamycin C and clavulanic acid production in *Streptomyces clavuligerus* is mistranslated in a bldA mutant. *Microbiology* 2002;148:643–656.
21. **Guthrie EP**, **Chater KF**. The level of a transcript required for production of a *Streptomyces coelicolor* antibiotic is conditionally dependent on a tRNA gene. *J Bacteriol* 1990;172:6189–6193.
22. **Gramajo HC**, **Takano E**, **Bibb MJ**. Stationary-phase production of the antibiotic actinorhodin in *Streptomyces coelicolor* A3(2) is transcriptionally regulated. *Mol Microbiol* 1993;7:837–845.
23. **Kieser BM**, **Bibb M**, **Buttner M**, **Chater K**, **Hopwood D**. *Practical Streptomyces Genetics*. Norwich, UK: John Innes Foundation; 2000.
24. **Feeney MA**, **Newitt JT**, **Addington E**, **Algora-Gallardo L**, **Allan C**, ***et al.*** ActinoBase: tools and protocols for researchers working on *Streptomyces* and other filamentous actinobacteria. *Microb Genom* 2022;8:mgen000824.
25. **Bentley SD**, **Chater KF**, **Cerdeño-Tárraga A-M**, **Challis GL**, **Thomson NR**, ***et al.*** Complete genome sequence of the model actinomycete *Streptomyces coelicolor* A3(2). *Nature* 2002;417:141–147.
26. **Deatherage DE**, **Barrick JE**. Identification of mutations in laboratory-evolved microbes from next-generation sequencing data using breseq. *Methods Mol Biol* 2014;1151:165–188.
27. **Tawfik DS**, **Gruic-Sovulj I**. How evolution shapes enzyme selectivity - lessons from aminoacyl-tRNA synthetases and other amino acid utilizing enzymes. *FEBS J* 2020;287:1284–1305.
28. **Blin K**, **Shaw S**, **Kloosterman AM**, **Charlop-Powers Z**, **Wezel GP van**, ***et al.*** antiSMASH 6.0: improving cluster detection and comparison capabilities. *Nucleic Acids Res* 2021;49:W29–W35.
29. **Chater KF**, **Bruton CJ**, **Foster SG**, **Tobek I**. Physical and genetic analysis of IS110, a transposable element of *Streptomyces coelicolor* A3(2). *Mol Gen Genet* 1985;200:235–239.
30. **Taguchi T**, **Awakawa T**, **Nishihara Y**, **Kawamura M**, **Ohnishi Y**, ***et al.*** Bifunctionality of ActIV as a cyclase-thioesterase revealed by *in vitro* reconstitution of actinorhodin biosynthesis in *Streptomyces coelicolor* A3(2). *Chembiochem* 2017;18:316–323.
31. **Gomez-Escribano JP**, **Song L**, **Fox DJ**, **Yeo V**, **Bibb MJ**, ***et al.*** Structure and biosynthesis of the unusual polyketide alkaloid coelimycin P1, a metabolic product of the cpk gene cluster of *Streptomyces coelicolor* M145. *Chem Sci* 2012;3:2716.
32. **Limauro D**, **Avitabile A**, **Cappellano C**, **Puglia AM**, **Bruni CB**. Cloning and characterization of the histidine biosynthetic gene cluster of *Streptomyces coelicolor* A3(2). *Gene* 1990;90:31–41.
33. **Barbosa JARG**, **Sivaraman J**, **Li Y**, **Larocque R**, **Matte A**, ***et al.*** Mechanism of action and NAD+-binding mode revealed by the crystal structure of L-histidinol dehydrogenase. *Proc Natl Acad Sci USA* 2002;99:1859–1864.
34. **Redenbach M**, **Kieser HM**, **Denapaite D**, **Eichner A**, **Cullum J**, ***et al.*** A set of ordered cosmids and a detailed genetic and physical map for the 8 Mb *Streptomyces coelicolor* A3(2) chromosome. *Mol Microbiol* 1996;21:77–96.
35. **Cumsille A**, **Durán RE**, **Rodríguez-Delherbe A**, **Saona-Urmeneta V**, **Cámara B**, ***et al.*** GenoVi, an open-source automated circular genome visualizer for bacteria and archaea. *PLoS Comput Biol* 2023;19:e1010998.
36. **Galperin MY**, **Wolf YI**, **Makarova KS**, **Alvarez RV**, **Landsman D**, ***et al.*** COG database update: focus on microbial diversity, model organisms, and widespread pathogens. *Nucleic Acids Res* 2021;49:D274–D281.

Appendix 6: Python and R scripts used for bioinformatic experiments

Carbon and nitrogen utilization in *Streptomyces* (see Section 2.12)

CSV file melting (performed in Python v3.11.5)

```
import panda as pd


df = pd.read_csv( "../data/M145_PM1.csv ")


melted_df = pd.melt(df, id_vars= ['Hour'], var_name='Type', value_name='Value')


melted_df.to_csv( "../data/M145_PM1_melted.csv ", index=False)
```

Carbon and Nitrogen utilization visualization and figure generation (R v4.5.0)

```
if (!requireNamespace('BiocManager', quietly = TRUE))
 install.packages('BiocManager')

# Install ggplot2 and load the library
install.packages('ggplot2')
library('ggplot2')

# read csv data from files into a variable
data01 <- read.csv('//Users/Jack/Documents/Biolog/M145_PM1_melted.csv')
data02 <- read.csv('//Users/Jack/Documents/Biolog/bldA_PM1_melted.csv')


# Create a PDF file for saving the plot (smaller file size)
pdf(file='//Users/Jack/Documents/Biolog/bldA_PM1_data_annotated.pdf', width=30, hei
ght=15)

# Create the plot with the first data set
p <- ggplot(data01, aes(y = Value, x = Hour)) +
 geom_jitter(alpha = 0.2) +
 facet_wrap(Type ~ ., scales = 'free_x', nrow = 8, dir = 'h')

# Add lines for additional data sets
p <- p +
 geom_point(data = data02, aes(y = Value, x = Hour), color = 'red')
 geom_jitter(alpha = 0.2)

# Print the plot
print(p)

# Close the PDF device (saves the file)
dev.off()



########## Heatmaps
install.packages('pheatmap')
library('pheatmap')

##setwd to folder

#combining dataframes
```

```
combined_results_1= read_csv = read.csv('//Users/Jack/Documents/Biolog/Carbon_ut_M1
45_bldA.csv')

#changing column and row names
colnames(combined_results_1) = c('M145', 'JWS-ΔbldA')
rownames(combined_results_1) = c('A2: L-Arabinose',
         'A3: N-Acetyl-D Glucosamine',
         'A4: D-Saccharic Acid',
         'A5: Succinic Acid',
         'A6: D-Galactose',
         'A7: L-Aspartic Acid',
         'Repeat for A8 to H3, with specific BioLog well compounds',
         'H4: Tyramine',
         'H5: D-Psicose',
         'H6: L-Lyxose',
         'H7: Glucuronamide',
         'H9: L-Galactonic Acid-γ-Lactone',
         'H10: D-GalacturonicAcid',
         'H11: Phenylethylamine',
         'H12: 2-Aminoethanol')

#default clustering with heatmap
Heatmap_combined_results_1 = pheatmap(combined_results_1,
          main = 'Carbon utilization in S. coelicolor M145 and S. coelicolor JWS-Δb
ldA',
          angle_col = 0,
          cluster_rows=FALSE,
          cluster_cols = FALSE,
          display_numbers = TRUE,
          fontsize_row = 4,
          fontsize = 4,
          fontsize_col = 8,
          filename = '//Users/Jack/Documents/Biolog/Carbon_ut_M145_bldA.tiff')

#removing clustering form heatmap
Heatmap_combined_results_1 = pheatmap(combined_results_1,
          cluster_rows=TRUE,
          cluster_cols = FALSE,
          main = 'Carbon utilization in S. coelicolor M145 and S. coelicolor JWS-Δb
ldA',
          angle_col = 45,
          cellwidth = 40,
          display_numbers = FALSE,
          fontsize_row = 4,
          fontsize = 4,
          fontsize_col = 8,
          filename = '//Users/Jack/Documents/Biolog/Carbon_ut_M145_bldA.tiff')
```

```
# Load required library
library(ggplot2)

# Read the data
data03 <- read.csv('//Users/Jack/Documents/Biolog/Carbon_ut_violin.csv')
data03$Strain <- as.factor(data03$Strain)
head(data03)

# Define the expression for the y-axis label with appropriate size and bold formatt
ing
y_label <- expression('Specific growth rate ' * mu * ' (h'^{-1}*')')

# Generate the violin plot
p_violin <- ggplot(data03, aes(x = Strain, y = OD.r)) +
 geom_violin(fill = 'white') +
 geom_jitter(width = 0.2, size = 1.5) +   # Add jittered points
 labs(x = 'Strain (n=1)',     # Change x-axis label
```

```
  y = y_label) +      # Change Y-axis label
 scale_x_discrete(labels = c('M145', 'JWS-ΔbldA')) + # Change x-axis labels
 scale_y_continuous(limits = c(0, 0.3)) +  # Set Y-axis limits
 coord_cartesian(ylim = c(0, 0.4)) +
 theme_minimal() + # Use minimal theme by default
 theme(
 text = element_text(size = 24),
 axis.line.x.bottom = element_line(size = 1),
 axis.line.y.left = element_line(size = 1),
 plot.background = element_rect(fill = 'white'),
 panel.background = element_rect(fill = '#ECECEC'),
 panel.grid.major = element_line(color = 'black'),
 panel.grid.minor = element_blank(),
 axis.line = element_line(color = 'black'),
 axis.text = element_text(color = 'black', size = 24), # Removed bold from axis tex
t
 axis.title = element_text(color = 'black'), # Removed bold from axis titles
 axis.title.x = element_text(size = 24), # X-axis title size 24
 axis.title.y = element_text(size = 24), # Y-axis title size 24
 axis.text.x = element_text(size = 24),  # X-axis text size 24
 axis.text.y = element_text(size = 24),  # Y-axis text size 24
 panel.border = element_blank() # Remove border around plot
 )

# Save the violin plot to a file with custom theme
ggsave('//Users/Jack/Documents/Biolog/Carbon_ut_violin_graph.png', plot = p_violin,
width = 10, height = 6, units = 'in', dpi = 300)

# Display the violin plot
print(p_violin)
```

Frequency of leucine codons in *S. coelicolor* CDS (Python 3.11.5)

```
from Bio import SeqIO
from Bio.Seq import Seq
import pandas as pd
import os

### your fasta sequence file
fasta_file = '/Users/Jack/Documents/Thesis/Streptomyces/S_coelicolor_A3_2_AL645882.
2.fasta'
### you gff3 file
gff3_file = '/Users/Jack/Documents/Thesis/Streptomyces/S_coelicolor_A3_2_AL645882.2
_cleaned.gff3'
gff3 = pd.read_csv(gff3_file, sep = '\t', names = ['ID', 'source', 'feature', 'star
t', 'end', 'score', 'strand', 'phase', 'attributes'])

### output file name
output_file = '/Users/Jack/Documents/Thesis/Streptomyces/TTA_genes.txt'
### load fasta file
with open(fasta_file, 'r') as f:
 lines = f.readlines()
lines = lines[1:]
lines = [l.replace('\n', '') for l in lines]
lines = ''.join(lines)

### function to reverse complement genes on reverse strand
def reverse_complement(sequence):
 complement_dict = {'A': 'T', 'T': 'A', 'C': 'G', 'G': 'C'}
reverse_seq = sequence[::-1]
complement_seq = ''.join([complement_dict[base] for base in reverse_seq])
return complement_seq

### Function to find check if DNA sequence contain a certain codon in the correct r
eading frame
```

```
def find_codon(DNA_sequence, codon):
 seq = Seq(DNA_sequence)
codon_list = [DNA_sequence[i:i+3] for i in range(0, len(DNA_sequence), 3)]
the_count = codon_list.count(codon)
return the_count
### make dataframe with fasta sequences for all coding genes
fasta_sequences = []
CDS_df = pd.DataFrame()
for index, row in gff3.iterrows():
 if row['feature'] == 'CDS':
 if row['strand'] == '+':
 fasta_sequences.append(lines[row['start'] - 1:row['end']])
else:
 fasta_sequences.append(reverse_complement(lines[row['start'] - 1:row['end']]))
CDS_df = pd.concat([CDS_df, gff3[gff3.index == index]])
# attributes.append(row['attributes'])
# locus_tags.append(f'{row['start']}_{row['end']}_{row['strand']}')

CDS_df['fasta'] = fasta_sequences
### find genes with codon: TTA
TTA_genes = pd.DataFrame()
counts = []
for index, row in CDS_df.iterrows():
 if find_codon(row['fasta'], 'TTA') != 0:
 TTA_genes = pd.concat([TTA_genes, CDS_df[CDS_df.index == index]], ignore_index = T
rue)
counts.append(find_codon(row['fasta'], 'TTA'))
TTA_genes['n_TTA'] = counts
### extract gene names or gene synonoms from dataframe
def extract_names(attributes, id, exclude):
 thelist = []
for att in attributes:
 att_list = att.split(';')
x = 0
for a in att_list:
 if a.find(id) == 0 and exclude not in a:
 thelist.append(a[len(id) + 1:])
x += 1
break
if x == 0:
 thelist.append(f'no_{id}_name')
return thelist

def extract_uni(attributes, id):
 thelist = []
for att in attributes:
 n = att.find(id)
if n != -1:
 thelist.append(att[n + len(id) + 1: n + len(id) + 7])
else:
 thelist.append('no_uniprot_id')
return thelist

TTA_genes['gene'] = extract_names(TTA_genes['attributes'], 'gene', 'gene_synonym')
TTA_genes['gene_synonym'] = gene_synonyms = extract_names(TTA_genes['attributes'],
'gene_synonym', '@')
TTA_genes['uniprot'] = extract_uni(TTA_genes['attributes'], 'UniProtKB/TrEMBL')
### save TTA genes as file
TTA_genes.to_csv(output_file, sep = '\t', header = True, index = False)
TTA_genes['uniprot'].to_csv(output_file + '_unitprot.txt', sep = '\t', header = Fal
se, index = False)
```

RNA-seq in *S. coelicolor* JWS- Δ*bldA*

Salmon:

```
$ salmon index -t M145.fa.gz -i M145_index


#!/bin/bash

samp="bldA"

echo "Processing sample ${samp}"


salmon quant -i M145 -l A \

     -1 /Users/Jack/Documents/RNA/${samp}_1.fastq.gz \

     -2 /Users/Jack/Documents/RNA/${samp}_2.fastq.gz \

     -p 8 --validateMappings -o /Users/Jack/Documents/RNA/${samp}_quan
```

R:

```
if (!requireNamespace('BiocManager', quietly = TRUE))
 install.packages('BiocManager')

## install software
BiocManager::install('tximport')
BiocManager::install('tximportData')
BiocManager::install('GenomicFeatures')
BiocManager::install('RSQLite')
BiocManager::install('DESeq2')
BiocManager::install('apeglm')
BiocManager::install('EnhancedVolcano')
install.packages('tidyverse')
#Venn diagrams - https://mkempenaar.github.io/gene_expression_analysis/chapter-5.ht
ml#venn-diagram
install.packages('VennDiagram')
install.packages('futile.logger')
install.packages('pheatmap')

# load libraries
library('DESeq2')
library('tximport')
library('readr')
library('tximportData')
library('dplyr')
library('magrittr')
library('apeglm')
library('EnhancedVolcano')
library('VennDiagram')
library('pheatmap')
library('ggkegg')
library('ggfx')
library('igraph')
library('tidygraph')
library('ggraph')
library('clusterProfiler')



######### Perform DEseq analysis
```

```
# Import conditional files (contain sample name and condition A or B) and provide c
onditional information
samples_m145_vs_bldA <- read.table(file.path('~/Downloads/X204SC24086605-Z01-F001/R
/samples_m145_vs_bldA.txt'), header=TRUE)
samples_m145_vs_bldA$Condition <- factor(rep(c('A','B'), each=2))
# Add rownames to the data frames
rownames(samples_m145_vs_bldA) <- samples_m145_vs_bldA$Run
# Select columns 'Run' and 'Condition' for each sample comparison
samples_m145_vs_bldA[,c('Run','Condition')]
# Get paths for all quantification files
files_samples_m145_vs_bldA <- file.path('~/Downloads/X204SC24086605-Z01-F001/quants
',samples_m145_vs_bldA$Run,'quant.sf')
# Assign names to the quant file paths based on sample names
names(files_samples_m145_vs_bldA) <- samples_m145_vs_bldA$Run
# Read in tx2gene file, which contains the mapping of transcript IDs to gene IDs
tx2gene <- read_csv(file.path('~/Downloads/X204SC24086605-Z01-F001/R/tx2gene.csv'))
# Perform tximport on salmon quantification files using tx2gene for gene IDs
txi_m145_vs_bldA <- tximport(files_samples_m145_vs_bldA, type='salmon', tx2gene = t
x2gene)
# Import the data and clarify it is for DESeq2, indicating the column (Condition) u
sed in differential analysis
ddsTxi_m145_vs_bldA <- DESeqDataSetFromTximport(txi_m145_vs_bldA, samples_m145_vs_b
ldA, ~Condition)
# Carry out differential expression analysis using DESeq
dds_m145_vs_bldA <- DESeq(ddsTxi_m145_vs_bldA)
# Carry out contrast differential expression analysis, specifying the base, factor
being compared, numerator, and denominator
res_m145_vs_bldA <- results(dds_m145_vs_bldA, contrast=c('Condition','B','A'))
# Perform differential expression analysis with independent filtering turned off to
include all results
no_filter_res_m145_vs_bldA <- results(dds_m145_vs_bldA, independentFiltering = FALS
E, contrast=c('Condition','B','A'))
# Summarize the results
summary(res_m145_vs_bldA)
# Output/write the DESeq2 results as CSV files
write.csv(res_m145_vs_bldA, 'm145_vs_bldA_deseq2.csv', row.names = TRUE)
######### generate a PCA plot
#extract count data
countData1 <- counts(dds_m145_vs_bldA)
#extract column data
colData1 <- colData(dds_m145_vs_bldA)
combinedCounts <- cbind(countData1)
combinedColData <- rbind(colData1)
# Combine count matrices and colData
dds_combined <- DESeqDataSetFromMatrix(countData = combinedCounts,
          colData = combinedColData,
          design = ~ Condition)
# Perform rlog transformation on combined dataset
rld_combined <- rlog(dds_combined)
# Plot PCA
pca <-plotPCA(rld_combined, intgroup = 'Condition')
pcaData <-plotPCA(rld_combined, intgroup = 'Condition', returnData = TRUE)
ggsave('~/Downloads/X204SC24086605-Z01-F001/R/pcaplot.tiff', pca, width = 7.18, hei
ght = 3, units = 'in')
######### Isolate Differentially Expressed Genes
#this is split into a log2fold change method for venndiagram and using p-values
pval_threshold <- 0.05
#Venn diagram with no independednt filtering
#testing out ways to remove basemean= 0 - https://stackoverflow.com/questions/99776
86/how-to-remove-rows-with-any-zero-value
no.res_m145_vs_bldA_sub_no_0 <- no_filter_res_m145_vs_bldA[no_filter_res_m145_vs_bl
dA$baseMean !=0,]
#Pull out row names for each file with a significant pvalue/padj based on threshold
degs.no.res_m145_vs_bldA <- row.names(no.res_m145_vs_bldA_sub_no_0[no.res_m145_vs_b
ldA_sub_no_0$padj <= pval_threshold,])
#Pull out row names for each file with a log2fc <-1 and >1
degs.no.res_m145_vs_bldA <- subset(no.res_m145_vs_bldA_sub_no_0, log2FoldChange < -
1 | log2FoldChange > 1)
```

```
#Pull out row names for each file with a significant pvalue/padj based on threshold
degs.no.res_m145_vs_bldA <- row.names(degs.no.res_m145_vs_bldA[degs.no.res_m145_vs_
bldA$padj <= pval_threshold,])
# Filter for degs.no.res:
filtered_m145_vs_bldA <- no_filter_res_m145_vs_bldA[rownames(no_filter_res_m145_vs_
bldA) %in% degs.no.res_m145_vs_bldA, ]
write.csv(filtered_m145_vs_bldA,'~/Downloads/X204SC24086605-Z01-F001/R/DEG_m145_vs_
bldA_RNA-seq.csv', row.names = TRUE)

########## Volcano plots
# Define the specific set of gene names to label
gene_labels <- c('') # Replace with your specific genes
# Function to create EnhancedVolcano plot with specific labels
create_volcano_plot <- function(res, gene_labels, subtitle) {
 EnhancedVolcano(res,
     lab = rownames(res),
     x = 'log2FoldChange',
     y = 'pvalue',
     title = NULL,
     subtitle = subtitle,
     legendPosition = 'none',
     caption = NULL,
     pCutoff = 0.05,
     FCcutoff = 1.0,
     pointSize = 2.0,
     labSize = 3.0,
     labCol = 'black',
     labFace = 'bold',
     boxedLabels = TRUE,
     colAlpha = 4/5,
     drawConnectors = TRUE,
     widthConnectors = 1.0,
     colConnectors = 'black',
     max.overlaps = Inf, # Ensure all labels are displayed
     selectLab = gene_labels) # Specify exact labels
}
# Create EnhancedVolcano plots with specific gene labels
P1 = create_volcano_plot(res_m145_vs_bldA, gene_labels, bquote(italic('S. coelicolo
r') ~ ' M145 - bldA'))
# Create a grid of the updated plots
library(gridExtra)
library(grid)
# Sets x and Y axis to the same scale
P1_1 = P1 +
 ggplot2::coord_cartesian(xlim=c(-10, 10), ylim=c(-10, 100)) +
 ggplot2::scale_x_continuous(breaks=seq(-10, 10, 1))

plot_final = grid.arrange(P1_1)
ggsave('~/Downloads/X204SC24086605-Z01-F001/R/volcano.tiff', plot_final, width = 16
.5, height = 11.7, units = 'in')
```